Surface Engineering of Algae and Synthesis of Pyrrolizidines for Carbon Dioxide Capture Applications

Inauguraldissertation

zur Erlangung der Würde eines Doktors der Philosophie

vorgelegt der
Philosophisch-Naturwissenschaftlichen Fakultät der
Universität Basel

von

Isabel Patrizia Kerschgens

aus Aachen, Deutschland

Basel 2016

Originaldokument gespeichert auf dem Dokumentenserver der Universität Basel edoc.unibas.ch

Genehmigt von der Philosophisch-Naturwissenschaftlichen Fakultät auf Antrag von:

Prof. Dr. Karl Gademann
Prof. Dr. Konrad Tiefenbacher

Basel, den 15. November 2016 Prof. Dr. Jörg Schibler

Dekan

Für Philipp
und meine Familie

Table of Contents

Summary

The three research projects presented in this thesis apply organic synthesis as the main tool to answer interdisciplinary scientific questions. In the first project, organic synthesis is the key to tailor molecules for direct interaction with living organisms. The second project comprises a new method for the preparation of biologically relevant lead structures. The last project examines the synthesis of bifunctional pyrrolizidine diamines and their application in the capture of carbon dioxide.

Chapter 1 starts with a general introduction to the field of chemical surface engineering on living cells. The different functionalization approaches are briefly introduced and selected illustrative examples are presented.

Chapter 2 describes the surface functionalization of the green alga *Chlamydomonas reinhardtii* with the antibiotic vancomycin. We used a peptide-anchor adhering to the surface glycopeptides of the algae. By synthetic means, we linked this anchor to vancomycin to give a conjugate with good antimicrobial activity. The conjugate adhered to the cell wall of *C. reinhardtii*, as verified by confocal fluorescent microscopy. Bacterial assays showed that the modified algae inhibited the growth of bacteria and led to complete inhibition of bacterial growth, after optimization. Delivery of the vancomycin-conjugate from the surface of the algae to the cell wall of the bacteria was mainly driven by diffusion.

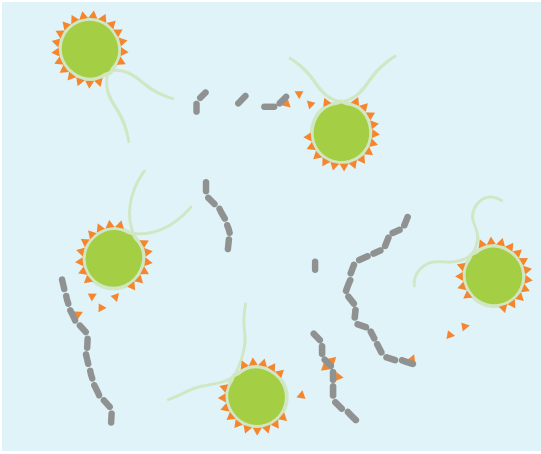

Illustration of vancomycin-modified algae with bacteria.

In **Chapter 3** we report on a method for the preparation of *7a*-substituted pyrrolizidine carboxamides. These compounds can be prepared by reaction of isonitriles with pyrrolines. Using a variety of isonitriles with different electronic and steric properties, we gained access to a diverse range of pyrrolizidine derivatives. An extension of this method by further functionalization of the pyrrolizidines as well as mechanistic studies are presented.

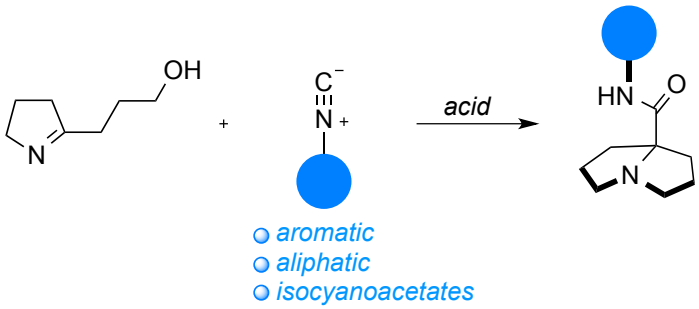

In **Chapter 4** our investigations of pyrrolizidines as scavengers for CO_2 are described. We quantified the efficiency of CO_2 uptake and elucidated the nature of the CO_2 adducts as well as the reversibility of the overall process.

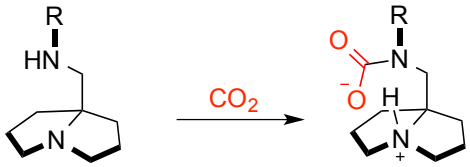

Zusammenfassung

Die drei Forschungsprojekte dieser Dissertation führen die herausragende Bedeutung organisch synthetischer Methoden für interdisziplinäre Fragestellungen vor Augen. Im ersten Projekt wird gezeigt, wie synthetische Methoden zur Herstellung maßgeschneiderter organischer Moleküle angewandt werden können, die direkt mit lebenden Organismen interagieren können. Das zweite Projekt ist eine neue Methode zur Synthese biologisch relevanter Moleküle. Im letzten Projekt haben wir bifunktionelle Pyrrolizidin Diamine in ihren Eigenschaften untersucht CO_2 zu binden.

Kapitel 1 gibt eine generelle Einführung in das Gebiet der chemischen Oberflächenmodifikation an lebenden Zellen. Die bekannten Verfahren werden kurz vorgestellt und anhand ausgewählter Beispiele veranschaulicht.

Kapitel 2 beschreibt unsere Resultate zur Oberflächenfunktionalisierung der Grünalge *Chlamydomonas reinhardtii* mit dem Antibiotikum Vancomycin. Hierzu haben wir einen Peptid-Anker benutzt, der Affinität zu den Oberflächenglykopeptiden der Zellwand aufweist. Der Peptid-Anker wurde über Festphasenpeptidsynthese hergestellt und anschließend mit Vancomycin verknüpft. Das resultierende Vancomycin-Konjugat zeigte weiterhin zufriedenstellende antimikrobielle Wirkung. Außerdem zeichnete es sich durch sehr gute Bindungseigenschaften an die Oberfläche der Algen aus, was mit Hilfe konfokaler Fluoreszenzmikroskopie nachgewiesen werden konnte. Wachstumsexperimente mit Bakterien und Algen zeigten, dass die zuvor modifizierten Algen das Bakterienwachstum hemmen und nach weiterer Optimierung sogar ganz unterbinden. Das Vancomycin-Konjugat wurde primär durch Diffusion von der Oberfläche der Algen auf die Zellwand der Bakterien übertragen.

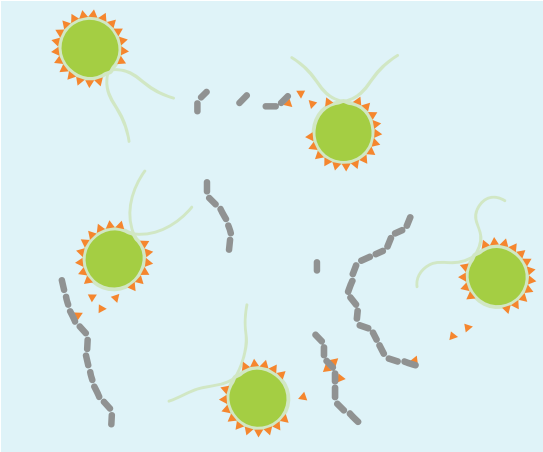

Illustration von Vancomycin-modifizierten Algen in Gegenwart von Bakterien.

In **Kapitel 3** beschreiben wir eine Methode zur Synthese *7a*-substituierter Pyrrolizidin-Carboxamide. Diese Substanzen sind durch direkte Reaktion von Isonitrilen mit Pyrrolinen zugänglich. Isonitrile mit verschiedenen sterischen und elektronischen Eigenschaften wurden erfolgreich als Startmaterialien eingesetzt und ermöglichten somit den effizienten Zugang zu einer Vielzahl von Pyrrolizidin-Derivaten. Darüber hinaus stellt dieses Kapitel mechanistische Studien zu dieser Reaktion und weitere Modifizierungen der Produkte vor.

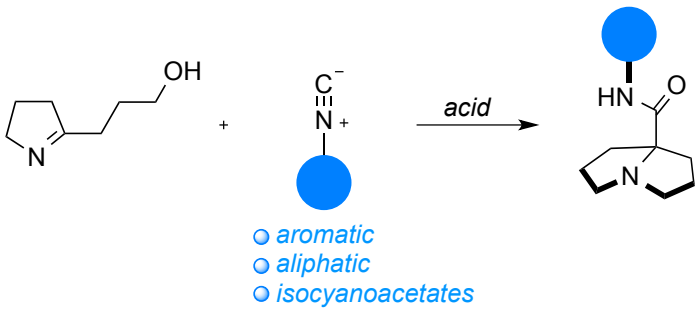

In **Kapitel 4** sind unsere Untersuchungen von Pyrrolizidinen als CO_2-bindende Moleküle beschrieben. Unsere Ergebnisse liefern Erkenntnisse zur Natur der CO_2-Addukte sowie der Effizienz und Reversibilität des Prozesses.

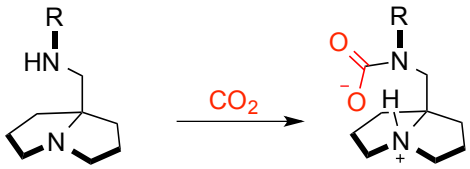

1 Introduction to Cell Surface Engineering

1.1 Cell surface engineering as a tool for the introduction of phenotypes

Cell therapy is the treatment of diseases by injection, transplantation or infusion of live cells. The cells can originate from the same patient (autologous) or from a different donor (allogeneic)[1] and cell therapies have emerged as standardized treatments in clinical use. Stem cell therapy is a fundamental technique for the treatment of leukemia with bone marrow transplants (hematopoietic stem cell transplants), but also non-hematopoietic stem cells are undergoing clinical evaluation. Among those are mesenchymal stem cells (MSCs) for the treatment of a number of diseases such as the Hurler syndrome[2], skeletal[3] and neurological disorders[4] or they can be used for the regeneration of bones[5], cartilage[6] or myocardia[7] tissue. Further cell treatments, such as neural stem cell therapy are still under investigation for the treatment of neurological disorders or human embryonic stem cells for the treatment of diabetes or Parkinson's disease, although the latter is highly controversial from an ethical standpoint of view.

Living cells can be engineered to improve their properties and function, enhancing cell survival, proliferation or differentiated function.[1] A traditional approach for this engineering is the preconditioning of cells *ex vivo* to later show enhanced effector function, self-renewal or longevity *in vivo*.[8] Further, the cell function can be modulated by appropriate drug treatment in addition to cell therapy, or the cells can be genetically engineered using synthetic biology to obtain genetically reprogrammed cells.[9]

More recently, another approach for the modification of living cells has emerged using the tools of molecular biology and chemistry to alter cell surfaces.[1] This approach directly remodels the cell itself for a very defined introduction of new phenotypes using techniques from chemistry, materials science or molecular biology. The cell surface plays the key role in all interactions of the cell with its environment and by manipulating it, properties such as adhesion, migration, tissue homing and cell-cell interactions can be altered.[1] Chemical surface engineering provides the opportunity to introduce functionality to the cell wall using synthetic materials, which are not accessible by genetic engineering. This is a vast advantage because it does not restrict the modification to originate from nature. In addition, it can be well defined where and at which time the cell is modified.

A major challenge of cell surface engineering is the loss of the cells' viability during the modification procedure or afterwards due to the modification. The experimental modification protocol needs to be carefully adapted to the cells needs because physical stress, change of pH, or

[1] For a review on the surface engineering of bacteria see: [10]

composition of the incubation solution can have severe effects on the well-being of the cell. The surface molecules for functionalization should be selected such that the cell can still exert its biological function and, for instance, essential surface proteins should remain intact. Another challenge is the internalization of the performed modification by cellular uptake mechanisms. And finally, the modified surface needs to be resistant to potential mechanical forces such as sheering, and the biochemical environment. There are several different techniques and approaches that have been used to modify the surface of living cells while addressing these challenges. The following sections will shortly introduce different cell surface engineering techniques from a chemical perspective.

1.2 Covalent modifications on naturally occurring functional groups

The most direct functionalization of a cell surface is the reaction of a functional material with the reactive groups of the cell surface (Figure 1). These groups usually are amine or thiol groups present on a cell membrane protein. The functional material contains reactive groups such as a succinimidyl ester or a maleimide group (Scheme 1).

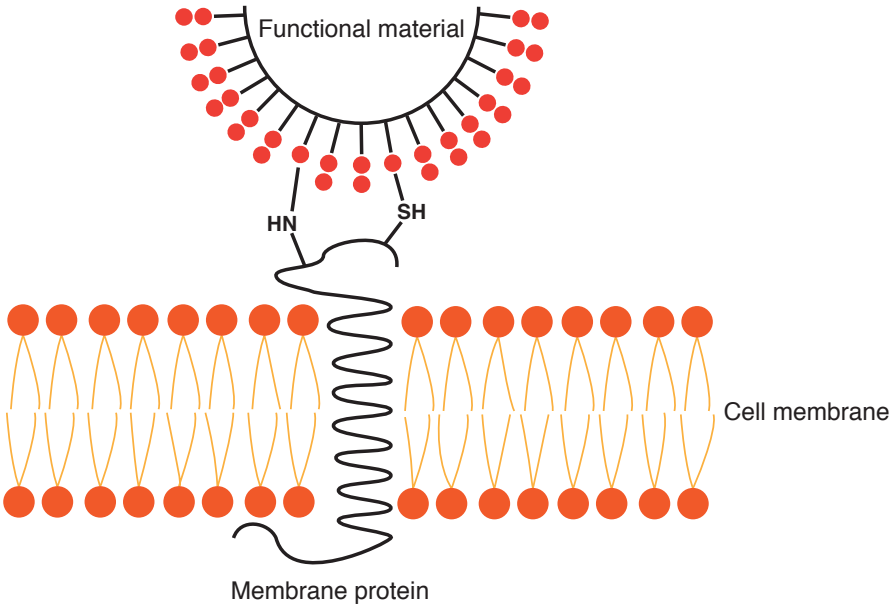

Figure 1: Direct functionalization by covalent attachment of naturally occurring functional groups.[2]

As an example *Lee* et al. modified pancreatic islets on the surface with a polyethylene glycol (PEG) chain using a succinimidyl ester functionalized PEG.[11] As a consequence, the cells were coated by a layer of PEG molecules. When injected into rats, the cells were tolerated by the im-

[2] Illustrations in this chapter were inspired by: [1]

mune system of the animals much longer as compared to the unmodified cells due to the coating. This example shows the potential application as immunogenic surface antigens.

Using the same attachment technique *Francis* and co-workers attached DNA strands to various cells including red blood cells and T-cells.[12] A bifunctional PEG chain was attached to the amine groups of the cell surface by reaction with a succinimidyl ester. On the other end, DNA was attached to a maleimide group *via* a thiol-decorated linker.

The reactivity of maleimides can also be used for the attachment to cells by reaction with free thiols of cysteines present in proteins on the surface. In their work, *Irvine* et al. used maleimide groups to link polymer nanoparticles to the surface of cells.[13]

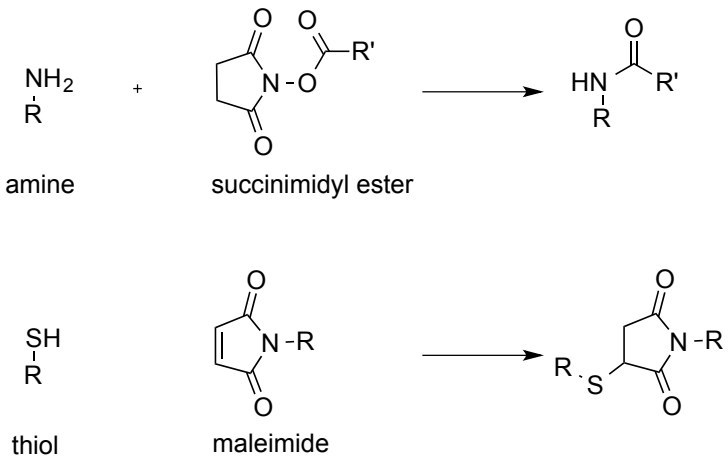

Scheme 1: Amines and thiols on the cell surface can be reacted with succinimidyl esters or maleimides.

Another technique for the attachment of a functional material is by reaction of a succinimidyl ester-functionalized biotin with the amine groups on the cell surface. This offers an advantage due to the wide range of biotinylated molecules that can be bound to a biotinylated cell surface *vi*a a streptavidin bridge (Figure 2). This technique has been used for the functionalization of MSC cells with Sialyl LewisX, a tetrasaccharide carbohydrate which drastically improved the rolling, adhesion and finally overall "homing" of the cells in a foreign environment.[14]

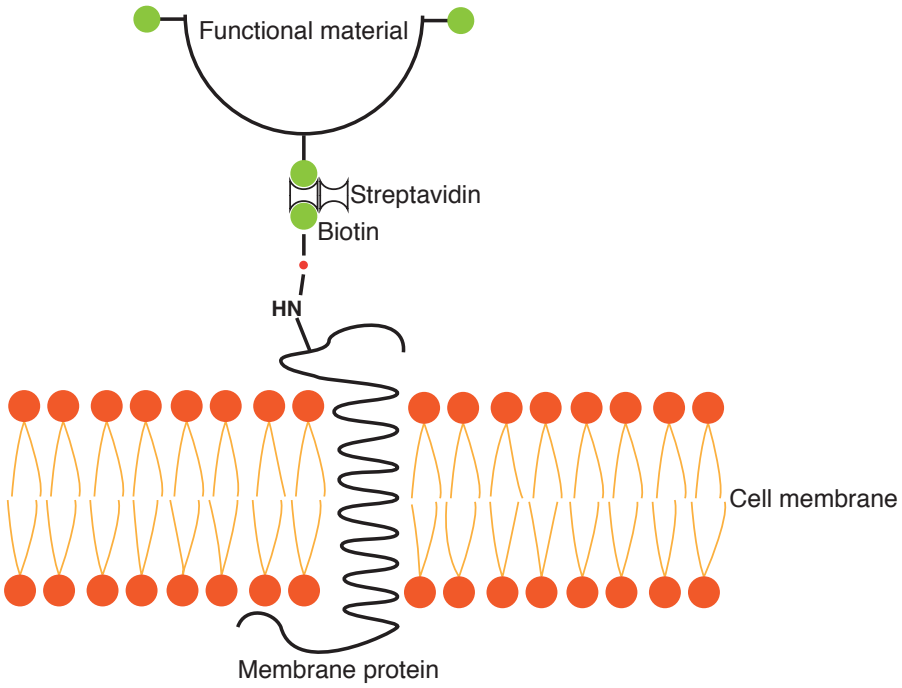

Figure 2: Direct functionalization of cell surfaces by biotin allows for the attachment of an array of biotinylated materials *via* a streptavidin bridge.

1.3 Modifications by hydrophobic insertion into the cell membrane

Membrane proteins function as receptors and play key roles in cellular signaling or nutrient uptake of the cell. Smaller membrane proteins control processes such as endocytosis or adhesion. They are either made up of protein alpha helices and span the plasma membrane, or are comprised of covalently linked lipids, which insert and interact with the lipid bilayer.[15] The latter binding principle has been used to engineer cells with artificial receptors. Molecules or nanoparticles can be decorated with hydrophobic chains and are able to spontaneously insert into the lipid bilayer in the presence of cells (Figure 3). Functional anchors such as glycoinositol phospholipids (GPIs) can be combined with virtually any protein by heterologous expression to give a recombinant protein. This protein is then isolated and used for surface engineering of target cells.[16,17]

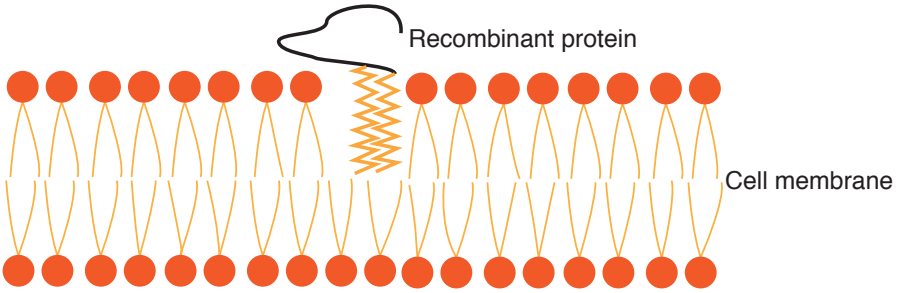

Figure 3: Recombinant proteins produced by heterologous expression can insert into the lipid bilayer of target cells.

A variation of this approach is the use of palmitated protein A or protein B, which can be prepared by reaction of the proteins with the *N*-hydroxy-succinimid ester of palmitic acid (Figure 4).[18] These proteins bind immunoglobins through their Fc region and allow for the fixation of antibodies on cell surfaces thereby broadening the functionalization possibilities with only one anchoring system.

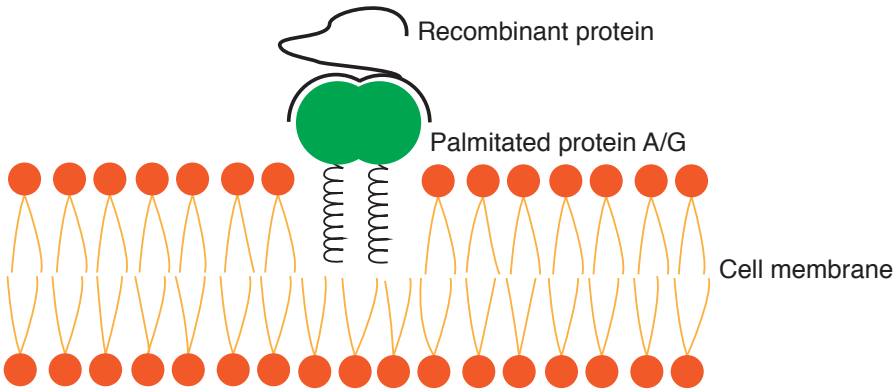

Figure 4: Inserted palmitated proteins can be functionalized with a variety of antibodies binding to their epitope.

In addition to the previously mentioned protein functionalization, hydrophobic insertion has also been done with chemically synthesized analogues. This allows for the functionalization of the surface with small molecules and even the delivery of otherwise cell-impermeable molecules.[1,15] *Bertozzi* and co-workers synthesized functionalized glycopolymers such as **1.1** that inserted into the lipid bilayer with a hydrophobic chain to mimic cell surface mucins (Figure 5).[3] Once in the cell membrane, the artificial compounds showed analogous behavior to natural mucins.[19]

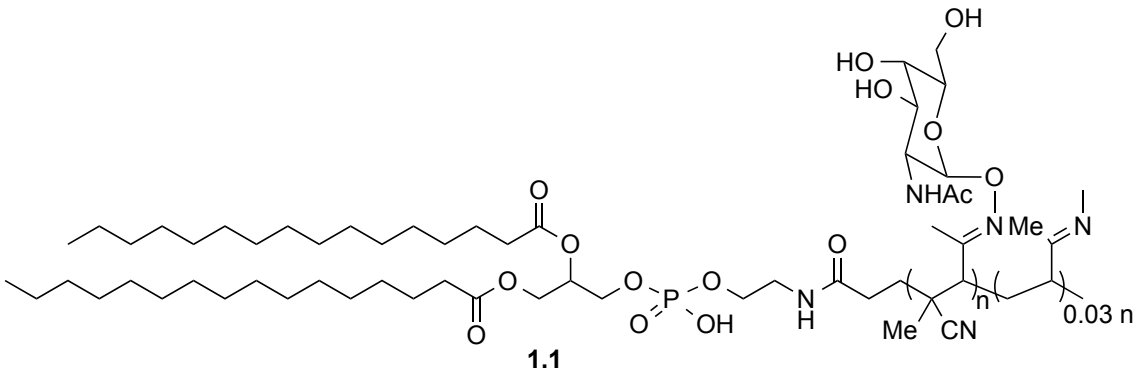

1.1

Figure 5: Chemically synthesized mucin-mimic polymer.

[3] Mucins are highly glycosylated proteins.

1.4 Surface modification by adsorption

The surface of mammalian cells is charged due to biomolecules such as phospholipids carrying phosphate groups or proteins and glycoproteins with carboxylate groups that contribute to an overall net negative charge. This charge is not able to form stable complexes to monovalent partners, but nanomaterials with multiple cationic sides can bind relatively strongly to such surfaces via multivalent electrostatic interactions (Figure 6).[1] Using this principle, *Chaikof* et al. engineered islets with various biocompatible reactive groups such as a biotin tag, an azide or a hydrazine (Figure 7).[20] A key feature of this study is a positively charged polylysine peptide **1.2** adhering to cell surfaces. Special feature of the peptide is that 40% of the lysine groups are PEGylated. The introduction of the PEG groups was necessary to decrease the cytotoxicity of the compound.[4]

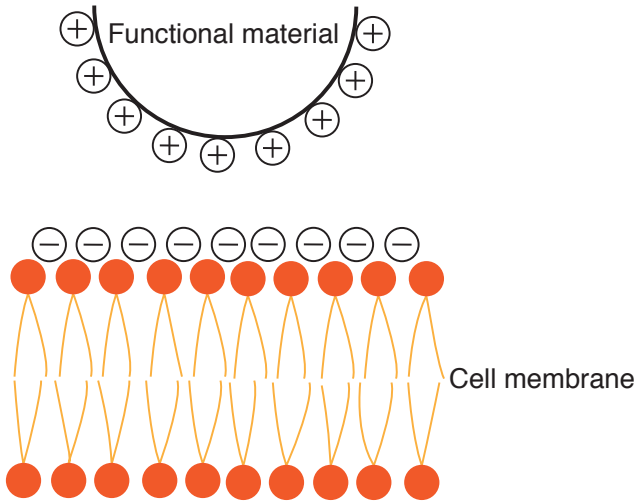

Figure 6: Surface modification by adsorption triggered by positively charges functional materials.

[4] Polycations can induce the formation of pores in the plasma membrane. These pores allow for the transport of small molecules through the plasma membrane into the cell that can lead to cell death.[21-23]

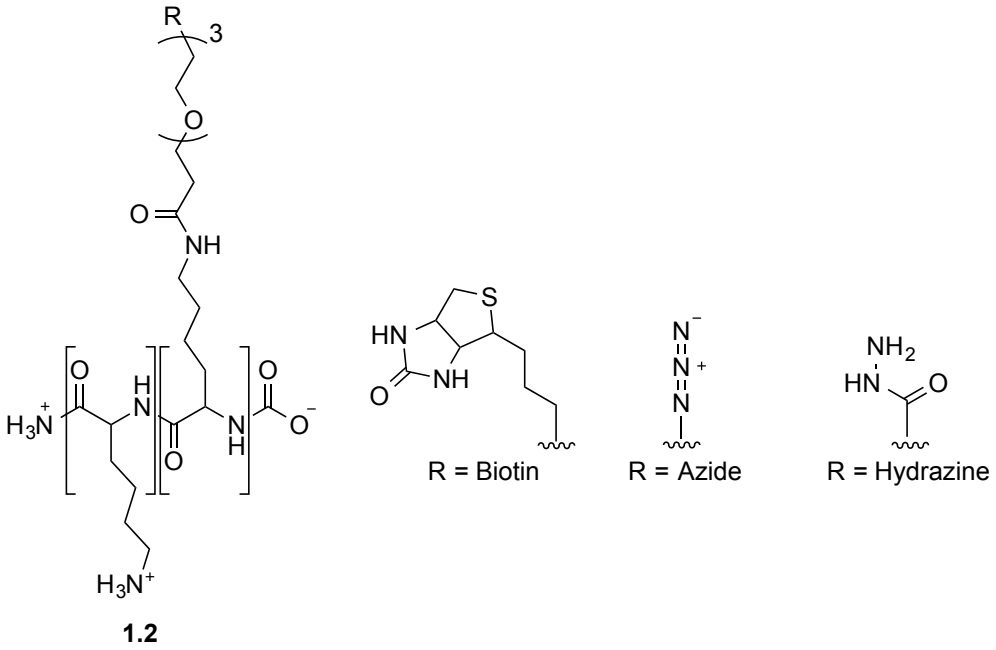

Figure 7: Positively charged polylysine **1.2** attaches to negatively charged cell membranes via electrostatic interactions. Reactive groups such as biotin, azide or hydrazine are attached to the peptide and can be used for further functionalization.

1.5 Modifications by attachment to naturally occurring receptors

Another technique for the functionalization of living cells is the attachment of modified ligands to naturally occurring receptors on the cell surface (Figure 8). A challenge to use this approach is the often-transient nature of these ligand-receptor interactions, as the ligand can dissociate from its receptor leading to a less stable attachment.

However, there are a number of examples using multivalent ligand binding and thereby exemplifying the utility of this approach. *Rubner* and co-workers used CD44 receptors and its natural ligand (hyaluronic acid) for the attachment of magnetic nanoparticles.[24] Notably, the cells could be functionalized only on one side of the cell, due to prior attachment of the cells to a polyelectrolyte multilayer patch. In another example, *Bertozzi* et al. used a hexavalent lectin termed *Helix pomatia* agglutinin (HPA) for the binding of carbon nanotubes to cell surfaces.[25] The carbon nanotubes were functionalized with α-GalNAc residues that are specific receptors for HPA. In addition, HPA is also capable of binding to cells and cross-linking glycoproteins, so that the carbon-nanotube-HPA complex could be fixed to the cell.

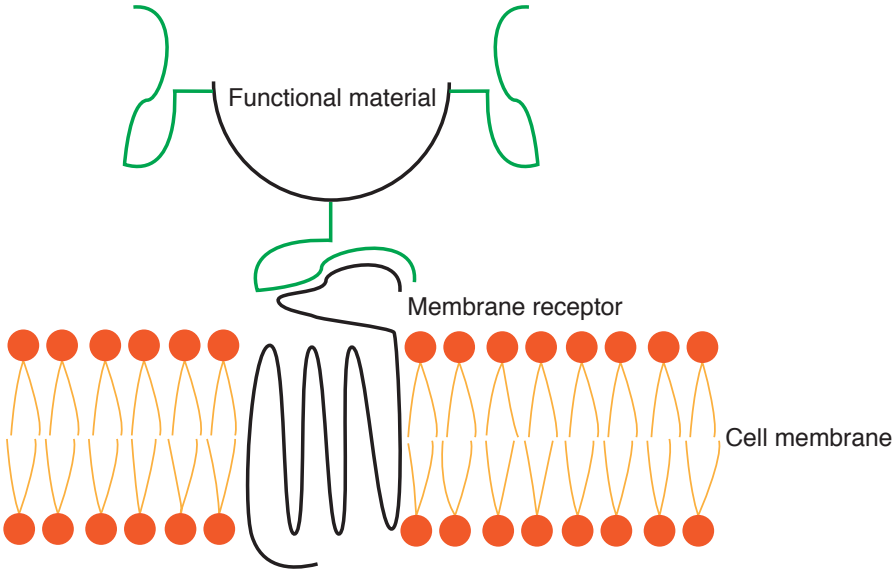

Figure 8: Naturally present membrane receptors can bind to modified ligands for surface engineering.

1.6 Metabolic introduction of functional groups for further modification

The metabolic introduction of bioorthogonal groups[5] to the cell surface represents a very elegant way for the functionalization of living cells. This approach uses biosynthetic precursors that carry bioorthogonal groups such as alkynes, azides, ketones or aldehydes and are incorporated into the living organism using its own biochemical machinery. After incorporation, the products carry the artificial tag that was previously installed on the precursor (Figure 9). These biosynthetic precursors can be amino acids for the functionalization of proteins,[27-30] sugars for the functionalization of cell surface glycans[31,32] or farnesyl and farnesol pyrophosphates to be used for lipid modification.[33] A precondition for this approach is that the enzymes involved in the biosynthetic processes tolerate the modifications on the precursors. After the modified precursor has been implemented into the cell it can be reacted in a mild way using bioorthogonal chemical reactions.[26] For example, azides can be reacted with phosphines in a Staudinger ligation[32,34] or by "Click"-reaction with alkynes.[35] Aldehydes or ketones can be reacted with hydrazines to hydrazones.[31] This approach offers the possibility to introduce functional molecules to the cell surface such as fluorescent probes[32] or viral receptors.[36]

[5] Bioorthogonal groups are non-native, non-perturbing chemical handles that are unreactive with groups present in biological systems. Bioorthogonal groups can later be modified with exogenously delivered probes.[26]

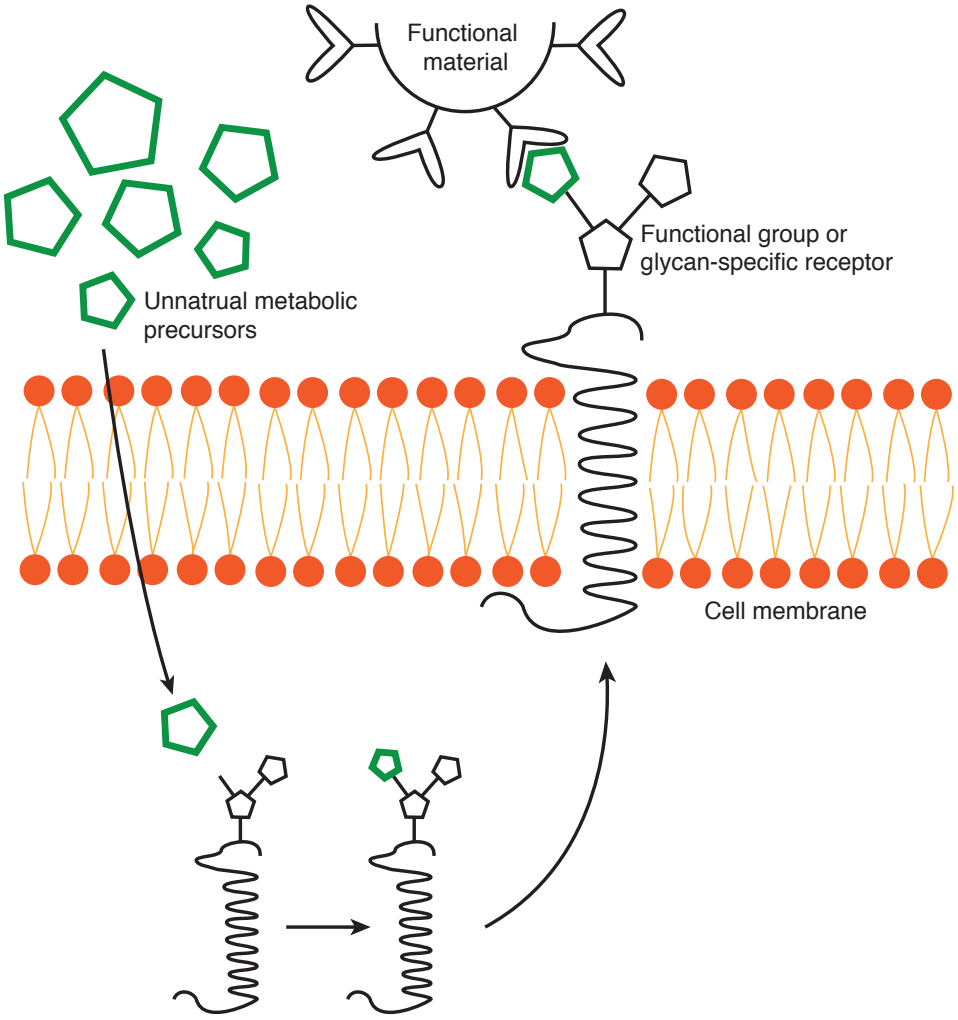

Figure 9: Metabolic incorporation of modified biosynthetic precursors that are later used to engineer cell surfaces.

An example closer related to the research in this thesis is the metabolic functionalization of a living diatom with thiol moieties (Figure 10).[37] Diatoms are unicellular algae with a cell wall comprised of silica.[38] Although the exact mechanisms of biomineralization are unknown *Finn* and co-workers were able to use thiol-functionalized silanes for the introduction of the functional group. The artificial building blocks are first hydrolyzed in the medium and then implemented in the silica framework of the organism. The utilization of the altered building block led to an overall similar morphology of the algae. However, differences in pore size were observed leading to a decreased density of the organism. Further functionalization of the modified diatom is not reported.

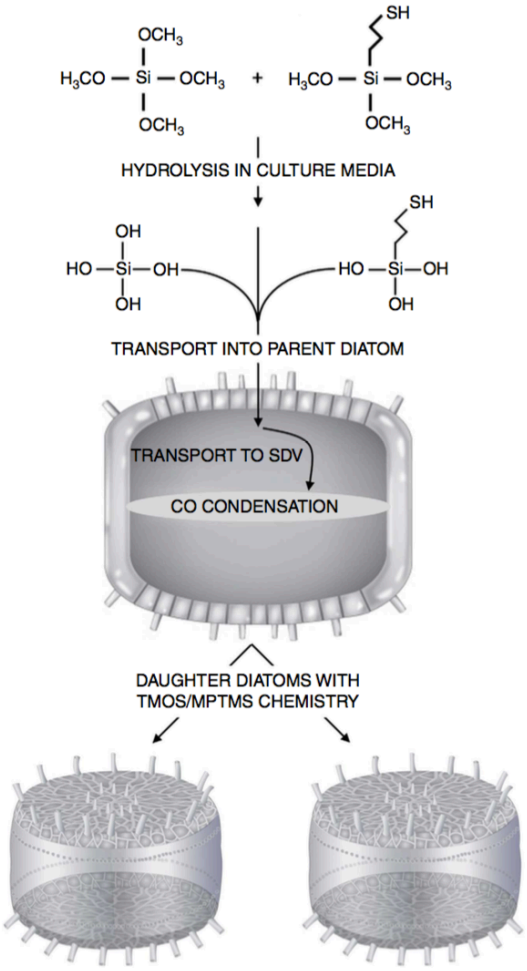

Figure 10: Metabolic introduction of thiol groups to diatoms.[37]

1.7 Conclusion

This introduction into cell surface engineering spotlighted the different classes of the chemical modification of living cell surfaces. We showed that there are a number of approaches to engineer these surfaces including covalent and non-covalent binding, the use of natural receptors or the introduction of non-natural binding sites on the surface. Most of the approaches are still in the early stage of development and to become more relevant to real clinical applications, they need to be implemented for a concrete therapeutic benefit. There are situations where chemical modification approaches are clearly beneficial over other techniques. For instance, chemical engineering is much less severe and non-permanent than the sometimes-unpredictable consequences of genetic engineering. There are also cases in which genetic engineering is very difficult or even impossible and in these situations, chemical surface engineering can serve as a useful tool. Overall, chemical surface engineering has emerged as a vibrant field of research in the interface of chemistry, biology and nanotechnology with the potential to solve fundamental problems in an interdisciplinary way.

2 Surface Engineering of Algae

2.1 The green alga *Chlamydomonas reinhardtii*

The unicellular green alga *Chlamydomonas* is one of the most frequently used model organisms in laboratory research, offering a simple platform to study fundamental processes in life with an easy life cycle and cellular features such as phototaxis and photosynthesis.[39] Figure 11 shows a light microscopy image of a *C. reinhardtii* culture. The genus consists of 459 species with *Chlamydomonas reinhardtii* being its most prominent representative.[40] The ellipsoid alga consists of a single basal chloroplast surrounding a nucleus that is located in center and contains a prominent nucleolus (Figure 12). The cell is encased by a cell wall in close proximity to the plasma membrane. Notably, the cell features two anterior flagella with which the cell is able to move and turn in aqueous environment triggered by phototaxis response.

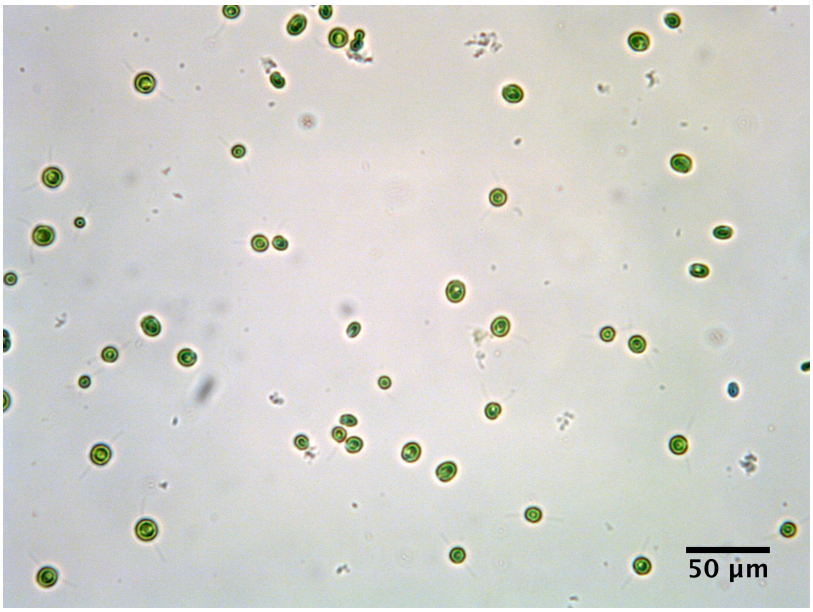

Figure 11: Light microscopy image of a *C. reinhardtii* culture.

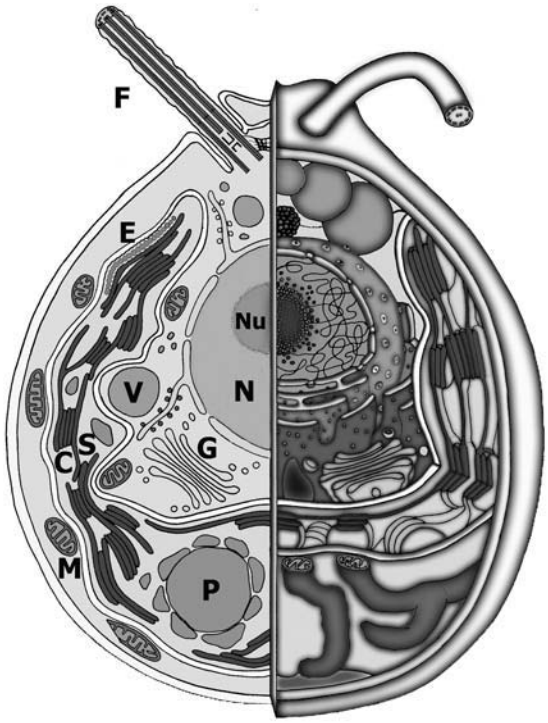

Figure 12: Cellular architecture of *C. reinhardtii*. The cell comprises the central nucleus (N) with the nucleolus (Nu), two isoform flagella (F), the cup-shaped chloroplast (C) including an eyespot (E), the starch-containing pyrenoid (P) and the mitochondria (M). It also contains the Golgi vesicle (G), starch grains (S), and vacuoles (V).[40,41]

2.1.1 Cell wall architecture

The cell wall of *C. reinhardtii* has been identified to consist of a dense arrangement of hydroxyproline-rich glycopeptides with arabinose, mannose, galactose and glucose showing the highest abundance of the sugars.[40] These glycoproteins show similarities to those of higher plant species but are also clearly distinctive in their sugar composition and molecular organization.[40,42-45] The cell wall is divided into seven sub-compartments showing different morphology (Figure 13).[46,47] The innermost layer (W1) consists of an irregular network of fibers with differing thickness that radiate outwards the cell. The thickness of this layer has been identified to vary from 30 to 200 nm. The next layer (W2) shows a very similar composition as W6, both consisting of a dense network of fibers. For the W2 layer the fibers lie mostly parallel to the cell surface, whereas a more crystalline arrangement of thick fibers is observed for W6, flanked by thin crossfibrils and an open-weave lattice. The layer in between (W4) is of granular consistency. Layers W2, W4 and W6 are often termed as the ‘central triplet’ and show high consistency independent from culture conditions or fixation techniques. The electron-transparent layers W3 and W5 are assumed to be spaces instead of true wall components.[40,47] The outer layer W7 is composed of granular fibers resembling layer W1.

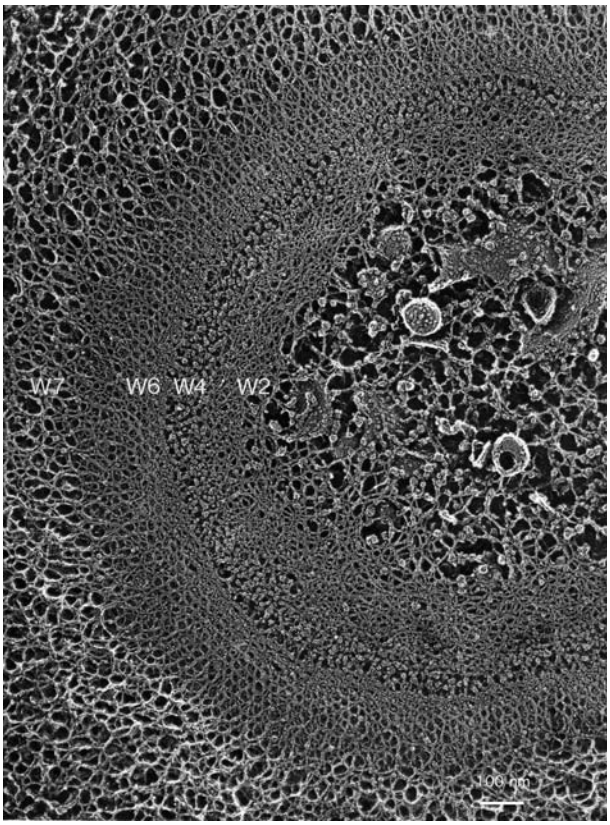

Figure 13: Cell wall of detergent-treated *C. reinhardtii*. Courtesy of U. W. Goodenough and J. E. Heuser.[40]

2.1.2 Chloroplast

Chloroplasts are organelles present in plants and algal cells and mainly provide the cell with energy through the process of photosynthesis. The photosynthetic dye is chlorophyll that also gives the cell the characteristic green color.[6] In *C. reinhardtii*, the chloroplast takes a cup-shape configuration, which appears like a U-shaped structure surrounding the nucleus (Figure 14, a). The pyrenoid is embedded in the chloroplast and is acting as the central unit for CO_2-fixation, providing sufficient supply for photosynthesis.[48,49] Besides a strong UV/VIS absorption chlorophyll also shows strong fluorescence in the red region. This is a useful tool in fluorescence microscopy for the identification and location of the algae (Figure 14, b).

[6] The green color results from strong UV/VIS absorption in the UV and blue region and in the yellow and red region of the visible light spectrum.

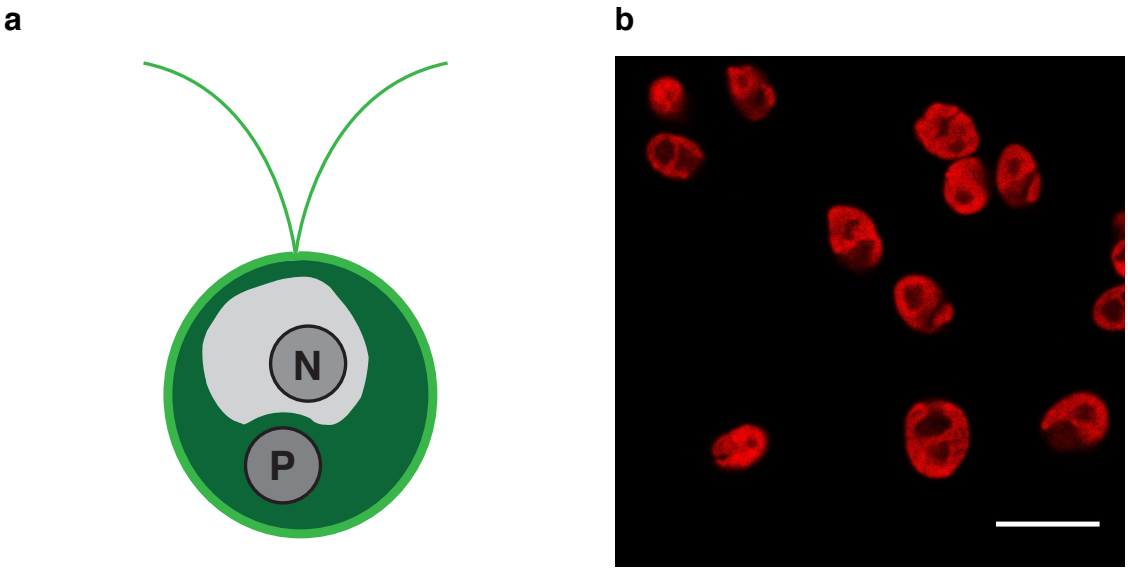

Figure 14: Chloroplast of *C. reinhardtii*. **a)** Arrangement of the chloroplast inside the cell. **b)** Fluorescent single confocal image of the chloroplast. Scale bar equals 10 µm.

2.1.3 Phototaxis

Phototaxis is the movement of an organism towards or away from a stimulus of light. Phototaxis can be positive, when the organism is moving in the direction of the light source or negative, when it is moving in the opposite direction. For organisms conducting photosynthesis, this is a highly advantageous stimulus because the organism can arrange itself most efficiently to receive energy.[50] The green alga *C. reinhardtii* moves using the two flagella. The phototactic behavior of *C. reinhardtii* is very complex and is influenced by a variety of factors. First, it strongly depends on the strength of the light source whether the algae react with positive or negative phototaxis. With low to moderate light intensities ($<10^3$ ergs/cm^2) the algae accumulate in a light beam, with high light intensities they avoid light.[51] Further, the cells behave differently depending on environmental influences such as culture medium, temperature and stage of life cycle.[52,53] The algae strain used for the experiments, as well as the age of the culture, have significant influence on the phototactic response. Cells of freshly inoculated algae cultures show negative phototaxis, whereas cells from older cultures are positively phototactic.[54] Further, phototactic behavior is maximal in the exponential growth phase and decreases in the stationary phase.[55] Overall, it can be concluded that a variety of factors need to be considered when strategically utilizing the phototaxis of the algae.

2.1.4 Surface functionalization of C. reinhardtii

The algae *C. reinhardtii* displays an interesting target for synthetic biology. Due to its easy life cycle, simple growth conditions and attractive features like phototaxis, it has been the objective on many genetic engineering approaches in the past.[56,57] However, to the best of our knowledge, only one example has been reported that documented surface functionalization of the green alga by non-genetic means. The report published by *Whitesides* and co-workers describes the surface modification of *C. reinhardtii* with a polystyrene bead.[58] The polystyrene bead was irreversibly attached to the surface, and the alga was able to cover distances of up to 20 cm with velocities of 100-200 µm·sec^{-1}. For the attachment of the bead to the surface, a 10-mer of 4-hydroxyproline was utilized that was connected to the polystyrene bead *via* a photocleavable linker (Figure 15). In first experiments, the authors demonstrated that the alga could transport the polystyrene bead through a microfluidic channel guided by LEDs that were alternately turned on (Figure 16). This served as a nice demonstration that the algae can function as a micro-bio-robot[59,60] controlled by the use of light. Later, the authors cleaved the polystyrene bead from the anchor with a 20 s light irradiation at 365 nm.

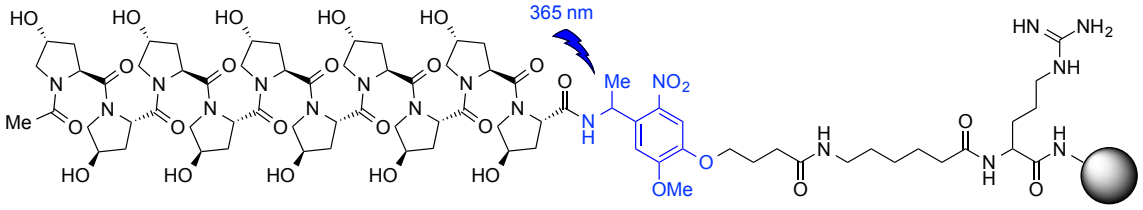

Figure 15: System used by *Whitesides* and co-workers for the immobilization of a polystyrene bead on the surface of *C. reinhardtii*.

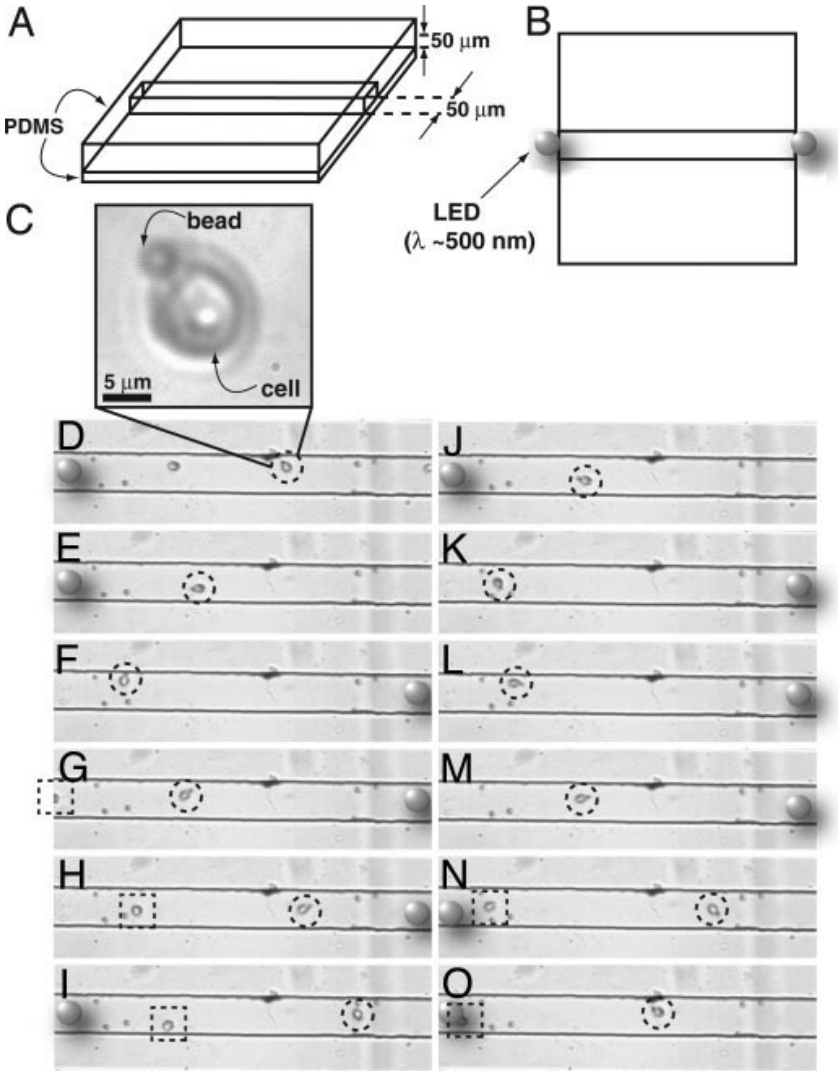

Figure 16: Transport of microloads by *C. reinhardtii* through a microfluidic channel triggered by a light stimulus.[58] Copyright (2005) National Academy of Sciences.

2.2 *Bacillus subtilis*

The Gram-positive bacterial strain *Bacillus subtilis* is a widely used model organism. The cells are 2.3 μm in length and 0.6 μm thick and the surface of the cells is fully flagellated allowing the bacteria to move quickly at velocities of up to 4 μm/sec (Figure 17).[61] The appearance of the cells during cell cultivation is not homogenous. Depending on the age of the culture single rod shapes or long chains composed of single cells are observed. The cell appearance of the bacteria depends strongly on the growth stage and on the bacterial strain[62-64]; we have observed the bacteria to appear mostly in single or double rods during the exponential phase and in chains during the stationary phase (see section 7.2.2, Figure 57 in the experimental part).

B. subtilis can be isolated from many environments, both of terrestrial and aquatic nature. The biofilm forming bacterium grows on plant roots[65,66] or can be isolated from the rhizosphere from a variety of plants.[67-69] In these environments it is often subjected to harsh conditions such

as nutrient deprivation, desiccation, heat, UV-light and pressure making it necessary for the organism to be flexible to survive.[70] As a response, it forms highly resistant dormant endospores that can spread through the air.[71,72] Once formed, the dormant cells can persist for long periods of time.

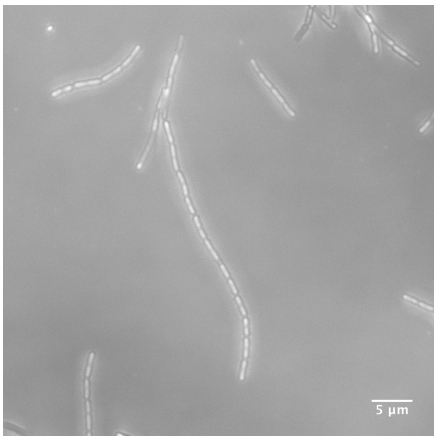

Figure 17: Bright field image of *B. subtilis* taken with a confocal microscope.

Bacterial cells consist of a cell wall surrounding inner components such as nucleoid (DNA) and ribosomes embedded in the cytoplasm. The cell wall in Gram-positive bacteria functions as protection from mechanical influences and allows them to live in hypotonic environments.[7] The cell wall consists of a relatively thick (20-80 nm) peptidoglycan or murein (Lat.: *murus*, wall) layer that lies on top of the cell membrane (Figure 18). Starting at the cell membrane, lipoteichoic acids pierce the peptidoglycan layer to the outside of the cell wall. In contrast, Gram-negative bacteria contain a thin peptidoglycan layer, which is covered by an outer membrane. Due to the second outer membrane and the thinner peptidoglycan, Gram-negative bacteria are not stained by Gram-stain, a chemical cocktail (crystal violet and iodine) for the detection of the peptidoglycan.

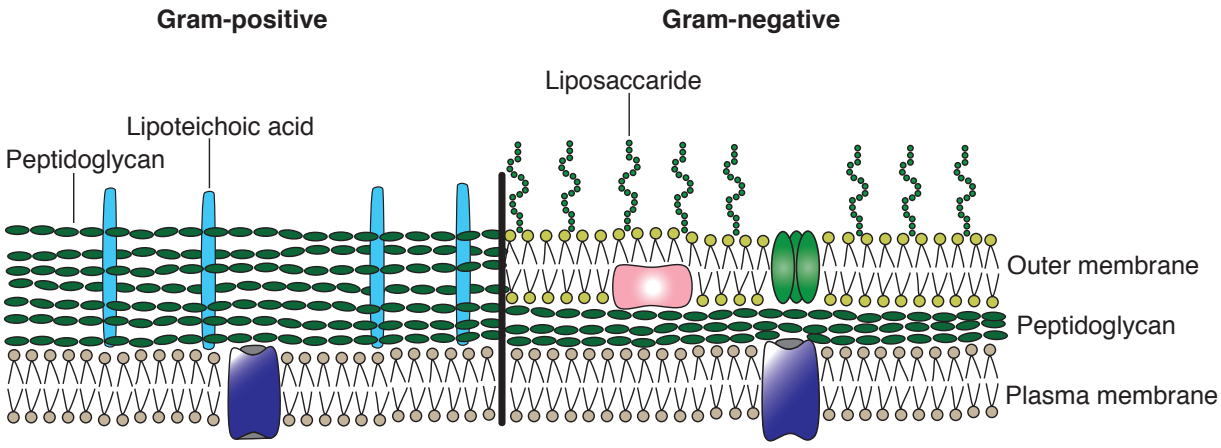

Figure 18: Comparison of the cell walls of Gram-positive bacteria and Gram-negative bacteria.

[7] Hypotonic: The salt concentration of the environment is lower than the intracellular salt concentration.

The life cycle of *B. subtilis* involves two mechanisms. The first one is the vegetative cycle, which occurs under normal growth conditions and serves the reproduction of bacteria. The second is the sporulation cycle that takes place under starvation conditions and ends in the formation of dormant endospores (Scheme 2).[73] The vegetative cycle starts with segregation of the chromosome inside the bacterial cell, which proceeds to the formation of a binucleate. Further, the cell wall of the bacteria starts to form a cross-wall initiating the separation of the cells; and further proceeds by segregation to finally release a second cell.[74] This cycle takes 120 min for *B. subtilis*, while it only takes 20 min for the Gram-negative bacteria *Escherichia Coli*. Opposed to this, the process of sporulation is mainly initiated by starvation, when the cell sees the need to transform into a highly resistant version. The stimulus of starvation triggers a complex cascade of biochemical reactions that involve the synthesis of the transcriptional regulator Spo0A that activates the transcription of several key sporulation-specific genes.[75] Based on this, the cell divides asymmetrically and a smaller cell, the prespore, is engulfed. This process involves the segregation of chromosome in the prespore and the mother cell. Next, the prespore is encapsulated by formation of the cortex, cell membrane and cell wall. At the same time the cell is dehydrated and mineralized. Finally, a multilayered coat of proteins is assembled around the cortex. During this process, the ability of the spore to respond to suitable environments for vegetative growth is included. Lysis of the mother cell releases the dormant endospore that is able to react to specific germinants to shed its protective layers and rehydrate.

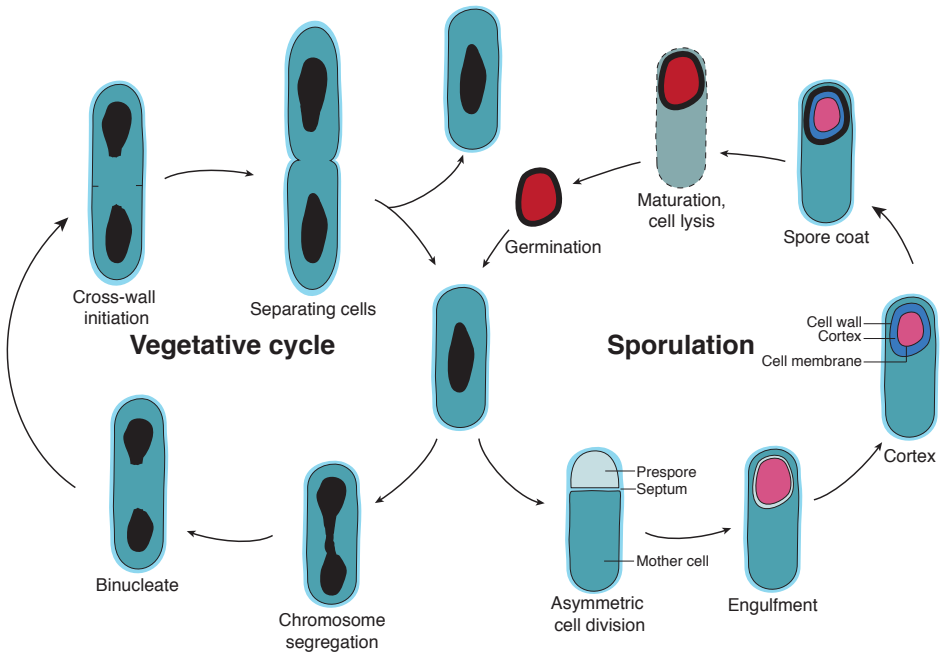

Scheme 2: Simplified schematic representation of the vegetative and sporulation cycle of *B. subtilis*. Chromosome segregation is not shown for the sporulation cycle.

2.3 Vancomycin – a glycopeptide antibiotic

Vancomycin is a glycopeptide antibiotic isolated from a soil sample in the mid 1950s by Eli Lilly in the USA and first used clinically in 1959 (Figure 19).[76] It is produced by the Gram-positive bacteria *Amycolatopsis orientalis*. At the beginning, the clinical use of the isolate caused a number of side effects, which hampered its application.[77] Later, it was recognized that the side effects were mainly caused by impurities present in the isolates, which could be removed by an improved purification procedure. Vancomycin and its relatives ristocetin A and teicoplanin have been the antibiotics of last resort against methicillin-resistant *Staphylococcus aureus* and other pathogens for a long time.[78] Unfortunately, the frequent prescription of vancomycin has led to a wide-spread resistance of bacterial strains in hospital.[79]

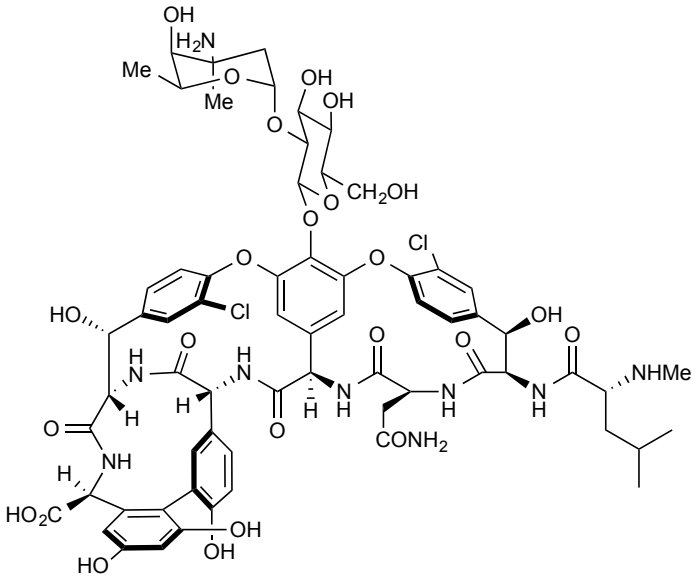

Figure 19: Structure of vancomycin.

The molecular structure of vancomycin involves a peptide backbone constituted from seven amino acids. Other characteristic features are the chlorine atoms attached to the aromatic rings of the side chains and the atropisomeric biaryl ring-system. The structural elucidation has first been investigated by NMR spectroscopy[80-83] and finally by X-Ray crystal structure analysis.[84,85]

Vancomycin is a potent antibiotic against Gram-positive bacteria and used for treatment of patients that are allergic to β-lactam antibiotics. Its mode of action is the complexation to the peptidoglycan precursor and thereby inhibiting the maturation of the cell wall.[86] As a consequence the bacteria lyse.[87] The complex formed between the cell wall fragment D-Ala-D-Ala and the peptide backbone of the antibiotic is stabilized by an array of van der Waals interactions and five key H-bonds (Figure 20).[88]

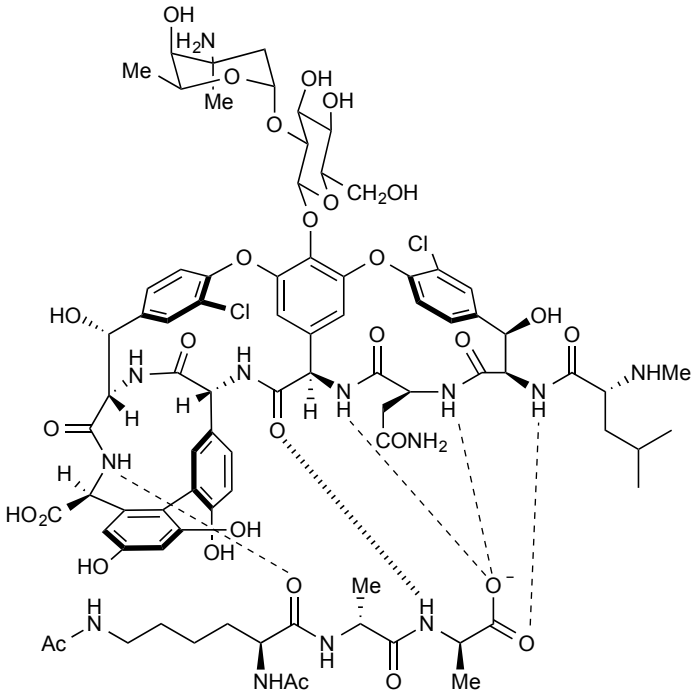

Figure 20: Complex between vancomycin and the peptidoglycan precursor.

Drug-resistant bacteria such as enterococci have developed mutations that defend themselves against vancomycin. The structural basis for the resistance lies in the exchange of the D-Ala-D-Ala terminus to D-Ala-D-Lac. This simple substitution (N→O) results in a 1000-fold decrease in binding of vancomycin to the cell wall fragment.[89] Basis for this is the loss of the central H-bond present in the D-Ala-D-Ala complex (Figure 21). In contrast, the new complex contains a repulsive lone-pair interaction between the carbonyl of vancomycin and the ester oxygen of lactic acid that mainly contributes to the loss of activity. Overall, this mutation leads to an increase of the MIC of vancomycin by a three-fold of magnitude.[90]

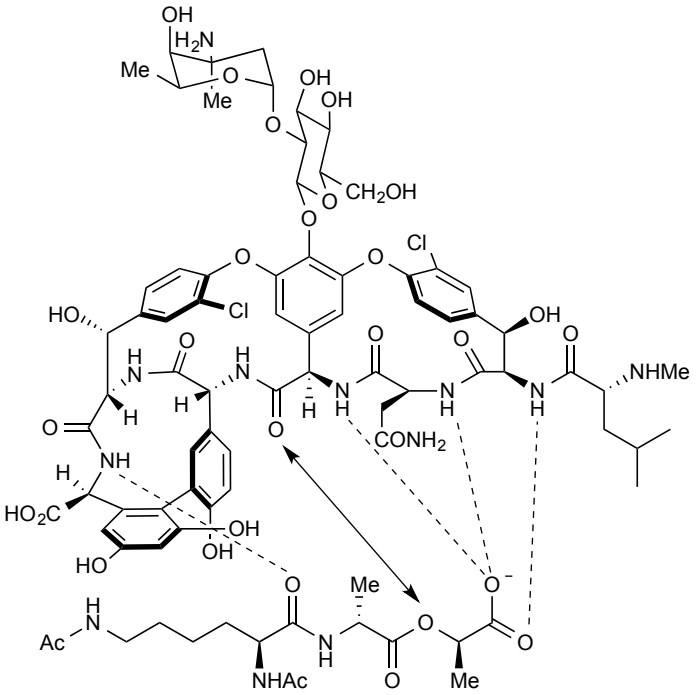

Figure 21: Interactions of vancomycin with the modified cell wall fragment.

2.4 Project outline

The objective of this project was the surface functionalization of the green algae *C. reinhardtii* with the antibiotic vancomycin. In a first step, a system had to be designed which allows for attachment of the antibiotic to the surface (Scheme 3). In a second step, the algae were tested on their antimicrobial activity against the Gram-positive bacteria *Bacillus subtilis*.

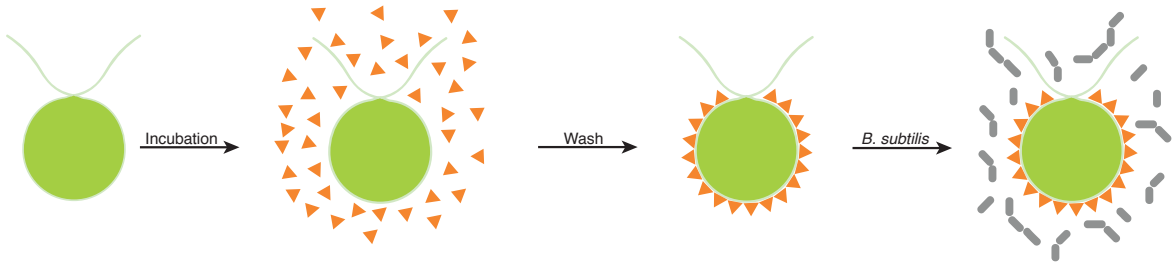

Scheme 3: Schematic representation of surface modification of *C. reinhardtii* with vancomycin followed by antimicrobial tests against *B. subtilis*.

Several challenges are addressed here: First, the coating needs to be sufficiently adhesive to remain on the surface after removal of the incubation solution and wash of the algae. Second, the properties of the algae in terms of general appearance and motility should not be severely impaired. Third, the operational procedure should be easy and practical. Finally, the amount of substance on the surface needs to be sufficiently high to exert an antimicrobial effect.

2.5 Preliminary work

Earlier work was carried out in our group by a former postdoc, *Prof. Dr. Chandan Kumar Jana*. He investigated a 4-hydroxyproline oligomer, which was fluorescently labeled by reaction with fluorescein isothiocyanate to give compound **2.01**.

The attachment of the substance to the algae was tested by incubation of the algae with **2.01**. The algae were washed and examined under a fluorescence microscope using different filters.[8] The images show the autofluorescence of *C. reinhardtii* in **a** and **a'** in green color; and the fluorescence of substance **2.01** in **b** and **b'** in red color **(**Figure 22).[9] The bright field images **c** and **c'** show the sample with transmitted light. The irregularities, especially visible in **c**, result from salt residues, which remain after the sample has dried out. The overlay images **d** and **d'** show that the red and green fluorescence is localized on the same position and from this we conclude, that compound **2.01** is localized on the alga.[10]

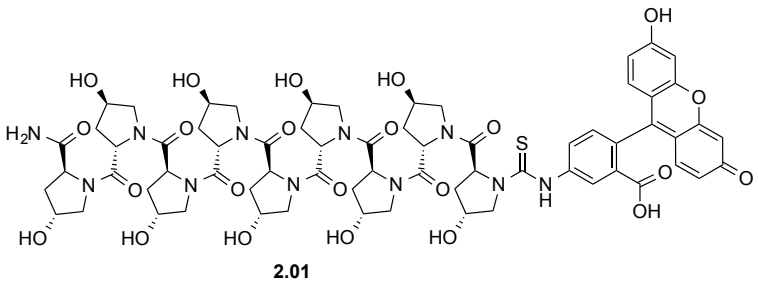

2.01

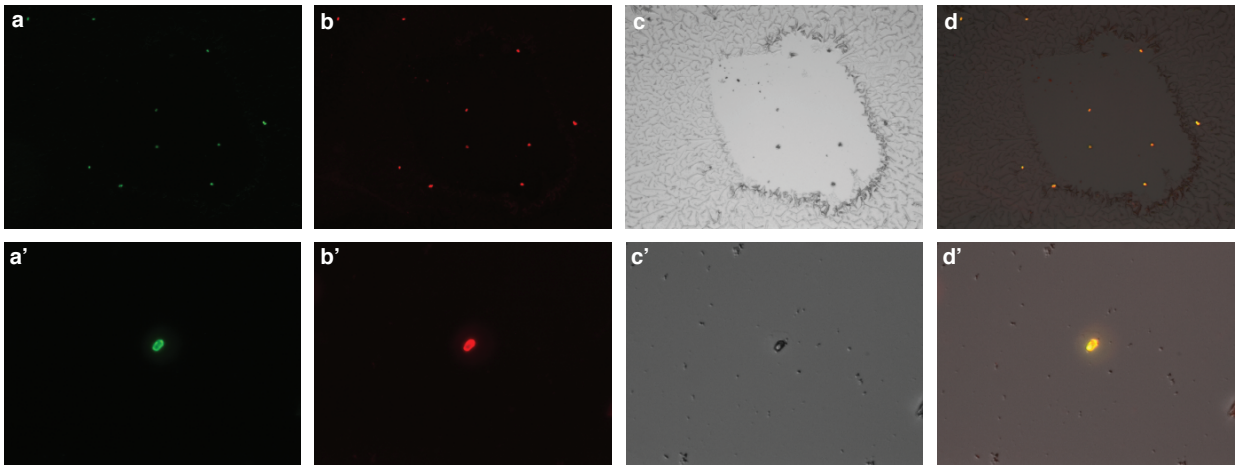

Figure 22: Algae *C. reinhardtii* modified with **2.01**. **a)** Autofluorescence of algae. **b)** Immobilized substance. **c)** Bright-field image. **d)** Merged image of **a**, **b** and **c**. Pictures indicated with ' are magnified images of the same samples. Images were taken by *Chandan Kumar Jana.*

[8] Imaging was performed on a widefield microscope (Leica DMI 4000), not listed in the instrumental part.
[9] The convention to choose the color of the fluorescent signal according to the emission wavelength of the fluorophore, was not followed in this case. For the upcoming images the convention was implemented.
[10] The overlay of red and green results in yellow color in the merged image.

2.6 Synthesis of 4-hydroxyproline oligomer derivatives and their interaction with *C. reinhardtii*

For the immobilization of vancomycin on the surface of the algae, 4-hydroxyproline oligomer was utilized as the anchor for attachment to the cell surface.[58] On the 4-hydroxyproline oligomer, a linker was installed which carried the fluorescent tag. The primary amine of the linker was used for the attachment of the antibiotic. Vancomycin offers several functional groups suitable for modification, for instance a carboxylic acid, a primary or a secondary amine.[91] The carboxylic acid group has been proven earlier to be a suitable site for functionalization[92,93] because it is not directly involved in the hydrogen bonding complex with the precursor peptidoglycan peptide terminus *N*-acyl-D-Ala-D-Ala (see section 2.3).

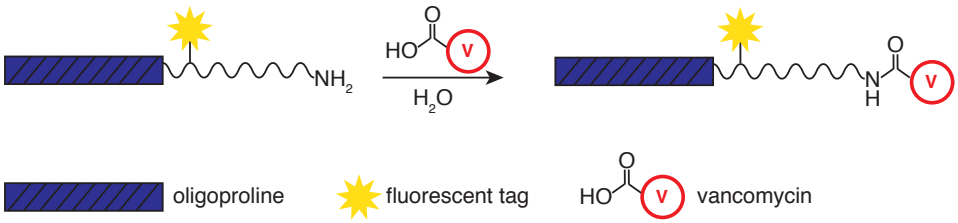

Scheme 4: Schematic representation of the 4-hydroxyproline oligomer-vancomycin conjugate.

We started with the reproduction of the results obtained earlier (see 2.5 Preliminary work), which involved the synthesis of the 4-hydroxyproline oligomer. In addition to fluorescently labeled 9-mer (compound **1**), we also decided to prepare the corresponding 10-mer. First, the 4-hydroxyproline oligomer was synthesized by solid phase peptide synthesis using Fmoc-protected amino acids, which were coupled on the C-terminus to a Rink amide resin. The resin had a relatively high loading of 0.59 mmol/g, which means a close proximity of the reactive groups on the polystyrene bead. The synthesis was performed with a solid phase peptide synthesizer that performed the following steps in nine cycles: (1) coupling, (2) Fmoc deprotection and (3) capping.

The peptide (**2.03**) was cleaved from the resin using a cocktail consisting of TFA, TIS and water. Due to the polarity of the compound, HPLC purification was not possible. Instead, the solid was dissolved in water and filtered over a SPE column previously equilibrated with water. Remaining components from the resin[11] could be removed in this way.

[11] One component was identified as this diphenyl ketone: 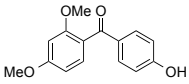

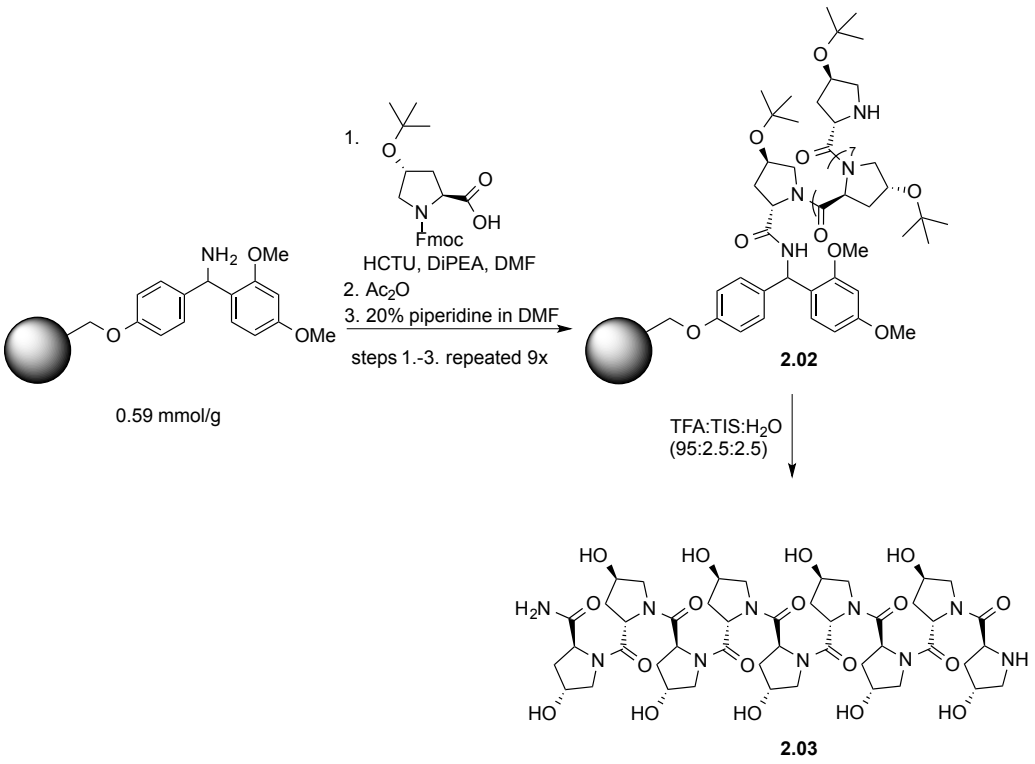

Figure 23: Synthesis of the 4-hydroxyproline oligomer **2.03** by solid phase peptide synthesis.

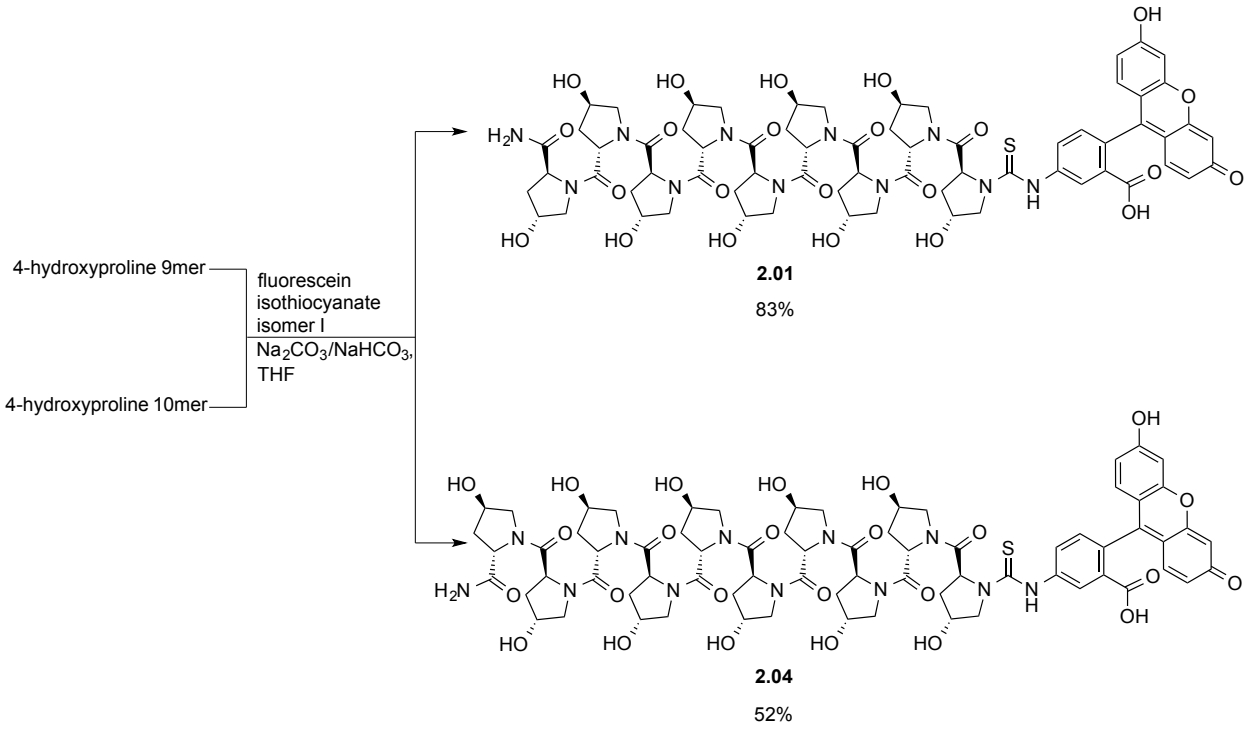

Scheme 5: Synthesis of fluorescently labeled 4-hydroxyproline oligomer connected by thiourea-bridge.

The fluorescent label was installed by addition of the 9-mer or the 10-mer to fluorescein isothiocyanate in a mixture of buffer and THF. At this stage, the 4-hydroxyproline oligomer was dissolved in water and THF was added to dissolve the fluorescent reagent.

LC-MS analysis of the crude mixtures revealed that the products partially had reacted according to a reaction named *Edman degradation* to release a fluoresceinthiohydantoin **2.08** as well as the peptide shortened by one amino acid unit **2.07** (Scheme 6). This reactivity of peptides that are α-substituted with a thiourea is well known and commonly used for the determination of amino acid sequences of peptides.[94,95] In our case, the fluoresceinthiohydantoin could be separated from the product by HPLC purification, but overall this side reaction shows that the compounds are not entirely stable in aqueous media.

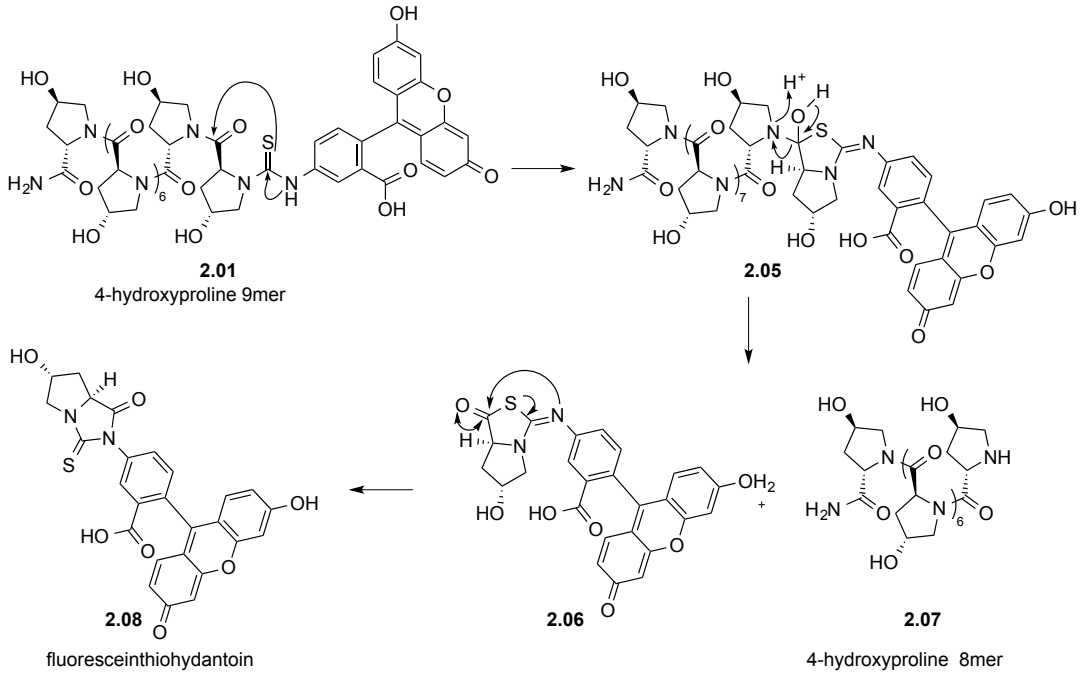

Scheme 6: Thiourea substituted peptides such as **2.01** can decompose according to the Edman degradation.

Next, we incubated the algae with compounds **2.01** and **2.04** for 48 h at a concentration of $4.67 \cdot 10^{-3}$ mmol/mL.[12] The algae were first concentrated by centrifugation and the medium was removed, such that the algae density was about 10x higher than in the culture they have been raised in. Then the substances were added as a solution in the culture medium of the algae. After 48 h, the algae were washed with medium and imaged on a confocal microscope (Scheme 7). The fluorescence images revealed that both compounds **2.01** and **2.04** were attached to the algae. The images taken are single layers of the center of the algae, so that the distribution of the compound inside the algae is visualized. Both compounds were clearly internalized by the algae, so that attachment solely to the surface can be excluded. Additionally, there was no significant difference in adherence between **2.01** and **2.04**, both substances attached equally well to the algae.

[12] The attachment of the compound to the algae was strongly dependent on the concentration. The concentration used was adapted from earlier protocols.

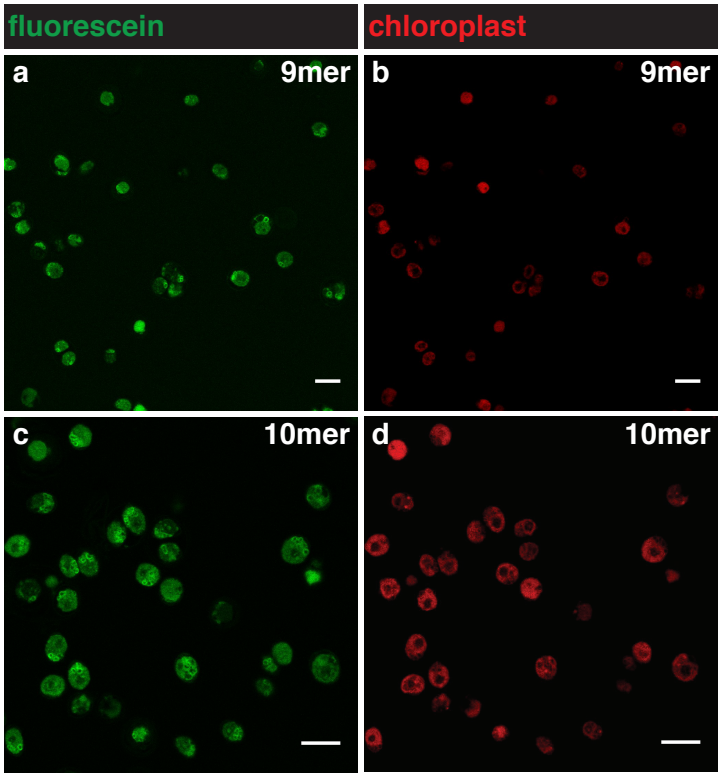

Scheme 7: Single layer confocal microscopy images of algae incubated with **2.01** or **2.04. a)** and **b)** Algae incubated with **2.01**. **c)** and **d)** Algae incubated with **2.04**. Scale bars equal 10 µm.

Encouraged by these results, we proceeded with the syntheses of anchor systems according to Scheme 4. Scheme 8 shows the two anchor systems that contain a fluorescent marker and allow for functionalization on the free amine. Anchor **2.09** includes a lysine unit as a linker that allows for attachment of fluorescein on the *N*-terminus and connection of vancomycin to the free amine on the side chain. Fluorescein is connected through an amide bond to ensure a chemically stable connection, in contrast to compounds **2.01** and **2.04**. Additionally, we also prepared compound **2.10**, which contains an additional spacer group.[13]

[13] In case that the space between oligoproline and fluorophore in compound **2.09** would be insufficient and would lead to a decreased binding ability of the anchor to the algae.

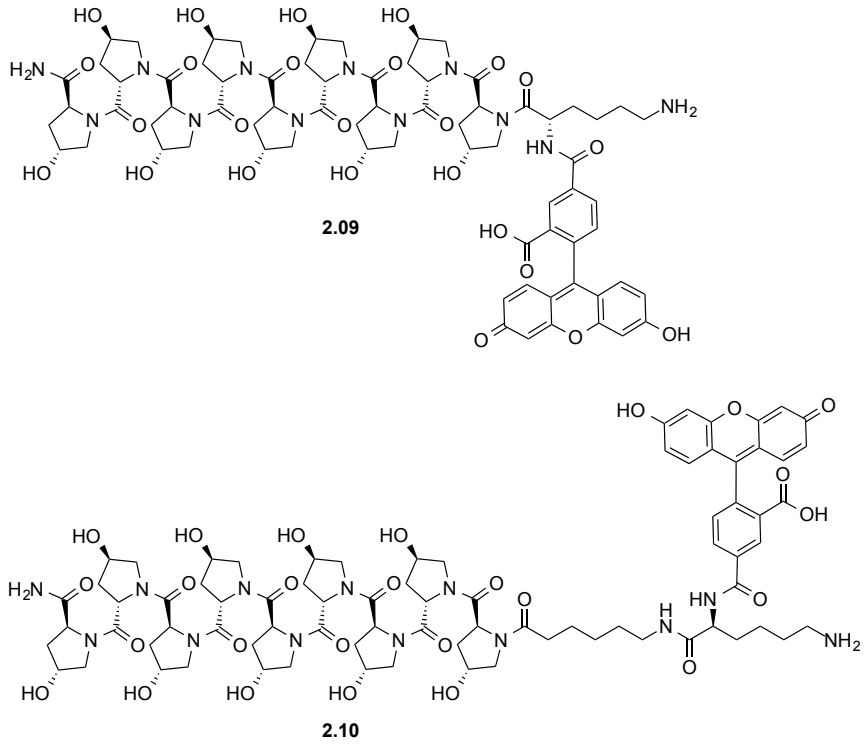

Scheme 8: Anchors **2.09** and **2.10** for functionalization.

The synthesis of the anchors **2.09** and **2.10** required the preparation of the 4-hydroxyproline oligomer fragment and the additional couplings of the linkers and the fluorophore. Instead of performing the linker and fluorophore couplings with 4-hydroxyproline oligomer in solution, we decided to perform the entire synthesis on the solid phase, which has the advantage that only one final HPLC purification is necessary. In a first approach, we used a conventional Rink amide resin with a loading of 0.59 mmol/g and performed a lysine coupling at room temperature followed by deprotection (Scheme 9). As a next step, we tried to couple 5-carboxyfluorescein to the free amine group of the lysine. Unfortunately, the coupling could not be brought to full completion, even after a second, new set of reagents was added. Finally, we succeeded to bring the reaction to full completion only by heating to 110 °C for 30 min in the microwave. Cleavage from the resin under acidic conditions delivered **2.09** in 10% yield after HPLC purification.

The synthesis of anchor **2.10** started with coupling of Fmoc-6-AHX, followed by capping, deprotection and coupling to lysine (Scheme 10). For both couplings, elevated temperatures under microwave irradiation were necessary to achieve full completion. The same was true for coupling of **2.13** with 5-carboxyfluorescein whose reaction progress was monitored by TNBS[14] and Kaiser[15] test of the peptide resin.

[14] Incomplete reaction: red beads. Complete reaction: colorless beads.
[15] Incomplete reaction: blue beads and solution. Complete reaction: colorless beads and solution.

The explanation for the required elevated temperatures presumably has two reasons. First, oligoprolines arrange in helices and are highly rigid, sterically demanding peptides.[96] This property is even enhanced by the *tert*-Butyl groups of the 4-hydroxyproline units. Second, the additional Fmoc-6-AHX linker of **2.13**, provides flexibility to the linker chain that can entangle and make the free amine inaccessible for reaction.

The accelerating effect of microwave irradiation in peptide synthesis is believed to be based on the direct interaction with the amide dipole moments of peptides thereby leading to more efficient heating.[97] Although the reactions were complete and product was isolated, elevated temperatures are not ideal with regard to the thermal lability of fluorescein and its bioconjugates. Therefore, we were aiming for conditions that were milder for the peptide and that delivered the product in higher yield.

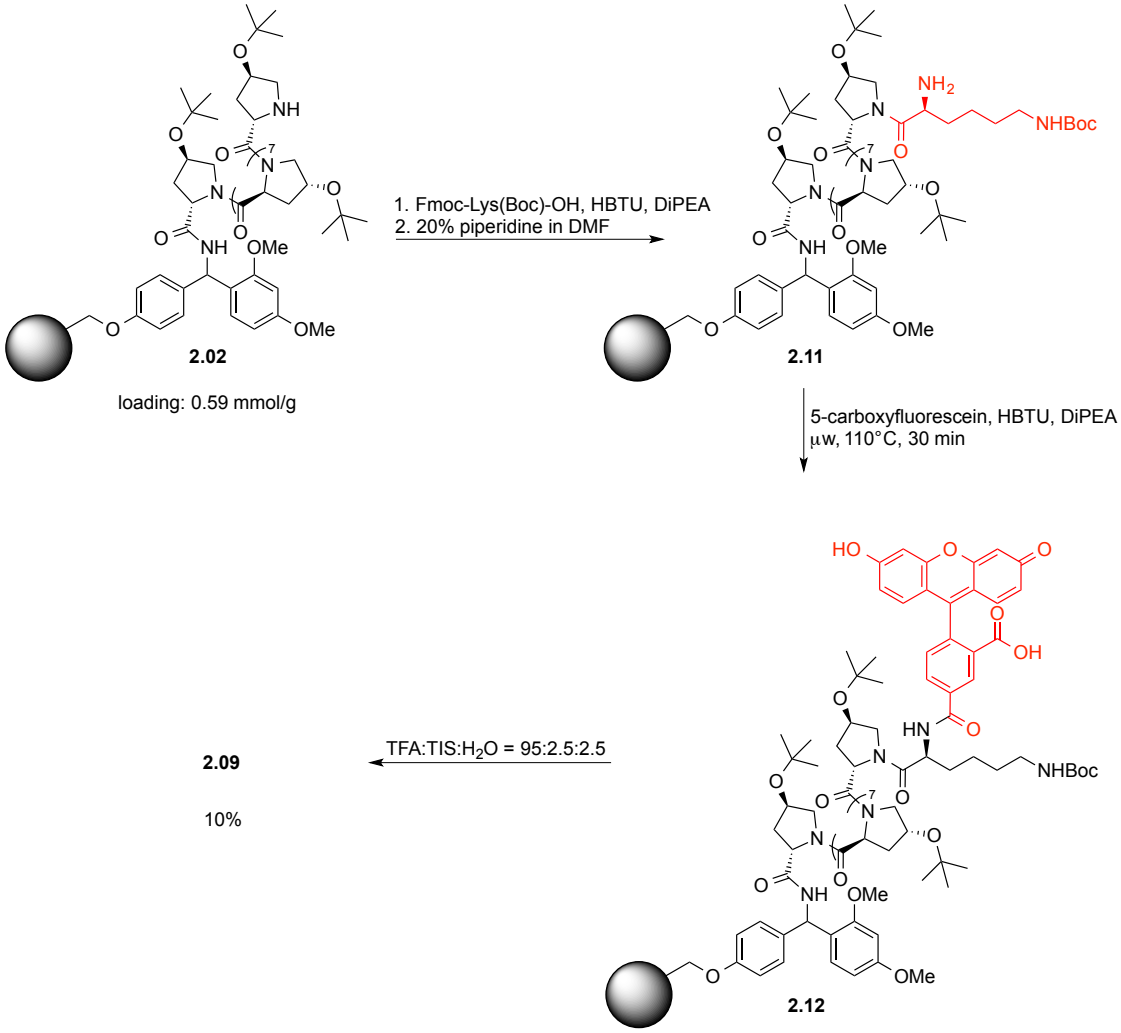

Scheme 9: Synthesis of anchor **2.09**.

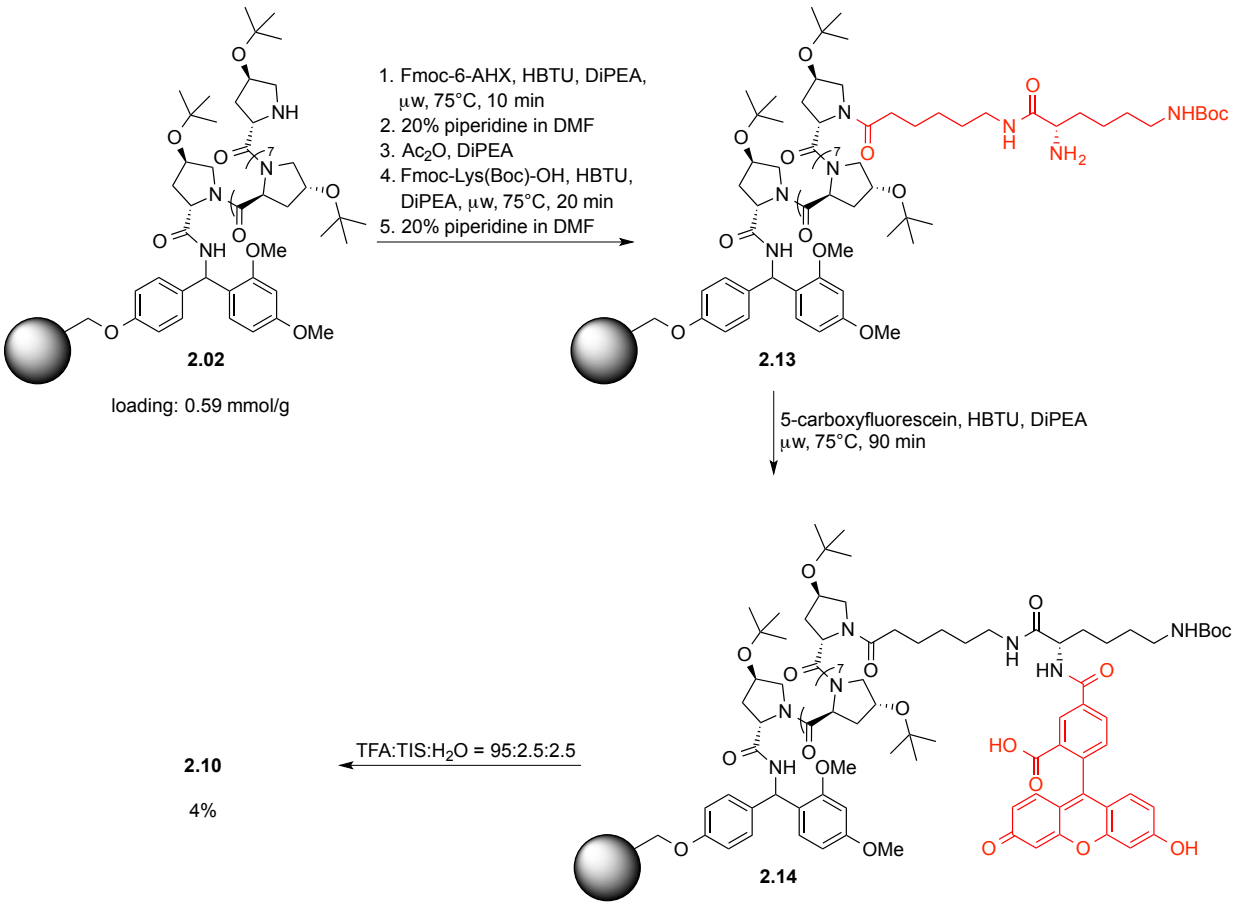

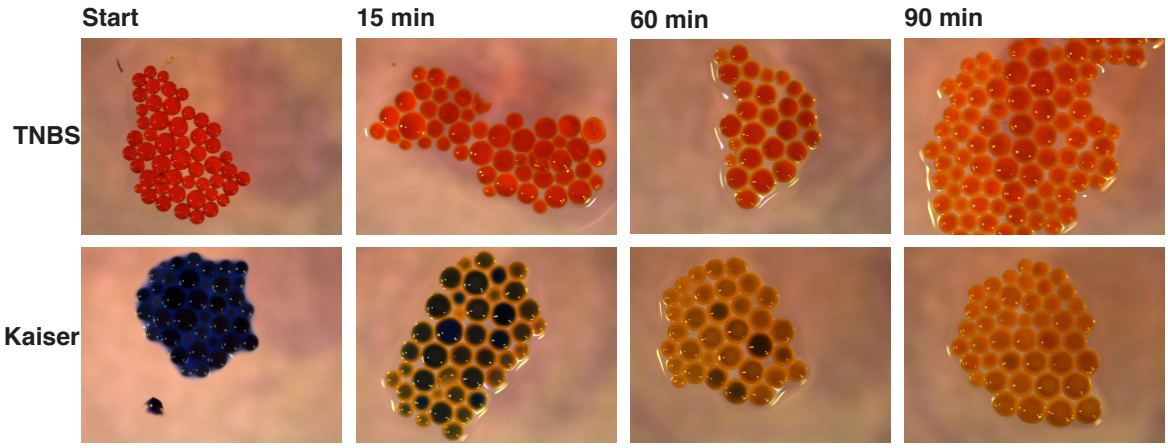

Scheme 10: Synthesis of anchor **2.10** and reaction progress of 5-carboxyfluorescein coupling using TNBS (top) and Kaiser (bottom) test.

For improvement of the synthesis we switched to a resin that provides more space for the peptide on the solid phase. In contrast to the previously used resin with a loading of 0.59 mmol/g the Rink Amide NovaPEG resin provides significantly more space for the peptide because it comprises a PEG chain between the polystyrene bead and the Rink Amide group (Scheme 11). Thereby this resin provides an environment during the synthesis almost like in solution. In addition, the loading of the resin (0.39 mmol/g) is significantly lower than for the previously used resin. Indeed, using this resin and slightly modified coupling conditions for the fluorescein coupling, the product was obtained in higher yield and purity. The couplings were all carried out at room temperature, especially important for the fluorescein coupling to maintain of the fluorescent brightness.

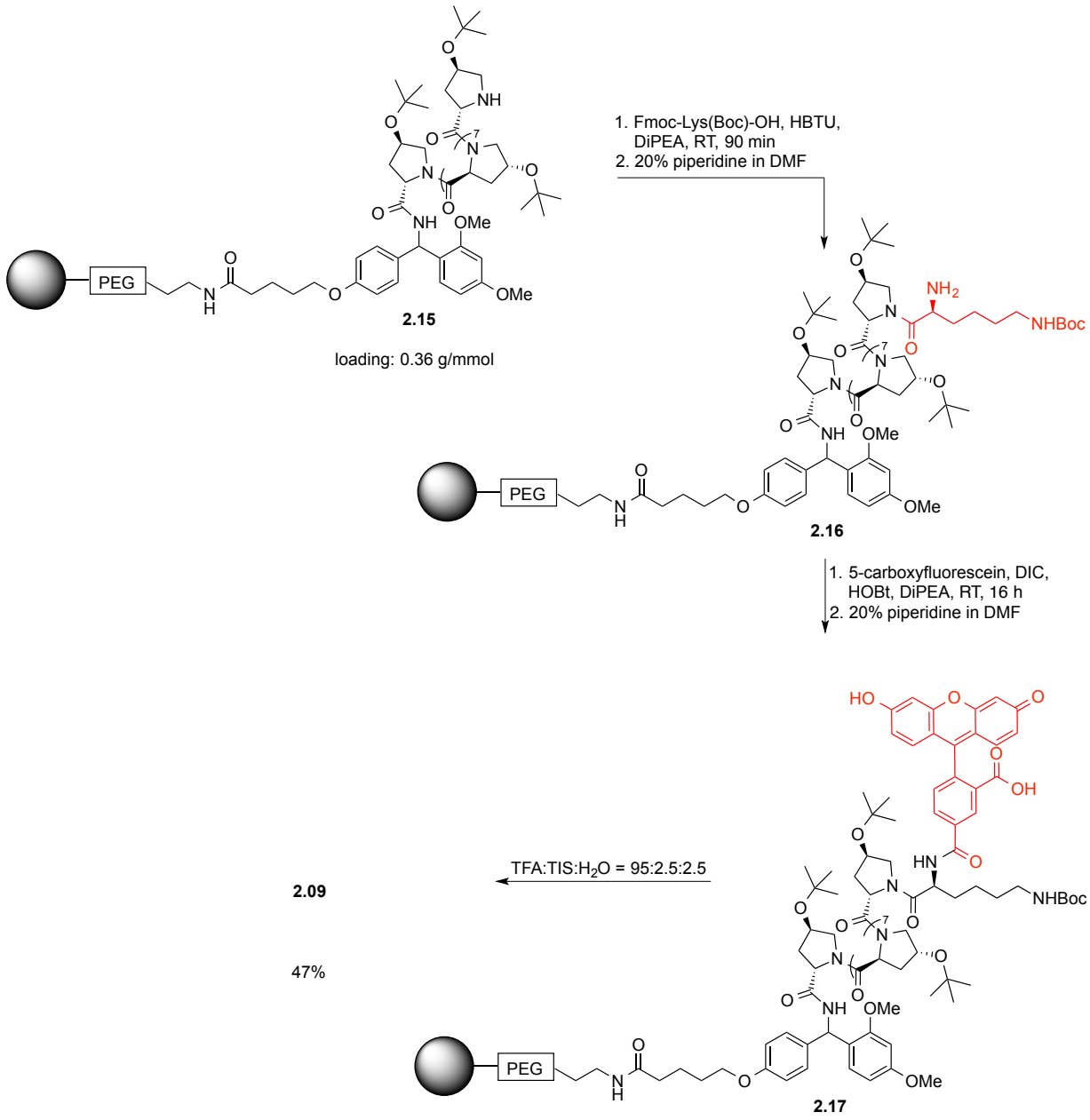

Scheme 11: Improved synthesis of anchor **2.09** using a Rink amide NovaPEG resin.

Next, we measured the fluorescent properties of compound **2.09** (Figure 24) and compared them to the fluorescence of a suspension of *C. reinhardtii* originating from the chlorophyll of the chloroplast (Figure 25). Compound **2.09** shows an excitation maxium at 486 nm and an emission maximum at 523 nm. *C. reinhardtii* shows an excitation maximum of 489 nm and an emission maximum at 689 nm. Importantly, the emissions of both, compound **2.09** and the algae, lie at different wavelengths. There is only minor emission of *C. reinhardtii* from 500-600 nm, so that both algae and **2.09** can be monitored without strong interference in fluorescence. In addition, both can be excited with a 488 nm argon laser, which makes a parallel acquisition possible.

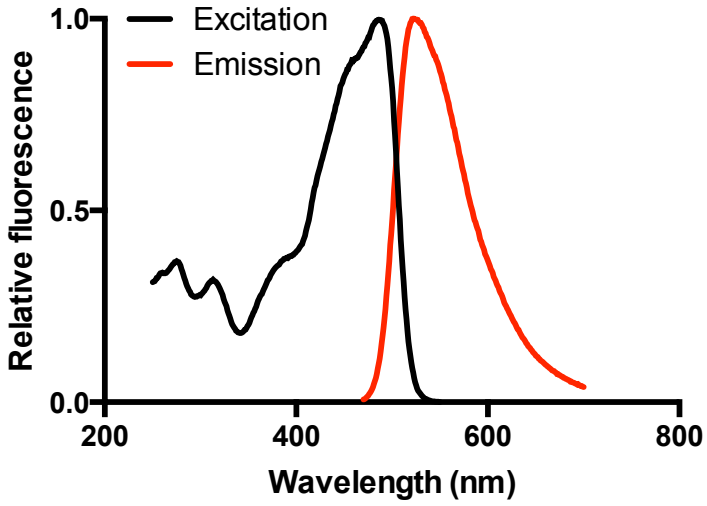

Figure 24: Fluorescence spectrum of **2.09**.

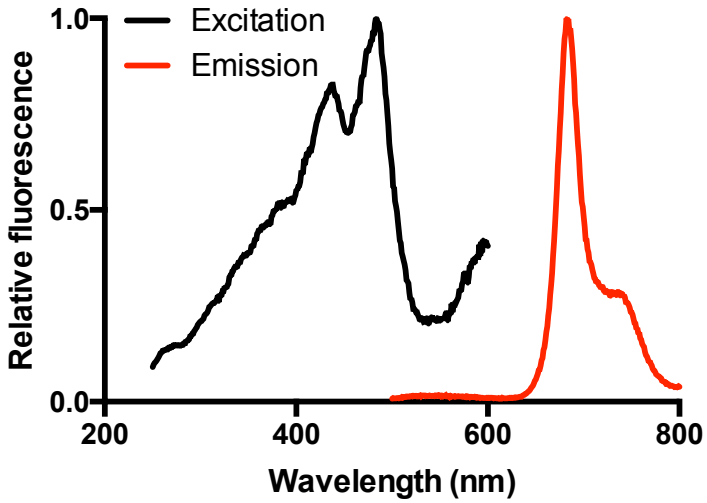

Figure 25: Fluorescence spectrum of *C. reinhardtii*.

With compounds **2.09** and **2.10** in hand, we investigated the immobilization of both conjugates on *C. reinhardtii*. The algae were incubated at a concentration of $4.67 \cdot 10^{-3}$ mmol/mL for 48 h under shaking. The cells were washed and investigated with a confocal microscope (Scheme 12). Both anchors **2.09** and **2.10** were attached to the algae and in both cases, the compounds penetrated inside the cell. However, the amount of substance appeared to be much less, than for anchors **2.01** and **2.04** (see Scheme 7). The apparent fluorescence was rather weak and dead cells appeared to be even stronger labeled than cells that were still alive (indicated by white arrows).[16] We were wondering whether the strong labeling for compounds **2.01** and **2.04** was caused by the fluoresceinthiohydantoin formed by Edman degradation during the incubation procedure. Fluoresceinthiohydantoin is a small molecule and might be able to penetrate inside the algae or react with the cell's components. As an alternative explanation, the presence of a primary amine in compounds **2.09** and **2.10** possibly caused the weak labeling by an increased water solubility of the substances.

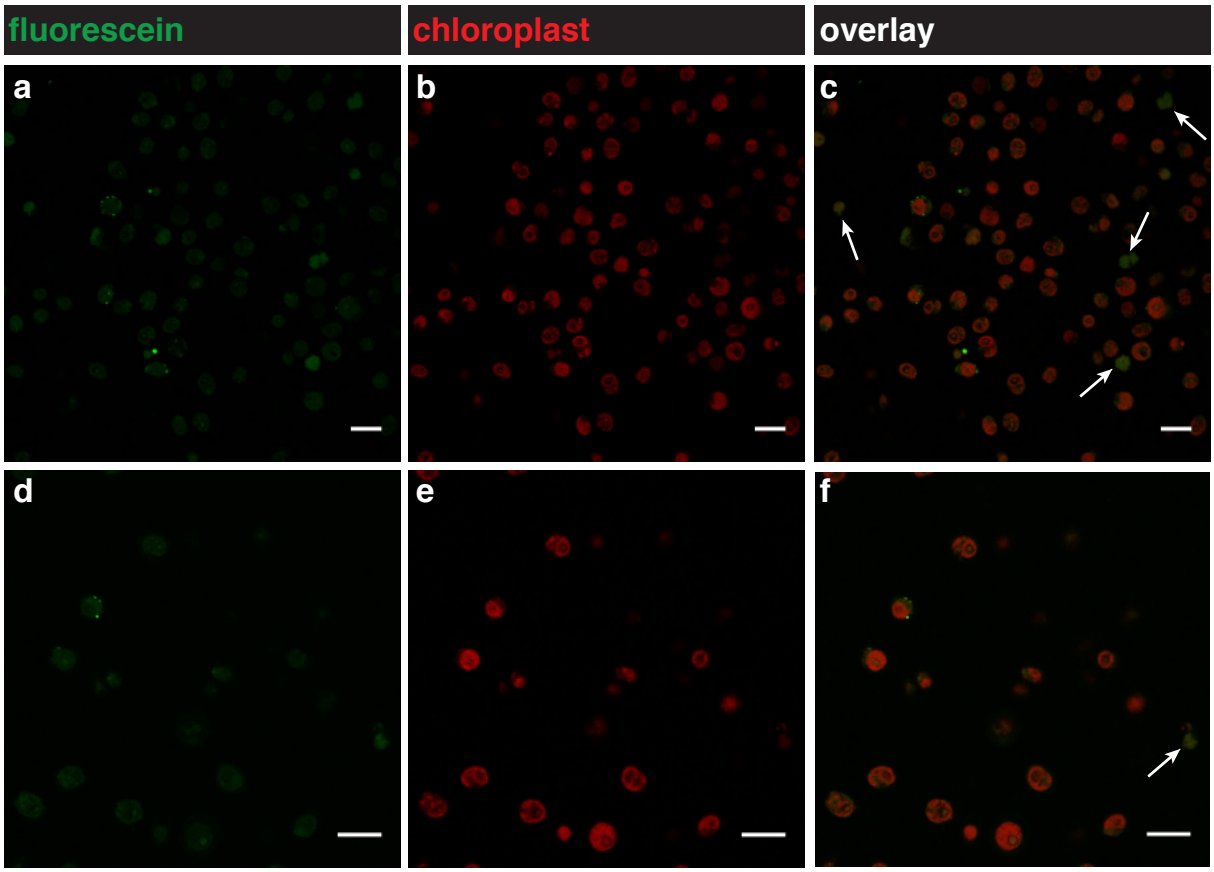

Scheme 12: Incubation of algae with compounds **2.09** and **2.10**. **a)-c)** Algae with compound **2.09**. **d)-f)** Algae with compound **2.10**. Scale bars equal 10 µm.

[16] Dead cells show very weak or no autofluorescence of the chloroplast.

To investigate an increased labeling by the possible decomposition products of **2.01** and **2.04**, we prepared compound **2.18** by coupling of **2.03** with 5-carboxyfluorescein in solution (Scheme 13). Compound **2.18** connects the fluorescein unit by an amide group, but should display very similar polarity to **2.01** and **2.04**. Incubation of the algae with **2.18** under the previous conditions showed similar labeling as anchor **2.09** and **2.10**, and much weaker attachment to the algae than **2.01**. This leads to the assumption that strong labeling of compound **2.01** is based on the formation of its degradation product fluoresceinthiohydantoin. In control experiments we did not see any attachment of the fluorescent reagents 5-carboxyfluorescein or fluorescein isothiocyanate to the algae. However, the structurally similar fluorescein diacetate is a common cell permeation agent used for the staining of live cells.[17] In this respect, it is clearly possible that fluoresceinthiohydantoin also permeates cells.

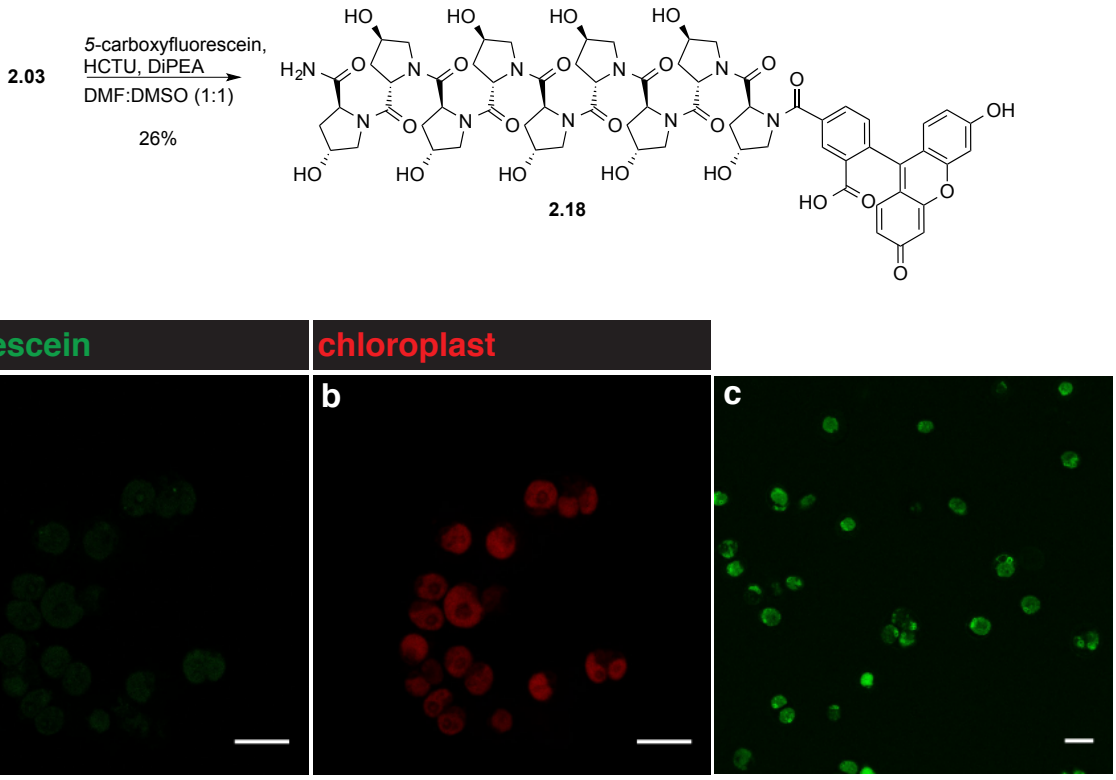

Scheme 13: Synthesis of **2.18** and incubation of algae. **a)** and **b)** Incubation with **2.18**. **c)** Algae incubated with compound **2.01** for comparison. Scale bars equal 10 µm.

[17] Fluorescein diacetate: 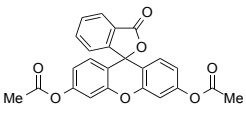

2.7 Synthesis of vancomycin conjugate

Vancomycin was coupled to anchor **2.09** in solution. The conditions tested for the coupling of vancomycin to anchor **2.09** are summarized in Table 1.

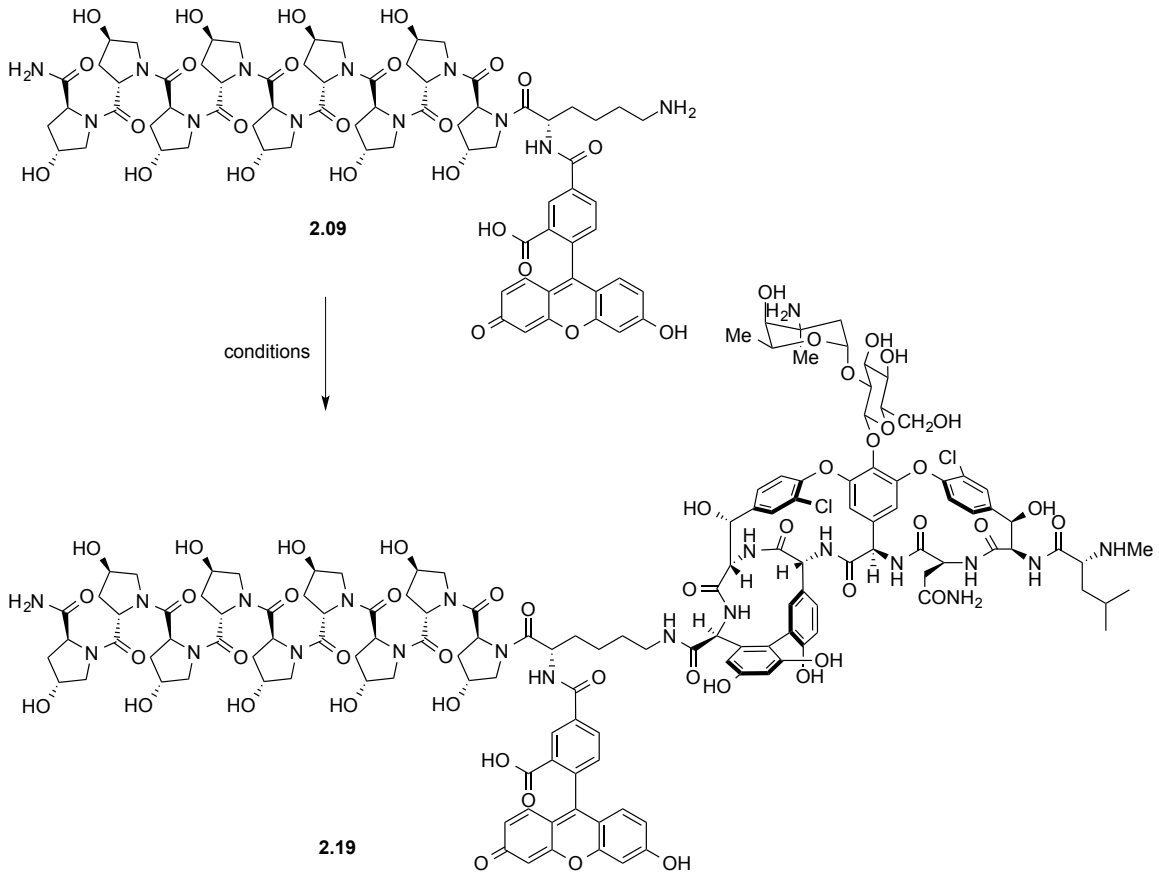

Table 1: Conditions for the coupling of vancomycin to anchor **2.09**.

Entry	Coupling reagent	Vancomycin/coupling reagent	Time	SM : product	Isolated yield
1	HATU	1.5/1.4	19 h	4.7 : 1	n. d.
2	HATU	1.5/1.4	5 d	4.4 : 1	n. d.
3	PyBOP	3/3	5 d	0.67 : 1	n. d.
4	PyBOP	6/6	4 h	0 : 1	n. d.
5	HATU	6/6	16 h	0.63 : 1	n. d.
6	PyBOP	3/3	14 h	2 : 1	n. d.
7	PyBOP	3/6	2.5 h	0 : 1	19%
8	PyBOP	3/3 + 3 equiv. HOBt	2 h	0 : 1	44%
9	PyBOP	1.2/1.2 + 1.2 equiv. HOBt	1.5	1.8 : 1	n. d.

The challenge of the coupling between vancomycin and compound **2.09** resided in incomplete conversions of **2.09**. This was often observed with HATU as the coupling reagent. When the coupling reagent was changed to PyBOP, this could be improved. However, care had to be taken as over-coupling was observed when using large excess of vancomycin resulting in the coupling of two vancomycin molecules to each other (Table 1, entry 4). With short activation time of vancomycin and excess of coupling reagent, the reaction was brought to completion without significant over-coupling (Table 1, entry 7). This could be further improved by use of HOBt as an additive resulting in cleaner reaction mixtures and higher isolated yield (Table 1, entry 8). At least 2 equiv. of vancomycin, coupling reagent and HOBt were required to bring the reaction to completion.

The fluorescence spectrum of compound **2.19** shows an excitation maximum at 497 nm and an emission maximum at 525 nm (Figure 26). This makes compound **2.19** suitable for simultaneous imaging with *C. reinhardtii* (for the fluorescence spectrum of *C. reinhardtii* see Figure 25).

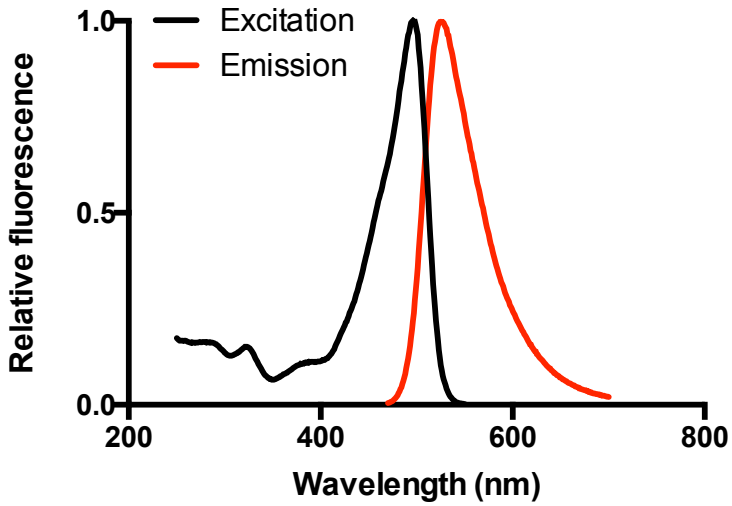

Figure 26: Fluorescence spectrum of **2.19**.

In addition to the fluorescently labeled vancomycin derivative, we also prepared a derivative without fluorophore, which we wanted to utilize later in the bacterial growth experiments. For this, we applied the chemistry used towards the synthesis of compound **2.13** by preparation of linker **2.20** on the resin followed by cleavage from the resin. The anchor **2.20** was dissolved in water, purified by filtration over a SPE column, and lyophilized. The lyophilized product was of sufficient purity to be coupled to vancomycin with the same conditions as for the synthesis of compound **2.19 (**Scheme 14**)**.

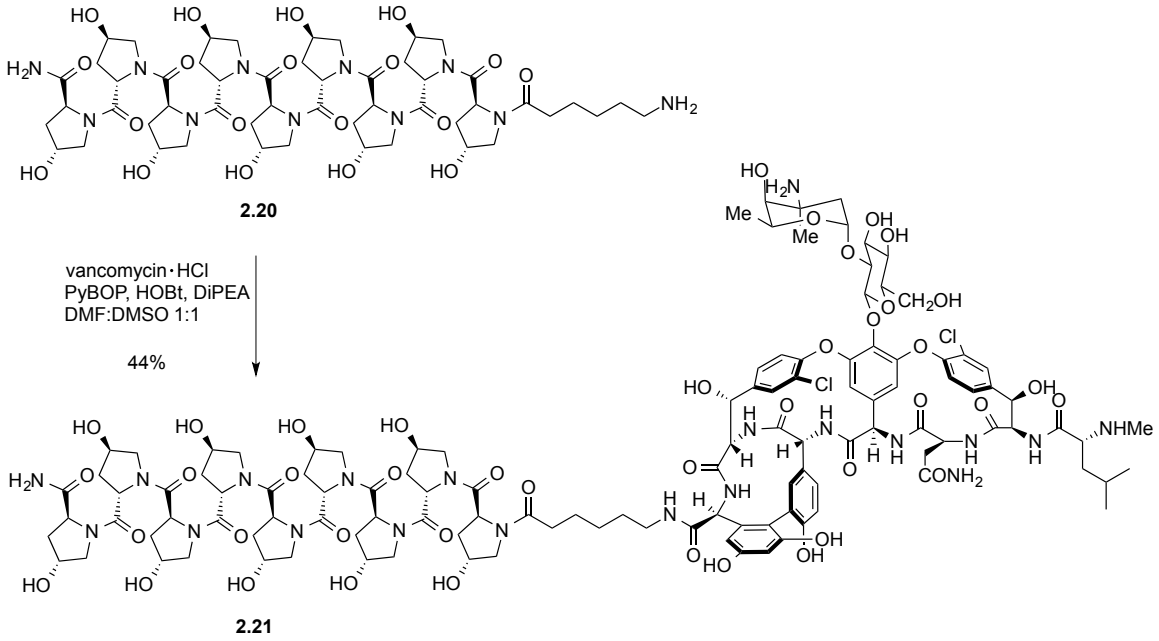

Scheme 14: Synthesis of vancomycin conjugate **2.21**.

2.8 Immobilization of vancomycin conjugate on algae

The immobilization of conjugate **2.19** was realized by incubation of the algae in a solution of **2.19** with mild shaking followed by a simple washing protocol. Time and concentration of the incubation solution determined the extent of loading on the algae. With high concentrations of **2.19** ($4.5 \cdot 10^{-3}$ mmol/mL) very strong labeling was observed within 3 h (Scheme 15, **a**-**e**). However, these conditions strongly affected the behavior of the algae in that the algal motility completely stopped even after seconds of exposure. On the other hand, the autofluorescence was still maintained, which indicates that the cells were still living. Dead cell material showed almost no autofluorescence of the chloroplast, but strong adhesion of compound **2.19** (indicated by arrow). By lowering the incubation concentration ($1 \cdot 10^{-3}$ mmol/mL), the motility of the algae could be maintained compared to the control algae that was incubated under the same conditions but with algae medium instead of a solution of **2.19** (Scheme 15, **f-j**). At this concentration, the algae were clearly covered with compound **2.19** after 12 h of incubation time, as visible in the confocal z-stack image (Scheme 15, **i**) and in the merged image with the autofluorescence of the chloroplast (Scheme 15, **h**). A single confocal layer reveals that the substance has been mainly deposited on the cell wall. However, also a considerable amount of substance penetrated the cell, with a concentration enhancement especially at the side of the flagellar collar.

The motility of the algae could be increased drastically by lowering the concentration of the incubation solution from $4.5 \cdot 10^{-3}$ mmol/mL to $1 \cdot 10^{-3}$ mmol/mL. However, the mobility was still decreased compared to fresh algae from the culture bottles. We, therefore, postulated that not only the concentration of the substance, but also the algae density in comparison to the incubation solution had an influence on the motility. Indeed, by lowering the algae amount in relation to incubation solution, the algae completely maintained their motility as in a fresh culture (Scheme 15, **k-o**). Conjugate **2.19** showed strong adhesion to the flagella, making the presence of the flagella easily observed (for enlarged images see Scheme 15, **p**-**t**). The concentration of the conjugate could be lowered even further ($c = 1.5 \cdot 10^{-4}$ mmol/mL) with an incubation time of 24 h, but the substance loading was not sufficiently high for the antibacterial assay application performed later (Figure 27).

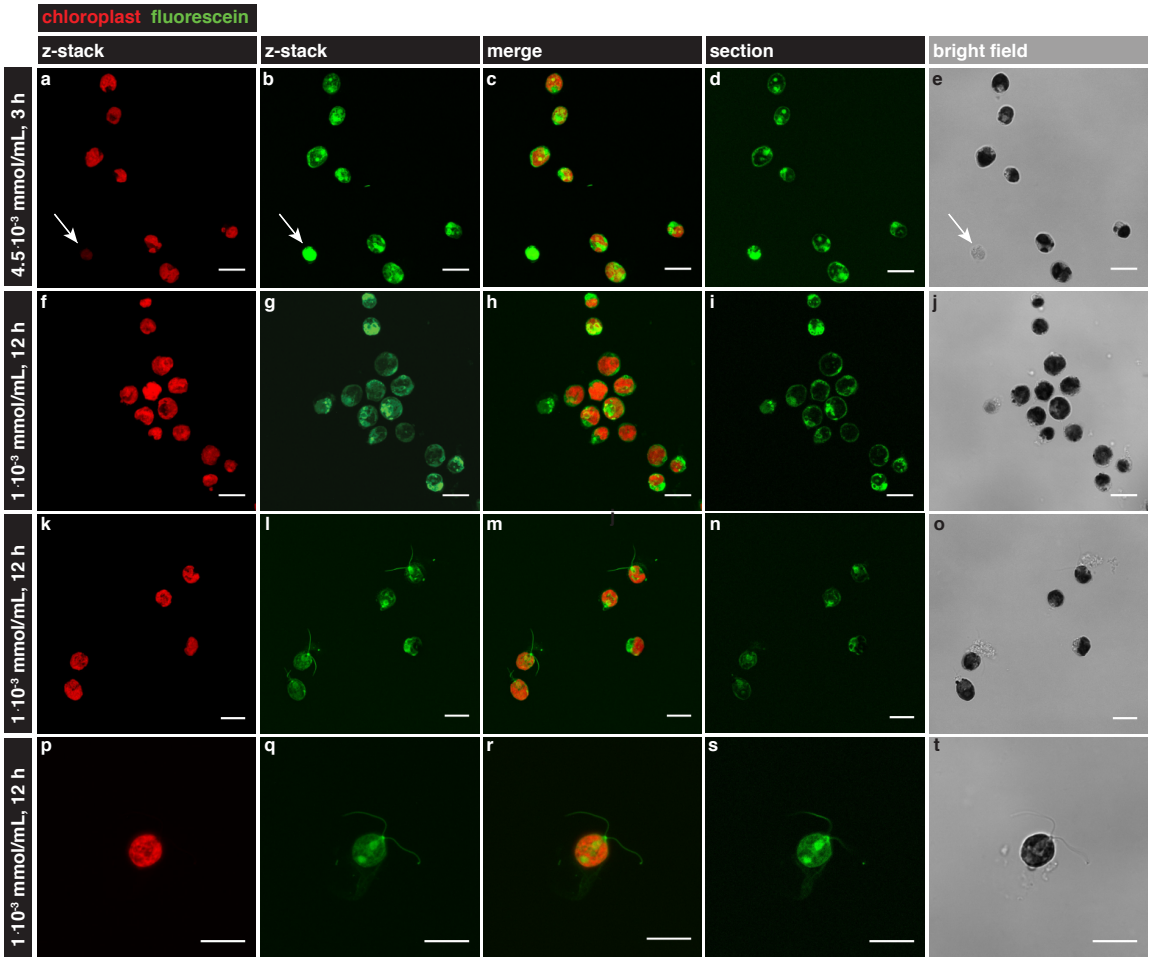

Scheme 15: Fluorescence microscopy images of *C. reinhardtii* treated with **2.19**.
a)-e) *C. reinhardtii*, treated with **2.19** at $4.5 \cdot 10^{-3}$ mmol/mL for 3 h. **f)-j)** *C. reinhardtii*, treated with **2.19** at $1 \cdot 10^{-3}$ mmol/mL for 12 h. **k)-o)** *C. reinhardtii* incubated with **2.19** at lower algae concentration in comparison to solution (c = $1 \cdot 10^{-3}$ mmol/mL). **p)-t)** Enlarged image of *C. reinhardtii* incubated with **2.19** at lower algae concentration in comparison to solution (c = $1 \cdot 10^{-3}$ mmol/mL). Scale bars equal 10 µm.

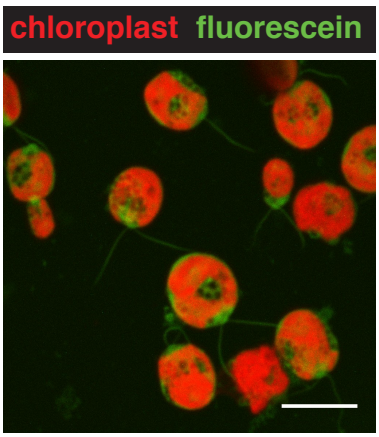

Figure 27: Incubation at $1.5 \cdot 10^{-4}$ mmol/mL for 24 h. Scale bar equals 10 µm.

2.9 Investigations on the binding affinity of vancomycin to *C. reinhardtii*

Overall the binding affinity of conjugate **2.19** was clearly higher than for anchor **2.09**. Our first presumption was that vancomycin itself also binds to the surface of the algae thereby increasing the overall binding affinity of conjugate **2.19**. To investigate the binding of vancomycin to *C. reinhardtii* we performed two different experiments. In the first experiment we labeled vancomycin with a fluorescent tag, to trace the behavior of the conjugate on the algae. In the second experiment we performed immunofluorescence for the detection of vancomycin.

2.9.1 Fluorescently-labeled vancomycin

The attempt to directly attach a fluorophore to vancomycin by reaction with 6-aminofluorescein failed because a very complex mixture was obtained. Therefore, we decided to use the fluorescent linker **2.22** instead. The linker was attached under similar conditions as used before for the synthesis of the oligoproline vancomycin conjugate **2.19** (Scheme 16).

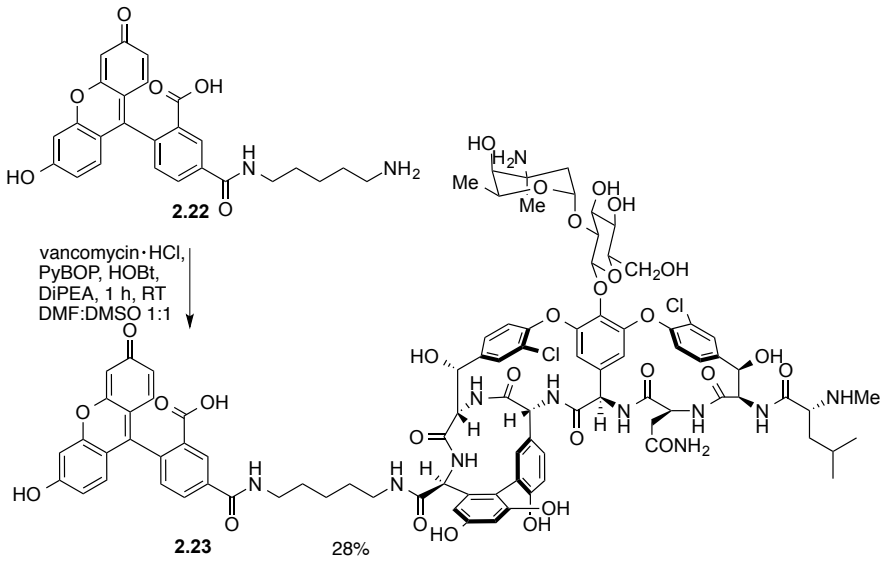

Scheme 16: Synthesis of fluorescently labeled vancomycin.

Unfortunately, **2.23** displayed drastically reduced water solubility in comparison to vancomycin. The substance was well soluble in DMSO but could not be dissolved in the algae culture medium even when 20% DMSO was added. The concentration of the substance was chosen as in the incubation conditions, but even by lowering the concentration, the substance did not dissolve. Similar results were obtained with a commercially available BODIPY-vancomycin conjugate (Thermo Fischer Scientific, Molecular Probes). Overall, the poor water solubility of the substances prevented this approach to be a suitable study for the adhesion of vancomycin to *C. reinhardtii*.

2.9.2 Immunolabeling of vancomycin

A second possibility to trace vancomycin with fluorescence is by immunolabeling. In this approach, an antibody is used that specifically binds to vancomycin. There are two general techniques: direct and indirect immunofluorescence. In direct immunofluorescence the specific primary antibody (1° antibody) is covalently linked to a fluorochrome and allows for direct visualization of the substance. In indirect immunofluorescence a two-step incubation is performed. First, a 1° antibody is used that specifically binds to the target structure. Secondly, a fluorochrome-coupled secondary antibody (2° antibody) is applied that specifically binds to the 1° antibody. The specificity results from direct binding of the 2° antibody to the species in which the 1° antibody was raised. Indirect immunofluorescence offers two main advantages over direct immunofluorescence: 1) More flexibility is obtained regarding the choice of fluorophore because the primary antibody is not necessarily produced with a range of different fluorochromes. The secondary antibody is usually available with several fluorophores and like this the right fluorochrome can be chosen for the individual experiment. 2) A signal amplification is obtained because multiple 2° antibodies can bind to one primary antibody. This leads to an increase in fluorescence, requiring less primary antibody and overall increases the sensitivity of the method. The drawback of indirect immunofluorescence lies in the extended working procedure requiring a second antibody incubation and more wash cycles. However, because of the flexible combinations of the 1° with 2° antibodies it is often preferred over direct immunolabeling. Indirect immunofluorescence was therefore chosen for the detection of vancomycin on *C. reinhardtii*, schematically illustrated in Scheme 17.

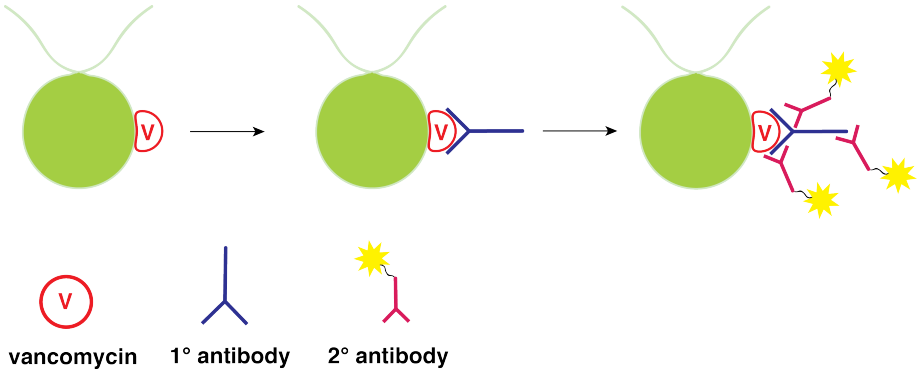

Scheme 17: Indirect immunolabeling of vancomycin with a 1° and 2° antibody on *C. reinhardtii*.

The algae were incubated overnight with vancomycin at a concentration of $1 \cdot 10^{-3}$ mmol/mL. The cells were washed, immobilized and fixed/permeabilized on cover slips for microscopy.[98] The algae cells were blocked with goat serum to minimize unspecific binding of the 1° antibody with the cell.

The immunolabeling was carried out with a 1° antibody binding specifically to vancomycin, which was raised in mouse (IgM). For the 2° antibody we used a goat anti-mouse IgM heavy chain antibody Alexa Fluor® 350 conjugate. Table 2 summarizes the working conditions used as well as those that are recommended by the supplier or the standard conditions. Incubation experiments involving vancomycin were carried out in duplicates. However, staining of the duplicates was performed in one batch.

Table 2: Comparison of applied conditions with standard/recommended conditions.

Antibody	Conditions used	Standard/recommended conditions
1° antibody	1:250 dilution	1:250:1:500 dilution
	3 h 37 °C	1-4 h 37 °C
2° antibody	5 µg/mL	1-10 µg/mL
	2 h 37 °C	1-2 h 37 °C

The experiments performed are summarized in Table 3. To allow for reasonable interpretation, a number of control experiments were necessary. The first control experiment (**a**) was the determination of the cellular autofluorescence, by refrain from using any antibody treatment in this sample. The second control experiment (**b**) is the use of only the 2° antibody for visualization of unspecific binding of the 2° antibody to cellular structures. The binding specificity of the 1° antibody can be controlled by using algae that have not been incubated with vancomycin (**c**). Unspecific binding of the 1° antibody would result in a signal in this control. As a positive control we chose to incubate the algae with conjugate **2.19**, whose presence on the algae can be identified by observation of green fluorescence (**d**). In addition to this, the algae were incubated with **2.21**, to visualize a potential attachment of this conjugate to the algae (**e**). Finally, the algae were incubated with vancomycin (**f**).

Table 3: Control experiments and samples prepared for immunofluorescence.

Experiment	Sample preparation	Purpose
a *Autofluorescence* Incubated with vancomycin 12 h, $1 \cdot 10^{-3}$ mmol/mL	· Fixation/Permeabilization · Blocking	Control for visualization of cellular autofluorescence
b *2° Antibody* Incubated with vancomycin 12 h, $1 \cdot 10^{-3}$ mmol/mL	· Fixation/Permeabilization · Blocking · 2° Antibody	Control for unspecific binding of 2° antibody
c *Untreated algae*	· Fixation/Permeabilization · Blocking · 1° Antibody · 2° Antibody	Control for binding specificity of 1° antibody
d *2.19* Incubated with **2.19** 12 h, $1 \cdot 10^{-3}$ mmol/mL	· Fixation/Permeabilization · Blocking · 1° Antibody · 2° Antibody	Sample to visualize attachment of **2.19** to *C. reinhardtii*
e *2.21* Incubated with **2.21** 12 h, $1 \cdot 10^{-3}$ mmol/mL	· Fixation/Permeabilization · Blocking · 1° Antibody · 2° Antibody	Sample to visualize attachment of **2.21** to *C. reinhardtii*
f *Vancomycin* Incubated with vancomycin 12 h, $1 \cdot 10^{-3}$ mmol/mL	· Fixation/Permeabilization · Blocking · 1° Antibody · 2° Antibody	Sample to visualize attachment of vancomycin to *C. reinhardtii*

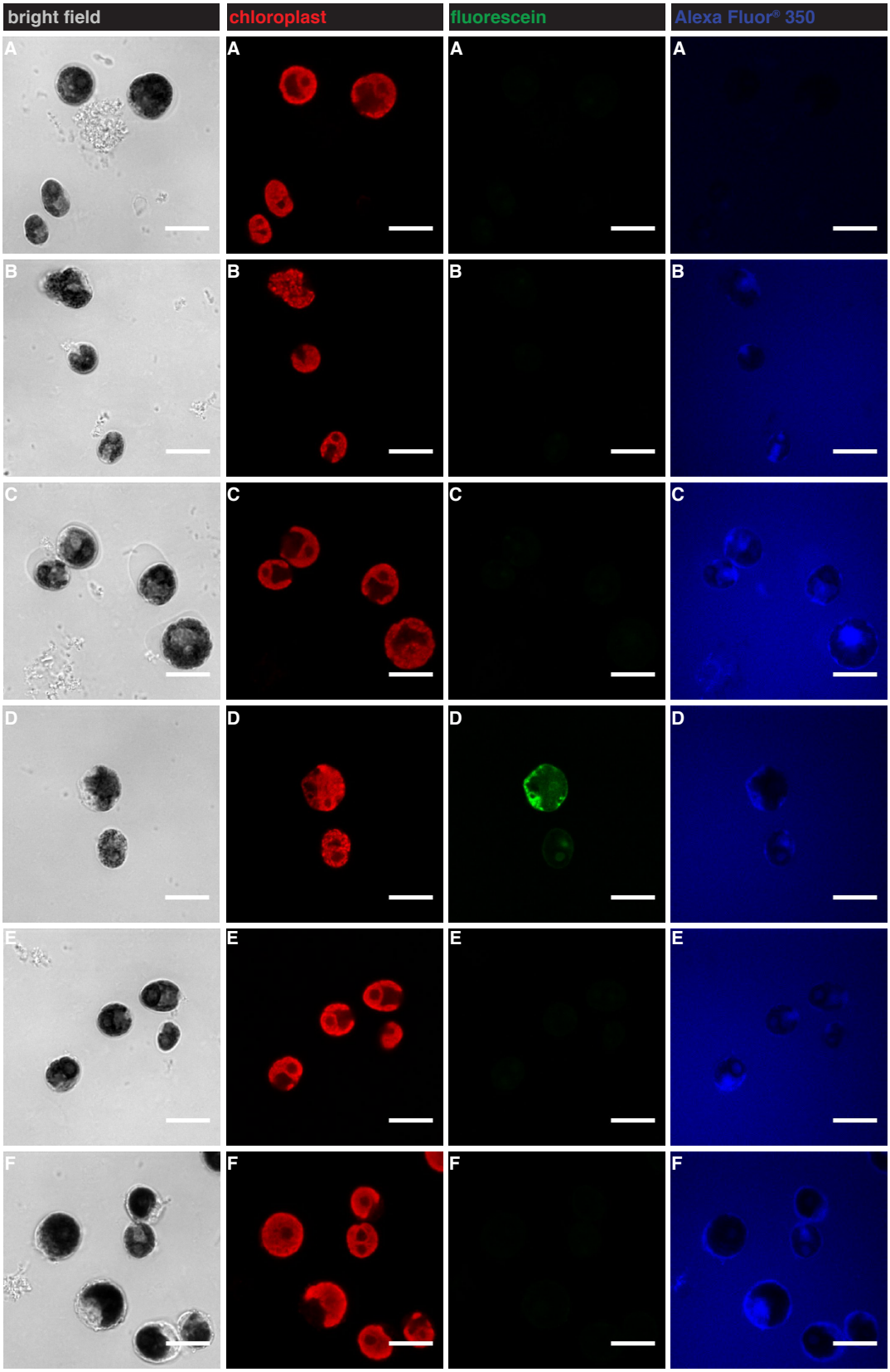

Scheme 18: Immunolabeling of *C. reinhardtii*. **a)** Algae incubated with vancomycin but not stained with antibodies. **b)** Algae incubated with vancomycin but only stained with 2° antibody. **c)** Algae that have not been modified but stained with 1° and 2° antibody. **d)** Algae incubated with **2.19** and stained with 1° and 2° antibody. **e)** Algae incubated with **2.21** and stained with 1° and 2° antibody. **f)** Algae incubated with vancomycin and stained with 1° and 2° antibody. Scale bars equal 10 µm.

The results obtained from the immunolabeling of *C. reinhardtii* are shown in Scheme 18. The images represent single layers of the algae, taken with a confocal laser scanning microscope. The images were recorded in a sequential mode with the bright field, chloroplast and fluorescein being taken in one sequence using the 488 nm laser. The Alexa Fluor® 350 antibody was excited with a 355 nm UV laser and detected in the second sequence. The intensity for the UV laser had to be set to high intensity (65%, 76 mV) to observe any signal for the blue fluorescent dye. All images shown were acquired using the same settings on the microscope and the same parameters during the image processing. This allows for direct comparison between the different experiments.

In the autofluorescence control (**a**) neither green nor blue fluorescence were observed as expected because the sample has been incubated with non-fluorescent vancomycin and no antibody treatment was performed. Image series **b** represents the sample that has been incubated with vancomycin followed by staining only with the 2° antibody. The sample shows no fluorescence in the green channel, but shows some signal in the blue channel. The signal observed is a faint blue background with some labeling of the algae. The signal observed is mainly localized in the area of the flagellar collar of the algae. This sample has not been treated with the anti-vancomycin 1° antibody, therefore the signal observed is the unspecific binding of the 2° antibody. Usually the acquisition parameters are adjusted so that there is no signal visible in this control. In this case we decided to maintain the parameters to visualize possible differences in the signal distribution.

The algae that have not been incubated with any compound overnight, but have been subjected to the immunofluorescence protocol (**c**), showed the same distribution of signal in the blue channel as in experiment **b**. This indicates that the signal observed is indeed resulting from unspecific binding of the 2° antibody with the sample. In addition to this, the 2° antibody may bind to the coating of the cover slip (background signal). The next sample (**d**) were algae, which have been incubated with the fluorescently tagged vancomycin conjugate **2.19**. We expected that sample **d**, algae that have been incubated with the fluorescently tagged vancomycin conjugate **2.19**, would act as positive control as we can trace the presence of the compound on the algae in the green channel. Against our expectations, the compound showed no significant signal enhancement compared to the control samples. This might be due to the fact that the antibody lost its affinity towards vancomycin when the oligoproline anchor was covalently attached to the antibiotic. Another possibility might be the internalization of the compound to the surface of the organism. A similar result was observed for sample **e**, where the algae have been incubated with vancomycin conjugate **2.21**. We also expected an increased signal, although we had not proved

the adherence of the sample to the surface in advance. The algae that have been incubated with vancomycin and subjected to the complete immunolabeling protocol are shown in series **f**. Compared to **b**, **d** and **e**, a slight enhancement of the signal at the surface of the algae is noticeable. Compared to control experiment **c** the difference is less pronounced. Therefore, it is difficult to formulate a clear statement regarding the binding of vancomycin to the surface of the algae. The method seems to be not very sensitive, resulting in harsh parameters[18] necessary for the imaging of the samples. In addition, the absence of a reliable positive control complicates the interpretation of the results. Immunolabeling often involves extensive optimization to find the optimal conditions for the specimen with the applied antibodies. For future experiments we could also investigate the effect of different incubation concentrations and times. An alternative would be the use of a 1° vancomycin antibody covalently attached to a microbead which has been shown to effectively trace the presence of vancomycin on magnetic nanoparticles.[99] This would allow a better quantification of traced vancomycin molecules; on the other hand difficulties could arise by non-specific interactions of the nanoparticle-antibody with the surface of the algae.

2.10 Antimicrobial activity of vancomycin conjugates

To confirm, that the synthesized vancomycin conjugates still possess antimicrobial activity, we tested their inhibitory activity against the Gram-positive bacteria *Bacillus subtilis*. First, we performed disk diffusion tests (Kirby Bauer) on agar plates previously inoculated with *B. subtilis* (Figure 28). The compounds were applied on paper disks and the agar plates were incubated overnight at 37 °C. As can be seen from the inhibition zones, the antibacterial potency of the conjugates clearly decreased in comparison to vancomycin itself. This result is also reflected in the MIC (Minimal Inhibitory Concentration) of the compounds. The MIC values of the vancomycin conjugates **2.19** (MIC = 8-4 μg mL^{-1}) and **2.21** (MIC = 4 μg mL^{-1}) was reduced in comparison to vancomycin (MIC = 0.125-0.06 μg mL^{-1}), but still displayed acceptable activity.[19] This decrease in activity is likely due to the decreased binding potential to the *N*-acyl-D-Ala-D-Ala fragment of the target bacterial cell wall because of the 4-hydroxyproline oligomer anchors. We found that the 4-hydroxyproline oligomer anchor alone displayed no antibacterial activity (see experimental part).

[18] High laser intensity.
[19] MIC values were determined by Myriam Gwerder.

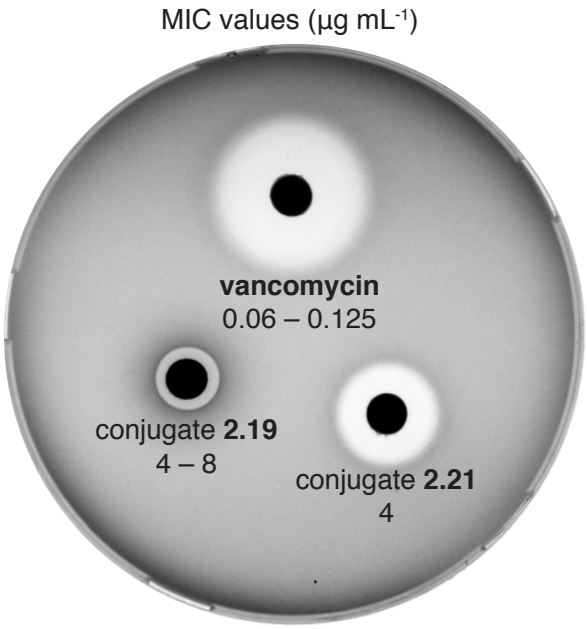

Figure 28: Antimicrobial activity of conjugates **2.19** and **2.21** against *B. subtilis.*

2.11 Antimicrobial activity of modified *C. reinhardtii* against *B. subtilis*

To evaluate the concept of chemical surface engineering as a possibility to introduce new phenotypes to an organism, we had to show that the modified algae are able to kill bacteria. In the following section, our investigations on the antimicrobial activity of *C. reinhardtii* modified with vancomycin conjugates are presented.

The antibacterial tests were performed in liquid culture to ensure homogeneous distribution and free diffusion of the modified algae and bacteria and to allow for easy contact. Bacterial growth was quantified by measuring the optical density at 600 nm (OD_{600}).[100] The determination of the optical density is a sensitive and established quantification method for bacterial growth. We grew the cultures in a 1:1 mixture of *B. subtilis* medium and algae medium in conical tubes that were shaken in an incubator at 37 °C and 200 r/min. Samples from the cultures were taken every hour and optical density was determined. For each experiment we established a reference growth curve by measuring the bacterial growth in the presence of unmodified algae. Experiments were performed at least in triplicates.

We started our experiments by incubating the algae for 3 h and 12 h at a concentration of $4.5 \cdot 10^{-3}$ mmol/mL in solutions of the respective compounds. For the compounds we chose parent vancomycin and both vancomycin conjugates **2.19** and **2.21**. The algae were washed with Kuhl medium (5x), diluted in fresh medium and inoculated with *B. subtilis*. The resulting growth curves are depicted in Scheme 19.

Figure **a** shows that for algae previously incubated with vancomycin (3h and 12h), the bacterial growth is not inhibited compared to the control of unmodified algae. For compound **2.21** a slight inhibition of bacterial growth is obtained (**b**). Surprisingly, for compound **2.19**, the bacterial growth is completely inhibited only after 3 h incubation time (**c**). After 1 h of incubation time, the growth was initially inhibited, but evolved later. This result showed, that *C. reinhardtii* could indeed be turned into an antimicrobial killer cell and that compound **2.19** was much more effective for this purpose than conjugate **2.21**. As already pointed out in section 2.8, at high incubation concentration the algae have the tendency to loose their flagella. During the preparation of the algae samples we observed, that for both compounds **2.19** and **2.21** the algae showed no motility at all. In contrast to this, algae incubated with vancomycin showed comparable motility to the untreated algae. A possible reason for this might be that vancomycin is not able to cross the algal cell wall. With the attached 4-hydroxyproline oligomer vancomycin is transported inside the cell. Another explanation is that the flagella apparatus reacts sensitive upon coating of the surface and sheds the flagella. This appears not be the case for vancomycin.

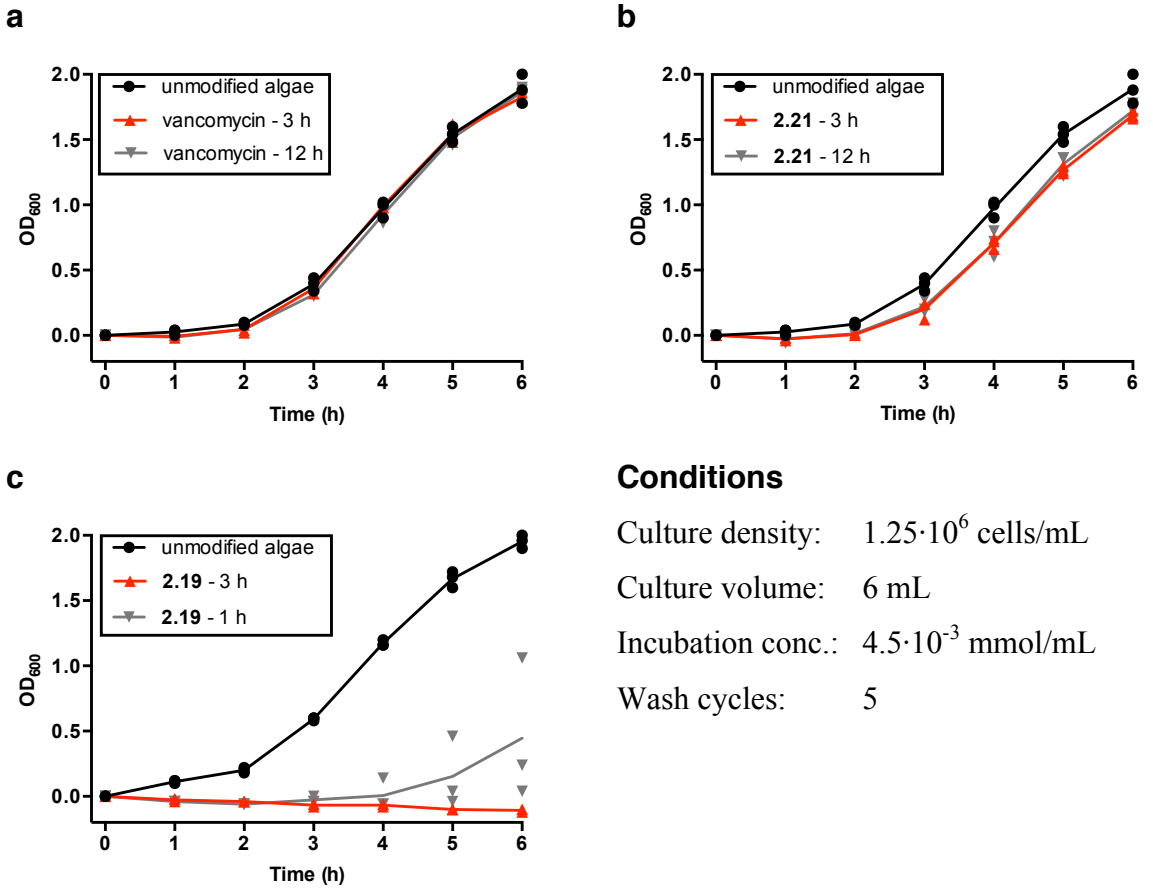

Scheme 19: Growth curves for *B. subtilis* in the presence of algae modified with vancomycin, **2.21** and **2.19**. Data points show individual replicates.

Next, we investigated different incubation concentrations of compound **2.19**. As can be seen from Scheme 20, the bacterial growth increased with decreasing incubation concentration. This is in alignment with the conception that the higher the incubation concentration, the more substance is deposited on the algae. The motility of the algae was completely suppressed for incubation concentrations of $3 \cdot 10^{-3}$ mmol/mL and $2 \cdot 10^{-3}$ mmol/mL. At $1 \cdot 10^{-3}$ mmol/mL the algae behaved like the untreated algae. Therefore we decided to continue our investigations at a concentration of $1 \cdot 10^{-3}$ mmol/mL.

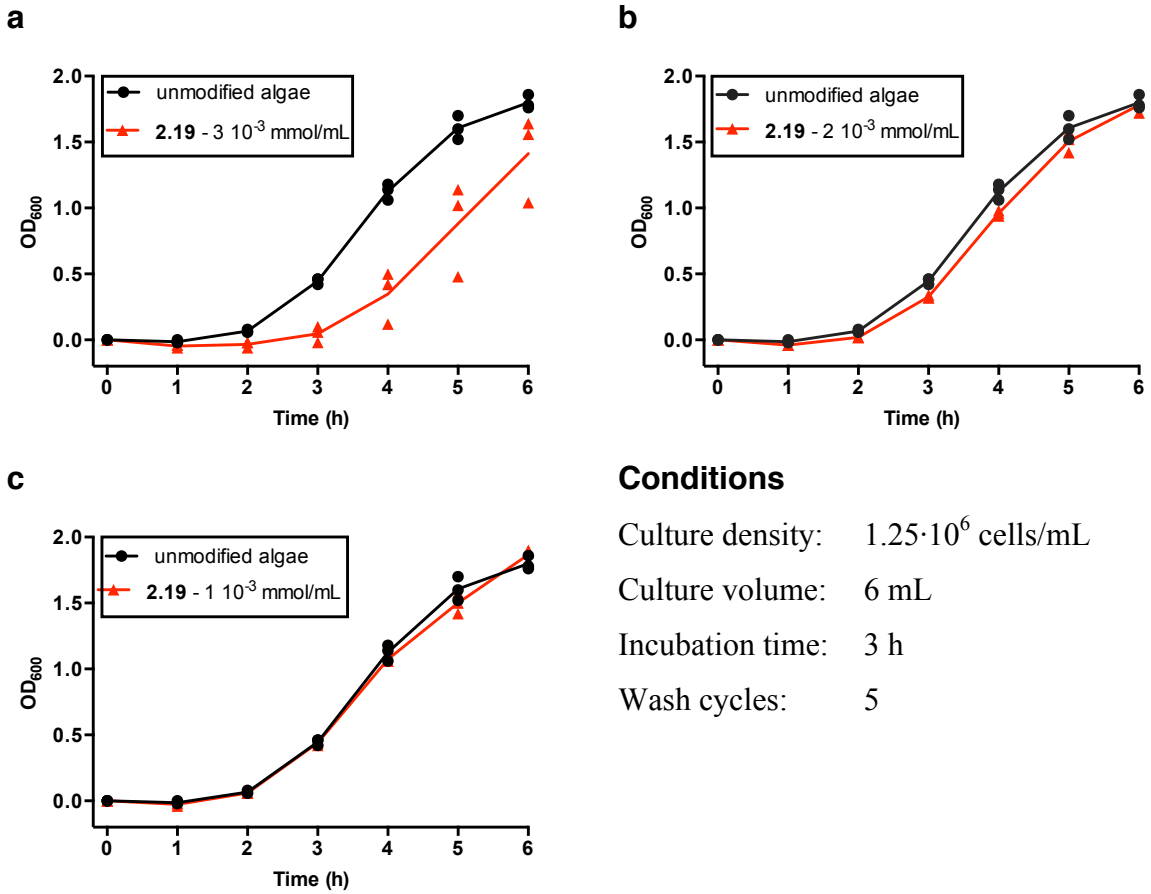

Scheme 20: Growth curves for *B. subtilis* in the presence of algae incubated at different concentrations. Data points show individual replicates.

The adhesion of the compounds to the surface of the algae might be a reversible process that can also be influenced by the extent of washing after the incubation. Therefore, we next investigated the effect of washing on the bacterial growth by reducing the number of wash cycles, at the same time increasing the amount of algae.[20] Changing the washing protocol to 1x (Scheme 21, a) instead of 5x (Scheme 20, a) resulted in complete inhibition of the bacterial growth. The same conditions but two wash cycles did not significantly inhibit the growth anymore, (Scheme 21, b) indicating that one wash cycle is not enough for removal of the compound from solution. As a control experiment, algae incubated with vancomycin and washed 2x, did not inhibit growth, showing that two wash cycles were enough to remove excess antibiotic.

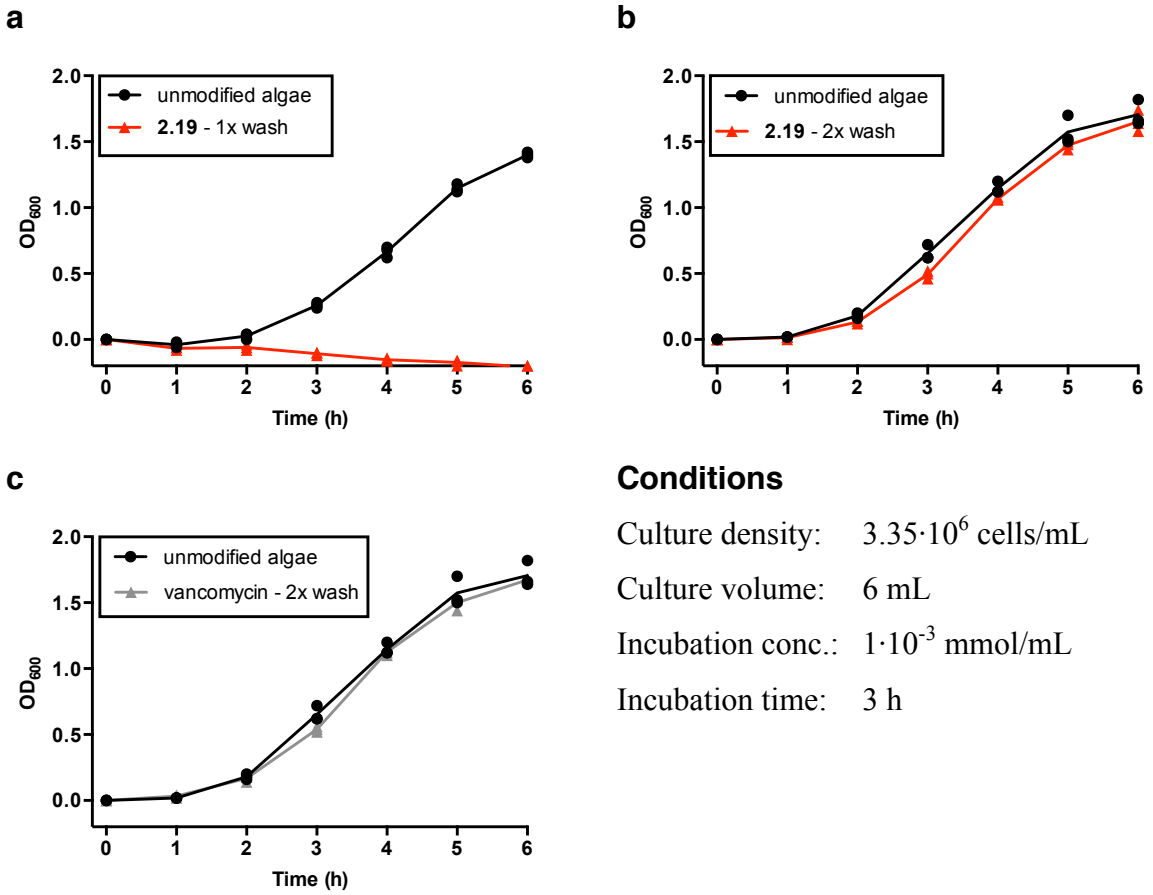

Scheme 21: Growth curves for *B. subtilis* in the presence of algae previously washed to different extent. Data points show individual replicates.

[20] Concerning the washing protocol is has to be mentioned that after the incubation, the algae were diluted with medium (~10-fold). The supernatant was removed and then the number of wash cycles started.

From the previous experiments we have learned that with 3 h of incubation time and two wash cycles, the loading of substance on the algae was not sufficiently high. Therefore, we extended the incubation time of the algae from 3 h to 12 h (Scheme 22). Interestingly, after 12 h incubation, the algae completely inhibited bacterial growth. We also incubated the algae under the same conditions with vancomycin as a control. Under these conditions, there was also complete inhibition of growth with vancomycin. Even after washing three times, the bacteria were completely killed. When the algae were incubated for 6 h instead of 12 h, the same result was obtained (data not shown). This indicates that there must be some kind of adhesion of vancomycin to the surface of the algae.This effect must evolve with longer incubation times and at higher algae densities compared to the first experiments.[21]

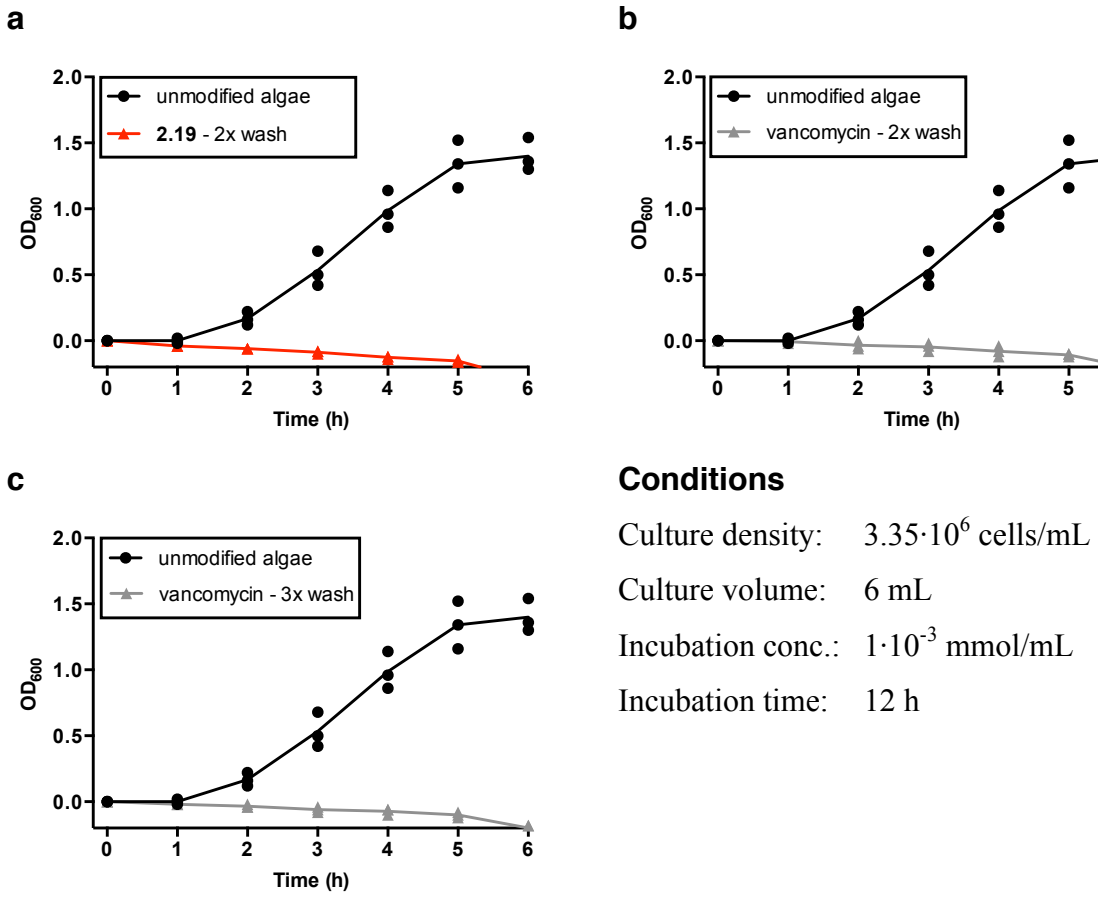

Scheme 22: Growth curves for *B. subtilis* in the presence of algae incubated for 12 h. Data points show individual replicates.

[21] Increasing from $1.25 \cdot 10^6$ cells/mL to $3.35 \cdot 10^6$ cells/mL with respect to earlier experiments.

After the finding that vancomycin probably also adheres to the surface of *C. reinhardtii*, we wanted to find conditions at which the difference between **2.19** and vancomycin became apparent. Based on the experiments depicted in Scheme 22, we had to reduce the amount of antibiotic present in the culture mixture. As learned from the experiments earlier, this can be done in two ways: 1) Reduce the incubation time of the algae so that there is less substance adhered to the surface or 2) reduce the amount of algae added to the culture mixture. We had already adjusted the incubation conditions for the algae, so that their motility was nicely maintained, so we decided to adjust the amount of algae in the culture (Scheme 23). Using an algae culture with a density of $1.5 \cdot 10^6$ cells/mL instead of $3.35 \cdot 10^6$ cells/mL revealed a difference between algae incubated with conjugate **2.19** (Scheme 23, a) and vancomycin (Scheme 23, b) by slight inhibition of bacterial growth for **2.19**-modified algae.

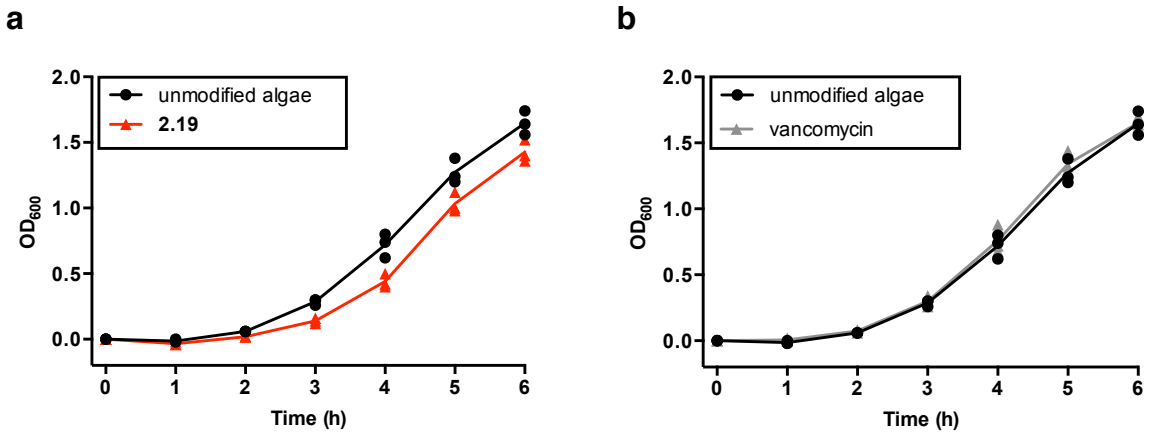

Conditions

Culture density:	$1.5 \cdot 10^6$ cells/mL
Culture volume:	6 mL
Incubation conc.:	$1 \cdot 10^{-3}$ mmol/mL
Incubation time:	12 h
Wash cycles:	3

Scheme 23: Growth curves for *B. subtilis* at an algal culture density of $1.5 \cdot 10^6$ cells/mL. Data points show individual replicates.

To further enhance this effect, we used an algae culture with slightly higher density. By utilizing a culture with $2.5 \cdot 10^6$ cells/mL, conjugate **2.19** fully inhibited bacterial growth (Scheme 24, a). Under these conditions, algae modified with vancomycin showed slight inhibition (Scheme 24, b). In addition to this, we also were interested in the effect that conjugate **2.21** had under these conditions. Surprisingly, algae previously incubated with **2.21** could not inhibit the growth of the bacteria at all. This confirms the results obtained in the initial experiments (see Scheme 19) that showed that algae incubated with **2.21** showed drastically less antibacterial potency than algae modified with **2.19**. This indicates that the fluorophore plays a crucial role for the adhesion of the substance to *C. reinhardtii*. On the other hand, under the earlier conditions, algae modified with **2.21** showed a higher inhibition of bacterial growth than vancomycin. This effect was reversed with lower concentration of the incubation solution. An explanation for this might be the higher potency of vancomycin opposed to **2.21** that has to be taken into account, as the effect seen in the growth curve is not only proportional to the adhesion of the substances but also their antimicrobial potency. Further, as we have presumed earlier, vancomycin shows some adhesion to the algae that becomes more apparent with long incubation times.

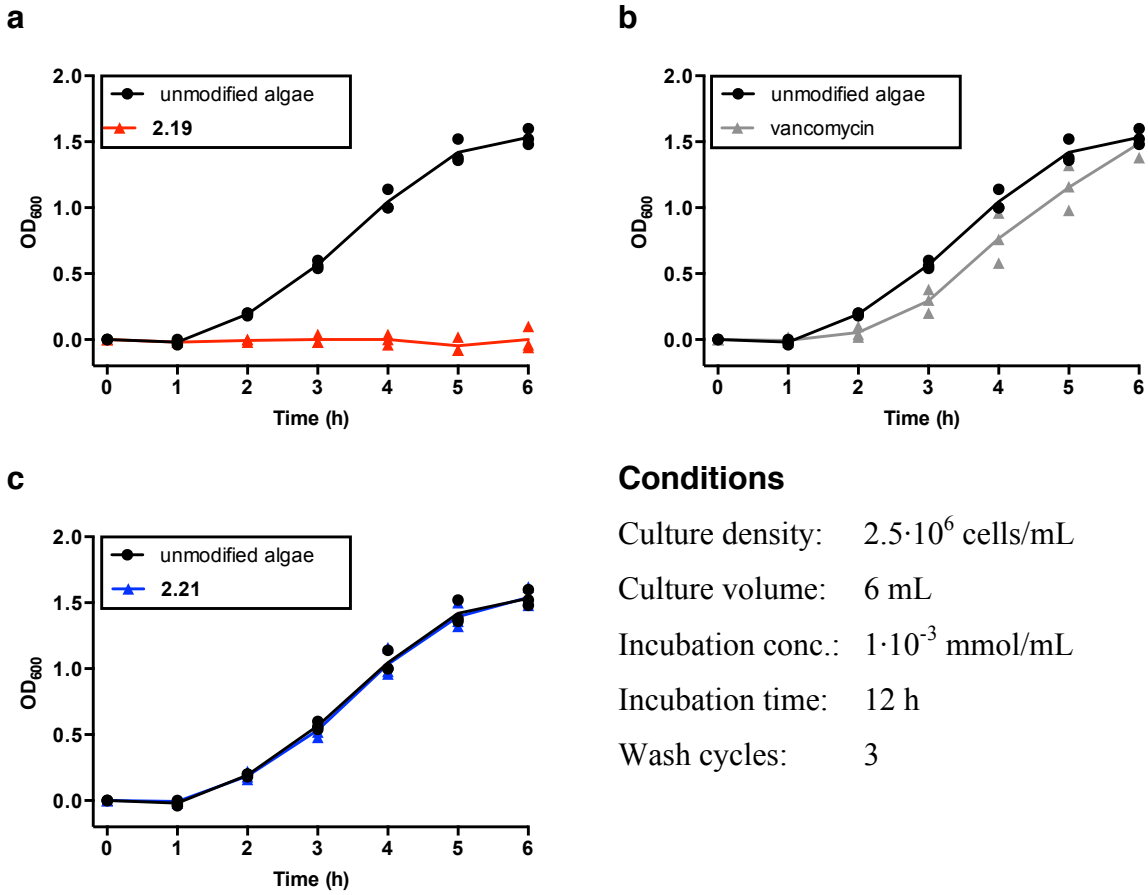

Scheme 24: Growth of *B. subtilis* at an algal culture density of $2.5 \cdot 10^6$ cells/mL. Data points show individual replicates.

2.12 Live/dead staining of bacteria

As an additional proof to the growth curves, we performed live/dead staining of the bacteria with the samples shown in Figure 29, b after 6 h incubation. Viable bacteria are stained by hydrolysis of the cell permeable calcein-AM to calcein, which shows green fluorescence. Dead bacteria were stained with propidium iodide, which emit red fluorescence. When bacteria were grown with unmodified algae, mainly living but also dead cells were observed (Figure 29, a). This is because the bacterial growth had already entered a stationary phase. Important, the cells either emit green or red fluorescence as indicated by the merged image of the red and green channel. The merged image of the bacteria grown with modified algae showed an overlay of red and green fluorescence at the same spots (Figure 29, b). Separation of the merged image showed that all bacteria emit red fluorescence, which confirmed all cells being dead (Figure 29, c). At the same time, compound **2.19** (Figure 29, d) adhered to the surface of the bacteria and is visualized on the green channel resulting in an overlay of red and green in the merged image.

These experiments show, that the substance is transferred from the algae to the bacteria and kill them. Attachment of **2.19** to the algae is reversible and binding of the compound to the bacterial cell wall is probably stronger than to the algae.

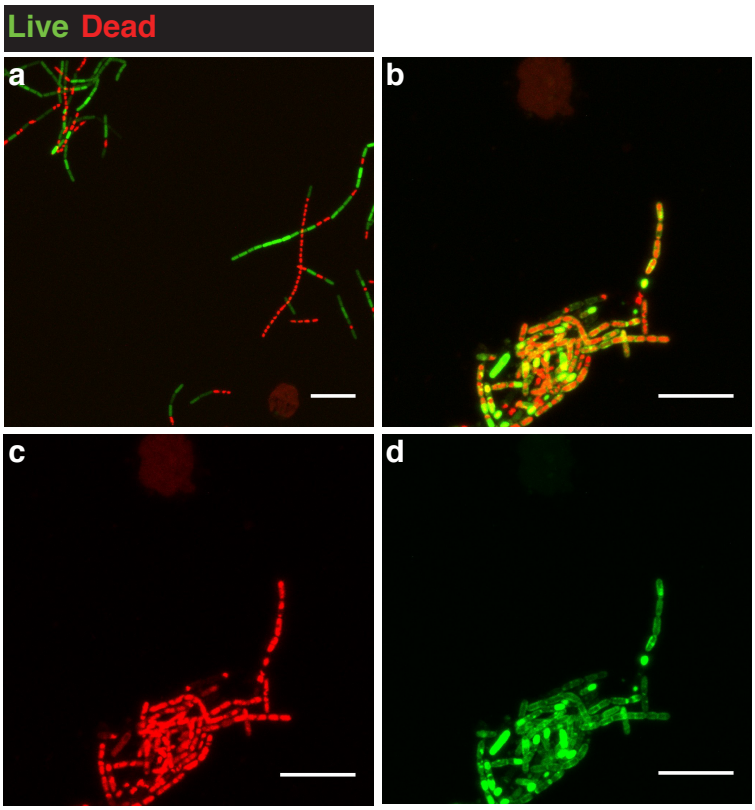

Figure 29: Fluorescence microscopy images of Live/Dead staining of bacteria after exposure to algae for 6 h. Living bacteria show green fluorescence, dead bacteria show red fluorescence. **a)** Bacteria in the presence of unmodified algae, red and green channel overlay. **b)** Bacteria in the presence of algae modified with **2.19**, red and green channel overlay. **c**) Bacteria in the presence of algae modified with **2.19**, red channel. **d**) Bacteria in the presence of algae modified with **2.19**, green channel.

2.13 Mechanistic investigations

Mechanistically, there are two possibilities how conjugate **2.19** is transferred from the algae to the bacteria: (**i**) by diffusion, where the compound is first released into the medium and then adheres to the bacteria, or (**ii**) by direct contact of the bacteria with the algae (Scheme 25). In case of the first mechanism, the attachment of the substance to the algae must be fully reversible in solution. Therefore, we designed an experiment in which we first equilibrated the modified algae for a defined period of time under the conditions with which we usually performed the bacterial growth curve experiments. Later, we separated the supernatant from the algae and with both, algae and supernatant, we investigated bacterial growth.

The growth curves suggest that both vancomycin and compound **2.19** are removed from the algae after 1 h of equilibration in the medium. For compound **2.19**, the amount released was sufficiently high enough to fully inhibit the bacterial growth, **a**), and at the same time, slightly inhibited growth by the remaining algae was also observed (Scheme 26, **c**). For vancomycin alone, partial inhibition of bacterial growth was achieved in the supernatant (Scheme 26, **b**), but no inhibition of the remaining algae could be observed (Scheme 26, **c**). These results indicate an overall lower loading of vancomycin and its fully reversible detachment from the algae, as opposed to an incomplete release of compound **2.19**. Overall, a mechanism proceeding only over pathway (ii) can be excluded and, instead, diffusion (i) is likely playing a crucial role in the delivery mechanism.

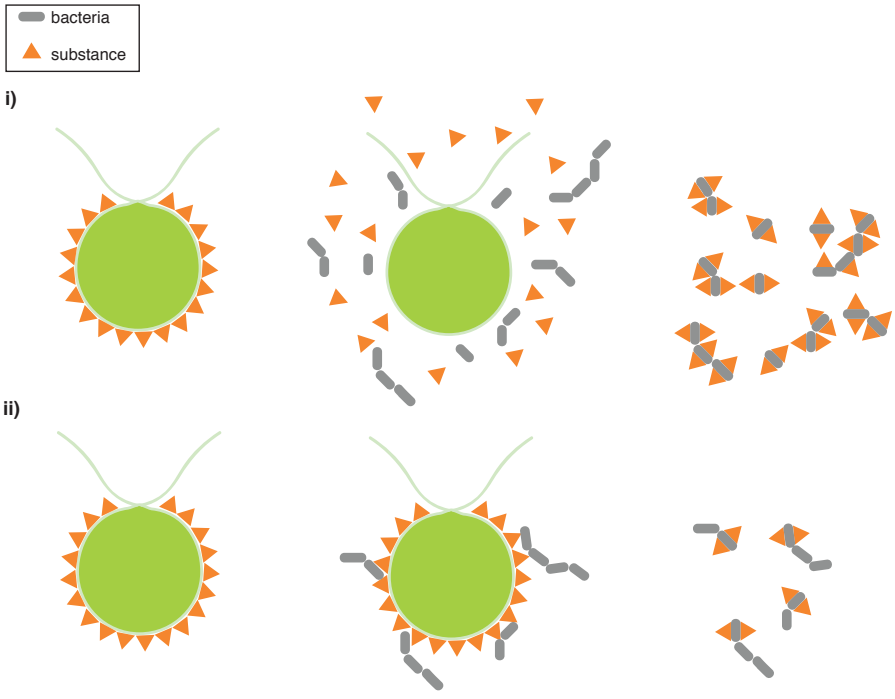

Scheme 25: Possible mechanisms for delivery of substances from the algae to the bacteria.

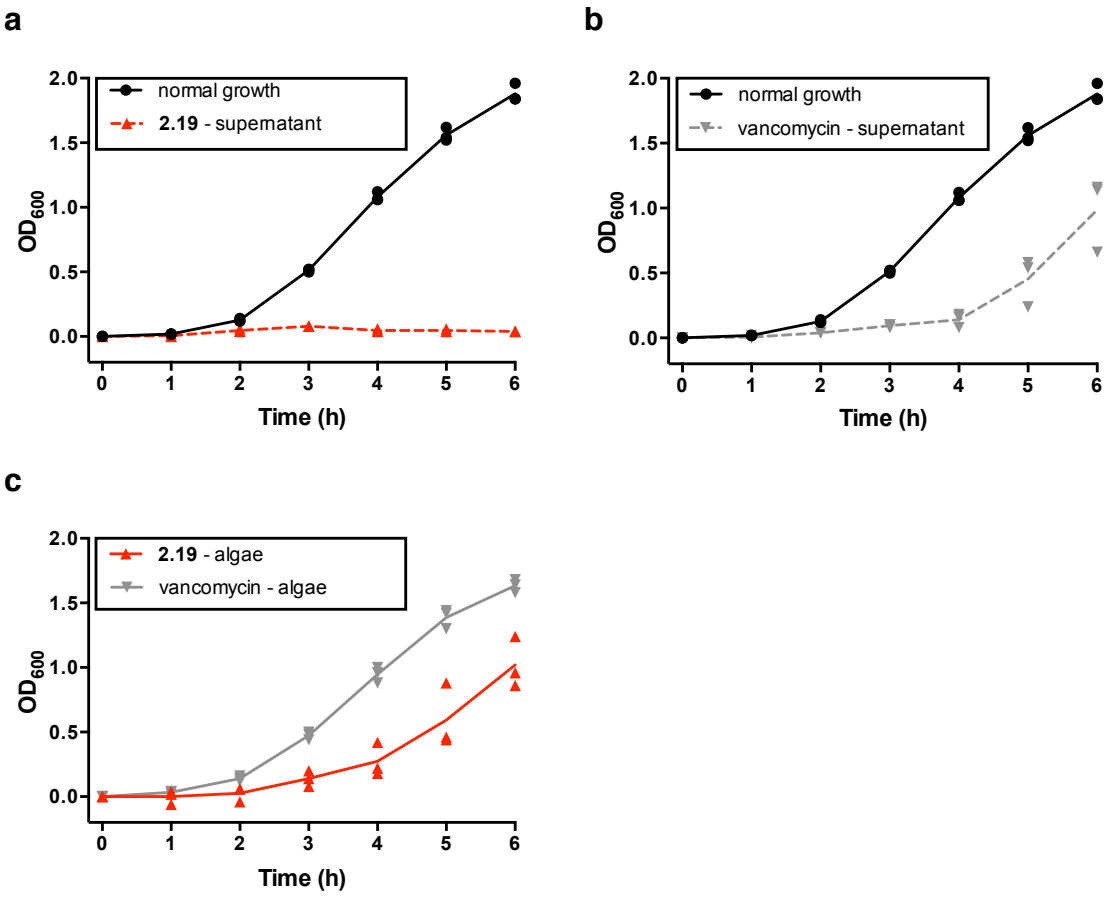

Scheme 26: Mechanistic investigations on substance delivery.

2.14 Quantification of conjugate 2.19 on *C. reinhardtii*

The quantification of substance **2.19** on *C. reinhardtii* was realized by UV/VIS absorption spectroscopy. The UV/VIS absorption spectrum of the alga shows a broad absorption with maxima located at 434 nm and 678 nm. The UV/VIS absorption spectrum of compound **2.19** shows high absorbance at 497 nm. The alga also shows UV/VIS absorption at 497 nm, so that the amount of substance can only be quantified by subtracting the UV/VIS absorption of the unmodified alga at 497 nm. By measuring the increase of UV/VIS absorption at the λ_{max} of **2.19** relative to the absorption at this wavelength of the unmodified algae, the amount of substance on the modified algae was determined.

In this context, we also need to determine the algae density or also termed algae concentration (in cells/mL). The algae concentration can also be identified by UV/VIS spectroscopy. The algae concentration was determined by measuring the absorption at 550 nm. At this wavelength, the light is scattered by the algae that is proportional to cell density.[101] Importantly, compound **2.19** shows no absorption at 550 nm (UV/VIS absorption spectrum of compound **2.19** depicted in Figure 31).

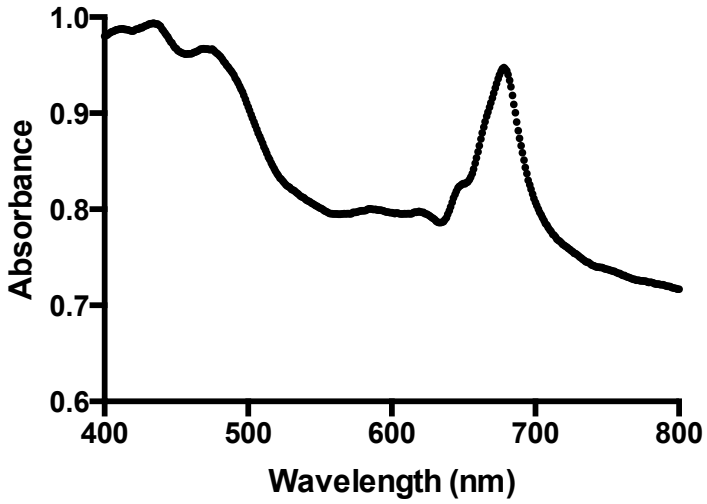

Figure 30: UV absorption spectrum of *C. reinhardtii.*

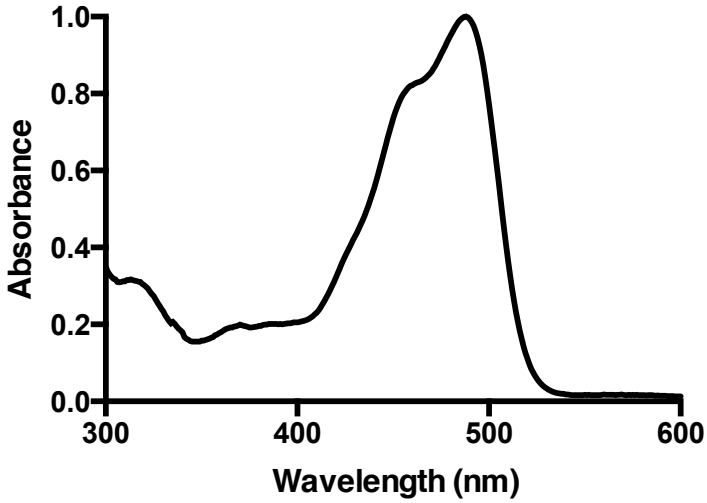

Figure 31: UV/VIS absorption spectrum of **2.19**.

When the UV/VIS absorption of unmodified *C. reinhardtii* at 497 nm and 550 nm was measured as a function of algae concentration, a linear relation was obtained for both wavelengths. The plots do not cross an absorption of 0 because of scattering of living and dead algae cells.[101]

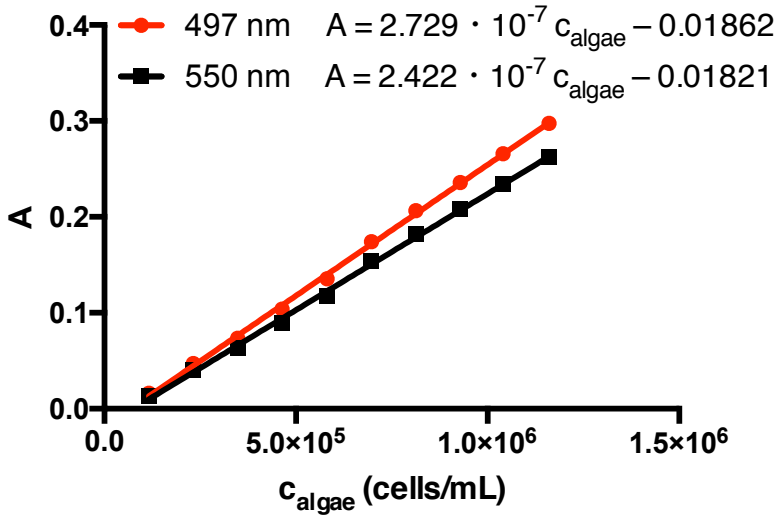

Figure 32: UV/VIS absorptions of unmodified algae at 497 nm and 550 nm at different algae concentrations.

Next, the UV/VIS absorption of the modified algae was measured at 550 nm for the determination of algae concentration, and at 497 nm for the determination of compound **2.19** in triplicates (Table 4).

Table 4: Measured UV/VIS absorption of modified algae at 497 nm and 550 nm.

Sample	550 nm	497 nm
1	0.159	0.212
2	0.159	0.212
3	0.177	0.243

The measured UV/VIS absorption at 550 nm and the equation obtained from Figure 32 was used to calculate the algae concentration (c_{algae}).

$$A_{550} = 2.422 \cdot 10^{-7} \cdot c_{algae} - 0.01821$$

$$c_{algae} = \frac{A_{550} + 0.01821}{2.422 \cdot 10^{-7}}$$

With the algae concentration, the UV/VIS absorption of the unmodified algae at 497 nm can be calculated.

$$A_{497} = 2.729 \cdot 10^{-7} \cdot c_{algae} - 0.01861$$

The UV/VIS absorption at 497 nm resulting from compound **2.19** can be calculated by subtraction of A_{497} from the determined value (A_{mod}).

$$\Delta A = A_{mod} - A_{497}$$

From ΔA the concentration of **2.19** can be calculated using Lambert Beer's Law.
Lambert-Beer law:

$$c = \frac{E_\lambda}{\varepsilon_\lambda \cdot d}$$

With the extinction coefficient of ε_λ = 16300 L·mol^{-1}·cm^{-1}, ΔA can be used to calculate the concentration of **2.19** on the modified algae.

$$c = \frac{\Delta A}{16300\ L \cdot mol^{-1} \cdot cm^{-1} \cdot 1\ cm}$$

The table below shows the values for the intermediate calculation steps and the final concentration of the substance per volume algae culture in µg·mL^{-1}.

Table 5: Intermediate calculation values and final concentrations of **2.19** in an algae suspension.

	c_{algae} (cells/ml)	A_{497}	ΔA	c (mmol·ml^{-1})	c (µg·ml^{-1})
1	7.38·10^5	0.183	0.0297	1.82·10^{-6}	5.38
2	7.36·10^5	0.182	0.0294	1.80·10^{-6}	5.32
3	8.14·10^5	0.204	0.0395	2.42·10^{-6}	7.15

The amount of compound attached to the algae lies in the low µg range for culture densities of 0.7-0.8·10^6 cells/mL. In initial experiments we found that the minimal inhibitory activity of vancomycin for our experimental setup is 1 µg/mL (see section 7.2.2).

With the determined loading of ~10-20 µg/mL for a culture of 1.5·10^6 cells/mL, this lies in good agreement.

2.15 Cell wall-deficient mutant

The interaction between anchor **2.19** and *C. reinhardtii* is of fundamental importance for the realization of the surface modification. We were interested in whether the interaction really takes place between components present in the cell wall of *C. reinhardtii* as postulated by *Whitesides* and co-workers,[58] or whether the plant material inside the cell also provides a basis for adhesion of the compound. To investigate this, we cultivated a cell wall-deficient mutant of *C. reinhardtii* that lacks the major components of the cell wall (W2-W6) but contains fibers that resemble the outer layer of the wild type (Figure 33).

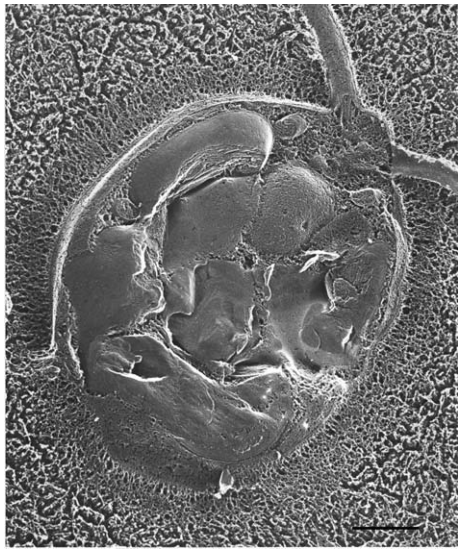

Figure 33: Electron microscopy image of *C. reinhardtii* prepared by quick-freeze deep-etch technique. The cell wall-deficient cw15 mutant lacks the central triplet W2-W6 layers.[40]

The cell wall-deficient mutant was incubated in a $4.5 \cdot 10^{-3}$ mmol/mL solution of **2.19** for 3 h. As a control, the cell wall containing algae were incubated under the same conditions. The cells were washed, fixed and prepared for microscopy. The difference of the two samples was clearly well apparent. After 3 h, the cell wall containing mutant was fully covered with conjugate **2.19** (Scheme 27). On the contrary, the cell wall-deficient mutant lacked any adhesion of **2.19**. As a control, we also imaged cell wall-deficient algae that have not been incubated with **2.19**. The image processing parameters were set the way that we did not see any fluorescence in this control. The results obtained with this experiment lead to the conclusion that compound **2.19** adheres to components belonging to the cell wall of the algae.

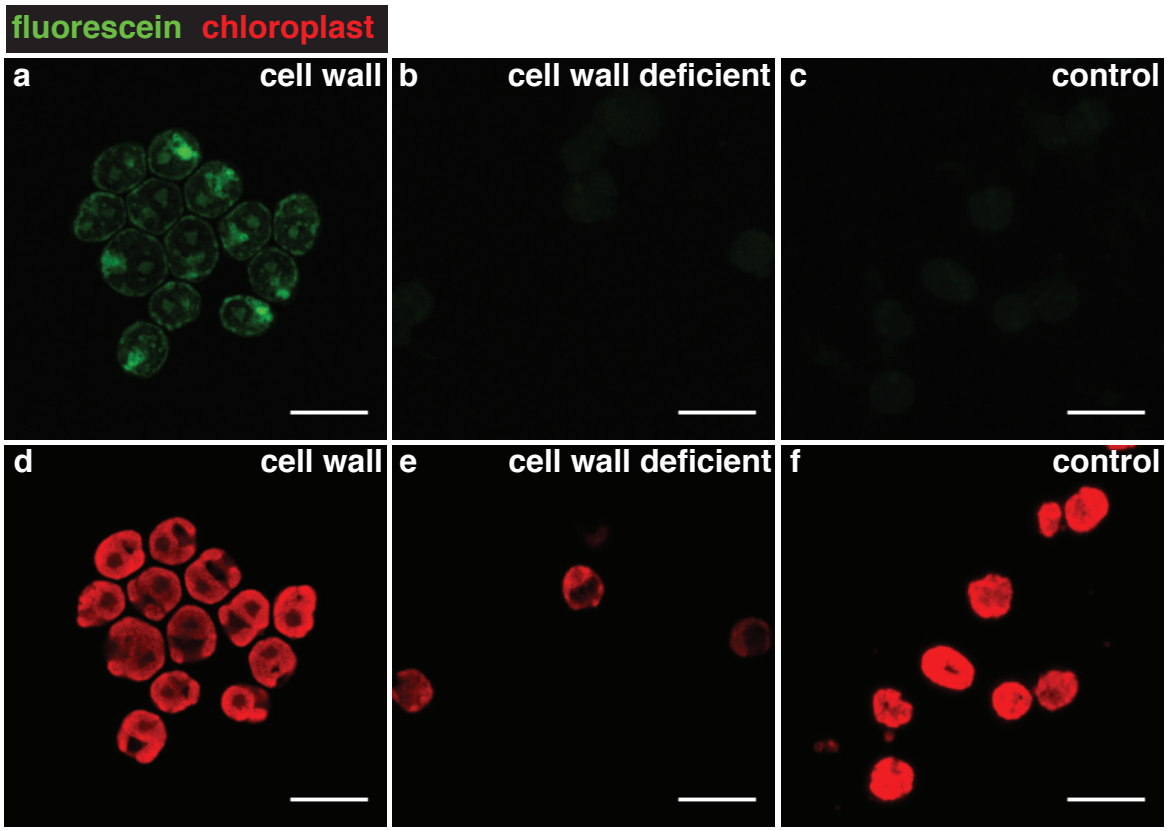

Scheme 27: Incubation of algae with and without cell wall for 3 h at $4.5 \cdot 10^{-3}$ mmol/mL with **2.19**. **a)** Algae with cell wall (11-32b). **b)** Cell wall-deficient algae (CC-406 cw15 mt-). **c)** Untreated cell wall-deficient algae. Scale bars equal 10 µm. **d)** Fluorescence of chloroplast of algae with cell wall previously treated with **2.19**. **e)** Fluorescence of chloroplast of algae without cell wall previously treated with **2.19**. **f)** Fluorescence of chloroplast of algae without cell wall.

2.16 Towards the crystal structure of a 4-hydroxyproline oligomer

Along with our studies in that the 4-hydroxyproline oligomer played such an important role, we were also interested in the architectural arrangement of the 4-hydroxyproline oligomer linker. It has been reported that polyprolines can arrange in helical structures,[96] and it has been calculated that the 4-hydroxy-variant does as well, however,[102] this has never been proven by X-ray structure analysis. Knowledge about the secondary structure of our 4-hydroxyproline oligomer anchor would provide us with more information, how the anchor might interact with the surface of the algae.

For a more facilitated crystallization we introduced a *p*-bromobenzoyl group to the 4-hydroxyproline oligomer, as this group was used in the crystallization of a 6-mer of 4-hydroxyproline oligomer in earlier reports (Figure 34).[96] The resulting 4-hydroxyproline oligomer **2.24** was hygroscopic and very polar, so that the substance was already hardly soluble in MeOH. A number of attempts to obtain crystals from MeOH, MeOH/H_2O, EtOH/H_2O, Diglyme/H_2O[103] and other mixtures using various techniques, were unsuccessful because most of the time, only oily residues were obtained.

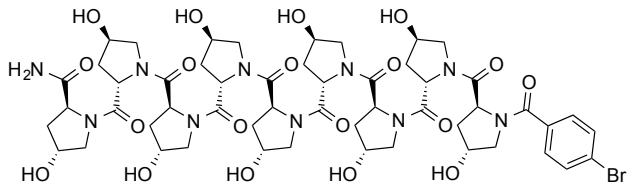

2.24

Figure 34: 4-Hydroxyproline oligomer functionalized with *p*-bromobenzoyl group to facilitate crystallization.

We then decided to utilize a method that is used in protein crystallization: the sitting drop method. A drop of protein solution in water is exposed to a chamber containing a reservoir, which is filled with a precipitant solution (mostly salts). From this reservoir a drop is added to the protein drop. The concentration difference between the reservoir filled with precipitant and the protein/precipitant drop causes evaporation of solvent from the drop to the precipitant reservoir, resulting in an increase of concentration in the protein drop. This increase of protein and salt concentration in the drop, can lead to a crystallization of the protein. Advantage of this method is the crystallization from aqueous solutions and the operationally simple screening method because crystallization sets are commercially available and robots place the drops and reservoir solutions in specially designed well plates. Disadvantage is false alarm crystallizations in which the salt from the precipitant crystallized instead of the protein.

We decided to carry out our experimentation at the protein crystallization facilities of the Universität Zürich. The screens used were general screens with a diverse combination of different conditions. We started with a concentration of 10 mg/mL of peptide dissolved in water, but after we did not see any precipitation we gradually went up to 60 mg/mL. Although we used several screen sets with each contained 96 different conditions, we were not able to get suitable crystals for X-ray analysis. Typical results were the precipitation of a solid from the drop (**a**, Figure 35) or a phase separation in the drop, in which the protein separated from the aqueous layer (**b**). Sometimes we also obtained promising crystals such as depicted in **c**, and the enlargement in cross-polarized light in **d**, but always the crystals were salts resulting from the precipitant and no peptide.

Further attempts for the crystallization should consider modifications on the 4-hydroxyproline oligomer anchor such as different rigid groups on the amine or replacement of the amide group on the C-terminus by a carboxyl group.

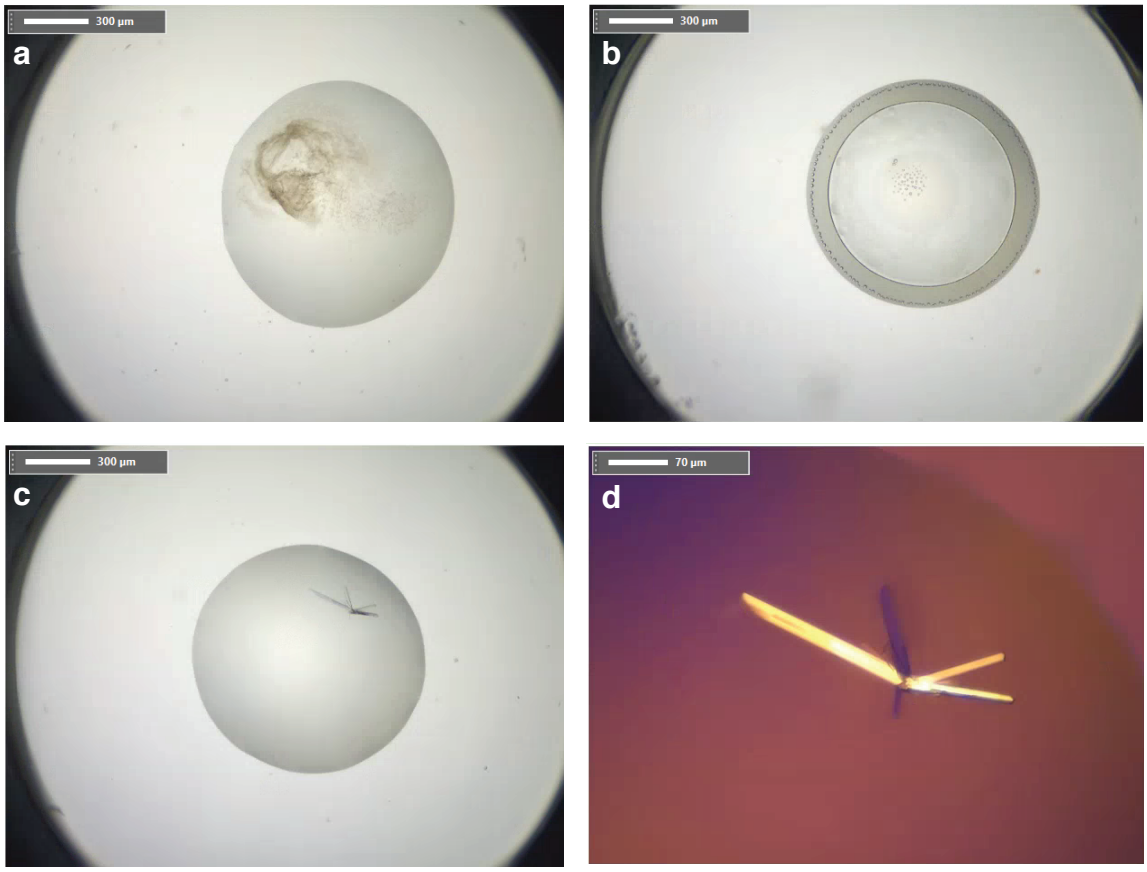

Figure 35: Representative images of drops containing 4-hydroxyproline oligomer **2.24. a)** 0.1 M NaOAc 4.5 pH, 0.2 M ZnOAc 10 %w/v PEG 3K. **b)** 1.6 M Na_3Cit. **c)** 0.17 M $(NH_4)_2SO_4$, 15 %v/v glycerol, 25.5 %w/v PEG 4K. **d)** Enlargement of c) imaged with cross polarized light.

2.17 Conclusion

Our results demonstrate the functionalization the alga *C. reinhardtii* with the antibiotic vancomycin. We prepared conjugates between vancomycin and a 4-hydroxyproline oligomer by a combination of solid- and solution-phase peptide synthesis. The antimicrobial activity against the Gram-positive bacteria *B. subtilis* decreased in comparison to the parent antibiotic vancomycin, but still showed satisfying activities (MIC = 4—8 μg/mL). We immobilized the conjugates on the surface of the algae by a simple incubation protocol followed by washing of the cells. Important parameters for attachment to the surface were concentration of the incubation solution and incubation time. Both parameters also affected the motility of algae to great extent, so that the parameters had to be optimized until loading of compound on the surface was sufficient and the cells still showed good viability.

The modified algae were tested in bacterial assays against *B. subtilis* for their antimicrobial properties. It was shown that the modified algae were able to kill the bacteria by transferring the substance from the surface of the algae to the cell wall of the bacteria. This process was mainly regulated by diffusion, as we observed reversibility for the attachment of the substance to the surface. Fluorescently-labeled conjugate **2.19** showed much stronger attachment to the surface compared to unlabeled conjugate **2.21**, indicating that the 4-hydroxyproline oligomer alone is not the main contributor for the attachment of the substances to the cell wall. On the contrary, the binding of the conjugates is more complex and the compounds as a whole contribute to this.

Overall we have shown, that the cell wall of a living cell can be modified by chemical means. Our system might be transferred to different cells or viruses resulting in the introduction of different phenotypes. Further research is necessary to better understand the factors that contribute to the binding of the conjugates. This could be investigated by the replacement of vancomycin by other therapeutic materials or by modification of the 4-hydroxyproline oligomer anchor (introduction of other functional groups to the peptide e.g. free amines).

3 Synthesis of Pyrrolizidines

3.1 Introduction

3.1.1 Biological relevance of pyrrolizidine alkaloids

Pyrrolizidine alkaloids are a large class of natural products with about 600 representatives known.[104-106] Exclusively produced in plants, these natural products are found in about 6000 different species, meaning that 3% of all flowering plants contain pyrrolizidine alkaloids. The majority of these compounds are isolated from the distantly related angiosperm plant families: *Asteraceae*, *Boraginaceae* and *Fabaceae*.[107] Central motif of pyrrolizidine alkaloids is two fused cyclopentane rings with a nitrogen atom at the bridgehead (Figure 36). Many of these heterocycles occur in oxidized forms such as the *N*-oxide or the 1,2-unsaturated and a fair amount of alkaloids also have a 3*H*-pyrrolizin-3-one substructure.

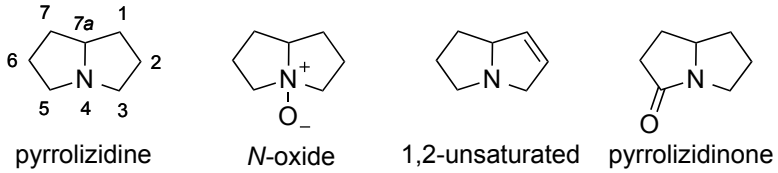

Figure 36: Pyrrolizidine alkaloids substructures in natural products.

With their isolation source often playing an important role in traditional medicine, pyrrolizidine alkaloids are often biologically relevant, exhibiting a variety of activities such as hepatotoxic, pulmotoxic, antimitotic, mutagenic or carcinogenic. For example, cremastrine **3.01** has been shown to be one of few compounds binding selectively to muscarinic M3 receptors,[108] and it has been proposed that selective blockade of M3 receptors might be useful in the treatment of respiratory disorders (Figure 37).[109] UCS1025A **3.02** was isolated from the fungus *Acremonium sp*. KY917[110] and showed antiproliferative activity against human tumor cell lines.[111]

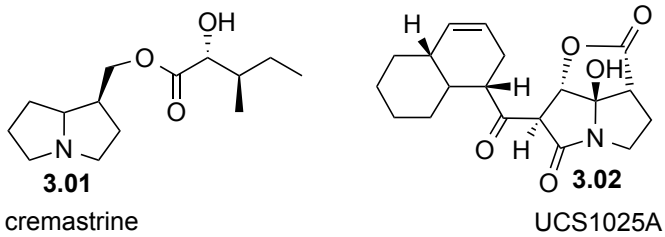

Figure 37: Biologically active pyrrolizidines.

1,2-Dehydropyrrolizidines such as monocrotaline **3.03** are potent hepatotoxins because they are readily oxidized to the corresponding pyrrole intermediates (Scheme 28). This reaction is catalyzed by microsomal cytochrome P450 enzymes mainly localized in the liver and lung tissues. The highly reactive intermediates subsequently mediate the interstrand cross-linking of DNA to form bis-alkylated adducts such as **3.05** (Scheme 28).[112,113] To protect themselves against these toxic alkaloids, arctiids[114] and *Zonocerus*[115] store pyrrolizidines exclusively in the *N*-oxide state.[116]

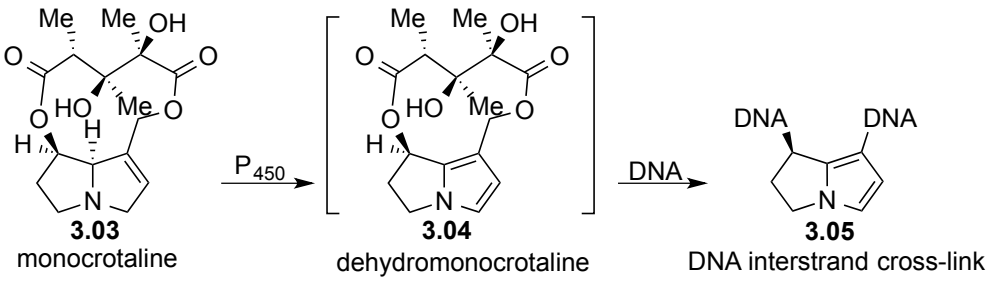

Scheme 28: Crosslinking of DNA with formation of reactive pyrrole intermediates.

Another way of preventing this aromatization is the introduction of a substituent on the *7a*-position of the pyrrolizidine ring. Biologically relevant structures with this feature are the muscarinic receptor antagonist **3.06** identified by *Suzuki* et al.[117] or the mixed α7-nicotinic receptor antagonist **3.07** prepared and tested by *Reymond* and co-workers (Figure 38).[118,119]

3.06
muscarinic antagonist

M1 receptor ([3H] pirenzepine):
IC_{50} = 0.1 mM
M2 receptor ([3H] quinuclidinyl benzilate):
IC_{50} = 8.3 mM

3.07
mixed a7-nicotinic
receptor antagonist

IC_{50} = 7.2 mM

Figure 38: Biologically active *7a*-substituted pyrrolizidine alkaloids.

3.1.2 Known synthetic methods for the preparation of 7a-substituted carboxamides

In the course of a study on the synthesis of a natural product, we became interested in structures such as **3.08**, which carry an amide group directly connected to the pyrrolizidine core. These *7a*-substituted pyrrolizidine carboxamides, are interesting structural motifs that lack direct approaches for their synthesis.

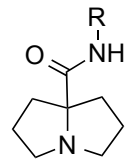

3.08

7a-substituted
pyrrolizidine carboxamide

There have been indirect syntheses of precursors reported towards *7a*-substituted pyrrolizidine carboxamides. The first reaction sequence towards the precursors was reported by *Suzuki* and co-workers and starts with the synthesis of nitrile-substituted pyrrolizidine **3.10** by condensation and reaction of ketone **3.09** with ammonia and potassium cyanide (Scheme 29).[120] For the synthesis of a *7a*-substituted carboxamide, the nitrile group of pyrrolizidine **3.10** needs to be hydrolyzed to the acid followed by peptide coupling to the corresponding amide.

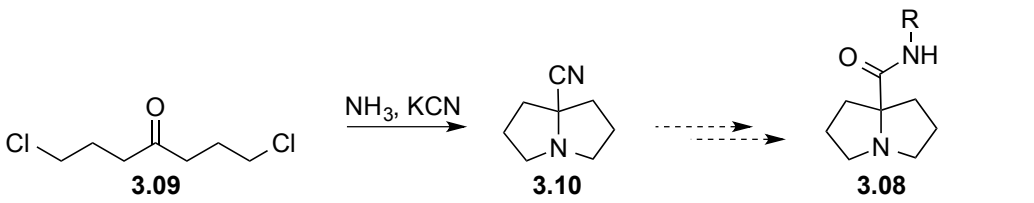

3.09 **3.10** **3.08**

7a-substituted
pyrrolizidine carboxamide

Scheme 29: Synthesis of *7a*-substituted pyrrolizidine by *Suzuki* and co-workers.

Another strategy furnished pyrrolizidines substituted with an ester group at the *7a*-position by *Cordero* et al. The reaction sequence started with a 1,3-dipolar cycloadditon of α,β-unsaturated amide **3.11** with pyrroline *N*-oxide **3.12** to furnish the isoxazolidine **3.13** (Scheme 30). These compounds are then hydrogenated with a palladium hydroxide catalyst on charcoal to open pyrrolidine **3.14**, which subsequently cyclized to the pyrrolizidinone **3.15**. Hydrolysis of the ester group, followed by peptide coupling would give the desired amide functionality as in the previous example.

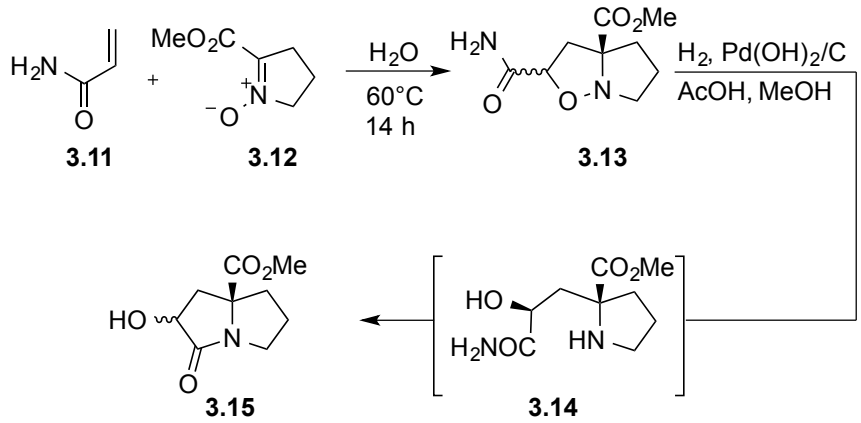

Scheme 30: Synthesis of pyrrolizidinone with ester group on the *7a*-position.

A third preparation procedure was published by *Sansano* et al. and utilizes a three component reaction involving proline ester **3.16**, an α,β-unsaturated aldehyde **3.17** and methyl acrylate **3.19** (Scheme 31). This reaction involves the *in situ* preparation of an iminium ion **3.18**, which forms a 5-membered ring by addition to methyl acrylate. In one step, highly substituted pyrrolizidines (**3.20**) can be obtained with good regio-and diasteroselectivity. An interesting extension of this method would be the exchange of the proline ester by an amide-functionalized proline. This would provide *7a*-substituted pyrrolizidines in a very concise manner.

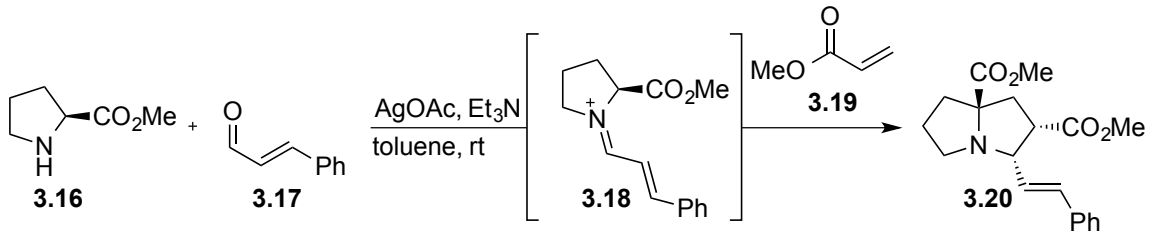

Scheme 31: Three-component reaction for the preparation of **3.20**.

3.2 Project outline

The objective of the project was to evaluate the direct preparation of *7a*-substituted pyrrolizidine alkaloids from simple building blocks. The building blocks we wanted to employ were pyrrolines, carrying a hydroxyl group on the side chain and isonitriles as the reaction partner (Scheme 32). The primary goal was the investigation of the reaction scope, as it is desirable to have direct access to pyrrolizidines with different steric and electronic properties. Furthermore, we wanted to investigate the functionalization of the final molecules to access oxidized and reduced derivatives at a late stage. Finally, it was desirable to extend the reaction to elaborated pyrroline precursors to give access to functionalized derivatives of the pyrrolizidine core.

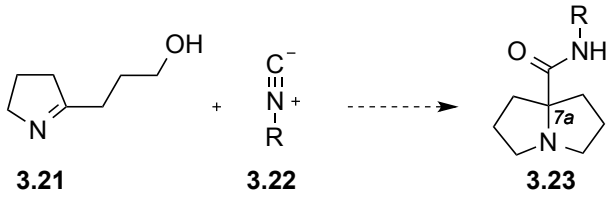

3.21 **3.22** **3.23**

Scheme 32: Synthesis of *7a*-substituted pyrrolizidines from pyrroline imines and isonitriles

3.3 Synthesis of the pyrroline building block

We started with the synthesis of pyrroline **3.21** of which a synthetic route had been reported in the literature (Scheme 33).[121,122] Ester **3.24** was hydrolyzed with potassium hydroxide to **3.25**, which was esterified using sulfuric acid and methanol. Next, *N*-vinylpyrrolidinone was reacted with ester **3.26** in a Claisen condensation to yield *N*-vinylpyrrolidine-2-one **3.28** in 40% yield instead of the reported 96%.[123] This compound was treated with HCl under reflux to hydrolyze the vinyl group, decarboxylate, deprotect and form the pyrroline. This reaction has been performed only one time and difficulties occurred with the addition of **3.28** to boiling hydrochloric acid with a syringe pump because the needle started to corrode. The reported yield of 95% was not reached.

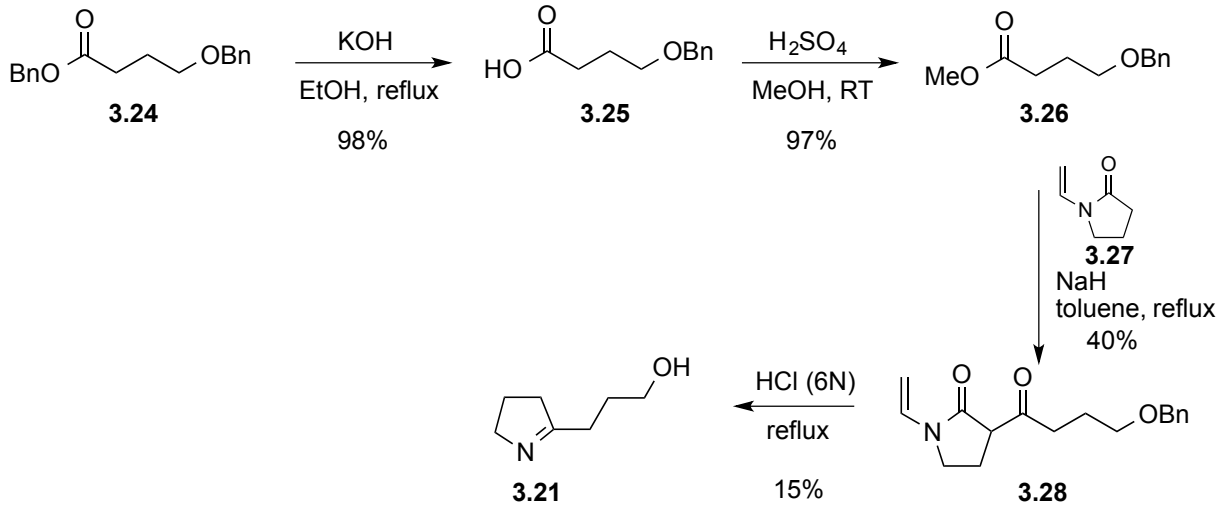

Scheme 33: Literature known route to pyrroline **3.21**.[123]

Due to the long procedure, difficulties with the last step and low yields for the last two steps, we decided to investigate a more direct access to **3.21**. We found that when 2-methyl pyrroline was deprotonated with LDA and ethylene oxide as a solution in THF was added, imine **3.21** was obtained in reasonable yield (Scheme 34). This demonstrates a very direct method for the synthesis of the precursor.

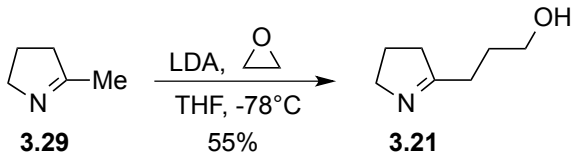

Scheme 34: More convenient synthesis of pyrroline **3.21**.

3.4 Initial cyclization experiments

For an initial test of the reaction we prepared phenylisonitrile **3.31** by Hofmann carbylamine reaction using tetrabutylammonium bromide as a phase transfer catalyst, sodium hydroxide as a base and chloroform (Scheme 35).

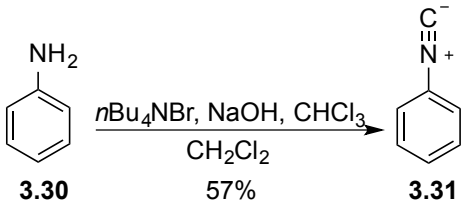

Scheme 35: Synthesis of phenylisonitrile **3.31** by Hofmann carbylamine reaction.

Next, we reacted pyrroline **3.21** with **3.31** under acidic conditions and elevated temperatures (Scheme 36). Fortunately, pyrrolizidine **3.32** could be isolated, but rather in low yield. The structure of **3.32** was confirmed by a single X-ray crystal structure (Figure 39).

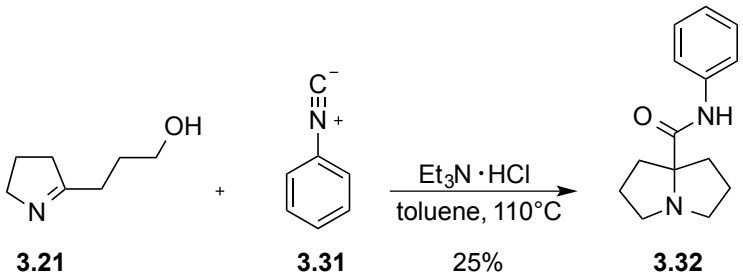

Scheme 36: Initial attempt for the synthesis of *7a*-substituted pyrrolizidine.

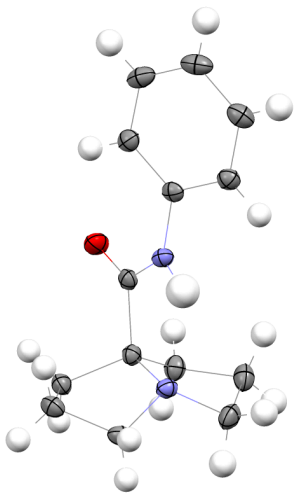

Figure 39: Single crystal X-ray structure of **3.32**.

To improve the yield, we tried other mild acids such as secondary ammonium salts as well as pyridinium chloride. The best yields were obtained with tertiary ammonium salts, with the initial triethylamine hydrochloride giving the best results.[124,125] To get the reaction to completion, high temperatures were required, but DMF or DMSO gave lower yields than toluene. With an adjustment of the reactant equivalents we were able to improve the yield from 25% to 46% for compound **3.32**.

3.5 Synthesis of the isonitrile building block

To investigate the scope of the pyrrolizidine synthesis we prepared a number of aromatic isonitriles by the previously used method. We chose electron withdrawing as well as electron rich substituents and those that had different steric effects (Scheme 37).

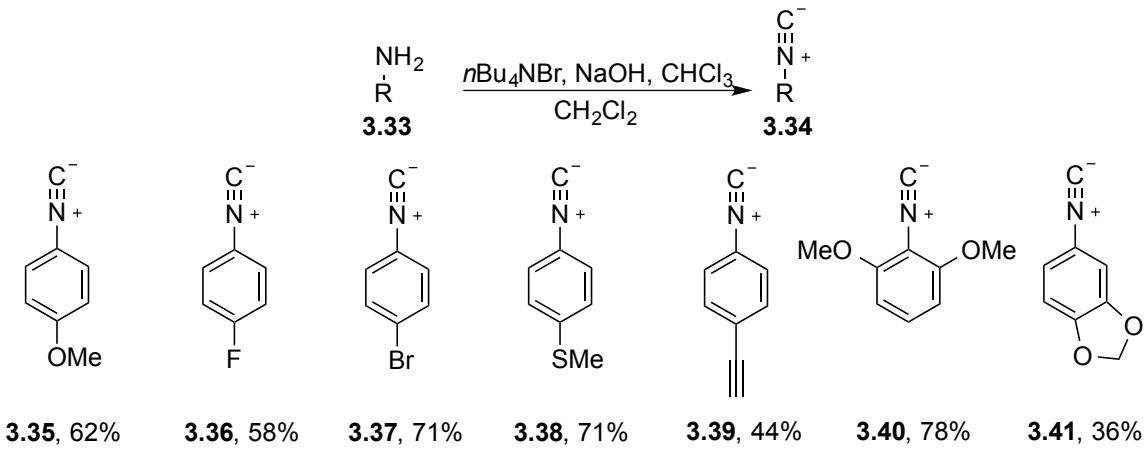

Scheme 37: Aromatic isonitriles prepared by the Hoffman carbylamine synthesis.

Further, we prepared isonitriles from L-amino acids (also isocyanoacetates) in a two-step procedure (Scheme 38). First, the amino group was formylated using either peptide coupling conditions with formic acid, dicyclohexylcarbodiimide and base[125] or by subjection to trimethyl orthoformate.[126] Dehydration of the formylamines was executed with the use of triphosgene at -78 °C. Phosphoryl chloride can also be used for this transformation, but in the case of chiral substrates led to racemic isonitriles.[127]

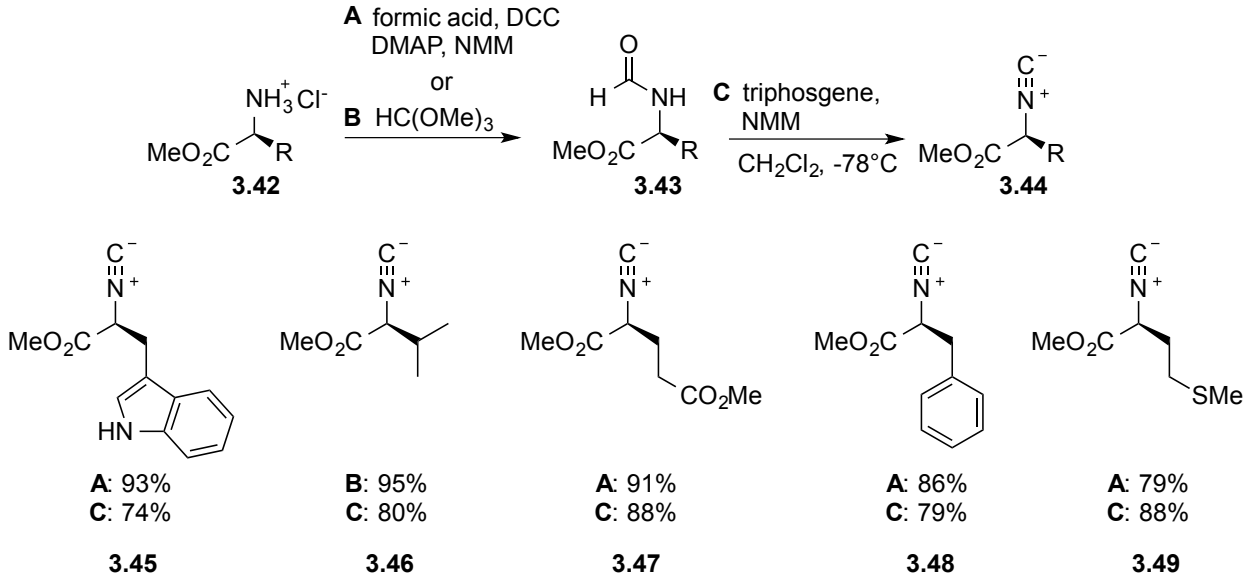

Scheme 38: Amino acid-based isonitriles.

In addition to the afore mentioned isonitriles, we purchased the commercially available compounds **3.50**, **3.51** and **3.52** and prepared the sterically demanding derivative **3.53** according to a literature known procedure in three steps and 73% overall yield (Scheme 39).[128] Isonitrile **3.54** was prepared in two steps and 24% overall yield.

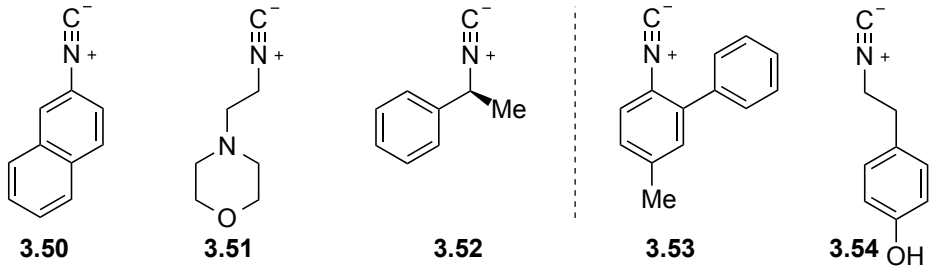

Scheme 39: Commercial isonitriles and sterically demanding isonitrile **3.53** and isonitrile **3.54**.[128]

3.6 Reaction scope[22]

With the isonitriles in hand we investigated the scope of the reaction (Scheme 40). The reaction was found to tolerate a variety of isonitriles. For aromatic isonitriles the yield varied from good to moderate depending on the electronic properties. The reaction with electron-donating isonitriles gave the products **3.55**, **3.56**, **3.57**, and **3.58** in higher yields than electron-poor isonitriles, which delivered the products **3.59**, **3.60**, **3.61**, and **3.62**. Surprisingly, the sterically demanding example **3.63** was observed in higher yield than product **3.32** from the reaction with phenyl isonitrile. A reason for this might be the positive inductive effect of the methyl group in the para-position, and of the phenyl group in the ortho-position on the aromatic ring. Aliphatic isonitriles were also tolerated in this reaction, albeit in lower yield. For example, compound **3.64** bearing a morpholine ring was obtained in low yield. In contrast, unprotected phenols such as **3.56** or benzyl-substituted pyrrolizidine carboxamide **3.66** could be obtained in good yield. Further, the sterically more demanding α-methylbenzyl isocyanide gave product **3.67** in slightly lower yield than benzyl isocyanide indicating that steric factors influence the outcome of the reaction to some extent. On average the best yields were obtained using isocyanoacetates. In this respect, the highest yield was obtained for the tryptophan related product **3.68** as well as for valine derivative **3.73**. The reaction towards pyrrolizidine **3.73** could be performed in the presence of 10 equivalents of water and product formation was still observed, albeit in lower yield (45%). Aromatic (to deliver product **3.70**), as well as aliphatic amino acids containing heteroatoms (to deliver products **3.71** and **3.72**) were also reacted in good yields.

[22] These results were published in I. P. Kerschgens, K. Gademann *Synthesis* **2015**, 47, 3153-3160.

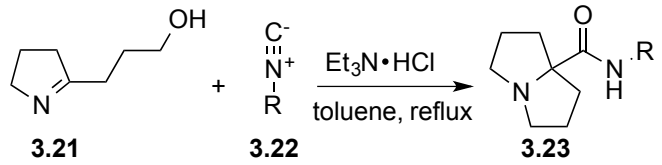

3.21 **3.22** **3.23**

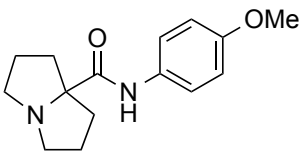

3.55, 48 h, 68%

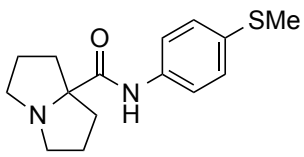

3.56, 24 h, 47%

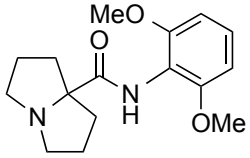

3.57, 23 h, 50%

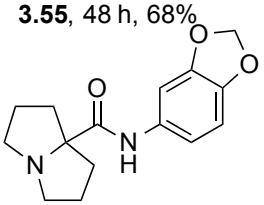

3.58, 25 h, 49%

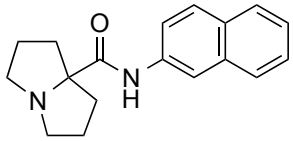

3.59, 23 h, 41%

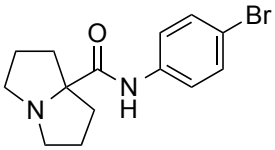

3.60, 23 h, 30%

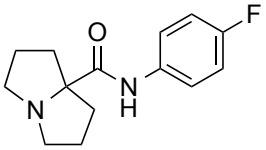

3.61, 22 h, 41%

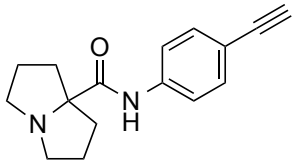

3.62, 17 h, 18%

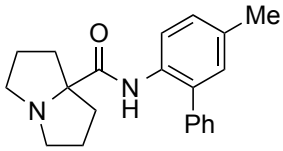

3.63, 18 h, 63%

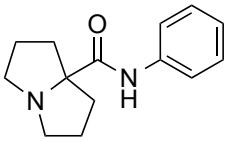

3.32, 18 h, 46%

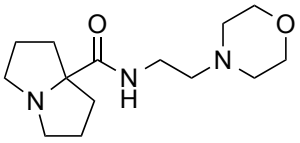

3.64, 23 h, 32%

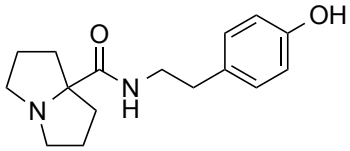

3.65, 17 h, 51%

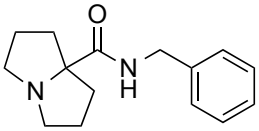

3.66, 17 h, 71%

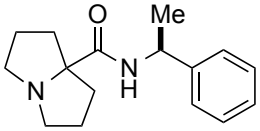

3.67, 24 h, 69%

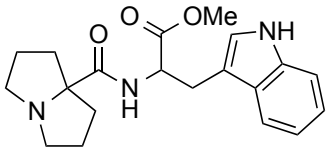

3.68, 16 h, 77%

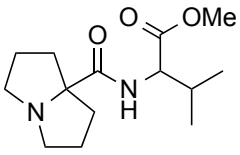

3.69, 16 h, 69%

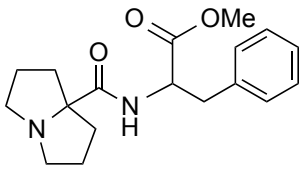

3.70, 23 h, 63%

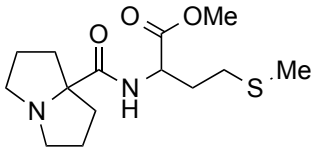

3.71, 24 h, 63%

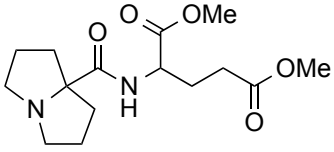

3.72, 16 h, 51%

Scheme 40: Scope of isonitriles for the construction of *7a*-substituted pyrrolizidine carboxamides.

Unfortunately, the isocyanoacetates suffered from complete racemization under the reaction conditions which is known to be a common issue in other similar transformations such as the *Ugi* reaction.[129] Due to the two electron withdrawing groups, the α-CH has a moderate acidity (pK_a = 9–11) and can be easily deprotonated by weak bases (Scheme 41). Mechanistically, the racemization can occur directly on the isocyanoacetates by enolization (**A**) or during the reaction (**B**). In the latter, racemization occurs after formation of the nitrilium ion **3.76** by attack of the isonitrile on an iminium ion and during oxazole formation **3.77**. The oxazole formation is reversible so that the racemic isocyanoacetate is obtained in the end. To investigate whether racemization potentially takes place before the reaction, we subjected optically pure isonitrile **3.80** to the reaction conditions without pyrroline **3.21** and heated it for 24 h under reflux (Scheme 42). Chiral HPLC revealed that complete racemization occurs already on the isonitrile precursors. It can be concluded that full racemization occurs even before product formation. Isonitrile **3.52**, however, is configurationally stable and pyrrolizidine **3.67** is observed in optically pure form.[23]

Limitations of the scope displayed isonitriles with strong electron withdrawing substituents such as nitro- or CF_3-groups.

[23] Isonitrile **3.52** has a drastically reduced α-CH acidity, due to lack of the ester group.

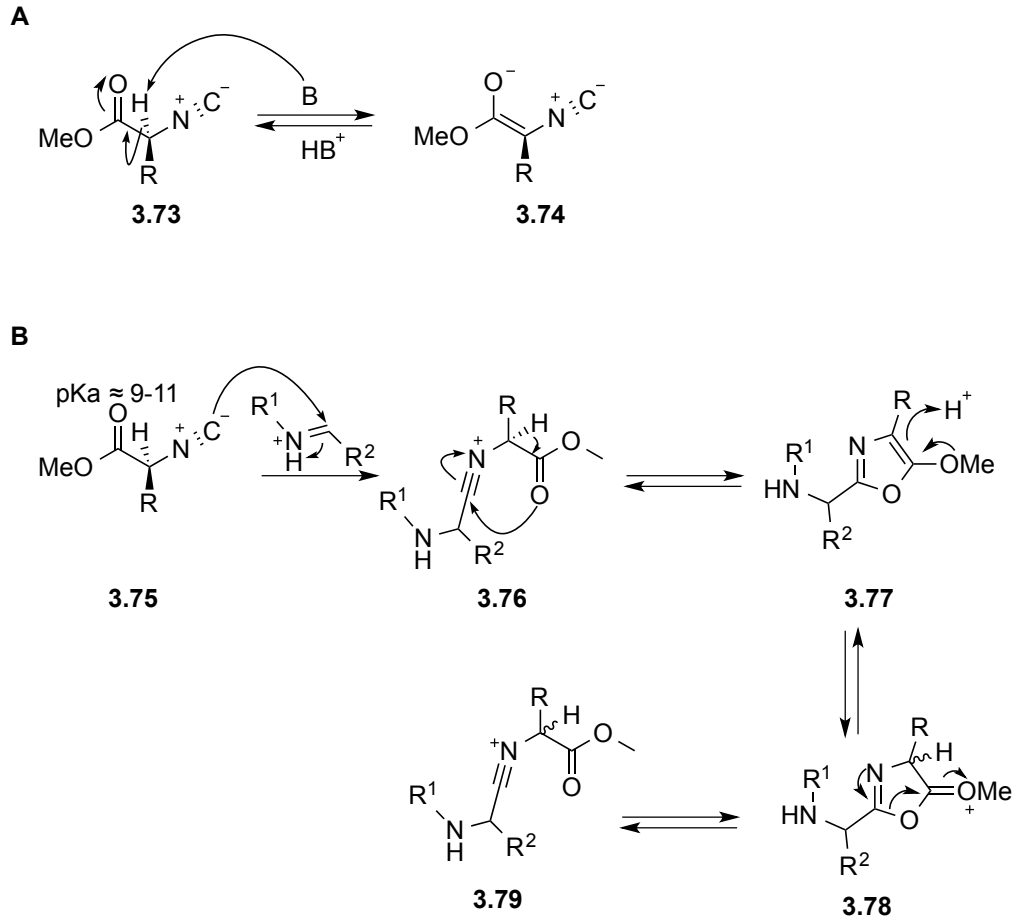

Scheme 41: Two mechanisms for the racemization of isocyanoacetates substrates.

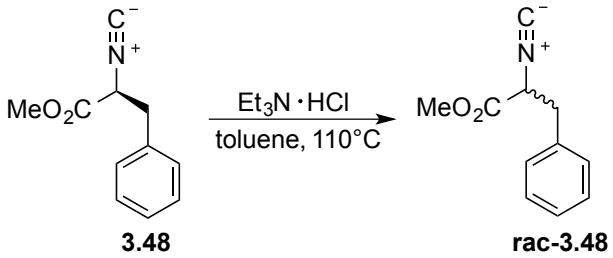

Scheme 42: Racemization of isocyanoacetate **3.48.** Racemization already takes place without addition of the pyrroline.

3.7 Mechanistic investigations

Mechanistically, the reaction can proceed *via* several pathways, of which two are shown in Scheme 43. Pathway **A** starts with protonation of the pyrroline to the corresponding iminium ion **3.80** and subsequent attack of the isonitrile resulting in nitrilium ion **3.81**. This intermediate could be intramolecularly trapped by the primary alcohol to give Spiro-intermediate **3.82**. To proceed to the pyrrolizidine, intermediate **3.82** needs to be opened by the pyrrolidine nitrogen on the C-O-bond of the imidate. Another possible mechanistic pathway involves protonation of the

alcohol (to **3.83**) followed by elimination of water to pyrrolizidinium salt **3.84**. The isonitrile can then proceed *via* nucleophilic attack on pyrrolizidinium ions, as has been shown previously with cyanide.[130,131] The resulting nitrilium ion **3.85** can be converted to the amide with water that was liberated earlier in the sequence. Both mechanisms involve certain unusual transformations. Whereas pathway **A** requires a HOMO-LUMO interaction of the N lone-pair and the σ*-orbital of the C-O bond in intermediate **3.82** for a successful outcome of the intramolecular reaction, pathway **B** involves formation of the highly reactive intermediate **3.84** with loss of water.

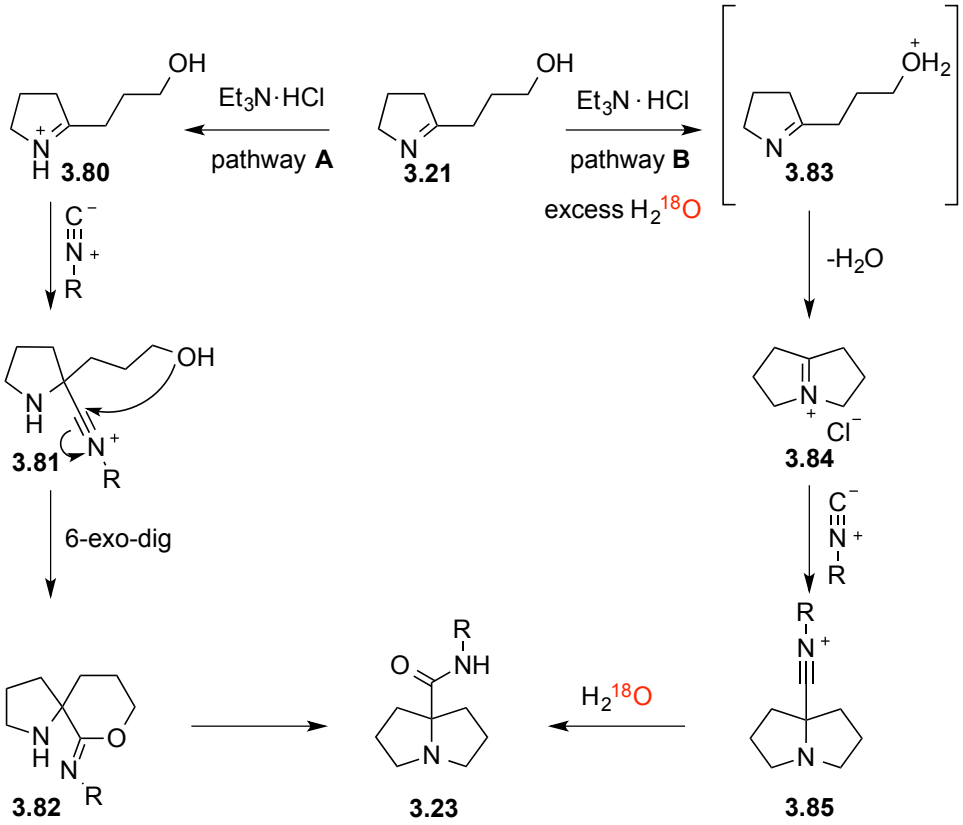

Scheme 43: Two possible mechanistic pathways for the formation of *7a*-substituted pyrrolizidines.

To investigate whether one of the two mechanisms applies to our reaction we performed a series of stable isotope labeling experiments and mass spectrometric detection. Key feature of our analysis is the performance of our reaction in presence of excess ^{18}O-labeled water. Following pathway **B**, incorporation of $H_2{}^{18}O$ would be obtained by hydrolysis of nitrilium ion **3.83**. On the other hand, following pathway **A**, the amide bond is formed intramolecularly thus excluding incorporation of external water. The reaction was performed using 10 equiv. of ^{18}O-labeled water under the normal reaction conditions. The product was purified and analyzed by HR-MS (ESI) (Scheme 44).

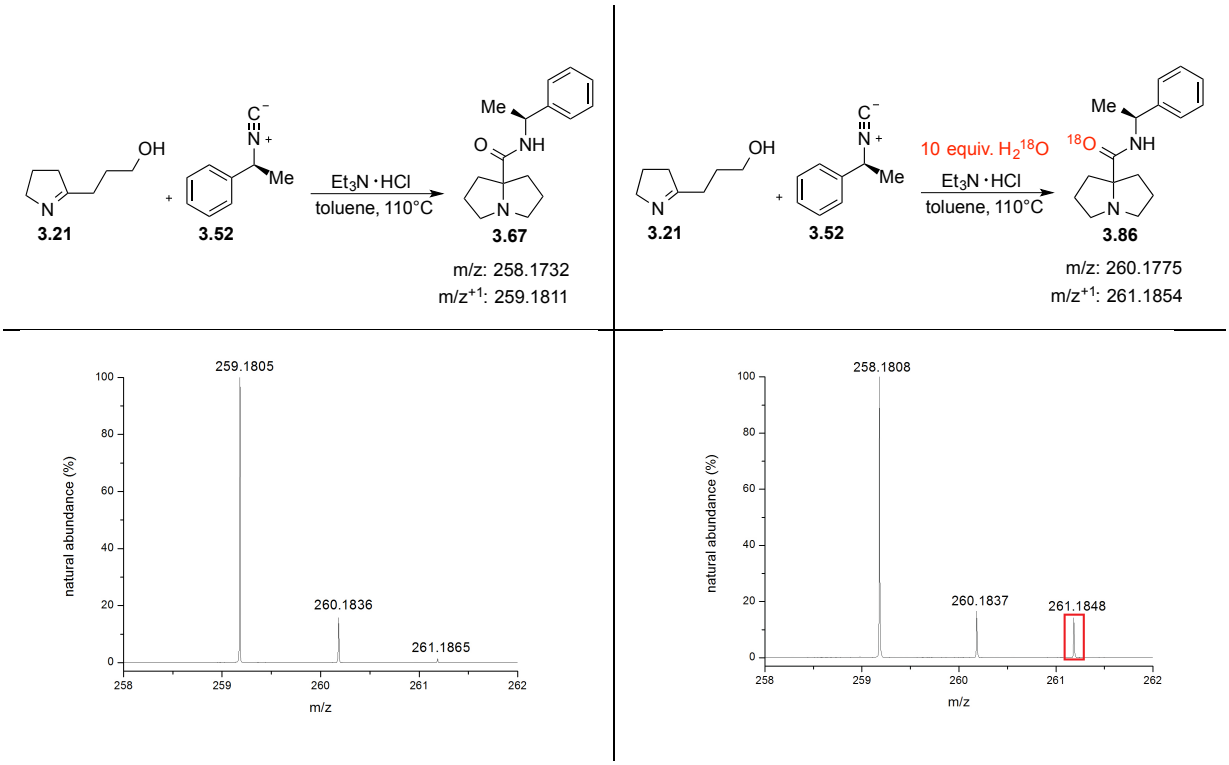

Scheme 44: Isotope incorporation experiments.

The mass spectra show an enhanced isotope peak of 261.18, which corresponds to a ~13% increased isotope peak of the ^{18}O-labeled derivative (Scheme 44). This indicates that the reaction more likely proceeds *via* pathway **B** involving pyrrolizidinium ion formation. This finding is supported by earlier reports describing the formation of stable pyrrolizidinium salts, although from different precursors.[130-132]

To further prove this hypothesis, we designed a number of control experiments that primarily pursued the goal of isolation of the pyrrolizidine salt **3.84** or its reduced form. In the first experiment, we reacted imine **3.21** under the reaction conditions of our pyrrolizidine formation reaction (Scheme 45). Subsequently, we added lithium aluminum hydride to potentially isolate the corresponding pyrrolizidine **3.87**. Unfortunately, the reaction only resulted in a complex mixture, which indicated towards a decomposition of the starting material under these conditions.

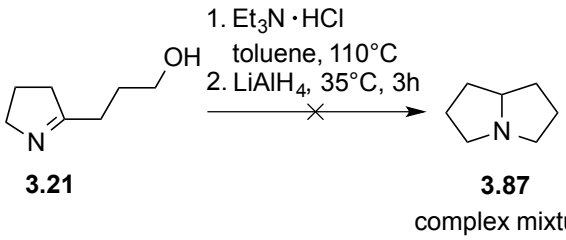

Scheme 45: Attempted formation of the pyrrolizidinium salt followed by reduction.

Further we attempted to isolate pyrrolizidinium salt **3.88** by subjection to the reaction conditions followed by NMR analysis (Scheme 46). The proton NMR showed exclusively the presence of starting material and not cyclized product in the mixture.

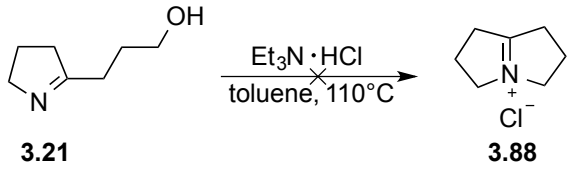

3.21 **3.88**

Scheme 46: Attempted isolation of pyrrolizidinium salt **3.88**.

Another experiment to discriminate between pathway **A** and **B** is the isotopic labeling of pyrroline **3.21** with an ^{18}O-isotope to give pyrroline **3.89** (Scheme 47). Pyrroline **3.89** would be used as a normal substrate in the reaction, but the reaction would be carried out in the presence of unlabeled water (e.g. 10 equiv.). Following pathway **A** would result in a 100% incorporation of ^{18}O into the product, because the oxygen never leaves the substrate. In pathway **B**, however, water is released during the mechanism, which later re-attacks on intermediate **3.85**. When the reaction is performed in the presence of unlabeled water we would observe a mixture of isotopes of the product.

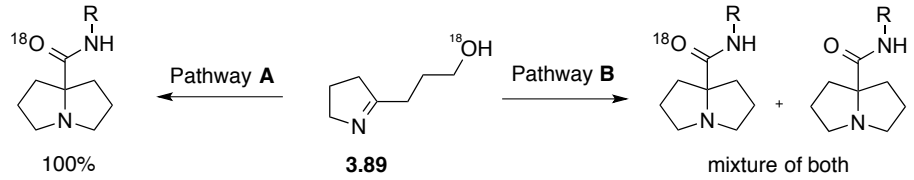

100% **3.89** mixture of both

Scheme 47: Isotopic discrimination between pathway A and B with isotopically labeled pyrroline **3.89**.

We assumed that the ^{18}O-labeled pyrroline **3.89** could be synthesized by mesylation of pyrroline **3.21** *in situ*, followed by addition of ^{18}O-labeled water. The heavy water could substitute the mesylated hydroxyl group to give isotopically labeled **3.89** (Scheme 48).

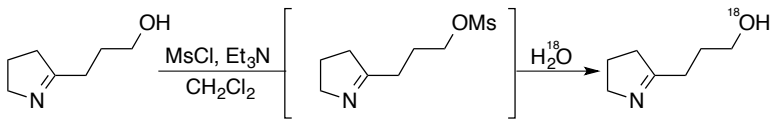

3.21 **3.90** **3.89**

Scheme 48: Planned synthesis of ^{18}O-labeled pyrroline.

We subjected pyrroline **3.21** with freshly distilled MsCl to form mesylated pyrroline **3.90** (Table 6). To see if the reaction led to the desired outcome without using expensive ^{18}O-labeled water we performed the quenching with normal water. We started by addition of MsCl at 0 °C,

stirred for 30 min at 0 °C and then warmed the reaction mixture to room temperature. The crude NMR of the reaction mixture was very complex, even though no water was added at this point. In the next experiment, we lowered the temperature to –20 °C and quenched with water after stirring for 30 min. The crude NMR revealed the presence of a pyrrolizidinium salt **a** and the pyrroline **b**, although it was not clear whether the pyrroline was unreacted starting material or resulted from replacement of the mesyl-group by water. Encouraged by this result we wanted to increase the product ratio in favor of the pyrroline **b**. We assumed an improvement would be to lower the freezing point of the aqueous solution so that it does not freeze the moment when it is added to the reaction mixture. We used a 4 N $CaCl_2$ solution and the more nucleophilic KOH (20%) solution. For both cases we observed formation of the pyrrolizidinium salt and only minor amounts of the pyrroline. Attempts to isolate the pyrroline were not successful.

Table 6: Initial experiments towards isotope incorporation.

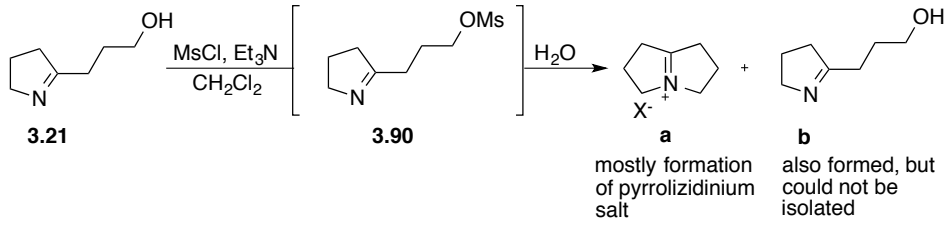

Entry	Conditions	**a** : **b**
1	0 °C to RT	Complex mixture
2	-20 °C, quenched with H_2O	2.6:1
3	-20 °C, quenched with $CaCl_2$ (4N)/MeCN, 4 h	2.8:1
4	-20 °C, quenched with KOH (20%)/MeCN, 2 h	Complex mixture
5	-20 °C, quenched with KOH (20%)/MeCN, 5 min	1:0

3.8 Other related transformations

3.8.1 Pyrrolidine synthesis

Extending this method to pyrroline **3.91** carrying a tertiary hydroxy group on the side chain, pyrrolidine derivatives **3.92** and **3.93** were obtained as a 2.1:1 mixture of prenylated pyrrolidine and its Δ3,4-isomer, respectively, instead of pyrrolizidine formation (Scheme 49).

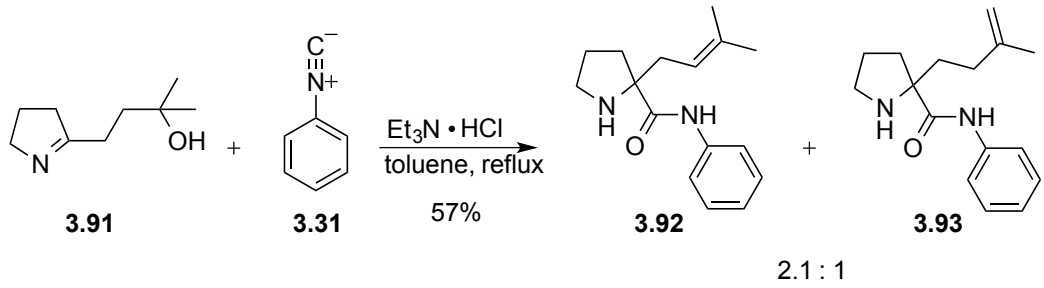

Scheme 49: Reaction of pyrroline **3.91** leads to pyrrolidine formation.

Mechanistically, this transformation could proceed similar to the formation of pyrrolizidines by an intramolecular mechanism involving an imidate intermediate **3.96** (pathway **A**), or by elimination of water and hydrolysis of nitrilium ions **3.98** and **3.99** (pathway **B**) (Scheme 50). Pathway **A** would be facilitated by a *Thorpe-Ingold* effect of intermediate **3.97**. To investigate the mechanism we applied the previous conditions and performed the reaction with 10 equivalents ^{18}O-labeled water. The ^{18}O-isotope was only enhanced by 0.1%. This strongly indicates for pathway **A**, as for pathway **B** we would expect a higher ^{18}O-abundance caused hydrolysis in the last step.

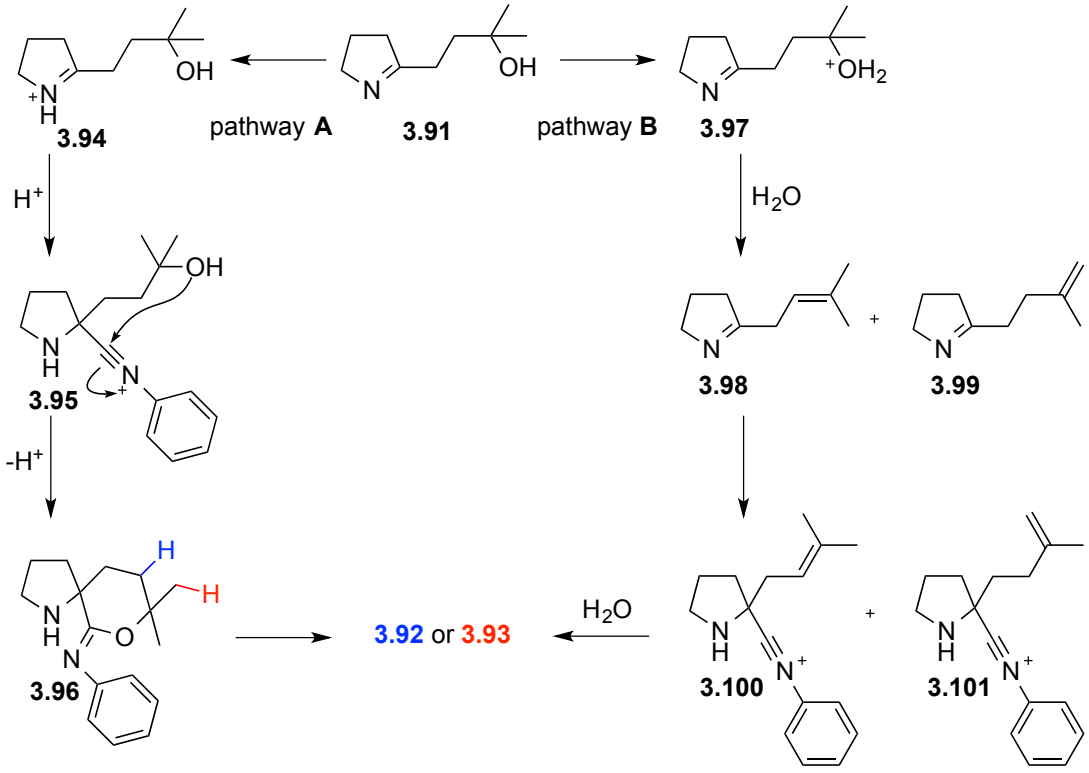

Scheme 50: Two mechanisms for the formation of pyrrolidines from pyrrolines.

Further, we tried to isomerize the double bond of isomer **3.93** to the thermodynamically more stable isomer **3.92**. We performed NMR-experiments in deuterated solvents using dimethyl terephthalate as an internal standard. The results are shown in Table 7. First, we attempted the isomerization with *p*-toluene sulfonic acid, a common reagent for the isomerization of double bonds.[133,134] At stoichiometric amounts of acid in benzene at 60 °C we observed decomposition of isomer **3.93** but no isomerization. In methanol under similar conditions no reaction occurred. When the temperature was raised and toluene was used for a longer reaction time, we observed decomposition of both isomers. Changing to catalytic amounts of acid only led to decomposition of isomer **3.93**. Then we changed the isomerization reagent to $RhCl_3$[135] and observed similar results as with the *p*-toluene sulfonic acid, as that no successful isomerization was observed.

Table 7: Isomerization attempts of **3.93** to **3.96**.

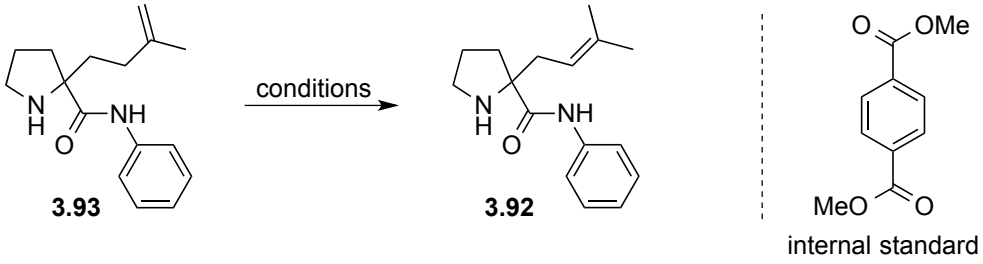

Entry	Reagent	Solvent	T	t	Heating	Observation
1	*p*TSA (4.0 equiv)	Benzene-*d*6	60	1 h	Δ	**3.93** decomposed
2	*p*TSA (4.0 equiv)	CD_3OD	60	24 h	Δ	No reaction
3	*p*TSA (2.2 equiv)	CD_3OD	40	24 h	Δ	No reaction
4	*p*TSA (1.0 equiv)	Toluene-*d*8	110	5 d	Δ	Decomposition
5	*p*TSA (0.05 equiv)	Toluene-*d*8	110	3 d	Δ	**3.93** decomposed
6	$RhCl_3$ (1.2 equiv.)	CD_3OD	60	24 h	Δ	No reaction
7	$RhCl_3$ (0.5 equiv.)	CD_3OD	100	1 h	μw	Decomposition
8	$RhCl_3 \cdot H_2O$	CD_3OD	65	1 d	Δ	**3.93** decomposed

3.8.2 Indolizidine synthesis

Next, we attempted an extension of our method to the related indolizidine alkaloids. This group of 5/6-fused cyclic alkaloids represents a large class of natural products and biologically relevant lead structures.[136,137]

For their synthesis we first had to prepare the imine precursor. We envisioned the synthesis of two precursors: 1) tetrahydropyridine **3.102** with three CH_2 units on the side chain and 2) pyrroline **3.103** with four CH_2 units on the side chain (Scheme 51). For the first precursor we wanted to start from 6-methyl-2,3,4,5-tetrahydropyridine by deprotonating and opening of ethylene oxide according to the synthesis of **3.21**. Under various conditions, using Lewis acids, and dif-

ferent bases, only very complex reaction mixtures were obtained. We then proceeded to the synthesis of pyrroline **3.103**, which was prepared by subjection to LDA, oxetane and boron trifluoride diethyl etherate, albeit in low yield.

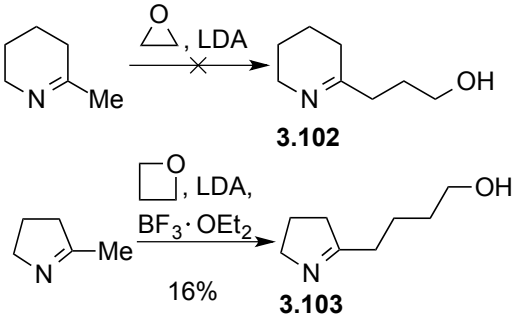

Scheme 51: Synthesis of imine precursor.

We then subjected pyrroline **3.103** to isonitrile **3.46** under the reaction conditions previously developed (Scheme 52). The indolizidine could be isolated in low yield and with minor contaminations.[24] Although the desired product was formed, we decided not to proceed further with the investigation of indolizidines, because of the low yield and difficulty with the preparation of the starting material.

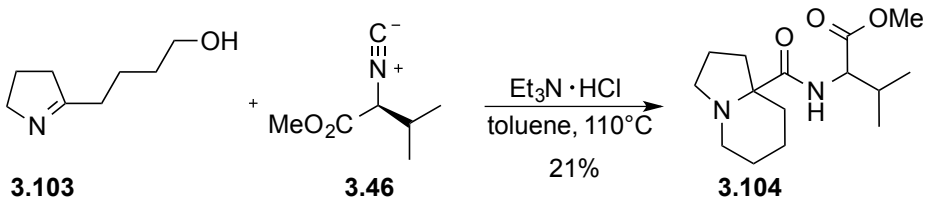

Scheme 52: Formation of indolizidine **3.104** with pyrroline **3.103**.

3.9 Further transformations

As an extension of the pyrrolizidine formation reaction, we were able to further functionalize pyrrolizidine **3.32** (Scheme 53). The first transformation is the oxidation of the pyrrolizidine core at the 3-position according to a procedure developed by *Schäfer* and co-workers using benzyltriethylammonium permanganate.[138] In this publication, the authors describe the oxidation of simple long-chain alkyl amines as well as *N*,*N*-alkylanilines. A direct oxidation at the 3-position on the pyrrolizidine core has not been previously described and makes our report the first of its kind. As a mild oxidant, benzyltriethylammonium permanganate delivers the 3H-pyrrolizin-3-one product **3.105** in good yield, allowing rapid access to these biologically relevant oxidized alkaloids.[114,115]

[24] Analysis by NMR and HR-MS (ESI).

Further, the tertiary nitrogen can be oxidized to furnish the corresponding *N*-oxide **3.106**. Functionalization based on the *N*-oxide derivative by *Polonovski-Portier* or *Cope* elimination protocols showed no reactivity of **3.106**. This might be due to the stability of the pyrrolizidine core that could have to be transferred to the strained unsaturated form in both reactions. In addition, in the case of a *Cope* elimination, the proton on the 2-position might be intramolecularly inaccessible for the nitroxide.

Further, we reduced the amide functionality of **3.32** with Red-Al® to the secondary amine in quantitative yield.[111] As highlighted in the introduction of this chapter, these structures have been identified to show binding affinities for the central muscarinic cholinergic receptor and therefore represent lead structures for the treatment of neurodegenerative diseases.[139]

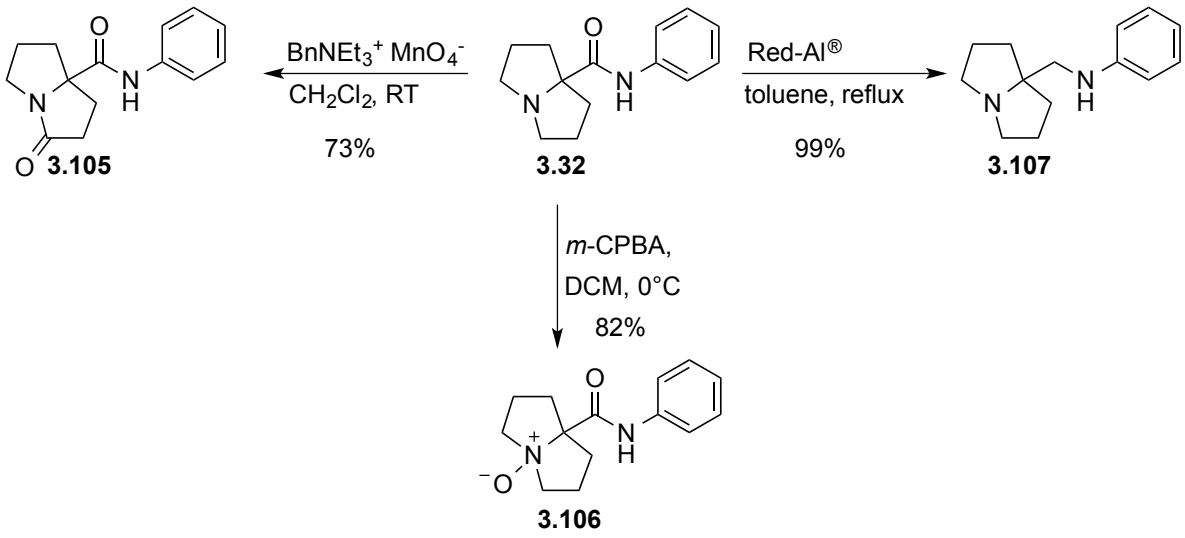

Scheme 53: Further functionalization of pyrrolizidine **3.32**.

3.10 The NMR that did not match

During studies towards the synthesis of **3.107** we discovered a mismatch of the NMR spectroscopy data between two different experiments, which actually should result in the same product. In one experiment we purified **3.107** by column chromatography using a CH_2Cl_2/MeOH eluent, in the other experiment no chromatographic purification was necessary after extraction with NaOH/Et_2O. When we compared the analytical data of the two experiments we found that, the proton NMR spectrum of the first experiment differed significantly from the second experiment in that the protons next to the amine were shifted downfield by 0.5 ppm. In addition, the CH_2-protons next to the aniline nitrogen were also shifted. After some experimentation we found that when the non-chromatographed sample was subjected to a CO_2 stream in deuterated methanol the resulting NMR spectrum corresponded to the sample that had been chromatographed (Scheme 55). In the ^{13}C-NMR spectra differences were also visible in the change of some of the peaks and the appearance of a new peak at 161.6 ppm (Scheme 56). From this we concluded that diamine **3.107** reacts with CO_2 (Scheme 54). We also found that this process is reversible because when the solution previously charged with CO_2 was heated to 65 °C for 15 min we obtained back the starting material before CO_2 treatment. CO_2 binding of amines generally occurs in two ways, either as a carbamate **3.108** or by bicarbonate formation (**3.109**) when water is present. The ^{13}C-chemical shift of a carbamate and bicarbonate are very similar, so that from the NMR analysis at this stage it cannot be determined in which form CO_2 is fixed by **3.107**. Our investigation on the CO_2-binding properties of pyrrolizidine diamines will be described in the next chapter.

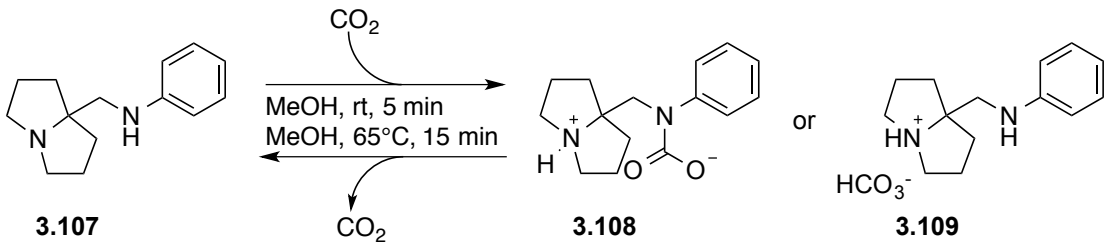

Scheme 54: Pyrrolizidine **3.107** reacts reversibly with CO_2.

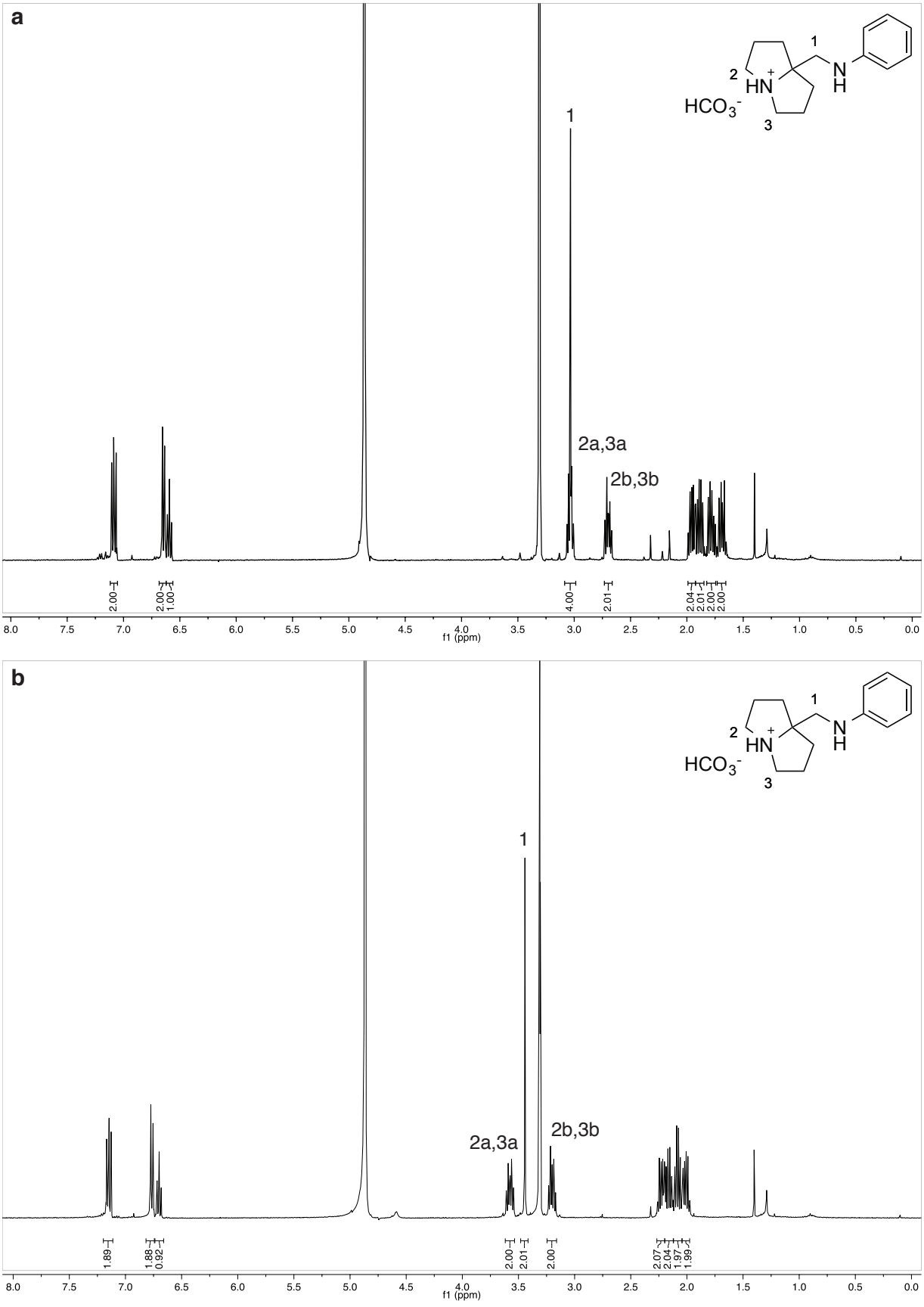

Scheme 55: ^{1}H-NMR spectra of pyrroline **3.107**. **a)** Before CO_2-treatment. **b)** After CO_2-treatment, with the bicarbonate salt form shown.

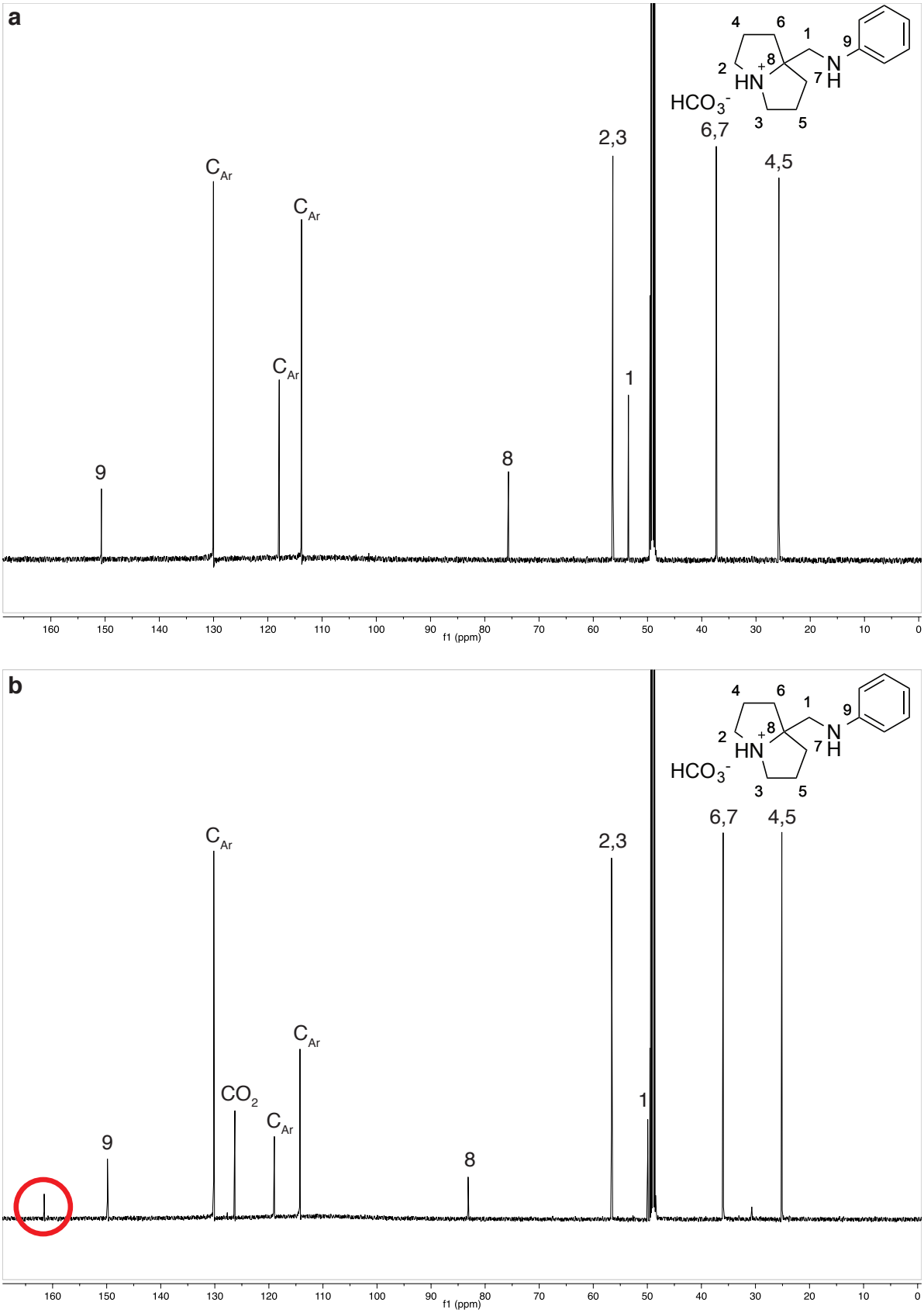

Scheme 56: ^{13}C-NMR spectra of pyrroline **3.107**. **a)** Before CO_2-treatment. **b)** After CO_2-treatment, with the bicarbonate salt form shown. The additional ^{13}C-signal at 126.3 ppm is CO_2 dissolved in CD_3OD.

3.11 Conclusion

This chapter described our efforts towards the construction of *7a*-substituted pyrrolizidines. Due to their broad diversity and their crucial role in plants and animals pyrrolizidine alkaloids have been relevant in medicine and biology, and were also an interesting target for chemical synthesis at the same time. However, very few methods for the construction of *7a*-substituted pyrrolizidines have been reported and there was no previous example that allowed for the direct preparation of *7a*-substituted pyrrolizidine carboxamides.

We have demonstrated that these structures can be synthesized in a single step starting from a pyrroline and with various isonitriles. The reaction was robust and tolerated a wide scope of isonitriles, affording a diverse variety of pyrrolizidine alkaloids within few synthetic operations. The products were further functionalized by oxidation and reduction protocols, and were able to extend the reaction principle using modified imine precursors for the construction of pyrrolidines and indolizidines. And finally, the diamine resulting from reduction of the amide group reacted with CO_2 in a reversible manner. The binding properties of CO_2 for this and related pyrrolizidines are investigated in the next chapter.

4 Application of Pyrrolizidines in Carbon Dioxide Capture

4.1 Introduction

The drastic increase of the global atmospheric and oceanic temperature since the beginning of the industrial revolution, will potentially lead to severe consequence for the environment and human beings.[140] In the northern hemisphere, the last three decades have been the warmest since 1400 years (Figure 40, a). The largest contribution to global warming is caused by atmospheric CO_2[140] that increased by almost one third in the last 40 years and shows a clear correlation between CO_2 emission and increase in global temperature (Figure 40, b). Major reason for the drastically raised CO_2 level is the combustion of fossil fuels such as coal, oil and natural gas.[141] On the other hand, tropical forests and other woods and green surfaces are cleared,[142] which leads to an even stronger imbalance in our atmosphere. The development of sustainable alternatives is a strongly developing field, however, many processes and applications still depend on the use of fossil fuels.[143] On the other hand, CO_2 is an important feedstock, which can be used directly in applications such as fire extinguishers, solvent for extraction of substances and fragrances or as a cleaner of electronics.[144] These applications only provide a short-term removal of CO_2 from the air, but no reduction of the global CO_2-levels. More effective in this respect is the conversion of CO_2 into products with added value thereby utilizing CO_2 as a C1-building block for chemical synthesis.[145]

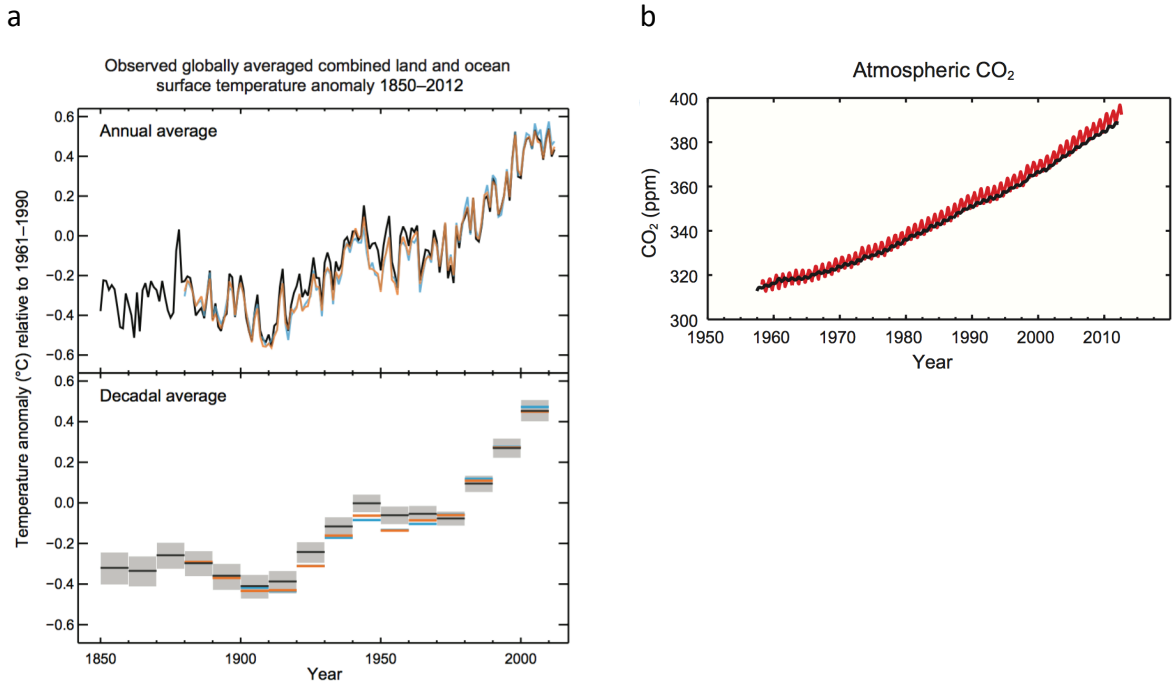

Figure 40: a) Temperature anomaly in land and ocean (1850-2012) by annual and decadal average. **b)** Increase of atmospheric CO_2 over the last three decades. Source: IPCC report 2013.[140]

4.1.1 Capture of CO_2

The starting point for all utilization applications is the isolation of CO_2 from the atmosphere (or a flue gas stream) also termed Carbon Capture and Storage (CCS). Among several techniques available for this process,[146] the major industrial technology for the capture of CO_2 from gas streams is the use of chemical absorbents. The most efficient absorbents are amine solutions that can consist of only one component but can also be combined with each other to form mixtures. A general flow chart of this process is depicted in Scheme 57. The CO_2-enriched gas enters the reactor containing the amine solution, most of the time in a solution of water. The CO_2 content of the gas is captured by the amine absorbent and the remaining gas is released to the atmosphere or used for further purposes. The amine solution, now enriched with CO_2, is transferred *via* a heat exchanger to the stripper, thereby being warmed to some extent. In the stripper, the amine solution is heated up to 120 °C to release the captured CO_2 which is cooled down and exits the plant for further purposes. Passing the heat exchanger and one further amine cooler lowers the temperature of the hot amine solution. The solution is finally transferred back to the amine reactor to reenter the absorption/desorption cycle.

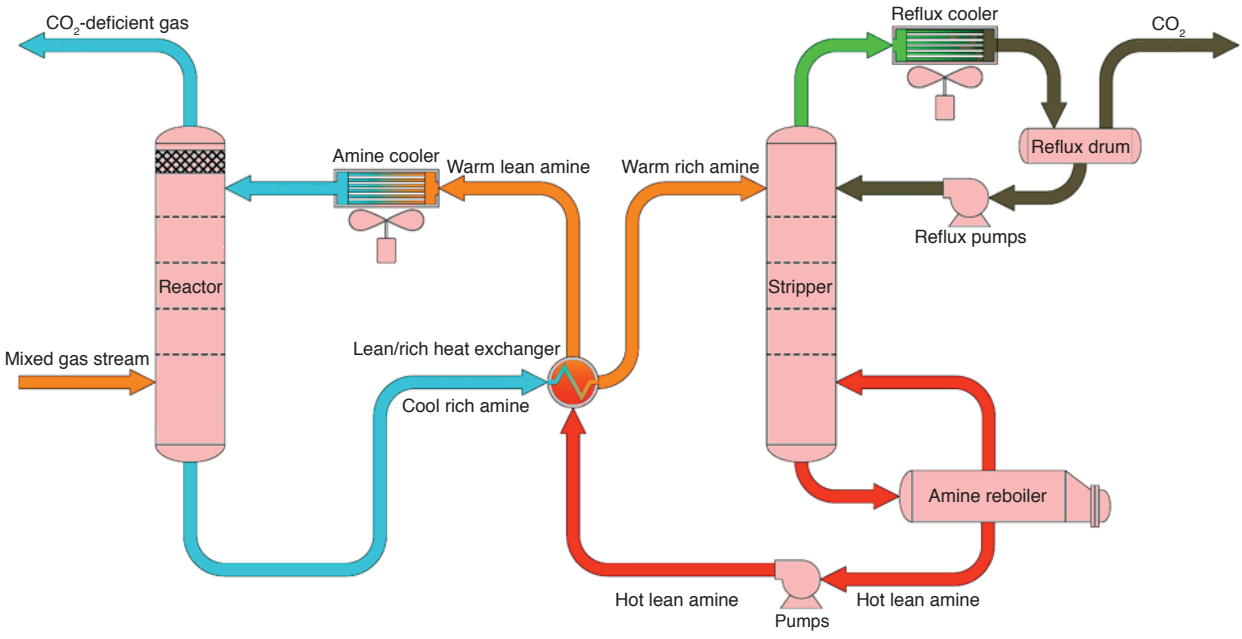

Scheme 57: Representation of an amine plant used for the removal of CO_2 from gas mixtures or flue gas.[25]

The process is widely established and serves for the purification of flue gas, natural gas or gas streams for the chemical industry. Main drawback of this process is the degradation of the amine solution resulting in solvent loss, corrosion and generation of volatile degradation com-

[25] http://www.jouleprocessing.com/products/treating/amine-plants (2.12.2016)

pounds.[147,148] Further, high temperatures are usually required for removal of CO_2 from the amine solution leading to immense energy costs and make this system inapplicable for the purification of flue gas from coal-fired power plants. It has been estimated that a coal plant needs to take a 81% increase of its electricity costs to capture 90% of its flue gas CO_2 using a standard amine absorbent.[149] Thus, the high energy costs prevent this process from being used for the removal of CO_2 from the flue gas of its biggest producers.

4.1.2 Amines for CO_2-capture

The amines used for the capture of CO_2 are usually simple, linear amines such as (methylamino)propylamine (MAPA) or alcoholamines such as aminoethylethanolamine (AEEA), diethanolamine (DEA) or the most common CO_2-absorbent monoethanolamine (MEA) (Figure 41). Some amines are also branched such as triethanolamine (TEA) or cyclic such as piperazine (PZ). Besides the already established absorbents, there have been a number of new compounds with different binding concepts developed. These structures involve heterocycles such as melamine[150], ionic liquids including pyridines[151], or the use of amidine bases in combination with alcohols.[152] The substances employ different mechanisms for the formation of the CO_2-adducts. In general, CO_2 can be fixed by amines in two ways either as a carbamate or as a bicarbonate salt (Scheme 58). For the first binding mode with primary amines, two molecules of amine absorbent are required to fix one molecule CO_2. This is based on the fact that one amine molecule binds CO_2 as a carbamate and the other acts as a base, together they form a counterion pair. When CO_2 is fixed as a bicarbonate salt, usually tertiary amines are employed in the presence of water. This sort of binding leads to a 1:1 stoichiometry requiring only one molecule of amine absorbent to capture one molecule of CO_2. However, because the binding is ionic, these absorbents do not always reach an equimolar uptake.

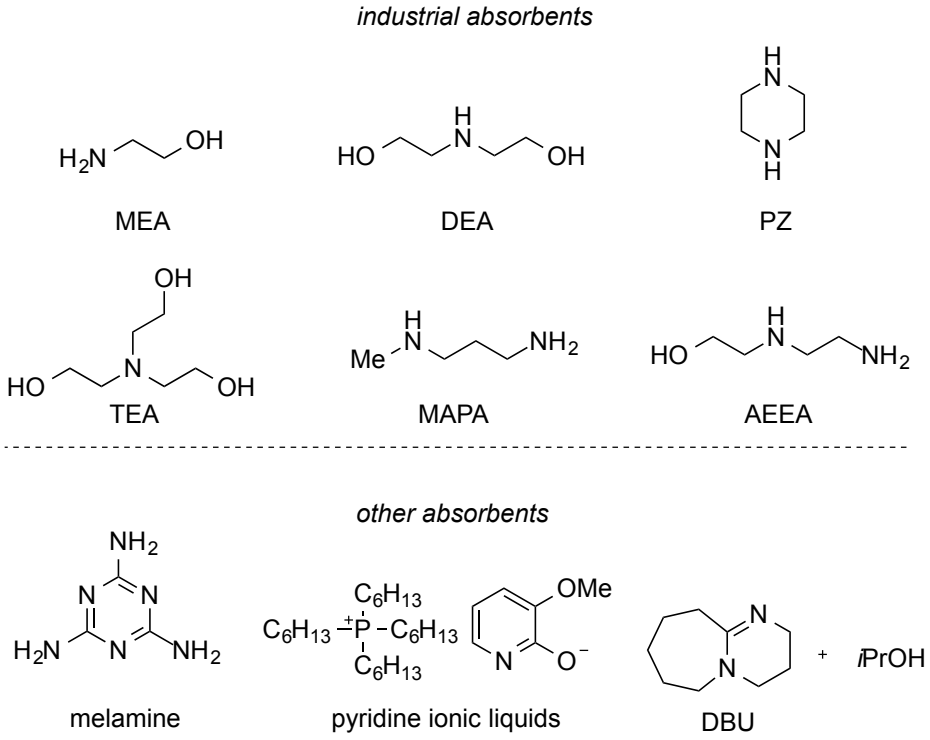

Figure 41: Industrially used absorbents and other absorbents for the capture of CO_2.

1. Carbamate formation:

monoamines: 2:1 stoichiometry

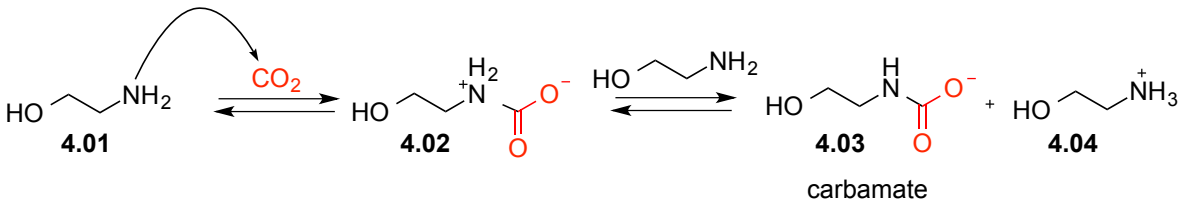

2. Bicarbonate formation:

tertiary amines: 1:1 stoichiometry

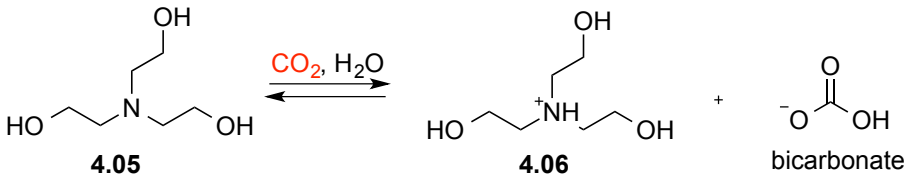

Scheme 58: CO_2-Binding modes by different classes of amine absorbents.

4.1.3 Pyrrolizidines for CO_2-capture

In the previous chapter we described the capture of CO_2 by pyrrolizidine diamine **3.107**. In principle, CO_2 can be bound by **3.107** in two ways, either as a carbamate or as a bicarbonate salt (Scheme 59).

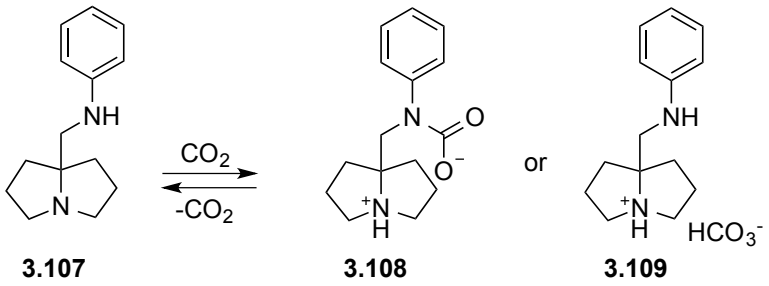

Scheme 59: Pyrrolizidine **3.107** can bind CO_2 by formation of a carbamate or a bicarbonate.

In the literature, the pyrrolizidine alkaloid temuline, isolated from the plant *Lolium temulentum*, has been reported to bind CO_2 in the carbamate form as has been confirmed by X-ray crystallography (Scheme 60).[153]

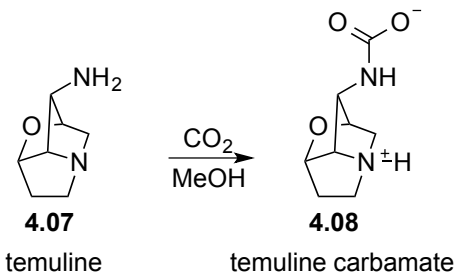

Scheme 60: Reaction of pyrrolizidine alkaloid temuline leads to carbamate **4.08**.

Pyrrolizidines such as the ones reported above provide a nucleophilic nitrogen and a basic amine, which both can assist each other in the fixation of CO_2. This would lead to a 1:1 stoichiometry by binding of one CO_2 unit per equivalent absorbent (Scheme 61). An additional advantage in comparison to conventional absorbents such as monoethanolamine is the three-dimensional architecture of the molecule provided by the pyrrolizidine backbone, generating a certain rigidity in the molecule. Besides the report on pyrrolizidine temuline, pyrrolizidines are completely unexplored for the capture of CO_2.

pyrrolizidine diamines: 1:1 stoichiometry

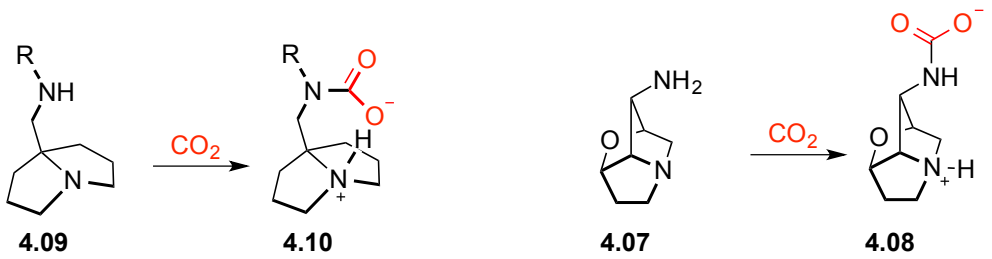

4.09 **4.10** **4.07** **4.08**

Scheme 61: Pyrrolizidines provide bifunctionality and a molecular architecture that might be beneficial for the capture of CO_2.

4.2 Project outline

This project takes up the finding of the previous chapter, where we discovered that compound **3.107** reacts with CO_2 in a reversible manner. Naturally, the question on the nature of the pyrrolizidine-CO_2 adduct arises. Further, the efficiency of the CO_2 uptake has not been investigated. We presumed that the three-dimensional architecture of the pyrrolizidine derivative with its pyrrolizidine backbone and the bended side-chain with a second amine could be beneficial for the CO_2 uptake. An additional feature could be that the two amine groups assist each other in the uptake process and may provide advantage compared to linear analogues.

Our first aim for this project was to synthesize derivatives of pyrrolizidine **3.107** with different substituents on the amine and with different CH_2-chain lengths. Further, we wanted to investigate to which extent and in which form these derivatives bind CO_2. An important parameter in this investigation was the reversibility of the CO_2-binding and the required energy for this process.

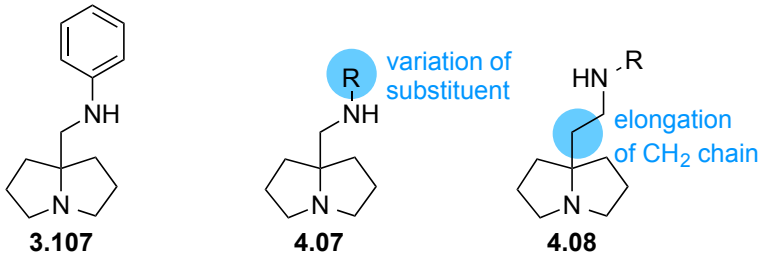

Figure 42: Modifications of pyrrolizidine absorbents.

4.3 Synthesis[26]

For the preparation of pyrrolizidine derivatives we chose to generally prepare compounds with one CH_2 group and two CH_2 groups on the *7a*-position. At this stage of the project we did not know if the distance between tertiary amine and the amine on the side chain would play any role. For this reason we prepared the primary amines **4.13** and **4.15** and the secondary amines **4.14** and **4.16** (Scheme 62). In addition, we wanted to synthesize anilines **4.17** and **3.107** on larger scale, to investigate if there was any difference in CO_2 uptake and the nature of binding in comparison to the primary and secondary derivatives. As an electron poor variant of **3.107**, we chose pyrrolizidine **4.18** carrying a strongly electron-deficient substituent on the aniline nitrogen.

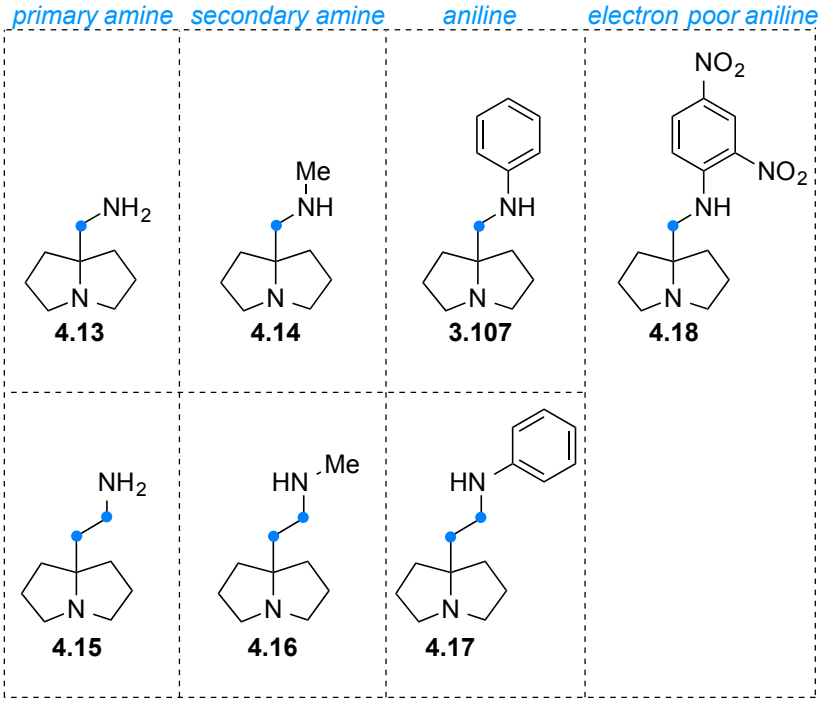

Scheme 62: Choice of derivatives for the evaluation of the CO_2 binding capacity.

For the preparation of the pyrrolizidine derivatives it was important that the synthetic route provides sufficient material for the CO_2 uptake experiments. In addition it is desirable to include as few purification steps as possible to demonstrate the applicability to industrial syntheses. For the diversification we decided to perform late-stage modifications on intermediates **4.13** and **4.15** (Scheme 63). These two intermediates can be prepared from ketone **4.19** by a literature known procedure.[117,120] The ketone can be prepared from the bulk chemical γ-butyrolactone.[154]

[26] The substances presented in this chapter were prepared by Jan Hanusch in the course of his master thesis under my supervision.

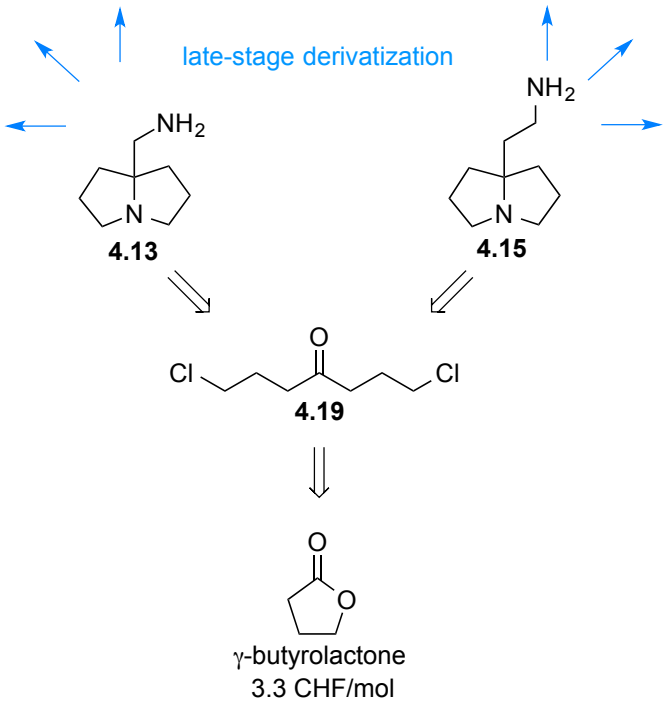

Scheme 63: Synthetic strategy for the preparation of pyrrolizidines.

We started with the synthesis of dichloroheptanone **4.19** from γ-butyrolactone after a protocol published by *Curtis* et al. (Scheme 64).[154] The cyclic lactone was subjected to a sodium methanolate solution and heated to 100 °C in a *Dean-Stark* reaction apparatus. Without isolation and purification, condensed product **4.20** is treated with HCl to furnish heptanone **4.19** in an overall yield of 68%. The reaction could be carried out at high substrate concentrations for the first step and no solvent for the second step, so that the reaction could be scaled up to 200 g with usual chemical synthesis equipment.

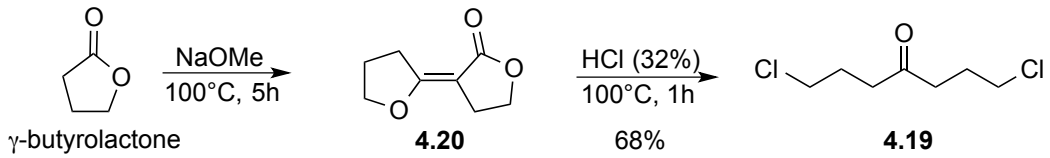

Scheme 64: Synthesis of heptanone **4.19** from γ-butyrolactone.

Synthesis of the first pyrrolizidine derivative **4.13** was performed using heptanone **4.19** (Scheme 65).[120] The ketone was reacted with aqueous ammonium hydroxide, ammonia gas and potassium cyanide. The resulting crude mixture was used in the next step without purification.[27] The mixture was reduced using lithium aluminum hydride followed by recrystallization of the corresponding hydrochloride salt. Following this procedure the by-product could be fully separated from the product.

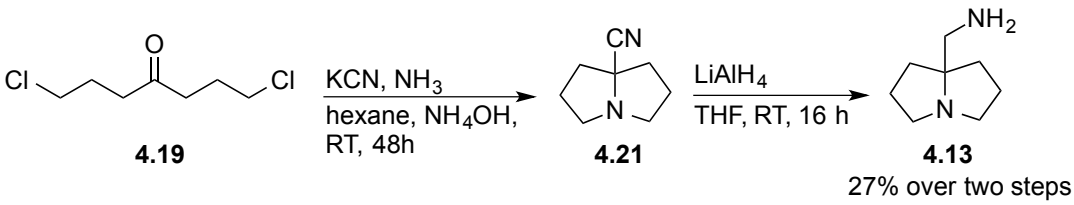

Scheme 65: Synthesis of the pyrrolizidine derivative **4.13**.

For the introduction of the methyl group we first formylated **4.13** with ethyl formate under basic conditions, followed by reduction of the formyl group using lithium aluminum hydride (Scheme 66).

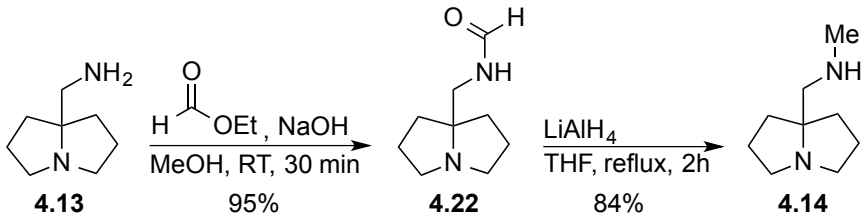

Scheme 66: Formylation of **4.13** followed by reduction provides methylated derivative **4.14.**

For the introduction of an electron-deficient substituent on the free amine of **4.13** we reacted the pyrrolizidine with *Sanger* reagent **4.23**. The reagent is used for peptide sequencing in that it is reacted with the amine group of a peptide. The resulting dinitrophenyl peptides are generally unstable under acid hydrolysis conditions and the terminal amino acid is released from the peptide.[155] In our case we benefited from the electron poor nature of the reagent, so that **4.13** can easily undergo displacement of the fluoride by nucleophilic aromatic substitution (Scheme 67). In contrast to the other pyrrolizidine derivatives carrying primary and secondary amines, the product could be purified by column chromatography and was isolated in 63% yield.

[27] The crude mixture contained the product and this pyrroline by-product as a 70:30 (product:by-product) mixture.

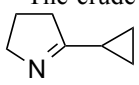

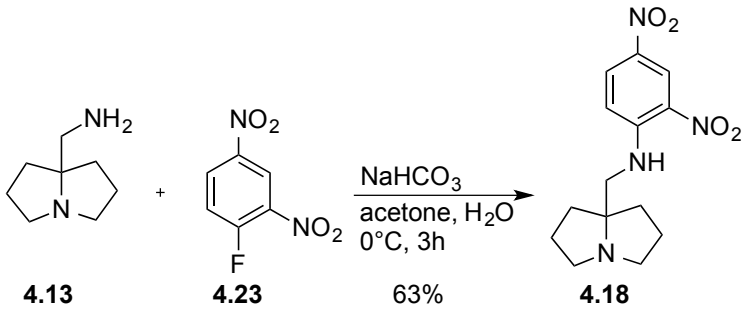

Scheme 67: Introduction of a 2,4-dinitrophenyl group using the *Sanger* reagent.

For the synthesis of the pyrrolizidine derivative carrying two CH_2-groups, we followed a literature known protocol starting from heptanone **4.19**.[120] The ketone was subjected to ammonia gas and treated with α-cyanoacetic acid (Scheme 68). The resulting nitrile **4.24** was reduced without purification to the corresponding amine in 25% over two steps.

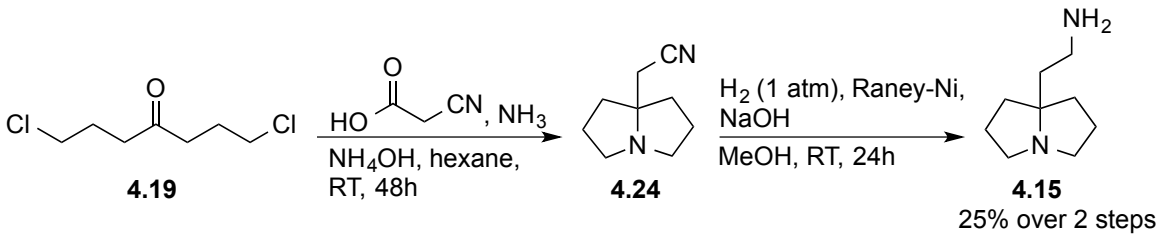

Scheme 68: Synthesis of pyrrolizidine derivative **4.15** from heptanone **4.19**.

The methylation of pyrrolizidine **4.15** was carried out analogous to the preparation of **4.14** by formylation and reduction (Scheme 69).

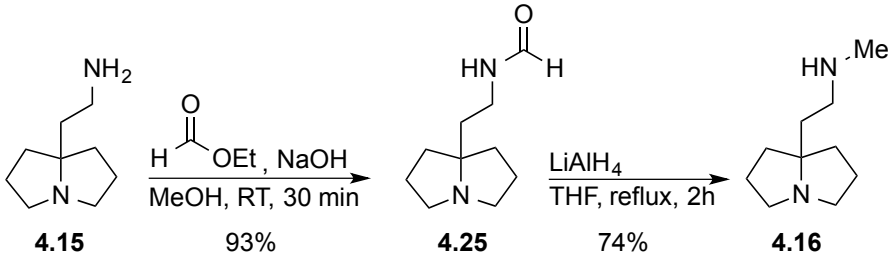

Scheme 69: Synthesis of methylated pyrrolizidine derivative **4.16** by formylation and reduction.

Next, we prepared the aniline derivatives **3.107** and **4.17** from pyrrolizidines **4.13** and **4.15** using a *Buchwald-Hartwig* coupling.[156] Under elevated temperatures the primary amines were reacted with chlorobenzene and the depicted precatalyst functionalized with the Brettphos ligand (Scheme 70).[157,158] For the preparation of derivative **4.17** a quantitative the yield was obtained. However, for derivative **3.107** the yield was significantly lower. This could be based on complexation of the formed diamine to the catalyst and thereby causing catalyst-deactivation. For derivative **3.107** the complex formed between the diamine and the palladium catalyst would en-

counter a 5-membered ring. On the other hand, with diamine **4.17** the complexation would involve formation of a 6-membered ring, which is less easily formed than a five membered ring. The difficulties obtained in the preparation of **3.107** highlight the power of our method established for the synthesis of *7a*-substituted pyrrolizidines, with which compound **3.107** was prepared in less steps and higher overall yield.[28]

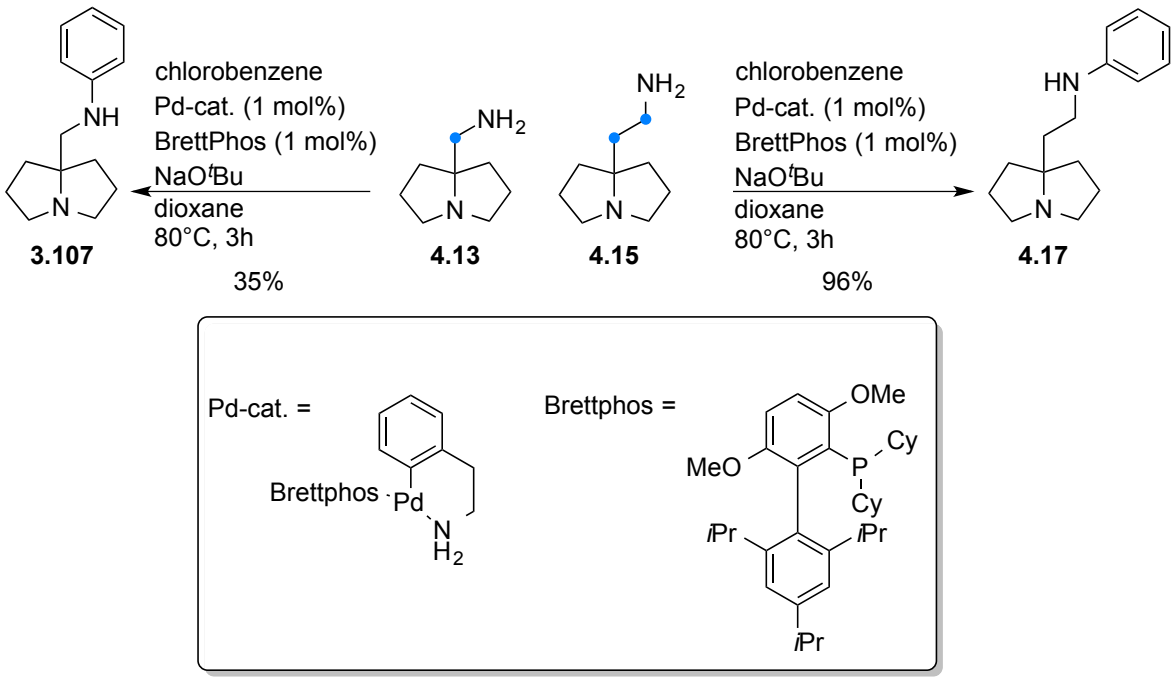

Scheme 70: *Buchwald-Hartwig* coupling of primary amines resulting in aniline derivatives **3.107** and **4.17**.

[28] As the amount of **3.107** prepared by *Buchwald-Hartwig* coupling was not sufficiently high, we used our method described in Chapter 3 for the preparation of the material.

4.4 CO_2-Capture

In the following section we report our studies on the CO_2-binding of the pyrrolizidine derivatives prepared in the previous section of this chapter. The CO_2-capture has been approached from different perspectives. Initial studies were devoted to NMR-analysis as it can give a preliminary indication if a substance is capable of binding CO_2. Further, we attempted the crystallization of the CO_2-adducts to analyze them by X-ray diffraction. Finally, for the quantification of the CO_2 uptake, we performed gravimetric experiments.

4.4.1 NMR-studies

With the first derivative **4.13** we performed NMR studies similar to the ones described in section 3.10. The amine was dissolved in CD_3OD and subjected to a CO_2 stream produced from dry ice until the solvent was almost evaporated. The residue was dissolved in CD_3OD and ^{1}H-NMR and ^{13}C-NMR analysis was performed. As observed earlier for pyrrolizidine **3.107** (section 3.10), a clear shift of ~0.5 ppm towards lower field was obtained for the protons (Figure 43).

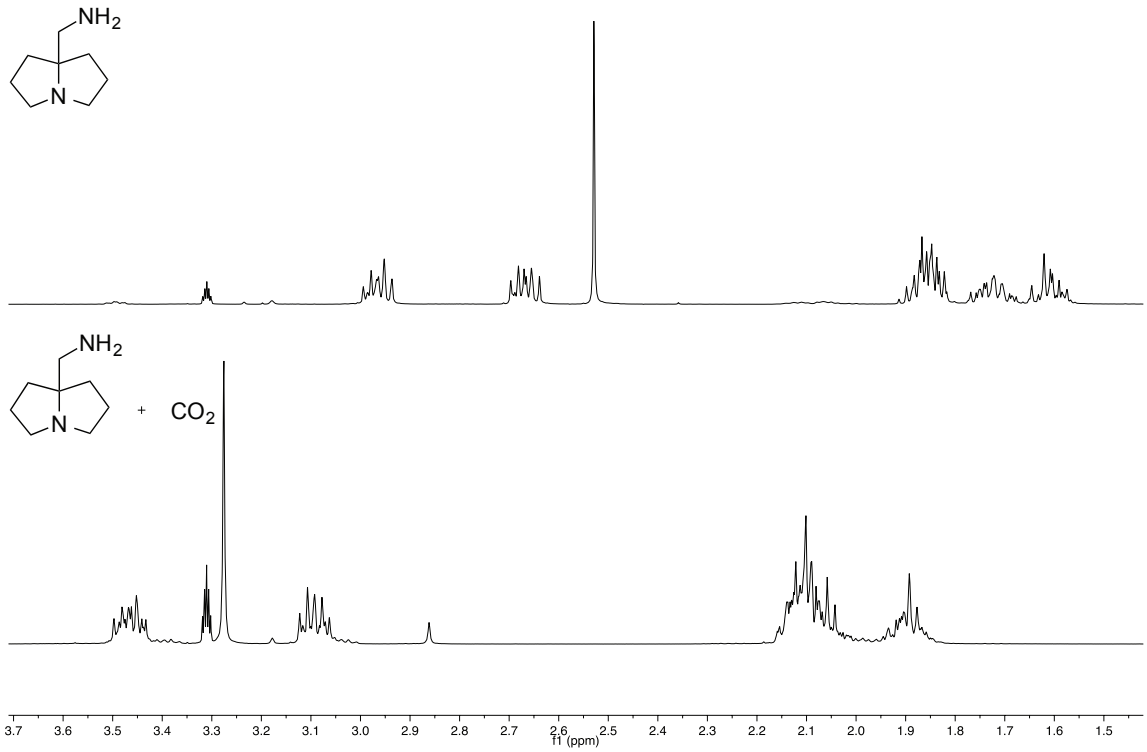

Figure 43: ^{1}H-NMR spectra of pyrrolizidine **4.13** before reaction (top) with CO_2 and after reaction with CO_2 (bottom).[29]

[29] NMR spectra recorded by Jan Hanusch during his master thesis under my supervision.

In the carbon ^{13}C-NMR we observed similar peak shifts as for **3.107**, and in addition, a new peak at 166.8 ppm appeared (Figure 44). This peak was shifted a little to lower field than for **3.107** with 161.6 ppm. Compared to other CO_2-adducts reported in the literature the obtained value of 166.8 ppm was slightly shifted to lower field as well. For instance, ionic liquid **4.26** was reported to bind CO_2 as a carbamic acid and a corresponding ^{13}C-shift of 158 ppm measured in deuterated DMSO (Figure 45).[159] Further, Cobalt-complex **4.27** showed a ^{13}C-NMR shift for CO_2 of 159 ppm in CD_2Cl_2[160] and amino acid derivative **4.28** was reported to bind CO_2 as a carbamic acid with a ^{13}C-shift of 161 ppm in CD_3OD.[161] For ammonium bicarbonate in CD_3OD we measured a ^{13}C-NMR shift of 161.5 ppm, indicating that a shift of 166 ppm rather belongs to a carbamate than a bicarbonate. Long-range correlations in the HMBC-spectra between the carbamate carbon and protons adjacent to the nitrogen were never observed for both **3.107** and **4.13**.

It has to be mentioned, that a shift of the signals in the ^{1}H-NMR is no proof of the CO_2-capture for a compound. For electron poor analogue **4.18** we observe ^{1}H-NMR shifts of the peaks towards lower field, but in the ^{13}C-NMR no shifts as well as no newly appearing peak in the carbamate region was observed. From this we concluded that **4.18** is most likely too electron-deficient for CO_2-capture.

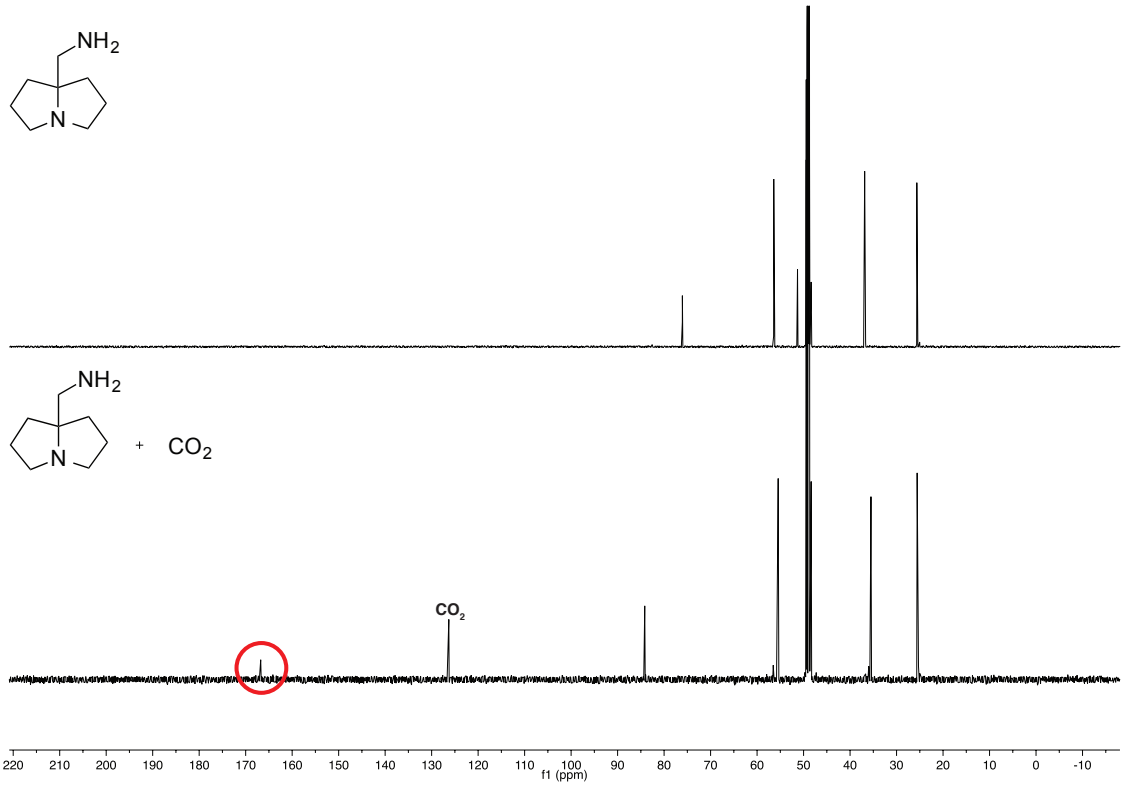

Figure 44: ^{13}C-NMR spectra of pyrrolizidine **4.13** before reaction (top) with CO_2 and after reaction with CO_2 (bottom).[30]

[30] NMR spectra recorded by Jan Hanusch during his master thesis under my supervision.

Brennecke et al.

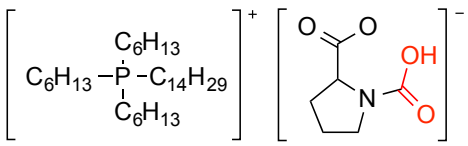

4.26

^{13}C-NMR = 158 ppm (*d*-DMSO)

Aresta et al.

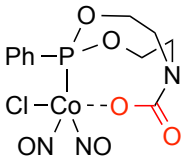

4.27

^{13}C-NMR = 159 ppm (CD_2Cl_2)

Liu et al.

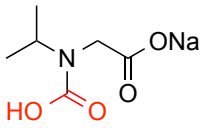

4.28

^{13}C-NMR = 161 ppm (CD_3OD)

Figure 45: Other CO_2-adducts and their ^{13}C-NMR shifts.

4.4.2 X-ray crystal structure analysis

During our studies we realized that when the neat primary and secondary amine absorbents were treated with CO_2, they instantaneously turn into a (usually white) solid. The microscopy images in Figure 46 show a drop of absorbent **4.15** placed on a microscopy slide. When the drop was subjected to a CO_2 stream the drop immediately turned into a solid.[31] Dissolving the substance in methanol and evaporating the solvent by CO_2 stream can also generate the solid. For a more complete conversion of the amine to the CO_2-adduct we prepared the solids from solution so that no unreacted material is enclosed in the solid. The growth of crystals for X-ray analysis is important because it would clarify the question how CO_2 is bound to our compounds. It has to be mentioned that attempts to turn anilines **3.107** and **4.18** into solids were not successful.

Before CO_2 stream

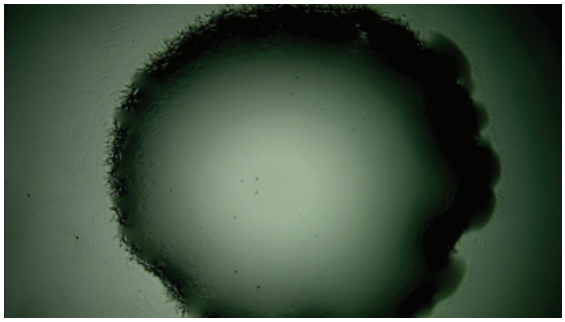

After CO_2 stream

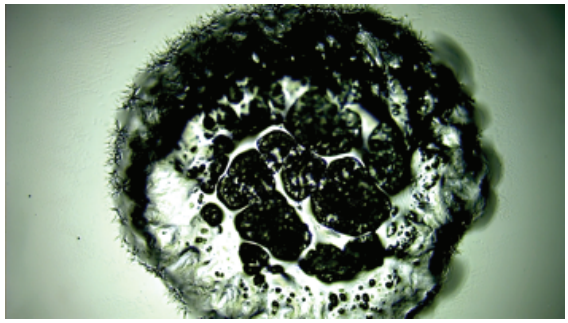

Figure 46: Microscopic image of a drop of **4.15** on a microscopy slide before a CO_2 stream (left) and after a CO_2 stream (right).

According to the above-mentioned procedure we prepared solids of the free amines (**4.13** and **4.15**) and the methylated compounds (**4.14** and **4.16**). The difficulty to obtain suitable crystals was that by evaporation procedures the CO_2 fixed by the amine was released along with evaporation of the solvent. We also had problems using batch-seeding techniques. After some experi-

[31] On the left image it can be noticed that crystallization has already started at the edges of the drop, probably because of CO_2 from the atmosphere.

mentation, we succeeded by dissolving the white solid in diisopropyl ether with one drop of *i*PrOH followed by slow evaporation of the solvent at 4 °C. For the compounds **4.13** and **4.16**, one primary and one methylated derivative, we obtained suitable crystals and from these the corresponding single crystal X-ray structures (Scheme 47). The crystal structure for compound **4.13** revealed that CO_2 is bound as a carbamate. The compound crystallized with four molecules of the same kind in one space group including water molecules that were placed in between the carbamate groups of two pyrrolizidine molecules providing a network of hydrogen bonds. **4.16** also bound CO_2 as a carbamate and crystallized as one molecule in the space group surrounded by four water molecules. As apparent from the crystal structures of **4.29** and **4.30** the carbamate is not directed towards the ammonium ion. We had expected this orientation as an effect of counter ion attraction. However, the supramolecular packing of carbamate **4.29** shows that the carbamate is directed towards the ammonium of a second carbamate molecule showing that the orientation of the carbamate is strongly influenced by the intermolecular interactions (Figure 48). The crystal structure of temuline in the work of *Trauner* et al. also did not show an orientation of the carbamate towards the positively charged nitrogen. Moreover, the authors observed strong intermolecular hydrogen bonds in the supramolecular packing.[153]

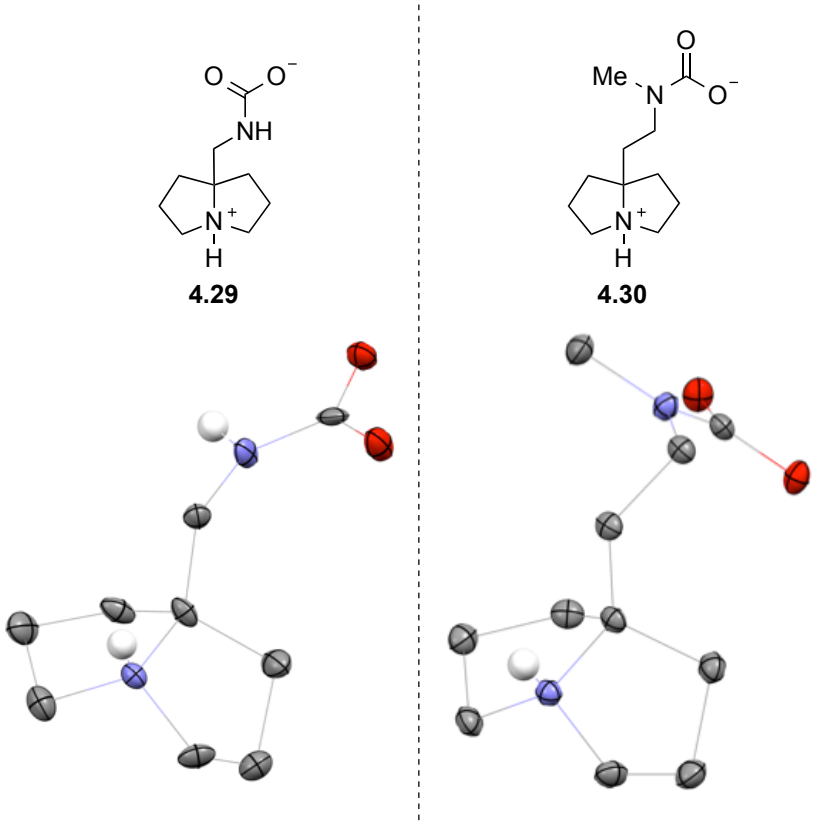

Figure 47: Single crystal X-ray structures of carbamates **4.29** and **4.30**.

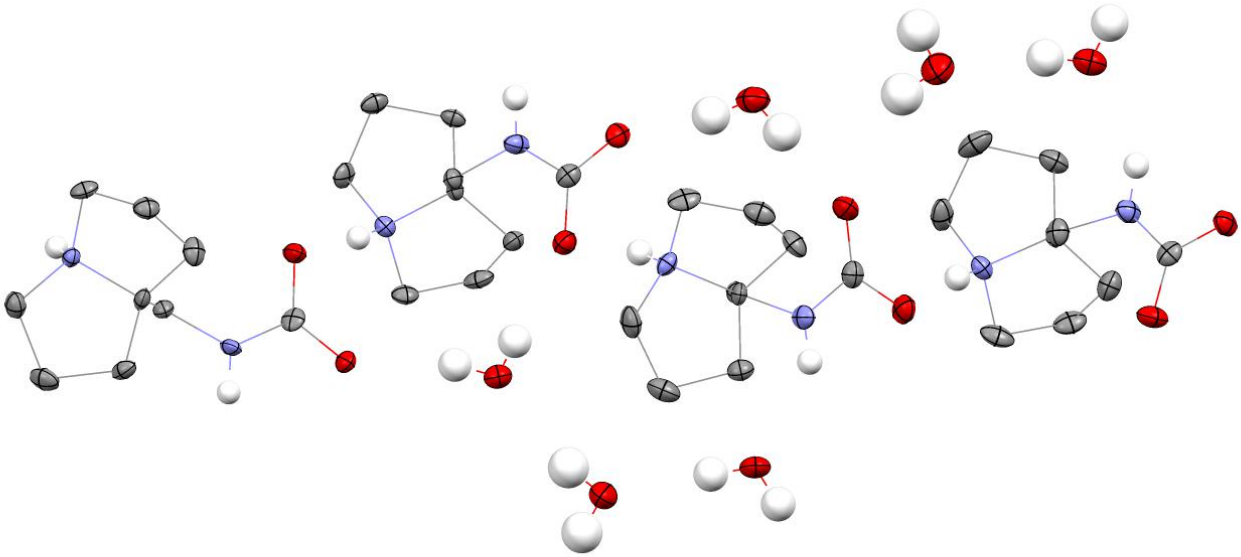

Figure 48: Unit cell of the single crystal X-ray structure of carbamate **4.29**. Carbamate **4.29** crystallized with four carbamates and six water molecules in one space group and reveals that the orientation of the carbamate is controlled by intermolecular interactions with other carbamate molecules and water.

Interestingly, the architecture of the pyrrolizidine ring of the two carbamates changed compared to pyrrolizidine **3.32**. The ring geometry changed from a *cis*-configuration in **3.32** to a *trans*-configuration of the carbamates **4.29** and **4.30** (Figure 49). Usually, for unsubstituted pyrrolizidines mainly the *cis*-conformer is observed, due to angular strain present in the *trans*-isomer, which is absent in the *cis*-isomer (Figure 50). Substituents on the pyrrolizidine ring, however, can strongly influence this equilibrium. The reason for the shift of the equilibrium in our case might be the protonation of the tertiary amine in the two carbamates **4.29** and **4.30**, as it has been reported that protonation can alter the geometry of the pyrrolizidine ring.[162,163]

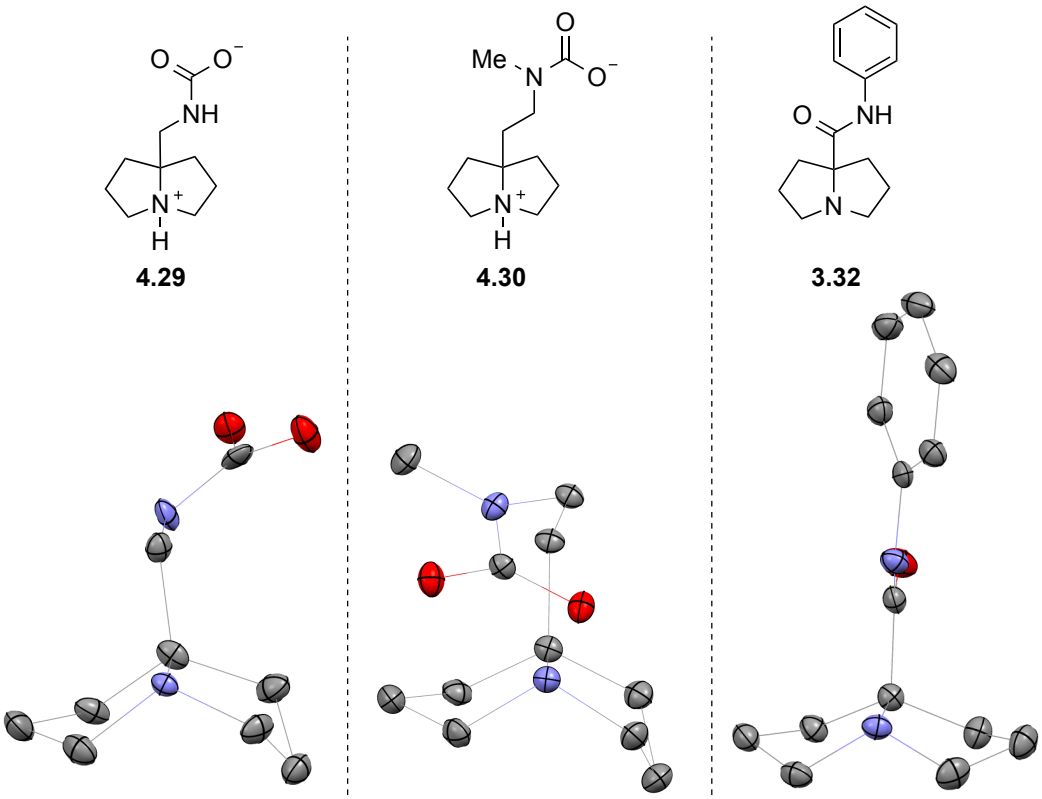

Figure 49: Crystal structures of **4.29, 4.30** and **3.32.** The carbamates adopt a *trans*-orientation of the pyrrolizidine core in contrast to **3.32** that show a *cis*-geometry.

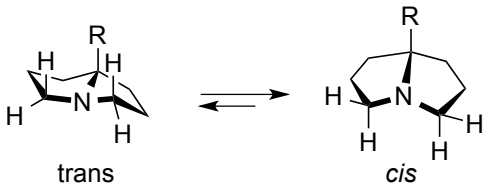

Figure 50: The equilibrium between the *trans*-geometry and the *cis*-geometry lies on the side of the *cis*-form for unsubstituted pyrrolizidines.

4.4.3 Gravimetric analysis

The following section describes the quantification of the CO_2 uptake for our pyrrolizidine derivatives. For its determination we chose to use a gravimetric method because a stoichiometric uptake results in a weight increase of 34%. A sample size of 3 mmol for the pyrrolizidine derivatives results in a weight increase of 132 mg (Scheme 71). This increase in weight is well measurable on an analytical balance. Besides the sufficient sensitivity, this established setup[161,164] does not require expensive equipment, such as other methods using calorimetry[159,165] or GC-analysis[166].

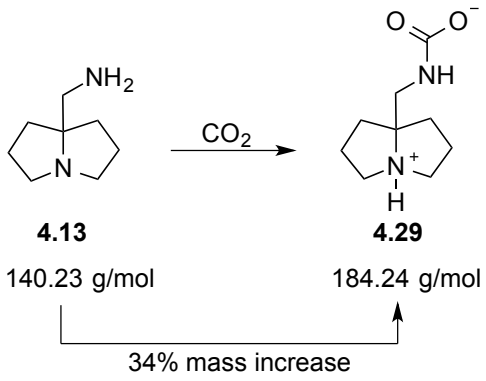

Scheme 71: Mass increase of pyrrolizidine **4.13** by CO_2.

A schematic representation of the setup is depicted in Scheme 72. We decided to build a unit that contains both, a CO_2- and a N_2-stream. This allows for the possibility to apply gas mixtures in our experiments, for instance to mimic the composition of flue gas from a power plant, or pure N_2 to assist in the release of the captured CO_2. Two individual flow controllers adjusted the two gas flows. Both gas flows can be merged together in a mixing chamber and then delivered to the absorbent sample, whose weight is measured on an analytical balance. Before each absorption measurement, the apparatus needs to be flooded with CO_2 to ensure for a homogeneous gas flow. In advance to the absorption measurement, the atmosphere of the sealed tube containing the pyrrolizidine absorbent and the solvent, was replace by CO_2 to prevent any falsified increase in weight caused by CO_2 from the atmosphere in the tube.[32] Placing the needle with the gas flow into the solution started the measurement. As a solvent for the amine absorbents we chose PEG_{200} because auf its high boiling point[33] which does not falsify the result by evaporation. In addition, PEG_{200} itself has a very low CO_2-absorption. In the beginning of our studies, we placed the sealed tube containing the absorbent on the balance and measured the increase in weight con-

[32] Density of air: 1.275 kg/m^3. Density of gaseous CO_2: 1.977 kg/m^3.
[33] >250 °C

tinuously using the program Balance Link®. The computer running the program was connected to the balance and recorded the weight every minute. The setup was very comfortable because no manual data collection was necessary. However, we encountered several problems with this set-up: 1) The container had to stand freely on the balance and any contact to the needle had to be avoided. This made the setup very sensitive to interruptions by the environment. 2) The airflow in the room sometimes contributed to fluctuations of weight because the balance could not be fully closed as it was attached to the CO_2-apparatus. 3) The CO_2 flow from the needle was not continuous as the needle was placed in the viscous solution. This resulted in strong variations of the sample weight and significant fluctuations in the resulting absorbance curves were obtained. In addition to this, the starting weight of the measurement was hard to determine, as in the beginning of the measurement it was already strongly fluctuating. As a result of this we obtained falsified end values of the overall absorption. Because of these encountered problems, we decided to determine the increase in weight manually.

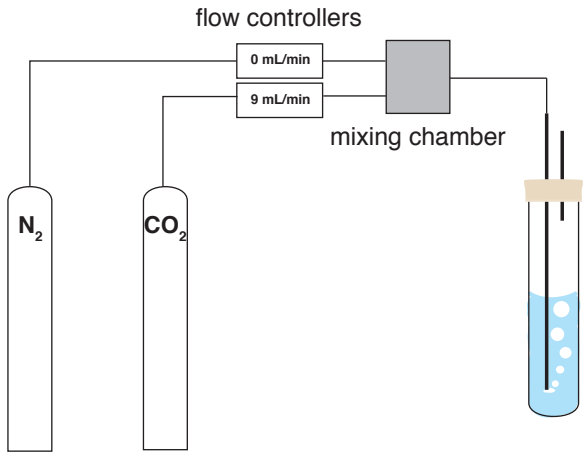

Scheme 72: Schematic representation of the CO_2-absorption apparatus, which also allows for the use of nitrogen gas for the release experiments.

An absorption curve of the absorbents **4.14** and **4.16** is shown in Scheme 73. To our delight, the pyrrolizidine absorbents showed a quantitative CO_2 uptake with ≥ 1 equiv. CO_2 captured by 1 equiv. amine absorbent. Interestingly, amine **4.14** showed a much faster uptake than **4.16** showing that the distance between the two amine groups plays an important role in the uptake kinetics. The closer proximity of the secondary and the tertiary amine in derivative **4.14** could contribute to a more efficient delivery of the proton and thereby leading to a faster uptake (Scheme 74). Most likely, CO_2 also needs to be activated by hydrogen bonding through solvent molecules, as we did not see any uptake in aprotic solvents (toluene-*d*8, $CDCl_3$) in earlier exper-

iments. In comparison to monoethanolamine, the most conventional absorbent in industry, our amines showed a clearly improved uptake.

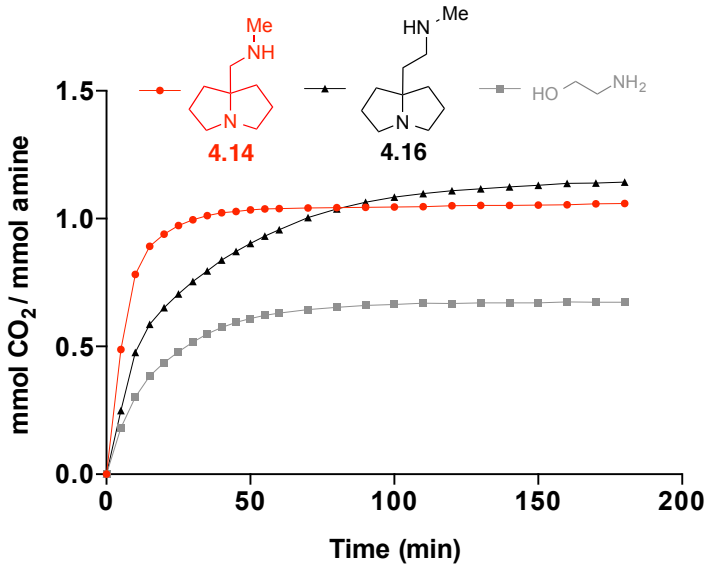

Scheme 73: CO_2-absorption curve of pyrrolizidines **4.14**, **4.16** and monoethanolamine.[34]

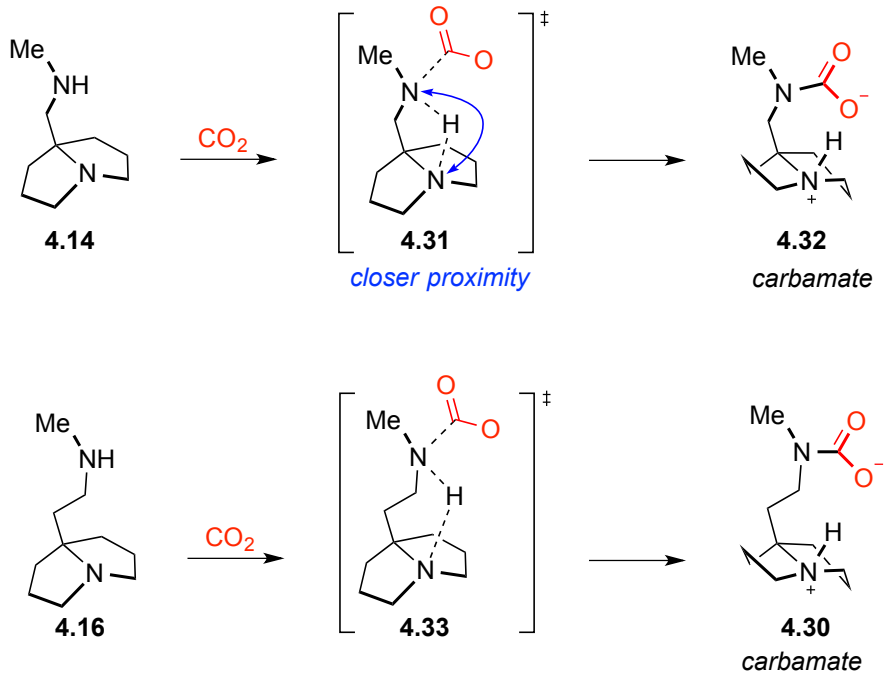

Scheme 74: The faster uptake of **4.14** compared to **4.16** could be explained by the closer proximity of the secondary and the primary amine.

[34] Absorption curve measured by Jan Hanusch.

Table 8: CO_2 absorption of pyrrolizidine derivatives and commercially available absorbents

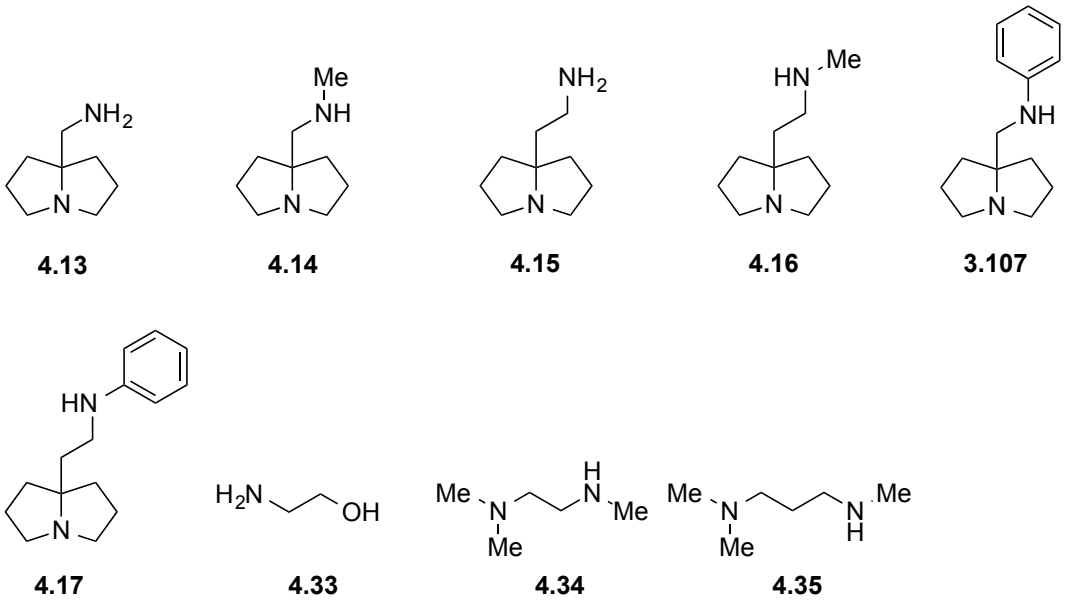

Absorbent	pK_a[b]	CO_2 absorption[d]
PEG_{200}	-	0.08[e]
4.13	10.7, 6.2	1.04
4.14	10.6, 6.6	1.06
4.15	11.2, 8.4	1.17
4.16	11.3, 8.6	1.14
3.107	10.5[c]	0.45
4.17	11.4	0.42
4.33	9.6	0.72
4.34	10.0, 6.1	0.65
4.35	10.6, 7.8	0.96

[a] Conditions: PEG_{200} (12 mmol) and absorbent (3 mmol), 25 °C, CO_2 stream 9 mL/min. [b] pK_a was determined by titration of the aqueous amine solutions with HCl. [c] Amine was dissolved in methanol and titrated with aqueous HCl [d] Moles of CO_2 per mol of absorbent, absorption by PEG_{200} is included. [e] CO_2 absorbed per 4 mmol of PEG_{200}.

Table 8 summarizes the results of the absorption experiments of all our derivatives. The pK_a values for the substances were also determined to examine on a possible correlation between CO_2-absorption and basicity. In general, the CO_2 uptake for all pyrrolizidines with secondary (**4.14** and **4.16**) and primary amine (**4.13** and **4.15**) side chains is stoichiometric which means that our proposed equimolar uptake is fulfilled. The observed over-stoichiometry of 5-17% is not fully clarified yet. Certainly, one part is because the amount of CO_2 absorbed by PEG_{200} is not

subtracted from these values. Another part may result from salt formation with water present in the solvent. An additional possibility is the formation of undefined pyrrolizidine-CO_2 adducts such as formation of carbamic acid and bicarbonate salt at the same time. The differences between the pyrrolizidines with primary and secondary amines are marginal, but the substances differ in their absorption kinetics as highlighted earlier in this chapter. On the other hand, aniline derivatives **3.107** and **4.17** show a significantly lower absorption compared to the other derivatives.

Interestingly, for linear diamine **4.34**, which shows the same amine connectivity as **4.14**, a significantly lower absorption was obtained. For this example the three-dimensional architecture of the pyrrolizidine might contribute positively to the CO_2-absorption. On the other hand for linear diamine **4.35** showing the same connectivity as **4.16**, this effect is less pronounced.

For the primary and secondary amine derivatives seems to be a dependency of the basicity on the CO_2-absorption because the more basic derivatives showed a slightly higher uptake. However, a general statement involving all the measured compounds cannot be formulated as has already been pointed out for other amine absorbents.[167]

4.5 Release

Next, we investigated the reversibility for the CO_2 uptake with compound **4.14** by measuring absorption-and-release-cycles. The uptake measurement was not continued until full saturation; instead we stopped at a ratio of 0.6-0.7 mmol CO_2/mmol amine. Absorption was performed at room temperature, desorption was performed at 65 °C and N_2-flow (9 mL/min). As can be seen from Figure 51 the compound showed full reversibility even after eleven cycles of absorption/desorption. The application of lower desorption temperatures with different solvents, is currently under investigation.

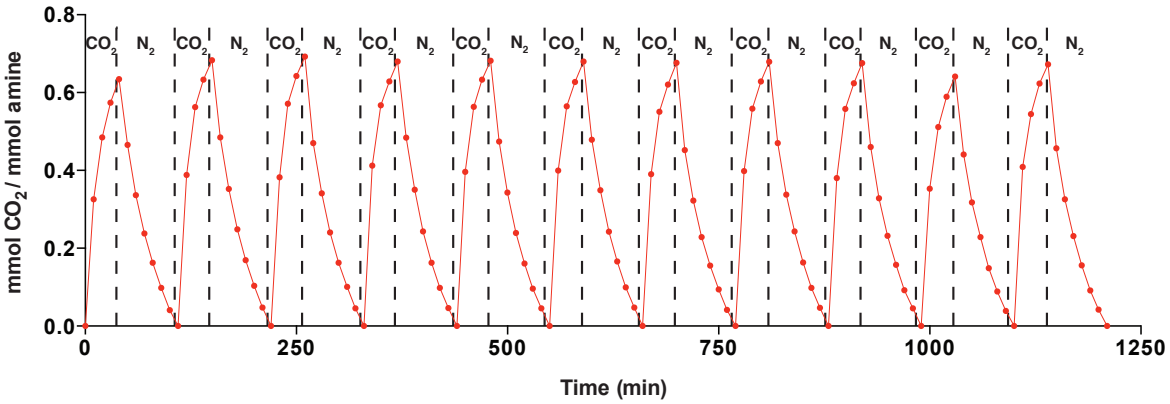

Figure 51: Absorption and desorption cycles of pyrrolizidine **4.14** at 9 mL/min CO_2 for the uptake and 65 °C / 9 mL/min N_2 for the release.[35]

[35] Absorption/Desorption experiments were performed by Jan Hanusch.

4.6 Determination of pK_a values

For the pK_a values shown in Table 8 we titrated the diamines with aqueous HCl. The methylated pyrrolizidine **4.14** was well soluble in water, the aniline derivative **3.107** had to be dissolved in MeOH and was then titrated with hydrochloric acid. The deviation in the resulting pK_a caused by the solvent mixture was corrected to a pK_a in pure water according to a literature known report.[168] The resulting titration curves are depicted in Figure 52.

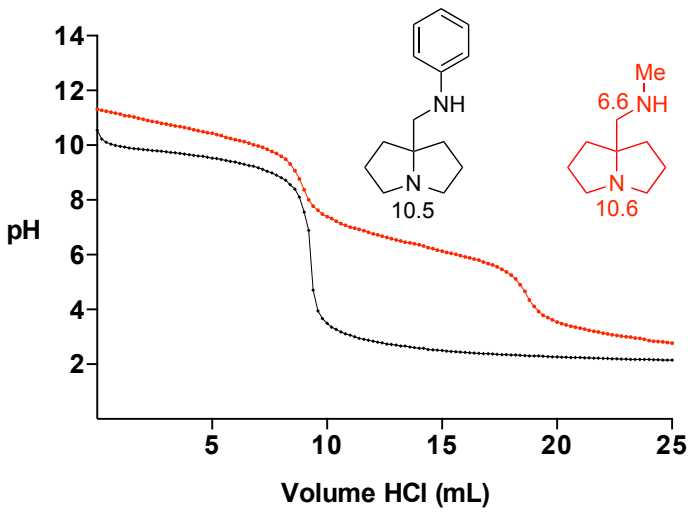

Figure 52: Titration curves of aniline **3.107** and methylated derivative **4.14**.

Interestingly, the aniline shows a typical titration curve of a buffer system with a buffer zone in the beginning (0-8 mL HCl) and one equivalent point, indicating that there is only one protonation. From this we can conclude that only the tertiary nitrogen is protonated and that there is no second protonation of the aniline nitrogen.[36] In contrast, the methylated pyrrolizidine shows two distinct protonations, so that both amines are protonated in this case.

This acid/base behavior of the substances may indicate that aniline **3.107** does not bind CO_2 as a carbamate. If the aniline nitrogen is not nucleophilic enough to attack a proton, it is most likely also not nucleophilic enough to attack a carbon atom (in this case CO_2). Further indications are a ^{13}C-NMR shift of 161 ppm in CD_3OD,[37] the low CO_2 uptake in the absorption measurements and the fact that a solid was never obtained for the compound when charged with a CO_2 stream.

[36] Because of its higher basicity the tertiary nitrogen is protonated first.
[37] We measured a ^{13}C-NMR shift of 161.5 ppm in CD_3OD for ammonium bicarbonate (see section 8.4)

4.7 Conclusion

Our results demonstrate that pyrrolizidine alkaloids can serve as useful agents for the capture of CO_2. Derivatives functionalized with a primary and a secondary amine bind CO_2 as a carbamate as shown by single crystal X-ray structure analysis. The uptake of CO_2 for these derivatives was equimolar and by that exceeded almost twice the capacity of conventional amines. In addition, the uptake was faster, especially for the derivatives **4.13** and **4.14** with one CH_2 group. As factors contributing to these properties we identified the proximity of the two amine groups and the three-dimensional architecture of the derivatives to be important. In general the low-lying pyrrolizidine backbone and the amine side-chain sticking out has been shown to be beneficial for the overall uptake of the absorbents. In addition, binding of CO_2 has been shown to be reversible with up to 11 cycles. The aniline derivatives **3.107** and **4.17** showed a significantly lower uptake of CO_2 than the other absorbents. Titration of these compounds revealed that the aniline nitrogen is not protonated, which leads to the presumption that the aniline is also not nucleophilic enough for the formation of a carbamate by nucleophilic attack on CO_2. From this we conclude that anilines of this kind most probably bind CO_2 as a bicarbonate salt, which seems to occur with lower efficiency thereby leading to a lower overall uptake.

5 Conclusion

This thesis entitled “Surface Engineering of Algae and Synthesis of Pyrrolizidines for Carbon Dioxide Capture Applications” highlights the utility of organic synthesis as a tool to tackle scientific problems. The investigations presented in this thesis were placed in the areas of chemical biology, synthetic method development and the design of molecules for the capture of CO_2.

In the second chapter, we demonstrate engineering of the green alga *Chlamydomonas reinhardtii* with an antibiotic, thereby turning the alga into an antimicrobial killer cell. It was shown that attaching the glycopeptide antibiotic vancomycin to the surface induced the new antimicrobial phenotype. We found that the compound **2.19**, consisting of a 4-hydroxyproline oligomer, a fluorophore for visualization and vancomycin was most effective for this purpose.[38] The compound was immobilized on the surface during an incubation time of 12 h without affecting the motility of the algae. The algae were then tested for their antimicrobial potency against the Gram-positive bacteria *Bacillus subtilis*. By monitoring the bacterial growth over time, we showed that **2.19**-modified algae are able to kill bacteria, and that the degree of overall culture growth can be controlled by variation of the amount of algae. Using laser scanning confocal fluorescence microscopy, we visualized the transfer of the substance from the surface of the algae to the cell wall of the bacteria.

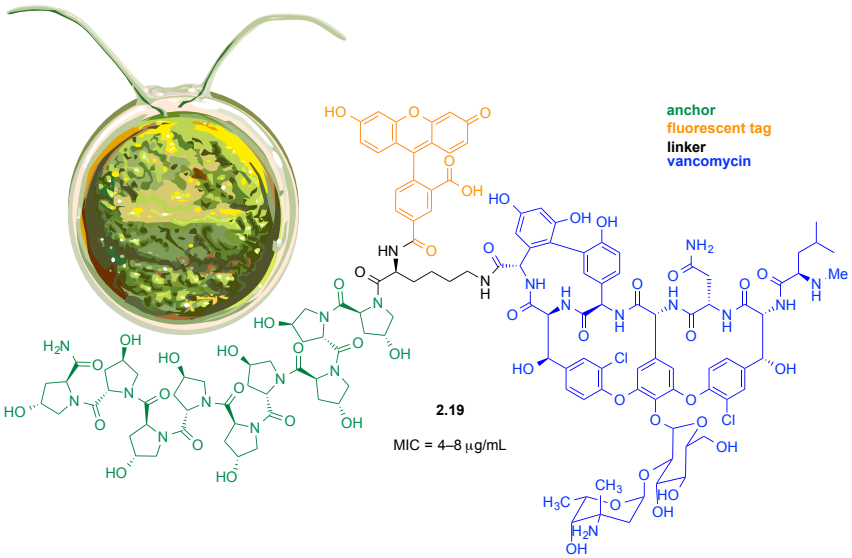

Our results demonstrate the first functionalization of the cell wall of *C. reinhardtii* with a therapeutic material. To the best of our knowledge this is also the first example in which a natively harmless organism is equipped with the feature to dispatch other organisms by chemical means. Our studies might deliver the basis for further functionalization resulting in the introduction of different phenotypes e.g. other therapeutic materials or catalysts. Further, this concept could be

[38] Image: modified from: http://www.pflanzenforschung.de/de/themen/pflanzen-im-fokus/chlamydomonas/ (2.12.2016)

transferred to different organisms that show similar surface compositions and architecture. Overall, we provided an example for the reversible modification of living cells without intervention into the organism's biosynthetic pathways.

In the third chapter, we describe the synthesis of *7a*-substituted pyrrolizidines from simple imine and isonitrile precursors. We showed that hydroxyl-functionalized pyrrolines react with isonitriles under acidic conditions and elevated temperatures to deliver direct access to these bicyclic heterocycles. The reaction tolerates a wide scope of isonitriles with aromatic and aliphatic substituents. Mechanistic investigations indicated that the reaction probably proceeds *via* a pyrrolizidinium intermediate. The products could be further functionalized by oxidation and reduction protocols. Our method demonstrates the first example for the direct preparation of these heterocycles with few synthetic operations and excellent atom economy.

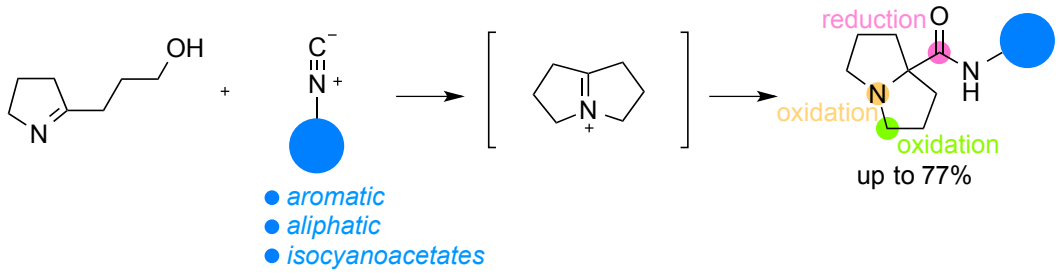

The last chapter described our investigations on the CO_2-binding properties of pyrrolizidines. We prepared a number of pyrrolizidine derivatives with different substituents on the side chain amine. We found that there were significant differences between amines substituted with aromatic groups and primary and secondary amines. Pyrrolizidines containing primary or secondary amines were able to bind CO_2 quantitatively, whereas the anilines did not reach even half of the binding capacity. This finding can be explained by the fact that primary and secondary amines bind CO_2 as a carbamate, leading to a 1:1 stoichiometry of amine:CO_2, on the other hand, anilines probably bind CO_2 as a bicarbonate salt. These findings are supported by crystal structures for both primary and secondary amines and by NMR studies and titration experiments for the anilines. The reversibility of CO_2 uptake was demonstrated by absorption-and-release-cycles that where repeated multiple times without loss of binding capacity. Overall, CO_2-binding pyrrolizidines might emerge as a useful alternative to existing CO_2-absorbents. Moreover, they might be useful tools to assist in the conversion of CO_2 to substances with higher value.

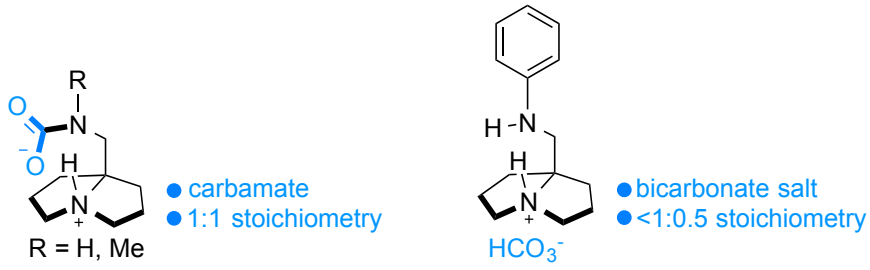

6 Abbreviations

A	absorbance
Ac	acetyl
AcOH	acetic acid
AHX	aminohexanoic acid
Ala	alanyl
aq.	aqueous
B.	*Bacillus*
BF	bright field
Boc	*tert*-butyloxycarbonyl
BODIPY	1,3,5,7-tetramethyl-8-phenyl-4,4-difluoroboradiazaindacene
BSA	bovine serum albumin
bs	broad singlet
Bu	butyl
°C	degrees Celsius
C.	*Chlamydomonas*
c	concentration
cat.	catalytic
CCS	carbon capture and storage
CF	carboxyfluorescein
δ	chemical shift
d	dublet
D	deuterium
DBU	1,8-diazabicyclo[5.4.0]undec-7-ene

DCC	*N,N'*-dicyclohexylcarbodiimide
DIC	*N,N'*-diisopropylcarbodiimide
DiPEA	*N,N'*-diisopropylethylamine
DMAP	4-dimethylaminopyridine
DMF	dimethylformamide
DMSO	dimethyl sulfoxide
DNA	deoxyribonucleic acid
EA	elemental analysis
e.e.	enantiomeric excess
EI	electron impact ionization
e.g.	*exempli gratia*
Et	ethyl
equiv.	equivalent
e.r.	enantiomeric ratio
ESI	electron spray ionization
FA	formic acid
FITC	fluorescein isothiocyanate
Fmoc	fluorenylmethyloxycarbonyl
FTIR	*Fourier* transform infrared spectroscopy
g	gram(s)
Gal	galactose
GC	gas chromatography
GPI	glycoinositol phospholipid
h	hour(s)
HATU	1-[bis(dimethylamino)methylene]-1H-1,2,3-triazolo[4,5-b]pyridinium 3-

	oxid hexafluorophosphate
HBTU	*N,N,N′,N′*-tetramethyl-*O*-(1*H*-benzotriazol-1-yl)uronium hexafluorophosphate
HCTU	2-(6-chlor-1*H*-benzotriazol-1-yl)-1,1,3,3-tetramethylaminium-hexafluorophosphat
HMBC	heteronuclear multiple-bond correlation spectroscopy
HOBt	1-hydroxybenzotriazole hydrate
HPA	*Helix pomatia* agglutinin
HPLC	high performance liquid chromatography
HR-MS	high resolution mass spectrometry
HyD	Hybrid detector
Hyp	hydroxyl proline
Hz	herz (s^{-1})
IC_{50}	50% inhibition concentration
IgM, IgG	immunoglobin mice, immunoglobin goat
J	coupling constant
Lac	lactate
LDA	lithium diisopropylamide
m	multiplet
L	liter(s)
LC	liquid chromatography
M	molarity
m	multiplet
m-CPBA	3-chloroperbenzoic acid
Me	methyl
min	minute(s)

m.p.	melting point
Ms	mesyl
MTBE	*tert*-butyl methyl ether
mV	milli volt
n.d.	not determined
NMM	*N*-methylmorpholine
MIC	minimum inhibitory concentration
MS	mass spectrometry
MSC	mesenchymal stem cell
NMR	nuclear magnetic resonance
LED	light-emitting diode
OD	optical density
p	para
p	quintet
PBS	phosphate buffered saline
PEG	polyethylene glycol
Ph	phenyl
ppm	parts per million
Pr	propyl
PyBOP	(benzotriazol-1-yloxy)tripyrrolidinophosphonium hexafluorophosphate
q	quartet
quant.	quantitative
R_f	retention factor
RT	room temperature
R_t	retention time

s	singlet
sat.	saturated
sec	second(s)
SM	starting material
sp.	*species*
SPE	solid phase extraction
t	triplet
THF	tetrahydrofuran
TIS	triisopropyl silane
TLC	thin layer chromatography
TNBS	picrylsulfonic acid
TFA	trifluoroacetic acid
TSA	toluene sulfonic acid
UHPLC	ultra high-performance liquid chromatography
UV	ultraviolet
ν	wavenumber
VIS	visible
X-Ray	X-radiation

7 Experimental Part

7.1 General

Confocal fluorescence microscopy was performed on an inverse confocal laser scanning microscope (CLSM SP5 Mid UV-VIS Leica) equipped with hybrid detectors. The microscope was operated using Leica Advanced Fluorescence software and images were processed by adjusting the brightness/contrast using Fiji.

Flash chromatography was performed using silica gel 60 (230-240 mesh) from Fluka using a forced flow eluent at 0.1-0.3 bar pressure.

GC-MS was measured on a Finnigan Trace GC Ultra (Thermo) equipped with a Finnigan Trace DSQ (Thermo) EI MS detector and a Zebron ZB-5MS (30m) column.

Glassware was dried in an oven at 120 °C over at least 24 h and for moisture sensitive reactions was heated with a heat gun under inert atmosphere.

Analytical and preparative HPLC was performed on a Shimadzu HPLC system (LC-20AP dual pump, CBM-20A Communication Bus Module, SPP-20,A UV/VIS Detector, FRC-10A Fraction collector).

IR-spectroscopy was performed on a *Varian 800 FT-IR ATR Spectrometer*.

Lyophilizations were performed on a *Cryst Freeze dryer ALPHA 1- 4 LD plus.*

High resolution mass spectra were recorded by the Mass Spectrometric Service of University of Basel on a *Bruker maXis 4G mass spectrometer* using electrospray ionization (HR-MS (ESI)) or a *Bruker ESQUIRE-LC* quadrupole ion trap instrument, equipped with a combined Hewlett-Packard Atmospheric Pressure Ion (API) source at the University of Zurich.

Melting points were determined using a *Büchi B-545 apparatus* in open capillaries and are uncorrected.

NMR-spectra were recorded either using a Bruker Avance 400 MHz, a Bruker Avance 250 MHz or a Bruker Avance DRX 500 MHz spectrometer at room temperature. Chemical shifts (δ-values) are reported in ppm, spectra were calibrated related to solvent's residual proton chemical shift ($CHCl_3$, δ = 7.26 ppm) or TMS ($CDCl_3$, δ = 0.00 ppm) and solvent's residual carbon chemical shift ($CDCl_3$, δ = 77.16 ppm). Multiplicity is reported as s = singlet, br. s = broad singlet, d = doublet, t = triplet, q = quartet, p = quintet, m = multiplet or unresolved and the coupling constant *J* in Hz. ^{19}F-NMR spectra were recorded using C_6F_6 as an internal reference ($CDCl_3$, δ = -164.9 ppm).

Optical rotations $[\alpha]_D^T$ were measured at the sodium D line using a 1 mL cell with a 1 dm path length on a *Jasco P-2000 digital polarimeter,* the concentration *c* is given in g/100 mL.

Reagents were purchased from Sigma-Aldrich, Acros and Fluka and used without further purification. ^{18}O-labeled (97%) water was purchased from Eurisotop.

Solid phase peptide synthesis was performed with a Syro I (Biotage) or a CS136XT (CS Bio) fully automated peptide synthesizer.

Solvents for work-up and chromatography were technical quality and distilled. Solvents used for chemical transformations were either puriss. quality or dried by filtration through activated Al_2O_3 under nitrogen (H_2O content < 10 ppm, *Karl-Fischer* titration).

SPE columns were DSC-18 purchased from *Supelco*.

Thin layer chromatography was performed on Merck silica gel 60 F254 plates (0.25 mm thickness) precoated with fluorescent indicator.

Titration curves were recorded using a Mettler Toledo Seven Easy pH-meter equipped with an InLab®409 pH-electrode.

X-ray data collection was performed at low temperature (123 K) using Mo K_a radiation on a *Bruker KappaAPEX diffractometer*. Integration of the frames and data reduction was carried out

using APEX2.[39] The structures were solved by direct methods using SIR92.[40] All non hydrogen atoms were refined using anisotropically by full-matrix least-squares on *F using CRYSTALS.*[41] Hydrogen atoms were placed in their calculated positions by means of the 'riding' model.

7.2 Surface engineering of algae

7.2.1 Microbiology

Cultivation of algae

Chlamydomonas reinhardtii (11-32b) was purchased from EPSAG (Experimentelle Phykologie und Sammlung von Algenkulturen der Universität Göttingen) and grown in Kuhl medium (1011.1 mg L^{-1} KNO_3, 621 mg L^{-1} $NaH_2PO_4 \cdot H_2O$, 89 mg L^{-1} $Na_2HPO_4 \cdot 2\ H_2O$, 246.5 mg L^{-1} $MgSO_4 \cdot 7\ H_2O$, 14.7 mg L^{-1} $CaCl_2 \cdot 2\ H_2O$, 6.95 mg L^{-1} $FeSO_4 \cdot 7\ H_2O$ (Fe-EDTA complex), 1 mL L^{-1} micronutrient solution (61.0 mg L^{-1} H_3BO_3, 169.0 mg L^{-1} $MnSO_4 \cdot H_2O$, 287.0 mg L^{-1} $ZnSO_4 \cdot 7\ H_2O$ mg L^{-1}, 2.5 mg L^{-1} $CuSO_4 \cdot 5\ H_2O$, 12.5 mg L^{-1} $(NH_4)_6Mo_7O_{24} \cdot 4\ H_2O$))[42] at 20 °C under medium light (30V).

Cultivation of cell wall-deficient algae

The cell wall deficient mutant (CC-406 cw15 mt-) was purchased from the Chlamydomonas Research Center, University of Minnesota and grown in Tris minimal medium (2.42 g L^{-1} Trizma® base, 25 mL salt solution (15 g L^{-1} NH_4Cl, 4 g L^{-1} $MgSO_4 \cdot 7H_2O$, 2 g L^{-1} $CaCl_2 \cdot 2H_2O$) 0.375 mL phosphate solution (28.8 g L^{-1} K_2HPO_4, 14.4 g L^{-1} KH_2PO_4), 1 mL Fe-EDTA complex (6.95 mg L^{-1} $FeSO_4 \cdot 7\ H_2O$)) at 20 °C under medium light (30V).

Surface modification of algae:

Modification of algae with OCV for bacterial growth curves

6 mL of a *C. reinhardtii* culture with a cell density of $3.3 \cdot 10^6$ cells/mL was centrifuged and the supernatant removed. The algae were resuspended in fresh Kuhl medium to a volume of 160 µL. 35 µL of a solution of **2.19** (c = $5.57 \cdot 10^{-3}$ mmol/mL) was added to the algae suspension to reach a final overall concentration of $1 \cdot 10^{-3}$ mmol/mL. The algae were shaken for 12 h at room temperature at 350 r/min.

[39] Bruker Analytical X-ray Systems, Inc., **2006**. *Apex2*, Version 2 User Manual, M86-E01078, Madison, WI.
[40] Altomare, A.; Cascarano, G.; Giacovazzo, C.; Guagliardi, A.; Burla, M. C.; Polidori, G.; Camalli, M. *J. Appl. Cryst*. **1994**, *27*, 435.
[41] Betteridge, P. W.; Carruthers, J. R.; Cooper, R. I.; Prout, K.; Watkin, D. J. *J. Appl. Cryst*. **2003**, *36*, 1487.
[42] Kuhl, A. Lorenzen, H. Handling and culturing of Chlorella. In: D. M. Prescott, ed., Methods in cell physiology, Vol. I, p. 152-187, Academic Press, New York and London, 1964.

The algae were diluted with 1 mL of Kuhl medium, centrifuged at 2000 r/min for 5 min and the supernatant was removed. The algae were washed 3x by addition of 1 mL Kuhl medium, centrifugation and removal of the medium. The algae pellet was resuspended in 2.5 mL Kuhl medium for the bacterial growth experiments.

Modification of algae with 2.19 for flagellar preservation

2 mL of algae culture with a cell density of $3.3 \cdot 10^6$ cells/mL was centrifuged and the supernatant removed. The algae were resuspended in fresh Kuhl medium to a volume of 65 µL. The algae suspension was added to 192 µg ($6.5 \cdot 10^{-5}$ mmol) of **2.19** and mixed well (final concentration: c = $1 \cdot 10^{-3}$ mmol/mL). The algae were shaken for 12 h at room temperature at 350 r/min.
The algae were diluted with 1 mL of Kuhl medium, centrifuged at 2000 r/min for 5 min and the supernatant was removed. The algae were washed 3x by addition of 1 mL Kuhl medium, centrifugation and removal of the medium. The algae pellet was resuspended in Kuhl medium for fixation on microscopy slides.

Preparation of fixed microscopy samples

Cover slips were coated with 0.1% gelatin solution for 15 min and air-dried. One drop of algae suspension was applied on the coverslip and the water was evaporated without the cells being dried out. Fixation solution (9% formaldehyde, 3% glutaraldehyde, 0.1% NaCl) was mixed 1:1 with Kuhl medium, placed on the cells and left for 5 min at room temperature. The fixation solution was rinsed away with Kuhl medium and the sample was mounted with ProLong® Diamond Antifade Mountant.

Bacterial strains and growth conditions

The bacterial strain used was *Bacillus subtilis* (ATCC 6633) from DSMZ (Deutsche Sammlung von Mikroorganismen und Zellkulturen, Braunschweig Germany). The bacteria were cultivated in Medium 1 (5 g l^{-1} peptone, 3 g l^{-1} meat extract, 10 mg l^{-1} $MnSO_4 \cdot 7\ H_2O$) at 37 °C (pH = 6).

Antibacterial activity and bacterial growth curves

Overnight cultures of *B. subtilis* were grown in a Erlenmeyer flask while vigorous shaking with 200 r/min at 37 °C. 2% of an overnight culture with OD_{600} = 6.00 (added volume was adjusted according to the OD_{600} of varying overnight cultures) was added to a 15 mL conical tube containing 2.5 mL of algae suspension and 2.4 mL of Medium 1. Bacteria were grown in an incubator at 37 °C and 200 r/min and the increase in bacterial growth (600 nm) was measured every hour. Graphs were background-corrected by subtracting the OD_{600} at time 0.

Live/Dead staining of bacteria

1 mL of the bacteria/algae suspension was transferred into an Eppendorf vial and centrifuged at 2000 r/min for 5 min. The medium was removed and 0.5 mL of PBS was added. To the suspension was added 100 µL Live/Dead staining solution (previously prepared by adding 10 µL of solution A and 5 µL of solution B to 1 mL PBS). The cell suspension was mixed by vortex shaking and incubated at 37 °C for 30 min at 200 r/min. 10 µL of cell suspension was placed on an agarose patch (previously prepared from a hot 1% agarose solution) and covered with a cover slip. Imaging was performed subsequently.

MIC values

B. subtilis (ATCC 6633) was inoculated from a fresh agar plate into a 0.9% NaCl aqueous solution. The turbidity of the bacterial suspension was adjusted to McFarland standard 0.5, and diluted 1 to 200 in cation-adjusted Mueller-Hinton-II broth. (Note, the MIC values are typically 4-8 fold lower when the assays are performed in Mueller-Hinton-I broth in the presence of 0.02% BSA). The compounds were dissolved in 0.01% acetic acid at a concentration of 1 mg/ml (determined by UV-Vis). In 96 well microtiter plates, two fold serial dilutions of the compounds (normally ranging from 64 µg/ml to 0.0005 µg/ml) were prepared in Mueller-Hinton-II broth with 0.002% P80 in a final volume of 50 µl. Finally, the bacterial suspension (50 µl) was used to inoculate each well on the microtiter plate, corresponding to approximately 5x 105 CFU/ml in a final volume of 100 µl. The microtiter plates were covered and incubated overnight at 37 °C with shaking at 200 r/min. The MIC was determined by visual inspection and is defined as the minimal concentration of a compound that prevented microbial growth under the conditions described. MIC readouts done by Myriam Gwerder.

Kirby-Bauer disk diffusion test

An overnight culture of *B. subtilis* was raised in Medium 1 (OD_{600} = 6.15). On the next day a culture was raised using 2% of the overnight culture. The OD_{600} values were measured every hour until OD_{600}~1.00. Agar plates were prepared using 10% of the bacteria culture.

Paper disks (6 mm) were incubated with 10 µL of solutions of vancomycin (53 µg), **2.21** (87 µg) (shown in Figure 28), **2.19** (100 µg) and **2.09** (50 µg). The paper disks were placed on the agar plates and the plates were incubated at 37 °C overnight. Antibacterial activity was evaluated after 16 h.

Figure 53: Kirby-Bauer disk diffusion test using vancomycin, **2.19** and **2.09**.

7.2.2 Preliminary investigations on bacterial growth

The following experiments were performed in advance to the growth experiments described in Chapter 2. Growth of *B. subtilis* was investigated in 50 mL conical tubes. The conditions tested were:

***B. subtilis* medium:** *B. subtilis* grown in 100% Medium 1

1 µg/mL vancomycin: *B. subtilis* grown in 100% Medium 1 with 1 µg/mL vancomycin added to the medium

***B. subtilis* medium/Kuhl medium 1/1:** *B. subtilis* grown in 50% Medium 1 and 50% Kuhl medium

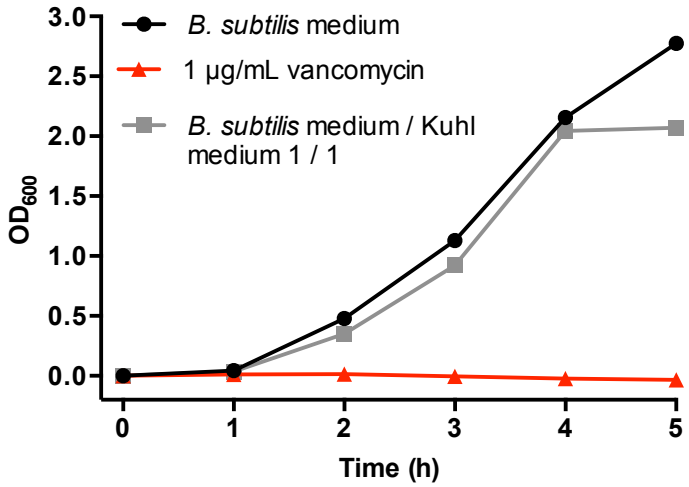

Figure 54: Growth of *B. subtilis* under different conditions.

As can be seen from Figure 54, the composition of the medium has a clear influence on the bacterial growth. Bacteria grown in a mixture of Medium 1 and Kuhl medium (1:1) stopped growing after 4 h. This can be explained by depletion of nutrients in the medium at this point.
Next, we investigated the effect of the vancomycin concentration in the medium. As can be seen in Figure 55, we observed full inhibition of growth with vancomycin in the range of 1 µg/mL–1 mg/mL

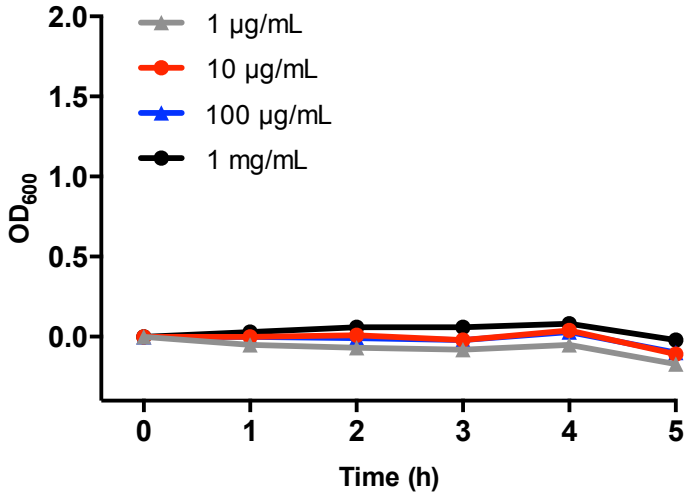

Figure 55: Growth of *B. subtilis* in the presence of vancomycin in the µg/mL range.

In the next set of experiments we lowered the antibiotic concentration to the ng/mL range. As can be seen in Figure 56 with these antibiotic concentrations the bacterial growth could not be inhibited anymore.

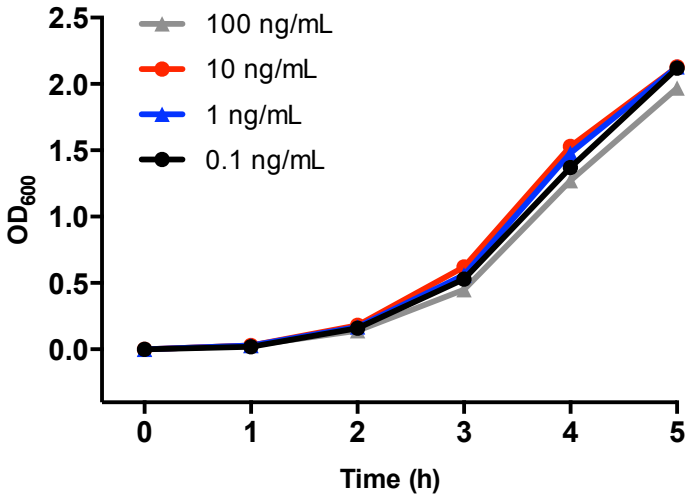

Figure 56: Growth of *B. subtilis* in the presence of vancomycin in the ng/mL range.

Figure 57 illustrates the different appearance of *B. subtilis* at different stages during growth. The curve shown in Figure 57 shows the growth of *B. subtilis* in the presence of unmodified (black curve) and with **2.19**-modified algae (red curve).[43] After 6 h of growth, Live/Dead staining was performed and investigated under a fluorescent microscope. The cells present in the beginning of the stationary phase (black curve) appeared as long chains that are partly wrapped up in ravels (b). On the contrary, the cells during the exponential phase (red curve) are mainly present in single or double rods (c). This highlights the different appearance of the cells dependent on the stage of growth (mentioned in section 2.2).

a

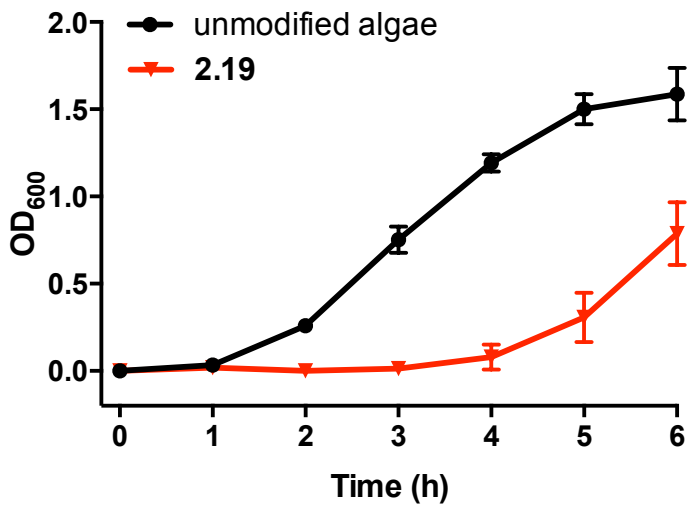

b

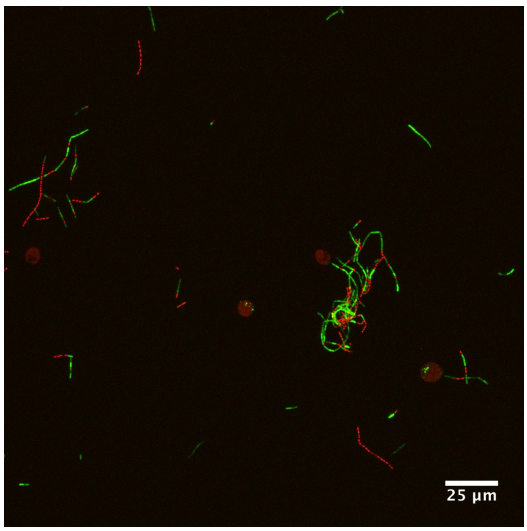

c

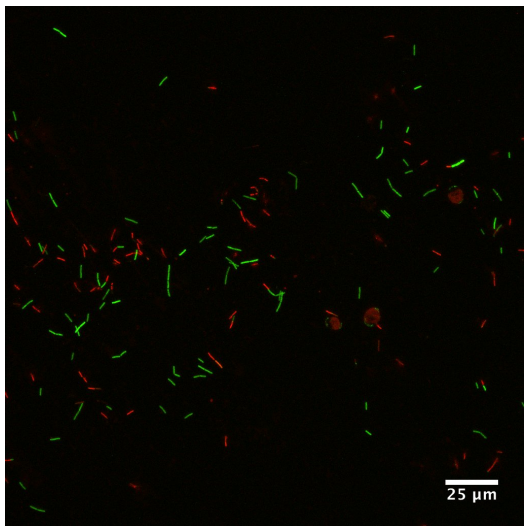

Figure 57: a) Growth curve for *B. subtilis* in the presence of algae both unmodified and modified with **2.19**. **b)** Live/Dead staining of the culture with unmodified algae after 6 h. The bacterial cells are in the beginning of the stationary phase and appear mostly as chains. **c)** Live/Dead staining of the culture with algae modified with **2.19** after 6 h. The bacterial cells were in the exponential phase and appear mostly as single and double rods.

[43] The algae were incubated at a concentration of $1 \cdot 10^{-3}$ mmol/mL for 12 h and washed 3x.

7.2.3 Synthesis

Hyp$_9$-FITC (2.01)

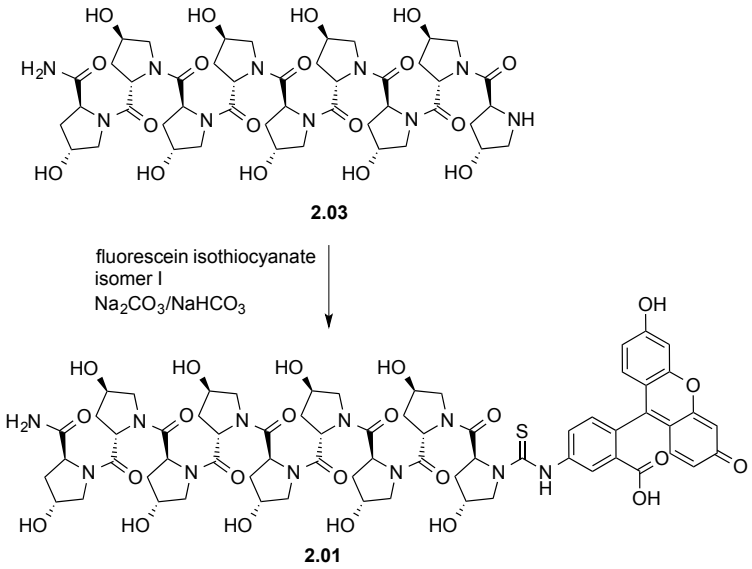

Hyp$_9$-NH_2 (8.3 mg, 8 µmol, 1.0 equiv.) and fluorescein isothiocyanate isomer I (4 mg, 10.3 µmol, 1.35 equiv.) were placed in a vial and 120 µL of Na_2CO_3/$NaHCO_3$ buffer (pH = 9.5) and 20 µL THF were added. The reaction mixture was stirred for 48 h at room temperature. The reaction mixture was diluted with 2 mL DMSO:H_2O (3:4) and filtered through a SPE column. The compound was purified by reversed phase HPLC using H_2O/MeCN + 0.1% FA (λ = 210 nm).

Column: Gemini-NX 10µ C18 110A, 250 mm x 21.2 mm

Method: 2-2–10–27–100%MeCN_0-6–9–23–25min, 20 mL/min. R_t = 25 min.

The MeCN was removed by rotary evaporation and the compound was lyophilized from water. The compound was obtained as a yellow foam in 83% yield (9.5 mg, 6.7 µmol).

The purity of the compound was analyzed by analytical reversed phase HPLC using H_2O/MeCN + 0.1% FA (λ = 210 nm).

Column: Gemini-NX 5µ C18 110A, 150 mm x 4.60 mm

Method: 2–2–10–45–100%MeCN_0–2–4–24–25min, 1 mL/min. R_t = 16.25 min.

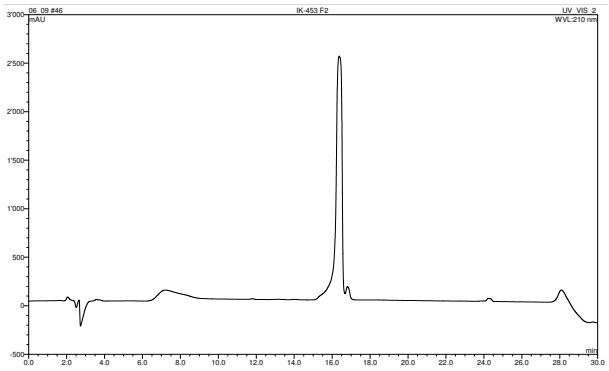

HR-MS (ESI) $C_{66}H_{79}N_{11}O_{23}S^{2+}$ $[M+2H]^{2+}$ calculated: 712.7530, found: 712.7536.

Hyp_9NH_2 (2.03)

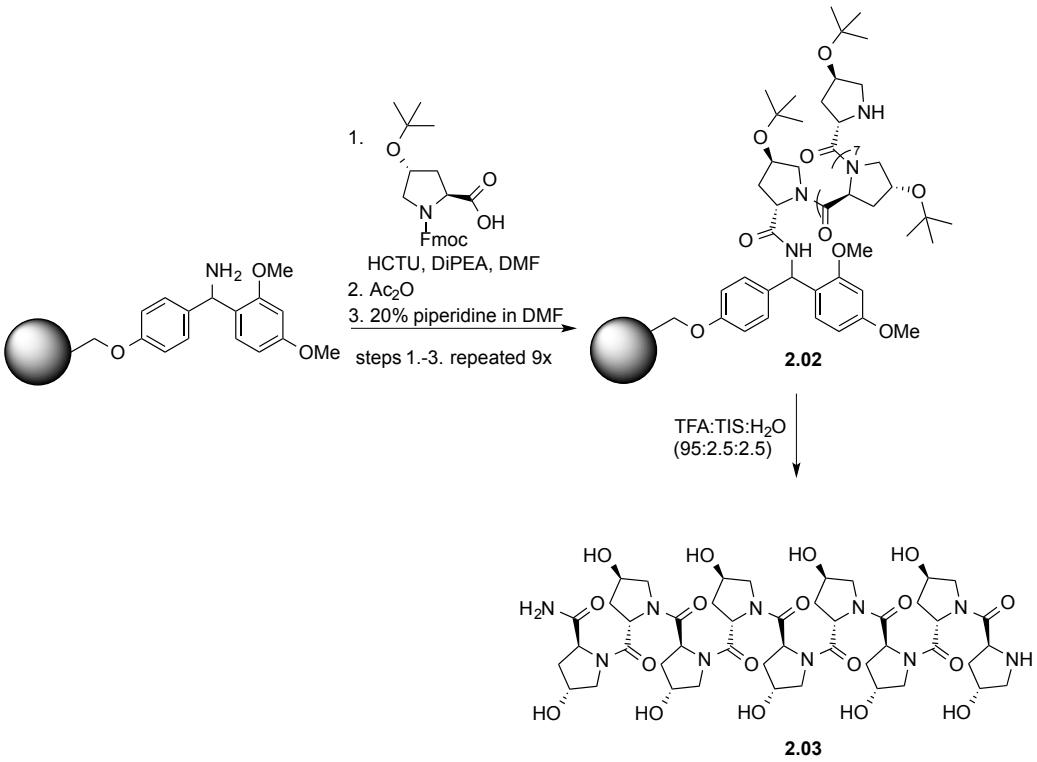

The synthesis of 4-hydroxyproline oligomer was performed on the solid phase using an automated peptide synthesizer (Syro I, Biotage). The synthesis was carried out on a Rink amide resin (Merck Millipore) with a loading of 0.59 mmol/g. The reagents used for the synthesis were: Fmoc-Hyp(*t*Bu)-OH (4.0 equiv.), HCTU (4.0 equiv.), DiPEA in NMP (4.0 equiv.), Ac_2O and DiPEA in DMF (50 equiv.), 20% piperidine in DMF. Coupling times were 1.5 h. From 0.1 g of the Rink amide resin, 0.25 g of resin was obtained after the synthesis. The peptide was either used for further transformations on the resin or cleaved using TFA:TIS:H_2O (95:2.5:2.5) (10 mL/g peptide resin). The cleaved peptide was dropped into MTBE at 0 °C (10 mL/g peptide), centrifuged and the MTBE was decanted. The peptide was washed following this sequence 3x. The solid was dried under a stream of N_2. The solid was dissolved in water and filtered through a SPE column using water. The filtrate was lyophilized to yield a white foam.

Hyp_{10}-FITC (2.04)

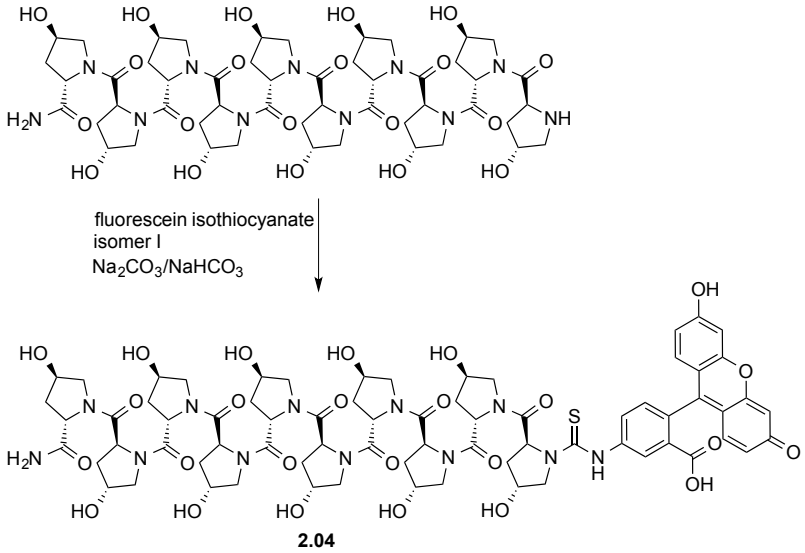

2.04

Hyp_{10}-NH_2 (9.2 mg, 8 µmol, 1.0 equiv.) and fluorescein isothiocyanate isomer I (4.3 mg, 11 µmol, 1.37 equiv.) were placed in a vial and 120 µL of $Na_2CO_3/NaHCO_3$ buffer (pH = 9.5) and 20 µL THF were added. The reaction mixture was stirred for 48 h at room temperature. The reaction mixture was diluted with 2 mL DMSO:H_2O (3:4) and filtered through a SPE column. The compound was purified by reversed phase HPLC using H_2O/MeCN + 0.1% FA (λ = 210 nm).

Column: Gemini-NX 10µ C18 110A, 250 mm x 21.2 mm

Method: 2-2–10–27–100%MeCN_0-6–9–23–25min, 20 mL/min. R_t = 24.75 min.

The MeCN was removed by rotary evaporation and the compound was lyophilized from water. The compound was obtained as a yellow foam in 52% yield (6.4 mg, 4.2 µmol).

The purity of the compound was analyzed by analytical reversed phase HPLC using H_2O/MeCN + 0.1% FA (λ = 210 nm).

Column: Gemini-NX 5µ C18 110A, 150 mm x 4.60 mm

Method: 2–2–10–45–100%MeCN_0–2–4–24–25min, 1 mL/min. R_t = 16.25 min.

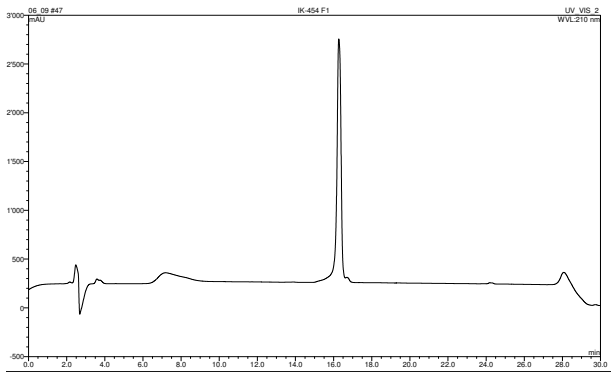

HR-MS (ESI) $C_{71}H_{86}N_{12}O_{25}S^{2+}$ $[M+2H]^{2+}$ calculated: 769.2768 found: 769.2764.

Hyp$_9$-Lys-CF (2.09)

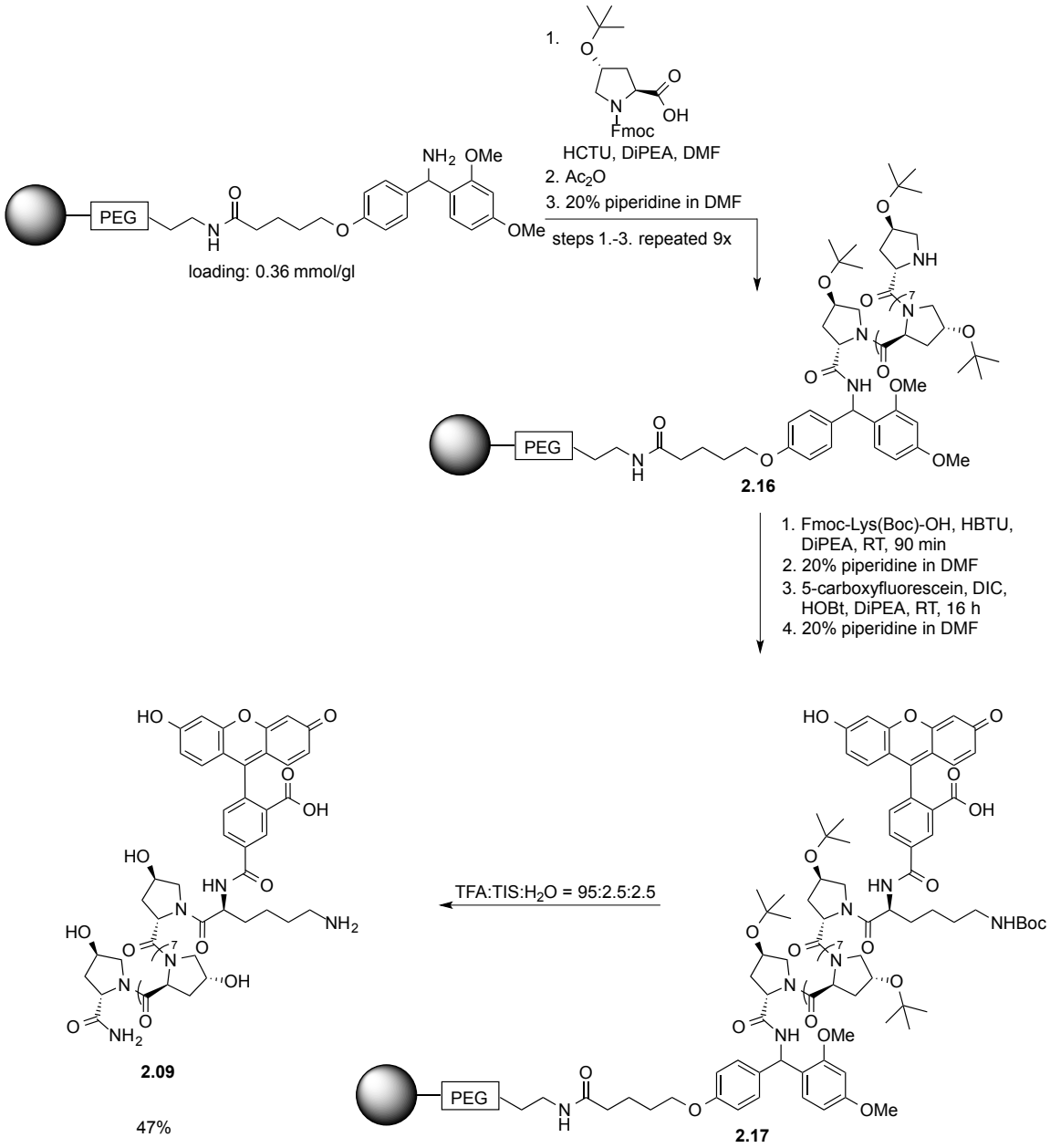

The synthesis of 4-hydroxyproline oligomer was performed on the solid phase using an automated peptide synthesizer (CS Bio, CS136XT). The synthesis was carried out on a Rink Amide-NovaPEG resin (Merck Millipore) with a loading of 0.36 mmol/g. The reagents used for the synthesis were: Fmoc-Hyp(*t*Bu)-OH (4.0 equiv.), HOBt/HBTU (4.0 equiv.), DiPEA in NMP (2.0 equiv.), 5% Ac_2O with 5% 2,6-lutidine in DMF and 20% piperidine in DMF. Each coupling was carried out for 1.5 h. From 0.25 g of the Rink-NovaPEG resin, ~0.4 g of resin was obtained after the synthesis. The following steps were performed manually.

Rink Amide-NovaPEG resin loaded with the 9-mer of 4-hydroxyproline was swelled in CH_2Cl_2 for 1 h and the solvent was replaced by DMF. In a separate flask Fmoc-Lys(Boc)-OH (127 mg, 270 µmol, 3.0 equiv.) was dissolved in 4 mL DMF/CH_2Cl_2 (1:1) and DiPEA (45 µL, 270 µmol,

3.0 equiv.) was added. To the reaction mixture was added HBTU (112 mg, 270 µmol, 3.0 equiv.) and the solution was stirred for 8 min at room temperature. The solution was added to the resin and the resin was shaken for 1.5 h at room temperature. Completion of the coupling was checked using the chloranil test. The resin was washed with DMF (7x). Deprotection was performed using 4 mL of 20% piperidine in DMF for 3 min and 2x 4 mL for 10 min. The resin was washed with DMF (7x). In a separate flask 5-carboxyfluorescein (2.5 equiv., 225 µmol, 85 mg) was dissolved in 4 mL DMF and DiPEA (35 µL, 225 µmol, 2.5 equiv.) was added. To the solution was added HOBt (33 mg, 225 µmol, 2.5 equiv.) and DIC (28 µL, 225 µmol, 2.5 equiv.) and the solution was stirred for 15 min at room temperature with exclusion of light. The solution was added to the resin and it was shaken for 16 h with the exclusion of light. Completion of the reaction was checked using the Kaiser test. The solution was removed and the resin was washed with DMF (7x). The beads were treated with 20% piperidine in DMF for 15 min and the beads were washed with DMF (5x) and CH_2Cl_2 (5x).[169] The beads were dried under a stream of N_2 until its weight remained constant. For cleavage of the peptide, the beads were treated with 8.4 mL of cleavage cocktail (8 mL TFA, 0.2 mL TIS, 0.2 mL H_2O) for 2 h. The solution was filtered through a pad of cotton and TFA was removed by N_2 stream. The residue was dissolved in MeCN/H_2O (1:1) and filtered through a SPE column. The MeCN was removed by rotary evaporation and the compound was purified by reversed phase HPLC using H_2O/MeCN + 0.1% FA (λ = 492 nm).

Column: Gemini-NX 10µ C18 110A, 250 mm x 21.2 mm

Method: 10–10–20–100%MeCN_0–2–25–33min, 20 mL/min. R_t = 14.25 min.

The MeCN was removed by rotary evaporation and the compound was lyophilized from water. The compound was obtained as a yellow foam in 47% yield (65 mg, 31 µmol).

The purity of the compound was analyzed by analytical reversed phase HPLC using H_2O/MeCN + 0.1% FA (λ = 492 nm).

Column: Gemini-NX 3µ C18 110A, 150 mm x 4.60 mm

Method: 10–10–20–100%MeCN_0–1–15–20min, 1 mL/min. R_t = 11 min.

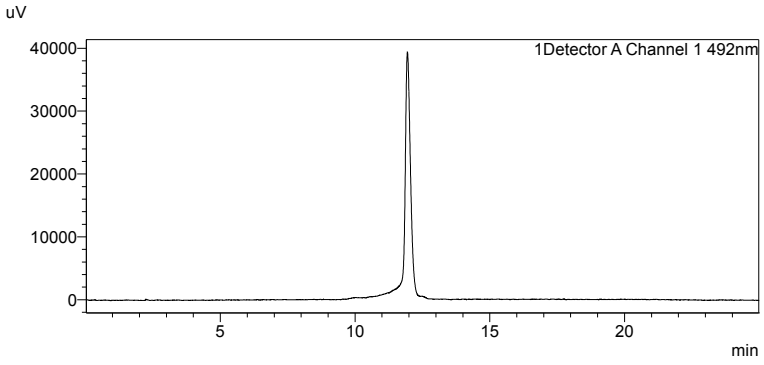

HR-MS (ESI) $C_{72}H_{91}N_{12}O_{25}^{3+}$ $[M+H]^{3+}$: calculated: 507.87340 found: 507.87365.

Hyp$_9$-AHX-Lys-CF adduct (2.10)

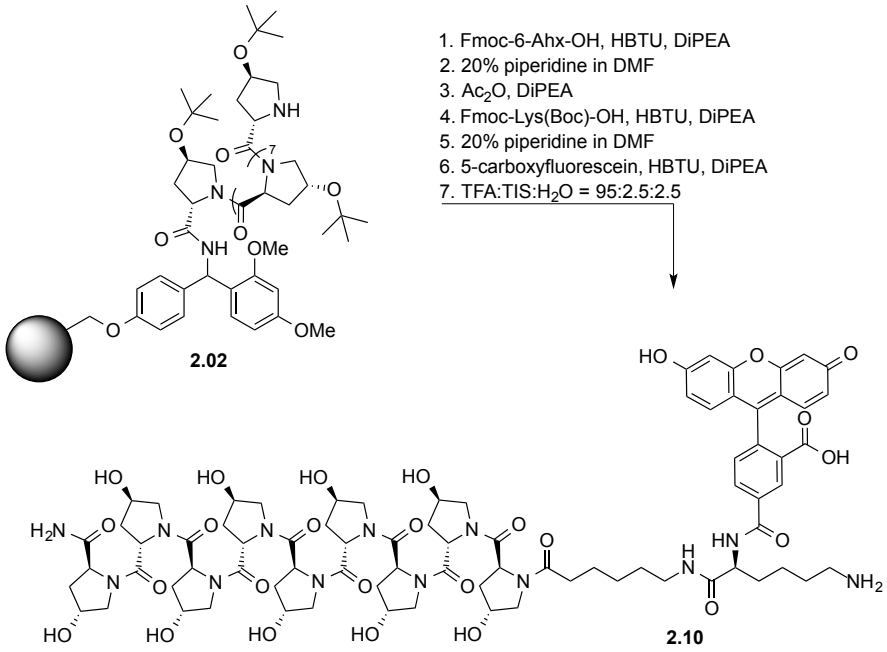

Rink amide resin loaded with Hyp$_9$-NH_2 was swelled in CH_2Cl_2 for 1 h. The solvent was removed and the beads were washed with DMF (5x). In a separate flask Fmoc-6-AHX-OH (94 mg, 266 µmol, 3.0 equiv.) was dissolved in 2.5 mL DMF by addition of DiPEA (44 µL, 266 µmol, 3.0 equiv.) and it was stirred until a clear solution was obtained. HBTU (101 mg, 266 µmol, 3.0 equiv.) was added and the solution was stirred for 8 min at room temperature. The solution was added to the beads and it was shaken at room temperature for 1 h 12 min. The reaction was not complete and the reagents were removed from the resin. The coupling step was repeated at room temperature using a new set of reagents and it was shaken at room temperature. After 4 h the reaction was still not complete and the beads and the solution were transferred into a microwave reaction vial and the mixture irradiated in the microwave for 10 min at 75 °C. Almost complete conversion was obtained and the beads were transferred back into a peptide reaction vessel containing a frit. The beads were washed thoroughly with DMF (7x) and capping was performed (0.54 mL Ac_2O and 0.97 mL DiPEA in 2 mL DMF) for 30 min at room temperature. The beads were washed with DMF (7x) and Fmoc deprotection was performed using 20% piperidine in DMF for 3 min and 2x 10 min. The beads were washed with DMF (7x). In a separate flask, Fmoc-Lys(Boc)-OH (124 mg, 266 µmol, 3.0 equiv.) was dissolved in 2.5 mL DMF, DiPEA (44 µL, 266 µmol, 3.0 equiv.) and HBTU (101 mg, 266 µmol, 3.0 equiv.) was added and it was stirred for 8 min at room temperature. The beads were transferred in a microwave reactor, the solution was added and it was heated to 75 °C for 20 min in the microwave while stirring

(entire completion of the reaction by TNBS and Kaiser test). The beads were transferred to a peptide reaction vessel and thoroughly washed with DMF (7x). Deprotection was performed with 20% piperidine in DMF for 3 min and 2x for 10 min. The beads were washed with DMF (7x). 5-Carboxyfluorescein (105 mg, 266 µmol, 3.0 equiv.) was dissolved in 2.5 mL DMF and DiPEA (44 µL, 266 µmol, 3.0 equiv.) and HBTU (101 mg, 266 µmol, 3.0 equiv.) was added. It was stirred at room temperature for 8 min. The solution was added to the beads that were previously transferred into a microwave reaction vessel. The mixture was irradiated for 90 min at 75 °C until the reaction was complete. The beads were washed with DMF (5x) and CH_2Cl_2 (5x).

Cleavage of the peptide was performed for 2 h using 1 mL of cleavage cocktail (0.95 mL TFA, 0.025 mL TIS, 0.025 mL H_2O). The solution was filtered and dropped into 30 mL of 0 °C MTBE and it was rinsed with 2x 0.2 mL TFA. The mixture was centrifuged (15 min, 3000 r/min) and the solvent decanted. The solid was washed with 30 mL MTBE (3x). After decanting, the residual MTBE was removed by N_2 stream and the resulting solid was purified by reversed phase HPLC using H_2O/MeCN + 0.1% FA (λ = 210 nm).

Column: Gemini-NX 10µ C18 110A, 250 mm x 21.2 mm

Method: 2-2–10–27–100%MeCN_0-6–9–23–25min, 20 mL/min. R_t = 20 min.

The MeCN was removed by rotary evaporation and the compound was lyophilized from water. The compound was obtained as a yellow foam in 3.8% yield (5.5 mg, 3.4 µmol).

The purity of the compound was analyzed by analytical reversed phase HPLC using H_2O/MeCN + 0.1% FA (λ = 210 nm).

Column: Gemini-NX 5µ C18 110A, 150 mm x 4.60 mm

Method: 2–2–10–45–100%MeCN_0–2–4–24–25min, 1 mL/min. R_t = 13.5 min.

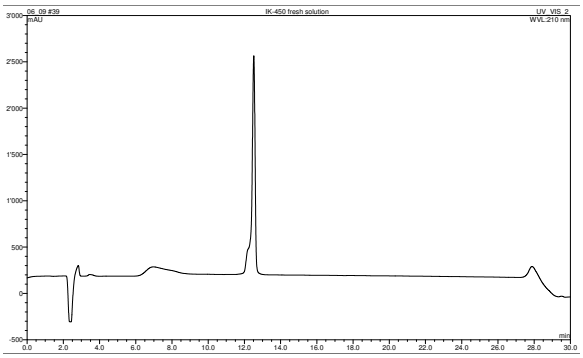

HR-MS (ESI) $C_{78}H_{101}N_{13}O_{26}^{2+}$ $[M+2H]^{2+}$ calculated: 817.8485 found: 817.8495.

Hyp$_9$-CF (2.18)

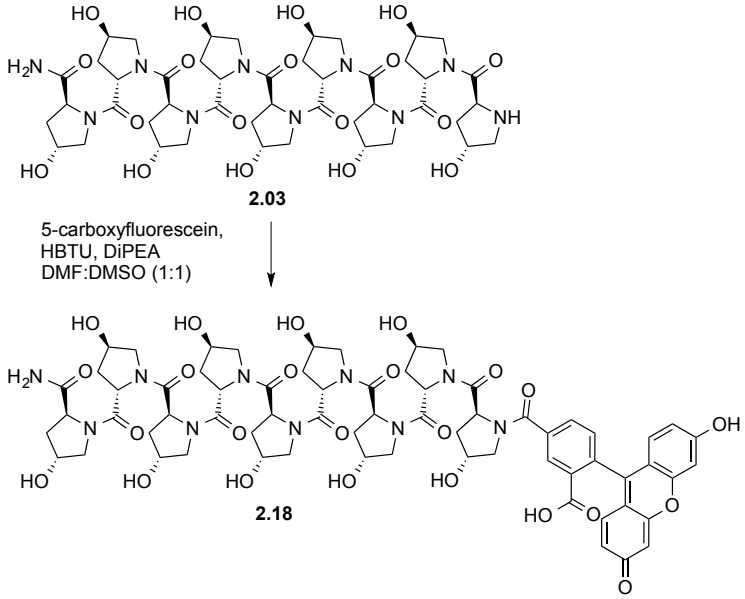

5-Carboxyfluorescein (9.6 mg, 26 µmol, 1.6 equiv.), HBTU (9.1 mg, 24 µmol, 1.5 equiv.) and DiPEA (8 µL, 48 µmol, 3.0 equiv.) were dissolved in 80 µL DMF and stirred for 8 min at room temperature. The solution was added to Hyp$_9$-NH$_2$ (16.6 mg, 16 µmol, 1.0 equiv.) in 80 µL DMSO and the reaction was stirred for 24 with exclusion of light. The reaction mixture was precipitated in 8 mL MTBE at 0 °C and the mixture was centrifuged, the solvent was decanted and the solid resuspended with MTBE (4x). The resulting solid was dried with an N_2 stream and purified by reversed phase HPLC using H_2O/MeCN + 0.1% FA (λ = 492 nm).

Column: Gemini-NX 10µ C18 110A, 250 mm x 21.2 mm

Method: 10–10–80–100%MeCN_0–1–20–21min, 20 mL/min. R_t = 9.2 min.

The MeCN was removed by rotary evaporation and the compound was lyophilized. The compound was obtained as a yellow foam in 26% yield (5.8 mg, 4 µmol).

The purity of the compound was analyzed by analytical reversed phase HPLC using H_2O/MeCN + 0.1% FA (λ = 254 nm).

Column: Gemini-NX 3µ C18 110A, 150 mm x 4.60 mm

Method: 10–10–80–100%MeCN_0–1–15–15.1min, 1 mL/min. R_t = 6.3 min.

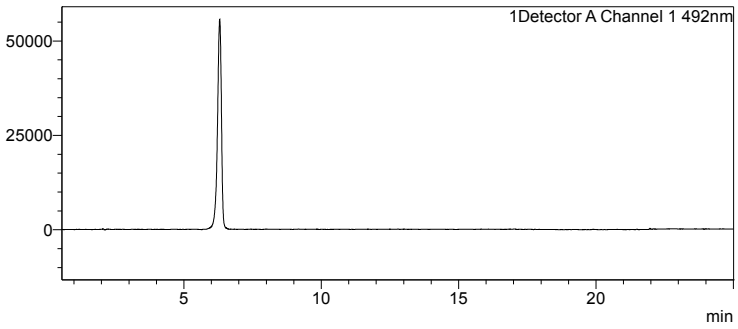

HR-MS (ESI) $C_{66}H_{78}N_{10}O_{24}^{2+}$ $[M+H]^{2+}$ calculated: 697.25897 found: 697.25890.

Hyp$_9$-Lys-CF-Vancomycin (2.19)

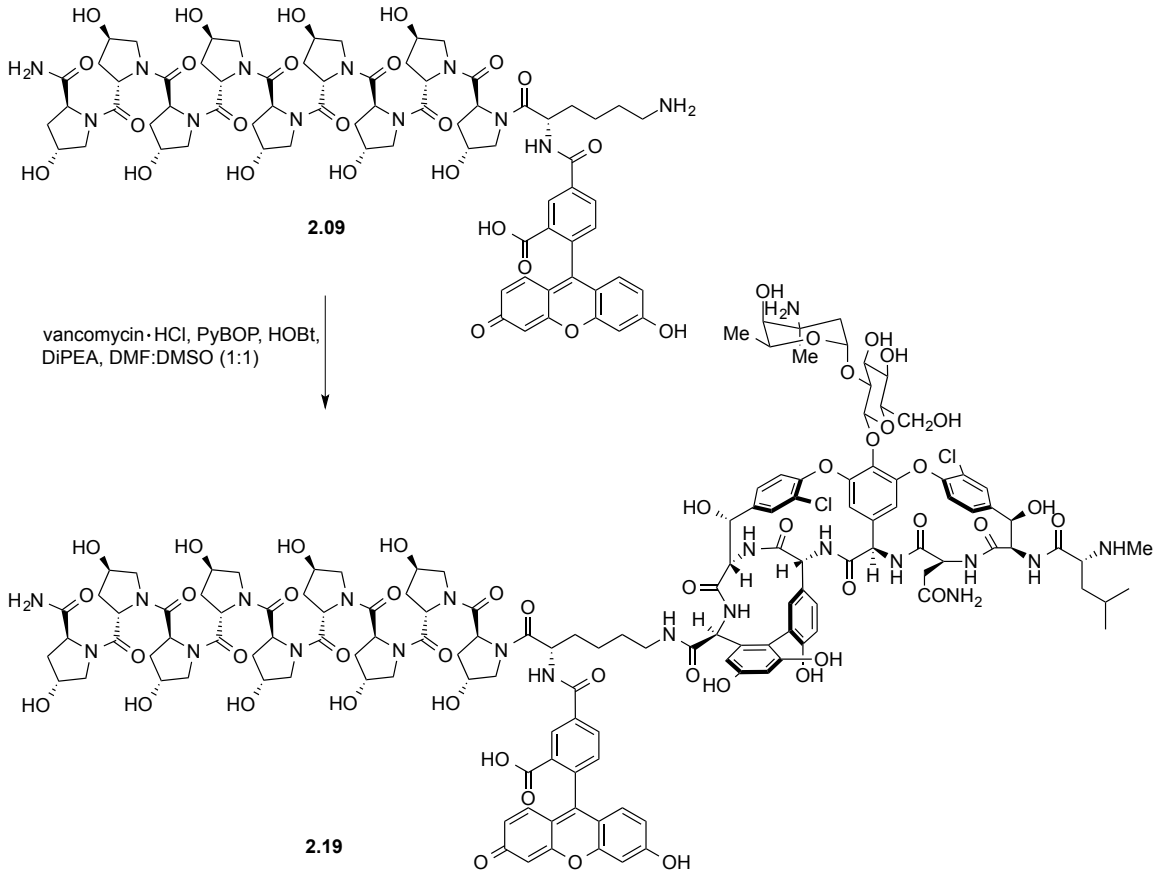

Vancomycin (58 mg, 39 µmol, 3.0 equiv.) was dissolved in 0.26 mL DMF:DMSO (1:1) and Di-PEA (13 µL, 79 µmol, 6.0 equiv.), HOBt (5.3 mg, 39 µmol, 3.0 equiv.) and PyBOP (21 mg, 39 µmol, 3.0 equiv.) were added and the reaction mixture was stirred for 8 min at room temperature. The solution was added to anchor **2.09** (20 mg, 13 µmol, 1.0 equiv.) and the mixture was stirred for 2 h at room temperature. The reaction mixture was dissolved in MeCN:H_2O (1:3) and filtered through a SPE column. The MeCN was evaporated and the compound was purified by reversed phase HPLC.

1st purification:

H_2O/MeCN + 0.1% FA (λ = 440 nm).

Column: Gemini-NX 10µ C18 110A, 250 mm x 21.2 mm

Method: 2–2–20–60–100%MeCN_0–3–33–41–50min, 20 mL/min. R_t = 26 min.

2nd purification:

H_2O/MeCN + 0.1% FA (λ = 440 nm).

Column: Gemini-NX 10µ C18 110A, 250 mm x 21.2 mm

Method: 13%MeCN_isocratic, 20 mL/min, R_t = 8 min.

The MeCN was removed by rotary evaporation and the compound was lyophilized from water. The compound was obtained as a yellow foam in 44% yield (17 mg, 6 μmol).

The purity of the compound was analyzed by analytical reversed phase HPLC using H_2O/MeCN + 0.1% FA (λ = 492 nm).

Column: Gemini-NX 3μ C18 110A, 150 mm x 4.60 mm

Method: 13%MeCN_isocratic, 1 mL/min. R_t = 7 min.

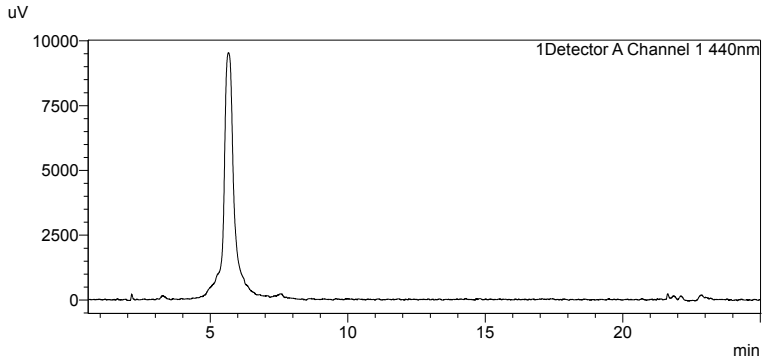

HR-MS (ESI) $C_{138}H_{164}N_{21}O_{48}Cl_2^{3+}$ $[M+3H]^{3+}$ calculated: 984.34661 found: 984.34605.

Hyp$_9$-*p*BrBzOH (2.24)

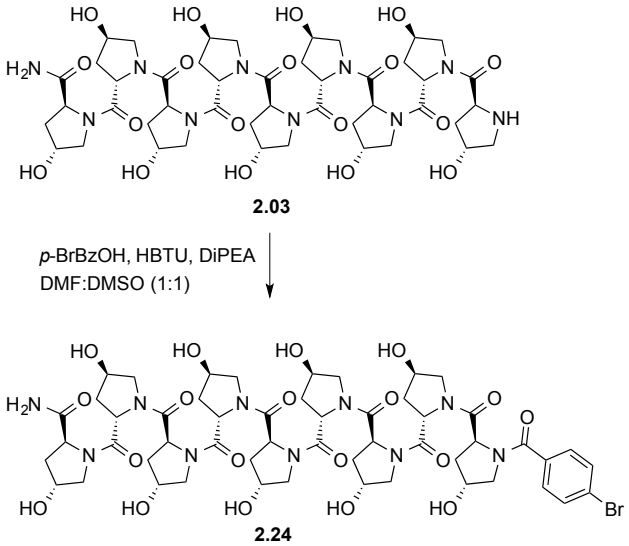

p-Bromobenzoic acid (9.3 mg, 46 µmol, 1.6 equiv.) DiPEA (14 µL, 87 µmol, 3.0 equiv.) and HBTU (17 mg, 44 µmol, 1.5 equiv.) were dissolved in 0.15 mL DMF and stirred for 8 min at room temperature. The solution was added to Hyp$_9$-NH$_2$ (30 mg, 29 µmol, 1.0 equiv.) dissolved in 0.15 mL DMSO. The mixture was stirred at room temperature for 41 h. The solution was precipitated in 20 mL 0 °C MTBE and the mixture was centrifuged, the solvent was decanted and the solid resuspended with MTBE (3x). The solid was dried with a N_2-stream and purified by reversed phase HPLC using H_2O/MeCN + 0.1% FA (λ = 254 nm).

Column: Gemini-NX 10µ C18 110A, 250 mm x 21.2 mm

Method: 10–10–60–100%MeCN_0–3–25–25.1min, 20 mL/min. R_t = 10.8 min.

The MeCN was removed by rotary evaporation and the compound was lyophilized from water. The compound was obtained as a white foam in 40% yield (14 mg, 12 µmol).

The purity of the compound was analyzed by analytical reversed phase HPLC using H_2O/MeCN + 0.1% FA (λ = 254 nm).

Column: Gemini-NX 3µ C18 110A, 150 mm x 4.60 mm

Method: 10–10–80–100%MeCN_0–1–15–15.1, 1 mL/min. R_t = 5.4 min.

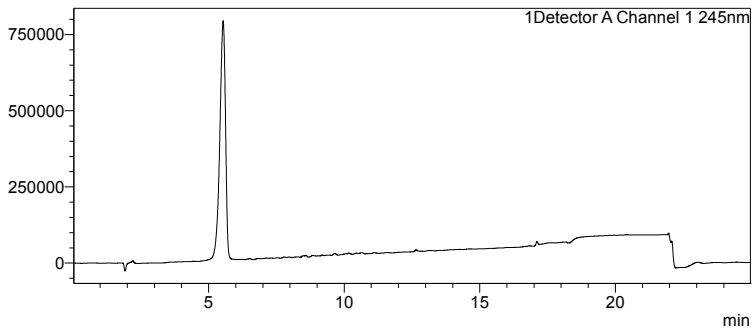

HR-MS (ESI) $C_{52}H_{71}N_{10}O_{19}Br^{2+}$ $[M+2H]^{2+}$ calculated: 609.20347 found: 609.20380.

Hyp$_9$-AHX (2.20)

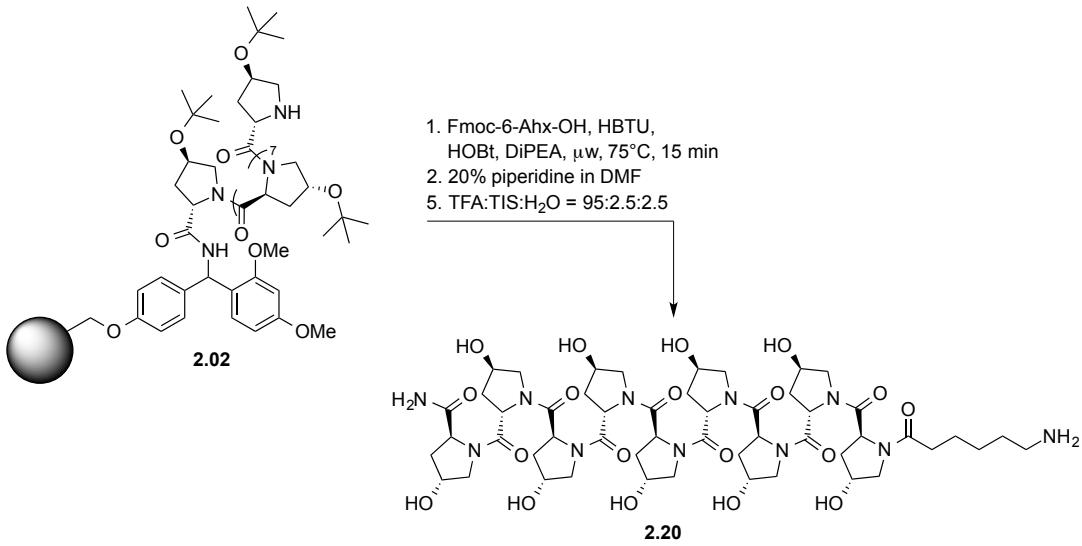

Hyp$_{10}$-NH$_2$ was used on Rink amide resin. 0.25 g of Resin was swelled in 2.5 mL CH_2Cl_2 for 2 h and the resin was washed with DMF (4x). Fmoc-6-Ahx-OH (102 mg, 0.29 mmol, 3.0 equiv.), HOBt (39 mg, 0.29 mmol, 3.0 equiv.), HBTU (110 mg, 0.29 mmol, 3.0 equiv.) and DiPEA (96 µL, 0.58 mmol, 6.0 equiv.) were stirred for 8 min at room temperature and then added to the resin. The resin was heated under stirring and microwave irradiation at 75 °C for 15 min. Completion of the reaction was checked using the chloranil test. The beads were transferred in a reaction frit and washed thoroughly with DMF and deprotection was performed using 20% piperidine in DMF for 3 min and 2x for 10 min. The resin was washed with DMF (5x) and CH_2Cl_2 (5x) and dried with N_2-stream. The peptide was cleaved from the resin using 2.5 mL TFA:TIS:H_2O (95:2.5:2.5) at room temperature for 2 h. The solution was filtered through a Pasteur pipette filled with a pad of cotton and dropped into MTBE at 0 °C. The precipitate was centrifuged and the solvent decanted (3x). Fresh MTBE was added and centrifugation was repeated (3x). The MTBE was removed by N_2 stream. The solid was dissolved in water and filtered through a SPE column and the column was flushed with water. The water was removed by lyophilization to obtain the product as a white foam in 74% yield (82 mg, 71 µmol). The compound was used without further purification in the next step.

HR-MS (ESI) $C_{51}H_{78}N_{11}O_{19}^+$ $[M+H]^+$ calculated: 1148.54700 found: 1148.54679.

Hyp$_9$-AHX-vancomycin (2.21)

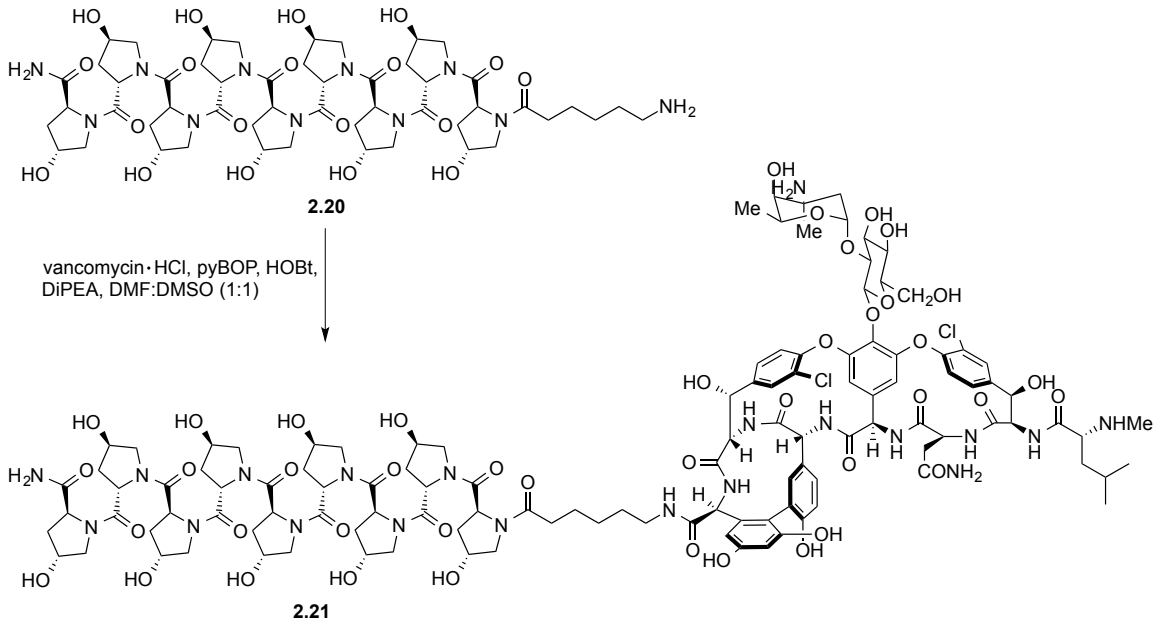

Vancomycin hydrochloride (30 mg, 20 µmol, 1.0 equiv.) and DiPEA (6.7 µL, 40 µmol, 2.0 equiv.) were added to 400 µL DMF:DMSO (1:1) and it was stirred until the vancomycin completely dissolved. HOBt (2.73 mg, 20 µmol, 1.0 equiv.) was added followed by pyBOP (11 mg, 20 µmol, 1.0 equiv.) and it was stirred for 8 min at room temperature. The solution was added to **2.20** (46 mg, 40 µmol, 2.0 equiv.) and it was stirred for 3 h at room temperature. Conversion was checked by LC-MS and the reaction mixture was dissolved in MeCN:H_2O (7:10) and filtered through a SPE column. The MeCN was removed by rotary evaporation and the crude mixture was purified by reversed phase HPLC.

1st purification:

H_2O/MeCN + 0.1% FA (λ = 225 nm).

Column: Gemini-NX 10µ C18 110A, 250 mm x 21.2 mm

Method: 5–5–100%MeCN_0–5–33min, 20 mL/min, R_t = 9.6 min.

2nd purification:

H_2O/MeCN + 0.1% FA (λ = 280 nm).

Column: Gemini-NX 10µ C18 110A, 250 mm x 21.2 mm

Method: 8%MeCN_isocratic, 20 mL/min, R_t = 6 min.

The MeCN was removed by rotary evaporation and the compound was lyophilized. The compound was obtained as a white foam in 44% yield (23.1 mg, 9 µmol).

The purity of the compound was analyzed by analytical reversed phase HPLC using H_2O/MeCN + 0.1% FA (λ = 492 nm).

Column: Gemini-NX 3µ C18 110A, 150 mm x 4.60 mm

Method: 5–5–100%MeCN_0–2–20min, 1 mL/min. R_t = 5.5 min.

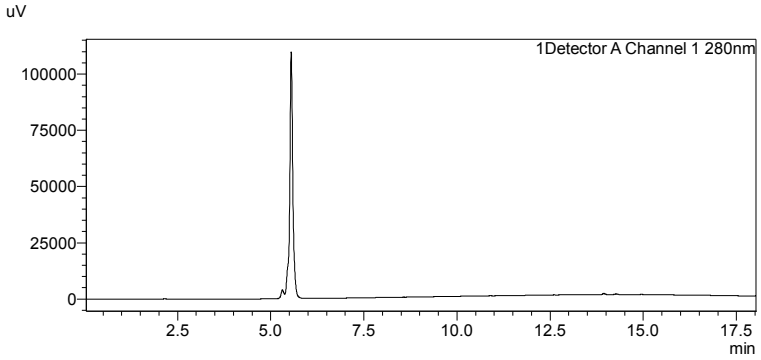

HR-MS (ESI) $C_{117}H_{153}N_{20}O_{42}Cl_2^{3+}$ $[M+H]^{3+}$ calculated: 859.99373 found: 859.99435.

CF-vancomycin adduct (2.23)

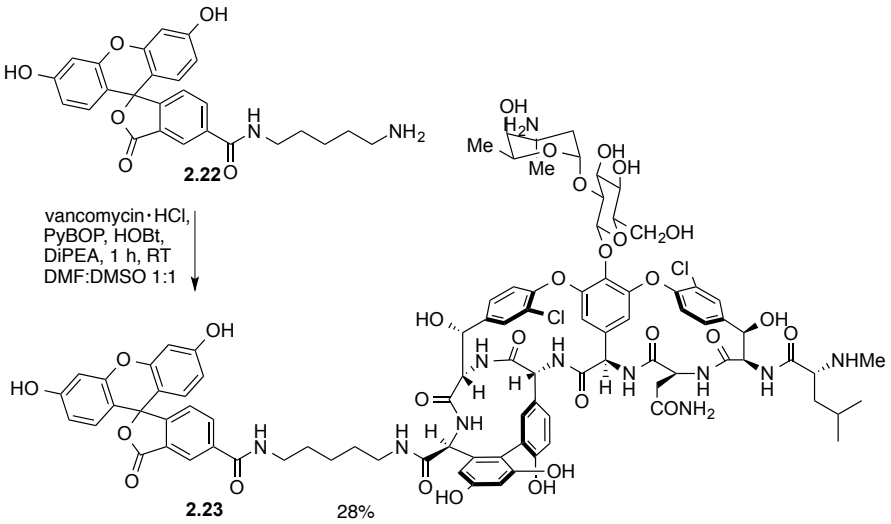

Vancomycin hydrochloride (15 mg, 10 µmol, 1.0 equiv.) and DiPEA (3.3 µL, 20 µmol, 2 equiv.) were added to 200 µL DMF:DMSO (1:1) and it was stirred until the vancomycin completely dissolved. HOBt (1.36 mg, 10 µmol, 1.0 equiv.) was added followed by pyBOP (5.26 mg, 10 µmol, 1.0 equiv.) and it was stirred for 8 min at room temperature. The solution was added to the fluorescein linker (9.3 mg, 20 µmol, 2.0 equiv.) and it was stirred for 1 h at room temperature. Conversion was checked by LC-MS and the reaction mixture was diluted with 60% MeCN in water and filtered through a SPE column. The MeCN was removed by rotary evaporation and the crude mixture was purified by reversed phase HPLC.

H_2O/MeCN + 0.1% FA (λ = 280 nm).

Column: Gemini-NX 10µ C18 110A, 250 mm x 21.2 mm

Method: 5–5–25–100%MeCN_0–3–33–33.1min, 20 mL/min, R_t = 25.5 min.

The MeCN was removed by rotary evaporation and the compound was lyophilized. The compound was obtained as a yellow foam in 28% yield (5.36 mg, 3 µmol).

The purity of the compound was analyzed by analytical reversed phase HPLC using H_2O/MeCN + 0.1% FA (λ = 280 nm).

Column: Gemini-NX 3µ C18 110A, 150 mm x 4.60 mm

Method: 5–5–25–100%MeCN_0–1–20–20.1min, 1 mL/min. R_t = 14.9 min.

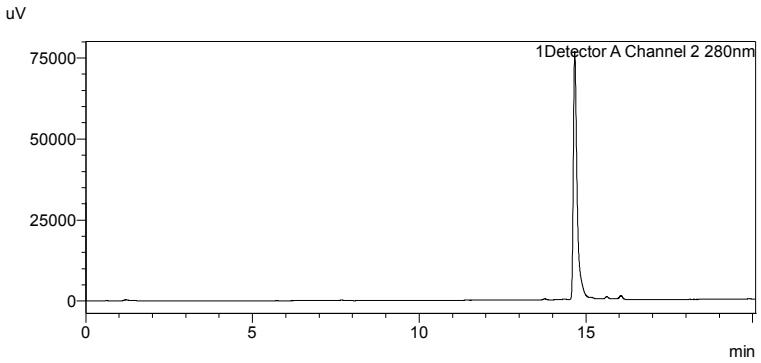

HR-MS (ESI) $C_{92}H_{100}N_{11}O_{29}Cl_2^{3+}$ $[M+3H]^{3+}$ calculated: 630.86830 found: 630.86989.

7.2.4 Manual crystallization of 2.24

No.	Substance	Method	solvent 1	solvent 2	result
1	**3**	Vapor diffusion	MeOH	-	Oil
3	**3**	Vapor dialysis	MeOH	Et_2O	Stiky residue
3	**2.24**	Batch, seeding	EtOH	H_2O	No evaporation
4	**2.24**	Batch, seeding	MeCN	H_2O	No evaporation
5	**2.24**	Vapor diffusion	H_2O	Diglyme	Amorphous solid
6	**2.24**	Batch + seeding	MeOH	H_2O	No evaporation
7	**2.24**	Vapor diffusion	H_2O	Dioxane	Oil
8	**2.24**	Vapor dialysis	H_2O	MeCN	Sticky residue

7.2.5 Screens used for the automated crystallization of 2.24

The following screens were used a the Protein Crystallization Facility, Universität Zürich:[44]

Compound	Screen	Temperature	Concentration
2.24	GS048	4 °C	10 mg/mL
2.24	GS048	20 °C	10 mg/mL
2.03	GS048	4 °C	10 mg/mL
2.03	GS048	20 °C	10 mg/mL
2.24	GS027	20 °C	20 mg/mL
2.24	GS028	20 °C	20 mg/mL
2.24	GS074	20 °C	20 mg/mL
2.24	GS075	20 °C	20 mg/mL
2.03	GS048	20 °C	60 mg/mL
2.24	GS027	20 °C	60 mg/mL

[44] The conditions for the individual screens can be downloaded from the website of the Protein Crystallization Center UZH:
https://www.bioc.uzh.ch/de/forschung/core-facilities/protein-crystalization-center/initial-screen/initial-xtal-screens/

7.3 Synthesis of pyrrolizidines

7.3.1 Synthesis

3-(3,4-Dihydro-2*H*-pyrrol-5-yl)propan-1-ol (3.21)

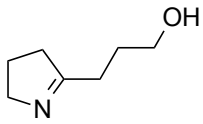

i-Pr_2NH (6.12 mL, 43.0 mmol, 1.2 equiv.) was dissolved in anhydrous THF (12 mL) and cooled to –78 °C. *n*-BuLi (25 mL of 1.6 mol/L solution in hexane, 40.0 mmol, 1.1 equiv.) was added dropwise and stirred for 40 min at –78 °C. 2-Methyl-1-pyrroline (3.4 mL, 36.0 mmol, 1.0 equiv.) was added and the reaction mixture was stirred for 1 h at –78 °C. Ethylene oxide (16 mL, 40.0 mmol, 2.5 mol/L solution in THF) was added at –78 °C and the mixture was stirred for 5 h. The reaction was quenched with sat. aq $NaHCO_3$ (20 mL) and the layers were separated. The aqueous layer was extracted with EtOAc (3 × 20 mL) and the combined organic layers were dried ($MgSO_4$). Evaporation of the solvents gave the crude product as a yellow oil. The residue was purified by distillation (bp 55 °C/$9.4 \cdot 10^{-3}$ mbar) to afford a colorless oil, which turned yellow upon standing; yield: 2.44 g (19 mmol, 53%).

^{1}H-NMR (250 MHz, $CDCl_3$) δ = 3.87–3.75 (m, 2H), 3.73–3.65 (m, 2H), 2.57–2.38 (m, *J* = 6.5 Hz, 4H), 1.96–1.82 (m, 4H) ppm. **^{13}C-NMR** (101 MHz, $CDCl_3$) δ = 179.57, 63.10, 60.43, 38.31, 32.58, 28.62, 22.68 ppm. **FTIR** (neat) ν = 2965, 2921, 2854, 1619, 1431, 1303, 1267, 1194, 1113 cm^{-1}. **HR-MS** (ESI) $C_7H_{14}NO^+$ $[M+H]^+$ calculated: 128.1070 found: 128.1070.

General procedure for the synthesis of isonitriles (GP 1):[170]

Aniline (4.50 mmol, 1.00 equiv.) was dissolved in 20 mL CH_2Cl_2 and tetrabutylammonium bromide (0.31 mmol, 0.069 equiv.) and aq. 50 w% NaOH (6.5 mL) was added. The mixture was stirred vigorously and $CHCl_3$ (6.7 mmol, 1.50 equiv.) was added and stirring was continued overnight. The reaction mixture was transferred in a separation funnel, the layers were separated and the organic layer was washed with water (2x) and brine (1x). The combined organic layers were dried over $MgSO_4$ and the solvent was carefully evaporated. The crude product was purified by column chromatography.

Isocyanobenzene (3.31)

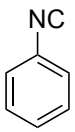

Purified by column chromatography on silica gel using Et_2O:pentane 1:7 (R_f = 0.8). The product was obtained as a greenish oil which darkens upon standing at room temperature in 57% yield (1.29 g, 12 mmol). **^{1}H-NMR** (400 MHz, $CDCl_3$) δ = 7.45–7.35 (m, 5H) ppm. The analytical data were in agreement with the literature.[170]

1-Isocyano-4-methoxybenzene (3.35)

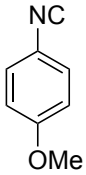

Purified by column chromatography on silica gel using Et_2O:pentane 1:2 (R_f = 0.67). The product was obtained as a brown oil in 62% yield (0.34 g, 2.5 mmol). **^{1}H-NMR** (400 MHz, $CDCl_3$) δ = 7.31 (d, *J* = 8.7 Hz, 2H), 6.90–6.84 (m, 2H), 3.82 (s, 3H) ppm. **^{13}C-NMR** (101 MHz, $CDCl_3$) δ = 160.02, 127.90, 114.71, 55.72 ppm.

1-Fluoro-4-isocyanobenzene (3.36)

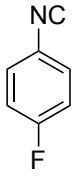

Purified by column chromatography on silica gel using Et_2O:pentane 1:1 (R_f = 0.78). The product was obtained as a yellow greenish oil which darkens upon standing in 58% yield (0.31 g, 2.6 mmol).

^{1}H-NMR (400 MHz, $CDCl_3$) δ = 7.38 (dd, *J* = 8.6, 4.7 Hz, 2H), 7.13–7.06 (m, 2H) ppm. **^{13}C-NMR** (101 MHz, $CDCl_3$) δ = 163.73, 161.23 (d, *J* = 251.79 Hz), 128.58, 128.49, 116.92, 116.69, 100.13 ppm. **^{19}F-NMR** (376 MHz, $CDCl_3$) δ = -111.81 ppm.

1-Bromo-4-isocyanobenzene (3.37)

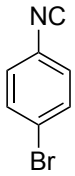

Purified by column chromatography on silica gel using Et_2O:pentane 1:5 (R_f = 0.83). The product was obtained as yellow crystals in 73% yield (0.38 g, 2.1 mmol).

^{1}H-NMR (400 MHz, $CDCl_3$) δ = 7.54 (d, *J* = 8.6 Hz, 2H), 7.29–7.22 (m, 2H) ppm.

1-Ethynyl-4-isocyanobenzene (3.39)

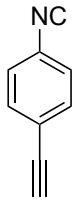

The product was purified by column chromatography on silica gel using Et_2O:pentane 1:2 (R_f = 0.8). The Product was obtained as a yellow solid in 44% yield (0.23 g, 1.8 mmol). **^{1}H-NMR** (400 MHz, $CDCl_3$) δ = 7.55–7.47 (m, 2H), 7.34 (d, *J* = 8.6 Hz, 2H), 3.20 (s, 1H) ppm. **^{13}C-NMR** (101 MHz, $CDCl_3$) δ = 166.14, 133.28, 126.53, 123.68, 82.03, 80.16 ppm.

2-Isocyano-1,3-dimethoxybenzene (3.40)

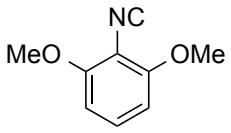

Purified by column chromatography on silica gel using Et_2O:pentane 1:2 (R_f = 0.32). The product was obtained as a white solid in 78% yield (0.25 g, 1.5 mmol). **^{1}H-NMR** (400 MHz, $CDCl_3$) δ = 7.25 (t, *J* = 8.5 Hz, 1H), 6.56 (d, *J* = 8.5 Hz, 2H), 3.91 (s, 6H) ppm. **^{13}C-NMR** (101 MHz, $CDCl_3$) δ = 156.47, 130.03, 103.88, 56.39 ppm. **FTIR** (neat) ν = 3008, 2945, 2841, 1588, 1479, 1264, 1104 cm^{-1}. **HRMS** (ESI) $C_9H_{10}NO_2^+$ $[M+H]^+$: calculated: 164.0706 found: 164.0704.

4-(2-Isocyanoethyl)phenol (3.54)

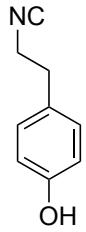

Formic acid (0.690 mL, 18.2 mmol, 5.00 equiv.) and acetic anhydride (0.69 mL, 7.30 mmol, 2.00 equiv.) were heated at 55 °C for 2 h. 4-(2-Aminoethyl)-phenol (500 mg, 3.64 mmol, 1.00 equiv.) was dissolved in THF (6.0 mL) and the freshly prepared formic anhydride was added dropwise at room temperature. The reaction mixture was stirred at room temperature overnight and quenched with aq. $NaHCO_3$ solution. The mixture was transferred to a separation funnel, the layers were separated and the aqueous layer was extracted with EtOAc (3x). The combined organic layers were dried over $MgSO_4$ and the solvents removed in *vacuo*.

The crude formamide mixture 0.321g (1.94 mmol, 1.00 equiv.) was dissolved in dry CH_2Cl_2 (7.9 mL) and cooled to -78 °C. Triphosgene (0.202 g, 0.68 mmol, 0.35 equiv.) was dissolved in dry CH_2Cl_2 (2.0 mL) and the solution was given dropwise to the formamide solution. After stirring for 5 min, *N*-methylmorpholine (0.42 mL, 3.80 mmol, 2.00 equiv.) was added slowly over the course of 10 min and the reaction mixture was stirred at -78 °C for 2 h. After 2 h the reaction conversion was monitored by TLC. The reaction was quenched with water and the heterogeneous mixture was allowed to warm to room temperature. The mixture was transferred to a separation funnel. The two layers were separated and the aqueous layer was extracted with CH_2Cl_2 (2x). The organic layers were combined, dried over $MgSO_4$ and the solvent was removed by evaporation. The compound was purified by column chromatography using Et_2O:pentane 1:1. The product was obtained as a brown solid in 24% yield (68.0 mg, 1.94 mmol). **^{1}H-NMR** (400 MHz, $CDCl_3$) δ = 7.14–7.06 (m, 2H), 6.84–6.77 (m, 2H), 4.84 (s, 1H), 3.57 (tt, *J* = 7.0, 1.8 Hz, 2H), 2.91 (tt, *J* = 7.2, 2.1 Hz, 2H) ppm. **^{13}C-NMR** (101 MHz, $CDCl_3$) δ = 154.93, 130.07, 115.78, 43.44, 34.99 ppm. **FTIR** (neat) ν = 3279, 3020, 2927, 1612, 1595, 1514, 1442, 1349, 1225 cm^{-1}. **HR-MS** (ESI) $C_9H_8NO^-$ $[M+H]^-$ calculated: 146.0611 found: 146.0612. M.p. = 44 °C.

General procedure for the synthesis of pyrrolizidines (GP 2):

Imine **3.21** (0.47 mmol, 1.0 equiv.) and isonitrile (0.47 mmol, 1.0 equiv.) were dissolved in dry toluene (3.6 mL) and $Et_3N{\cdot}HCl$ (0.94 mmol, 2.0 equiv.) was added. The suspension was heated under reflux and the reaction was monitored by TLC. The reaction mixture was diluted with water, the layers were separated and the aqueous layer was extracted using Et_2O (2x 5 mL). The combined organic layers were dried over $MgSO_4$. The solvents were removed in vacuo and the residue was purified by flash column chromatography on silica gel.

***N*-Phenyltetrahydro-1*H*-pyrrolizine-*7a*(5*H*)-carboxamide (3.32)**

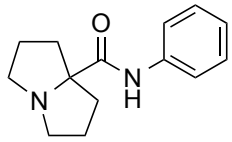

Purification by column chromatography on silica gel using CH_2Cl_2:MeOH 40:1 (R_f = 0.41). The product was obtained as a yellow solid in 46% yield (50 mg, 0.22 mmol). **^{1}H-NMR** (500 MHz, $CDCl_3$) δ = 10.07 (s, 1H), 7.61 (dd, *J* = 8.5, 1.0 Hz, 2H), 7.35– 7.28 (m, 2H), 7.11–7.05 (m, 1H), 3.22–3.13 (m, 2H), 2.71–2.62 (m, 2H), 2.34–2.25 (m, 2H), 1.89–1.78 (m, 4H), 1.78–1.69 (m, 2H) ppm. **^{13}C-NMR** (126 MHz, $CDCl_3$) δ = 176.11, 138.15, 129.06, 123.93, 119.31, 78.47, 56.01, 37.37, 26.37 ppm. **FTIR** (neat) ν = 3187, 2961, 2923, 2853, 1670, 1600, 1510, 1440, 1312 cm^{-1}. **HR-MS** (ESI) $C_{14}H_{19}N_2O^+$ $[M+H]^+$ calculated: 231.1492 found: 231.1494. M.p.: 105–108 °C.

***N*-(4-Methoxyphenyl)tetrahydro-1*H*-pyrrolizine-*7a*(5*H*)-carboxamide (3.55)**

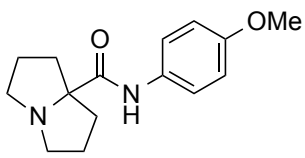

Purification by column chromatography on silica gel using CH_2Cl_2:MeOH = 40:1 (R_f = 0.19). The product was isolated as a yellow solid in 68% yield (83 mg, 0.32 mmol). **^{1}H-NMR** (400 MHz, $CDCl_3$) δ = 9.94 (s, 1H), 7.62–7.46 (m, 2H), 6.93–6.79 (m, 2H), 3.79 (s, 3H), 3.24–3.11 (m, 2H), 2.71–2.60 (m, 2H), 2.36–2.24 (m, 2H), 1.91–1.67 (m, 6H) ppm. **^{13}C-NMR** (101 MHz, $CDCl_3$) δ = 175.65, 156.10, 131.56, 120.81, 114.20, 78.38, 56.01, 55.65, 37.36, 26.39 ppm. **FTIR (neat)** ν = 3256, 2960, 2869, 1678, 1516, 1245 cm^{-1}. **HR-MS** (ESI) $C_{15}H_{21}N_2O_2^+$ $[M+H]^+$ calculated: 261.1598 found: 261.1601. M.p. = 84 °C.

***N*-(4-(Methylthio)phenyl)tetrahydro-1*H*-pyrrolizine-*7a*(5*H*)-carboxamide (3.56)**

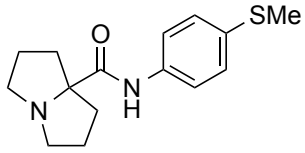

Purification by column chromatography on basic Al_2O_3 using EtOAc:pentane = 1:6 (R_f = 0.32). The product was obtained as a brown oil in 47 % yield (61 mg, 0.22 mmol). **^{1}H-NMR** (400 MHz, $CDCl_3$) δ = 10.05 (s, 1H), 7.60–7.51 (m, 2H), 7.30–7.20 (m, 2H), 3.17 (ddd, *J* = 10.3, 6.0, 4.6 Hz, 2H), 2.72–2.60 (m, 2H), 2.45 (s, 3H), 2.33–2.24 (m, 2H), 1.90–1.76 (m, 4H), 1.76–1.67 (m, 2H) ppm. **^{13}C-NMR** (101 MHz, $CDCl_3$) δ = 176.02, 135.99, 132.90, 128.43, 119.92, 78.47, 56.02, 37.37, 26.38, 17.16 ppm. **FTIR** (neat) ν = 3245, 2964, 2938, 2868, 1681, 1505 cm^{-1}. **HR-MS** (ESI) $C_{15}H_{21}N_2OS^+$ $[M+H]^+$ calculated: 277.1369 found: 277.1371.

***N*-(2,6-Dimethoxyphenyl)tetrahydro-1*H*-pyrrolizine-*7a*(5*H*)-carboxamide (3.57)**

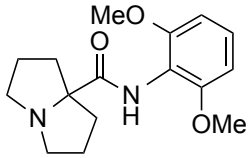

Purification by column chromatography on silica gel using CH_2Cl_2:MeOH = 30:1 (R_f = 0.22). The product was obtained as a yellow oil in 50 % yield (69 mg, 0.24 mmol). **^{1}H-NMR** (400 MHz, $CDCl_3$) δ = 9.26 (s, 1H), 7.13 (t, *J* = 8.4 Hz, 1H), 6.57 (d, *J* = 8.4 Hz, 2H), 3.80 (s, 6H), 3.21 (dt, *J* = 10.2, 5.2 Hz, 2H), 2.64 (dt, *J*

= 9.9, 7.1 Hz, 2H), 2.35 (dt, *J* = 11.6, 5.4 Hz, 2H), 1.92–1.83 (m, 4H), 1.83–1.73 (m, 2H) ppm. **^{13}C-NMR** (101 MHz, $CDCl_3$) δ = 176.49, 155.70, 127.19, 115.18, 104.75, 100.11, 78.47, 56.27, 55.97, 37.22, 26.58 ppm. **FTIR** (neat) ν = 3281, 2959, 2867, 1686, 1593, 1507, 1461, 1256, 1108 cm^{-1}. **HR-MS** (ESI) Exact mass calculated for $C_{16}H_{23}N_2O_3^+$ $[M+H]^+$ calculated: 291.1703 found: 291.1704.

***N*-(Benzo[*d*][1,3]dioxol-5-yl)tetrahydro-1*H*-pyrrolizine-*7a*(5*H*)-carboxamide (3.58)**

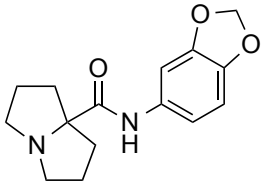

Purification by column chromatography on basic Al_2O_3 using EtOAc:pentane = 1:4 (R_f = 0.36). The product was obtained as a brown solid in 49 % yield (63 mg, 0.23 mmol). **^{1}H-NMR** (400 MHz, $CDCl_3$) δ = 9.97 (s, 1H), 7.36 (d, *J* = 2.1 Hz, 1H), 6.89 (dd, *J* = 8.3, 2.1 Hz, 1H), 6.74 (d, *J* = 8.3 Hz, 1H), 5.93 (s, 2H), 3.16 (ddd, *J* = 10.3, 5.9, 4.5 Hz, 2H), 2.65 (ddd, *J* = 10.0, 7.8, 5.6 Hz, 2H), 2.33–2.23 (m, 2H), 1.90–1.76 (m, 5H), 1.76–1.69 (m, 1H) ppm. **^{13}C-NMR** (101 MHz, $CDCl_3$) δ = 175.69, 147.91, 143.87, 132.73, 112.21, 108.14, 101.94, 101.25, 78.41, 56.00, 37.36, 26.39 ppm. **FTIR** (neat) ν = 3238, 2963, 2870, 1676, 1504, 1038 cm^{-1}. **HR-MS** (ESI) $C_{15}H_{19}N_2O_3^+$ $[M+H]^+$ calculated: 275.1390 found: 275.1389. M.p. = 106–108 °C.

***N*-(Naphthalen-2-yl)tetrahydro-1*H*-pyrrolizine-*7a*(5*H*)-carboxamide (3.59)**

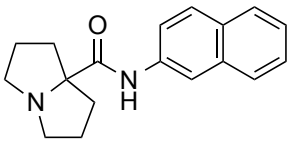

Purification by column chromatography on basic Al_2O_3 using EtOAc:pentane = 1:15 (R_f = 0.28). The product was isolated as a brown solid in 41% yield (54 mg, 0.19 mmol). **^{1}H-NMR** (400 MHz, $CDCl_3$) δ = 10.18 (s, 1H), 8.25 (d, *J* = 2.1 Hz, 1H), 7.71 (dd, *J* = 9.8, 7.4 Hz, 3H), 7.48 (dd, *J* = 8.8, 2.2 Hz, 1H), 7.37 (ddd, *J* = 8.2, 6.8, 1.4 Hz, 1H), 7.33–7.28 (m, 1H), 3.19–3.11 (m, 2H), 2.68–2.57 (m, 2H), 2.32–2.23 (m, 2H), 1.84–1.73 (m, 4H), 1.73–1.66 (m, 2H) ppm. **^{13}C-NMR** (101 MHz, $CDCl_3$) δ = 176.34, 135.59, 134.12, 130.59, 127.76, 127.65, 126.49, 124.82, 119.75, 115.76, 78.59, 56.08, 37.43, 26.42 ppm. **FTIR** (neat) ν = 3237, 3057, 2963, 2867, 1681, 1524, 1496 cm^{-1}. **HR-MS** (ESI) $C_{18}H_{21}N_2O^+$ $[M+H]^+$ calculated: 281.1648 found: 281.1650. M.p. = 108–110 °C.

***N*-(4-Bromophenyl)tetrahydro-1*H*-pyrrolizine-*7a*(5*H*)-carboxamide (3.60)**

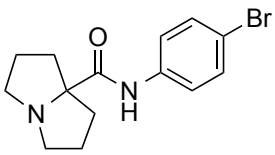

Purification by column chromatography on basic Al_2O_3 using EtOAc:pentane = 1:8 (R_f = 0.19). The product was isolated as a brown solid in 30% yield (43 mg, 0.14 mmol). **^{1}H-NMR** (400 MHz, $CDCl_3$) δ = 10.11 (s, 1H), 7.54–7.50 (m, 2H), 7.44–7.40 (m, 2H), 3.17 (ddd, *J* = 10.3, 6.1, 4.6 Hz, 2H), 2.70–2.62 (m, 2H), 2.32–2.24 (m, 2H), 1.89–1.78 (m, 4H), 1.77–1.69 (m, 2H) ppm.

ppm. **^{13}C-NMR** (101 MHz, $CDCl_3$) δ = 176.20, 137.23, 131.97, 120.92, 116.37, 78.51, 56.01, 37.36, 26.36. **FTIR** (neat) ν = 3236, 2965, 2869, 1684, 1503, 1396 cm^{-1}. **HR-MS** (ESI) $C_{14}H_{18}BrN_2O^+$ $[M+H]^+$ calculated: 309.0597 found: 309.0600. M.p. = 91 °C.

***N*-(4-Fluorophenyl)tetrahydro-1*H*-pyrrolizine-*7a*(5*H*)-carboxamide (3.61)**

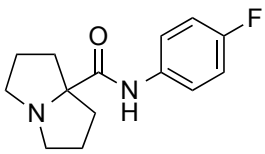

Purification by column chromatography on basic Al_2O_3 using EtOAc:pentane = 1:8 (R_f = 0.5). The product was isolated as a brown solid in 41% yield (48 mg, 0.19 mmol). **^{1}H-NMR** (400 MHz, $CDCl_3$) δ = 10.06 (s, 1H), 7.64–7.51 (m, 2H), 7.07–6.95 (m, 2H), 3.17 (ddd, *J* = 10.3, 6.1, 4.6 Hz, 2H), 2.66 (ddd, *J* = 9.9, 7.8, 5.4 Hz, 2H), 2.34–2.24 (m, 2H), 1.91–1.78 (m, 4H), 1.78–1.68 (m, 2H) ppm. **^{13}C-NMR** (101 MHz, $CDCl_3$) δ = 175.97, 159.2 (d, $J_{C,F}$ = 242.7 Hz), 134.29, 120.95, 120.87, 115.72, 115.50, 78.42, 56.00, 37.35, 26.37 ppm. **^{19}F NMR** (376 MHz, $CDCl_3$) δ = –122.03 ppm. **FTIR** (neat) ν = 3230, 2965, 2870, 1680, 1513, 1407, 1211 cm^{-1}. **HR-MS** (ESI) $C_{14}H_{18}FN_2O^+$ $[M+H]^+$ calculated: 249.1398 found: 249.1399. M.p. = 133-135 °C

***N*-(4-Ethynylphenyl)tetrahydro-1*H*-pyrrolizine-*7a*(5*H*)-carboxamide (3.62)**

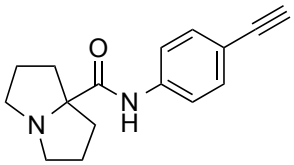

Purification by column chromatography on basic Al_2O_3 using Et_2O:pentane = 1:3 (R_f = 0.21). The product was obtained as a brown oil in 18 % yield (22 mg, 0.086 mmol). **^{1}H-NMR** (400 MHz, $CDCl_3$) δ = 10.17 (s, 1H), 7.63–7.54 (m, 2H), 7.49–7.40 (m, 2H), 3.24–3.12 (m, 2H), 3.03 (s, 1H), 2.71–2.62 (m, 2H), 2.33–2.24 (m, 2H), 1.90–1.78 (m, 4H), 1.78–1.67 (m, 2H) ppm. **^{13}C-NMR** (101 MHz, $CDCl_3$) δ = 176.25, 138.58, 133.03, 118.95, 117.22, 83.77, 78.53, 76.62, 56.01, 37.38, 26.36 ppm. **FTIR** (neat) ν = 3236, 2931, 2869, 1680, 1513 cm^{-1}. **HR-MS** (ESI) $C_{16}H_{19}N_2O^+$ $[M+H]^+$ calculated: 255.1492 found: 255.1494.

***N*-(5-Methyl-[1,1'-biphenyl]-2-yl)tetrahydro-1*H*-pyrrolizine-*7a*(5*H*)-carboxamide (3.63)**

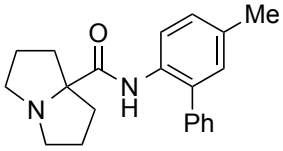

Purification by column chromatography on silica gel using CH_2Cl_2:MeOH = 20:1 (R_f = 0.28). The product was obtained as a white solid in 63 % yield (88 mg, 0.28 mmol). **^{1}H-NMR** (400 MHz, $CDCl_3$) δ = 10.24 (s, 1H), 8.27 (d, *J* = 8.3 Hz, 1H), 7.48–7.41 (m, 2H), 7.41–7.31 (m, 3H), 7.17 (dd, *J* = 8.3, 2.1 Hz, 1H), 7.06 (d, *J* = 2.1 Hz, 1H), 2.77–2.66 (m, 2H), 2.42–2.33 (m, 2H), 2.34 (s, 3H), 2.27–2.16 (m, 2H), 1.78–1.52 (m, 7H) ppm. **^{13}C-NMR** (101 MHz, $CDCl_3$) δ = 175.74, 139.00, 133.30, 132.89, 132.56, 130.47, 129.43, 128.97, 128.62, 127.53, 120.22, 78.56, 55.47, 37.11, 26.74, 21.01 ppm. **FTIR** (neat) ν = 3208, 2963, 2868, 1681, 1514, 1467 cm^{-1}. **HR-MS** (ESI) $C_{21}H_{25}N_2O^+$ $[M+H]^+$ calculated: 321.1961 found: 321.1960. M.p. = 89–91 °C.

N-(2-Morpholinoethyl)tetrahydro-1H-pyrrolizine-*7a*(5H)-carboxamide (3.64)

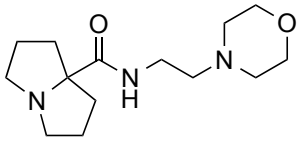

Purification by column chromatography on basic Al_2O_3 using EtOAc (R_f = 0.17). The product was obtained as a colorless oil in 32 % yield (41 mg, 0.15 mmol). **^{1}H-NMR** (250 MHz, $CDCl_3$) δ = 8.17 (s, 1H), 3.68 (d, *J* = 4.5 Hz, 4H), 3.31 (q, *J* = 6.2 Hz, 2H), 3.07 (ddd, *J* = 9.8, 6.5, 4.2 Hz, 2H), 2.62–2.52 (m, 2H), 2.44 (dd, *J* = 6.3, 3.4 Hz, 6H), 2.22–2.11 (m, 2H), 1.84–1.60 (m, 6H) ppm. **^{13}C-NMR** (101 MHz, $CDCl_3$) δ = 177.74, 161.24, 77.89, 67.18, 57.68, 55.88, 53.55, 37.17, 35.84, 26.37 ppm. **FTIR** (neat) ν = 3326, 2956, 2856, 2811, 1657, 1512, 1118 cm^{-1}. **HR-MS** (ESI) $C_{14}H_{26}N_3O_2^+$ $[M+H]^+$ calculated: 268.2020 found: 268.2023.

***N*-(4-Hydroxyphenethyl)tetrahydro-1*H*-pyrrolizine-*7a*(5*H*)-carboxamide (3.65)**

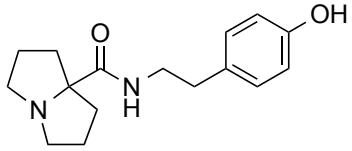

The reaction was performed using GP 2 on a 0.145 mmol scale. Purification by column chromatography on silica gel using CH_2Cl_2:MeOH = 20:1 (R_f = 0.05). The product was obtained as a white solid in 51 % yield (16 mg, 74 μmol). **^{1}H-NMR** (400 MHz, $CDCl_3$) δ = 8.11 (s, 1H), 7.04–6.96 (m, 2H), 6.78 (dd, *J* = 8.4, 1.6 Hz, 2H), 3.48 (q, *J* = 6.6 Hz, 2H), 2.96 (dt, *J* = 10.3, 5.8 Hz, 2H), 2.72 (t, *J* = 6.8 Hz, 2H), 2.51 (ddd, *J* = 9.8, 7.8, 5.6 Hz, 2H), 2.11–2.01 (m, 2H), 1.70 (m, 4H), 1.59–1.44 (m, 2H) ppm. **^{13}C-NMR** (101 MHz, $CDCl_3$) δ = 178.12, 155.40, 129.80, 115.56, 77.80, 55.81, 40.27, 37.07, 35.10, 29.84, 26.12 ppm. **FTIR** (neat) ν = 3279, 2922, 2867, 1640, 1513, 1451, 1241 cm^{-1}. **HR-MS** (ESI) $C_{16}H_{23}N_2O_2^+$ $[M+H]^+$ calculated: 275.1754 found: 275.1755. M.p. = 109–111 °C.

***N*-Benzyltetrahydro-1*H*-pyrrolizine-*7a*(5*H*)-carboxamide (3.66)**

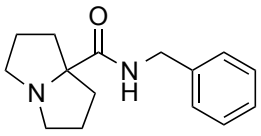

Purification by column chromatography on basic Al_2O_3 using EtOAc:pentane = 1:3 (R_f = 0.4). The product was obtained as a yellow oil in 71 % yield (82 mg, 0.34 mmol). **^{1}H-NMR** (400 MHz, $CDCl_3$) δ = 8.32 (s, 1H), 7.38–7.23 (m, 5H), 4.42 (d, *J* = 6.0 Hz, 2H), 3.10–3.00 (m, 2H), 2.63–2.52 (m, 2H), 2.29–2.20 (m, 2H), 1.86–1.72 (m, 4H), 1.73–1.64 (m, 2H) ppm. **^{13}C-NMR** (101 MHz, $CDCl_3$) δ = 177.72, 139.15, 128.74, 127.50, 127.31, 77.96, 55.94, 43.15, 37.35, 26.41 ppm. **FTIR** (neat) ν = 3322, 2961, 2868, 2362, 1667, 1508 cm^{-1}. **HR-MS** (ESI) $C_{15}H_{21}N_2O^+$ $[M+H]^+$ calculated: 245.1648 found: 245.1651.

(*S*)-*N*-(1-Phenylethyl)tetrahydro-1*H*-pyrrolizine-*7a*(5*H*)-carboxamide (3.67)

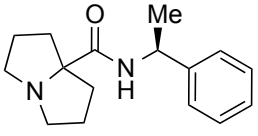

Purification by column chromatography on silica gel using CH_2Cl_2:MeOH = 20:1 (R_f = 0.07). The product was obtained as a yellow oil in 69 % yield

(69 mg, 0.33 mmol, *e.r.* 99:1 by HPLC). **^{1}H-NMR** (400 MHz, $CDCl_3$) δ = 8.30 (d, *J* = 6.7 Hz, 1H), 7.37–7.20 (m, 5H), 5.06 (dq, *J* = 13.9, 6.9 Hz, 1H), 3.14–3.01 (m, 2H), 2.64–2.53 (m, 2H), 2.28–2.20 (m, 1H), 2.19–2.11 (m, 1H), 1.85–1.63 (m, 6H), 1.47 (t, *J* = 6.3 Hz, 3H) ppm. **^{13}C-NMR** (101 MHz, $CDCl_3$) δ = 176.69, 144.08, 128.67, 127.10, 126.04, 77.88, 55.95, 47.98, 37.21, 37.19, 26.40, 22.47 ppm. **FTIR** (neat) ν = 3313, 2965, 2868, 2361, 1669, 1497 cm^{-1}. **HR-MS** (ESI) $C_{16}H_{23}N_2O^+$ $[M+H]^+$ calculated: 259.1805 found: 259.1805. $[\alpha]^{24}_D$ = -39.3° (*c* = 1.12, $CHCl_3$). Enantiomeric purity was determined by HPLC using a Chiracel 1A column (1 mLmin^{-1}, *i*PrOH:*n*-hexane 3:97, UV 225 nm): major enantiomer: R_t = 19.66 min, minor enantiomer R_t = 26.93 min.

Methyl-(hexahydro-1*H*-pyrrolizine-*7a*-carbonyl)-tryptophanate (3.68)

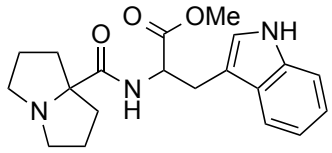

The reaction was performed using GP 2 on a 0.3 mmol scale. Purification by column chromatography on silica gel using EtOAc:pentane = 3:1 (R_f = 0.04). The product was obtained as a colorless oil in 76 % yield (21 mg, 60 µmol, *e.r.* 53:47 by HPLC). **^{1}H-NMR** (500 MHz, $CDCl_3$) δ = 8.46 (d, *J* = 8.6 Hz, 1H), 8.31 (s, 1H), 7.57 (d, *J* = 7.8 Hz, 1H), 7.34 (d, *J* = 8.1 Hz, 1H), 7.20–7.14 (m, 1H), 7.12–7.08 (m, 1H), 6.99 (d, *J* = 2.3 Hz, 1H), 4.87 (dt, *J* = 8.8, 6.1 Hz, 1H), 3.68 (s, 3H), 3.31–3.27 (m, 2H), 3.01–2.95 (m, 1H), 2.82–2.76 (m, 1H), 2.50–2.40 (m, 2H), 2.20–2.12 (m, 1H), 2.05–1.97 (m, 1H), 1.75–1.69 (m, 1H), 1.69–1.62 (m, 4H), 1.40 (m, 1H) ppm. **^{13}C-NMR** (126 MHz, $CDCl_3$) δ = 197.26, 182.60, 177.84, 172.79, 136.20, 127.83, 122.62, 122.19, 119.57, 118.75, 111.26, 110.69, 77.73, 55.82, 55.64, 52.77, 52.32, 37.27, 36.89, 27.87, 26.28, 26.21 ppm. **FTIR** (neat) ν = 3261, 2957, 2923, 2852, 1744, 1646, 1506 cm^{-1}. **HR-MS** (ESI) $C_7H_{14}NO^+$ $[M+H]^+$ calculated: 356.1969 found: 356.1972. The *e.r.* was determined of the Boc-protected derivative by HPLC using a Chiracel OD-H column (0.5 mLmin^{-1}, *i*PrOH:*n*-hexane 3:97, UV 225 nm): first enantiomer: R_t = 41.83 min, second enantiomer R_t = 61.73 min.

Methyl-(hexahydro-1*H*-pyrrolizine-*7a*-carbonyl)-valinate (3.69)

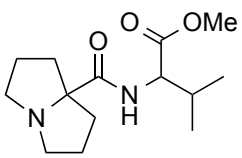

Purification by column chromatography on silica gel using EtOAc:pentane = 1:1 (R_f = 0.05). The product was obtained as a colorless oil in 69 % yield (55 mg, 0.26 mmol, *e.r.* 50:50 by HPLC). **^{1}H-NMR** (400 MHz, $CDCl_3$) δ = 8.48 (d, *J* = 8.9 Hz, 1H), 4.45 (dd, *J* = 9.6, 4.9 Hz, 1H), 3.71 (s, 3H), 3.19–3.08 (m, 2H), 2.65–2.56 (m, 2H), 2.23–2.13 (m, 3H), 1.83–1.69 (m, 6H), 0.92 (d, *J* = 6.8 Hz, 3H), 0.88 (d, *J* = 6.9 Hz, 3H) ppm. **^{13}C-NMR** (126 MHz, $CDCl_3$) δ = 177.80, 172.78, 77.95, 56.76, 55.88, 55.86, 52.11, 37.33, 37.14, 31.21, 26.57, 26.42, 19.38, 17.75 ppm. **FTIR** (neat) ν =

3322, 2961, 2932, 2870, 1741, 1673, 1499 cm^{-1}. **HR-MS** (ESI) $C_{15}H_{25}N_2O_5^+$ $[M+H]^+$ calculated: 269.1860 found: 269.1861. The *e.r.* was determined by HPLC using a Chiracel AD-H column (0.5 mL min^{-1}, *i*PrOH:*n*-hexane 5:95, UV 225 nm): first enantiomer: R_t = 16.73 min, second enantiomer R_t = 20.13 min.

Methyl-(hexahydro-1*H*-pyrrolizine-*7a*-carbonyl)-phenylalaninate (3.70)

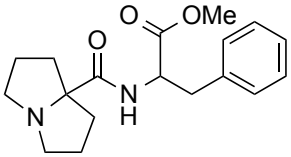

Purification by column chromatography on silica gel using CH_2Cl_2:MeOH = 40:1 (R_f = 0.48). The product was obtained as a yellow oil in 63 % yield (94 mg, 0.3 mmol, *e.r.* 53:47 by HPLC). **^{1}H-NMR** (400 MHz, $CDCl_3$) δ = 8.38 (d, *J* = 7.6 Hz, 1H), 7.35–7.18 (m, 3H), 7.17–7.08 (m, 2H), 4.85–4.75 (m, 1H), 3.72 (s, 3H), 3.18 (dd, *J* = 13.9, 5.5 Hz, 1H), 3.10–3.04 (m, 1H), 3.03 (dd, *J* = 13.9, 7.6 Hz, 1H), 2.98–2.88 (m, 1H), 2.57–2.46 (m, 2H), 2.19–2.13 (m, 1H), 2.01–1.93 (m, 1H), 1.76–1.71 (m, 1H), 1.70–1.63 (m, 4H), 1.51–1.40 (m, 1H) ppm. **^{13}C-NMR** (101 MHz, $CDCl_3$) δ = 172.40, 136.49, 129.35, 128.54, 127.07, 77.81, 55.85, 55.73, 52.73, 52.33, 38.19, 37.12, 36.97, 26.33, 26.23 ppm. **FTIR** (neat) ν = 3310, 2955, 2869, 1744, 1669, 1502 cm^{-1}. **HR-MS** (ESI) $C_{18}H_{25}N_2O_3^+$ $[M+H]^+$ calculated: 317.1860 found: 317.1865. The *e.r.* was determined by HPLC using a Chiracel OD-H column (0.5 mL min^{-1}, *i*PrOH:*n*-hexane 3:97, UV 225 nm): first enantiomer: R_t = 48.25 min, second enantiomer R_t = 58.35 min.

Methyl-(hexahydro-1*H*-pyrrolizine-*7a*-carbonyl)-methioninate (3.71)

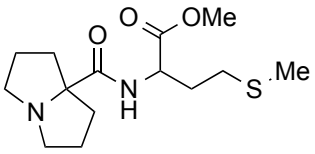

Purification by column chromatography on silica gel using CH_2Cl_2:MeOH = 20:1 (R_f = 0.38). The product was obtained as a yellow oil in 63 % yield (89 mg, 0.3 mmol, *e.r.* 52:48 by HPLC). **^{1}H-NMR** (400 MHz, $CDCl_3$) δ = 8.49 (d, *J* = 9.1 Hz, 1H), 4.63 (td, *J* = 8.3, 5.0 Hz, 1H), 3.73 (s, 3H), 3.19–3.06 (m, 2H), 2.65–2.56 (m, 2H), 2.52–2.46 (m, 2H), 2.24–2.12 (m, 3H), 2.10 (s, 3H), 2.02–1.91 (m, 1H), 1.88–1.78 (m, 2H), 1.78–1.63 (m, 4H) ppm. **^{13}C-NMR** (101 MHz, $CDCl_3$) δ = 177.80, 172.53, 77.70, 55.77, 55.76, 52.34, 51.09, 37.07, 31.98, 30.24, 26.41, 26.24, 15.56 ppm. **FTIR** (neat) ν = 3305, 2960, 2868, 1743, 1670, 1502, 1442, 1224, 1175 cm^{-1}. **HR-MS** (ESI) $C_{14}H_{25}N_2O_3S^+$ $[M+H]^+$ calculated: 301.1580 found: 301.1585. The *e.r.* was determined by HPLC using a Chiracel AD-H column (0.5 mL min^{-1}, *i*PrOH:*n*-hexane 5:95, UV 225 nm): first enantiomer: R_t = 37.20 min, second enantiomer R_t = 42.95 min.

Dimethyl-(hexahydro-1*H*-pyrrolizine-*7a*-carbonyl)-glutamate (3.72)

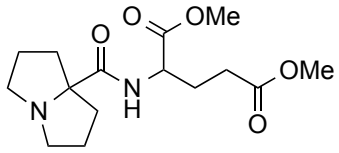

The reaction was performed using GP 2 on a 0.3 mmol scale. Purification by column chromatography on silica gel using EtOAc:pentane = 2:1 (R_f = 0.05). The product was obtained as a yellow oil in 51 % yield (47 mg, 0.15 mmol, *e.r.* 57:43 by HPLC). **^{1}H-NMR** (500 MHz, $CDCl_3$) δ = 8.44 (d, *J* = 8.7 Hz, 1H), 4.53 (td, *J* = 8.8, 5.2 Hz, 1H), 3.72 (s, 3H), 3.67 (s, 3H), 3.17–3.07 (m, 2H), 2.63–2.55 (m, 2H), 2.43–2.29 (m, 2H), 2.27–2.20 (m, 1H), 2.20–2.11 (m, 2H), 2.01–1.92 (m, 1H), 1.81–1.64 (m, 6H) ppm. **^{13}C-NMR** (126 MHz, $CDCl_3$) δ = 178.14, 173.14, 172.56, 77.80, 55.89, 55.84, 52.48, 51.92, 51.25, 37.22, 37.18, 30.36, 27.58, 26.46, 26.33 ppm. **FTIR** (neat) ν = 3261, 2957, 2923, 2852, 1744, 1646, 1506, 1439 cm^{-1}. **HR-MS** (ESI) $C_{15}H_{25}N_2O_5^+$ $[M+H]^+$ calculated: 313.1758 found: 313.1762. The *e.r.* was determined by HPLC using a Chiracel AD-H column (0.5 mL min^{-1}, *i*PrOH:*n*-hexane 5:95, UV 225 nm): first enantiomer: R_t = 63.66 min, second enantiomer R_t = 67.22 min.

4-(3,4-Dihydro-2*H*-pyrrol-5-yl)-2-methylbutan-2-ol (3.90)

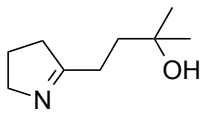

Diisopropylamine (0.97 mL, 6.86 mmol, 1.2 equiv.) was dissolved in anhydrous THF (6.3 mL) and cooled to -78 °C. n-BuLi (3.93 mL of 1.6 M solution in hexane, 6.29 mmol, 1.1 equiv.) was added dropwise and stirred for 40 min at -78 °C. A solution of 2-methyl-1-pyrroline (0.57 mL, 5.71 mmol, 1.0 equiv.) in THF (0.6 mL) was added dropwise at -78 °C and it was stirred for 1 h. Isobutylene epoxide (0.51 mL, 5.71 mmol, 1.0 equiv.) was added at -78 °C and it was stirred for further 60 min. The reaction mixture was allowed to warm to room temperature and stirred overnight.

The reaction was quenched with 10% NaOH, (6 mL) and the aqueous layer was extracted with CH_2Cl_2 (3x). The combined organic layers were dried over MgSO4 followed by evaporation gave the product as a yellow oil in 91% yield (0.803 g, 5.17 mmol). The product was of sufficient purity to be used for the next step.

^{1}H-NMR ($CDCl_3$, 400 MHz) δ = 4.92 (bs, 1H), 3.78 (ddq, *J* = 9.4, 5.9, 2.0 Hz, 2H), 2.48 (m, 4H), 1.91-1.86 (m, 2H), 1.83 (t, *J* = 6.8 Hz, 2H), 1.21 (s, 6H) ppm. **^{13}C-NMR** (101 MHz, $CDCl_3$) δ = 179.6, 69.4, 60.4, 38.9, 38.2, 29.7, 29.0, 22.6 ppm. **FTIR** (neat) ν = 3373, 2928, 2968, 2928, 2869, 2366, 1642 cm^{-1}. **HR-MS** (ESI) $C_9H_{18}NO^+$ $[M+H]^+$ calculated: 156.1383 found: 156.1382.

2-(3-Methylbut-2-en-1-yl)-*N*-phenylpyrrolidine-2-carboxamide ($\Delta^{2,3}$) and 2-(3-methylbut-3-en-1-yl)-*N*-phenylpyrrolidine-2-carboxamide ($\Delta^{3,4}$) (3.92 and 3.93)

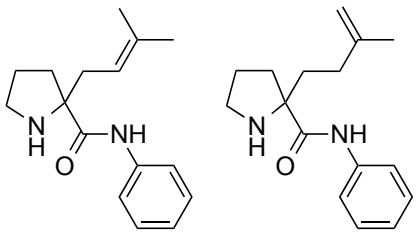

Imine (44 mg, 0.28 mmol, 1.0 equiv.) and isonitrile (29 mg, 0.28 mmol, 1.0 equiv.) were dissolved in dry toluene (2 mL) and $Et_3N{\cdot}HCl$ (77 mg, 0.56 mmol, 2.0 equiv.) was added. The suspension was heated under reflux for 17 h and the reaction was monitored by TLC. The reaction mixture was diluted with water, the layers were separated and the aqueous layer was extracted using EtOAc (2x). The combined organic layers were dried over $MgSO_4$. The solvents were removed in vacuo and the residue was purified by flash column chromatography on silica gel using CH_2Cl_2:MeOH 40:1, 0.1% Et_3N (R_f = 0.24). A mixture of two products ($\Delta^{2,3}$:$\Delta^{3,4}$ = 2.1:1) was obtained as a yellow oil in 57% yield (41 mg, 0.16 mmol).

$\Delta^{2,3}$: ^{1}H-NMR (400 MHz, $CDCl_3$) δ = 10.06 (bs, *J* = 12.0 Hz, 1H), 7.66-7.58 (m, 2H), 7.37-7.27 (m, 2H), 7.12-7.04 (m, 1H), 5.09 (tdt, *J* = 6.8, 2.9, 1.4 Hz, 1H), 3.16-3.03 (m, 1H), 2.99-2.89 (m, 1H), 2.79-2.67 (m, 1H), 2.44-2.32 (m, 1H), 2.28-2.20 (m, 1H), 1.86 – 1.73 (m, 3H), 1.68 (d, *J* = 27.2 Hz, 6H) ppm. **^{13}C-NMR** (101 MHz, $CDCl_3$) δ = 175.51, 138.28, 136.37, 129.04, 123.85, 119.29, 118.78, 70.12, 47.34, 36.73, 36.14, 26.56, 26.18, 18.14 ppm.

$\Delta^{3,4}$: ^{1}H-NMR (400 MHz, $CDCl_3$) δ = 10.06 (bs, *J* = 12.0 Hz, 1H), 7.66-7.58 (m, 2H), 7.37-7.27 (m, 2H), 7.12-7.04 (m, 1H), 4.73-4.65 (m, 2H), 3.16-3.03 (m, 1H), 2.99-2.89 (m, 1H), 2.44-2.32 (m, 1H), 2.28-2.20 (m, 1H), 2.02 (td, *J* = 9.8, 5.4 Hz, 2H), 1.86 – 1.73 (m, 4H), 1.72 – 1.70 (m, 3H) ppm. **^{13}C-NMR** (101 MHz, $CDCl_3$) δ = 175.01, 145.29, 138.15, 129.07, 123.96, 119.32, 110.33, 70.50, 47.34, 37.39, 37.21, 33.20, 26.33, 22.75 ppm. **FTIR** (neat) ν = 3244, 2967, 2872, 1681, 1600, 1516, 1441, 1310, 755 cm^{-1}. **HR-MS** (ESI) $C_{16}H_{23}N_2O^+$ $[M+H]^+$ calculated: 259.1805 found: 259.1809.

4-(3,4-Dihydro-2*H*-pyrrol-5-yl)butan-1-ol (3.103)

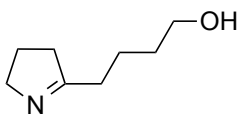

Freshly distilled diisopropylamine (0.2 mL, 1.4 mmol, 1.2 equiv.) was dissolved in THF (4.4 mL) and cooled to -78 °C. *n*-butyllithium (0.83 mL, 1.3 mmol, 1.1 equiv.) was added and it was stirred for 45 min at -78 °C. Freshly distilled 2-methyl pyrroline was added and it was stirred for 1 h at -78 °C. Freshly distilled trimethyleneoxide (0.081 mL, 1.2 mmol, 1.0 equiv.) was added followed by boron trifluoride diethyl etherate (0.18 mL, 1.4 mmol, 1.2 equiv.) at -78 °C. The reaction stirred for 22h slowly warming to room temperature, before it was quenched with NaOH (10%). The reaction mixture was extracted with EtOAc (3x) and the combined organic layers were dried with $MgSO_4$. The solvents were evaporated and the crude product was purified by column chromatography on

Al_2O_3 using EtOAc:pentane 7:1 (R_f = 0.1). The product was isolated as a brown oil in 16% yield (27 mg, 0.19 mmol).

^{1}H-NMR (500 MHz, $CDCl_3$) δ = 3.97 (s, 1H), 3.78–3.71 (m, 2H), 3.55 (t, *J* = 6.2 Hz, 2H), 2.44 (t, *J* = 8.2 Hz, 2H), 2.32 (t, *J* = 7.1 Hz, 2H), 1.83 (p, *J* = 7.7 Hz, 2H), 1.69 (p, *J* = 7.2 Hz, 2H), 1.55 (p, *J* = 6.4 Hz, 2H) ppm. **^{13}C-NMR** (126 MHz, $CDCl_3$) δ = 179.22, 61.33, 60.41, 37.57, 33.06, 32.47, 22.48, 21.82 ppm. **FTIR** (neat) ν = 3364, 33270, 2924, 2868, 1643, 1430, 1060 cm^{-1}. **HR-MS** (ESI) $C_8H_{16}NO^+$ $[M+H]^+$ calculated: 142.1227 found: 142.1226.

3-Oxo-*N*-phenyltetrahydro-1*H*-pyrrolizine-*7a*(5*H*)-carboxamide (3.105)

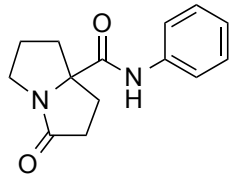

Oxidation of pyrrolizidine-*7a*-carboxamide 3.32.[138] Pyrrolizidine **3.32** (15 mg, 65 μmol, 1.0 equiv.) was dissolved in anhydrous CH_2Cl_2 (1.0 mL) under argon atmosphere. Benzyl(triethyl)ammonium permanganate[171] (61 mg, 0.195 mmol, 3.0 equiv.) was added and the suspension was stirred for 24 h at room temperature. Conversion was monitored by GC-MS. The suspension was filtered over cotton and the filtrate was transferred to a separation funnel. The solution was washed with water, the layers were separated and the aqueous layer was extracted with CH_2Cl_2 (2x 2 mL). The combined organic layers were dried over $MgSO_4$ and the solvent was evaporated. The crude extracts were purified by column chromatography on silica gel using CH_2Cl_2:MeOH = 30:1 (R_f = 0.2). The product was obtained as a white solid in 73% yield (11.6 mg, 47 μmol). **^{1}H-NMR** (400 MHz, $CDCl_3$) δ = 8.15 (s, 1H), 7.62 –7.54 (m, 2H), 7.40–7.31 (m, 2H), 7.19–7.12 (m, 1H), 3.86–3.75 (m, 1H), 3.21 (ddt, *J* = 12.3, 8.3, 4.5 Hz, 1H), 2.82 (dt, *J* = 17.1, 10.2 Hz, 1H), 2.68–2.57 (m, 2H), 2.50 (ddd, *J* = 17.1, 9.5, 2.4 Hz, 1H), 2.30–2.16 (m, 1H), 2.12–1.94 (m, 2H), 1.82–1.70 (m, 1H) ppm. **^{13}C-NMR** (101 MHz, $CDCl_3$) δ = 179.17, 172.36, 137.18, 129.27, 125.11, 120.05, 75.23, 43.92, 36.60, 33.58, 32.23, 26.02 ppm. **FTIR** (neat) ν = 3293, 2953, 1676, 1598, 1532, 1441 cm^{-1}. **HR-MS** (ESI) $C_{14}H_{17}N_2O_2^+$ $[M+H]^+$ calculated: 245.1285 found: 245.1281. M.p. = 172 °C.

***7a*-(Phenylcarbamoyl)hexahydropyrrolizine-4(1*H*)-oxide (3.106)**

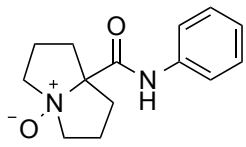

***N*-Oxide formation of pyrrolizidine-*7a*-carboxamide 3.32:** To a solution of pyrrolizidine **3.32** (10 mg, 43 μmol, 1.0 equiv.) in anhydrous CH_2Cl_2 (0.22 mL) at 0 °C was added a solution of *m*-CPBA (12 mg, 43 μmol, 1.0 equiv.) in anhydrous CH_2Cl_2 (0.22 mL). The solution was stirred at 0 °C and completion was monitored on TLC (CH_2Cl_2:MeOH = 40:1). After 5 h, the reaction mixture was quenched with sat. aqueous Na_2CO_3 solution (1 mL). The mixture was diluted with Et_2O (1 mL) and transferred

to a separation funnel. The organic layer was washed with Na_2CO_3 solution, the layers were separated and the organic layer was dried over $MgSO_4$. The crude extracts were purified by column chromatography on basic Al_2O_3 using CH_2Cl_2:MeOH 100:1 as an eluent (R_f = 0.16). The product was obtained as a colorless oil in 82% yield (8.8 mg, 36 μmol). **^{1}H-NMR** (400 MHz, $CDCl_3$) δ = 14.60 (s, 1H), 7.62 (dd, *J* = 8.2, 1.1 Hz, 3H), 7.35–7.25 (m, 2H), 7.07 (td, *J* = 7.3, 1.2 Hz, 1H), 3.87–3.76 (m, 2H), 3.76–3.66 (m, 2H), 2.97–2.86 (m, 2H), 2.38–2.25 (m, 2H), 2.18–2.00 (m, 4H) ppm. **^{13}C-NMR** (101 MHz, $CDCl_3$) δ = 167.96, 138.52, 128.98, 124.09, 120.43, 83.53, 68.40, 32.97, 19.87 ppm. **FTIR** (neat) ν = 3386, 3270, 2922, 1661, 1596, 1556, 1495, 1449 cm^{-1}. **HR-MS** (ESI) $C_{14}H_{19}N_2O_2^+$ $[M+H]^+$ calculated: 247.1441 found: 247.1444.

N-((Tetrahydro-1*H*-pyrrolizin-*7a*(5*H*)-yl)methyl)aniline (3.107)

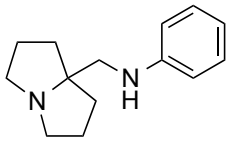

Reduction of pyrrolizidine-*7a*-carboxamide 3.32: In a two-neck round-bottom flask equipped with a reflux condenser under argon was dissolved pyrrolizidine **3.32** (65 mg, 0.28 mmol, 1.0 equiv.) in toluene (3 mL) and the solution was cooled to 0 °C. Red-Al®-solution (0.73 mL, 2.26 mmol, 60% in toluene) was added dropwise. The cooling bath was removed after addition and the reaction mixture was heated to reflux for 15 h. The reaction mixture was cooled to 0 °C and aqueous NaOH (c = 3 mol·L^{-1}, 6.5 mL) was added carefully. The reaction mixture was stirred at room temperature overnight. The reaction mixture was transferred into a separation funnel and diluted with ether. The aqueous layer was separated and the organic layer was washed with 10% NaOH solution and brine. The organic layer was dried over $MgSO_4$ and the solvent was evaporated to give the product as a pale yellow oil in 99% yield (60.7 mg, 0.28 mmol). **^{1}H-NMR** (400 MHz, Methanol-d_4) δ = 7.12–7.05 (m, 2H), 6.67–6.62 (m, 2H), 6.62–6.57 (m, 1H), 3.07–3.00 (m, 2H), 3.03 (s, 2H), 2.74–2.66 (m, 2H), 2.00–1.93 (m, 2H), 1.92–1.85 (m, 2H), 1.82–1.74 (m, 2H), 1.72–1.66 (m, 2H) ppm. **^{13}C-NMR** (101 MHz, Methanol-d_4) δ = 150.68, 130.03, 117.94, 113.83, 56.41, 53.52, 37.32, 25.77 ppm. **FTIR** (neat) ν = 3360, 2953, 2865, 2357, 1604, 1504, 1315, 1260 cm^{-1}. **HR-MS** (ESI) $C_{14}H_{21}N_2^+$ $[M+H]^+$ calculated: 217.1699 found 217.1703.

7a-((Phenylamino)methyl)octahydropyrrolizin-4-ium hydrogen carbonate (3.109)

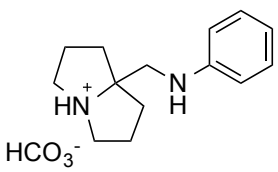

Pyrrolizidine **3.107** (19 mg, 88 μmol) was dissolved in 0.6 mL CD_3OD. A CO_2 stream generated from dry ice was bubbled through the solution for 5 min. The sample was submitted for NMR analysis. Mass analysis resulted in the same mass as **3.107**.

^{1}H-NMR (500 MHz, CD_3OD) δ = 7.19–7.11 (m, 2H), 6.78–6.74 (m, 2H), 6.70 (tt, *J* = 7.3, 1.1 Hz, 1H), 3.56 (dt, *J* = 11.8, 7.0 Hz, 2H), 3.43 (s, 2H), 3.19 (dt, *J* = 12.4, 6.3 Hz, 2H), 2.27–2.17

(m, 2H), 2.21–2.10 (m, 2H), 2.11–2.04 (m, 2H), 2.03–1.97 (m, 2H) ppm. **^{13}C-NMR** (126 MHz, CD_3OD) δ = 161.56, 149.86, 130.19, 118.98, 114.25, 83.15, 56.61, 49.92, 35.97, 25.12 ppm. **FTIR** (neat) ν = 2952, 2863, 1605, 1504, 1313, 1259 cm^{-1}.

7.3.2 $H_2{}^{18}O$-labeling experiment

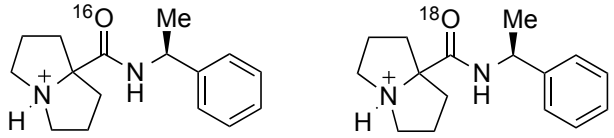

Exact mass = 259.1805 Exact mass = 261.1847

Incorporation of ^{18}O-labeled (97%) water was investigated as follows:

(*S*)-(–)-α-Methylbenzyl isocyanide (5.12 mg, 0.039 mmol, 1.0 equiv.) and imine **3.21** (5 mg, 0.039 mmol, 1.0 equiv.) were dissolved in toluene (0.18 mL) and suspended with triethylamine hydrochloride (10.7 mg, 0.078 mmol, 2.0 equiv.). ^{18}O-labeled water (7.00 µL, 0.39 mmol, 10 equiv.) was added and the reaction mixture was heated to 100 °C overnight. The reaction mixture was diluted with Et_2O and water and the aqueous layer was extracted using Et_2O (3x). The combined organic layers were dried over $MgSO_4$ and the solvent was evaporated. The residue was purified by column chromatography using CH_2Cl_2:MeOH = 20:1 (R_f = 0.07). The product was analyzed by HR-MS (ESI).

Table 9 shows the natural isotope distribution of **3.67** measured by HR-MS (ESI). The spectrum of the reaction in presence of ^{18}O-labeled is shown in Table 10. A clear enhancement of the isotope 261.18 is observed. The isotope corresponds to 14.2% of the main isotope 259.18 whereas the natural distribution includes only 1.4% of isotope 261.18. We therefore obtain 12.8% incorporation.

Table 9: HR-MS (ESI) report of 3.67.

Mass Spectrum List Report

Analysis Info

Analysis Name	N:\new acq data\IK-254 001.d	Acquisition Date	05.03.2014 17:39:39
Method	hn Direct_Infusion_pos mode_75-1500 mid 4eV.m	Operator	hn
Sample Name	Isabel Kerschgens, IK-254	Instrument / Ser#	maXis 4G 21243
Comment	IK-254, 10 ug / ml ACN		

Acquisition Parameter

Source Type	ESI	Ion Polarity	Positive	Set Nebulizer	0.4 Bar
Focus	Not active	Set Capillary	4500 V	Set Dry Heater	180 °C
Scan Begin	75 m/z	Set End Plate Offset	-500 V	Set Dry Gas	4.0 l/min
Scan End	1500 m/z	Set Collision Cell RF	500.0 Vpp	Set Divert Valve	Waste

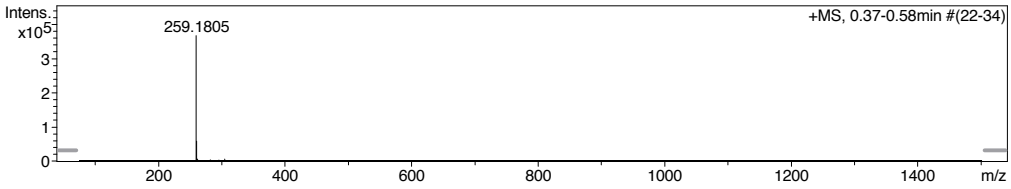

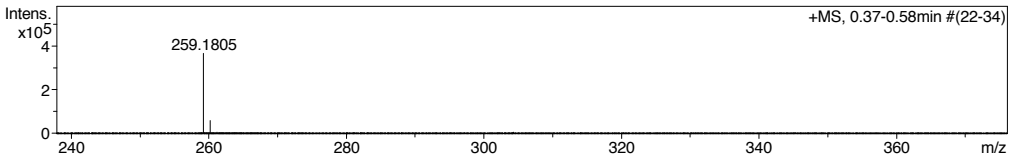

#	m/z	I %	I
1	152.6281	0.0	168
2	155.1175	0.1	225
3	159.6094	0.0	178
4	160.6166	0.3	938
5	161.1184	0.1	213
6	161.6066	0.0	171
7	168.6141	0.1	280
8	169.6221	0.2	657
9	173.1418	0.0	168
10	178.6272	0.1	442
11	181.1302	0.0	178
12	182.1462	0.0	182
13	186.9228	0.1	209
14	187.0940	0.1	416
15	190.1355	0.0	167
16	201.1017	0.0	166
17	205.0599	0.1	235
18	217.1048	0.2	661
19	223.0968	0.0	181
20	227.0952	0.0	174
21	229.1407	0.1	225
22	231.1199	0.2	807
23	239.0887	0.1	316
24	251.1616	0.1	214
25	254.2477	0.0	172
26	256.2630	0.1	258
27	259.0422	0.1	200
28	259.0819	0.1	236
29	259.1805	100.0	366197
30	260.1836	15.7	57658
31	261.1303	0.1	368
32	261.1865	1.4	5002
33	262.1894	0.1	365
34	265.1428	0.0	174
35	265.2142	0.1	210
36	267.1616	0.1	251
37	269.1654	0.1	201

Bruker Compass DataAnalysis 4.0 printed: 05.03.2014 17:47:03 Page 1 of 2

Table 10: HR-MS (ESI) report of 3.86.

Mass Spectrum List Report

Analysis Info

Analysis Name	N:\new acq data\IK-317-rep 002.d		
Method	hn Direct_Infusion_pos mode_75-1700 mid 4eV.m	Operator	hn
Sample Name	Isabel Kerschgens, IK-317-rep	Instrument / Ser#	maXis 4G 21243
Comment	IK-317-rep, ca. 10 ug/ml MeCN	Acquisition Date	09.10.2014 09:22:22

Acquisition Parameter

Source Type	ESI	Ion Polarity	Positive	Set Nebulizer	0.4 Bar
Focus	Not active	Set Capillary	3600 V	Set Dry Heater	180 °C
Scan Begin	75 m/z	Set End Plate Offset	-500 V	Set Dry Gas	4.0 l/min
Scan End	1700 m/z	Set Collision Cell RF	500.0 Vpp	Set Ion Energy (MS only)	4.0 eV

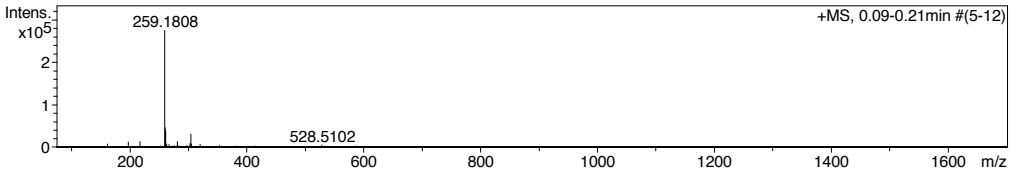

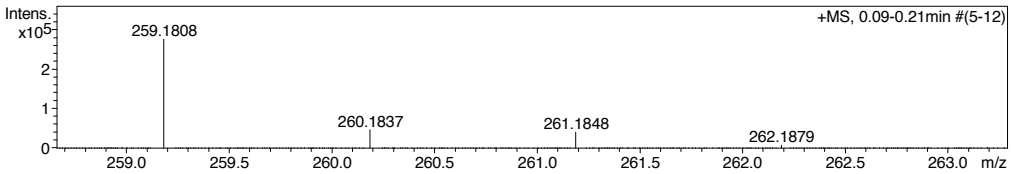

#	m/z	I %	I
1	120.9870	0.3	797
2	136.9611	0.3	938
3	147.0084	0.2	538
4	152.9349	0.5	1304
5	160.9796	0.2	488
6	161.0239	2.3	6413
7	162.0247	0.2	502
8	163.0386	0.2	489
9	170.1175	0.3	926
10	170.9613	0.2	592
11	172.0945	0.3	828
12	197.0783	4.2	11497
13	198.0816	0.4	1217
14	200.9721	0.3	747
15	217.0470	4.4	12165
16	217.1046	0.3	794
17	218.0505	0.5	1499
18	218.9851	0.2	674
19	228.9667	0.2	674
20	230.2475	0.2	482
21	233.0210	0.2	491
22	253.0170	1.0	2627
23	256.9623	0.2	593
24	258.9776	0.3	869
25	259.0712	0.2	494
26	259.1808	100.0	274958
27	260.1837	16.6	45553
28	261.1848	14.2	38931
29	262.1879	2.4	6504
30	263.1916	0.3	688
31	267.0323	2.0	5590
32	268.0337	0.3	822
33	269.0304	0.2	509
34	274.2735	0.9	2593
35	275.1246	0.3	781
36	275.2767	0.2	523
37	276.2295	0.8	2258

Bruker Compass DataAnalysis 4.0 printed: 09.10.2014 09:34:10 Page 1 of 2

7.4 Application of pyrrolizidines in carbon dioxide capture

7.4.1 Synthesis

(Tetrahydro-1*H*-pyrrolizin-*7a*(5*H*)-yl)methanamine (4.13)

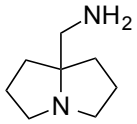

An oven-dried flask was charged with $LiAlH_4$ (8.40 g, 220 mmol, 4.0 equiv.) and was evacuated and backfilled with argon three times. Anhydrous THF (100 mL) was added and the reaction mixture was cooled to 0 °C. The crude mixture of nitrile **4.21** (7.69 g) was slowly added to the reaction mixture. The suspension was allowed to warm to room temperature and stirred for 15 h. The mixture was cooled to 0 °C and quenched with water (1 mL/g $LiAlH_4$), aqueous sodium hydroxide (15%, 1 mL/g $LiAlH_4$) and water (3 mL/g $LiAlH_4$). The suspension was stirred for 15 min and was diluted with diethyl ether (50 mL). Na_2SO_4 was added and the suspension was stirred for another 30 min. The mixture was filtered over a pad of Celite® and the solvent was removed under reduced pressure. The residue was treated with HCl·*i*PrOH (21%, 10 mL) and filtered. The resulting solid was refluxed in EtOH/*i*PrOH (7:1) to yield the dihydrochloride salt of the free amine. The salt was resuspended in diethyl ether and gaseous NH_3 was bubbled through the suspension to release the free amine. Filtration and subsequent removal of the solvent afforded the desired product (2.07 g, 14.8 mmol, 27% from **4.19**) as colorless oil. The analytical data are in agreement with the literature.[120,172]

^{1}H-NMR (400 MHz, CD_3OD): δ = 2.98–2.92 (m, 2H), 2.68–2.63 (m, 2H), 2.52 (s, 2H), 1.89–1.82 (m, 4H), 1.76–1.68 (m, 2H), 1.64–1.57 (m, 2H) ppm. **^{13}C-NMR** (101 MHz, CD_3OD): δ = 76.1, 55.4, 51.3, 36.9, 25.6 ppm.

2-(Tetrahydro-1*H*-pyrrolizin-*7a*(5*H*)-yl)ethan-1-amine (4.15)

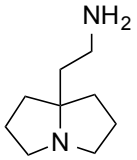

Crude (1-azabicyclo[3.3.0]octane-5-yl)acetonitrile (9.79 g) was dissolved in methanol (60 mL) and sodium hydroxide (5.26 g, 130 mmol, 2.0 equiv.) was added. Raney-Ni (50% in water, 4.12 g) was added and the reaction mixture was charged with hydrogen atmosphere (1 atm). The reaction mixture was stirred under hydrogen atmosphere for 24h until full conversion of the starting material was observed in the ^{1}H-NMR. The mixture was filtered over a pad of Celite® and the solvent was removed under reduced pressure. The resulting residue was resuspended in Et_2O and stirred for 30 min at room temperature. The precipitate was filtered off and the organic layer was concentrated under reduced pressure. The resulting crude amine (8.82 g, 88%) was treated with a HCl·*i*PrOH solution (21%) to precipitate the free amine. The resulting dihydrochloride salt (determined by EA) was recrystallized from EtOH/*i*PrOH (4:1) and resuspended in diethyl ether. NH_3 gas was bubbled through the suspension for 30 min and the mixture was stirred for 5h at room temperature. Filtra-

tion and subsequent removal of the solvent afforded the desired product as light yellowish oil in 42% yield (4.25 g, 27.6 mmol). The analytical data were in agreement with the literature.[120]

^{1}H-NMR (400 MHz, CD_3OD) δ = 3.02–2.91 (m, 2H), 2.68–2.54 (m, 2H), 2.60–2.52 (m, 2H), 2.36 (s, 2H), 1.90–1.67 (m, 6H), 1.70–1.56 (m, 4H) ppm. **^{13}C-NMR** (101 MHz, CD_3OD) δ = 74.0, 56.0, 49.0, 41.9, 38.2, 36.1, 25.5 ppm.

N-Methyl-1-(tetrahydro-1*H*-pyrrolizin-*7a*(5*H*)-yl)methanamine (4.14)

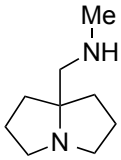

An oven-dried two-neck flask was charged with $LiAlH_4$ (195 mg, 5.14 mmol, 2.0 equiv.) and was three times evacuated and backfilled with argon. After cooling to 0 °C THF (5.0 mL) was added followed by **4.22** (428 mg, 2.54 mmol, 1.0 equiv.) in THF (10 mL) was added dropwise. The reaction mixture was heated to reflux for 2h. After cooling to 0 °C, remaining $LiAlH_4$ was quenched by the addition of water (1 mL/g $LiAlH_4$), NaOH (15%, 1 mL/g $LiAlH_4$) and water (3 mL/g $LiAlH_4$). The resulting slurry was diluted with diethyl ether (10 mL) and stirred for 5 min., treated with Na_2SO_4 and the suspension was stirred for 15 min. Filtration over Celite® and removal of the solvent afforded the desired product as a colorless oil in 84% yield (330 mg, 2.14 mmol).

^{1}H-NMR (400 MHz, $CDCl_3$): δ = 2.99–2.93 (m, 2H), 2.62 (m, 2H), 2.43 (s, 2H), 2.43 (s, 3H), 1.88–1.80 (m, 2H), 1.79–1.67 (m, 4H), 1.56–1.50 (m, 2H), 1.26 (br. s, 1H) ppm. **^{13}C-NMR** (101 MHz, $CDCl_3$): δ = 73.1, 62.7, 55.9, 37.4, 37.2, 25.3 ppm. **FTIR** (neat) ν = 3320, 2949, 2865, 2785, 2687, 1685, 1457, 1319, 1262, 1136, 1095, 1024, 904, 794, 700, 633 cm^{-1}.

HR-MS (ESI) $C_9H_{19}N_2^+$ $[M+H]^+$ calculated: 155.1543 found: 155.1544.

N-Methyl-2-(tetrahydro-1*H*-pyrrolizin-*7a*(5*H*)-yl)ethan-1-amine (4.16)

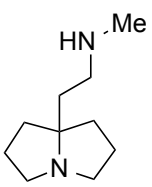

An oven-dried two-neck flask was charged with $LiAlH_4$ (154mg, 4.06 mmol, 2.0 equiv.) and was three times evacuated and backfilled with argon. After cooling to 0 °C THF (5 mL) was added followed by solution of **4.25** (370 mg, 2.03 mmol, 1.0 equiv.) in THF (14 mL) was added dropwise. The reaction mixture was heated to reflux for 2h. After cooling to 0 °C, remaining $LiAlH_4$ was quenched by the addition of water (1 mL/g $LiAlH_4$), NaOH (15%, 1 mL/g $LiAlH_4$) and water (3 mL/g $LiAlH_4$). The resulting slurry was diluted with Et_2O (15 mL), Na_2SO_4 was added and the mixture was stirred for 15 min. Filtration over Celite® and removal of the solvent afforded the crude product (348 mg, quant.) as a yellowish oil. The oil was treated with $HCl{\cdot}Et_2O$ (18%, 5-10 mL) under formation of a white solid which was identified as the dihydrochloride salt of the product (determined by EA). The solid was recrystallized from *i*PrOH/EtOH (1:4, 11 mL) and precipitated

with Et_2O leading to the HCl-salt of the desired product (413 mg, 84%). The HCl-salt was suspended in Et_2O and NH_3 gas was introduced for 1h. Filtration and subsequent removal of the solvent afforded the product colorless oil in 74% yield (254 mg, 1.51 mmol).

^{1}H-NMR (400 MHz, $CDCl_3$): δ = 3.00–2.95 (m, 2H), 2.61–2.53 (m, 4H), 2.42 (s, 3H), 1.78–1.67 (m, 6H), 1.62–1.58 (m, 2H), 1.55–1.49 (m, 2H) ppm. **^{13}C-NMR** (101 MHz, $CDCl_3$): δ = 77.4, 55.5, 49.3, 42.3, 37.8, 36.9, 25.1 ppm. **FTIR** (neat) ν = 3287, 2950, 2865, 1550, 1478, 1382, 1308, 1261, 1163, 1059, 929, 814, 706 cm^{-1}. **HR-MS** (ESI) $C_{10}H_{21}N_2^+$ $[M+H]^+$ calculated: 169.1700 found: 169.1702.

N-(2-(Tetrahydro-1*H*-pyrrolizin-*7a*(5*H*)-yl)ethyl)aniline (4.17)

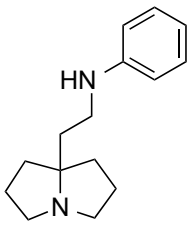

An oven dried Schlenk tube was charged with BrettPhos precatalyst (35.0 mg, 43.8 µmol, 1 mol%, Sigma Aldrich: 718750), BrettPhos ligand (24.0 mg, 44.7 µmol, 1 mol%) and NaO*t*Bu (838 mg, 8.72 mmol, 2.0 equiv.) and it was three times evacuated and backfilled with argon. Then amine **4.15** (803 mg, 5.21 mmol, 1.2 equiv.) was added as a solution in dioxane (15 mL). Chlorobenzene (0.45 mL, 4.44 mmol, 1.0 equiv.) was added and the mixture was heated to 80 °C for 1.5h until GC-MS showed full conversion. After cooling to room temperature ethyl acetate (10 mL) was added and the mixture was transferred into a separation funnel and washed with water (15 mL). The aqueous layer was extracted with ethyl acetate (2x) and the combined organic layers were dried over Na_2SO_4 giving the crude product. The mixture was treated with HCl·Et_2O (18%, 15 mL) and washed with Et_2O. The resulting solid was recrystallized in *i*PrOH/EtOH (1:3, 15 mL) and after cooling to room temperature treated with Et_2O. The resulting solid was washed with Et_2O, leading to the HCl-salt of the desired product. This was suspended in Et_2O and NH_3 gas was introduced for 1h. After stirring for 4h the solid was removed by filtration. Subsequent removing of the solvent afforded the desired product as a yellow oil in 96% yield (951 mg, 4.13 mmol).

^{1}H-NMR (400 MHz, CD_3OD): δ = 7.12–7.08 (m, 2H), 6.64–6.59 (m, 3H), 3.12–3.08 (m, 2H), 3.00–2.94 (m, 2H), 2.65–2.60 (m, 2H), 1.88–1.81 (m, 4H), 1.77–1.72 (m, 4H), 1.68–1.63 (m, 2H) ppm. **^{13}C-NMR** (101 MHz, CD_3OD): δ = 150.3, 130.0, 118.1, 114.2, 74.0, 56.0, 42.2, 41.7, 38.3, 25.6 ppm. **FTIR** (neat) ν = 3255, 3021, 2951, 2864, 1601, 1506, 1319, 1289, 1179, 1122, 864, 746, 690 cm^{-1}. **HR-MS** (ESI) $C_{15}H_{23}N_2^+$ $[M+H]^+$ calculated: 231.1856 found: 231.1859.

2,4-Dinitro-*N*-((tetrahydro-1*H*-pyrrolizin-7a(5*H*)-yl)methyl)aniline (4.18)

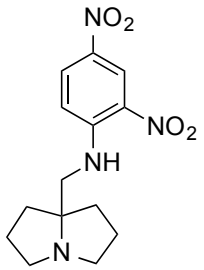

Amine **4.13** (480 mg, 3.42 mmol, 1.0 equiv.) was dissolved in acetone (39 mL) and water (16 mL) and treated with $NaHCO_3$ (439 mg, 5.23 mmol, 1.5 equiv.). The reaction mixture was cooled to 0 °C and 2,4-dinitrofluorobenzene (0.53 mL, 4.21 mmol, 1.2 equiv.) was added. The mixture was stirred at 0 °C for 3 h until TLC showed full conversion of amine **4.13**. Acetone was removed under reduced pressure and the aqueous layer was extracted with ethyl acetate (3x 35 mL). The combined organic layers were dried over $MgSO_4$ and the solvent was removed under reduced pressure. Purification by column chromatography (SiO_2, MeOH/CH_2Cl_2 1:10 with NEt_3 (1%), R_f = 0.47) afforded the desired product as yellow crystals in 61% yield (661 mg, 2.16 mmol).

^{1}H-NMR (400 MHz, CD_3OD): δ = 9.04 (d, *J*= 4.4 Hz, 1H), 8.28 (dd, *J*= 15.6 Hz, *J* = 4.4 Hz, 1H), 7.19 (d, *J* = 15.6 Hz, 1H), 3.39 (s, 2H), 3.15–3.07 (m, 2H), 2.80–2.71 (m, 2H), 1.96–1.75 (m, 8H) ppm. **^{13}C-NMR** (101 MHz, CD_3OD) δ = 150.1, 137.0, 131.6, 131.1, 124.8, 116.2, 74.3, 56.8, 52.5, 37.7, 25.9 ppm. **FTIR** (neat) *v* = 3314, 3106, 2956, 2867, 2342, 2171, 2027, 1620, 1525, 1417, 1334, 1137, 1097, 922, 817, 744 cm^{-1}. **HR-MS** (ESI) $C_{14}H_{19}N_4O_4^+$ $[M+H]^+$ calculated: 307.1401 found: 307.1401. **M.p.** = 111–114 °C.

1,7-Dichloroheptan-4-one (4.19)

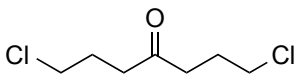

Methanol (180 mL) was cooled to 0 °C and sodium (14.8 g, 0.64 mol, 1.1 equiv.) was added in small portions. After the sodium was dissolved, γ-butyrolactone (90.0 mL, 1.17 mol, 2.0 equiv.) was added. The reaction mixture was heated to 100 °C and methanol was removed from the reaction mixture with a *Dean-Stark* apparatus. Towards the end of the reaction methanol was removed under reduced pressure to yield the desired product as a high viscous yellowish oil, which turned solid after cooling to room temperature.

The crude **4.20** was heated to 100 °C. Hydrochloric acid (32%, 270 mL) was slowly added *via* a dropping funnel with CO_2 being released from the mixture. After the addition was complete, the mixture was refluxed for another 30 min at 100 °C and then cooled to room temperature. The crude mixture was diluted with water (250 mL) until the solid had dissolved, transferred into a separation funnel and the aqueous layer was extracted with diethyl ether (3x 150 mL). The combined organic layers were washed with water (200 mL) and sat. aqueous $NaHCO_3$ (3x 150 mL). The combined aqueous layers were extracted with ether (100 mL) and the combined organic

layers were dried over $MgSO_4$. Removal of the solvent afforded the desired product as a brown oil in 68% yield (71.8 g, 392 mmol).

^{1}H-NMR (400 MHz, $CDCl_3$): δ = 3.58 (t, *J* = 6.4 Hz, 2H), 2.64 (t, *J* = 7.2 Hz, 2H), 2.05 (p, *J* = 6.8 Hz, 2H) ppm. **^{13}C-NMR** (101 MHz, $CDCl_3$): δ = 208.6, 44.5, 39.6, 26.4 ppm.

Tetrahydro-1*H*-pyrrolizine-*7a*(5*H*)-carbonitrile1,7-Dichloroheptan-4-one (4.21)

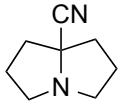

(30.1 g, 164 mmol, 1.0 equiv.) was dissolved in methanol (150 mL) and gaseous NH_3 was bubbled through the solution for 1.5 hours. The reaction mixture was stirred at room temperature for 3h until GC-MS showed full consumption of the starting material. Afterwards potassium cyanide (32.0 g, 492 mmol, 3.0 equiv.) was added and the mixture was stirred overnight at room temperature until GC-MS showed full conversion. Aqueous sodium hydroxide solution (20%, 200 mL) was added and the aqueous layer was extracted with CH_2Cl_2 (3x 150 mL). The combined organic layers were dried over Na_2SO_4 and the solvent was removed under reduced pressure to afford a crude mixture (16.1 g) of the desired product and 5-cyclopropyl-3,4-dihydro-2*H*-pyrrole in a 70:30 ratio as a brown oil. This mixture was used without further purification. The analytical data matches the literature. The analytical data are in agreement with the literature.[26][30]

^{1}H-NMR (250 MHz, $CDCl_3$): δ = 3.25–3.17 (m, 2H), 2.62–2.53 (m, 2H), 2.39–2.30 (m, 2H), 2.12–1.86 (m, 6H) ppm.

***N*-((Tetrahydro-1*H*-pyrrolizin-*7a*(5*H*)-yl)methyl)formamide (4.22)**

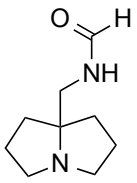

To a solution of 5-aminomethyl-1-azabicyclo[3.3.0]octane (377 mg, 2.69 mmol, 1.0 equiv.) and sodium hydroxide (244 mg, 6.10 mmol, 2.0 equiv.) in methanol (3.5 mL) was added ethylformate (1.10 mL, 13.5 mmol, 10 equiv.) was added and the mixture was stirred at room temperature for 30 min, until GC-MS showed full conversion. The solvent was removed under reduced pressure and diethyl ether (15 mL) was added to the residue and stirred for 10 min. Filtration and subsequent removal of the solvent afford the desired product as a mixture of *cis*- and *trans*-isomers as colorless oil in 95% yield (428 mg, 2.54 mmol).

^{1}H-NMR (400 MHz, $CDCl_3$): δ = 8.22 (m, 0.8H), 8.06 (d, *J* = 12.2 Hz, 0.2H), 6.15 (br. s, 0.8H), 5.95 (br. s, 0.2H), 3.20 (d, *J* = 6.6 Hz, 1.6H), 3.02 (d, *J* = 6.5 Hz, 0.4H), 2.99–2.93 (m, 2H), 2.65–2.58 (m, 2H), 1.84–1.77 (m, 2H), 1.75–1.65 (m, 4H), 1.63–1.58 (m, 2H) ppm. **^{13}C-NMR** (101 MHz, $CDCl_3$): δ = 161.5, 72.8, 55.8, 45.8, 36.4, 25.2 ppm. **FTIR** (neat) ν = 3291, 3058, 2955, 2867, 2361, 1669, 1539, 1455, 1384, 1239, 1091, 758, 698 cm^{-1}.

HR-MS (ESI) $C_9H_{17}N_2O^+$ $[M+H]^+$ calculated: 169.1335 found: 169.1338.

2-(Tetrahydro-1*H*-pyrrolizin-*7a*(5*H*)-yl)acetonitrile (4.24)

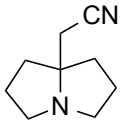

1,7-Dichloroheptan-4-one (20.1 g, 110 mmol, 1.0 equiv.) was dissolved in aqueous NH_3 (25%, 65 mL) and cyanoacetic acid (46.7 g, 549 mmol, 5.0 equiv.) was slowly added. NH_3 gas was bubbled through the reaction mixture for 1h. Hexane (20 mL) was added and the mixture was stirred for 48h at room temperature. After GC-MS showed full conversion, the aqueous NH_3 was removed under reduced pressure and sodium hydroxide (20%, 160 mL) was added to the residue. The aqueous layer was extracted with ethyl acetate (3x 150 mL) and the combined organic layers were dried over Na_2SO_4. Removal of the solvent afforded the crude product (9.79 g, 59 %) as brown oil. This crude product was used in the next step without further purification. The analytical data were in agreement with the literature.[120]

^{1}H-NMR (400 MHz, $CDCl_3$): δ = 3.13–3.08 (m, 2H), 2.63–2.57 (m, 2H), 2.41 (s, 2H), 1.94–1.80 (m, 6H), 1.75–1.71 (m, 2H) ppm.

***N*-(2-(Tetrahydro-1*H*-pyrrolizin-*7a*(5*H*)-yl)ethyl)formamide (4.25)**

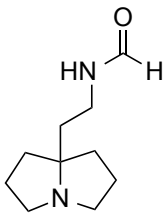

To a solution of amine **4.15** (741 mg, 4.80 mmol, 1.0 equiv.) and sodium hydroxide (401 mg, 10.0 mmol, 2.0 equiv.) in methanol (5.0 mL), ethylformate (1.90 mL, 23.5 mmol, 5.0 equiv.) was added and stirred for 30 min until GC-MS showed full conversion. The solvent was removed under reduced pressure and the resulting residue was resuspended in diethyl ether and stirred for 1h. Filtration and subsequent removal of the solvent afforded the crude product (764 mg, 93 %) as colorless oil. The purity was sufficiently high, so that no further purification was necessary.

^{1}H-NMR (400 MHz, $CDCl_3$): δ = 8.43 (br. s, 1H), 8.11 (s, 1H), 3.42–3.38 (m, 2H), 3.00–2.94 (m, 2H), 2.62–2.56 (m, 2H), 1.82–1.67 (m, 6H), 1.64–1.58 (m, 4H) ppm.

^{13}C-NMR (101 MHz, $CDCl_3$): δ = 161.1, 73.4, 55.4, 38.3, 37.9, 35.6, 25.0 ppm.

FTIR (neat) ν = 3463, 3276, 3058, 2953, 2867, 2137, 1667, 1540, 1457, 1384, 1244, 1088, 926, 833, 717 cm^{-1}. **HR-MS** (ESI) $C_{10}H_{19}N_2O^+$ $[M+H]^+$ calculated: 183.1492 found: 183.1491.

***N*-((Tetrahydro-1*H*-pyrrolizin-*7a*(5*H*)-yl)-methyl)aniline through *Buchwald-Hartwig* coupling (3.107)**

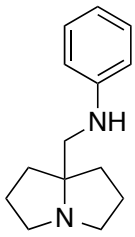

An oven-dried flask was charged with NaO*t*Bu (13.3 mg, 139 µmol, 2.0 equiv.), BrettPhos precatalyst (2.60 mg,, 3.25 µmol, 5 mol%, Sigma Aldrich: 718750), BrettPhos ligand (1.99 mg, 3.71 µmol, 6 mol%) and three times evacuated and backfilled with argon. Amine **4.13** (10.8 g, 76.0 µmol, 1.2 equiv.), dioxane (0.7 mL) and chlorobenzene (0.6 µL, 63.0 µmol, 1.0 equiv.) were added successively. The reaction mixture was heated to 80 °C for 2h until GC-MS showed full consumption of the chlorobenzene. After cooling to room temperature the reaction mixture was diluted with ethyl acetate (1.5 mL), washed with water (0.5 mL) and the aqueous layer was extracted with ethyl acetate (3x 1.5 mL). The combined organic layers were dried over Na_2SO_4, filtered and concentrated under reduced pressure. The crude residue was treated with HCl·*i*PrOH (21%, 1.0 mL) and the resulting dihydrochloride salt was recrystallized in EtOH/*i*PrOH (7:1, 0.1 mL) and treated with diethyl ether (0.5 mL). The resulting crystals were filtered off and resuspended in diethyl ether. NH_3 gas was bubbled through the reaction mixture until saturation occurred and the suspension was stirred for five hours at room temperature. Filtration and removal of the solvent afforded the desired product as colorless oil in 34% yield (4.3 mg, 0.02 mmol).

^{1}H-NMR (400 MHz, $CDCl_3$): δ = 7.18–7.14 (m, 2H), 6.69–6.65 (m, 1H), 6.64–6.62 (m, 2H), 4.15 (br. s, 1H), 3.06–3.00 (m, 2H), 2.55 (d, *J* = 5.6 Hz, 2H), 2.68–2.62 (m, 2H), 1.90–1.71 (m, 8H), 1.65–1.60 (m, 2H) ppm. **^{13}C-NMR** (101 MHz, $CDCl_3$): δ = 149.4, 129.3, 117.1, 113.1, 73.2, 55.8, 52.4, 36.9, 25.3 ppm.

7.4.2 CO_2 Uptake experiments

The carbon dioxide was purchased from PanGas Switzerland, with a purity of 5.3 (>99.9993%). Flow-controllers F-201CV-020-AGD-33-V were delivered from Bronkhorst Switzerland with a flow rate area of 0.18-9.0 mL/min. The inlet pressure was 2-6 bar and the outlet pressure was 1 bar. Gravimetric measurements were performed using Mettler-Toledo ME204 balance with a readability of 0.01/0.1 mg.

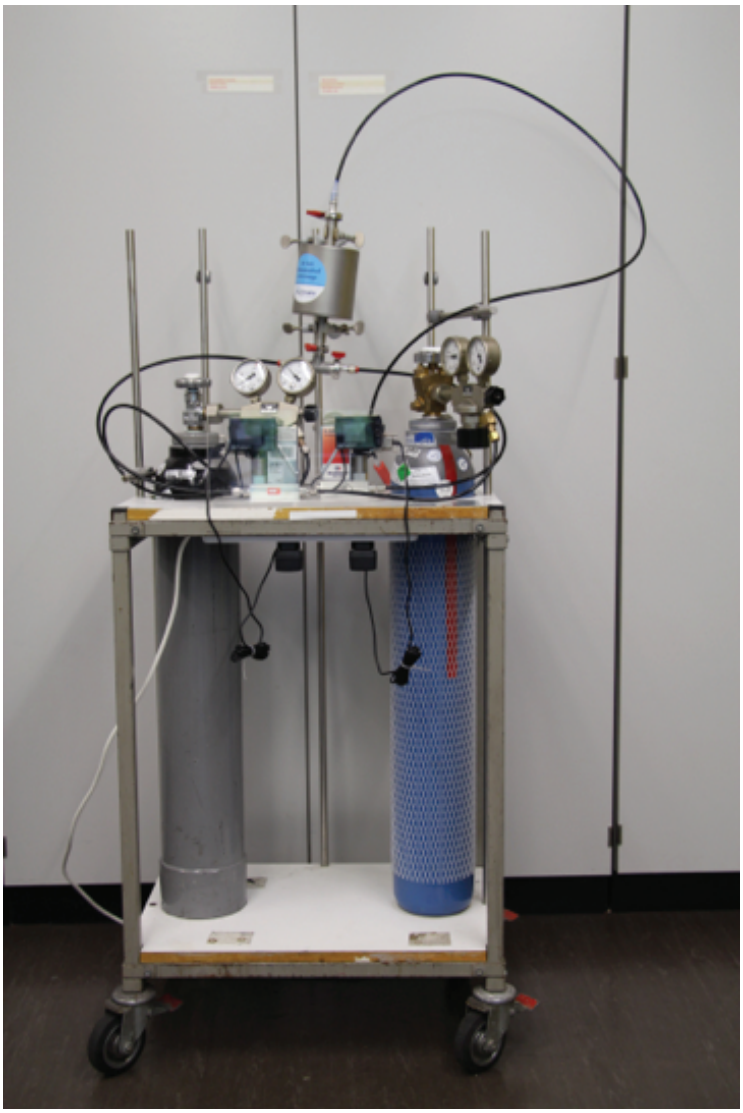

Figure 58: Apparatus for CO_2 experiments.

For the CO_2 uptake experiments we dissolved 3 mmol of amine absorbent and 12 mmol of PEG_{200} in a glastube and sealed it with a septum. A long needle was plunged through the septum and placed above the solution. A second but shorter needle served as an exit. The atmosphere in the tube was replaced by charging the container with CO_2 through the longer needle (no CO_2 was allowed to enter the solution at this point). After changing the atmosphere to CO_2, the weight of the glastube including septum and needles was determined. Placing the longer needle in the solution and the introducing a CO_2 stream through this needle started the measurement. The needle was disconnected every 5 min from the CO_2 stream and weight increase measured on an analytical balance. The absorption curves for the amine absorbents are depicted below.[45]

[45] Due to difficulties with the initial experimental setup described in section 4.4.3 we have no suitable absorption curve for compound **4.17**.

(Tetrahydro-1*H*-pyrrolizin-*7a*(5*H*)-yl)methanamine (4.13)

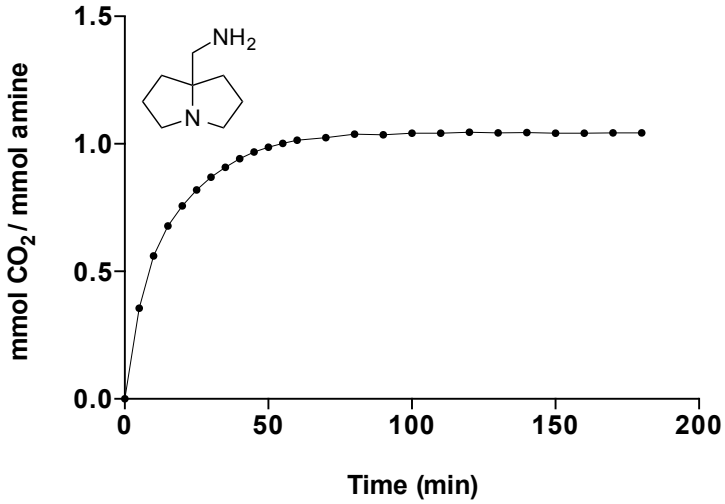

***N*-Methyl-1-(tetrahydro-1*H*-pyrrolizin-*7a*(5*H*)-yl)methanamine (4.14)**

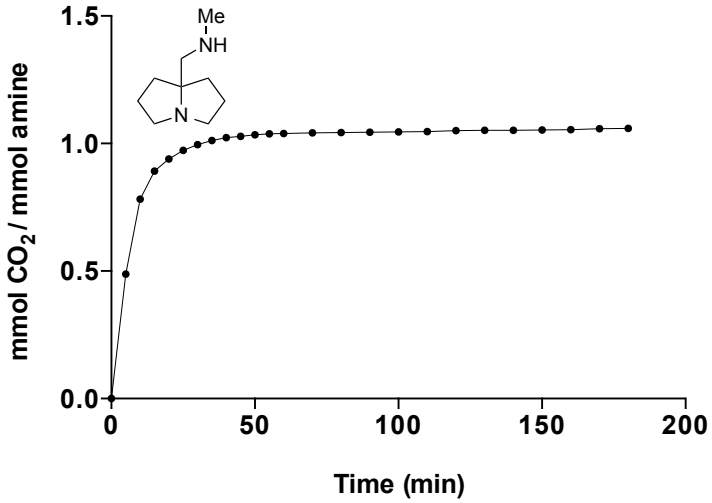

2-(Tetrahydro-1*H*-pyrrolizin-*7a*(5*H*)-yl)ethan-1-amine (4.15)

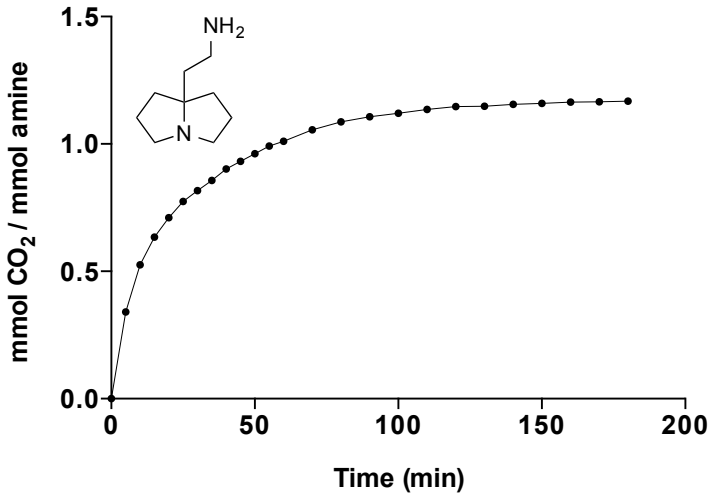

***N*-Methyl-2-(tetrahydro-1*H*-pyrrolizin-*7a*(5*H*)-yl)ethan-1-amine (4.16)**

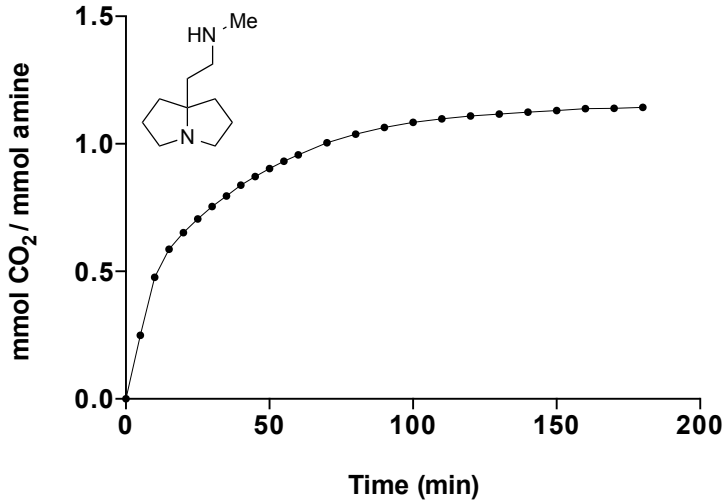

***N*-((Tetrahydro-1*H*-pyrrolizin-*7a*(5*H*)-yl)methyl)aniline (3.107)**

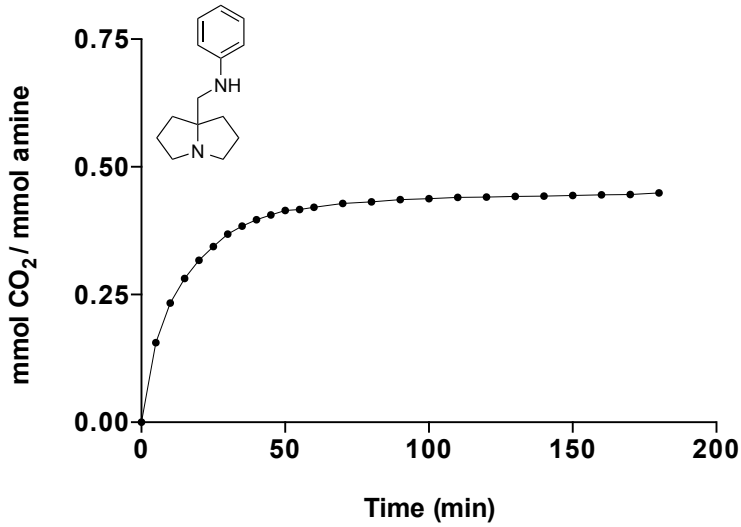

***N*^{1},*N*^{1},*N*^{2}-Trimethylethane-1,2-diamine**

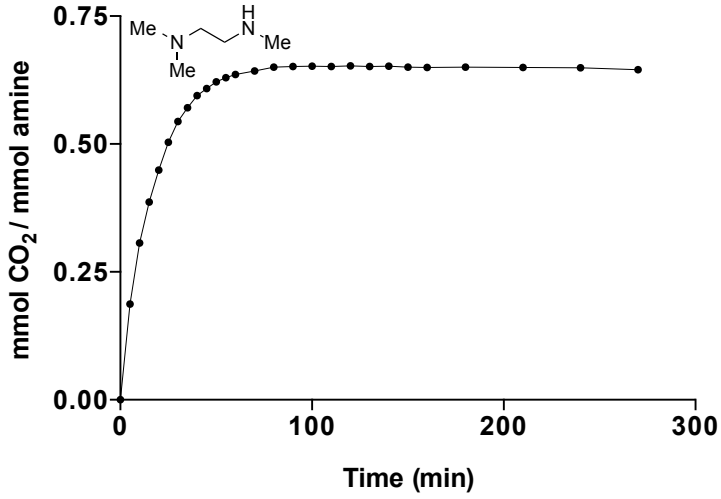

N^1,N^1,N^3-Trimethylpropane-1,3-diamine

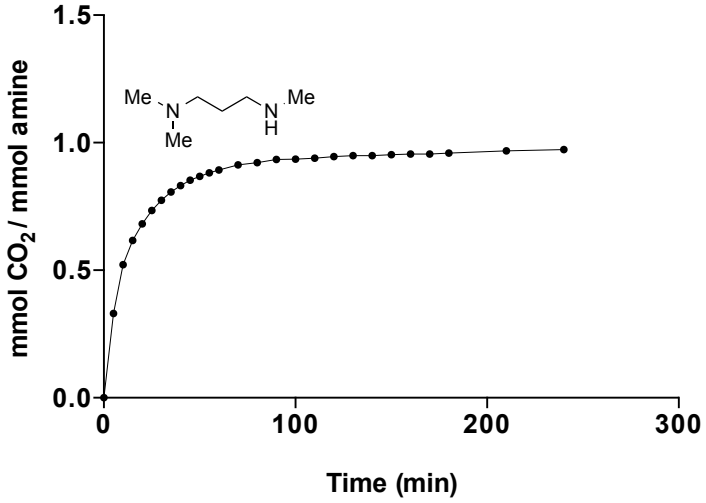

PEG_{200}

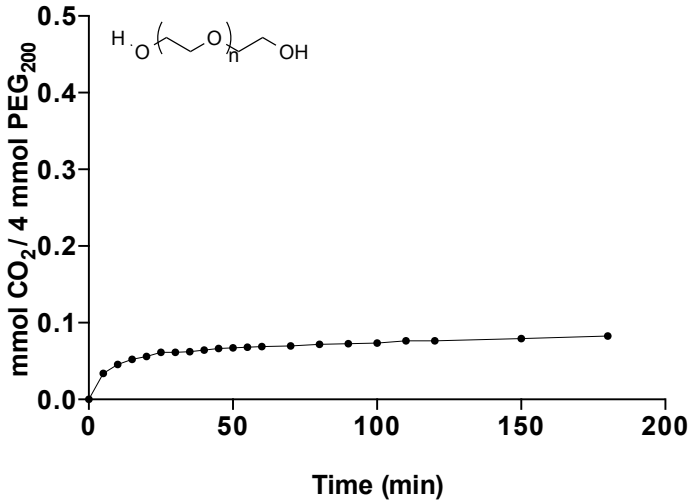

7.4.3 Titration of pyrrolizidine derivatives

A 0.01 M aqueous solution of diamine was prepared by dissolving 0.1 mmol diamine in 10 mL of water and filled in a flask equipped with a stirring bar. A pH-electrode (calibrated before each experiment) was placed in the flask. The amine solution was titrated using an aqueous 0.01 M HCl solution (0.2 mL portions) and the corresponding pH values were recorded.

(Tetrahydro-1*H*-pyrrolizin-*7a*(5*H*)-yl)methanamine (4.13)

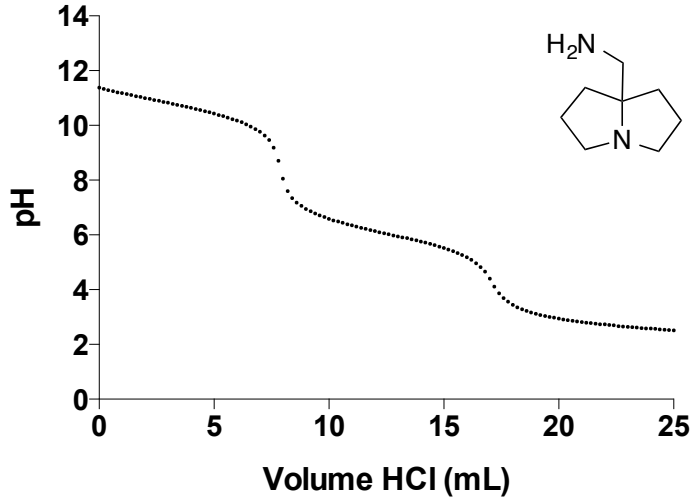

***N*-Methyl-1-(tetrahydro-1*H*-pyrrolizin-*7a*(5*H*)-yl)methanamine (4.14)**

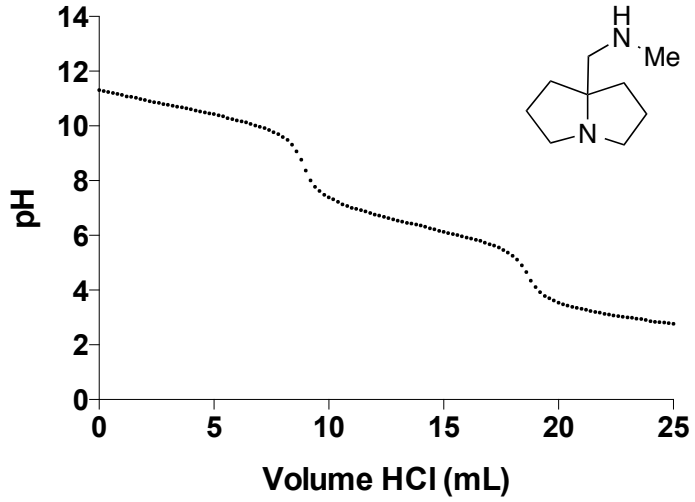

***N*-((Tetrahydro-1*H*-pyrrolizin-*7a*(5*H*)-yl)-methyl)aniline (3.107)**

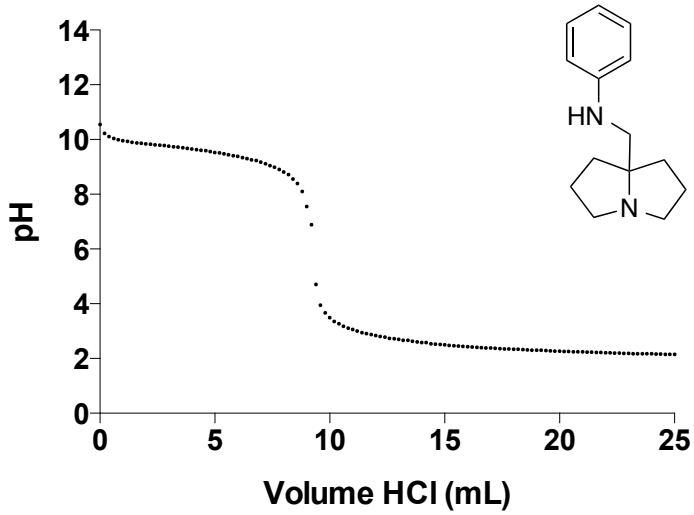

2-(Tetrahydro-1*H*-pyrrolizin-*7a*(5*H*)-yl)ethan-1-amine (4.15)

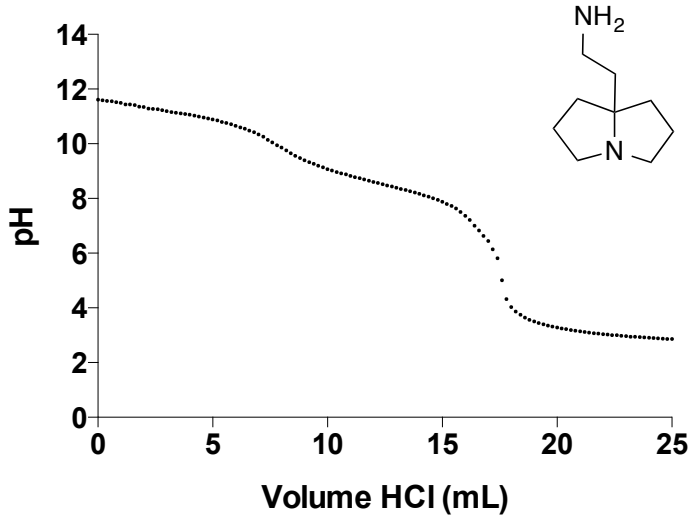

***N*-Methyl-2-(tetrahydro-1*H*-pyrrolizin-*7a*(5*H*)-yl)ethan-1-amine (4.16)**

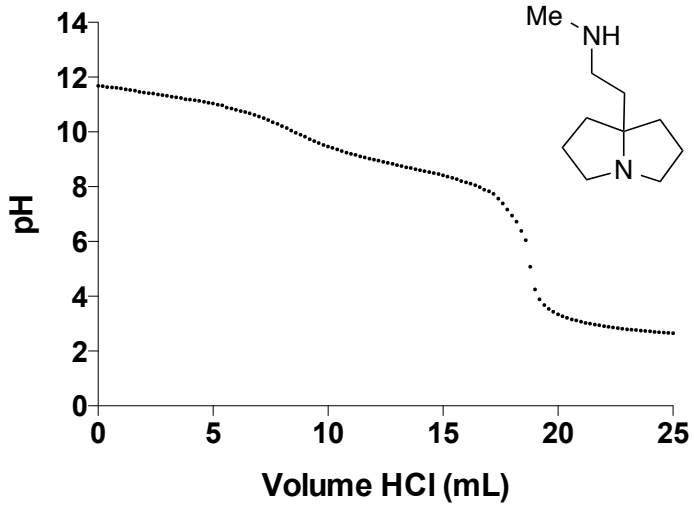

_N_-(2-(Tetrahydro-1_H_-pyrrolizin-_7a_(5_H_)-yl)ethyl)aniline (4.17)

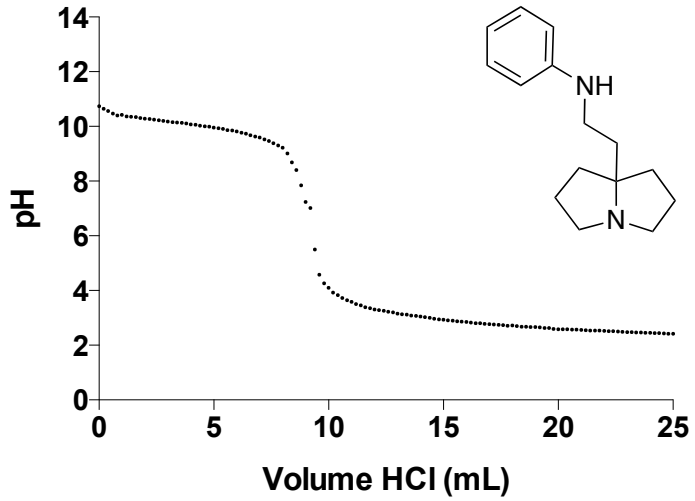

7.4.4 pK_a-value correction for water-insoluble derivatives

The phenyl-substituted diamines **3.107** and **4.17** were not soluble in water. Instead, the sample was dissolved in MeOH (10 mL) and titrated with 0.1 M aqueous HCl. The pK_a obtained with the solvent mixture was corrected to the corresponding pK_a to water using the following equations[168]

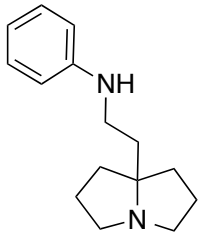

4.5 mL H_2O, 10 mL MeOH, $\Phi = 0.69$

$${}^{s}_{w}pK_a = 10.01$$

$${}^{w}_{w}pK_a = \frac{({}^{s}_{w}pKa - b_s - \delta)}{a_s}$$

$$\delta = \frac{0.09\,\Phi_{MeOH} - 0.11\Phi^2_{MeOH}}{1 - 3.15\Phi_{MeOH} + 3.15\Phi^2_{MeOH} - 1.35\Phi^3_{MeOH}}$$

$$a_s = \frac{1 + a_{s1}\Phi_{MeOH} + a_{s2}\Phi^2_{MeOH}}{1 + a_{s3}\Phi_{MeOH} + a_{s4}\Phi^2_{MeOH}}$$

$$b_s = \frac{b_{s1}\Phi_{MeOH} + b_{s2}\Phi_{MeOH}^2}{1 + b_{s3}\Phi_{MeOH} + b_{s4}\Phi_{MeOH}^2}$$

$$\delta = \frac{0.09 \cdot 0.69 - 0.11 \cdot 0.69^2}{1 - 3.15 \cdot 0.69 + 3.15 \cdot 0.69^2 - 1.35 \cdot 0.69^3} = \frac{0.062 - 0.0523}{1 - 2.17 + 1.50 - 0.44} = \frac{0.0097}{-0.11}$$

$$= -0.088$$

$$a_s = \frac{1 + (-0.476 \cdot 0.69) + (0.209 \cdot 0.69^2)}{1 + (-0.4 \cdot 0.69) + (0.158 \cdot 0.69^2)} = \frac{1 - 0.33 + 0.0995}{1 - 0.276 + 0.075} = \frac{0.769}{0.799} = 0.962$$

$$b_s = \frac{(-0.458 \cdot 0.69) + (0.477 \cdot 0.69^2)}{1 + (-1.674 \cdot 0.69) + (0.69 \cdot 0.69^2)} = \frac{-0.32 + 0.227}{1 - 1.15 + 0.33} = \frac{-0.093}{0.18} = -0.52$$

$${}^{w}_{w}pK_a = \frac{10.01 + 0.52 + 0.088}{0.962} = \frac{10.62}{0.962} = 11.04$$

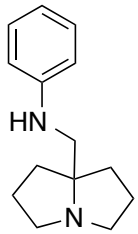

4.75 mL H_2O, 10 mL MeOH, $\Phi = 0.68$

$${}^{s}_{w}pK_a = 9.55$$

$$\delta = \frac{0.09 \cdot 0.68 - 0.11 \cdot 0.68^2}{1 - 3.15 \cdot 0.68 + 3.15 \cdot 0.68^2 - 1.35 \cdot 0.68^3} = \frac{0.061 - 0.051}{1 - 2.14 + 1.46 - 0.424} = \frac{0.01}{-0.104}$$

$$= -0.096$$

$$a_s = \frac{1 + (-0.476 \cdot 0.68) + (0.209 \cdot 0.68^2)}{1 + (-0.4 \cdot 0.68) + (0.158 \cdot 0.68^2)} = \frac{1 - 0.324 + 0.097}{1 - 0.272 + 0.073} = \frac{0.773}{0.801} = 0.965$$

$$b_s = \frac{(-0.458 \cdot 0.68) + (0.477 \cdot 0.68^2)}{1 + (-1.674 \cdot 0.68) + (0.69 \cdot 0.68^2)} = \frac{-0.311 + 0.221}{1 - 1.14 + 0.319} = \frac{-0.09}{0.179} = -0.503$$

$$_{w}^{w}pK_a = \frac{9.55 + 0.503 + 0.096}{0.965} = \frac{10.12}{0.965} = 10.49$$

8 Appendices

8.1 Image processing parameters

Images were processed using Fiji (ImageJ) by adjusting the brightness and contrast. In the table below the adjusted values for each image are listed. All images acquired are 8-bit images with a full display range of 0–255. Overlay images have not been corrected after merging the partial images and thus are not listed here.

Location	Image	Range	Location	Image	Range
Scheme 7, a	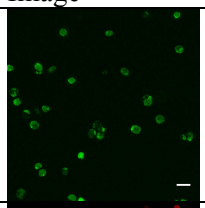	0–255	Scheme 12, e	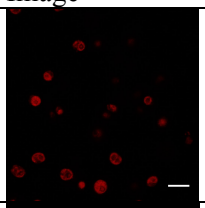	0–92
Scheme 7, b	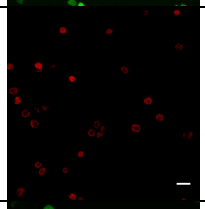	0–255	Scheme 13, a	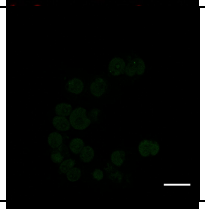	0–140
Scheme 7, c	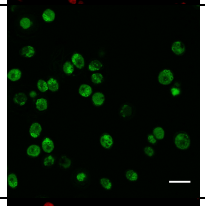	0–255	Scheme 13, b	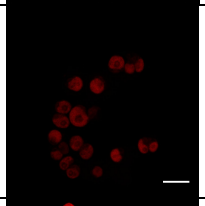	0–255
Scheme 7, d	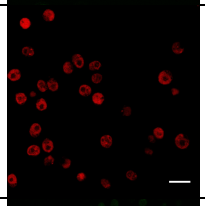	0–255	Scheme 15, a	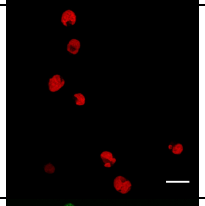	24–163
Scheme 12, a	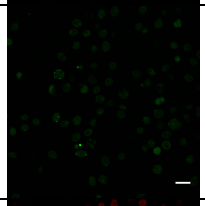	0–255	Scheme 15, b	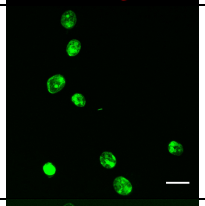	16–154
Scheme 12, b	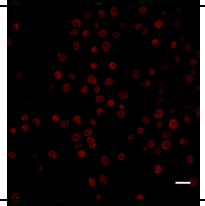	0–129	Scheme 15, d	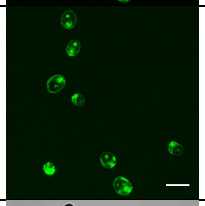	0–140
Scheme 12, d	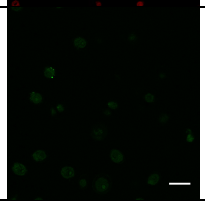	0–255	Scheme 15, e	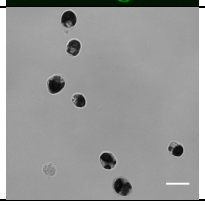	16–185

Scheme 15, f	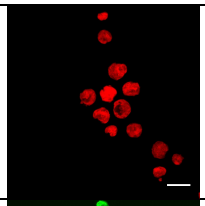	59–244	Scheme 15, q	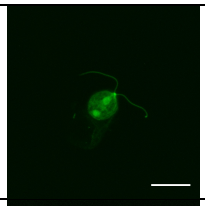	5–241
Scheme 15, g	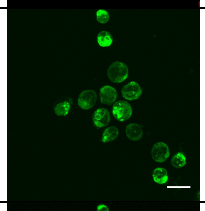	5–171	Scheme 15, s	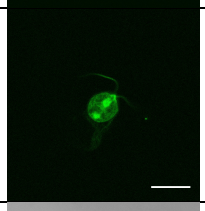	0–107
Scheme 15, i	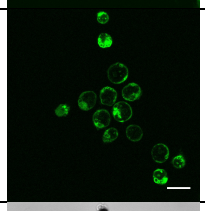	0–107	Scheme 15, t	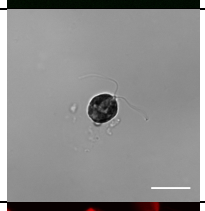	18–198
Scheme 15, j	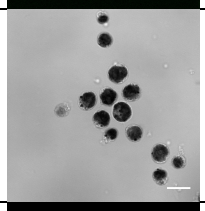	12–181	Figure 27	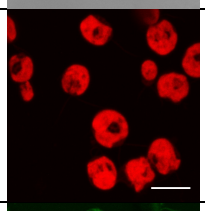	0–255
Scheme 15, k	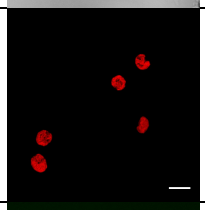	24–163	Figure 27	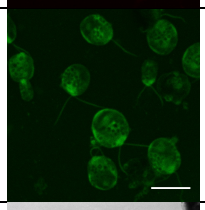	1–153
Scheme 15, l	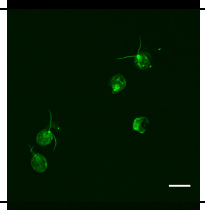	6–124	Scheme 18, BF		41–148
Scheme 15, n	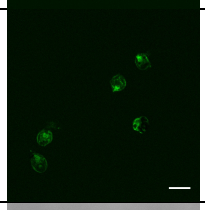	0–107	Scheme 18, chloroplast	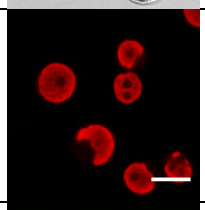	0–255
Scheme 15, o	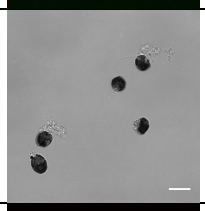	0–188	Scheme 18, fluorescein	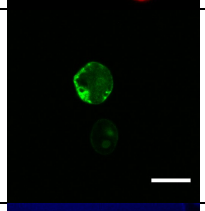	0–255
Scheme 15, p	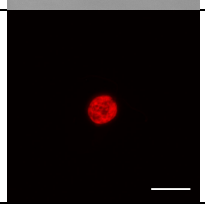	0–119	Scheme 18, vancomycin antibody	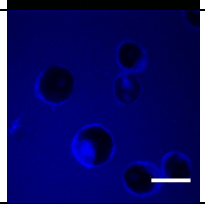	0–73

Location	Image	Range
Figure 29, a	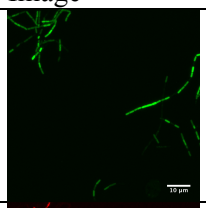	0–255
Figure 29, a	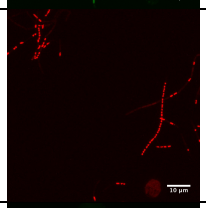	0–255
Figure 29, d	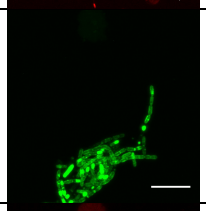	0–255
Figure 29, c	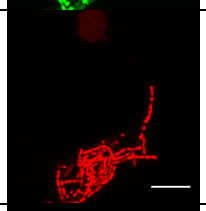	0–255
Scheme 27, a	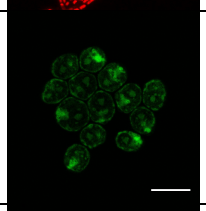	0–255
Scheme 27, b	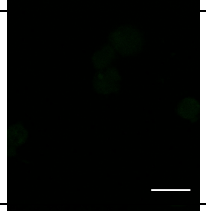	0–255
Scheme 27, c	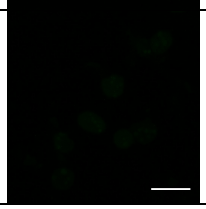	0–255

8.2 Imaging conditions

General:

Argon Laser: 20%

Temperature: room temperature

Resolution: 8 bits

Objective: HCX PL APO lambda blue 63.0x1.40 OIL UV

Aquisition software: Leica AF

Image	**Resolution (xyz)**	**Imaging medium**	**Laser**	**Detector 1**	**Detector 2**
Scheme 7, a, b	1024x1024x91 39.08x139.08x15.11 µm step size: 0.17 µm	Kuhl medium	λ_{ex} = 488 nm 8%	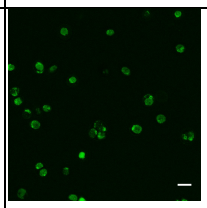 HyD 500-530 nm 20% gain	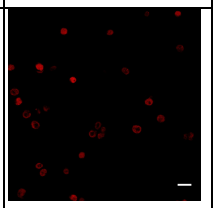 HyD 600-700 nm 10% gain
Scheme 7, c, d	1024x1024x92 90.35x90.35x15.27 µm step size: 0.17 µm	Kuhl medium	λ_{ex} = 488 nm 8%	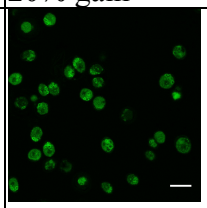 HyD 500-530 nm 20% gain	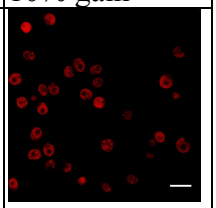 HyD 600-700 nm 10% gain
Scheme 12, a, b	1024x1024x1 129.17x129.17x0 µm	Kuhl medium	λ_{ex} = 488 nm 8%	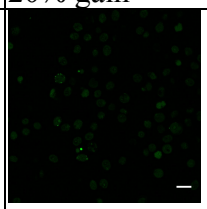 HyD 500-530 nm 20% gain	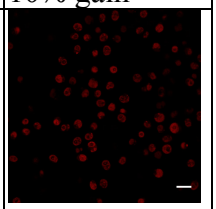 HyD 600-700 nm 10% gain
Scheme 12, c, d	1024x1024x1 90.35x90.35x0 µm	Kuhl medium	λ_{ex} = 488 nm 8%	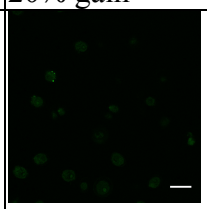 HyD 500-530 nm 20% gain	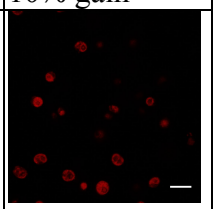 HyD 600-700 nm 10% gain

Scheme 13, a, b	1024x1024x1 72.63x71.63x0 µm	Kuhl medium	λ_{ex} = 488 nm 18%	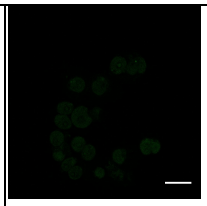 PMT 493.8-530 nm 60% gain	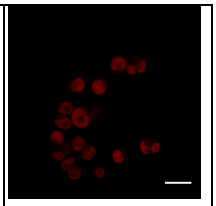 HyD 555-727 nm 28% gain
Scheme 15, a-e	1024x1024x63 pixel 82.01x82.01x7.8 µm step size: 0.13 µm	ProLong	λ_{ex} = 488 nm 5%	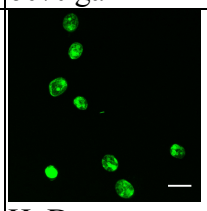 HyD 500-530 nm 12% gain	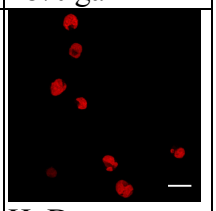 HyD 600-700 nm 10% gain
Scheme 15, f-j	1024x1024x64 82.01x82.01x7.93 µm step size: 0.13 µm	ProLong	λ_{ex} = 488 nm 8%	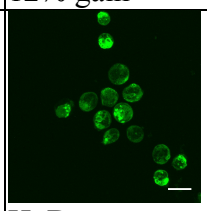 HyD 500-530 nm 34% gain	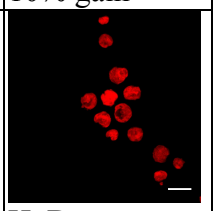 HyD 600-700 nm 10% gain
Scheme 15, k-o	1024x1024x42 89.64x89.64x5.16 µm step size: 0.13 µm	ProLong	λ_{ex} = 488 nm 5%	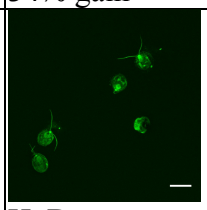 HyD 500-530 nm 15% gain	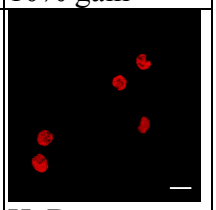 HyD 600-700 nm 10% gain
Scheme 15, p-t	1024x1024x42 49.21x49.21x5.16 µm step size: 0.13 µm	ProLong	λ_{ex} = 488 nm 8%	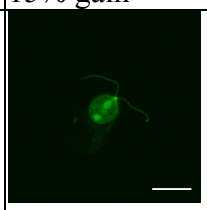 HyD 500-530 nm 34% gain	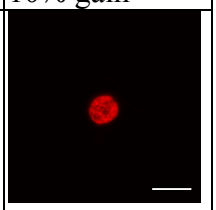 HyD 600-700 nm 10% gain
Figure 27	1024x1024x44 49.21x49.21x5.41 µm step size: 0.13 µm	ProLong	λ_{ex} = 488 nm 11%	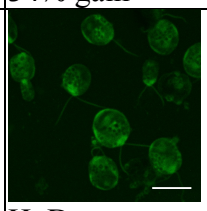 HyD 500-530 nm 39% gain	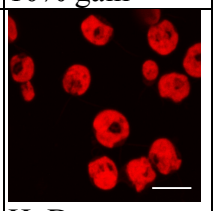 HyD 600-700 nm 57% gain

Figure 29, a	1024x1024x48 82.01x82.1x5.92 µm step size: 0.13 µm	Agarose patch	λ_{ex} = 488 nm 10%	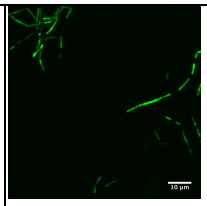 HyD 500-530 nm 37% gain	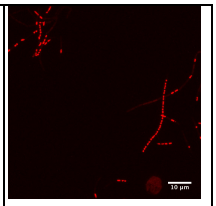 HyD 605-644 nm 104% gain
Figure 29, c, d	1024x1024x35 82.01x82.1x4.28µm step size: 0.13 µm	Agarose patch	λ_{ex} = 488 nm 10%	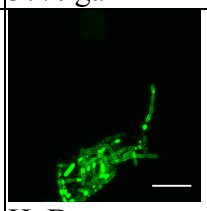 HyD 500-530 nm 37% gain	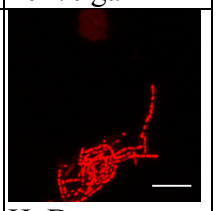 HyD 605-644 nm 104% gain
Scheme 27, a	1024x1024x39 49.21x49.21x4.78 µm step size: 0.13 µm	ProLong	λ_{ex} = 488 nm 5%	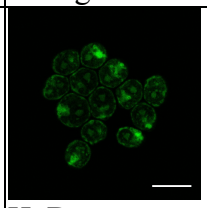 HyD 500-530 nm 41% gain	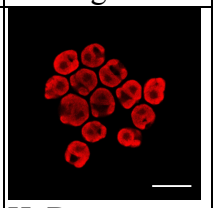 HyD 600-700 nm 12% gain
Scheme 27, b	1024x1024x1 49.21x49.21x0 µm	ProLong	λ_{ex} = 488 nm 5%	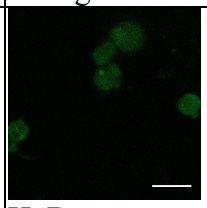 HyD 500-530 nm 41% gain	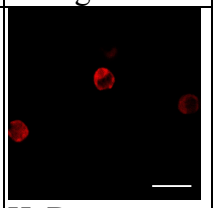 HyD 600-700 nm 18% gain
Scheme 27, c	1024x1024x1 49.21x49.21x0 µm	ProLong	λ_{ex} = 488 nm 5%	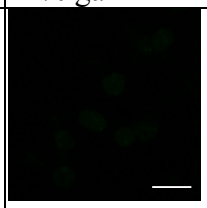 HyD 500-530 nm 41% gain	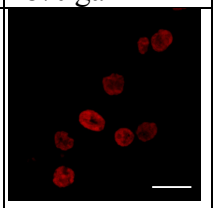 HyD 600-700 nm 18% gain

Immunolabeling:

Same conditions have been applied to all images in Scheme 18.

Resolution (xyz)	**Imaging medium**	**Laser 1**	**Detector 1**	
512x512x1 49.21x49.21x0 µm	ProLong	λex = 355 nm 65%	HyD 428-465 nm PhotonCount-ing	
			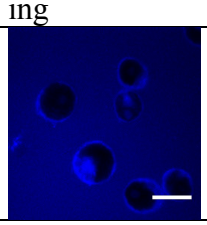	
		Laser 2	**Detector 2**	**Detector 3**
		λex = 488 nm 8%	HyD 506-535 nm PhotonCount-ing	HyD 600-700 nm PhotonCounting
			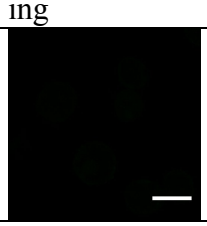	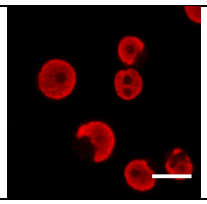

8.3 Single crystal X-ray structures

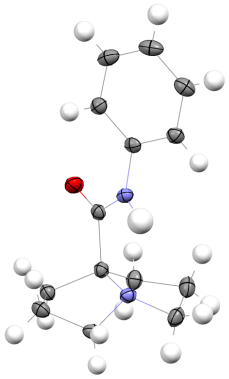

Table 11: Crystal data for pyrrolizidine **3.32**.

Formula	$C_{14}H_{18}N_2O$
Formula weight	230.31 g·mol^{-1}
Z, calculated density	8, 1.256 Mg · m^{-3}
F (000)	992
Description and size of crystal	colorless needle, 0.060 · 0.100 · 0.280 mm^3
Absorption coefficient	0.631 mm^{-1}
Min/max transmission	0.94 / 0.96
Temperature	123K
Radiation (wavelength)	Cu K_α (λ = 1.54178 Å)
Crystal system, space group	monoclinic, P 21/c
a	6.2225(4) Å
b	27.8281(16) Å
c	14.2974(8) Å
α	90°
β	100.432(2)°
γ	90°
V	2434.8(3) Å^3
Min/max Θ	3.176° / 68.386°
Number of collected reflections	23143
Number of independent reflections	4420 (merging r = 0.028)
Number of observed reflections	4369 (I>2.0σ(I))
Number of refined parameters	307
R	0.0346
rW	0.0391
Goodness of fit	1.1196

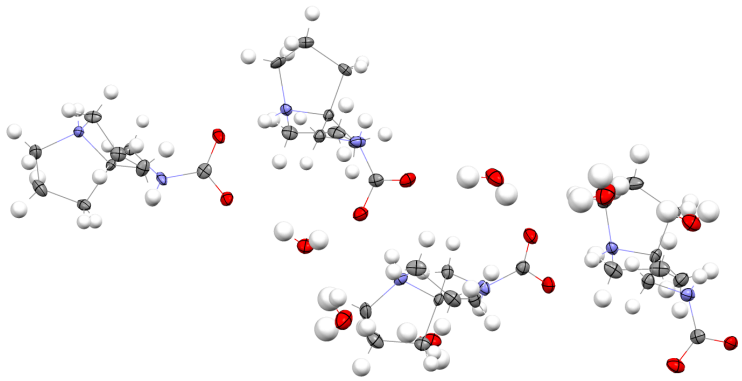

Table 12: Crystal data for carbamate **4.29**.

Formula	$C_{18}H_{38}N_4O_7$
formula weight	422.52
Z, calculated density	4, 1.343 Mg · m^{-3}
F(000)	919.991
description and size of crystal	colorless plate, 0.020 · 0.110 · 0.180 mm^3
absorption coefficient	0.854 mm^{-1}
min/max transmission	0.91 / 0.98
temperature	123K
radiation(wavelength)	Cu Kα (λ = 1.54178 Å)
Crystal system, space group	monoclinic, P n
a	7.8954(8) Å
b	22.637(2) Å
c	11.6950(11) Å
α	90°
β	90.952(7)°
γ	90°
V	2089.9(2) $Å^3$
min/max Θ	3.905° / 68.901°
number of collected reflections	15770
number of independent reflections	6655 (merging r = 0.070)
number of observed reflections	5647 (I>2.0σ(I))
number of refined parameters	584
r	0.0453
rW	0.0773
goodness of fit	1.1157

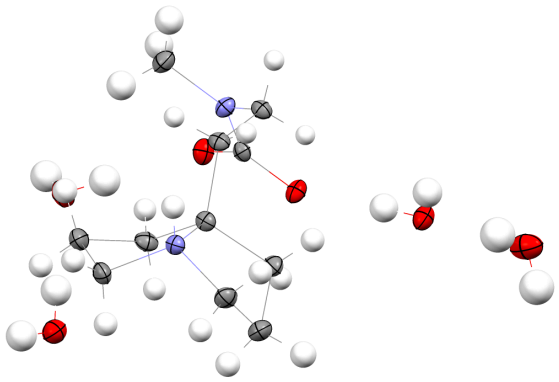

Table 13: Crystal data for carbamate **4.30**.

Formula	$C_{11}H_{28}N_2O_6$
formula weight	284.35
Z, calculated density	4, 1.273 Mg · m^{-3}
F(000)	624
description and size of crystal	colorless block, 0.040 · 0.110 · 0.230 mm^3
absorption coefficient	0.856 mm^{-1}
min/max transmission	0.91 / 0.97
temperature	123K
radiation (wavelength)	Cu Kα (λ = 1.54178 Å)
Crystal system, space group	monoclinic, P 21/n
a	7.0751(5) Å
b	16.6440(12) Å
c	13.0818(9) Å
α	90°
β	105.578(2)°
γ	90°
V	1483.89(10) $Å^3$
min/max Θ	4.401° / 69.119°
number of collected reflections	9721
number of independent reflections	2692 (merging r = 0.022)
number of observed reflections	2629 (I>2.0σ(I))
r	0.0319
rW	0.0360
goodness of fit	1.1204

8.4 ^{1}H and ^{13}C-NMR spectra

Synthesis of 3-(3,4-dihydro-2*H*-pyrrol-5-yl)propan-1-ol (3.21)

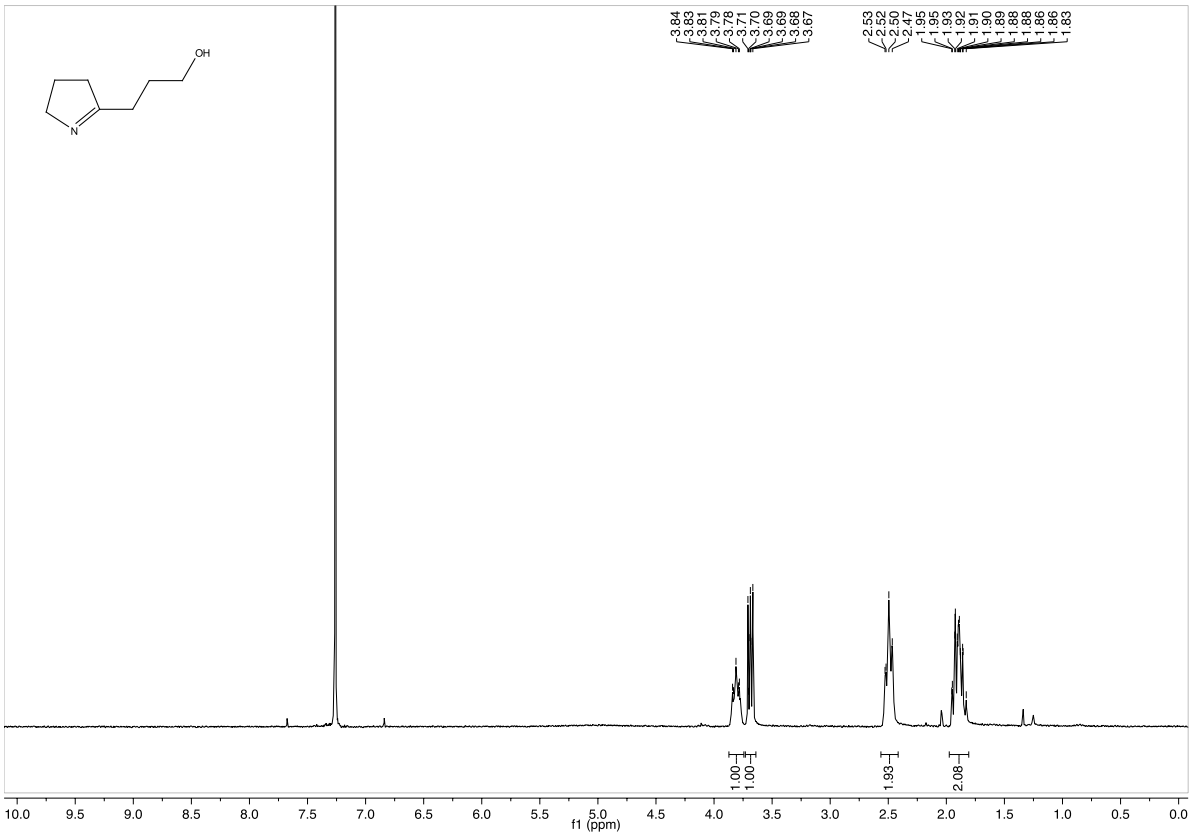

250 MHz ^{1}H-NMR in $CDCl_3$

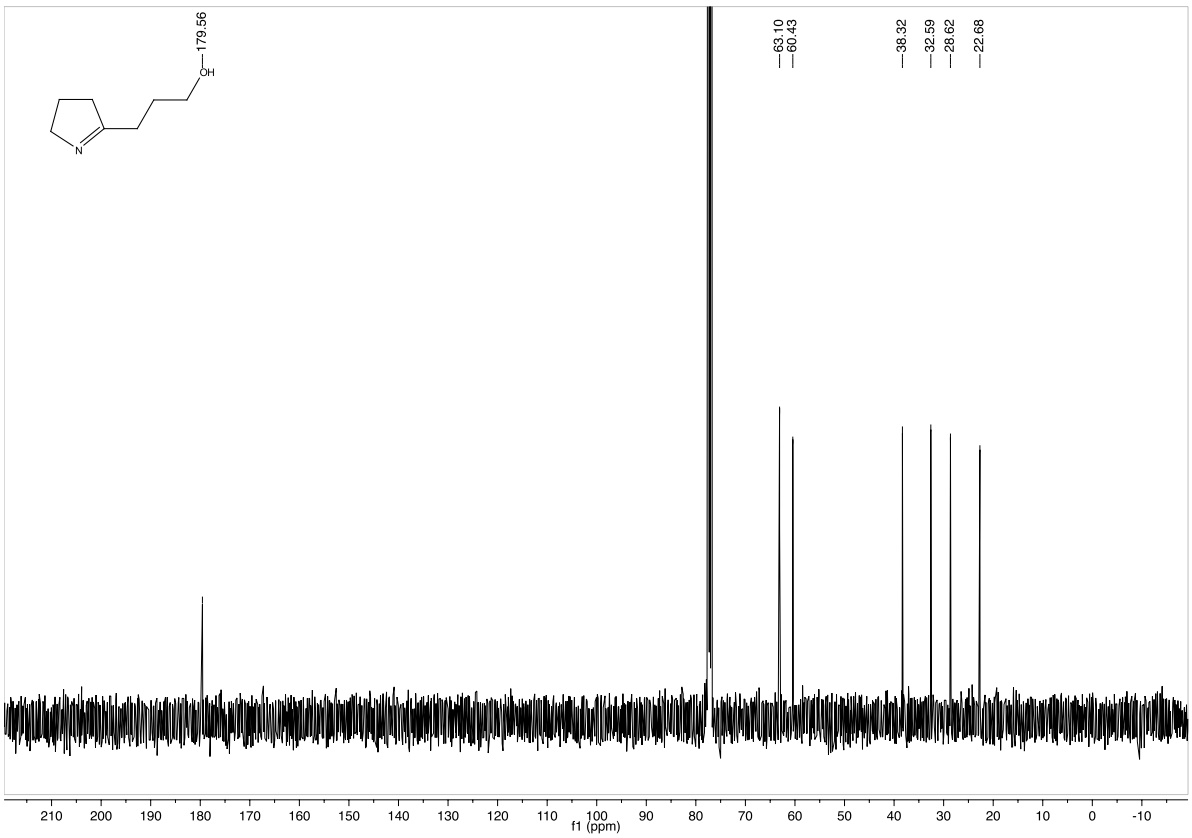

101 MHz ^{13}C-NMR in $CDCl_3$

1-Isocyano-4-methoxybenzene (3.35)

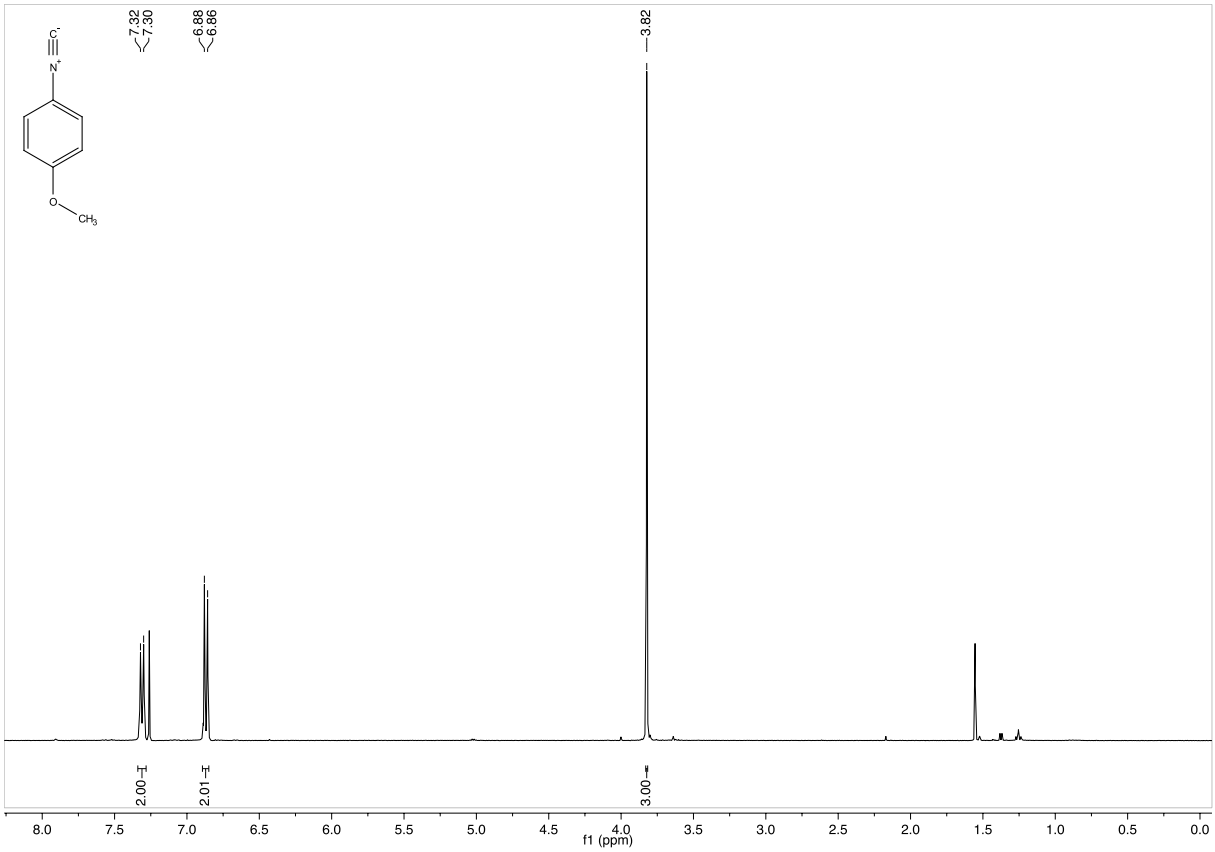

400 MHz ^{1}H-NMR in $CDCl_3$

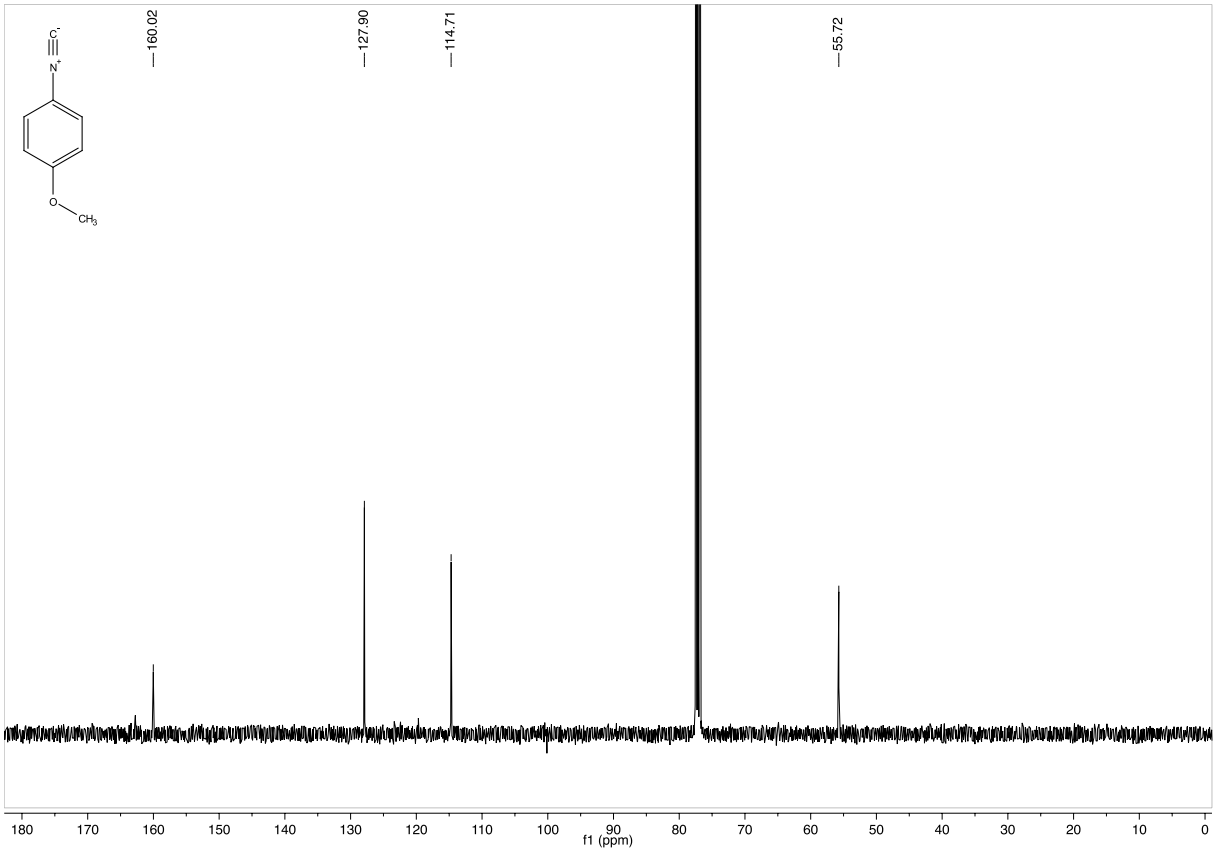

101 MHz ^{13}C-NMR in $CDCl_3$

1-Fluoro-4-isocyanobenzene (3.36)

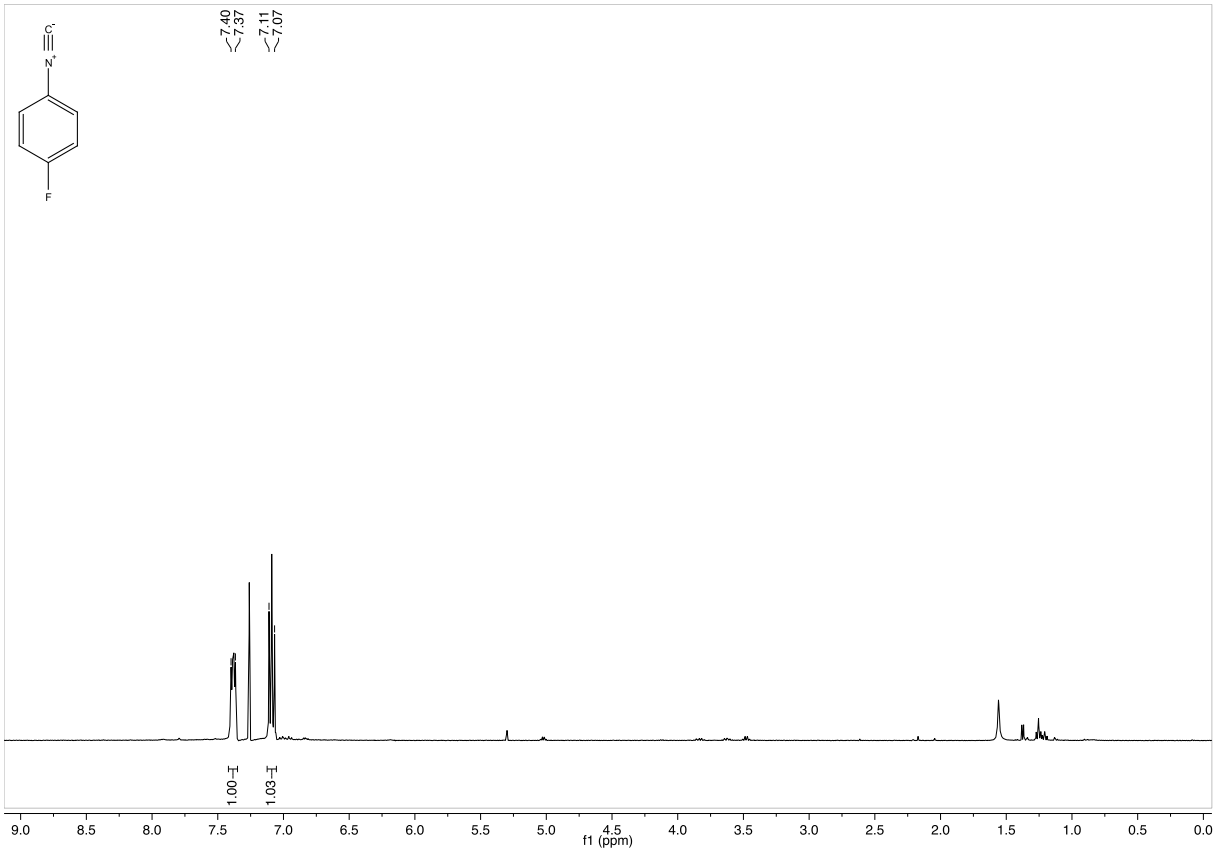

400 MHz ^{1}H-NMR in $CDCl_3$

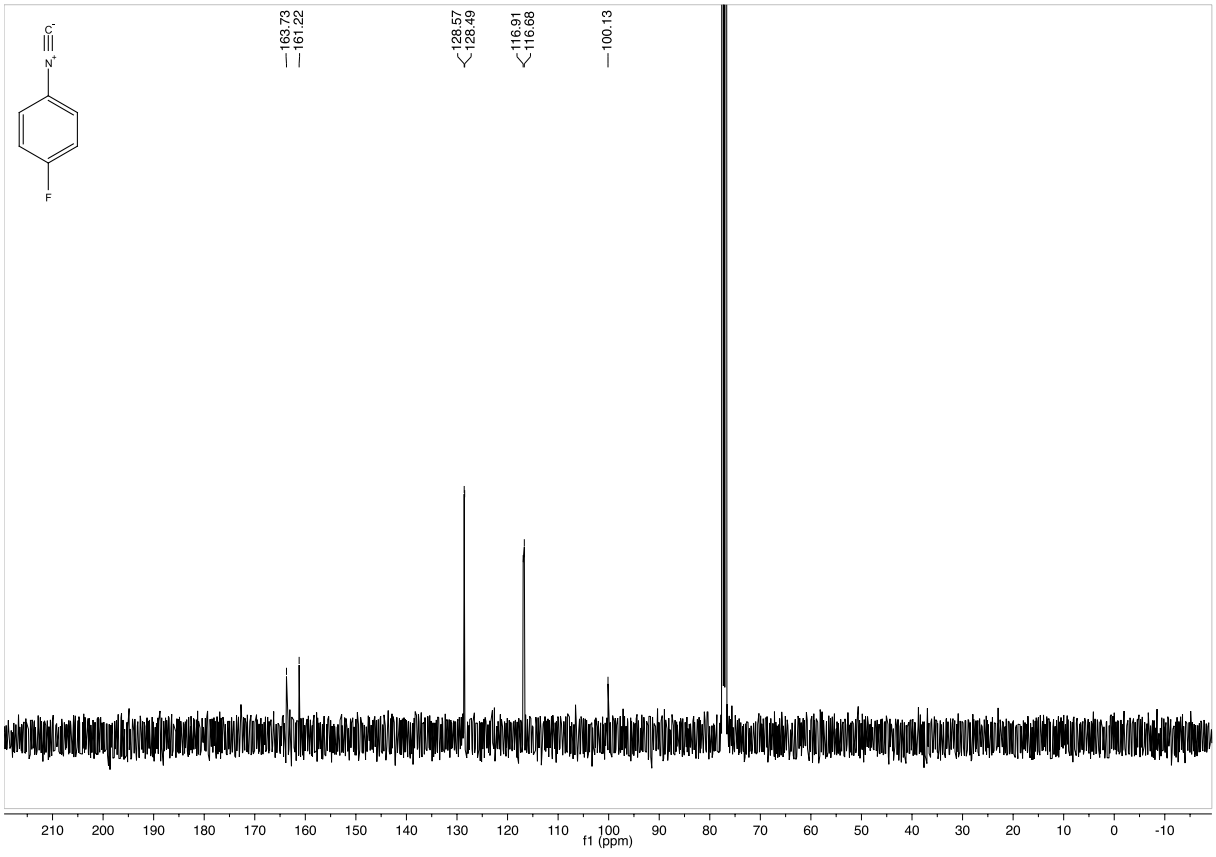

101 MHz ^{13}C-NMR in $CDCl_3$

2-Isocyano-1,3-dimethoxybenzene (3.40)

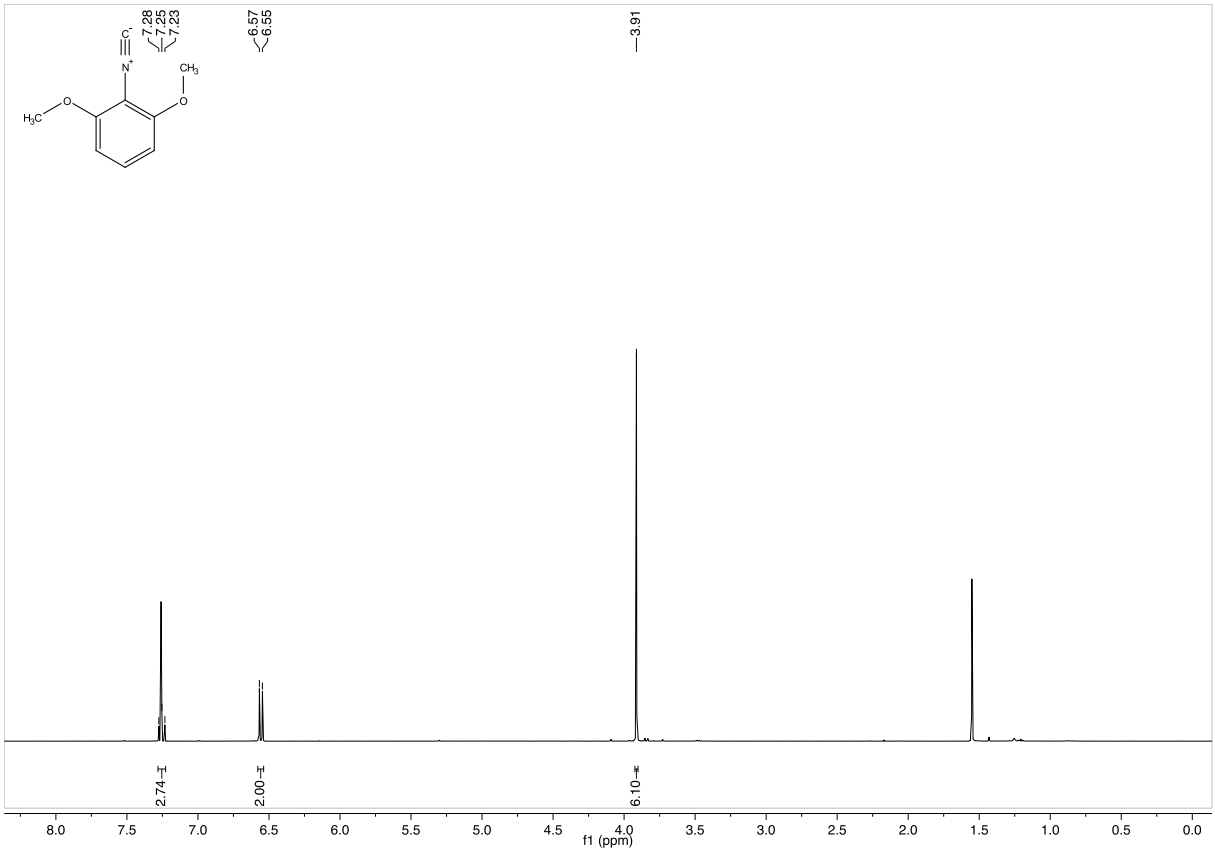

400 MHz ^{1}H-NMR in $CDCl_3$

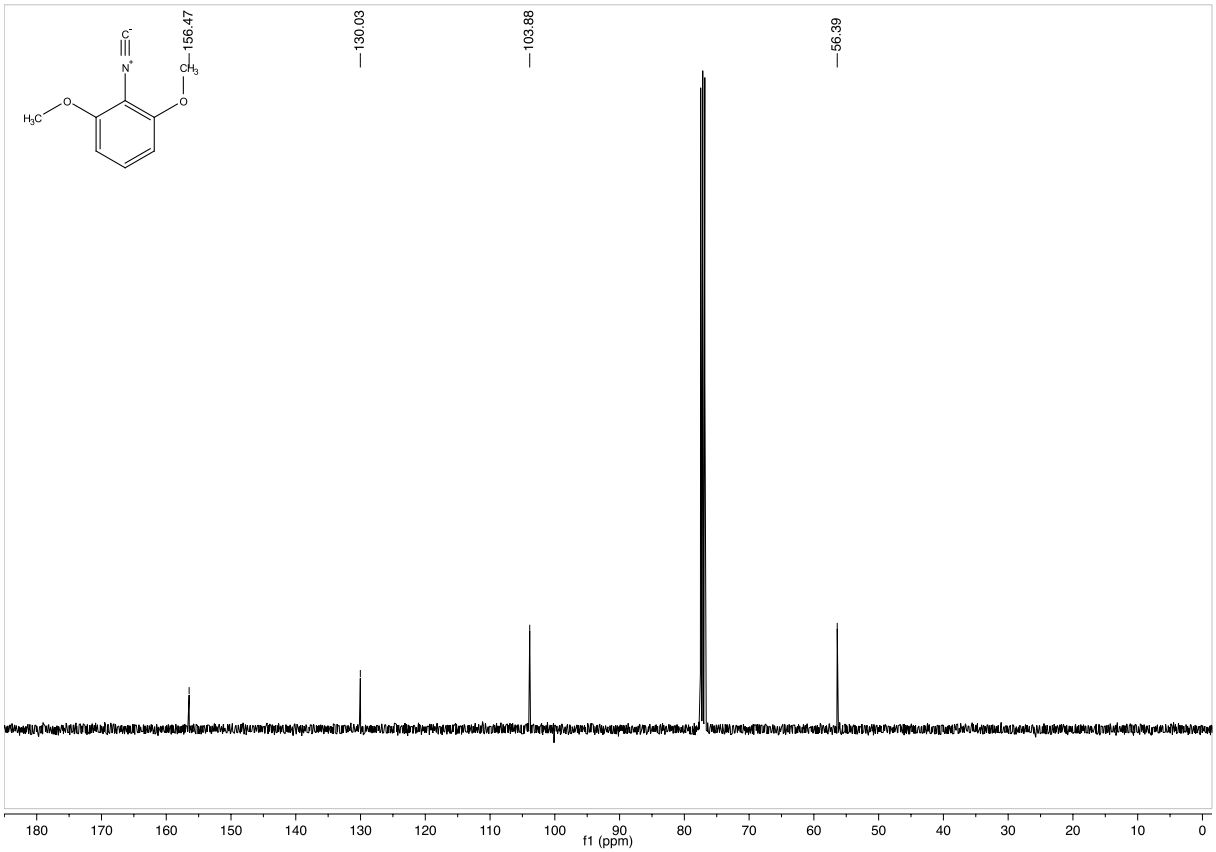

101 MHz ^{13}C-NMR in $CDCl_3$

4-(2-Isocyanoethyl)phenol (3.54)

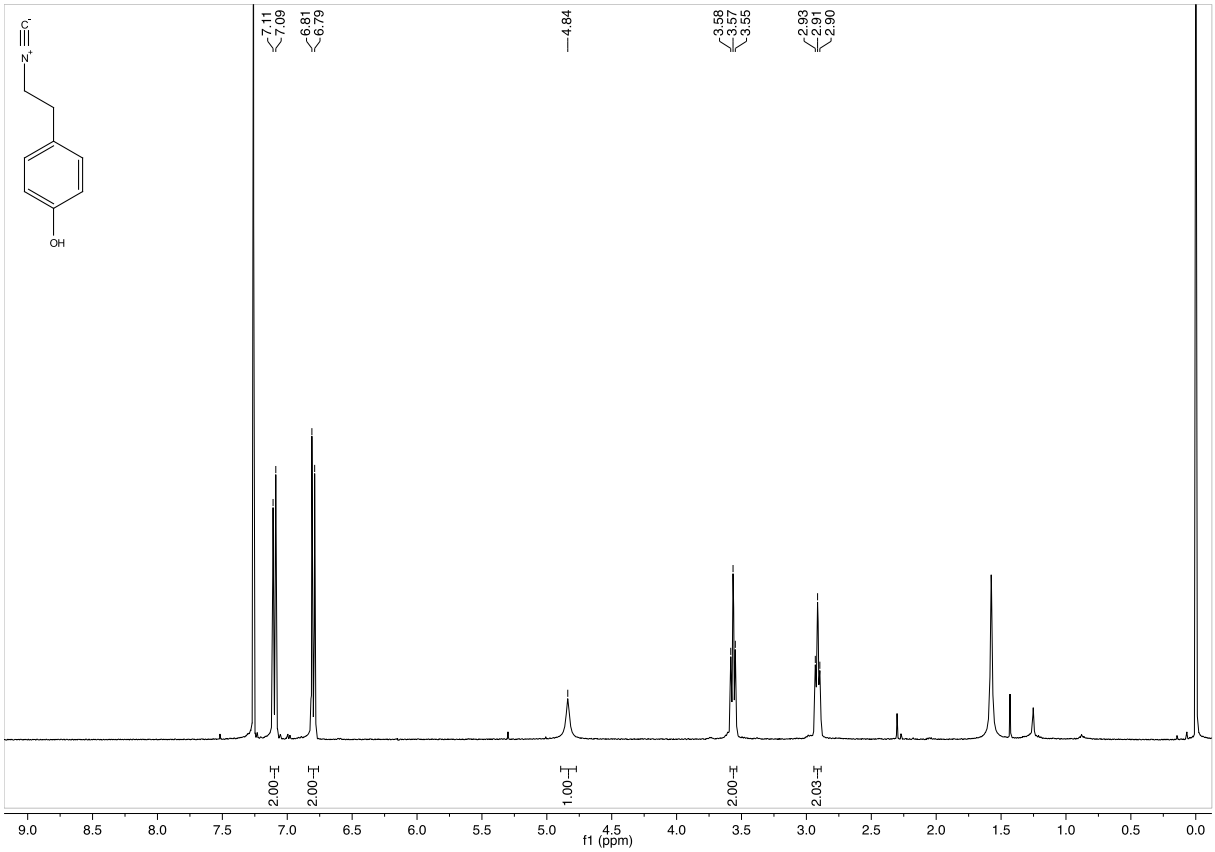

400 MHz ^{1}H-NMR in $CDCl_3$

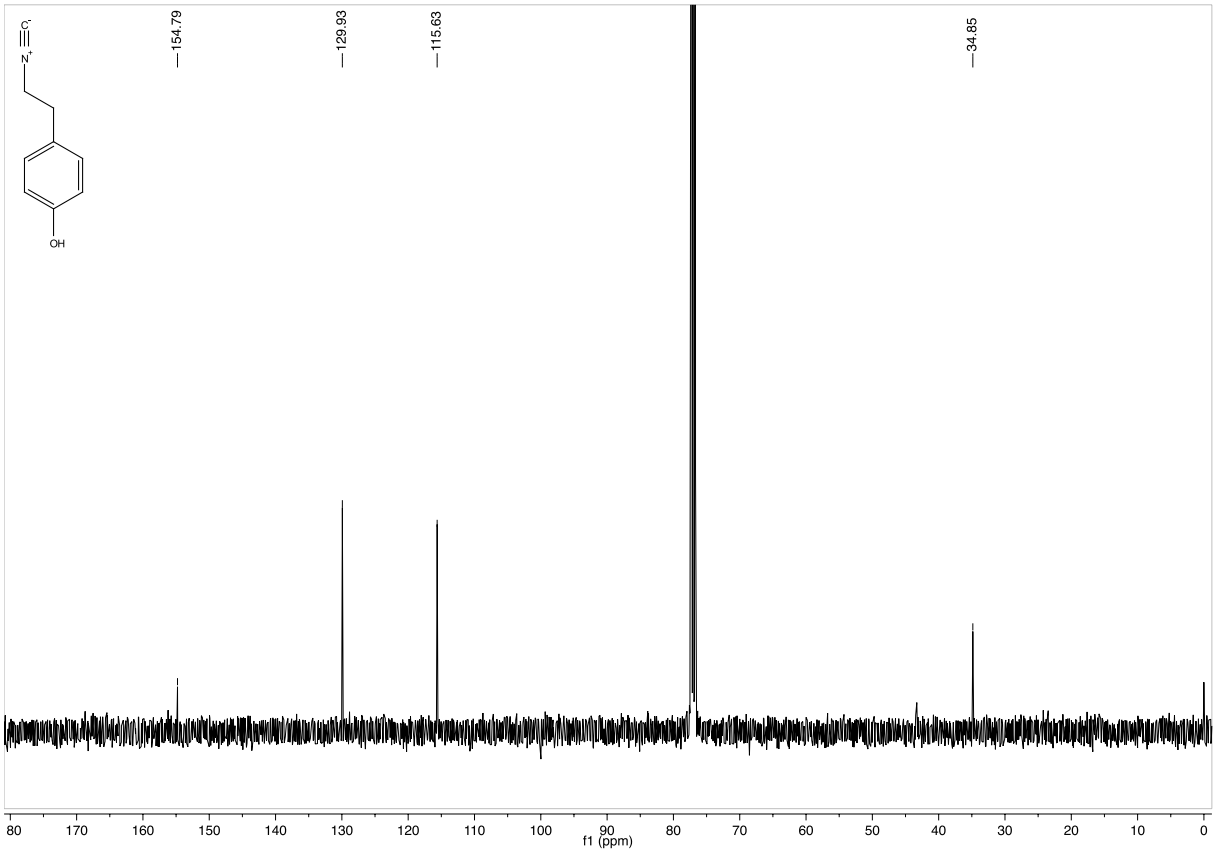

101 MHz ^{13}C-NMR in $CDCl_3$

N-Phenyltetrahydro-1*H*-pyrrolizine-7a(5*H*)-carboxamide (3.32)

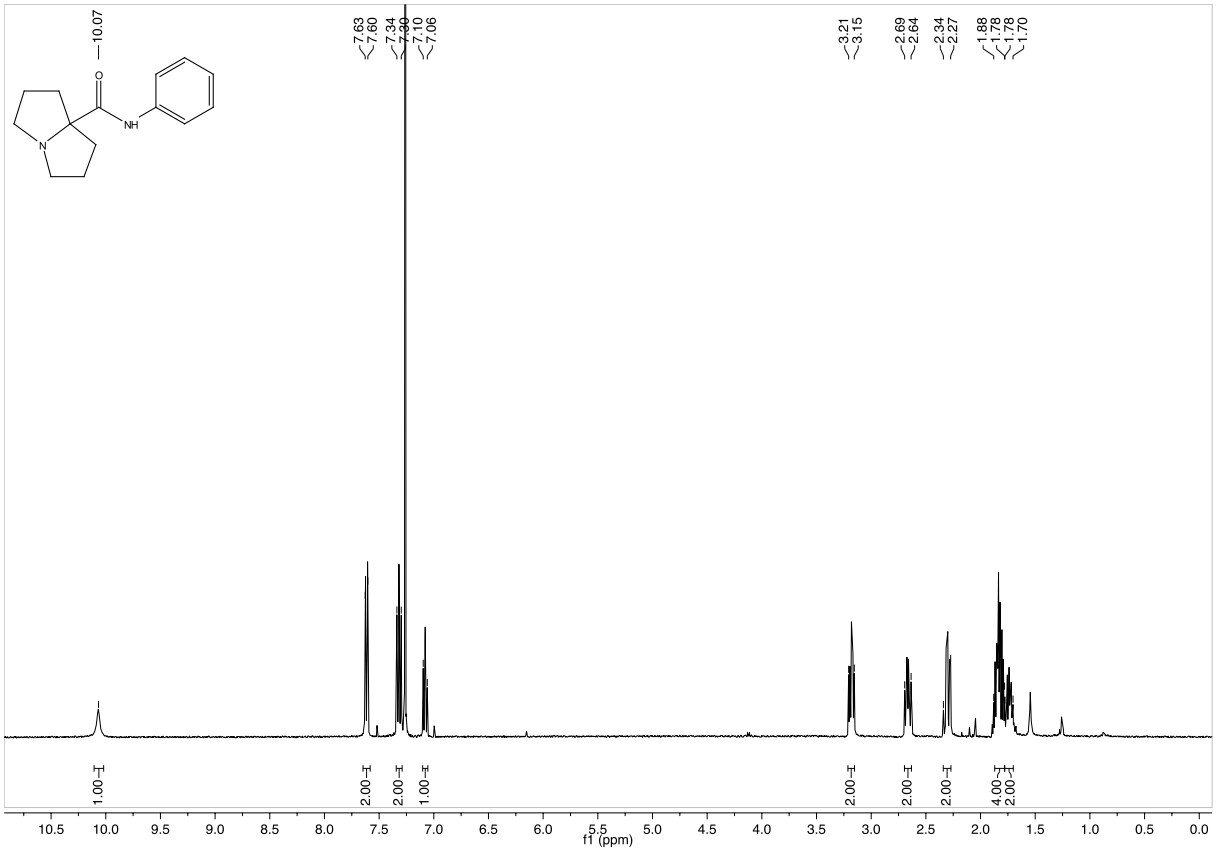

500 MHz ^{1}H-NMR in $CDCl_3$

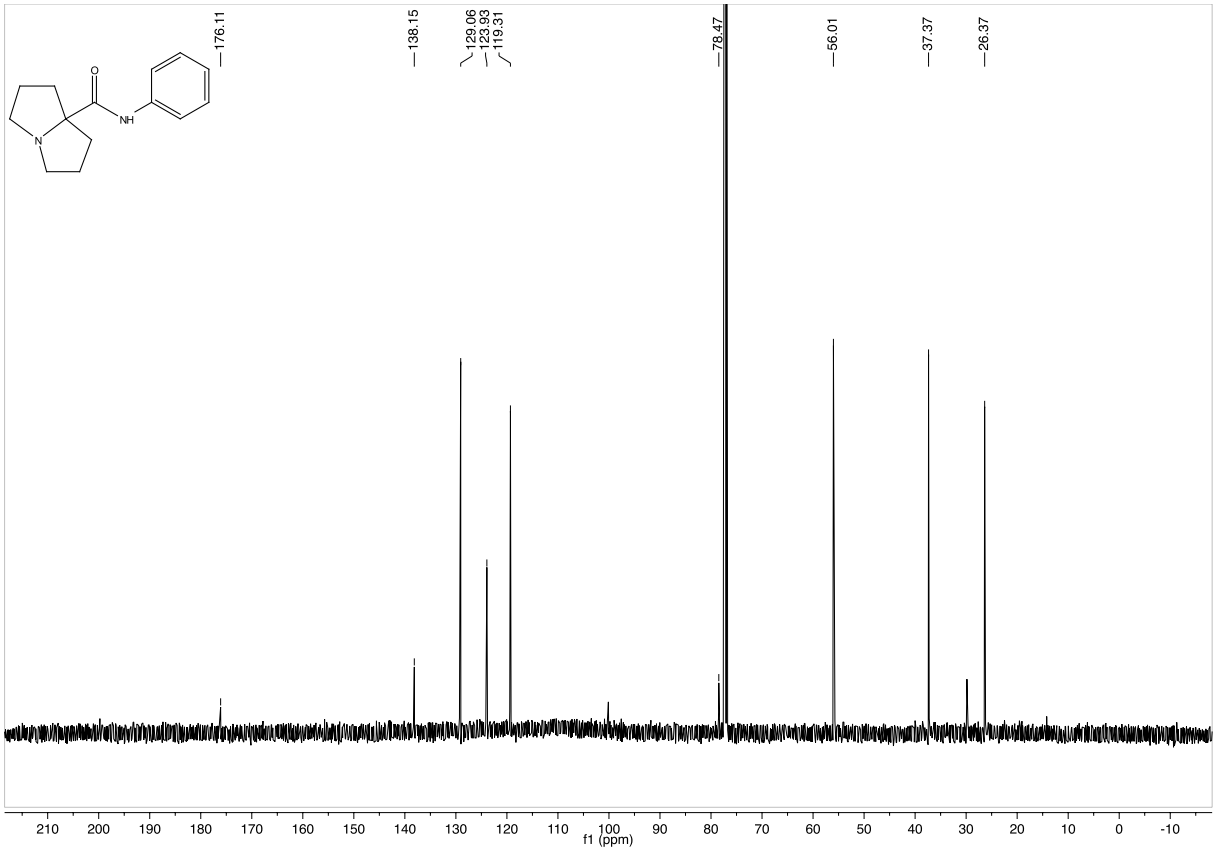

126 MHz ^{13}C-NMR in $CDCl_3$

N-(4-Methoxyphenyl)tetrahydro-1*H*-pyrrolizine-7a(5*H*)-carboxamide (3.55)

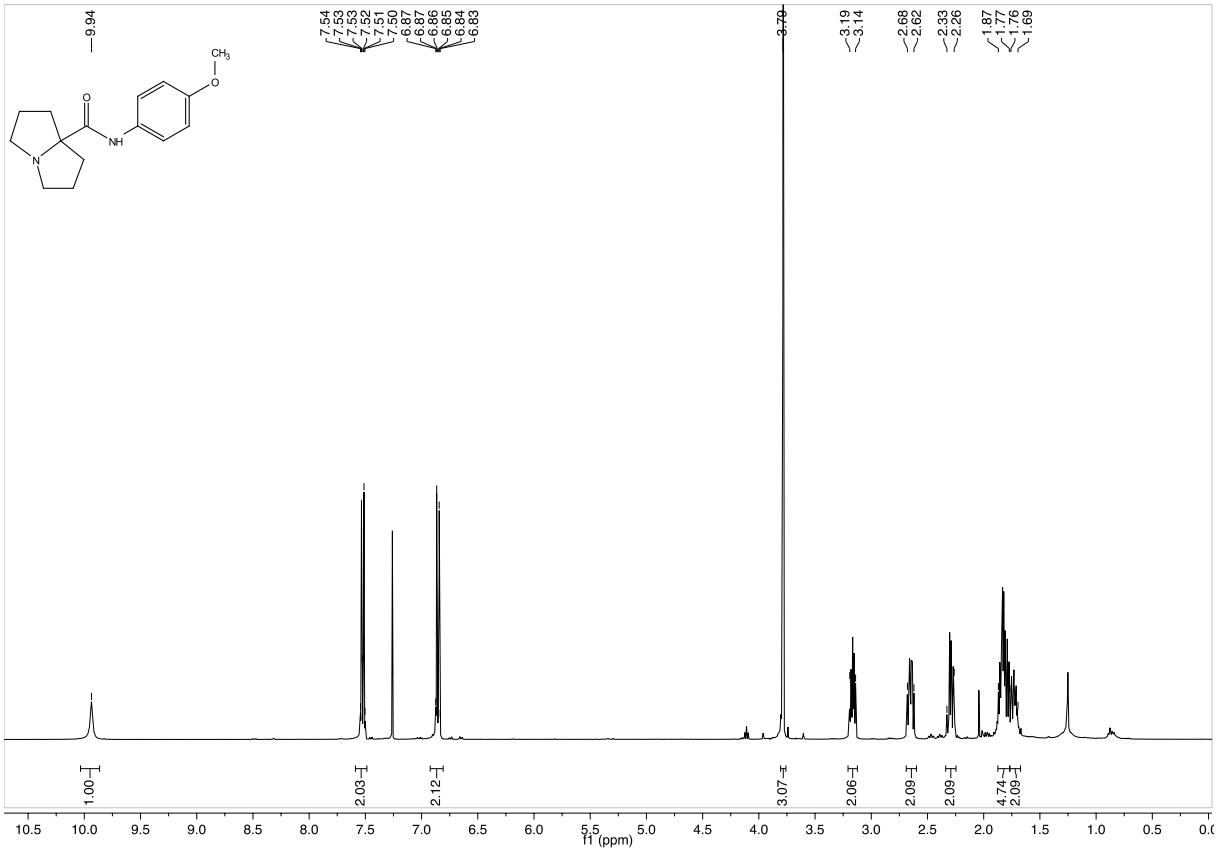

400 MHz ^{1}H-NMR in $CDCl_3$

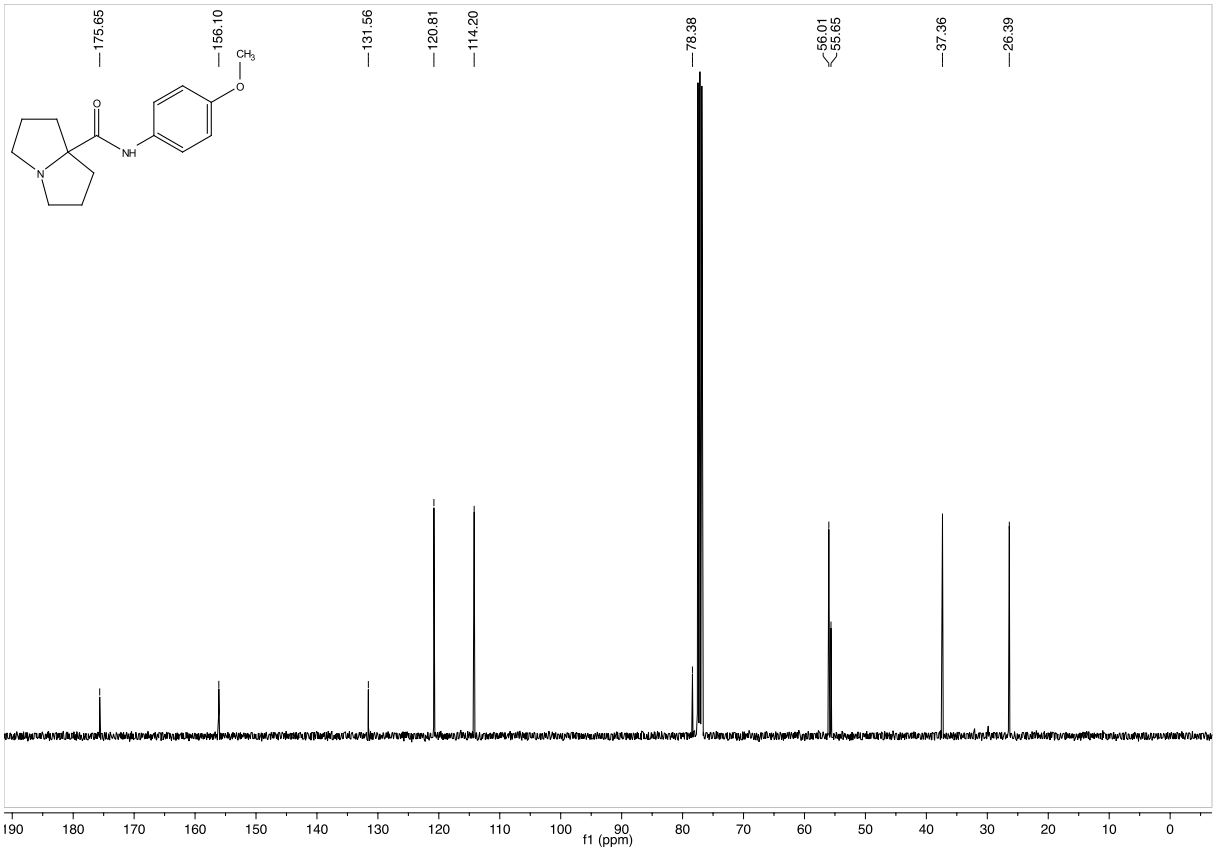

101 MHz ^{13}C-NMR in $CDCl_3$

N-(4-(Methylthio)phenyl)tetrahydro-1*H*-pyrrolizine-7a(5*H*)-carboxamide (3.56)

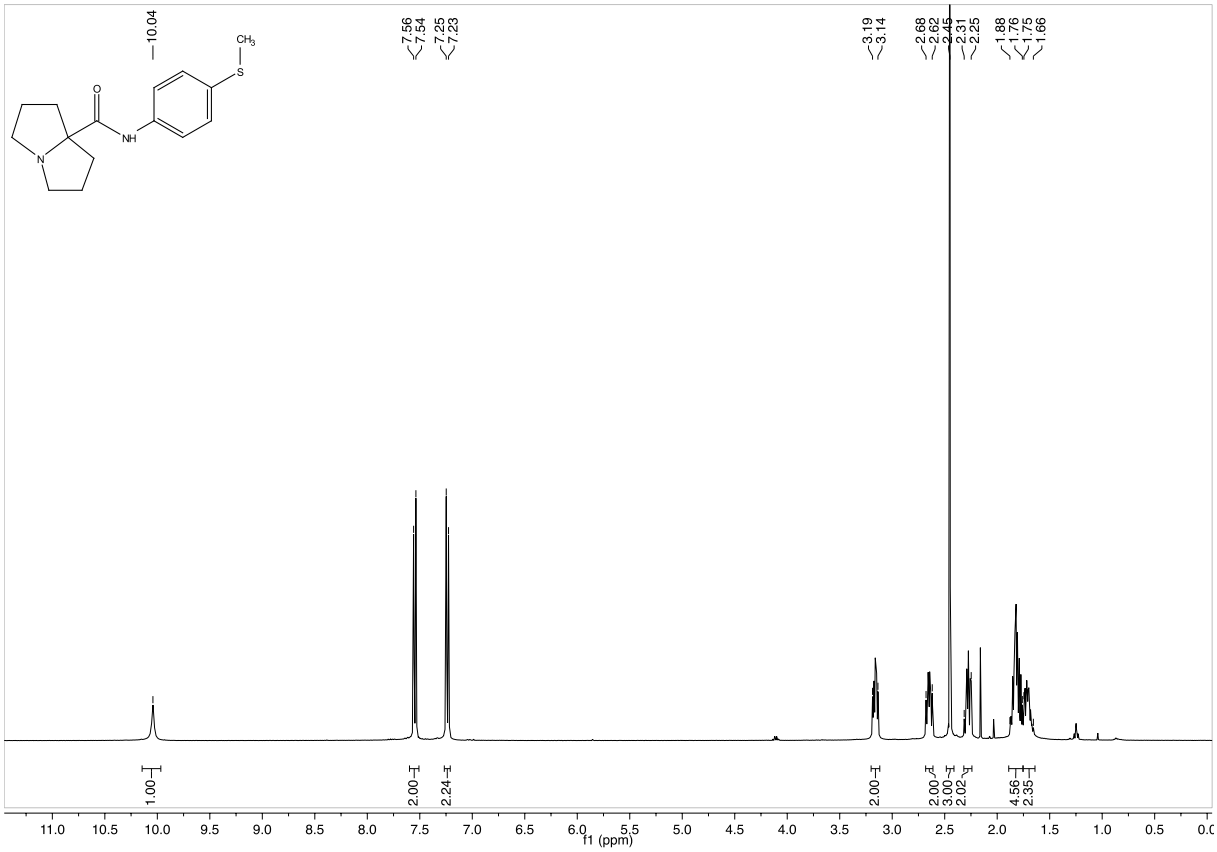

400 MHz ^{1}H-NMR in $CDCl_3$

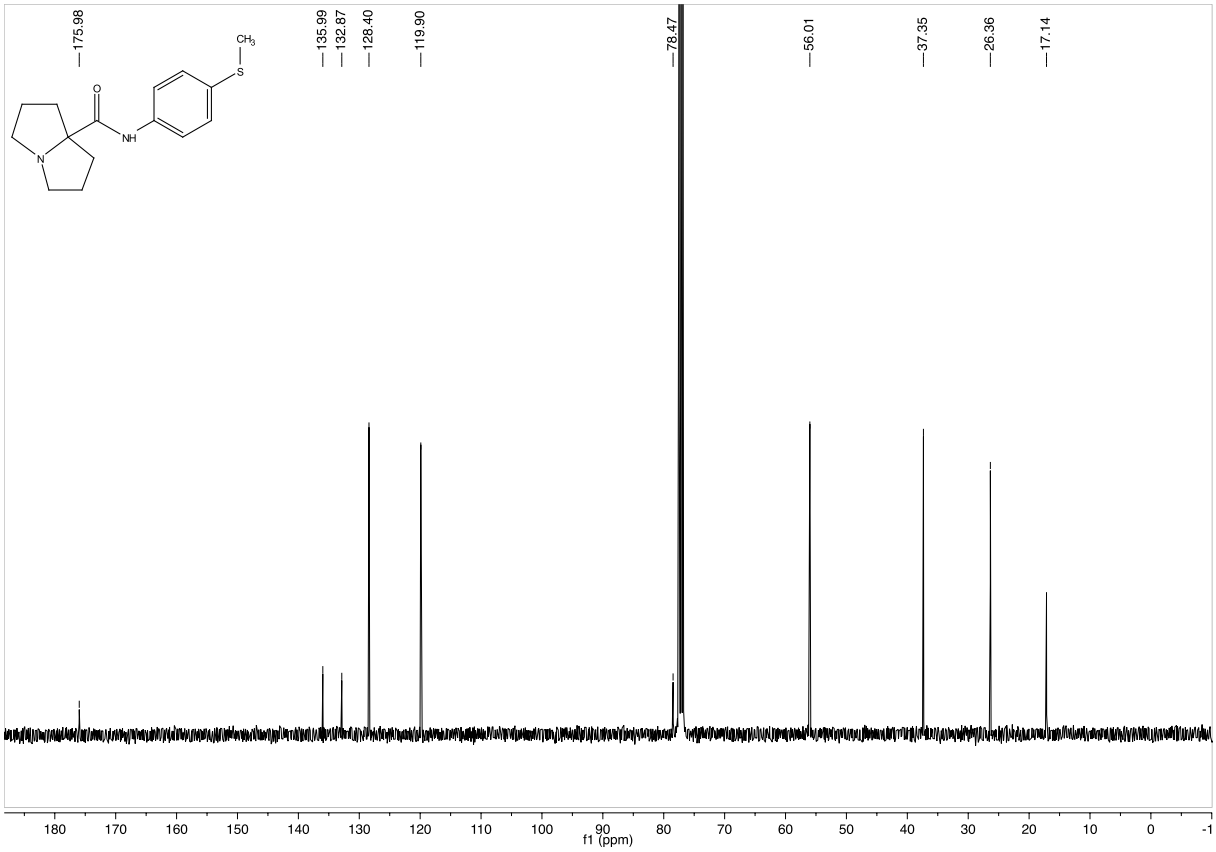

101 MHz ^{13}C-NMR in $CDCl_3$

***N*-(2,6-Dimethoxyphenyl)tetrahydro-1*H*-pyrrolizine-7a(5*H*)-carboxamide (3.57)**

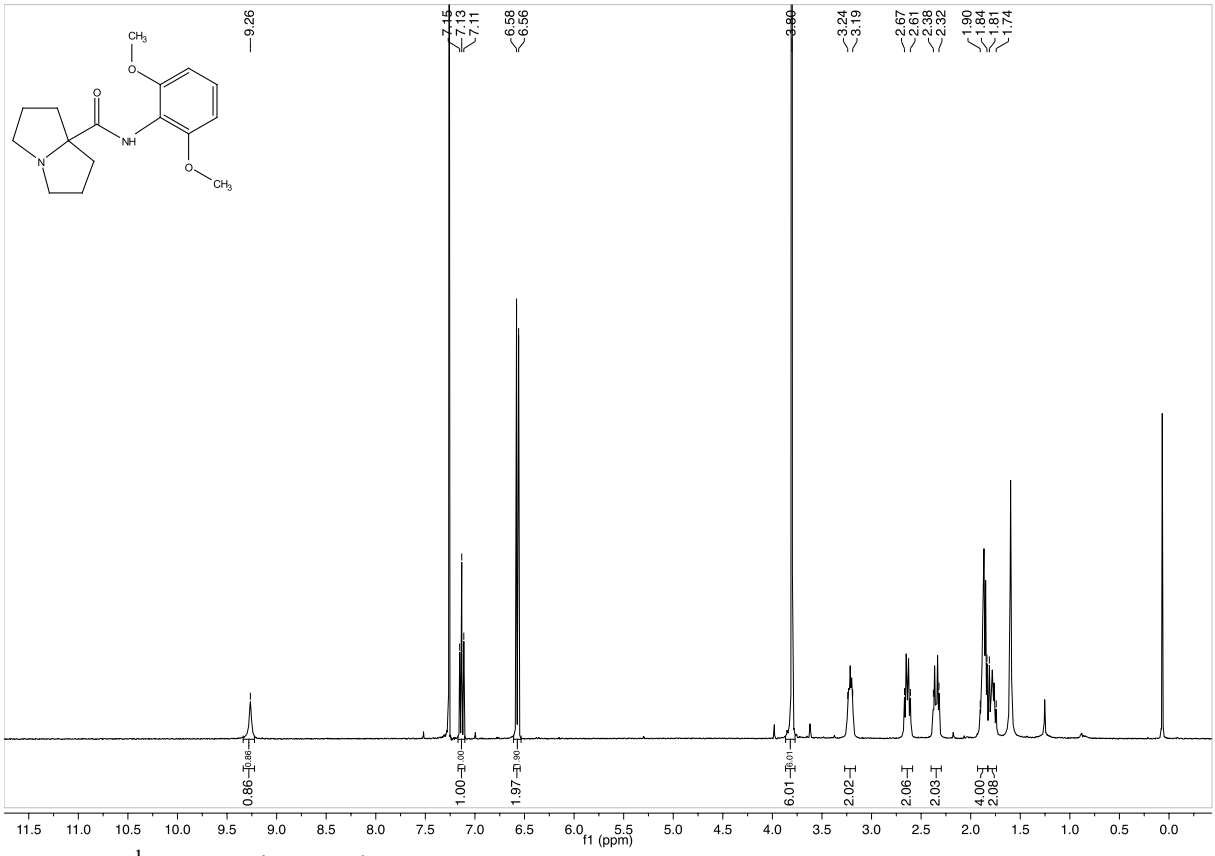

400 MHz ^{1}H-NMR in $CDCl_3$

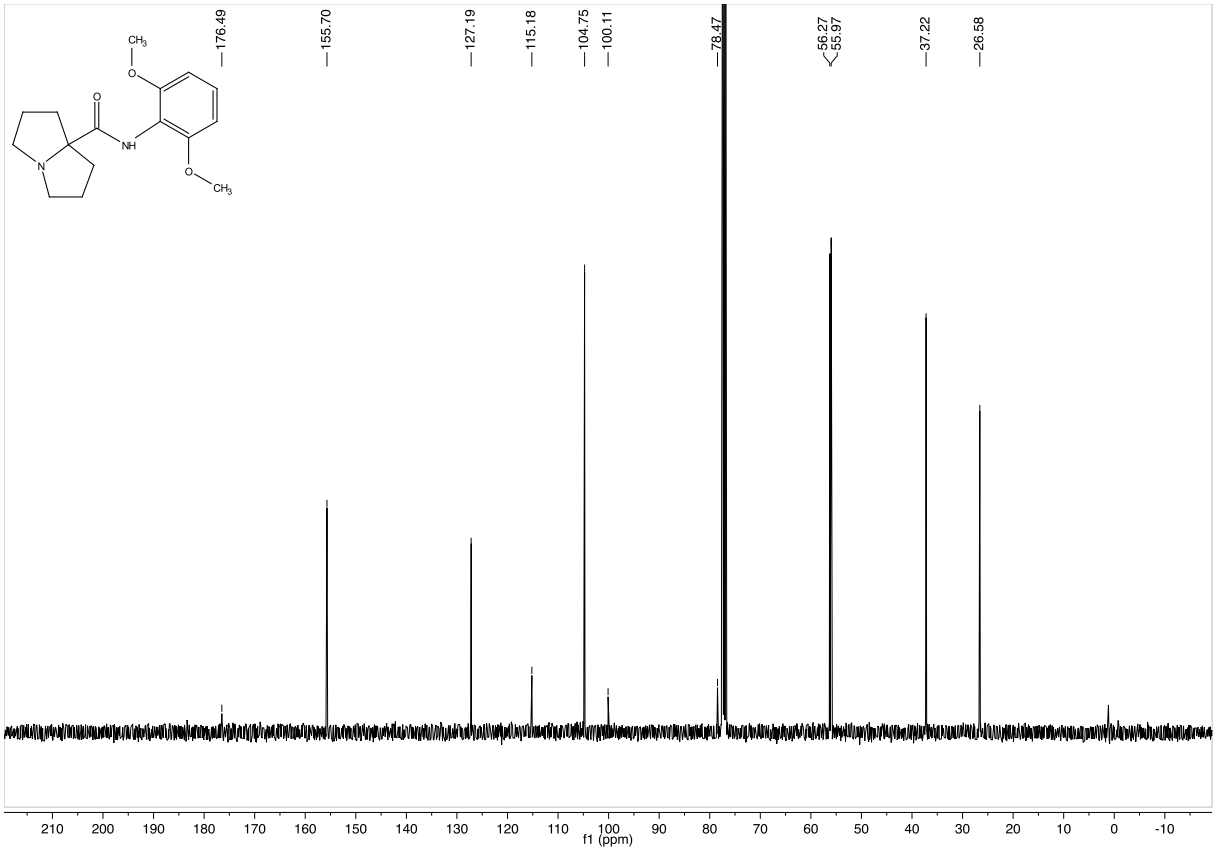

101 MHz ^{13}C-NMR in $CDCl_3$

_N_-(Benzo[_d_][1,3]dioxol-5-yl)tetrahydro-1_H_-pyrrolizine-7a(5_H_)-carboxamide (3.58)

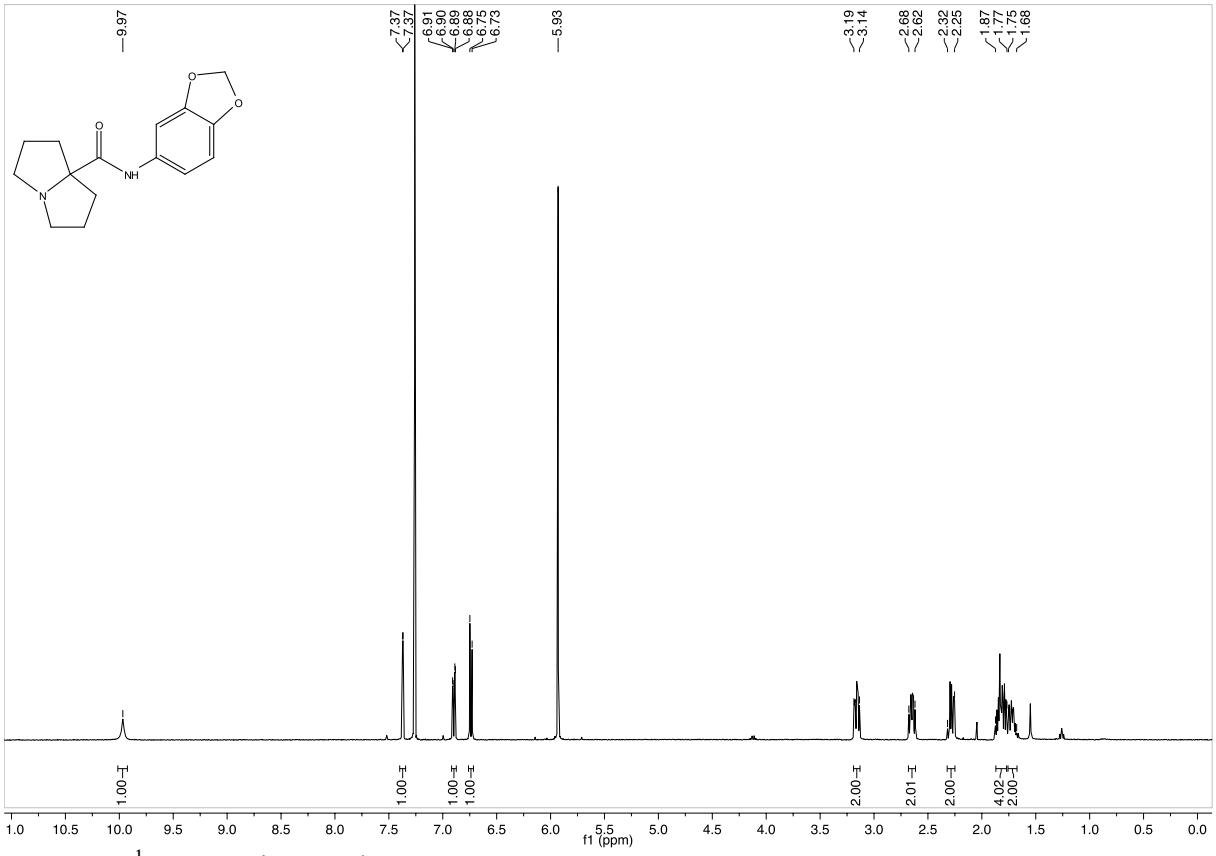

400 MHz ^{1}H-NMR in $CDCl_3$

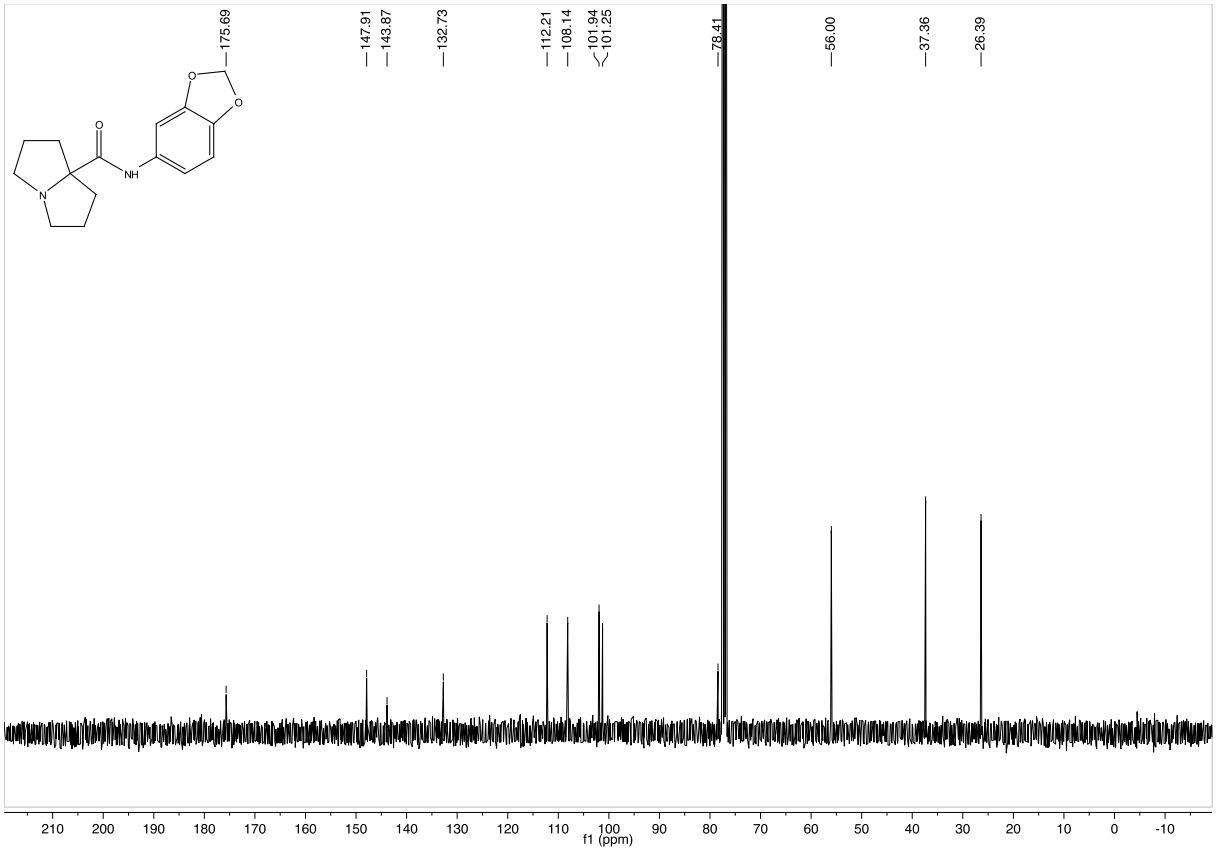

101 MHz ^{13}C-NMR in $CDCl_3$

_N_-(Naphthalen-2-yl)tetrahydro-1_H_-pyrrolizine-7a(5_H_)-carboxamide (3.59)

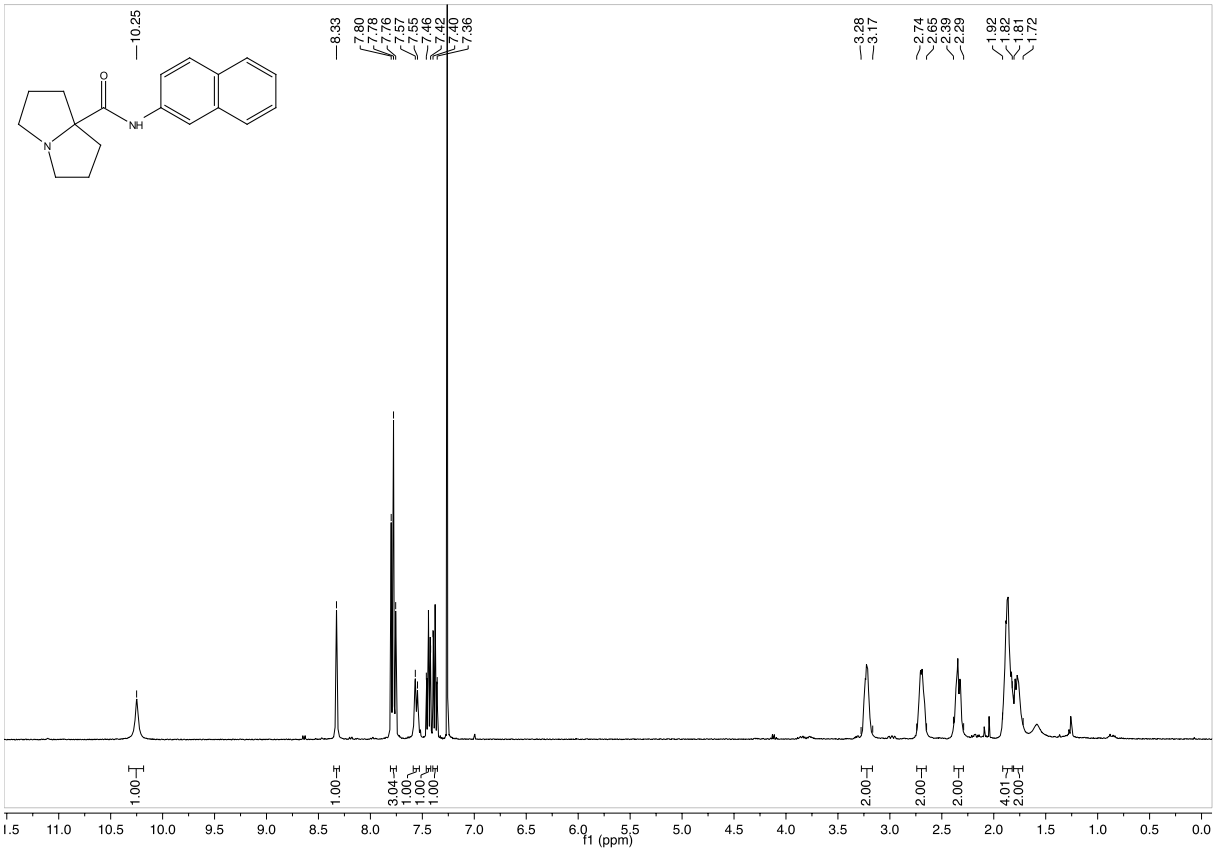

400 MHz ^{1}H-NMR in $CDCl_3$

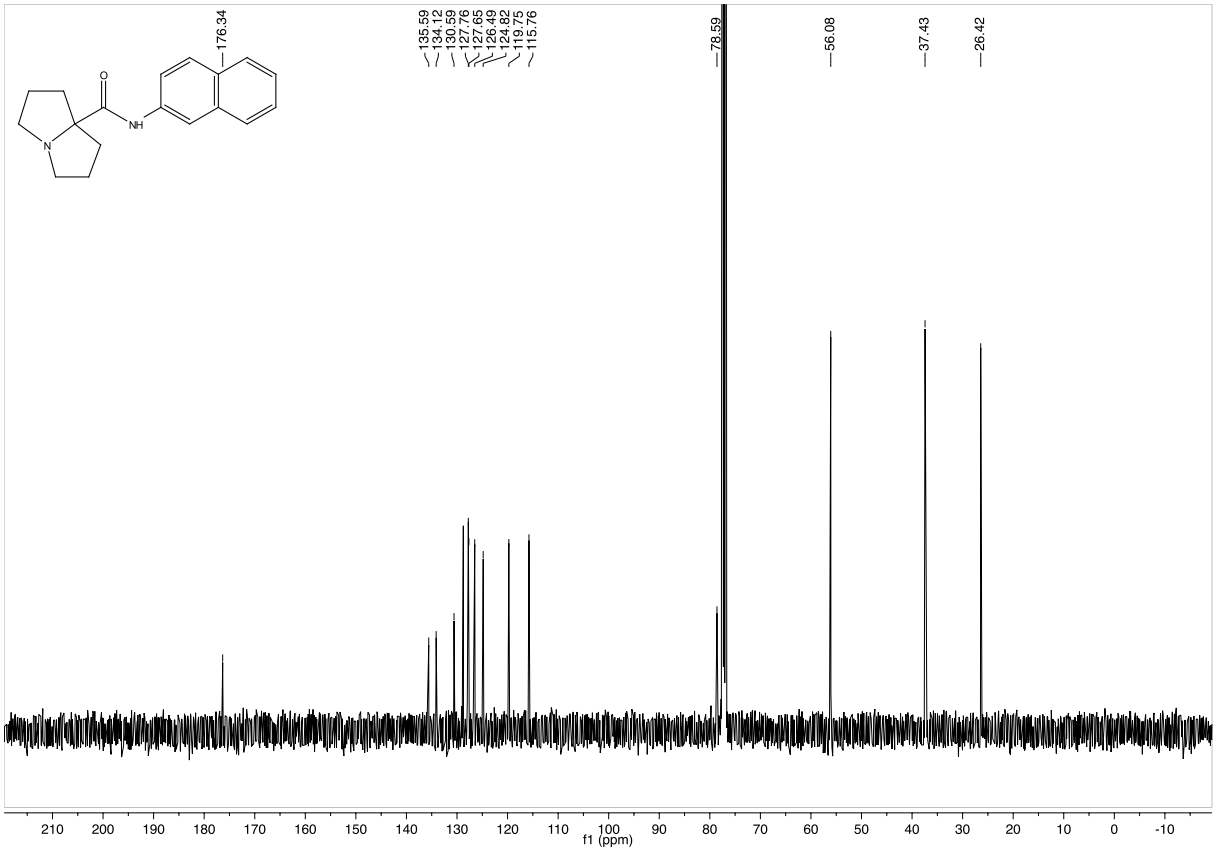

101 MHz ^{13}C-NMR in $CDCl_3$

_N_-(4-Bromophenyl)tetrahydro-1_H_-pyrrolizine-7a(5_H_)-carboxamide (3.60)

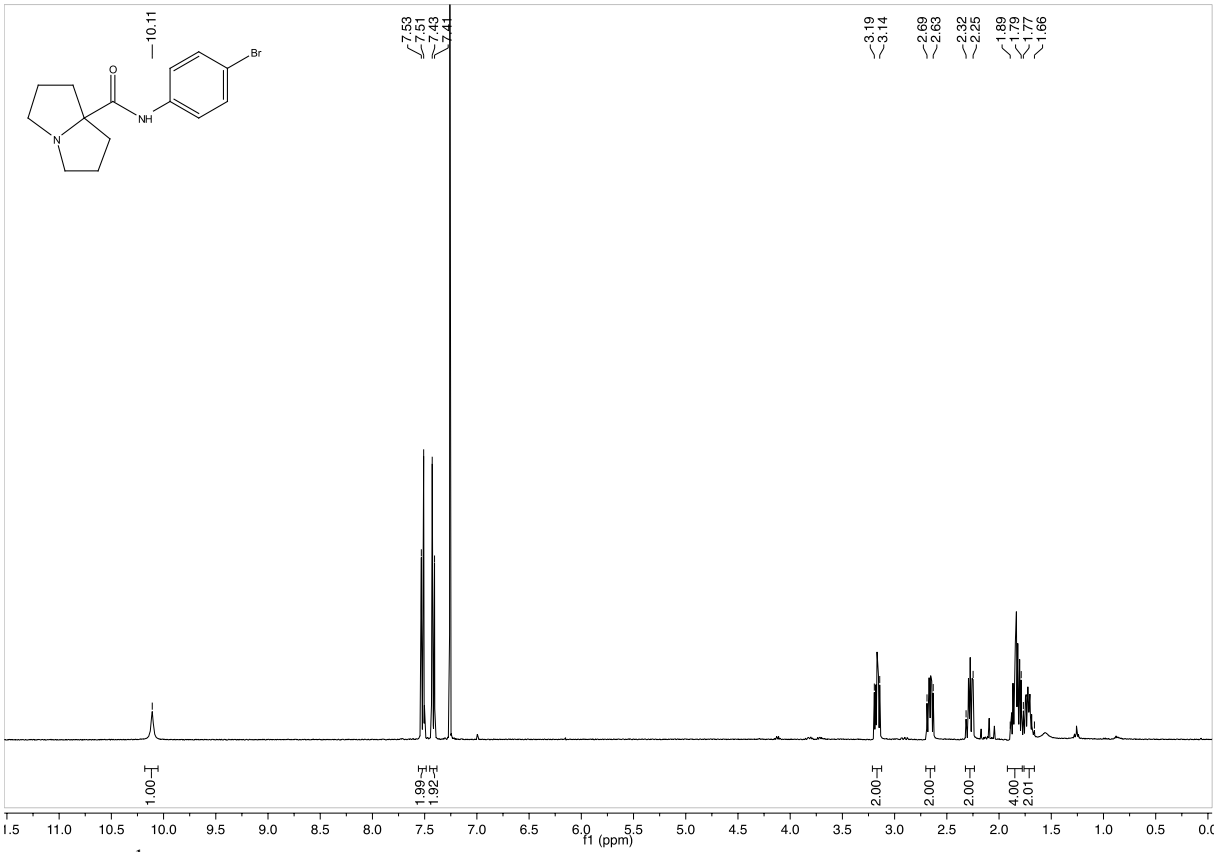

400 MHz ^{1}H-NMR in $CDCl_3$

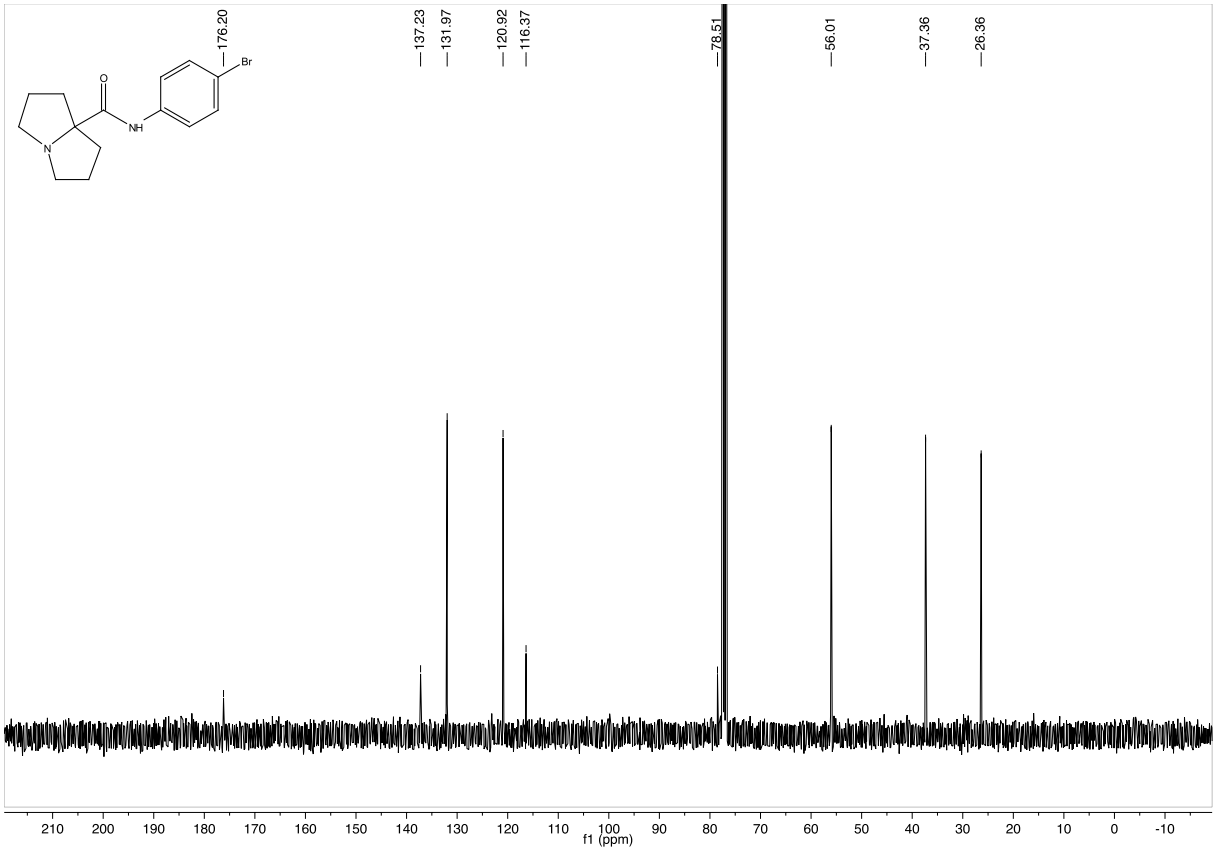

101 MHz ^{13}C-NMR in $CDCl_3$

_N_-(4-Fluorophenyl)tetrahydro-1_H_-pyrrolizine-7a(5_H_)-carboxamide (3.61)

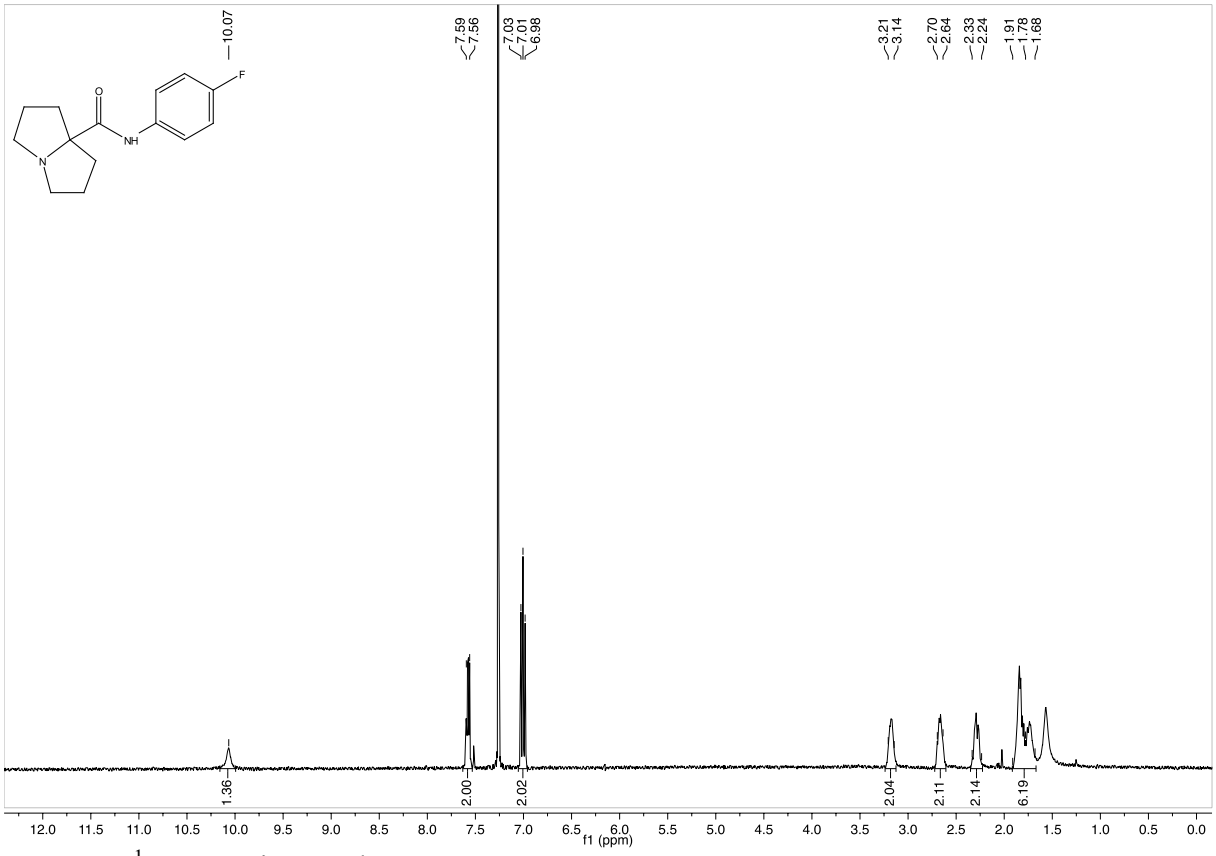

400 MHz ^{1}H-NMR in $CDCl_3$

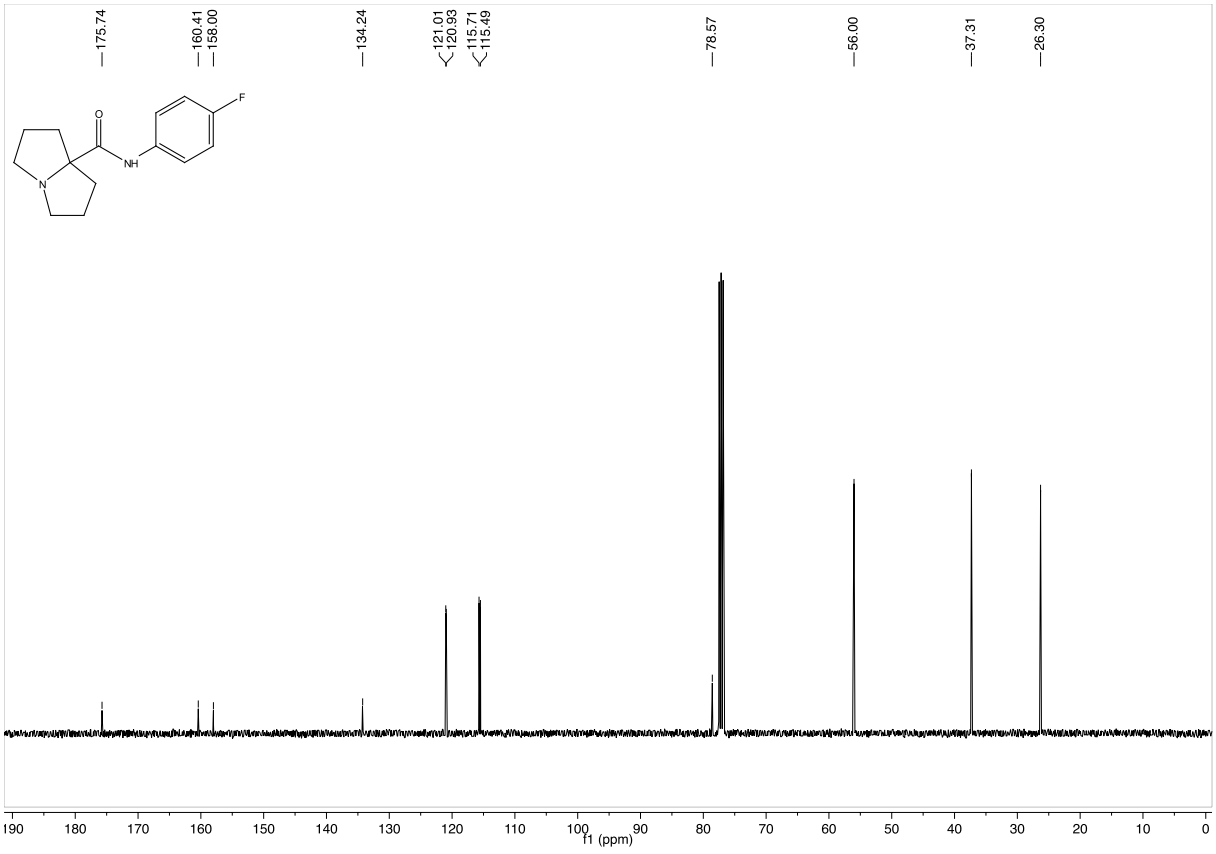

101 MHz ^{13}C-NMR in $CDCl_3$

_N_-(4-Ethynylphenyl)tetrahydro-1_H_-pyrrolizine-7a(5_H_)-carboxamide (3.62)

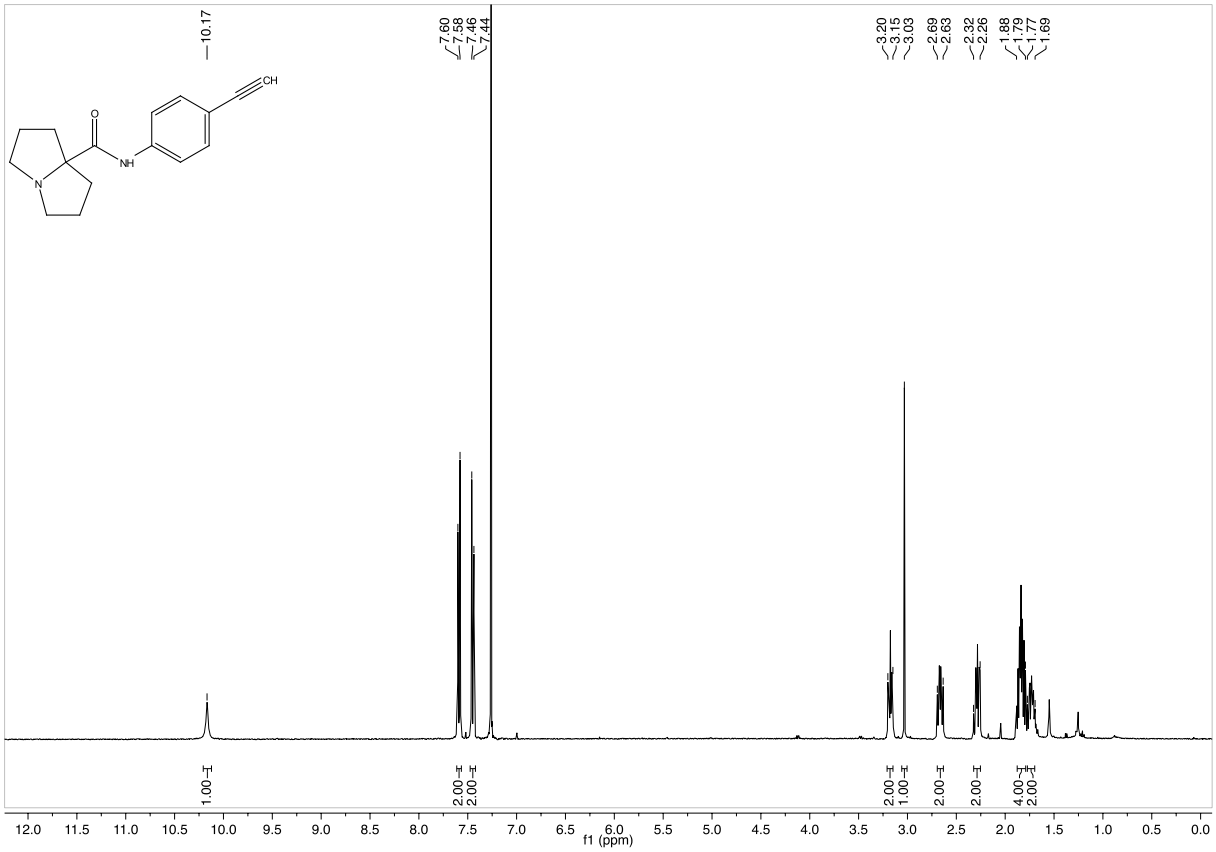

400 MHz ^{1}H-NMR in $CDCl_3$

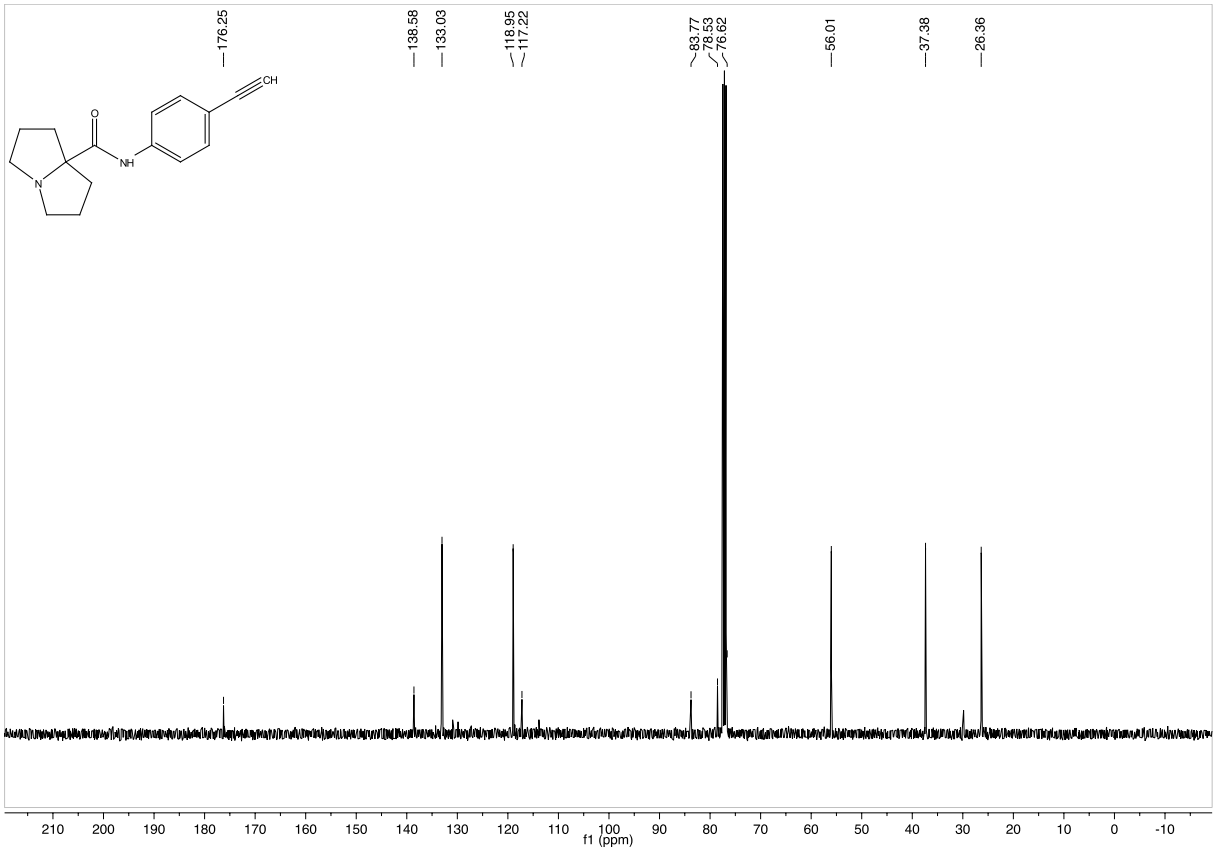

101 MHz ^{13}C-NMR in $CDCl_3$

_N_-(5-Methyl-[1,1'-biphenyl]-2-yl)tetrahydro-1_H_-pyrrolizine-7a(5_H_)-carboxamide (3.63)

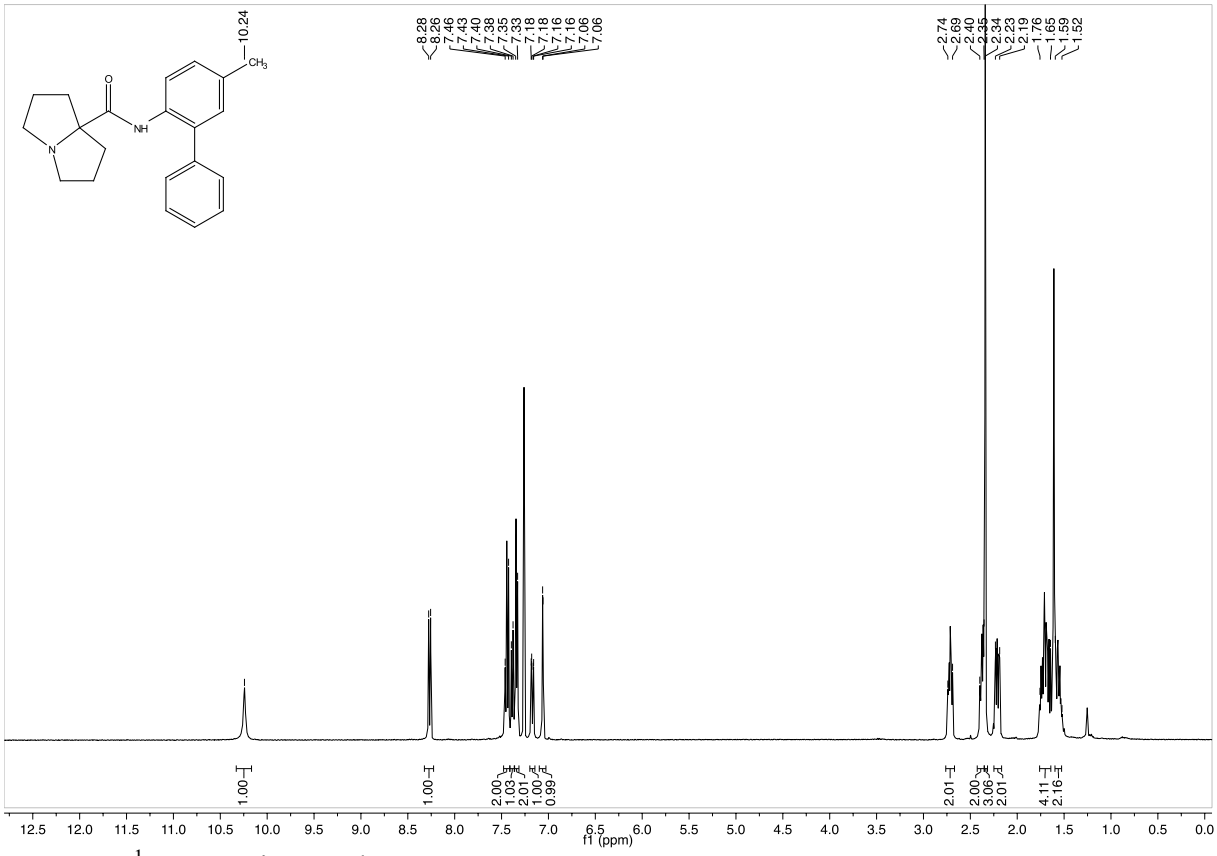

400 MHz ^{1}H-NMR in $CDCl_3$

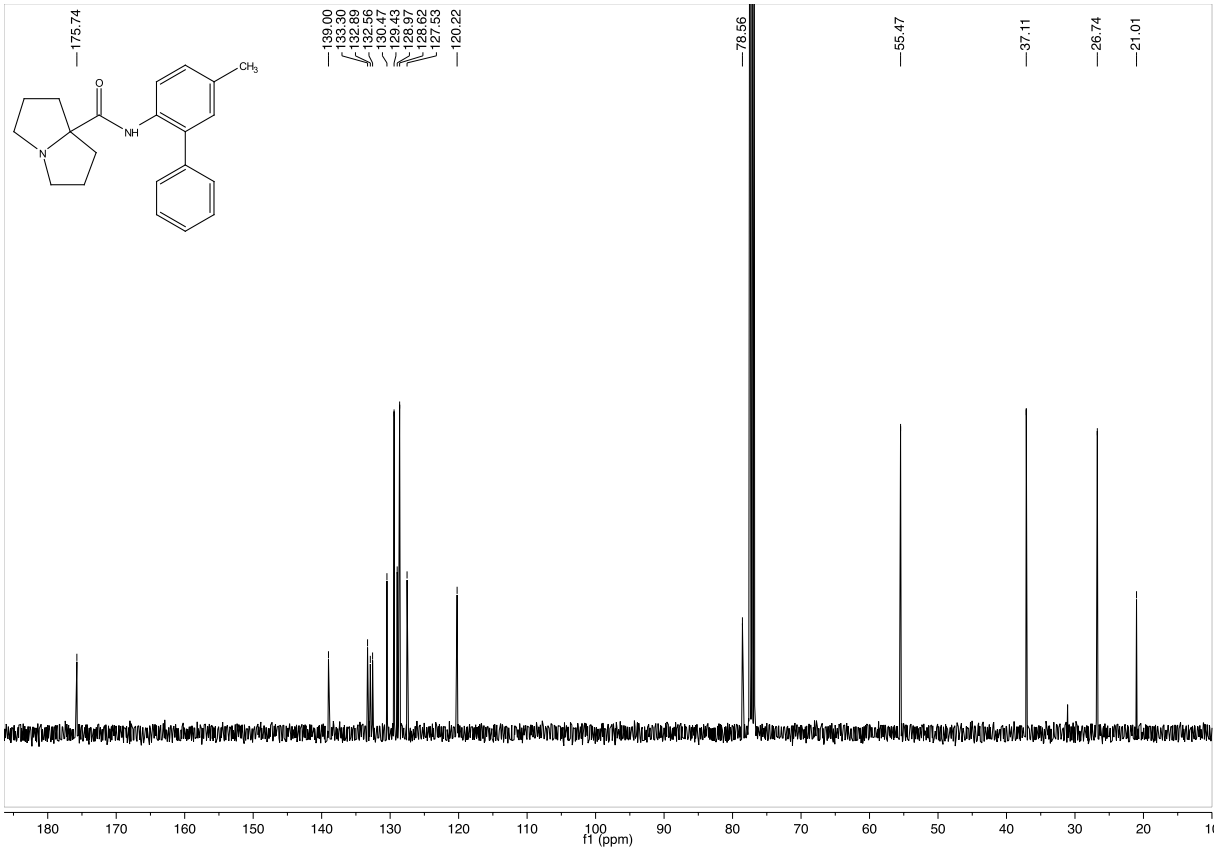

101 MHz ^{13}C-NMR in $CDCl_3$

N-(2-Morpholinoethyl)tetrahydro-1H-pyrrolizine-7a(5H)-carboxamide (3.64)

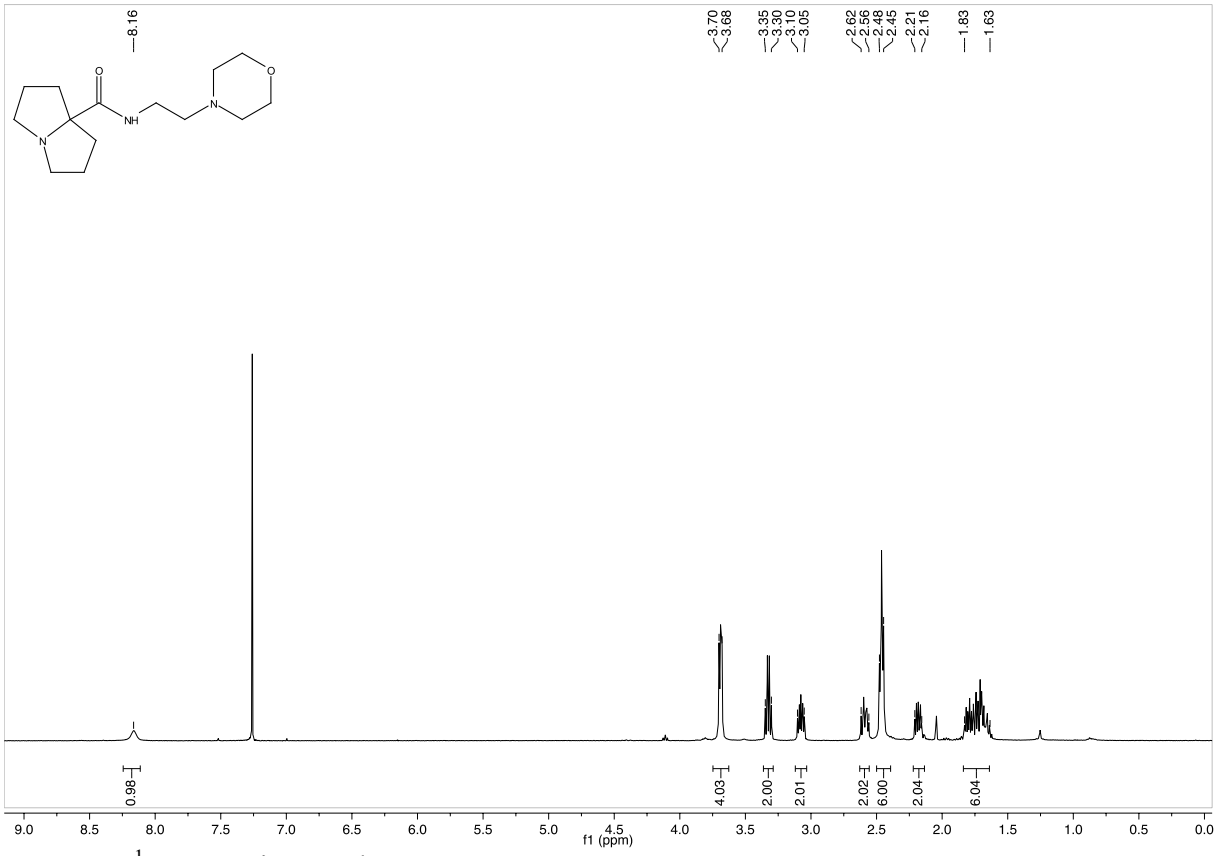

250 MHz ^{1}H-NMR in $CDCl_3$

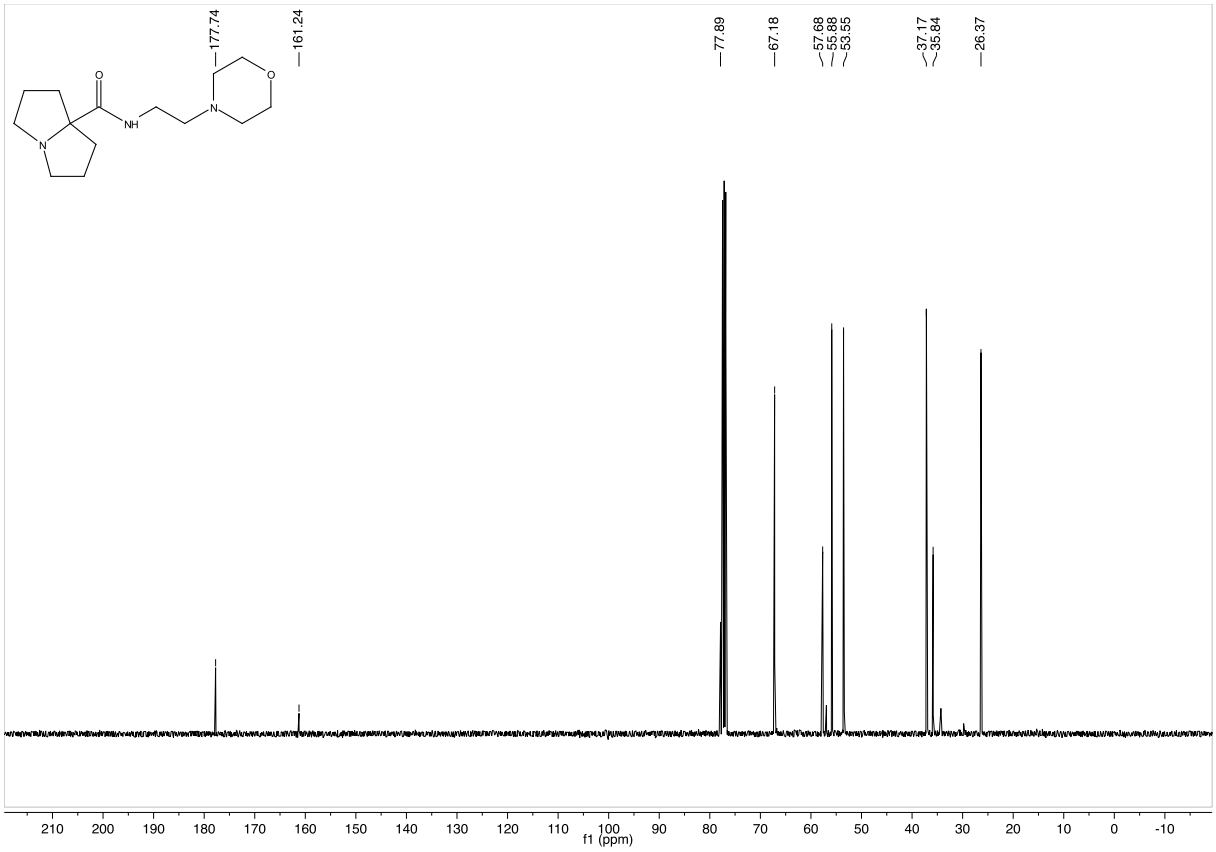

101 MHz ^{13}C-NMR in $CDCl_3$

N-(4-Hydroxyphenethyl)tetrahydro-1*H*-pyrrolizine-7a(5*H*)-carboxamide (3.65)

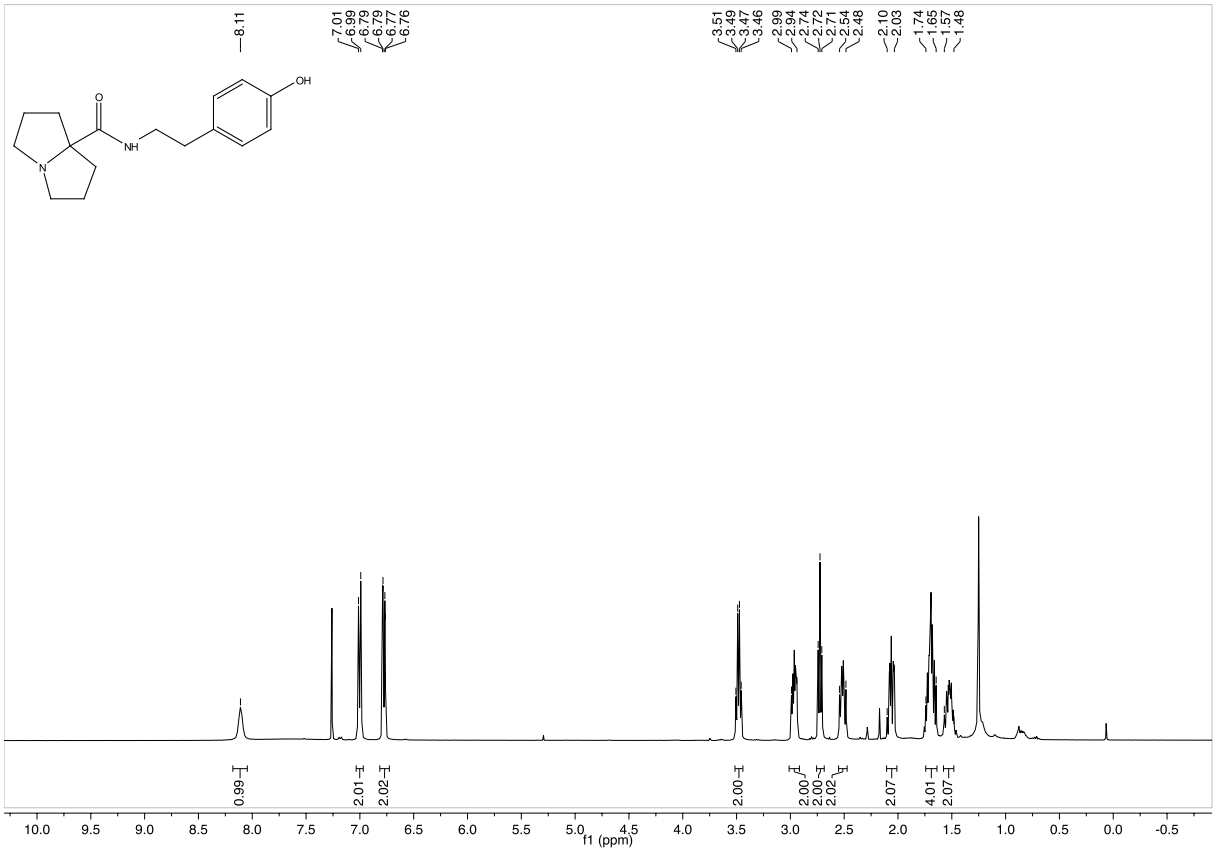

400 MHz ^{1}H-NMR in $CDCl_3$

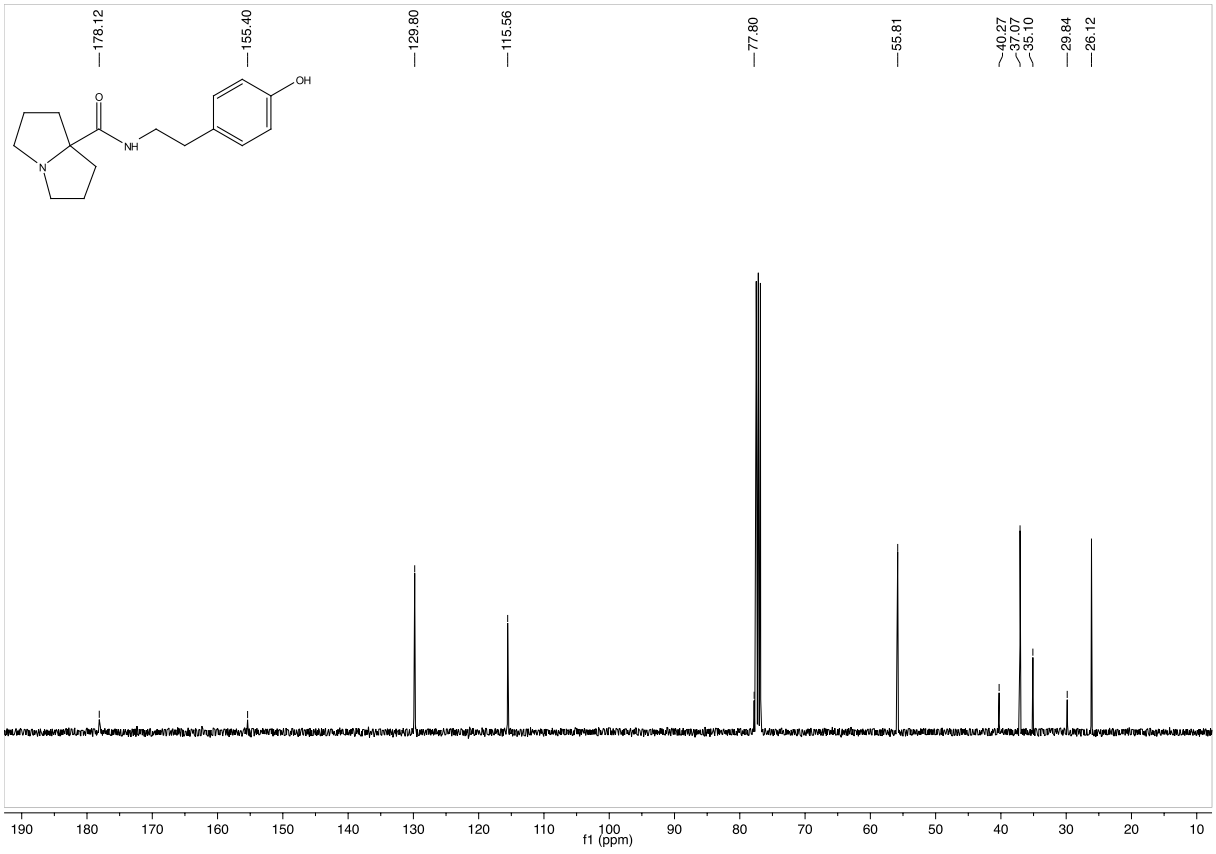

101 MHz ^{13}C-NMR in $CDCl_3$

N-Benzyltetrahydro-1*H*-pyrrolizine-7a(5*H*)-carboxamide (3.66)

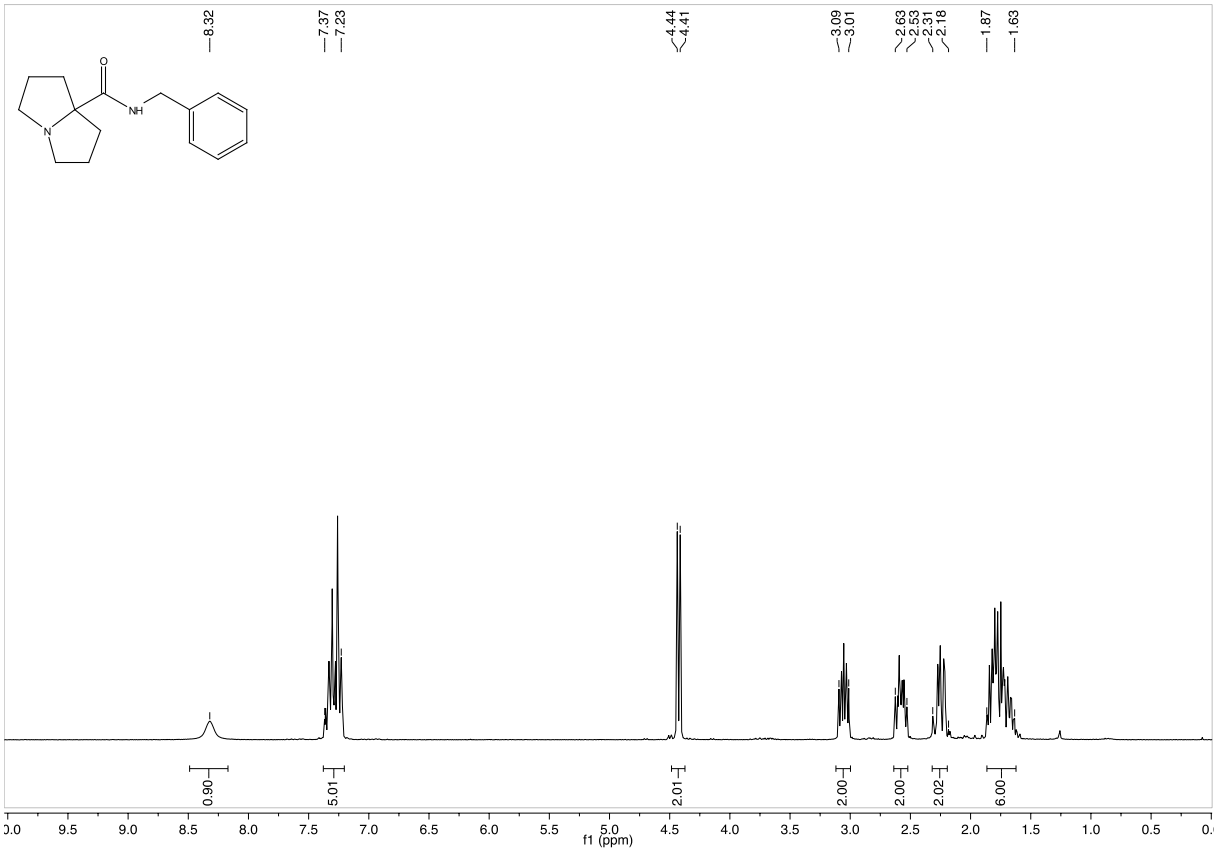

400 MHz ^{1}H-NMR in $CDCl_3$

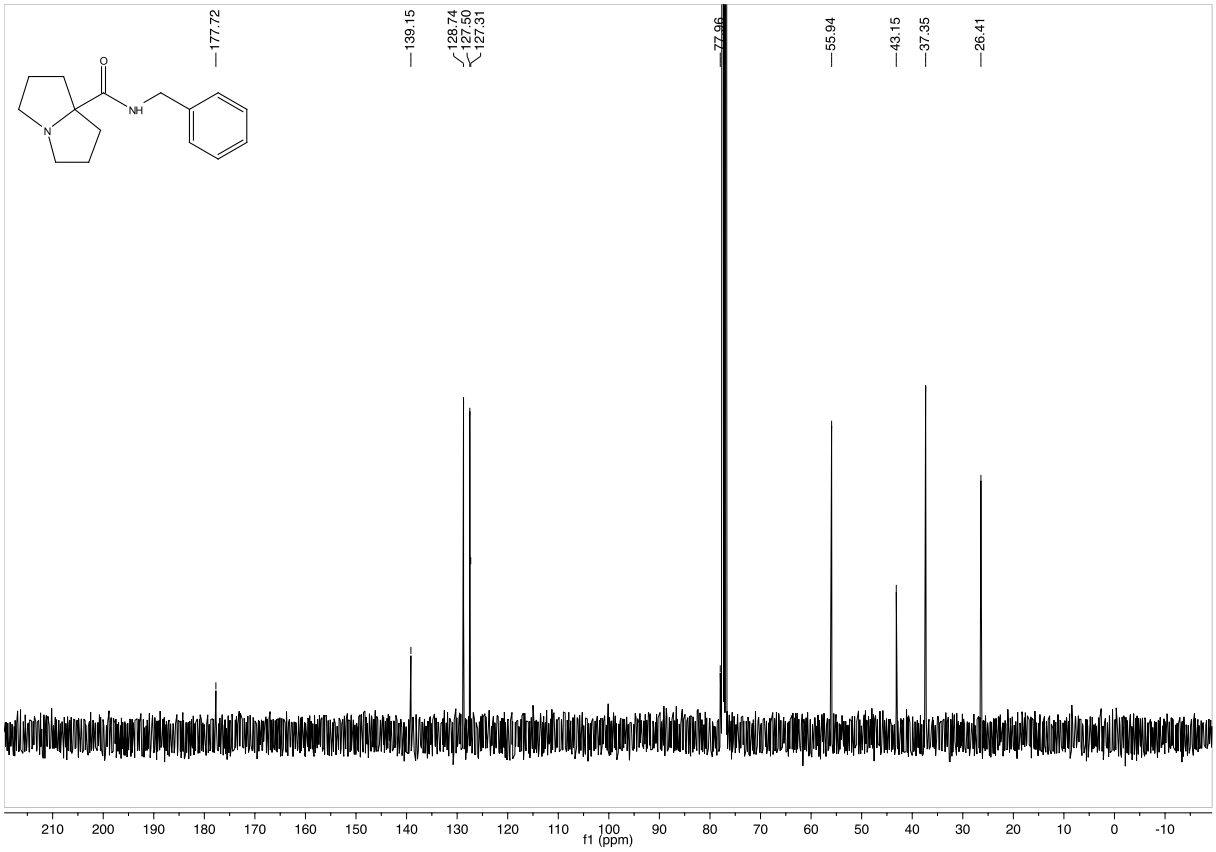

101 MHz ^{13}C-NMR in $CDCl_3$

(*S*)-*N*-(1-Phenylethyl)tetrahydro-1*H*-pyrrolizine-7a(5*H*)-carboxamide (3.67)

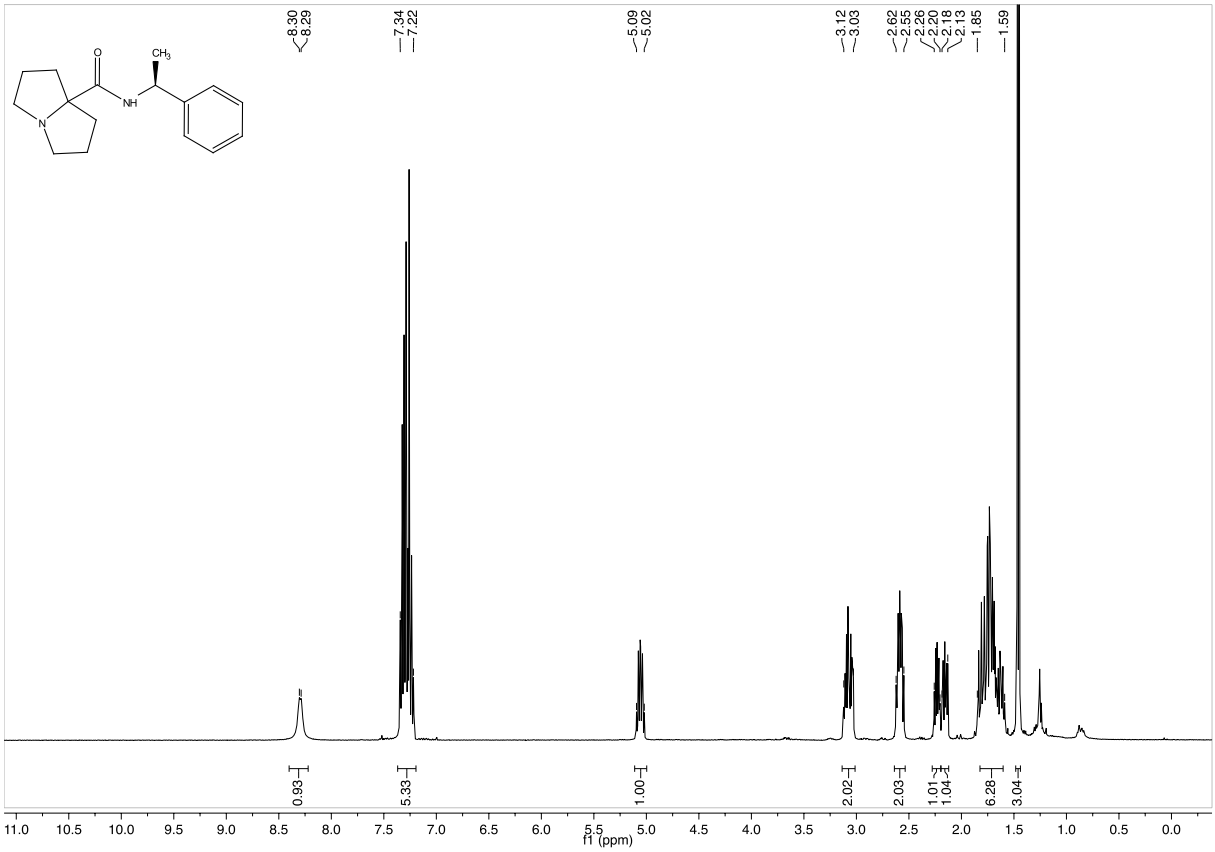

400 MHz ^{1}H-NMR in $CDCl_3$

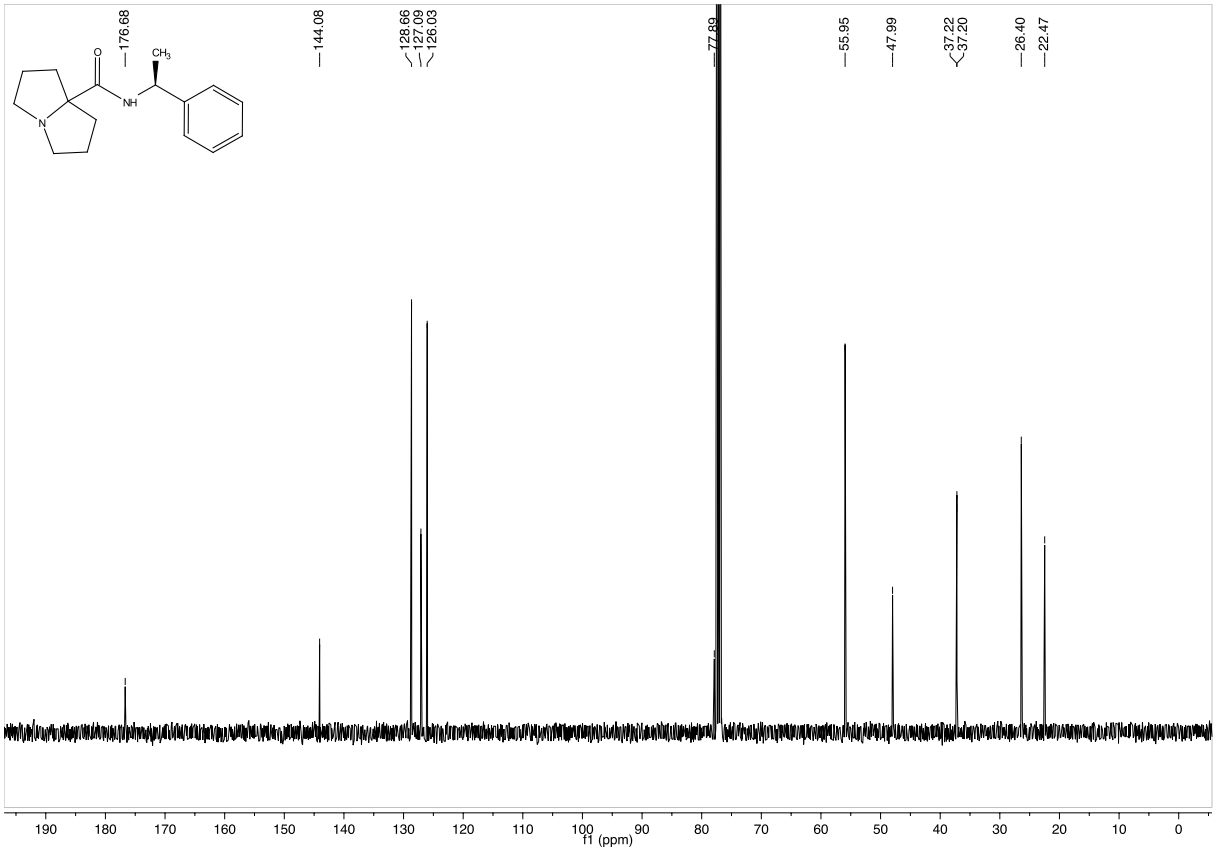

101 MHz ^{13}C-NMR in $CDCl_3$

Methyl-(hexahydro-1*H*-pyrrolizine-7a-carbonyl)-tryptophanate (3.68)

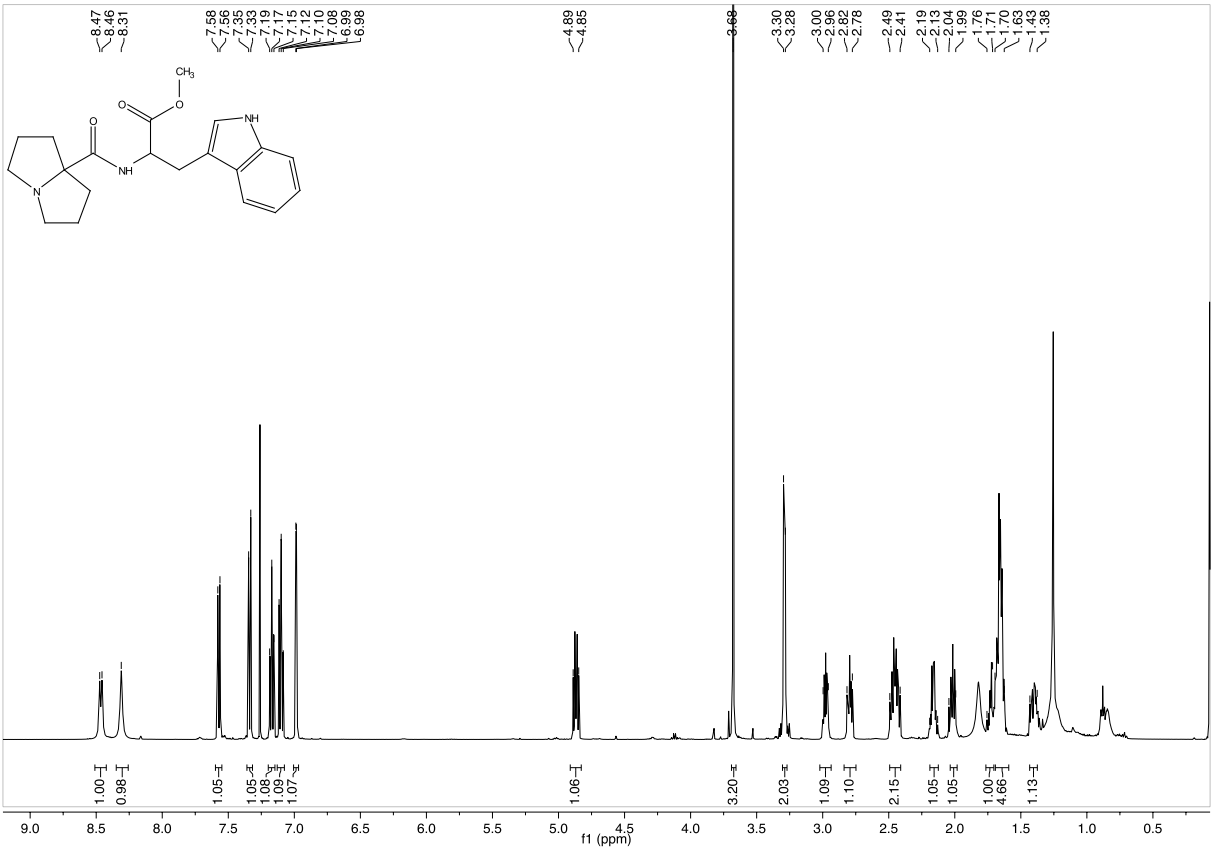

500 MHz ^{1}H-NMR in $CDCl_3$

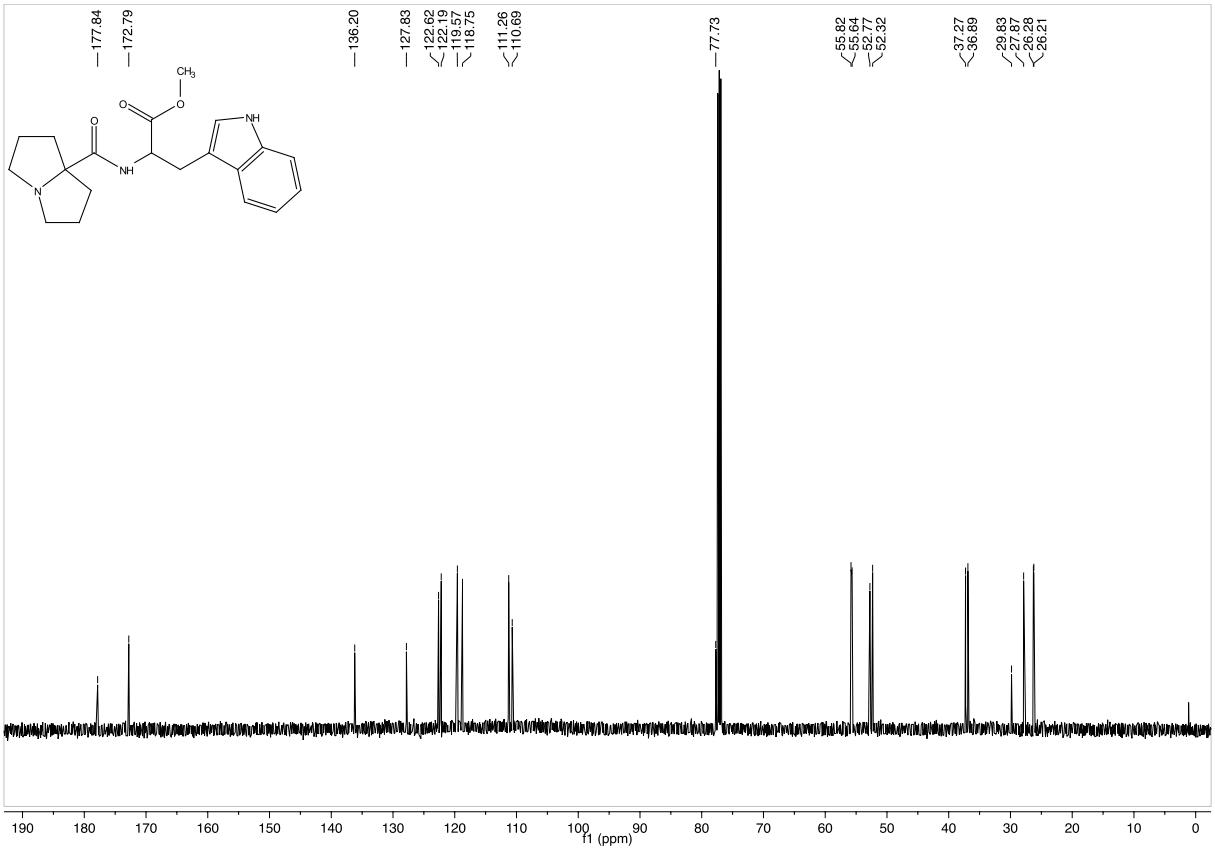

126 MHz ^{13}C-NMR in $CDCl_3$

Methyl-(hexahydro-1*H*-pyrrolizine-7a-carbonyl)-valinate (3.69)

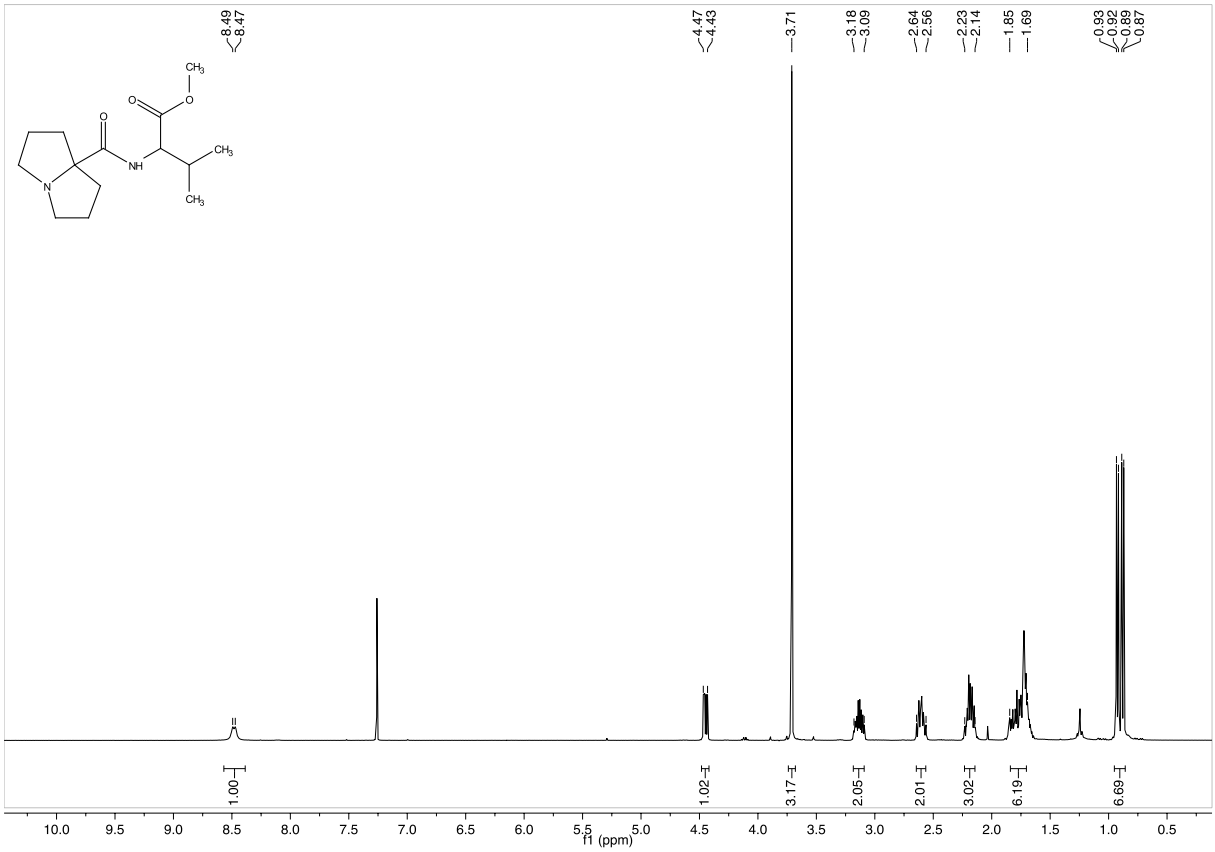

400 MHz ^{1}H-NMR in $CDCl_3$

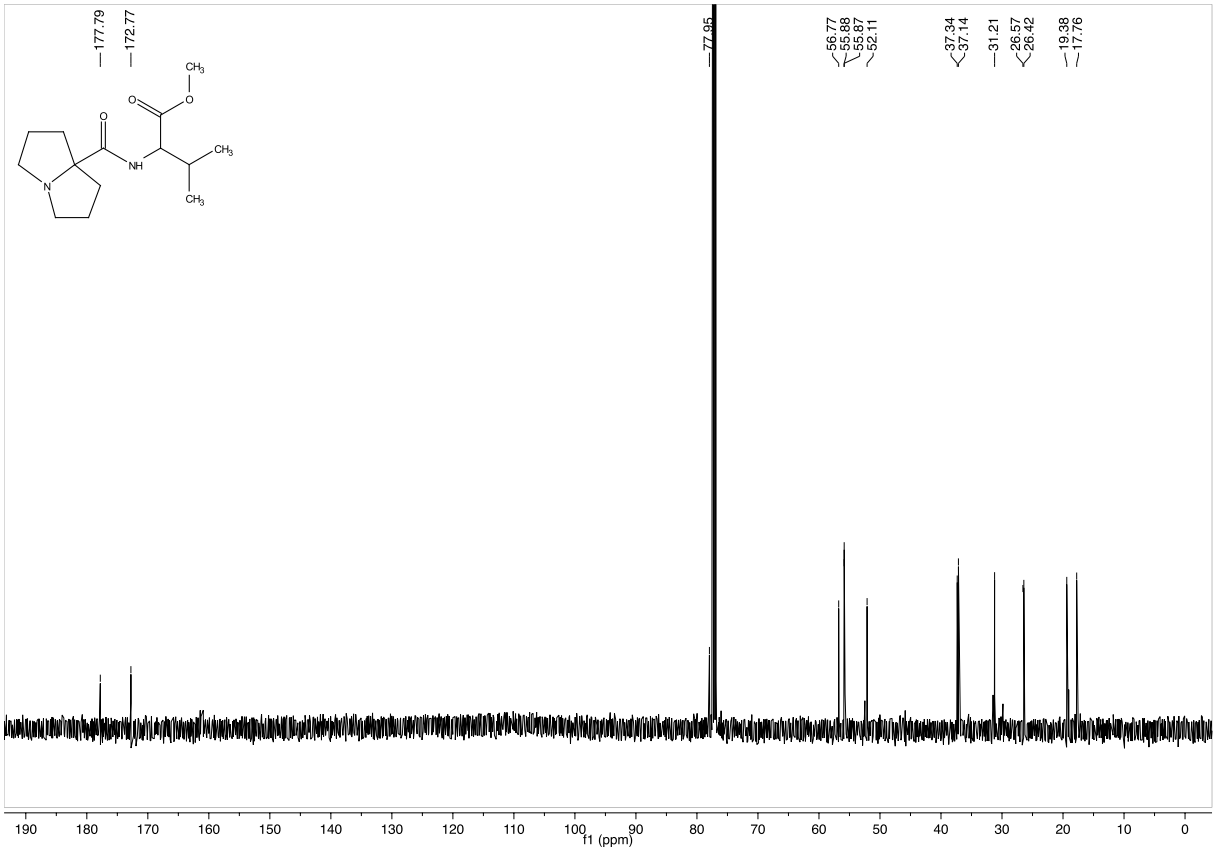

101 MHz ^{13}C-NMR in $CDCl_3$

Methyl-(hexahydro-1*H*-pyrrolizine-7a-carbonyl)-phenylalaninate (3.70)

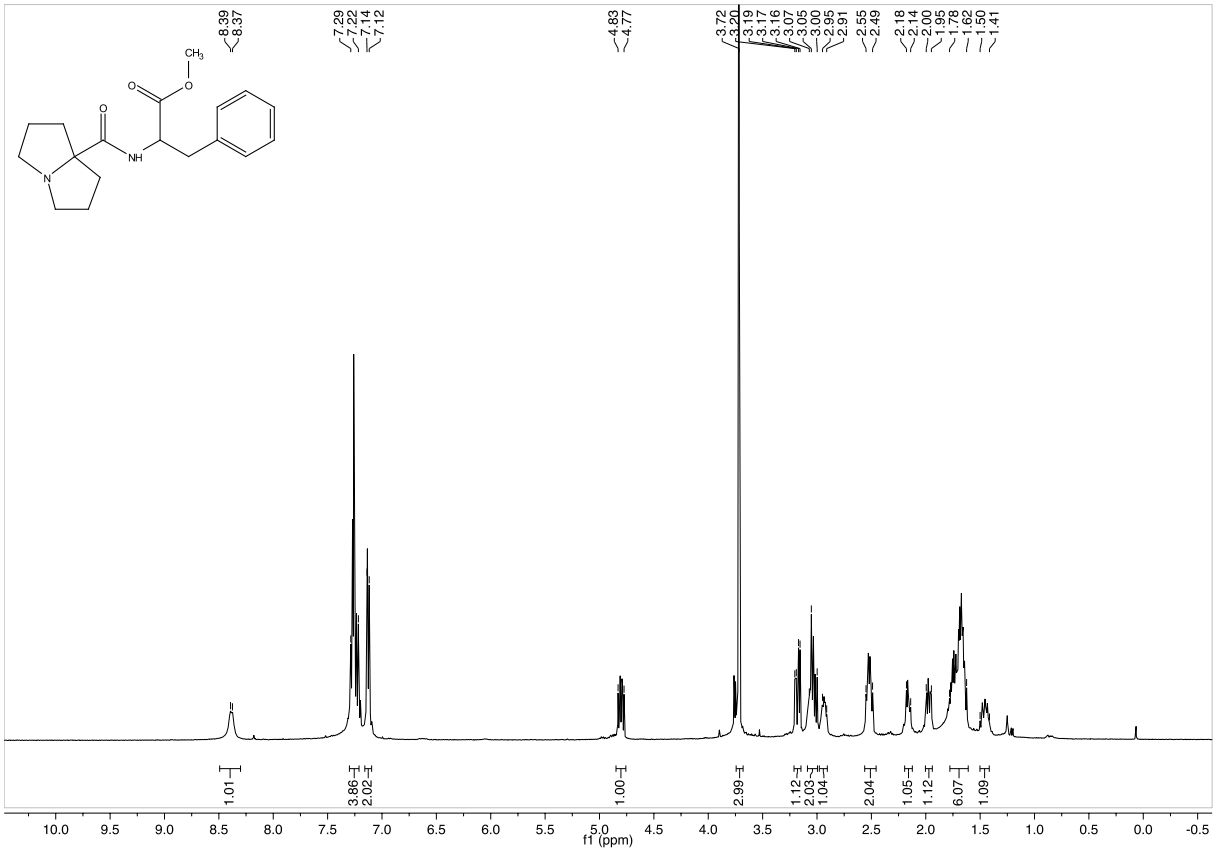

400 MHz ^{1}H-NMR in $CDCl_3$

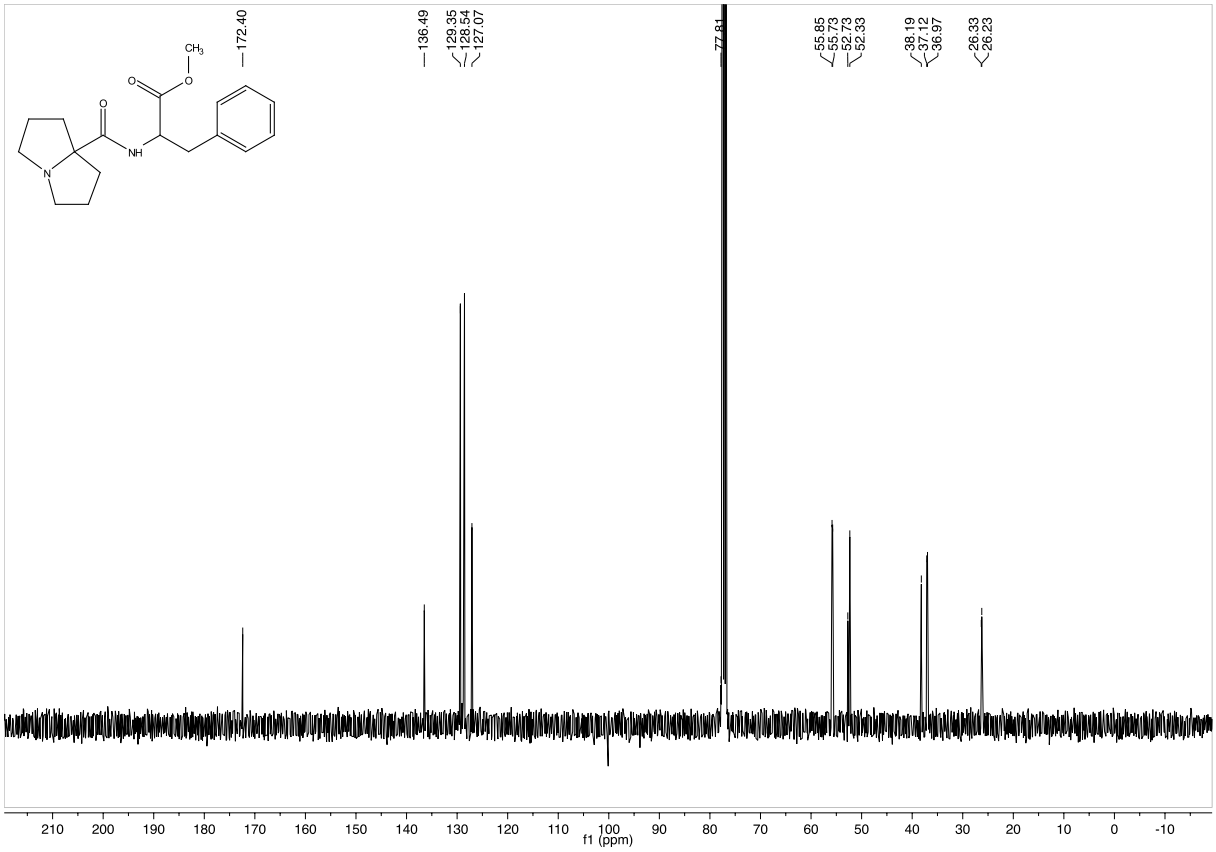

101 MHz ^{13}C-NMR in $CDCl_3$

Methyl-(hexahydro-1*H*-pyrrolizine-7a-carbonyl)-methioninate (3.71)

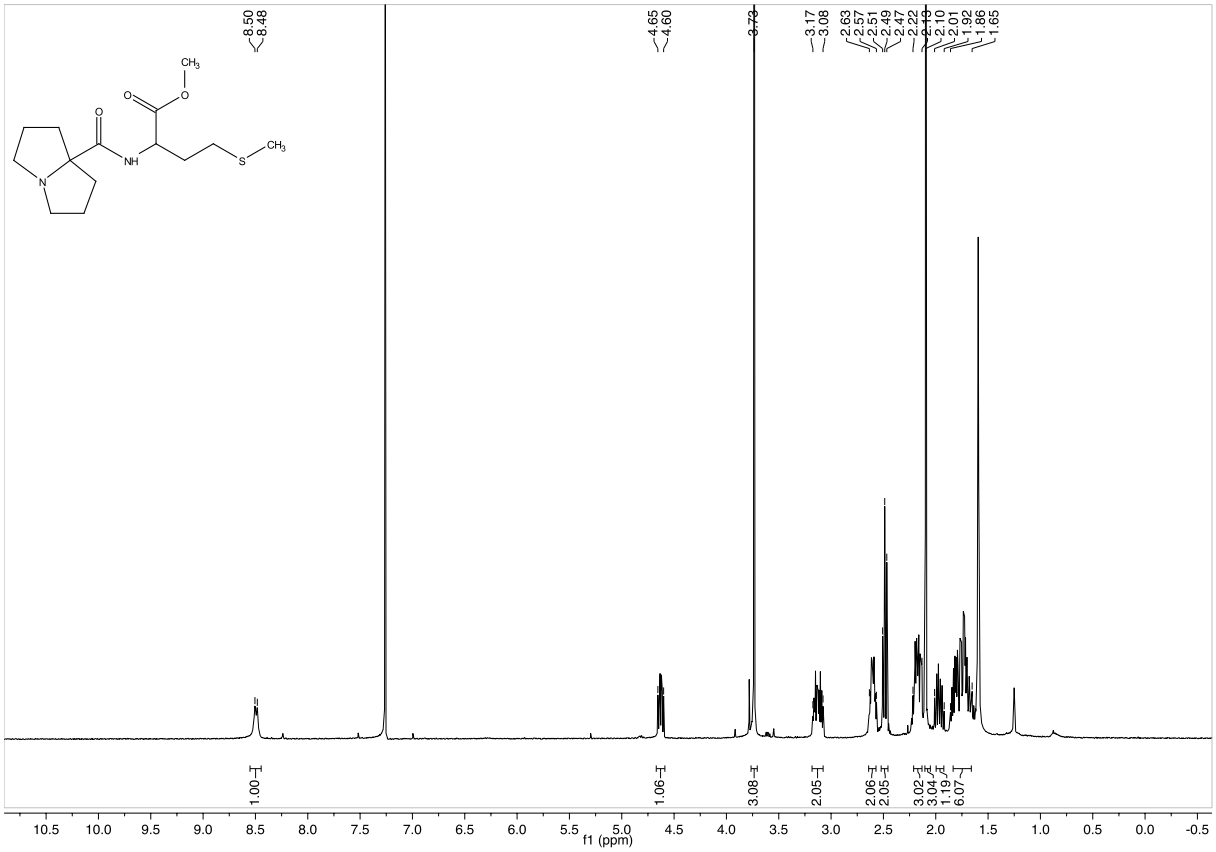

400 MHz ^{1}H-NMR in $CDCl_3$

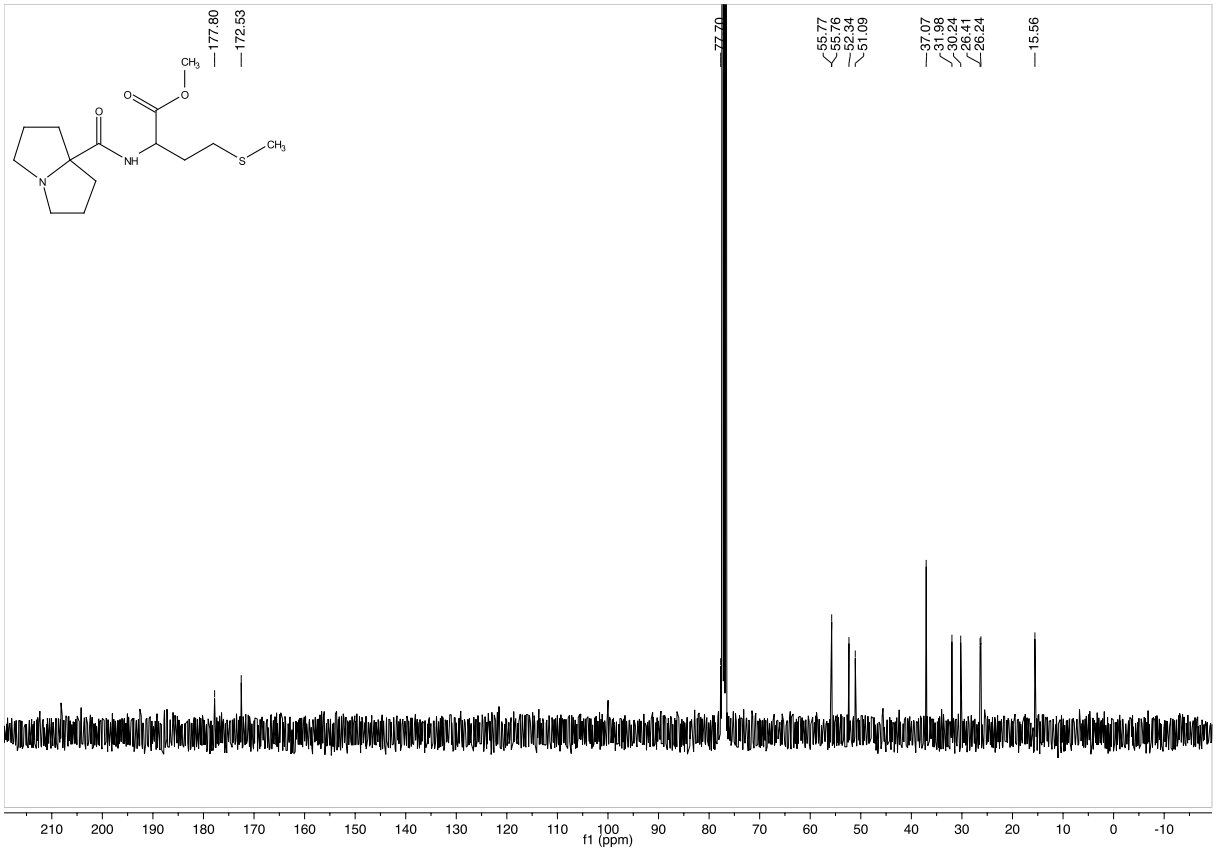

101 MHz ^{13}C-NMR in $CDCl_3$

Dimethyl-(hexahydro-1*H*-pyrrolizine-7a-carbonyl)-glutamate (3.72)

400 MHz ^{1}H-NMR in $CDCl_3$

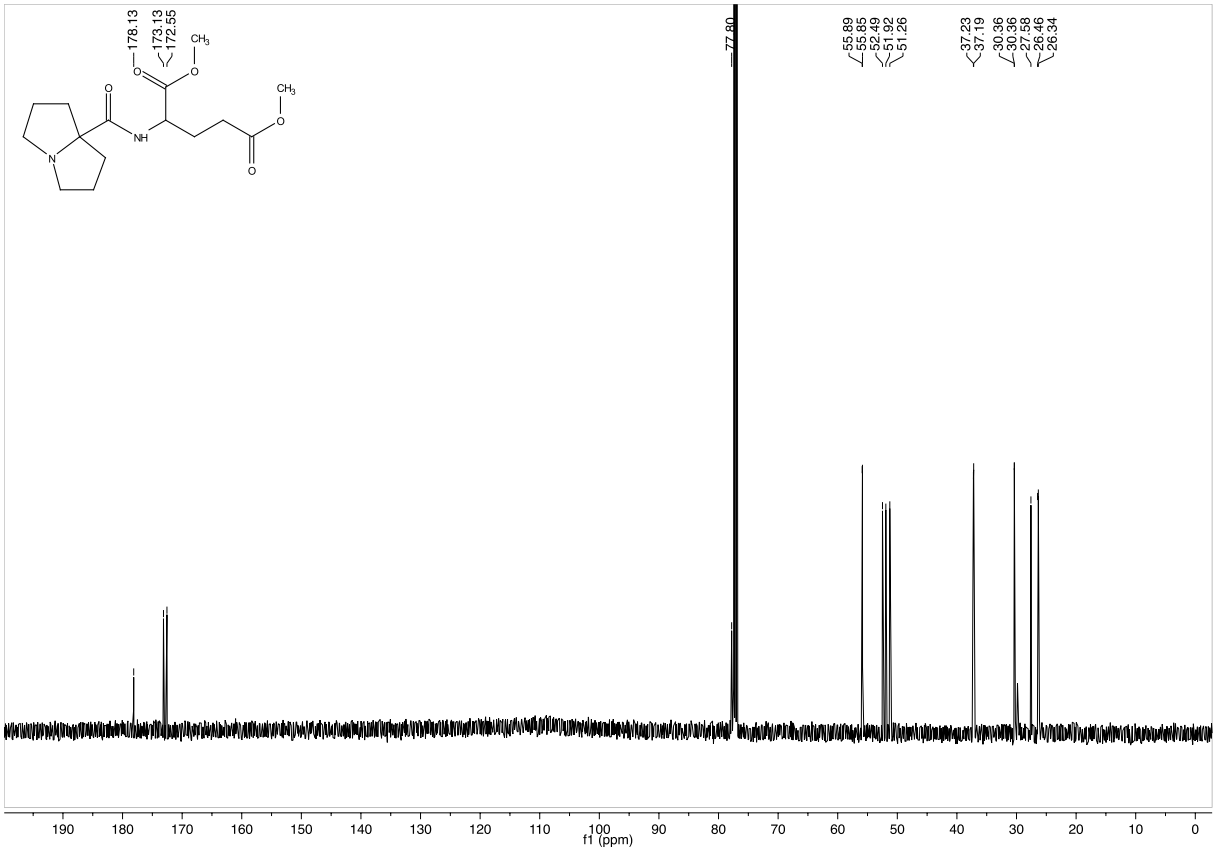

101 MHz ^{13}C-NMR in $CDCl_3$

4-(3,4-Dihydro-2*H*-pyrrol-5-yl)-2-methylbutan-2-ol (3.90)

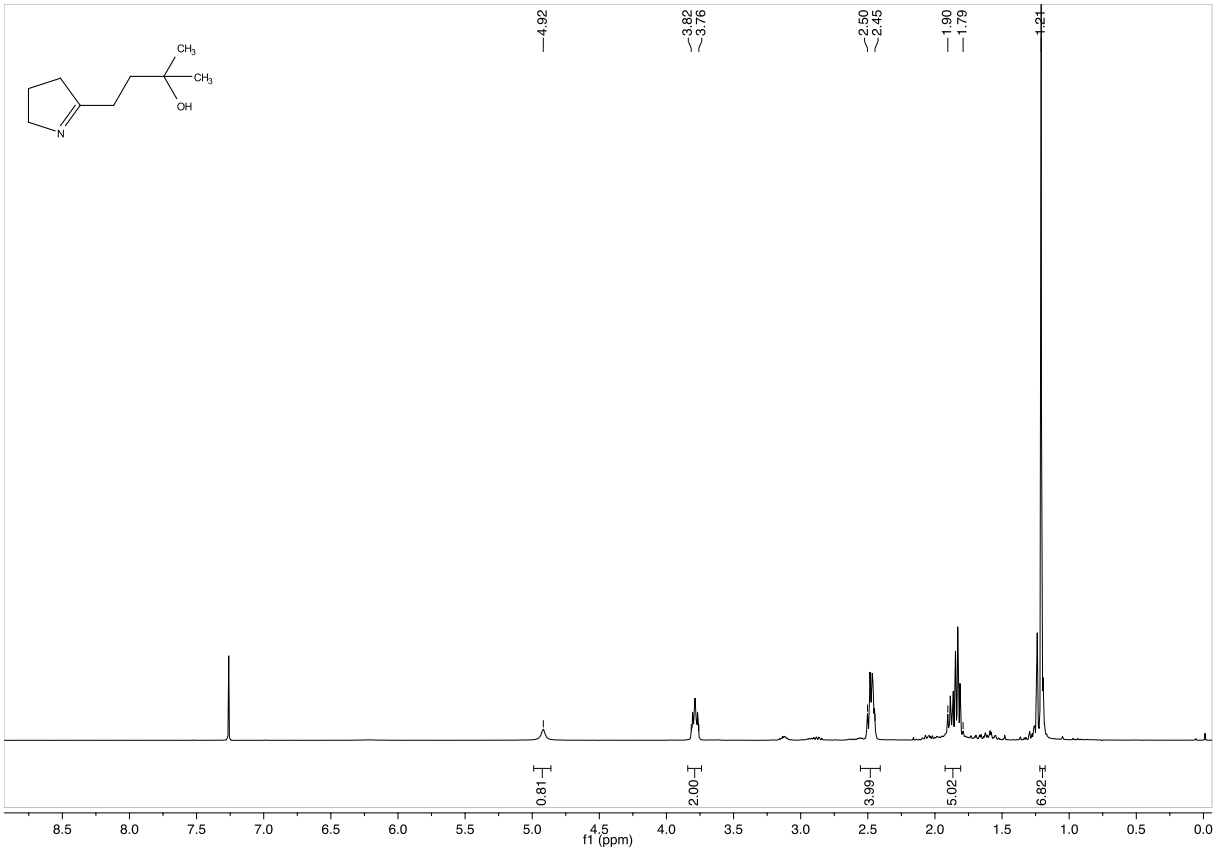

400 MHz ^{1}H-NMR in $CDCl_3$

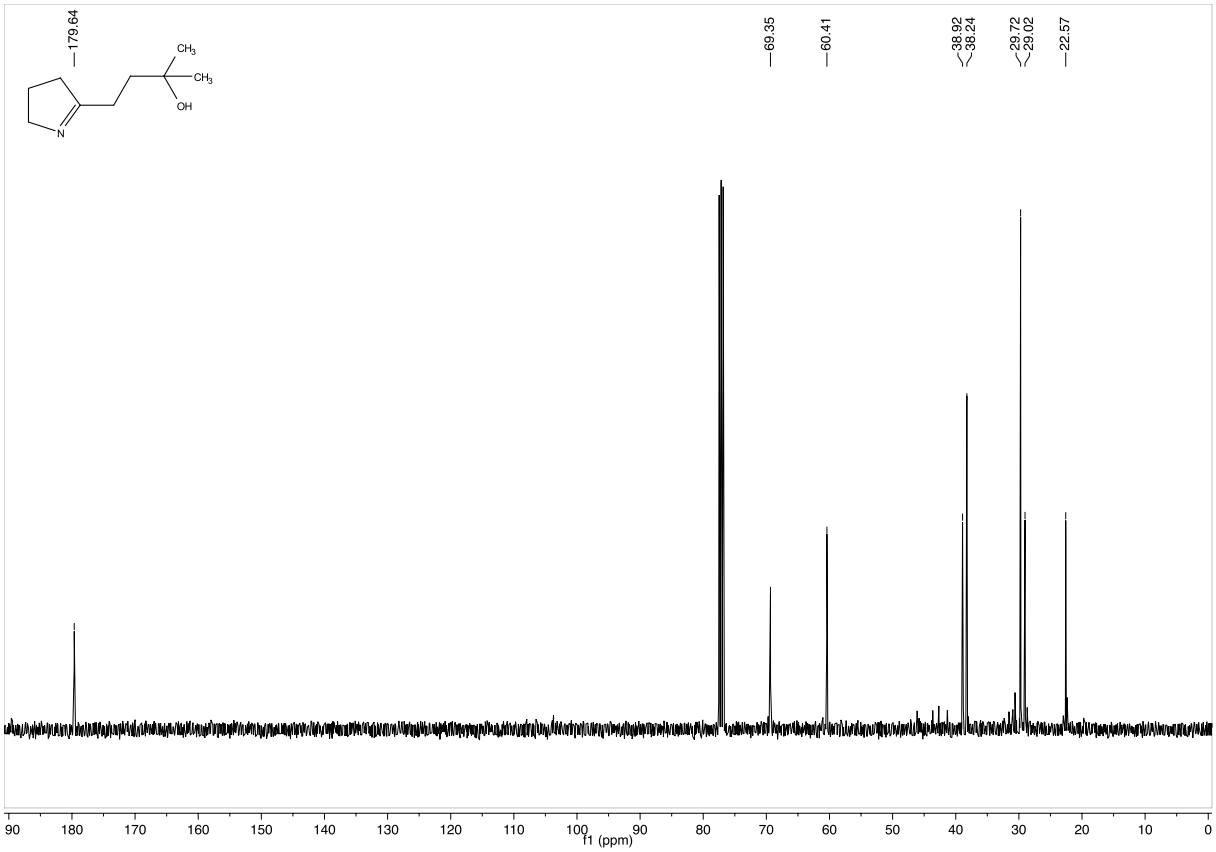

101 MHz ^{13}C-NMR in $CDCl_3$

2-(3-Methylbut-2-en-1-yl)-*N*-phenylpyrrolidine-2-carboxamide (3.92 and 3.93)

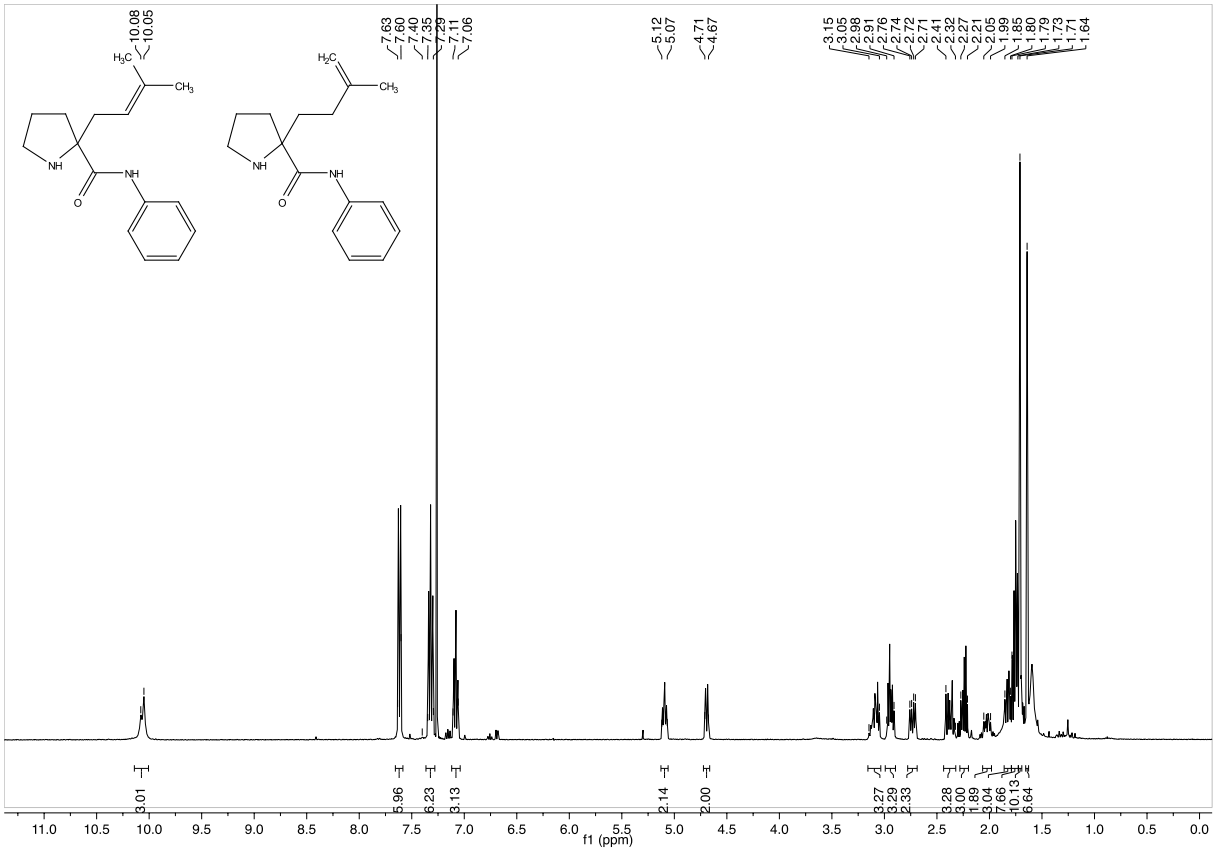

400 MHz ^{1}H-NMR in $CDCl_3$

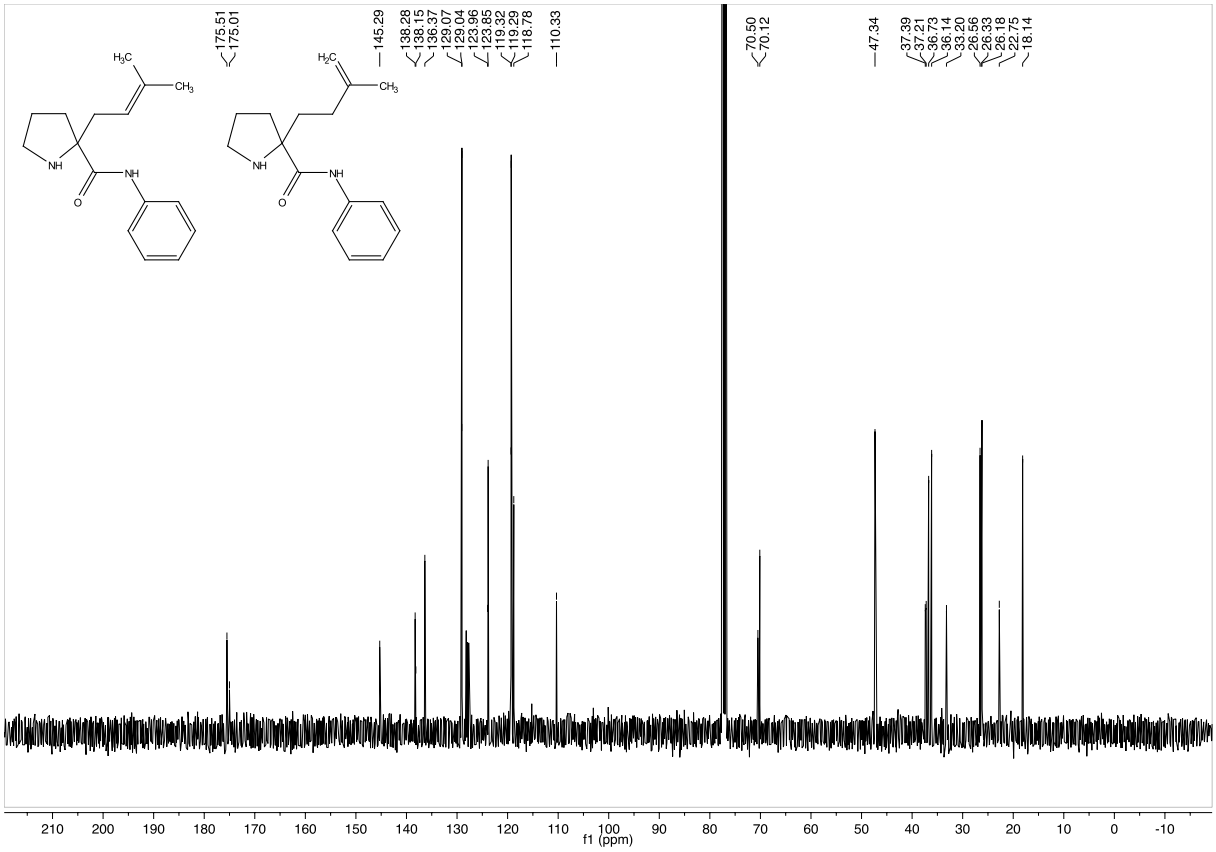

101 MHz ^{13}C-NMR in $CDCl_3$

4-(3,4-Dihydro-2*H*-pyrrol-5-yl)butan-1-ol (3.103)

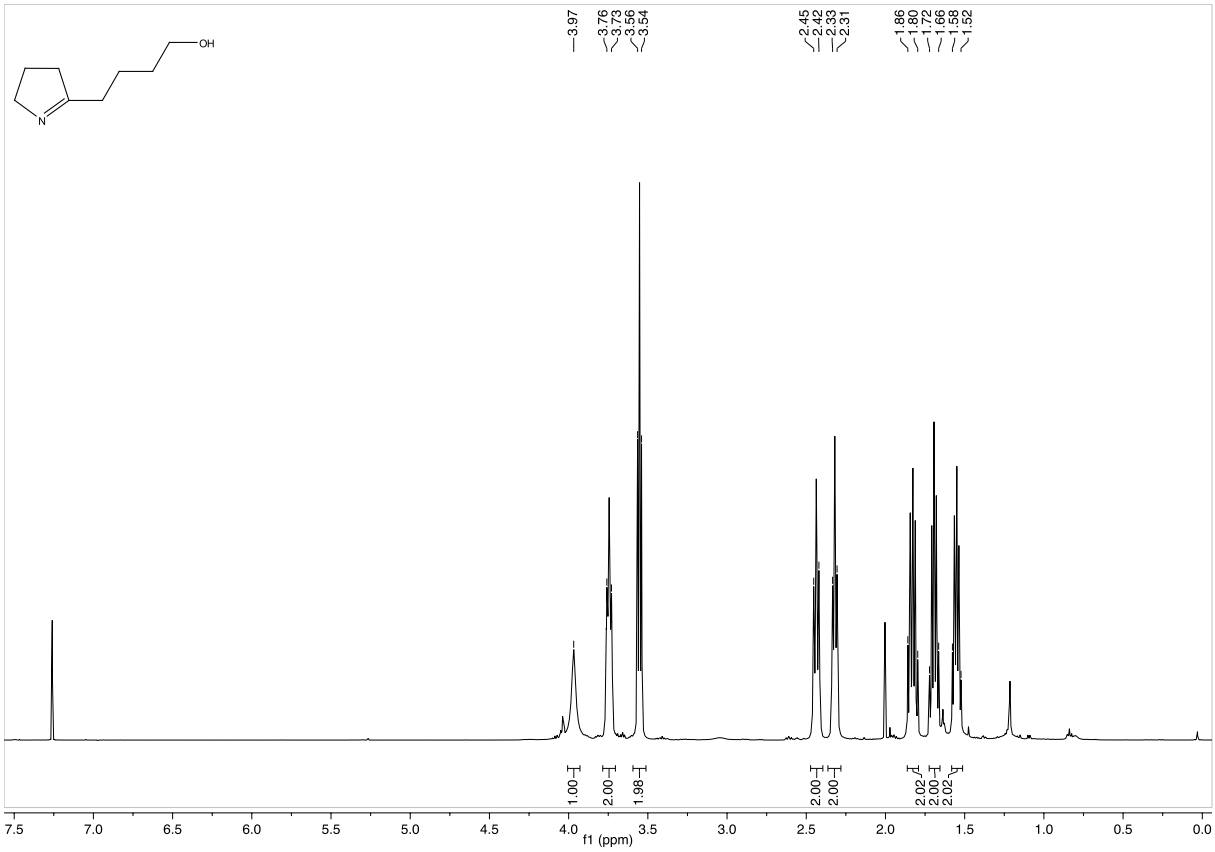

500 MHz ^{1}H-NMR in $CDCl_3$

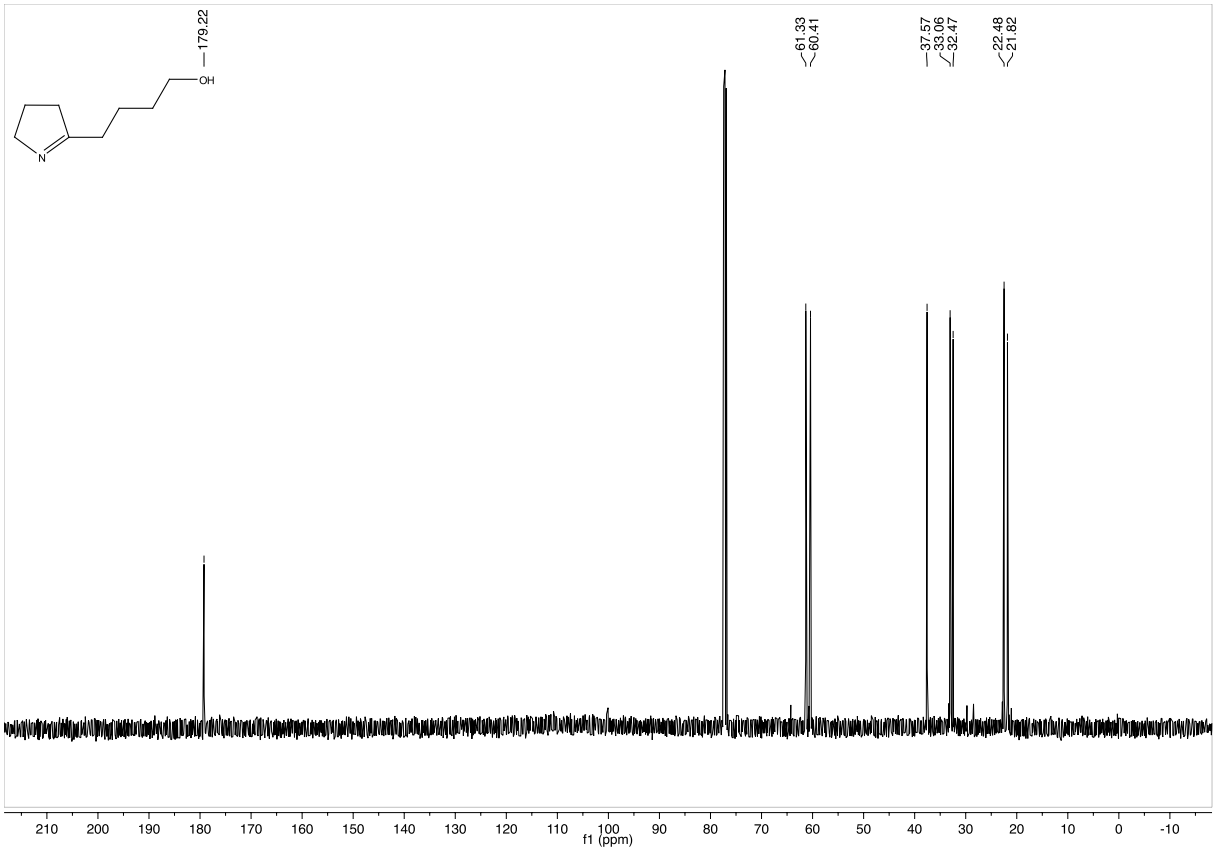

126 MHz ^{13}C-NMR in $CDCl_3$

3-Oxo-*N*-phenyltetrahydro-1*H*-pyrrolizine-7a(5*H*)-carboxamide (3.105)

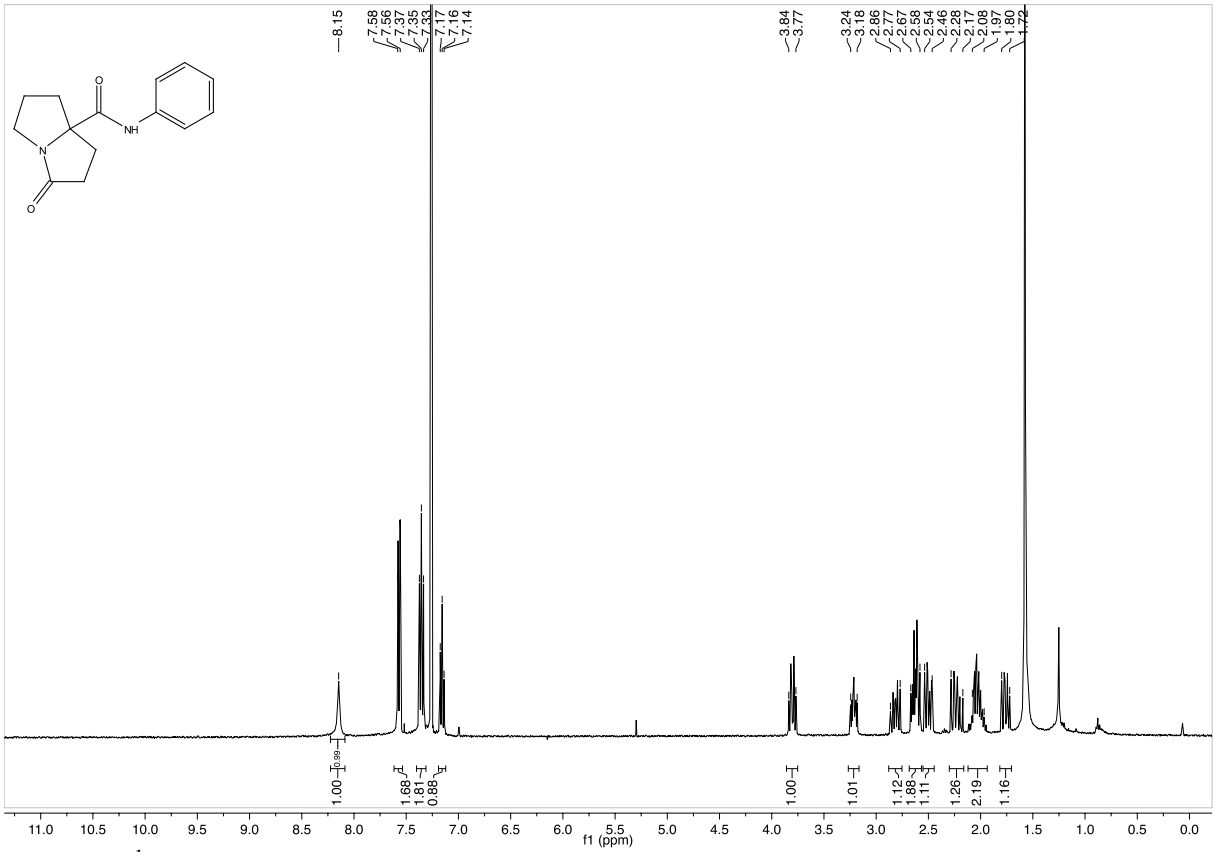

400 MHz ^{1}H-NMR in $CDCl_3$

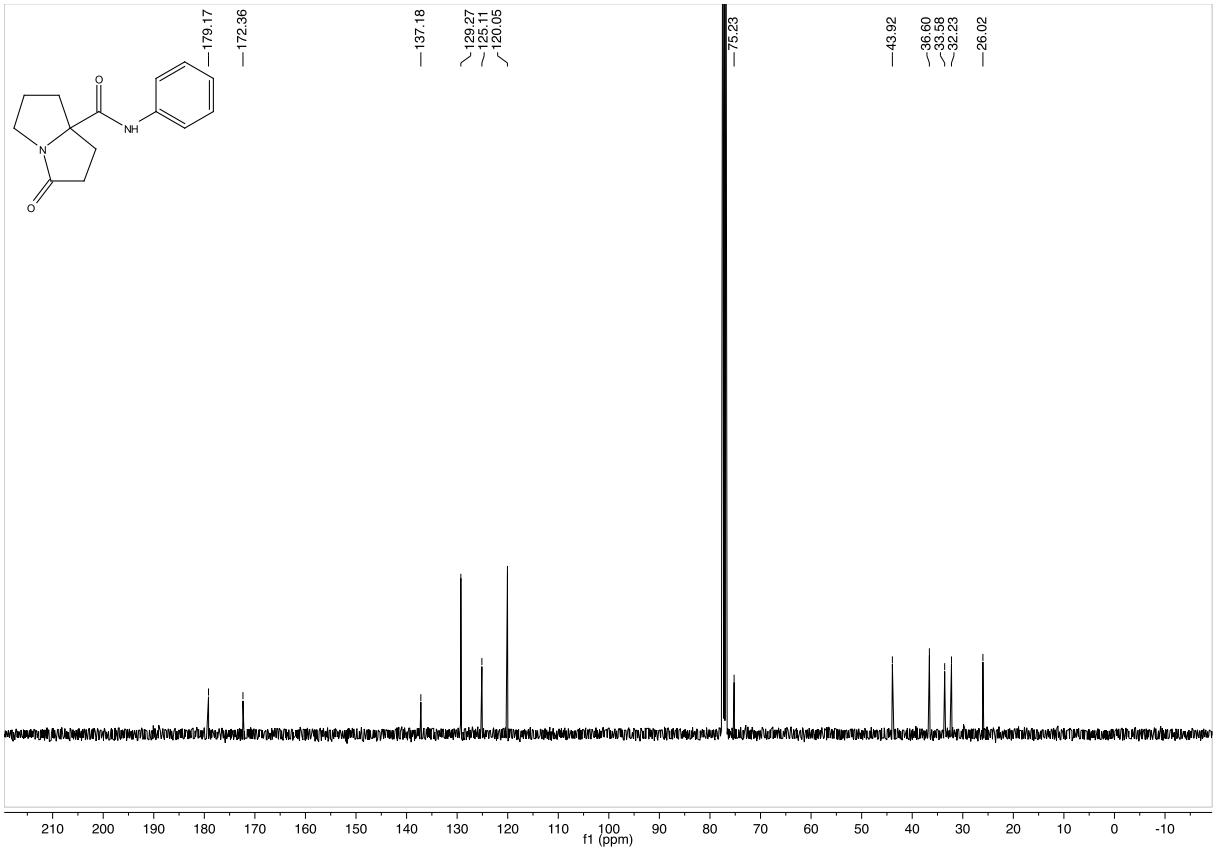

101 MHz ^{13}C-NMR in $CDCl_3$

7a-(Phenylcarbamoyl)hexahydropyrrolizine-4(1*H*)-oxide (3.106)

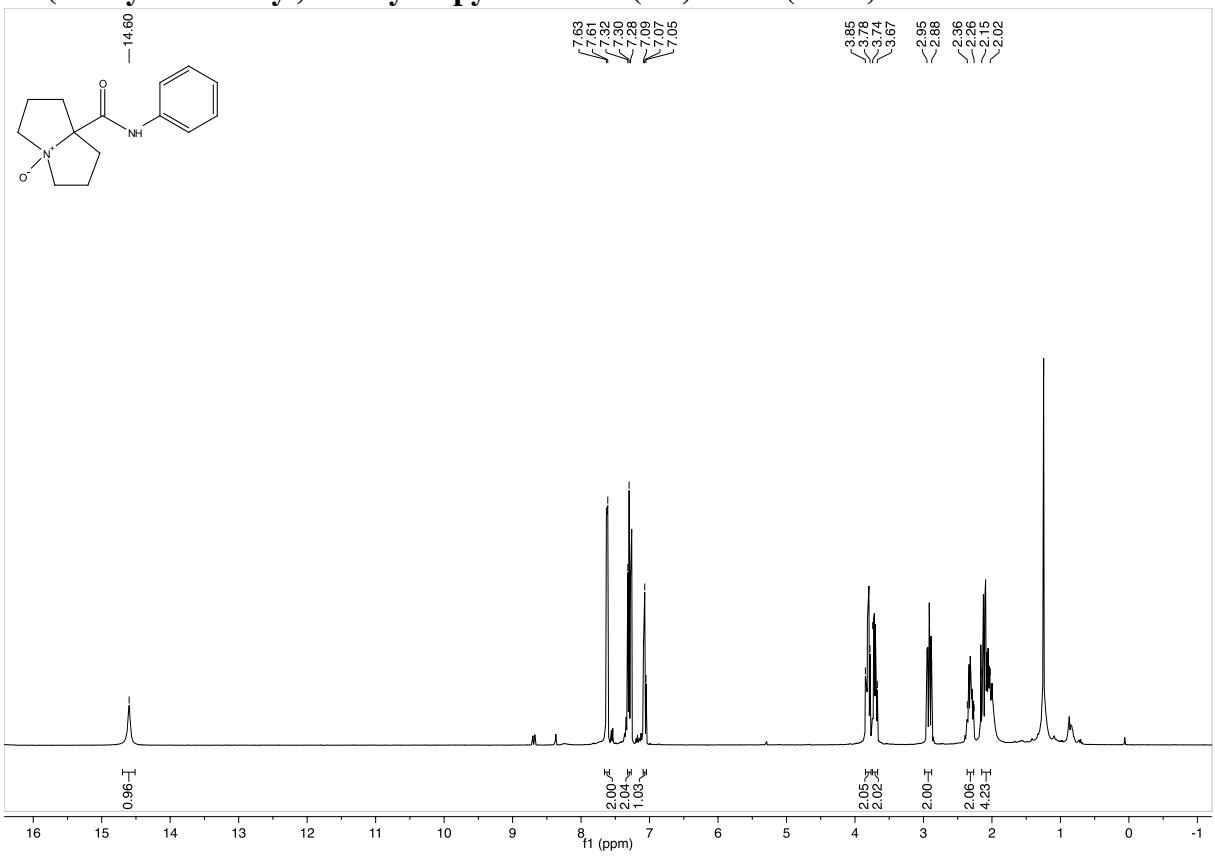

400 MHz ^{1}H-NMR in $CDCl_3$

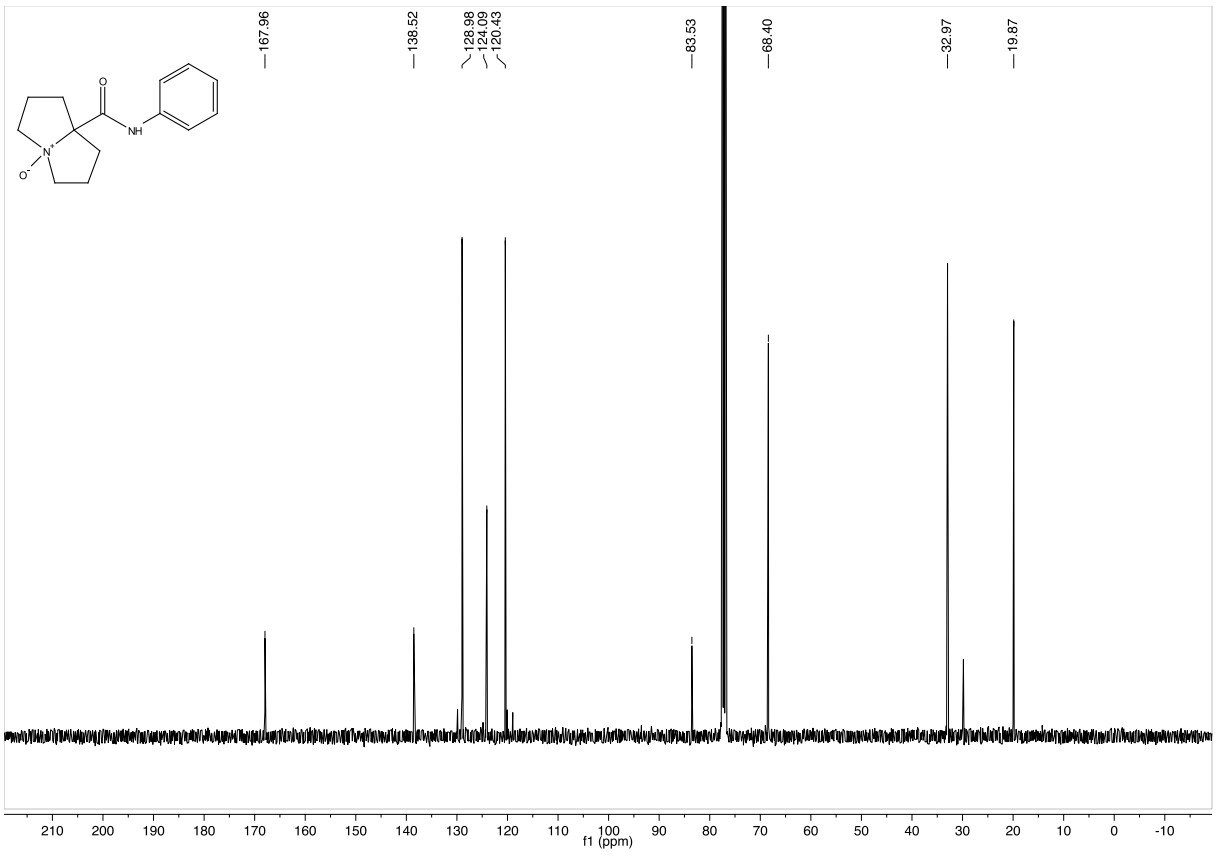

101 MHz ^{13}C-NMR in $CDCl_3$

_N_-((Tetrahydro-1_H_-pyrrolizin-7a(5_H_)-yl)methyl)aniline (3.107)

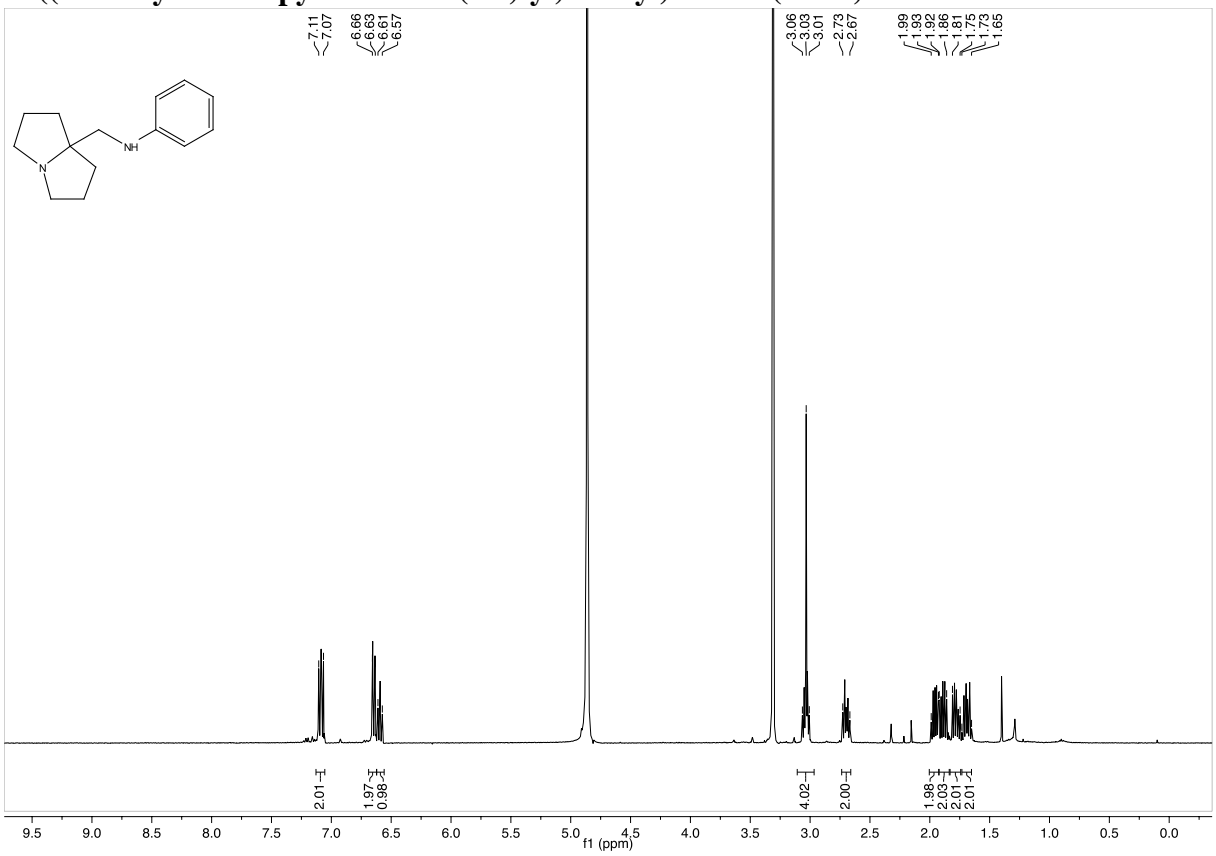

400 MHz ^{1}H-NMR in CD_3OD

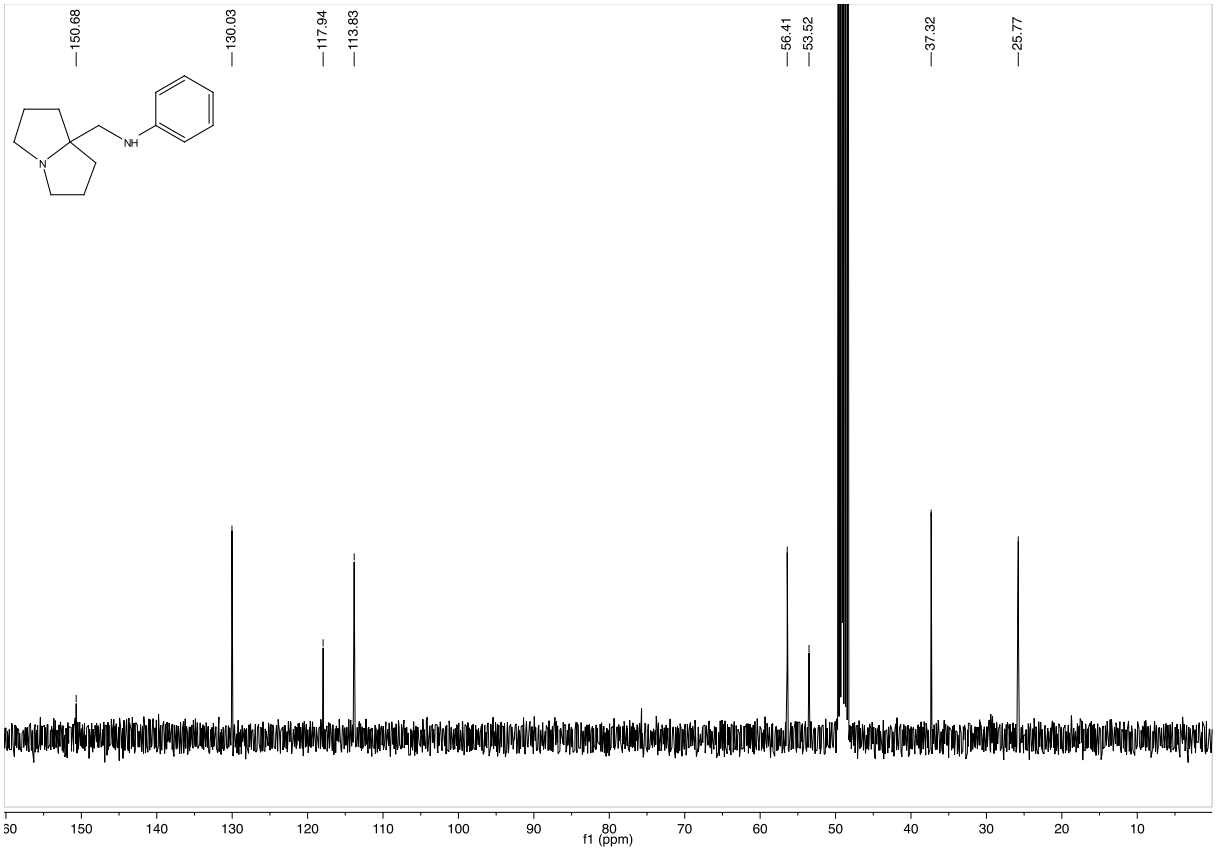

101 MHz ^{13}C-NMR in CD_3OD

7a-((phenylamino)methyl)octahydropyrrolizin-4-ium hydrogen carbonate (3.109)

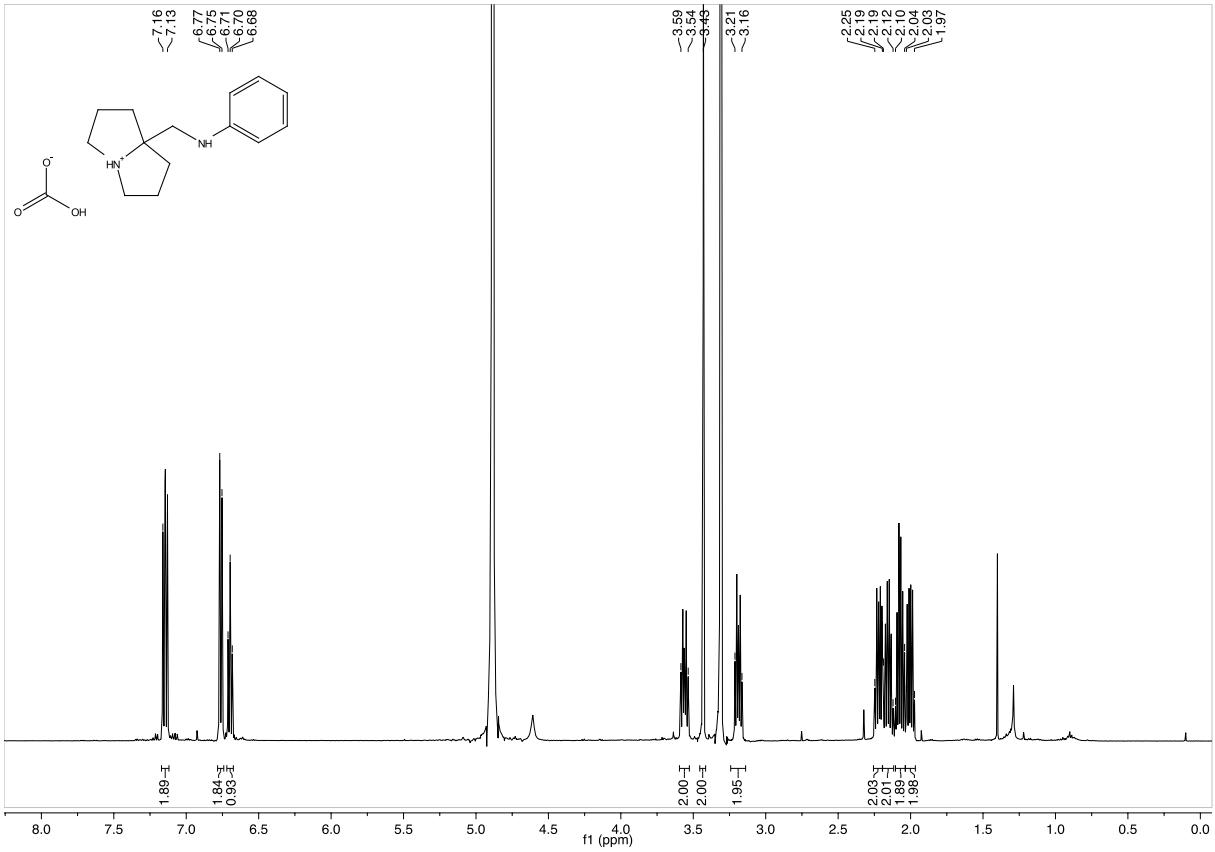

500 MHz ^{1}H-NMR in CD_3OD

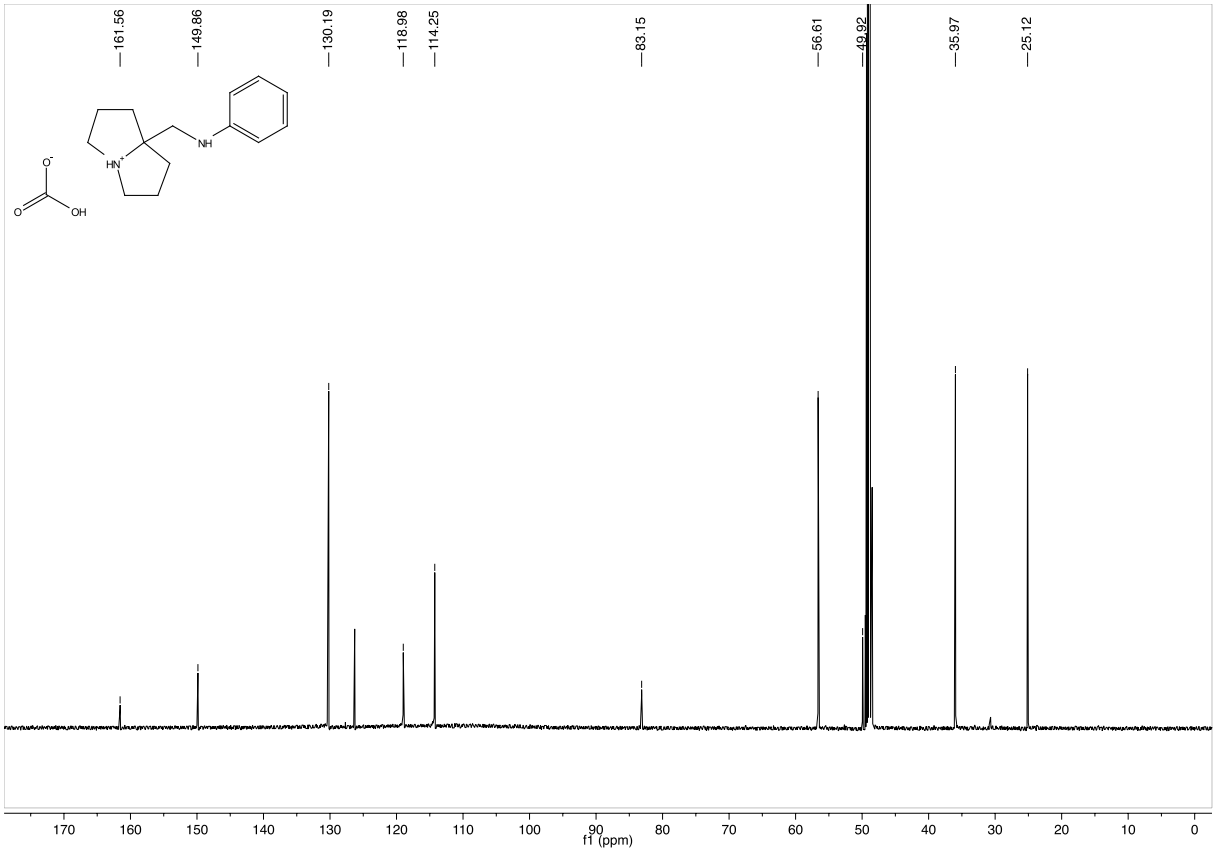

126 MHz ^{13}C-NMR in CD_3OD

(Tetrahydro-1*H*-pyrrolizin-7a(5*H*)-yl)methanamine (4.13)

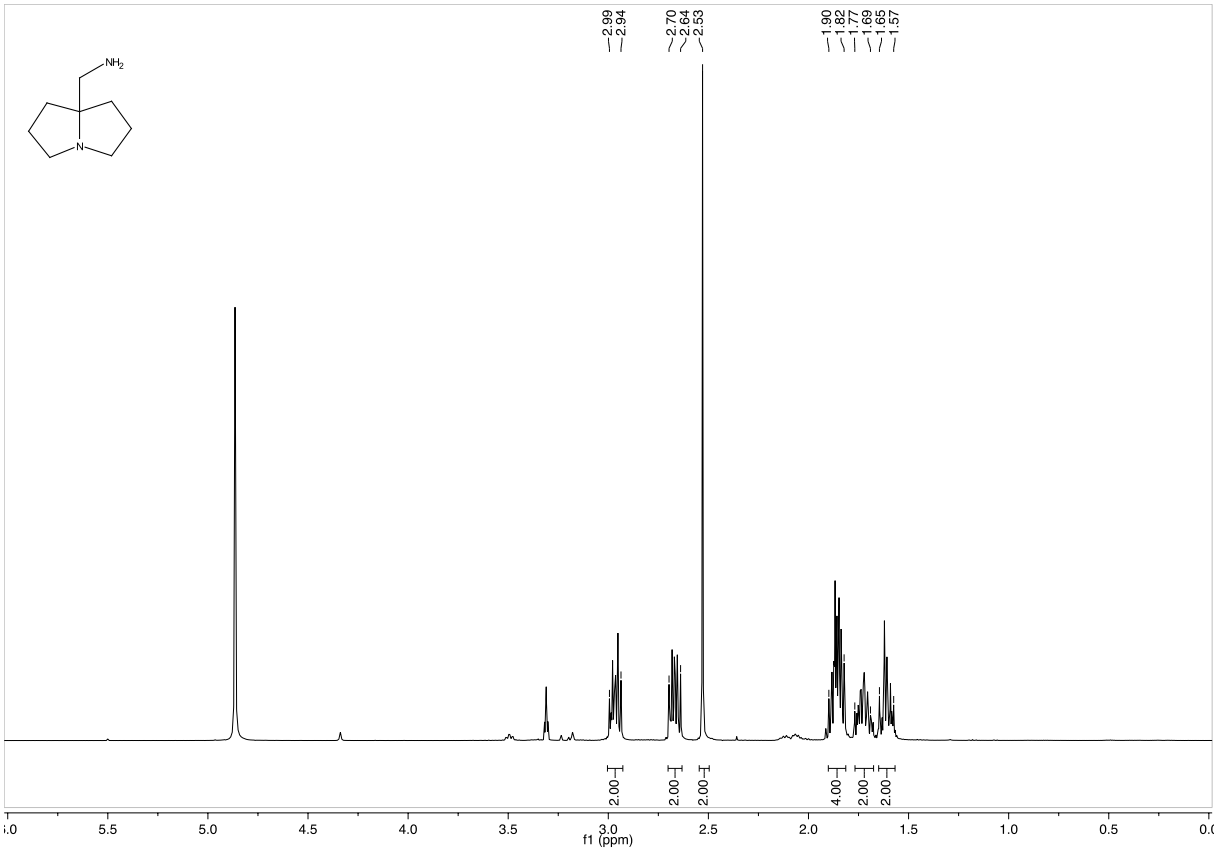

400 MHz ^{1}H-NMR in CD_3OD

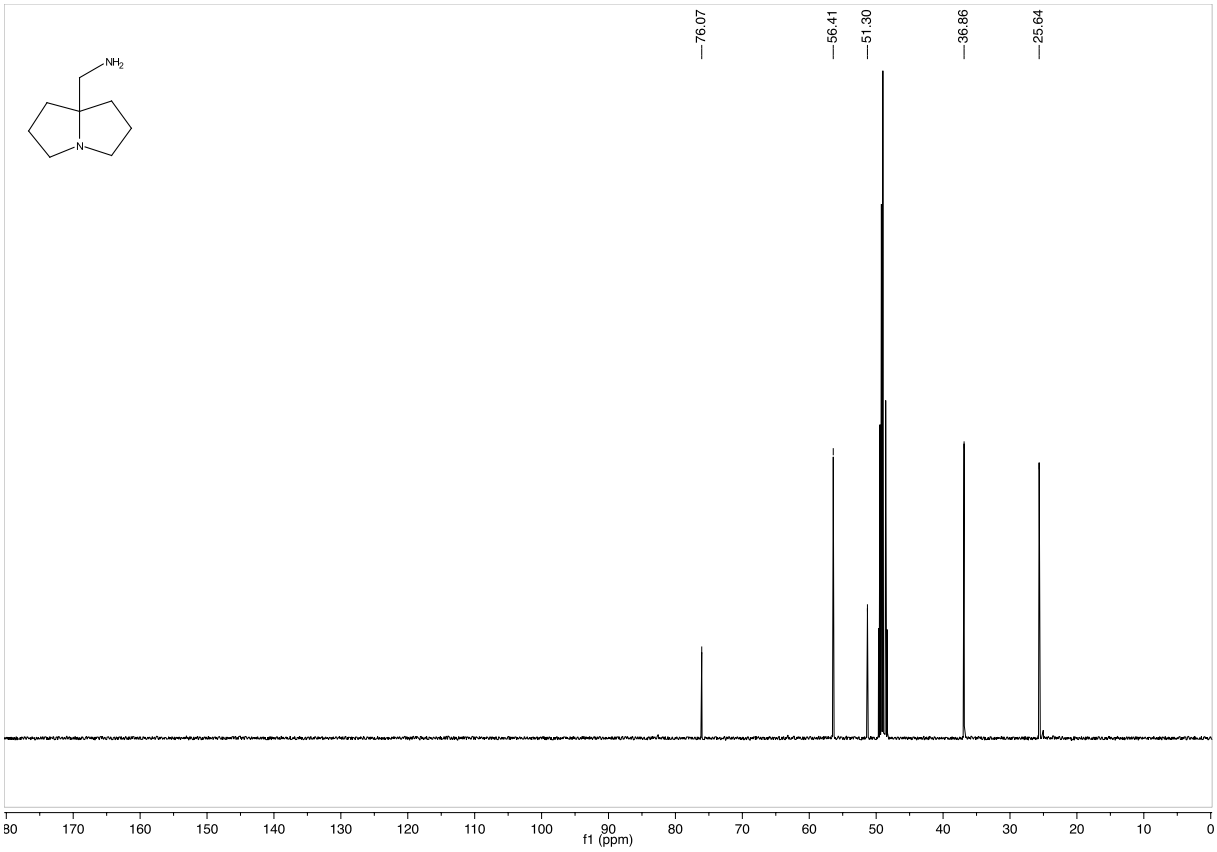

101 MHz ^{13}C-NMR in CD_3OD

((Hexahydropyrrolizin-4-ium-7a(1*H*)-yl)methyl)carbamate (4.29)

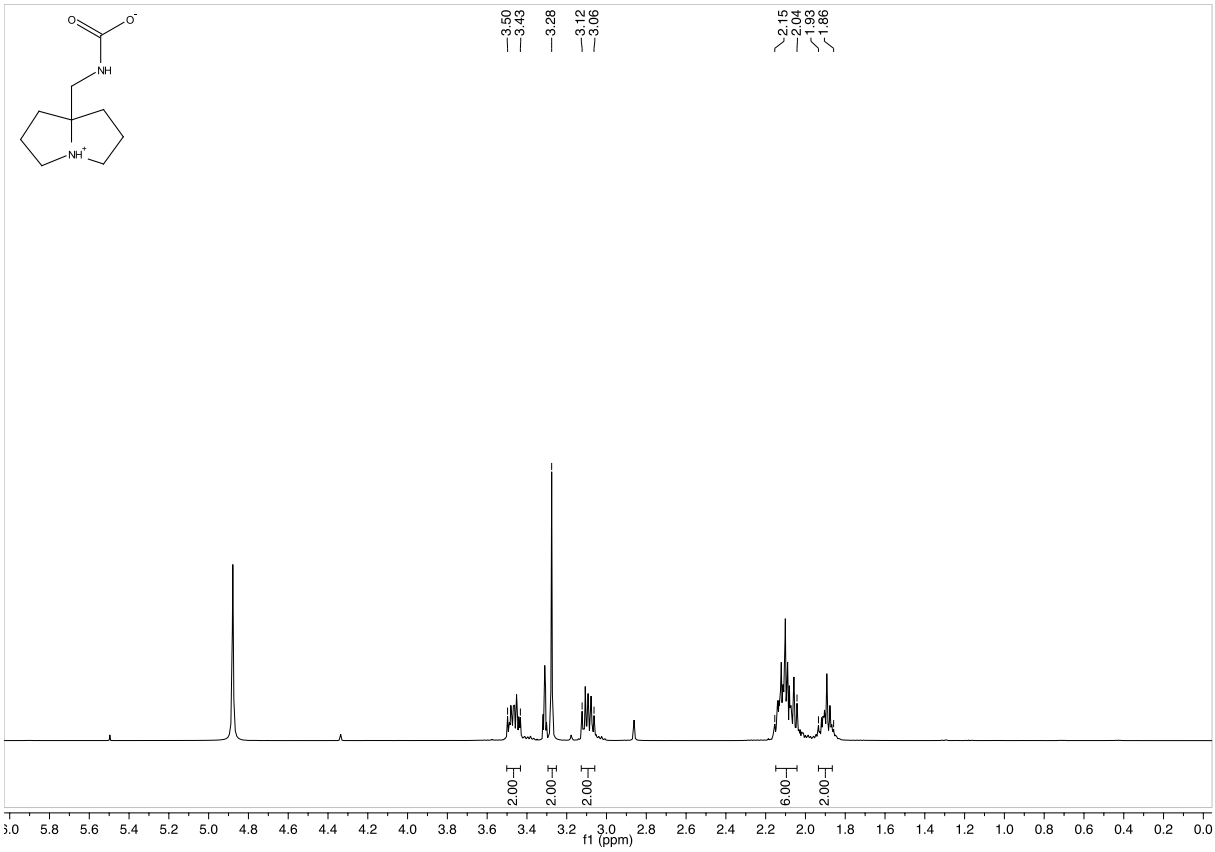

400 MHz ^{1}H-NMR in CD_3OD

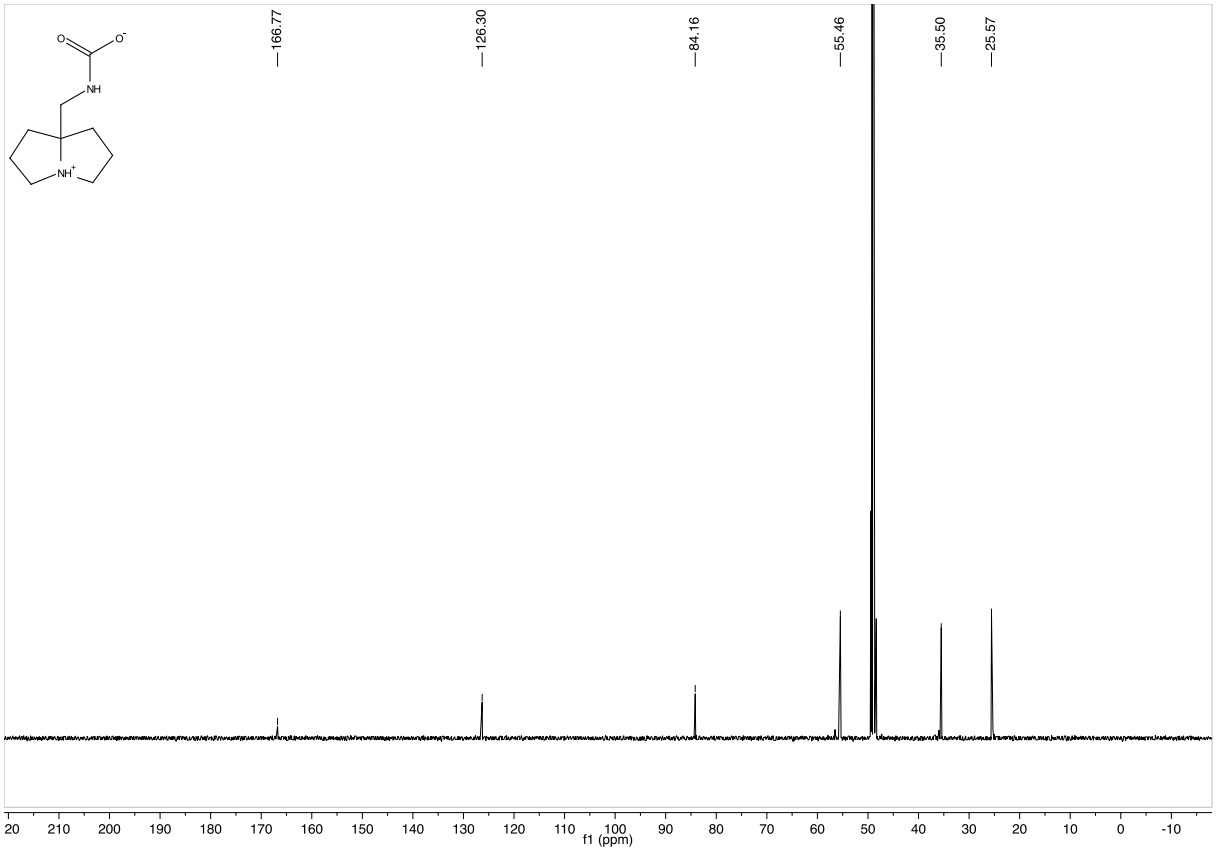

101 MHz ^{13}C-NMR in CD_3OD

2-(Tetrahydro-1*H*-pyrrolizin-7a(5*H*)-yl)ethan-1-amine (4.15)

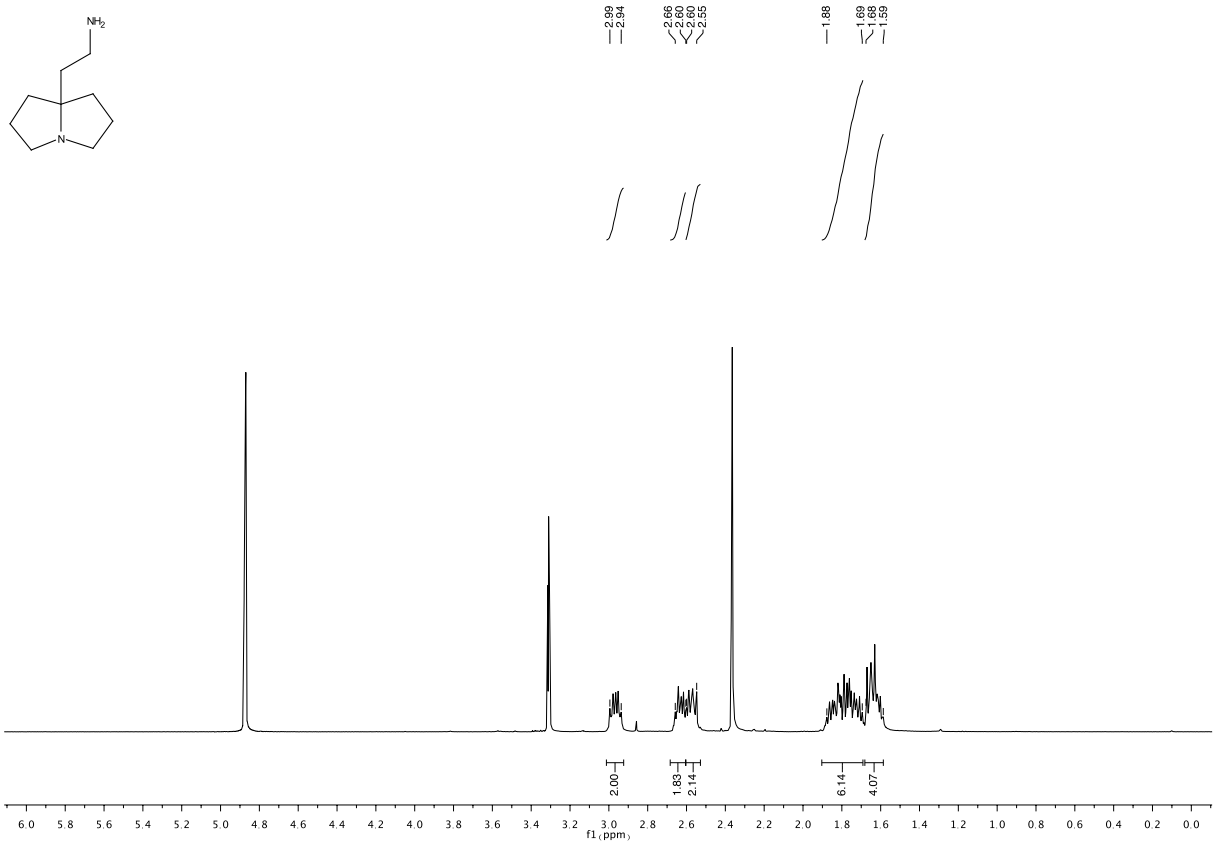

400 MHz ^{1}H-NMR in CD_3OD

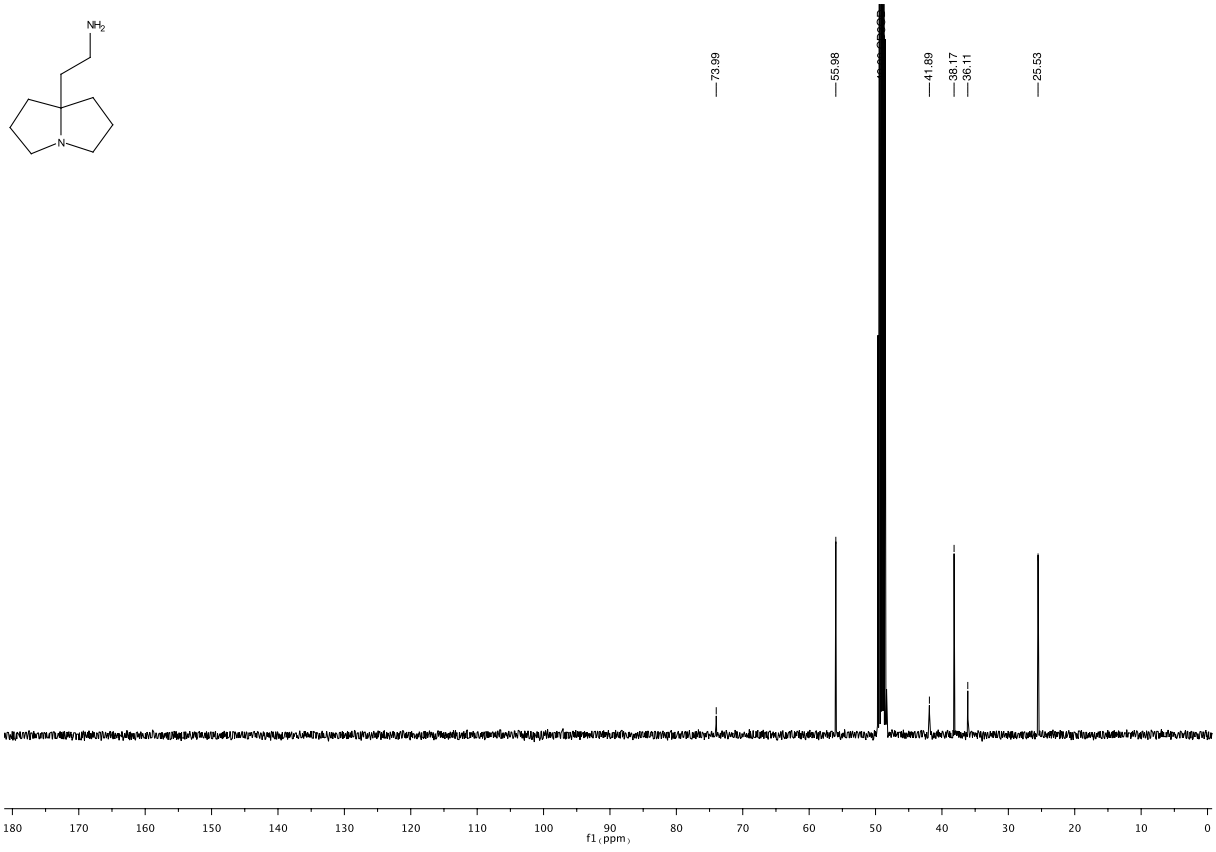

101 MHz ^{13}C-NMR in CD_3OD

N-Methyl-1-(tetrahydro-1*H*-pyrrolizin-7a(5*H*)-yl)methanamine (4.14)

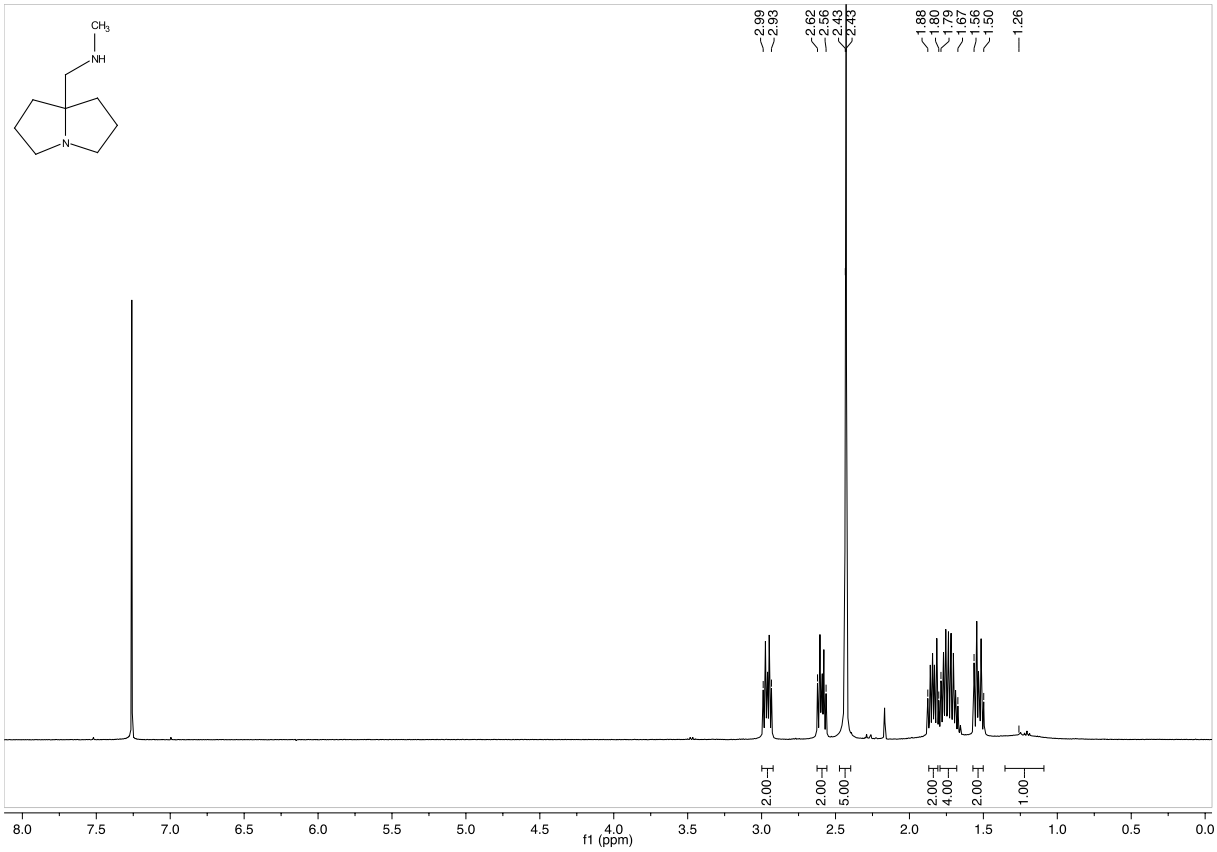

400 MHz ^{1}H-NMR in $CDCl_3$

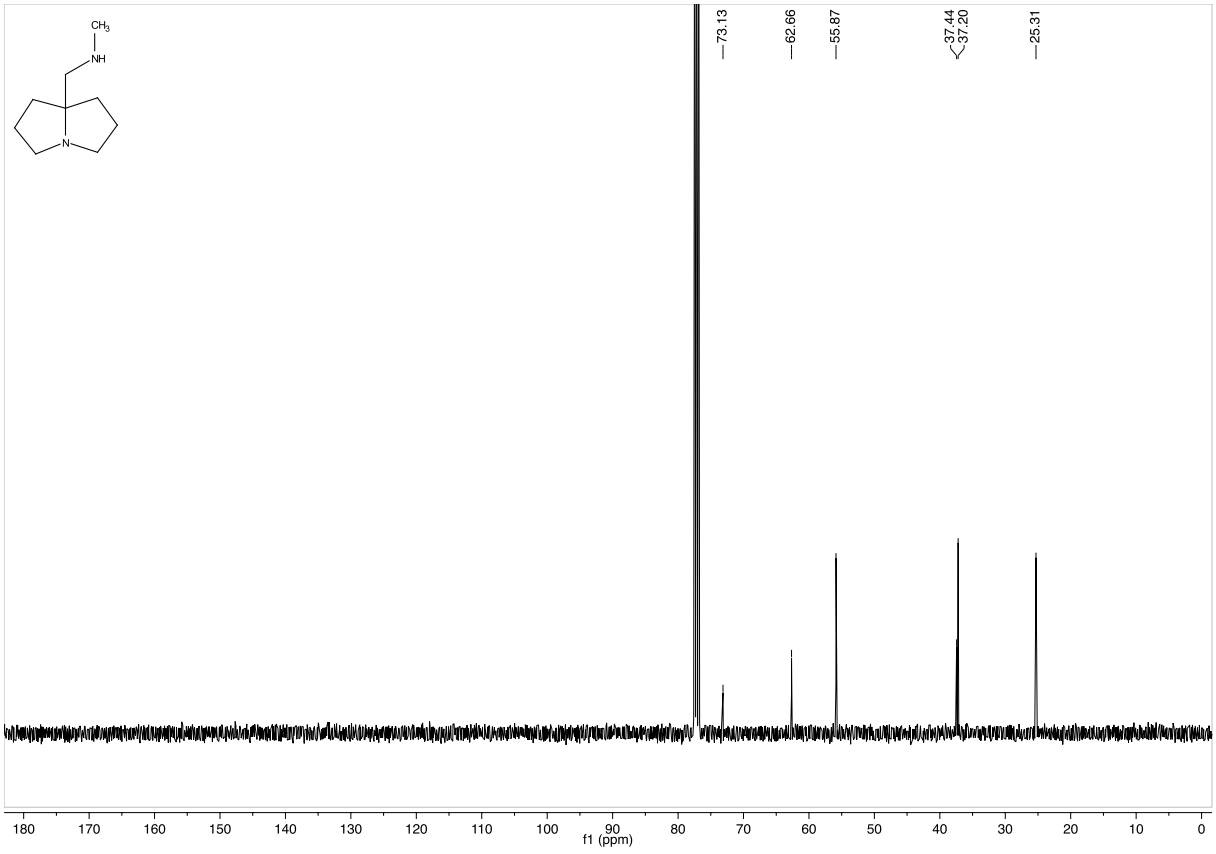

101 MHz ^{13}C-NMR in $CDCl_3$

2,4-Dinitro-*N*-((tetrahydro-1*H*-pyrrolizin-7a(5*H*)-yl)methyl)aniline (4.18)

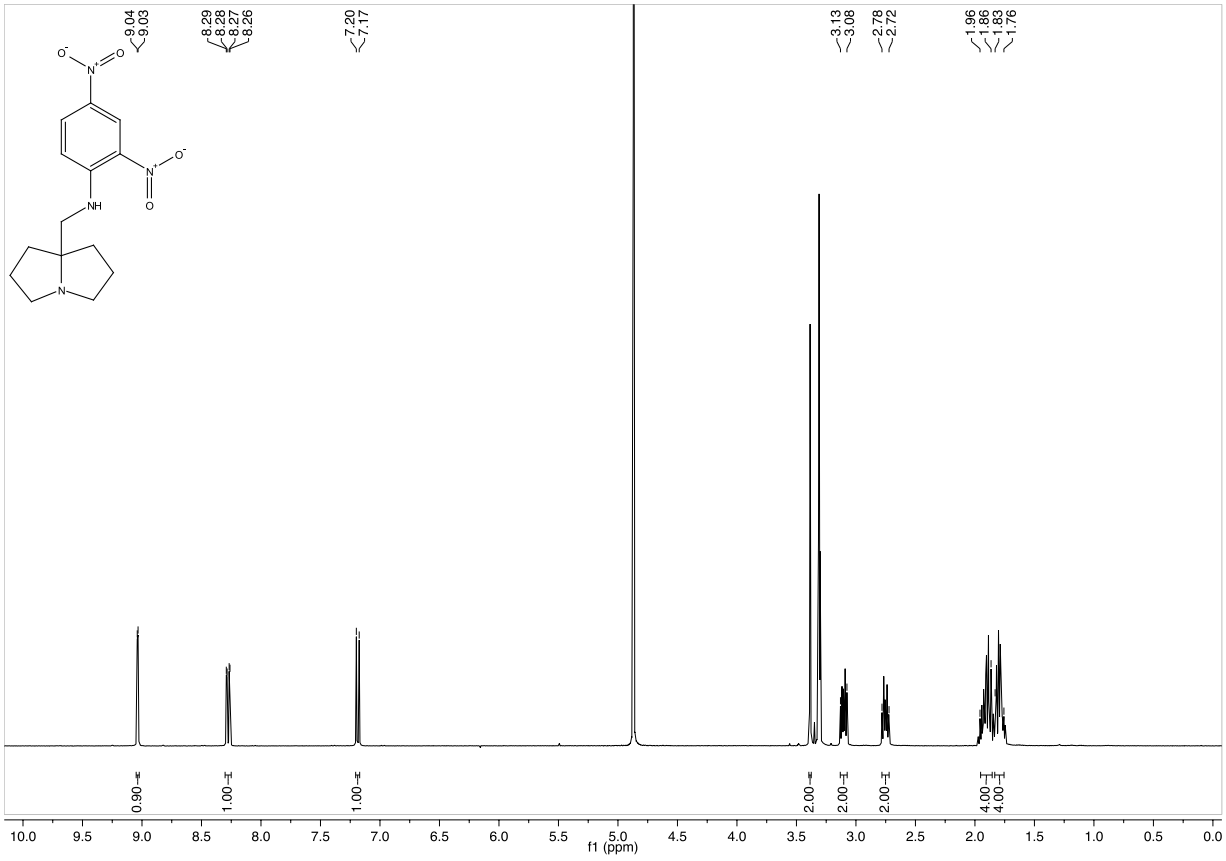

400 MHz ^{1}H-NMR in CD_3OD

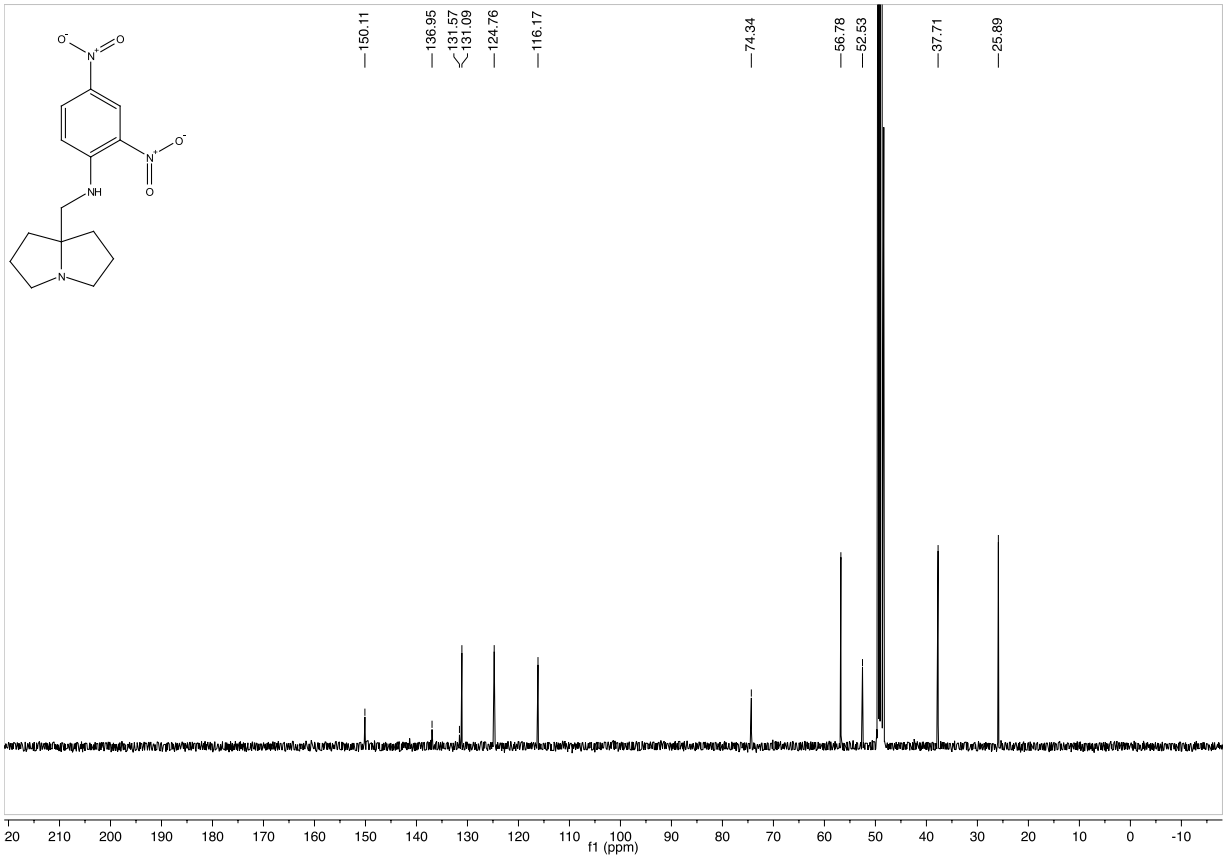

101 MHz ^{13}C-NMR in CD_3OD

N-Methyl-2-(tetrahydro-1*H*-pyrrolizin-7a(5*H*)-yl)ethan-1-amine (4.16)

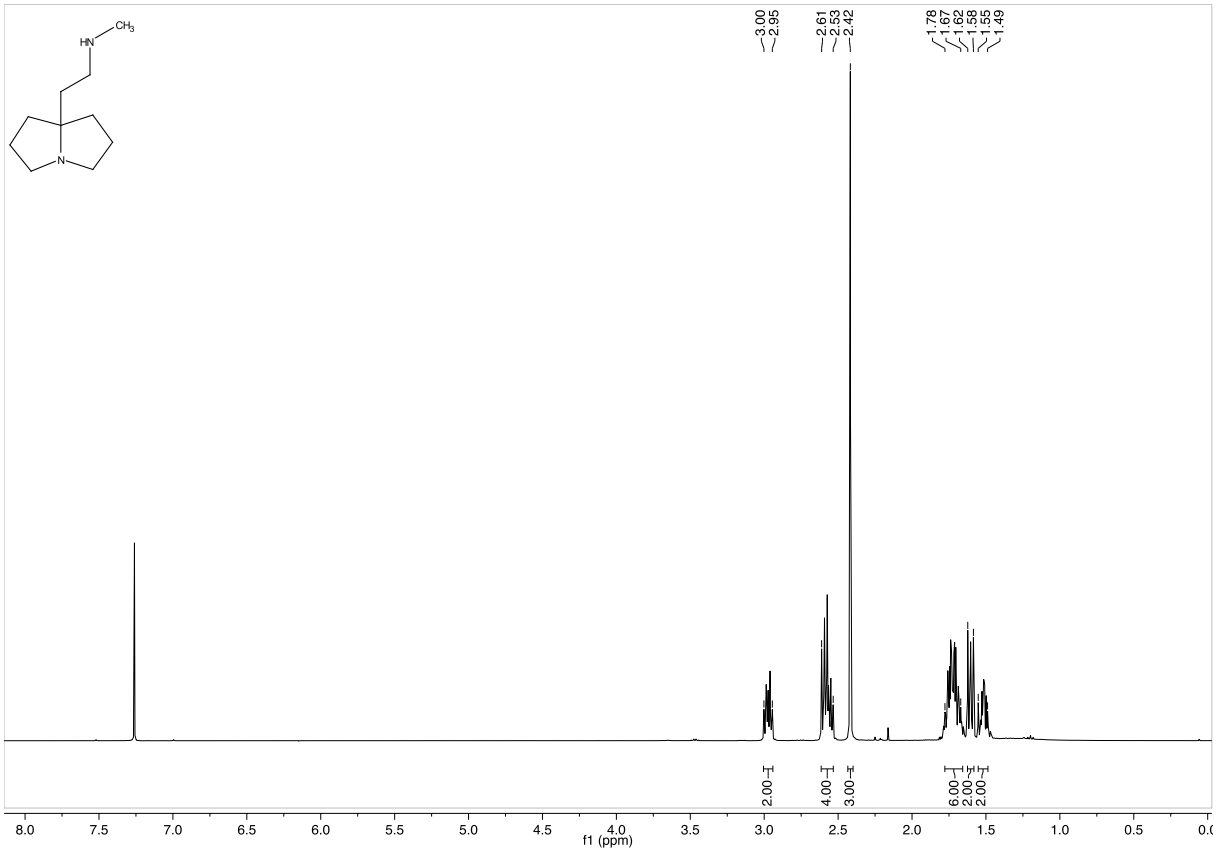

400 MHz ^{1}H-NMR in $CDCl_3$

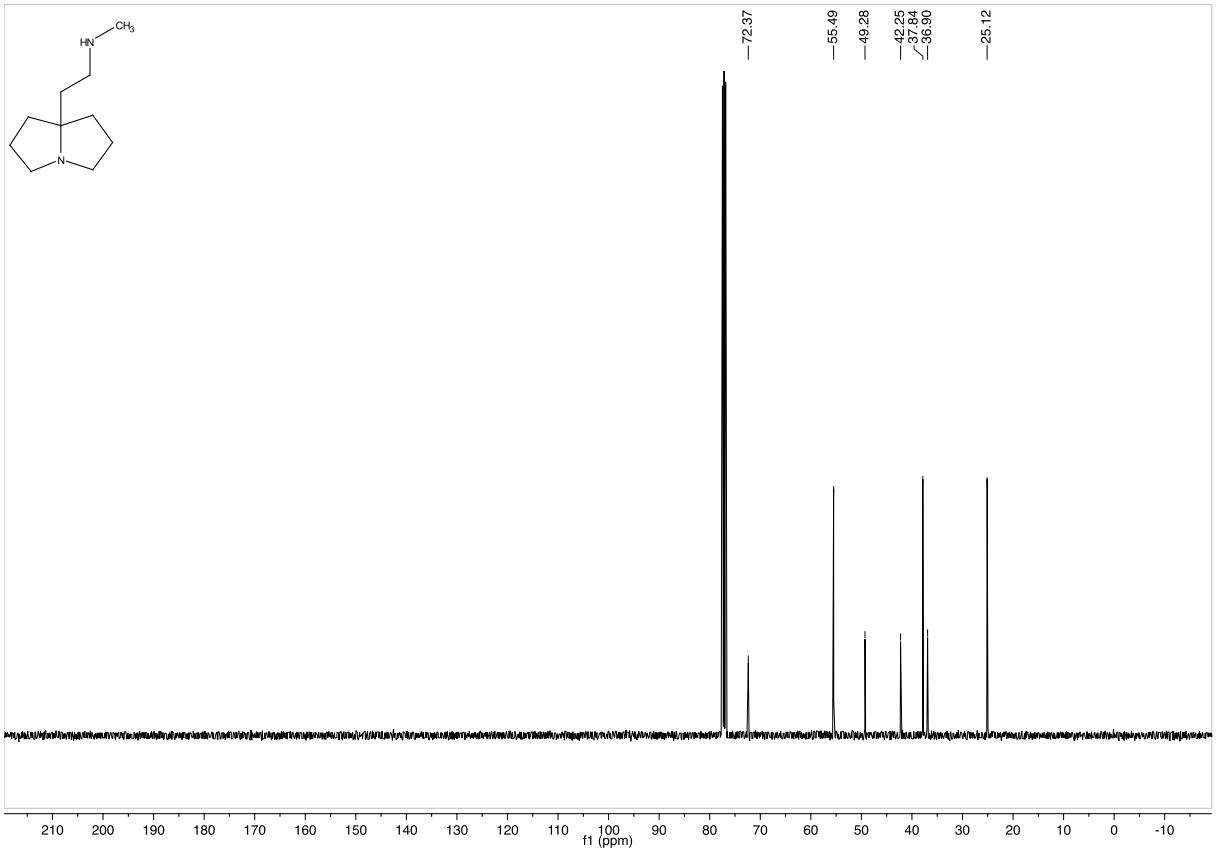

101 MHz ^{13}C-NMR in $CDCl_3$

N-(2-(Tetrahydro-1*H*-pyrrolizin-7a(5*H*)-yl)ethyl)aniline (4.17)

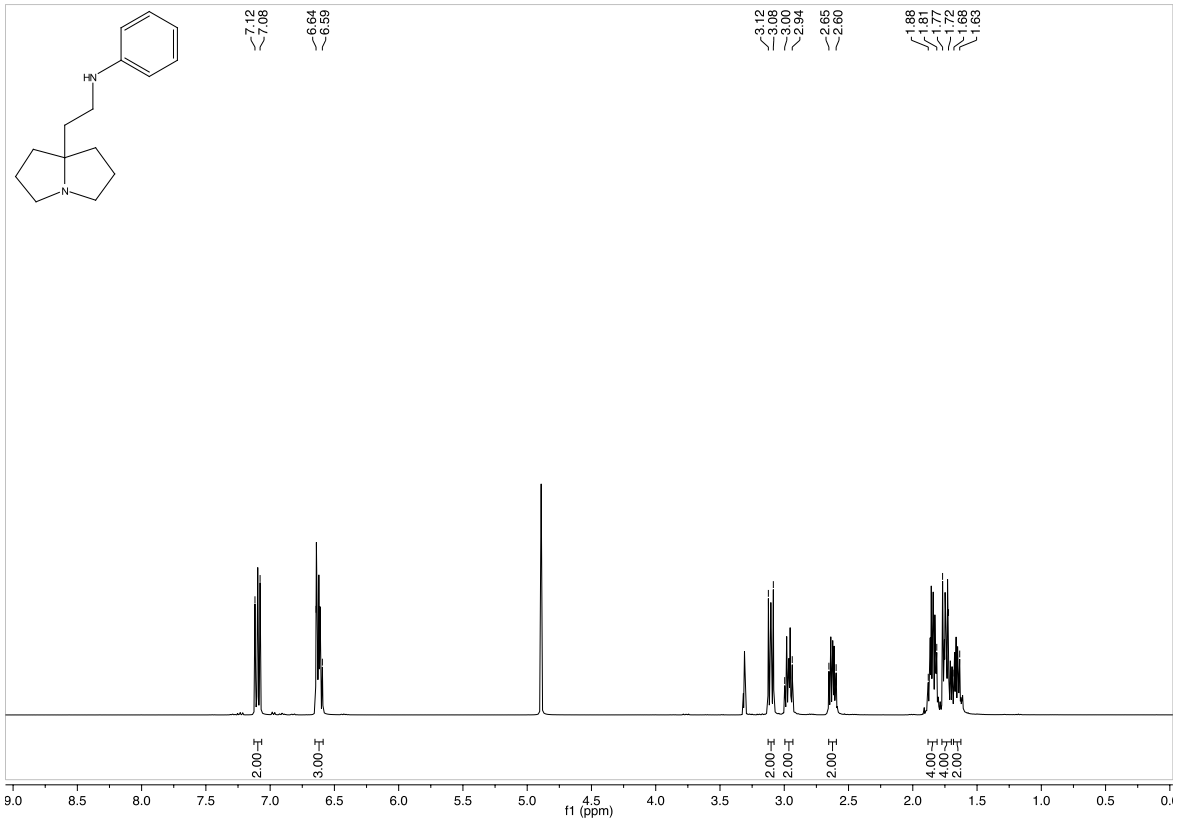

400 MHz ^{1}H-NMR in CD_3OD

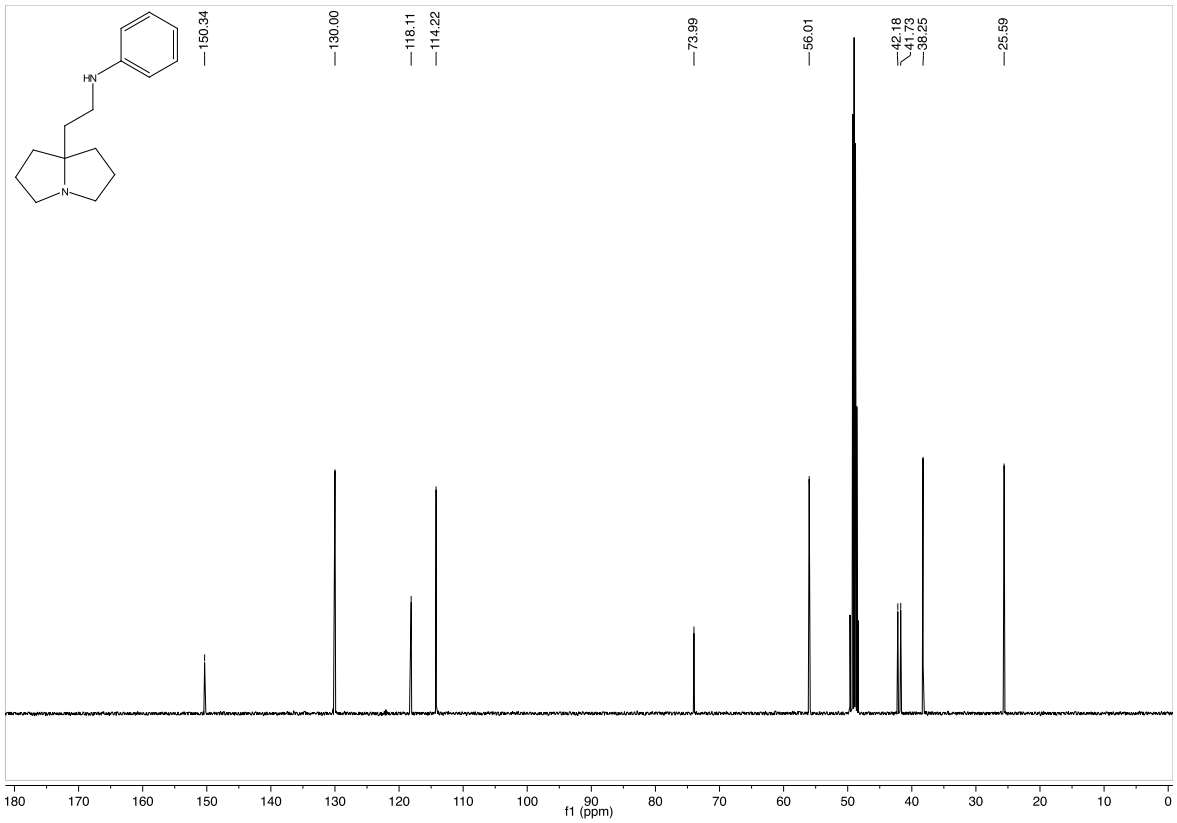

101 MHz ^{13}C-NMR in CD_3OD

Ammonium bicarbonate

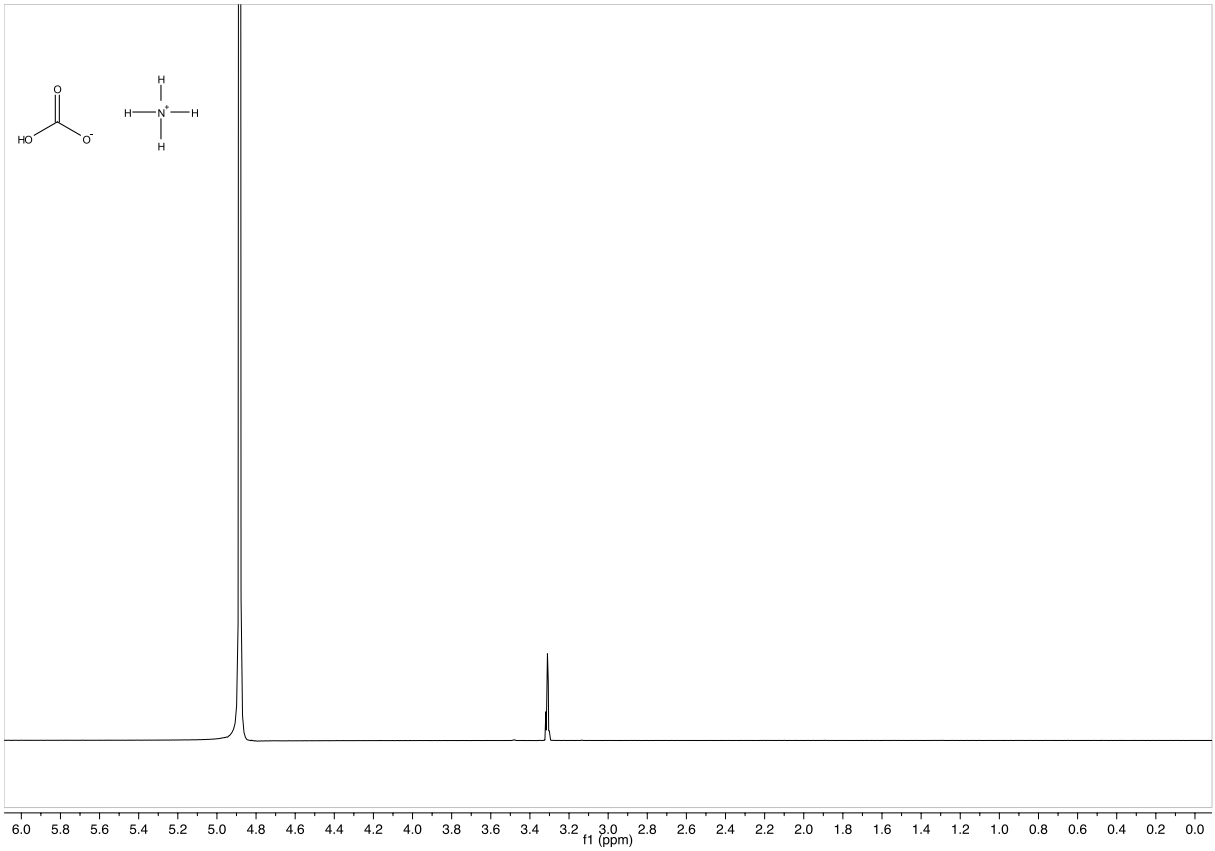

400 MHz ^{1}H-NMR in CD_3OD

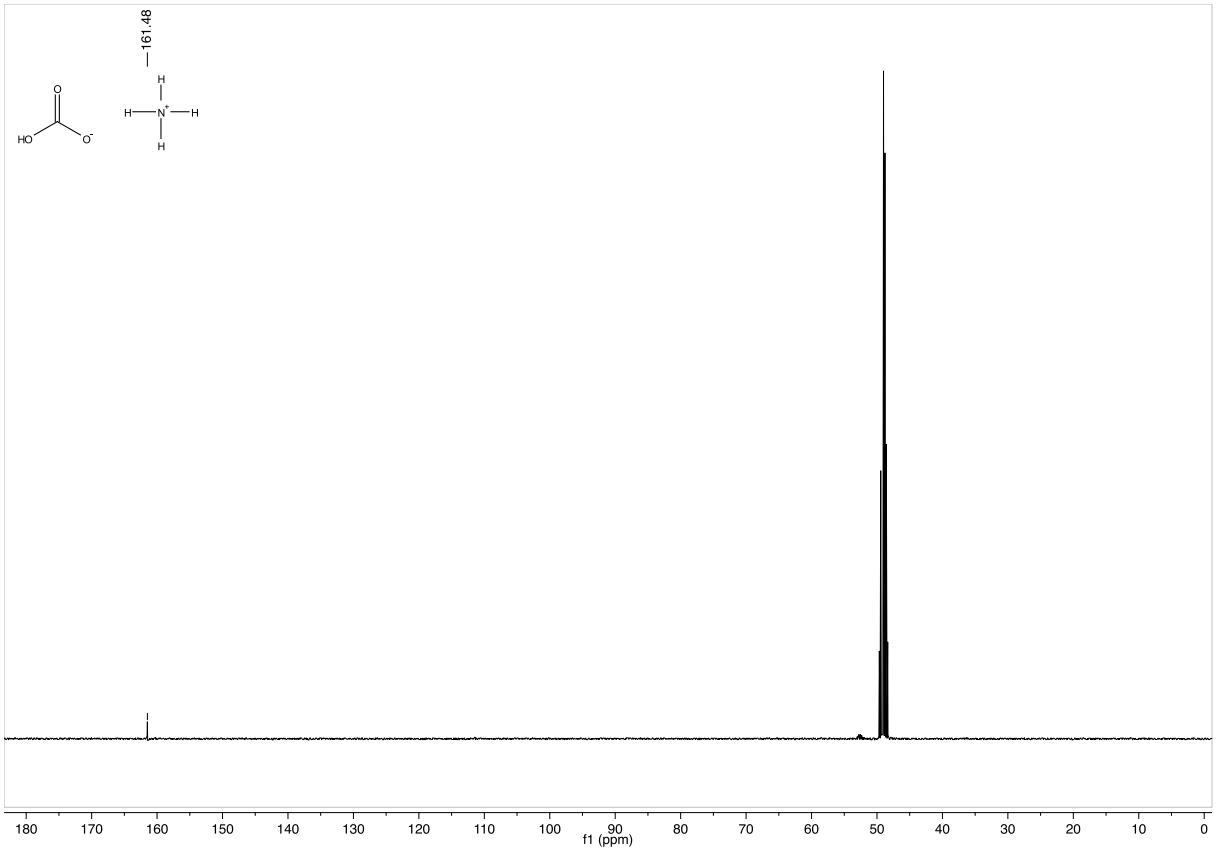

101 MHz ^{13}C-NMR in CD_3OD

9 Acknowledgements

First, I would like to thank “meinem Chef” *Prof. Dr. Karl Gademann* for his guidance and support during the last four years and his unbroken optimism. I value the excellent research conditions and opportunities you have provided us very highly. Thank you!

I thank *Prof. Dr. Konrad Tiefenbacher* for accepting the “Korreferat” of this thesis.

Prof. Dr. *Christof Sparr* is kindly acknowledged for the discussions we had during the major time of my PhD and for accepting to chair the defense.

I would like to thank Dr. *Erika Crane*, Dr. *Nadine Bohni*, Dr. *Florian Huber* and Dr. *Regina Berg* for critical proof-reading of my thesis thereby substantially contributing to its quality.

I would like to thank *Jan Hanusch* for his great work during his Master thesis and his internship. The discussions we had about our research mean a lot to me.

Dr. Katja Zerbe is kindly acknowledged for the introduction in the bacterial world and for advice during the experiments.

I thank the A-Team *Mathieu Szponarski*, *Simone Grendelmeier* and *Nadine Bohni* for the good discussions and the great exchange we had. Long lives the alga!

Prof. Dr. Suman de Sarkar is kindly acknowledged for his teaching and guidance throughout the first year of my PhD.

I would like to thank *Dr. Malika Makhlouf*, *Dr. Hideki Miyatake-Ondozobal*, *Dr. Chien-Chi Hsiao* and *Simone Grendelmeier* for the great time we had during chemical reaction mechanism problems. I really enjoyed our afternoon sessions a lot!

I thank the past members of Lab104 in Basel and present members of Lab92 in Zürich for the good time. Especially I would like to acknowledge *Raphael Liffert*, with whom I have shared the lab for three years, for the good discussions and his helpfulness.

I would like to thank the present and past members of the *Gademann group* for the great atmosphere in the lab and outside. You have made my PhD studies and my time in Switzerland very enjoyable.

Further, I would like to thank the technical staff at the University of Basel (especially *Hr. Koller* for constructing the CO_2-absorption apparatus) and at the University of Zurich (especially *Serkan* and *Hans-Peter* for building my beloved shelf).

The Center for Microscopy and Image Analysis at the University of Zurich (especially *Jana Doehner* and *Caroline Aemisegger*) is kindly acknowledged for the great maintenance of the instruments and their help in times of despair in front of the microscope.

Meiner Familie möchte ich ganz herzlich für die Unterstützung während des Studiums und der Promotion danken. In schwierigen Zeiten habt ihr mich perfekt aufgefangen und alles nochmal in Perspektive gerückt, in guten Zeiten habt ihr mit mir gefeiert.
Philipp danke ich dafür, dass er ein so toller Begleiter während Studium und Promotion war und ist, für seine Unterstützung und seinen Humor. Vielen Dank!

10 References

[1] M. T. Stephan, D. J. Irvine, *Nano Today* **2011**, *6*, 309–325.
[2] O. N. Koç, J. Day, M. Nieder, S. L. Gerson, H. M. Lazarus, W. Krivit, *Bone Marrow Transplant.* **2002**, *30*, 215–222.
[3] E. Jones, X. Yang, *Injury* **2011**, *42*, 562–568.
[4] N. Joyce, G. Annett, L. Wirthlin, S. Olson, G. Bauer, J. A. Nolta, *Regen. Med.* **2010**, *5*, 933–946.
[5] M. N. Knight, K. D. Hankenson, *Advances in Wound Care* **2013**, *2*, 306–316.
[6] P. K. Gupta, A. K. Das, A. Chullikana, A. S. Majumdar, *Stem Cell Res. Ther.* **2012**, *3*, 25.
[7] E. Przybyt, M. C. Harmsen, *Curr. Stem Cell Res. Ther.* **2013**, *8*, 270–277.
[8] S. P. Yu, Z. Wei, L. Wei, *Transl. Stroke Res.* **2013**, *4*, 76–88.
[9] S. Chakradhar, *Nat. Med.* **2015**, *21*, 1236–1238.
[10] S. Gautam, T. J. Gniadek, T. Kim, D. A. Spiegel, *Trends Biotechnol.* **2013**, *31*, 258–267.
[11] D. Y. Lee, S. J. Park, J. H. Nam, Y. Byun, *Tissue Eng.* **2006**, *12*, 615–623.
[12] S. C. Hsiao, B. J. Shum, H. Onoe, E. S. Douglas, Z. J. Gartner, R. A. Mathies, C. R. Bertozzi, M. B. Francis, *Langmuir* **2009**, *25*, 6985–6991.
[13] M. T. Stephan, J. J. Moon, S. H. Um, A. Bershteyn, D. J. Irvine, *Nat. Med.* **2010**, *16*, 1031–1037.
[14] D. Sarkar, P. K. Vemula, G. S. L. Teo, D. Spelke, R. Karnik, L. Y. Wee, J. M. Karp, *Bioconjugate Chem.* **2008**, *19*, 2105–2109.
[15] B. R. Peterson, *Org. Biomol. Chem.* **2005**, *3*, 3607.
[16] M. E. Medof, S. Nagarajan, *FASEB Journal* **1996**, *10*, 574–586.
[17] S. Nagarajan, P. Selvaraj, *Cancer Res.* **2002**, *62*, 2869–2874.
[18] I. K. Ko, T. J. Kean, J. E. Dennis, *Biomaterials* **2009**, *30*, 3702–3710.
[19] D. Rabuka, M. B. Forstner, J. T. Groves, C. R. Bertozzi, *J. Am. Chem. Soc.* **2008**, *130*, 5947–5953.
[20] J. T. Wilson, V. R. Krishnamurthy, W. Cui, Z. Qu, E. L. Chaikof, *J. Am. Chem. Soc.* **2009**, *131*, 18228–18229.
[21] S. Hong, P. R. Leroueil, E. K. Janus, J. L. Peters, M.-M. Kober, M. T. Islam, B. G. Orr, J. R. Baker Jr., M. M. Banaszak Holl, *Bioconjugate Chem.* **2006**, *17*, 728–734.
[22] F. M. Menger, V. A. Seredyuk, M. V. Kitaeva, A. A. Yaroslavov, N. S. Melik-Nubarov, *J. Am. Chem. Soc.* **2003**, *125*, 2846–2847.
[23] D. Fischer, B. Ahlemeyer, J. Kriegelstein, T. Kissel, *Biomaterials* **2003**, *24*, 1121–1131.
[24] A. J. Swiston, C. Cheng, S. H. Um, D. J. Irvine, R. E. Cohen, M. F. Rubner, *Nano Lett.* **2008**, *8*, 4446–4453.
[25] X. Chen, U. C. Tam, J. L. Czlapinski, G. S. Lee, D. Rabuka, A. Zettl, C. R. Bertozzi, *J. Am. Chem. Soc.* **2006**, *128*, 6292–6293.
[26] J. A. Prescher, C. R. Bertozzi, *Nat. Chem. Biol.* **2005**, *1*, 13–21.
[27] D. Datta, P. Wang, I. S. Carrico, S. L. Mayo, D. A. Tirrell, *J. Am. Chem. Soc.* **2002**, *124*, 5652–5653.
[28] K. Kirshenbaum, I. S. Carrico, D. A. Tirrell, *ChemBioChem* **2002**, *2-3*, 235–237.
[29] J. C. M. van Hest, K. L. Kiick, D. A. Tirrell, *J. Am. Chem. Soc.* **2000**, *122*, 1282–1288.
[30] A. J. Link, D. A. Tirrell, *J. Am. Chem. Soc.* **2003**, *125*, 11164–11165.
[31] L. K. Mahal, K. J. Yarema, C. R. Bertozzi, *Science* **1997**, *276*, 1125–1128.
[32] J. A. Prescher, D. H. Dube, C. R. Bertozzi, *Nature* **2004**, *430*, 873–877.
[33] Y. Kho, S. C. Kim, C. Jiang, D. Barma, S. W. Kwon, J. Cheng, J. Jaunbergs, C. Weinbaum, F. Tamanoi, J. Falck, et al., *Proc. Natl. Acad. Sci. U.S.A.* **2004**, *101*, 12479–

12484.
[34] E. Saxon, C. R. Bertozzi, *Science* **2000**, *287*, 2007–2010.
[35] N. J. Agard, J. A. Prescher, C. R. Bertozzi, *J. Am. Chem. Soc.* **2004**, *126*, 15046–15047.
[36] J. H. Lee, T. J. Baker, L. K. Mahal, J. Zabner, C. R. Bertozzi, D. F. Wiemer, M. J. Welsh, *J. Biol. Chem.* **1999**, *274*, 21878–21884.
[37] Y. Lang, F. del Monte, L. Collins, B. J. Rodriguez, K. Thompson, P. Dockery, D. P. Finn, A. Pandit, *Nat. Commun.* **2016**, *4*, 1–6.
[38] N. Kröger, N. Poulsen, *Annu. Rev. Genet.* **2008**, *42*, 83–107.
[39] E. H. Harris, *Annu. Rev. Plant Physiol. Plant Mol. Biol.* **2001**, *52*, 363–406.
[40] E. H. Harris, *The Chlamydomonas Sourcebook*, Elsevier, Kidlington, Oxford, **2009**.
[41] J. Nickelsen, U. Kück, *Naturwissenschaften* **2000**, *87*, 97–107.
[42] D. H. Miller, D. T. A. Lamport, M. Miller, *Science* **1972**, *176*, 918–920.
[43] M. A. O'Neill, K. Roberts, *Phytochemistry* **1981**, *20*, 25–28.
[44] J. P. Woessner, U. W. Goodenough, *Plant Physiol.* **1992**, *83*, 65–76.
[45] P. J. Ferris, J. P. Woessner, S. Waffenschmidt, S. Kilz, J. Drees, U. W. Goodenough, *Biochemistry* **2001**, *40*, 2978–2987.
[46] K. Roberts, M. Gurney-Smith, G. J. Hills, *J. Ultrastruct. Res.* **1972**, *40*, 599–613.
[47] U. W. Goodenough, J. E. Heuser, *J. Cell Biol.* **1985**, *101*, 1550–1568.
[48] F. Schötz, *Planta* **1972**, *102*, 152–159.
[49] J. Uniacke, W. Zerges, *Plant Physiol.* **2007**, *19*, 3640–3654.
[50] G. Jékély, *Phil. Trans. R. Soc. B* **2009**, *364*, 2795–2808.
[51] J. Buder, *Zur Kenntnis Der Phototaktischen Richtungsbewegungen*, Jahrb. Wiss. Bot., **1919**.
[52] W. Nultsch, *Arch. Microbiol.* **1977**, *112*, 179–185.
[53] W. Nultsch, *Arch. Microbiol.* **1979**, *123*, 93–99.
[54] M. E. H. Feinleib, G. M. Curry, *Physiol. Plant.* **1971**, *25*, 346–352.
[55] R. L. Stavis, R. Hirschberg, *J. Cell Biol.* **1973**, *59*, 367–377.
[56] M. Hippler, K. Redding, J.-D. Rochaix, *Biochim. Biophys. Acta* **1998**, *1367*, 1–62.
[57] M. A. Scaife, G. T. D. T. Nguyen, J. Rico, D. Lambert, K. E. Helliwell, A. G. Smith, *Plant J.* **2015**, *82*, 532–546.
[58] D. B. Weibel, P. Garstecki, D. Ryan, W. R. DiLuzio, M. Mayer, J. E. Seto, G. M. Whitesides, *Proc. Natl. Acad. Sci. U.S.A.* **2005**, *102*, 11963–11967.
[59] V. Magdanz, S. Sanchez, O. G. Schmidt, *Adv. Mater.* **2013**, *25*, 6581–6588.
[60] W. F. Paxton, S. Sundararajan, T. E. Mallouk, A. Sen, *Angew. Chem. Int. Ed.* **2006**, *45*, 5420–5429.
[61] M. Ito, N. Terahara, S. Fujinami, T. A. Krulwich, *J. Mol. Biol.* **2005**, *352*, 396–408.
[62] T. Nishihara, E. Freese, *J. Bacteriol.* **1975**, *123*, 366–371.
[63] J. E. Fein, *J. Bacteriol.* **1979**, *137*, 933–946.
[64] D. B. Kearns, R. Losick, *Genes Dev.* **2005**, *19*, 3083–3094.
[65] T. Rudrappa, W. J. Quinn, N. R. Stanley-Wall, H. P. Bais, *Planta* **2007**, *226*, 283–297.
[66] H. Pal Bais, R. Fall, J. M. Vivanco, *Plant Physiol.* **2004**, *134*, 307–319.
[67] R. Fall, R. F. Kinsinger, *System. Appl. Microbiol.* **2004**, *27*, 372–379.
[68] A. Pandey, L. M. Palni, *Microbiol. Res.* **1997**, *152*, 359–365.
[69] F. M. Cazorla, D. Romero, A. Pérez-García, B. J. J. Lugtenberg, A. de Vicente, G. Bloemberg, *J. Appl. Microbiol.* **2007**, *103*, 1950–1959.
[70] A. M. Earl, R. Losick, R. Kolter, *Trends Microbiol.* **2008**, *16*, 269–275.
[71] L. Merrill, J. Dunbar, J. Richardson, C. R. Kuske, *J. Forensic Sci.* **2006**, *51*, 559–565.
[72] R. Jaenicke, *Science* **2005**, *308*, 73–73.
[73] J. Errington, *Microbiol. Rev.* **1993**, *57*, 1–33.
[74] I. D. J. Burdett, T. B. L. Kirkwood, J. B. Whalley, *J. Bacteriol.* **1986**, *167*, 219–230.

[75] J. Errington, *Nat. Rev. Micro.* **2003**, *1*, 117–126.
[76] M. H. McCormick, W. M. Stark, G. E. Pittenger, R. C. Pittenger, J. M. McGuire, *Antibiot. Annu.* **1955**, *1*, 606–611.
[77] A. A. C. Dutton, P. C. Elmes, *Br. Med. J.* **1959**, *1*, 1144–1149.
[78] D. H. Williams, B. Bardsley, *Angew. Chem. Int. Ed.* **1999**, *38*, 1172–1193.
[79] P. Courvalin, *Clin. Infect. Dis.* **2006**, *42*, S25–S34.
[80] F. J. Marshall, *J. Med. Chem.* **1965**, *8*, 18–22.
[81] D. H. Williams, J. R. Kalman, *J. Am. Chem. Soc.* **1977**, *99*, 2768–2774.
[82] G. M. Sheldrick, P. G. Jones, O. Kennard, D. H. Williams, G. A. Smith, *Nature* **1978**, *271*, 223–225.
[83] D. H. Williams, *Acc. Chem. Res.* **1984**, *17*, 364–369.
[84] M. Schäfer, T. R. Schneider, G. M. Sheldrick, *Structure* **1996**, *4*, 1509–1515.
[85] P. J. Loll, A. E. Bevivino, B. D. Korty, P. H. Axelsen, *J. Am. Chem. Soc.* **1997**, *119*, 1516–1522.
[86] H. R. Perkins, *Pharmac. Ther.* **1982**, *16*, 181–197.
[87] M. A. Kohanski, D. J. Dwyer, J. J. Collins, *Nat. Rev. Micro.* **2010**, *8*, 423–435.
[88] D. H. Williams, M. P. Williamson, D. W. Butcher, S. J. Hammond, *J. Am. Chem. Soc.* **1983**, *105*, 1332–1339.
[89] T. D. H. Bugg, G. D. Wright, S. Dutka-Malen, M. Arthur, P. Courvalin, C. T. Walsh, *Biochemistry* **1991**, *30*, 10408–10415.
[90] C. C. McComas, B. M. Crowley, D. L. Boger, *J. Am. Chem. Soc.* **2003**, *125*, 9314–9315.
[91] J. H. Griffin, M. S. Linsell, M. B. Nodwell, Q. Chen, J. L. Pace, K. L. Quast, K. M. Krause, L. Farrington, T. X. Wu, D. L. Higgins, et al., *J. Am. Chem. Soc.* **2003**, *125*, 6517–6531.
[92] J.-Y. Wach, S. Bonazzi, K. Gademann, *Angew. Chem. Int. Ed.* **2008**, *47*, 7123–7126.
[93] V. Yarlagadda, P. Sarkar, S. Samaddar, J. Haldar, *Angew. Chem. Int. Ed.* **2016**, *55*, 7836–7840.
[94] P. Edman, *Acta Chem. Scand.* **1950**, *4*, 283–293.
[95] J. M. Berg, J. L. Tymoczko, L. Stryer, *Section 4.2: Amino Acid Sequences Can Be Determined by Automated Edman Degradation*, New York: W H Freeman, **2002**.
[96] P. Wilhelm, B. Lewandowski, N. Trapp, H. Wennemers, *J. Am. Chem. Soc.* **2014**, *136*, 15829–15832.
[97] S. L. Pedersen, A. P. Tofteng, L. Malik, K. J. Jensen, *Chem. Soc. Rev.* **2012**, *41*, 1826–1844.
[98] M. A. Sanders, J. L. Salisbury, *Methods Cell Biol.* **1995**, *47*, 163–169.
[99] A. J. Kell, B. Simard, *Chem. Commun.* **2007**, 1227–1229.
[100] W. A. Velema, J. P. van der Berg, M. J. Hansen, W. Szymanski, A. J. M. Driessen, Ben L Feringa, *Nat. Chem.* **2013**, 1–5.
[101] J. A. Myers, B. S. Curtis, W. R. Curtis, *BMC Biophysics* **2013**, *6*, 1–16.
[102] E. B. Naziga, F. Schweizer, S. D. Wetmore, *J. Phys. Chem. B* **2013**, *117*, 2671–2681.
[103] C. Garbay-Jaureguiberry, B. Arnoux, T. Prangé, S. Wehri-Altenburger, C. Pascard, B. P. Roques, *J. Am. Chem. Soc.* **1980**, *102*, 1827–1837.
[104] E. Roeder, *Pharmazie* **1995**, *50*, 83–98.
[105] A. R. Mattocks, *Chemistry and Toxicology of Pyrrolizidine Alkaloids*, Academic Press, London, **1985**.
[106] T. Hartmann, L. Witte, *Pyrrolizidine Alkaloids: Chemical, Biological and Chemoecological Aspects. in: Alkaloids: Chemical and Biological Perspectives*, Pergamon Press, Oxford, **1995**.
[107] *EFSA Journal*, **2011**, 9, 2406-2539.
[108] Y. Ikeda, H. Nonaka, T. Furumai, Y. Igarashi, *J. Nat. Prod.* **2005**, *68*, 572–573.

[109] R. M. Wallis, *Life Sci.* **1995**, *56*, 861–868.
[110] R. Nakai, H. Ogawa, A. Asai, K. Ando, T. Agatsuma, S. Matsumiya, S. Akinaga, Y. Yamashita, T. Miuzukami, *J. Antibiot.* **2000**, *53*, 294–296.
[111] T. Agatsuma, T. Akama, S. Nara, S. Matsumiya, R. Nakai, H. Ogawa, S. Otaki, S.-I. Ikeda, Y. Saitoh, Y. Kanda, *Org. Lett.* **2002**, *4*, 4387–4390.
[112] C. Kosogof, J. J. Tepe, R. M. Williams, *Tetrahedron Lett.* **2001**, *42*, 6641–6643.
[113] J. J. Tepe, R. M. Williams, *J. Am. Chem. Soc.* **1999**, *121*, 2951–2955.
[114] A. Ehmke, L. Witte, A. Biller, T. Hartmann, *Z. Naturforsch.* **1990**, *45c*, 1185–1192.
[115] A. Biller, M. Boppré, L. Witte, T. Hartmann, *Phytochemistry* **1994**, *35*, 615–619.
[116] T. Hartmann, C. Theuring, J. Schmidt, M. Rahier, J. M. Pasteels, *J. Insect Physiol.* **1999**, *45*, 1085–1095.
[117] T. Suzuki, M. Oka, K. Maeda, K. Furusawa, T. Mitani, T. Kataoka, *Chem. Pharm. Bull.* **1997**, *45*, 1218–1220.
[118] L. Bréthous, N. Garcia-Delgado, J. Schwartz, S. Bertrand, D. Bertrand, J.-L. Reymond, *J. Med. Chem.* **2012**, *55*, 4605–4618.
[119] N. Garcia-Delgado, S. Bertrand, K. T. Nguyen, R. van Deursen, D. Bertrand, J.-L. Reymond, *ACS Med. Chem. Lett.* **2010**, *1*, 422–426.
[120] T. Suzuki, M. Oka, K. Maeda, K. Furusawa, T. Mitani, T. Kataoka, *Chem. Pharm. Bull.* **1998**, *45*, 1218–1220.
[121] S. Udagawa, S. Sakami, T. Takemura, M. Sato, T. Arai, A. Nitta, T. Aoki, K. Kawai, T. Iwamura, S. Okazaki, et al., *Bioorg. Med. Chem. Lett.* **2013**, *23*, 1617–1621.
[122] S. Machida, N. Kato, K. Harada, J. Ohkanda, *J. Am. Chem. Soc.* **2011**, *133*, 958–963.
[123] K. L. Sorgi, C. A. Maryanoff, D. A. McComsey, B. E. Maryanoff, *Org. Synth.* **1998**, *75*, 215.
[124] P. Janvier, X. Sun, H. Bienaymé, J. Zhu, *J. Am. Chem. Soc.* **2002**, *124*, 2560–2567.
[125] D. W. Carney, J. V. Truong, J. K. Sello, *J. Org. Chem.* **2011**, *76*, 10279–10285.
[126] C. J. Gerack, L. McElwee-White, *Molecules* **2014**, *19*, 7689–7713.
[127] R. Obrecht, R. Herrmann, I. Ugi, *Synthesis* **1985**, 400–402.
[128] M. Tobisu, K. Koh, T. Furukawa, N. Chatani, *Angew. Chem. Int. Ed.* **2012**, *51*, 11363–11366.
[129] A. V. Gulevich, A. G. Zhdanko, R. V. A. Orru, V. G. Nenajdenko, *Chem. Rev.* **2010**, *110*, 5235–5331.
[130] N. J. Leonard, A. S. Hay, *J. Am. Chem. Soc.* **1956**, *78*, 1984–1987.
[131] K. A. Tehrani, M. D'hooghe, N. De Kimpe, *Tetrahedron* **2003**, *59*, 3099–3108.
[132] N. J. Leonard, A. S. Hay, R. W. Fulmer, V. W. Gash, *J. Am. Chem. Soc.* **1955**, *77*, 439–444.
[133] S. A. Popov, A. V. Rukavishnikov, A. V. Tkachev, *Synthesis* **1992**, 783–786.
[134] S. Menichetti, R. Amorati, M. G. Bartolozzi, G. F. Pedulli, A. Salvini, C. Viglianisi, *Eur. J. Org. Chem.* **2010**, *2010*, 2218–2225.
[135] D. S. Mueller, N. L. Untiedt, A. P. Dieskau, G. L. Lackner, L. E. Overman, *J. Am. Chem. Soc.* **2015**, 660–663.
[136] J. P. Michael, *Nat. Prod. Rep.* **2008**, *25*, 139–165.
[137] E. Gellert, *J. Nat. Prod.* **1982**, *45*, 50–73.
[138] H. J. R. Schmidt, H. J. Schäfer, *Angew. Chem. Int. Ed.* **1981**, *20*, 109–109.
[139] T. Suzuki, Oka, K. Maeda, K. Furusawa, K. Furusawa, H. Uesaka, T. Kataoka, *Chem. Pharm. Bull.* **1999**, *47*, 28–36.
[140] T. F. Stocker, D. Qin, G. K. Plattner, M. Tignor, J. Boschung, A. Nauels, V. Bex, P. M. Midgley, *Climate Change 2013: the Physical Science Basis. Contribution of Working Group I to the Fifth Assessment Report of the Intergovern- Mental Panel on Climate Change*, Ipcc, **2013**.
[141] O. Edenhofer, R. Pichs-Madruga, Y. Sokona, E. Farahani, S. Kadner, K. Seyboth, A.

Adler, I. Baum, S. Brunner, P. Eickemeier, et al., *Contribution of Working Group III to the Fifth Assessment Report of the Intergovernmental Panel on Climate Change*, IPCC Synthesis Report **2014**.
[142] J. Tollefson, *Nature* **2015**, *520*, 20–23.
[143] C. Song, *Catal. Today* **2006**, *115*, 2–32.
[144] M. Aresta, *Carbon Dioxide: Utilization Options to Reduce Its Accumulation in the Atmosphere*, Wiley-VCH Verlag GmbH & Co. KGaA, Weinheim, Germany, **2010**.
[145] Q. Liu, L. Wu, R. Jackstell, M. Beller, *Nat. Commun.* **2015**, *6*, 1–15.
[146] D. Y. C. Leung, G. Caramanna, M. M. Maroto-Valer, *Renewable Sustainable Energy Rev.* **2014**, *39*, 426–443.
[147] G. T. Rochelle, *Curr. Opin. Chem. Eng.* **2012**, *1*, 183–190.
[148] S. B. Fredriksen, K.-J. Jens, *Energy Procedia* **2013**, *37*, 1770–1777.
[149] C. Lastoskie, *Science* **2010**, *330*, 595–596.
[150] H. Yin, Y. Feng, H. Liu, M. Mu, C. Fei, *Langmuir* **2014**, *30*, 9911–9919.
[151] X. Luo, Y. Guo, F. Ding, H. Zhao, G. Cui, H. Li, C. Wang, *Angew. Chem. Int. Ed.* **2014**, *53*, 7053–7057.
[152] P. G. Jessop, D. J. Heldebrant, X. Li, C. A. Eckert, C. L. Liotta, *Nature* **2005**, *436*, 1102–1102.
[153] M. Cakmak, P. Mayer, D. Trauner, *Nat. Chem.* **2011**, *3*, 543–545.
[154] O. E. Curtis, Jr, J. M. Sandri, R. E. Crocker, H. H. C. B. V. Boekelheide, R. Taber, D. S. Tarbell, *Org. Synth.* **1958**, *38*, 19.
[155] F. Sanger, *Biochem. J.* **1945**, *39*, 507–515.
[156] D. S. Surry, S. L. Buchwald, *Chem. Sci.* **2010**, *2*, 27.
[157] B. P. Fors, D. A. Watson, M. R. Biscoe, S. L. Buchwald, *J. Am. Chem. Soc.* **2008**, *130*, 13552–13554.
[158] D. Maiti, B. P. Fors, J. L. Henderson, Y. Nakamura, S. L. Buchwald, *Chemical Science* **2010**, *2*, 57.
[159] B. E. Gurkan, J. C. de la Fuente, E. M. Mindrup, L. E. Ficke, B. F. Goodrich, E. A. Price, W. F. Schneider, J. F. Brennecke, **2010**, *132*, 2116-2117.
[160] M. Aresta, D. Ballivet-Tkatchenko, D. B. Dell'Amico, D. Boschi, F. Calderazzo, L. Labella, M. C. Bonnet, R. Faure, F. Marchetti, *Chem. Commun.* **2000**, 1099–1100.
[161] A.-H. Liu, R. Ma, C. Song, Z.-Z. Yang, A. Yu, Y. Cai, L.-N. He, Y.-N. Zhao, B. Yu, Q.-W. Song, *Angew. Chem. Int. Ed.* **2012**, *51*, 11306–11310.
[162] O. A. Subbotin, I. M. Skvortsov, *Chem. Heterocycl. Compd.* **1985**, *21*, 1347–1355.
[163] I. M. Skvortsov, *Chem. Heterocycl. Compd.* **2006**, *42*, 1247–1266.
[164] D. J. Heldebrant, C. R. Yonker, P. G. Jessop, L. Phan, *Energy Environ. Sci.* **2008**, 1, 487-493.
[165] F.-F. Chen, K. Huang, Y. Zhou, Z.-Q. Tian, X. Zhu, D.-J. Tao, D.-E. Jiang, S. Dai, *Angew. Chem. Int. Ed.* **2016**, *55*, 7166-7170.
[166] H. Liu, B. Liu, L.-C. Lin, G. Chen, Y. Wu, J. Wang, X. Gao, Y. Lv, Y. Pan, X. Zhang, et al., *Nat. Commun.* **2014**, *5*, 5147.
[167] G. Puxty, R. Rowland, A. Allport, Q. Yang, M. Bown, R. Burns, M. Maeder, M. Attalla, *Environ. Sci. Technol.* **2009**, *43*, 6427–6433.
[168] X. Subirats, M. Rosés, E. Bosch, *Sep. Purif. Rev.* **2007**, *36*, 231–255.
[169] R. Fischer, O. Mader, G. Jung, R. Brock, *Bioconjugate Chem.* **2003**, *14*, 653–660.
[170] Kim, J. M. Beebe, Y. Jun, X. Y. Zhu, C. D. Frisbie, *J. Am. Chem. Soc.* **2006**, *128*, 4970–4971.
[171] H. Karaman, R. J. Barton, B. E. Robertson, D. G. Lee, *J. Org. Chem.* **1984**, *49*, 4509–4516.
[172] M. Oka, Y. Matsumoto, K. Hirooka, T. Suzuki, *Chem. Pharm. Bull.* **2000**, *48*, 1121–1124.